HUNGARIAN

Journal of

INDUSTRIAL CHEMISTRY

Edited by

the Hungarian Oil & Gas Research Institute (MÁFKI),
the Research Institute for Heavy Chemical Industries (NEVIKI),
the Research Institute for Technical Chemistry of the
Hungarian Academy of Sciences (MÜKKI),
the Veszprém University of Chemical Engineering (VVE).
Veszprém (Hungary)



Volume 6. 1978 Number 1.

HU ISSN: 0133—0276
CODEN: HJICAI

Editorial Board:

R. CSIKÓS and GY. MÓZES
Hungarian Oil & Gas Research Institute
(MÁFKI Veszprém)

A. SZÁNTÓ and M. NÁDASY
Research Institute for Heavy Chemical Industries
(NEVIKI Veszprém)

T. BLICKLE and O. BORLAI
Research Institute for Technical Chemistry
of the Hungarian Academy of Sciences
(MÜKKI Veszprém)

A. LÁSZLÓ and L. PÉCHY
Veszprém University of Chemical Engineering
(VVE Veszprém)

Editor-in Chief:
E. BODOR

Assistant Editor:
J. DE JONGE

Veszprém University of Chemical Engineering
(VVE Veszprém)

The „Hungarian Journal of Industrial Chemistry" is a joint publication of the Veszprém scientific institutions of the chemical industry that deals with the results of applied and fundamental research in the field of chemical processes, unit operations and chemical engineering. The papers are published in four numbers at irregular intervals in one annual volume, in the English, Russian, French and German languages

Editorial Office:
Veszprémi Vegyipari Egyetem
„Hungarian Journal of Industrial Chemistry"
H–8201 Veszprém, P. O. Box: 28.
Hungary

Subscription price $ 45.– per volume/year Orders may be placed with
KULTURA
Foreign Trading Co. for Books and Newspapers
Budapest, 62. POB 149
or with its representatives abroad, listed on the verso of the cover

FELELŐS SZERKESZTŐ: DR. BODOR ENDRE

KIADJA A LAPKIADÓ VÁLLALAT, 1073 BP. VII., LENIN KRT. 9—11.
TELEFON: 221-285. LEVÉLCÍM: 1906 BP. PF. 223
FELELŐS KIADÓ: SIKLÓSI NORBERT IGAZGATÓ

HUNGARIAN

Journal of

INDUSTRIAL CHEMISTRY

Edited by

the Hungarian Oil & Gas Research Institute (MÁFKI),
the Research Institute for Heavy Chemical Industries (NEVIKI),
the Research Institute for Technical Chemistry of the
Hungarian Academy of Sciences (MÜKKI),
the Veszprém University of Chemical Engineering (VVE).
Veszprém (Hungary)



Volume 6. **1978** **Number 1—4.**

HU ISSN: 0133—0276
CODEN: HJICAI

Editorial Board:

R. CSIKÓS and GY. MÓZES
Hungarian Oil & Gas Research Institute
(MÁFKI Veszprém)

A. SZÁNTÓ and M. NÁDASY
Research Institute for Heavy Chemical Industries
(NEVIKI Veszprém)

T. BLICKLE and O. BORLAI
Research Institute for Technical Chemistry
of the Hungarian Academy of Sciences
(MÜKKI Veszprém)

A. LÁSZLÓ and L. PÉCHY
Veszprém University of Chemical Engineering
(VVE Veszprém)

Editor-in Chief:
E. BODOR

Assistant Editor:
J. DE JONGE

Veszprém University of Chemical Engineering
(VVE Veszprém)

The „Hungarian Journal of Industrial Chemistry" is a joint publication of the Veszprém scientific institutions of the chemical industry that deals with the results of applied and fundamental research in the field of chemical processes, unit operations and chemical engineering. The papers are published in four numbers at irregular intervals in one annual volume, in the English, Russian, French and German languages

Editorial Office:
Veszprémi Vegyipari Egyetem
„Hungarian Journal of Industrial Chemistry"
H—8201 Veszprém, P. O. Box: 28.
Hungary

Subscription price $ 45.—per volume/per year. Orders may be placed with
KULTURA
Foreign Trading Co. for Books and Newspapers
Budapest 62. POB 149
or with its represenatives abroad, listed on the verso of the cover

FELELŐS SZERKESZTŐ: DR. BODOR ENDRE

KIADJA A LAPKIADÓ VÁLLALAT, 1073 BP. VII., LENIN KRT. 9—11.
TELEFON: 221-285. LEVÉLCÍM: 1906 BP. PF. 223
FELELŐS KIADÓ: SIKLÓSI NORBERT IGAZGATÓ

Egyetemi Nyomda — 78.3547 Budapest, 1979. Felelős vezető: Sümeghi Zoltán igazgató

INDEX

Balla, L. and Sisak, Cs.: Studies on the Liquid-Phase Hydrodynamics in Bubble and Sieve-Plate Columns Equipped with Selective Partitions I. Liquid Mixing Processes in the Connecting Tubes and on the Selective Partitions Installed between Pairs of Bubble or Sieve-Plate Columns 383

Balla, L. and Sisak, Cs.: Studies on the Liquid Phase Hydrodynamics in Bubble and Sieve-Plate Columns Equipped with Selective Partitions II. Modelling of the Flow Conditions in Counter-Current Cascades 395

Báthory, J.: see Csikós, Cs.

Mrs. Bésán, J.: see Gór-Nagy, S.

Biehounek, J.: The Throughput Availability of a Capacity-Divided Parallel Connection with Internal Capacity Reserve 369

Blickle, T.: see Lakatos, B., Vajda, T.

Cherkashin, V. V.: see Gartsman, A. N.

Csikós, Cs. und Báthory, J.: Untersuchungen der zur Dehydrierung von n-Hexan verwendeten Katalysatoren (The Examination of Catalysts Used for Dehydrogenation of n-Hexane) 155

Csukás, B.: see Szentmarjay, T.

Dencs, B. and Ormós, Z.: Particle Formation from Solutions in Gas Fluidized Bed. I. Establishment of Steady State Conditions by Solid Material Feed-in 301

Dencs, B. and Ormós, Z.: Particle Formation from Solutions in Gas Fluidized Bed. II. The Effects of the Characteristics of the Solid Material and Solution Fed-in upon the Physical Properties of the Particles Formed 313

Dencs, B. and Ormós, Z.: Particle Formation from Solutions in Gas Fluidized Bed. III. The Effects of Bed Geometry, Mechanical Agitation and Material Properties upon the Physical Characteristics of the Particles Formed 323

Dencs, B. and Ormós, Z.: Particle Formation from Solutions in Gas Fluidized Beds. IV. Determination of Average Particle Size and Solid Material Feed Ratio ... 343

Fratzscher, W., Hebecker, D. und Gaffke, H.: Zur Gleichgewichtberechnung und Bewertung gasförmiger Energieträger bei Hochtemperaturprozessen (To the Equilibrium Calculation and Estimation of Gaseous Energy Carriers of High Temperature Processes) 351

Fratzscher, W. und Michalek, K.: Energetische und exergetische Analyse einer Rohöldestillationsanlage (Energetic and Exergetic Examination of Crude Oil Distillation Plant) 163

Gaffke, H.: see Fratzscher, W.

Gartsman, A. N., Cherkashin, V. V. and Rassadnikova, N. I.: Chemical Reaction Accompanied by Mass Transfer in Liquid-Gas System. II. Consecutive First and Second Order Chemical Reactions (in the Russian) 361

Gór-Nagy, S., Káldi, P., Mrs. Bésán, J. and Szántó, A.: The Solubility of Micronutrients in Ammonium Polyphosphate Solutions 259

Gruhn, G., Neumann, W. and Heining, H.: Reliability Analysis of Chemical Plants by Means of Markow Processes 275

Gupta, P. K. and Ravindram, M.: Vapour Phase Dehydration of Ethyl Alcohol over Alumina and Related Catalysts 115

Hakim, K. A. A., Zalai, A., Lechner, A. and Tóth, A.: Study on the Effect of a Detergent Additive, and Test Severity on Motor Oil Test Results 251

Halász, G.: Determination of the Filtrate Output of the Industrial Filtration Centrifuge with the aid of a Model Sized Centrifuge 435

Hebecker, D.: see Fratzscher, W.

Heining, H.: see Gruhn, G.

Holderith, J.: Some Linear Relations in Hierarchic Modelling of Multiphase Reactors 125

Mrs. Horváth, E., Pataki, K. and Ormós, Z.: Hydrodynamical Studies on Fluidized Beds. VI. Studies on the Hydrodynamical Properties of Gas-Fluidized Beds with Concial Inserts 93

Mrs. Horváth, E., Pataki, K. and Ormós, Z.: Studies on Particle Coating. I. Film-Coating of Urea Particles in Fluidized Bed 225

Iván, L.: see Várhegyi, Gy.

KÁLDI, P.: see GÓR-NAGY, S.
KEIL, G.: see NOWAK, S.
KIRILLOV, V. A. and OGARKOV, B. L.: The Examination of Heat and Mass Transfer in a Three Phase, Fixed Catalyst Bed (in the Russian) 175
KRAMARZ, J. and RADOSZ, M.: Prediction of Catalytic Reformer Yield by Chemical Equilibrium (Commercial Results) 243
KURIACOSE, J. C.: see SUBRAHMANYAM, M., YESODHARAN, E. P.
LAKATOS, B. and BLICKLE, T.: The Inhomogeneity Parameter and its Properties. I. Closed Systems 53
LAKATOS, B. and BLICKLE, T.: The Inhomogeneity Parameter and its Properties. II. Open Systems 67
LECHNER, A.: see HAKIM, K. A. A.
MICHALEK, K.: see FRATZSCHER, W.
MISKEI, M.: see VÁRHEGYI, GY.
MOHOS, F.: General Properties of Technological Systems. I. 21
MOHOS, F.: General Properties of Technological Systems. II. 39
MOHOS, F.: General Properties of Technological Systems. III. 131
MOHOS, F.: General Properties of Technological Systems. IV. 145
NEUMANN, W.: see GRUHN, G.
NOWAK, S., KEIL, G. and ZIMMERMANN, G.: Zur Pyrolyse höhersiedender technischer Erdölfraktionen. (The Pyrolysis of High Boiling Point Oil Fractions) 105
OGARKOV, B. L.: see KIRILLOV, V. A.
ORMÓS, Z.: see DENCS, B., MRS. HORVÁTH, E., SZENTMARJAY, T.
PARTI, M.: Transport Processes in Packed Beds 333
PATAKI, K.: see MRS. HORVÁTH, E.
RADOSZ, M.: see KRAMARZ, J.
RAMAKRISHNAN, V.: see YESODHARAN, E. P.
RASSADNIKOVA, N. I.: see GARTSMAN, A. N.
RAVINDRAM, M.: see GUPTA, P. K.
SEBESTYÉN, ZS.: see SZEPESY, K.
SISAK, CS.: see BALLA, L.
SUBRAHMANYAM, M. and KURIACOSE, J. C.: The Nature of the Reaction of Propan-2-ol on a Zn:Cr:Fe Catalyst 283
SZÁNTÓ, A.: see GÓR-NAGY, S.
SZENTMARJAY, T., CSUKÁS, B. and ORMÓS, Z.: Hydrodynamical Studies on Fluidized Beds. V. Studies on the Particle Mixing Phenomena in Dual-cell Fluidized Beds Using Isotope Tracer Techniques 81
SZEPESY, K., WELTHER, K. and SEBESTYÉN, ZS.: Efficient Catalytic Oxidation Process for Air Pollution Abatement 11
SZÉPVÖLGYI, J. and ÚJHIDY, A.: Studies on Ethylene Dichloride Formation in a Rotary Film Reactor I. Kinetical Investigations 187
SZÉPVÖLGYI, J.: Studies on Ethylene Dichloride Formation in a Rotary Film Reactor II. Investigations in a Reactor of Known Transfer Surface 195
SZÉPVÖLGYI, J. and ÚJHIDY, A.: Studies on Ethylene Dichloride Formation in a Rotary Film Reactor III. Investigation of Rotary Film Equipment as a Reactor 211
TÓTH, A.: see HAKIM, K. A. A.
ÚJHIDY, A.: see SZÉPVÖLGYI, J.
VAJDA, T.: Annähernde analytische Beschreibung einer Reaktion ersten Grades in einem Dünnschichtreaktor (Approximate Analytic Description of a First Order Reaction Carried out in a Rotary Film Reactor) 409
VAJDA, T. and BLICKLE, T.: Algorythm for the Analytical Approximation of a Diffusion Model of Diphasic Processes Occurring in Heat and Mass Transfer 423
VÁRHEGYI, GY., MISKEI, M. and IVÁN, L.: Intensive Methods for the Preparation of Vanadium Chlorides from Bauxite Ore 1
WELTHER, K.: see SZEPESY, K.
ZALAI, A.: see HAKIM, K. A. A.
ZIMMERMANN, G.: see NOWAK, S.
YESODHARAN, E. P., RAMAKRISHNAN, V. and KURIACOSE, J. C.: Reactions of Benzyl Alcohol on U-V Irradiated Zinc Oxide 293

HUNGARIAN JOURNAL
OF INDUSTRIAL CHEMISTRY
VESZPRÉM
Vol. 6. pp. 1—10 (1978)

INTENSIVE METHODS FOR THE PREPARATION OF VANADIUM CHLORIDES FROM BAUXITE ORE

GY. VÁRHEGYI, M. MISKEI and L. IVÁN

(Research Institute for Non-Ferrous Metals, Budapest)

Received: November 14, 1977.

The authors elaborated a technology for the production of vanadium (IV)-chloride and vanadium (V)-oxide-trichloride, starting from bauxite processing. On the basis of the results, model experimental reactors were constructed, such as a steel reactor for chlorination and a salt column for purification, from which impurities can be continuously removed in the form of complex double salts.

The production of vanadium(V)-oxide-trichloride was accomplished by partial oxidation of vanadium(IV)-chloride with air accompanied by ignition.

Reactors with high productivity can be constructed inexpensively. The energy consumption of the process is quite low.

The fifth group of the periodical system contains several rare metals, forming the vanadium group. New processes for their preparation were developed with the application of the latest results in the field of halogen-metallurgy.

Halogen-metallurgy—a steadily developing branch of metallurgy—produces metals by entirely new chemical reactions. The main results can be summarized as follows:

a) Various processes on an industrial scale for the preparation of metal-chlorides are known which can easily be developed and designed for automatic operation. Such processes cover the preparation of titanium-tetrachloride, uranium-tetrafluoride, and aluminium-trichloride, etc., plus numerous rare metal-chlorides.

b) A number of processes are used for the separation and purification of metal-chlorides, the majority of which are dependent on the difference in the melting and boiling point, and vapour pressure of metal-chlorides, respectively.

c) Chemical purification methods utilizing the formation of complex chlorides are also known, which surpass physical methods in simplicity and efficiency. These include the purification process based on the formation of double-chlorides of iron- and aluminium-chlorides with alkali metals. The change in the degree of oxidation of metal-chlorides also provides good separation.

d) Halogen-metallurgy opens up the possibility for the wide range processing of raw materials and thus also the extraction of rare metals.

e) The construction material problem can be considered as solved. In the majority of cases this is not relatively cheap, but a small-size, efficient reactor can be built at a favourable price.

f) The main advantage of halogen-metallurgy processes is that metal is more easily produced from metal halogenides, than from metal-oxides. In addition, a better possibility exists for making the processes more efficient. For example, bipolar cells of chloride-electrolysis, different Kroll syntheses, and reductions by hydrogen, etc.

g) Finally, the energy requirement of the processes for the preparation of chlorides, its separation and reduction is surprisingly low. Many chemical reactions involved are exothermic, for instance, the processes for the formation of some chlorides, the reduction by hydrogen, and the formation of complex-chlorides.

The production of metallic vanadium starting from bauxite ore goes through the preparation of vanadium-tetrachloride, vanadium trichloride and vanadium sponge. Vanadium oxide trichloride (VCl_3O) might also occur during the process. The aim of our work was to develop economic and efficient processes that can be readily developed, which can serve as the foundation for the development of technology for other rare metals.

The sequence of our work was as follows:

1. A suitable process was selected for the basis of the method.
2. Reaction kinetic measurements were carried out in model-experiments and the parameters of the continuous process were established.
3. On basis of the results obtained in this way, an experimental unit with a higher capacity was designed and operated for a longer time.

Preparation and Purification of Vanadium(IV)-Chloride

The main phases of the development work were following:

The synthesis was selected for vanadium(IV) chloride production, i.e. the product was made from primary vanadium produced by alumino-thermic reduction (approx. 80% purity) and elemental chlorine. The reaction involved is satisfactorily exothermic, fast and we can presume an almost complete conversion.

Based on the literature of the last hundred years, synthesis processes were summarized in *Table 1.*

Except for two methods, the processes involved are of laboratory-scale, carried out in a quartz tube unsuitable for development. The processes of FOLEY and co-workers [1] for the preparation of chlorides carried out in a furnace provided with a heat-resistant lining and that of W. THIEL [2] carried out in ceramic-lined reactor can already be considered small-scale technical-size methods. However, these are processes of a small specific output, and a bigger quantity of material cannot be burnt in them without the risk of sintering, and the lining of the furnace and reactor is subject to frequent replacement.

Table 1

Prepearation of vanadium(IV)-chloride by synthesis
Comparison of process in chronological order

Process	Initial raw materials	Temperature °C	Development stage	Construction material of the reactor	Year and remarks
Roscoe Koppel Ruff Meyer Voigt Starr Stschuckarev	$V + Cl_2$	600—1000	laboratory scale	quartz	1870 1905 1911 1924 1924 1940 1956
Tyczak Foley	synthesis	600—1000	laboratory semi-continuous technical scale	quartz	1957 1957 construction material unknown
Freiberg FNE[2]	Nb, $Ta + Cl_2$	600—1000	large scale laboratory process	ceramic lining	1964 unreliable construction material
FKI I.[1]	synthesis	600—800	large-scale laboratory process	quartz	1965 without continuous heat removal
FKI II.	synthesis	800—1000	small-scale plant size	cooled steel reactor	1970 with continuous heat removal

1. FKI = Fémipari Kutató Intézet (Research Institute for Non-Ferrous Metals) Budapest.
2. FNE = Forschungsinstitut f. Nichteisenmetalle Freiberg.

In developing our process, the results of the model tests (3) were carried out with raw vanadium and chlorine in a quartz boat. According to this, the formation of vanadium(IV)-chloride is more rapid and complete—as can be seen from *Fig. 1*—if we work above 600° C temperature.

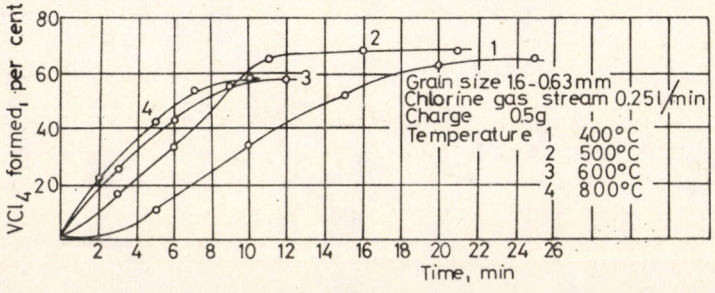

Fig. 1.

Quantity of vanadium(IV) chloride formed from raw vanadium at different temperatures as a function of time

Below 600° C temperature sigmoid-shape-curves were obtained, indicative of autocatalytic processes. The ignition temperature of vanadium in a chlorine atmosphere was found to be 600° C.

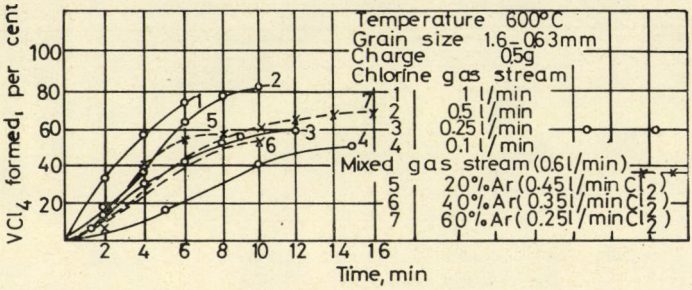

Fig. 2.

Quantity of vanadium(IV) chloride formed from raw vanadium at different gas velocities and chlorine gas concentration respectively as a function of time

In the next series of measurements, according to *Fig. 2* the rate of vanadium(IV) chloride formation increased depending on the velocity of the chlorine gas stream, which indicated that the reaction took place in the kinetic field, and was not hampered by diffusion processes.

Thus, in a continuous process it can be expected that we can work in the high-velocity range. In addition, the accumulation of a larger quantity of raw vanadium can be avoided and also the risk of sintering.

The tubular quartz reactor of a vertical arrangement on laboratory scale was designed on basis of the model test results. Chlorine gas was fed into the reactor from the bottom and led through the raw vanadium bed. The device was suitable for the production of vanadium(IV) chloride at the rate of 1 kg/h.

Modifications were necessary in two fields, one of them was the separator operated on the principle of fractional condensation used by FOLEY and coworkers [1] in which impurity metal chlorides were separated above the boiling point of vanadium(IV) chloride, at 200° C, and the other was the quartz reactor which inhibited technical scale operation due to its fragility.

A limitation in the efficiency of the separator is shown in *Fig. 3*. By this method it is possible to separate only 80 per cent of the iron-chloride (Fe_2Cl_6) and 40 per cent of aluminium-chloride (Al_2Cl_6). In addition iron-chloride and aluminium-chloride take part in the undesirable decomposition of vanadium (IV) chloride occurring during its condensation, which leads to clogging.

A process for quantitative separation was required, which was found in the formation of the chloride-complex composed of sodium-chloride, with iron- and aluminium-chlorides. The principle used by KORSHUNOV and MOROZOV [4] was applied in a vertical column filled with lumpy salt. In this column, at 300° C, reaction yielded—in quantitative way—a chloride-complex composed of iron and aluminium-chlorides, which in a melted condition drained out at the bottom of the column.

The replacement of the quartz tube by another—possible metal—construction material of good thermal conductivity was a major problem. The suggestion was put forward to keep our construction material close to room tem-

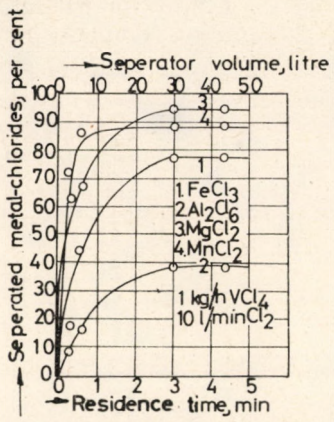

Fig. 3.
Separation of metal-chlorides in the separator as a function of holding time

perature to prevent its damage as it is subjected to strong corrosion at a high temperature. This was in complete agreement with our other objective, namely, the increase in efficiency is accompained by a proportional increase in exothermic heat, which we wanted to remove by a flowing cooling medium. Thus, the idea was reached of using a water-cooled, jacketed steel reactor, designed on the following basis:

The prerequisite for the maintenance of the process was to have the reaction heat as close as possible to the value, which a cylindrical steel wall could remove. For example a steel tube with a diameter of 100 mm and with a length of 300 mm, has a heat permeability of 4000 kcal/h. This was compared in *Table 2*, with the heat formed during the formation of vanadium(IV)

Table 2.
Comparison of reaction heat formed during different outputs with the heat that can be removed by a 100 mm diameter steel tube*

VCl_4 (kg/h)	Heat formation (kcal/h)	Removable heat (kcal/h)	Difference (kcal/h)	Remarks
1	890	4040	−3150	small, it freezes in
2	1780	4040	−2260	small, it freezes in
3	2670	4040	−1370	small, it freezes in
4	3560	4040	−480	in balance
5	4450	4040	+410	in balance
6	5340	4040	+1300	too high overheated
7	6230	4040	+2190	too high, overheated

* Wall thickness: 10 mm; temperature difference: 45 − 35° C = 10° C.

chloride on a scale of 1, 2, 3 kg/h, etc., minus heat needed for the warming up of raw materials and removed by metal chloride vapours and chlorine.

Thus, the thermal equilibrium of our imaginary test reactor is reached at an output of 4–5 kg/h. The accuracy of above calculation was verified by experiment. The warming up of the cooling water came up to our expectation and adapted itself entirely to the charging, thus charging could be controlled by a contact thermometer. *Fig. 4* shows the process flow sheet of an automatically operated bench-scale operation unit linked up with a salt column and condenser.

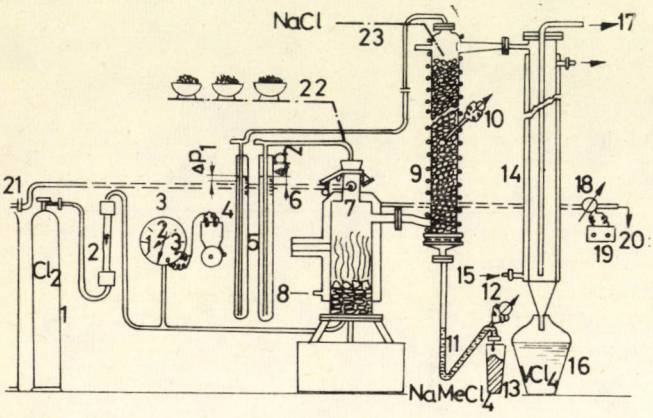

Fig. 4.

Process flow sheet of recovery and purification of vanadium(IV) chloride on scale of 15 kg/h
1 — chlorine gas cylinder, 2 — rotameter, 3 — contact manometer, 4 — indicator bell, 5 — pressure gauge, 6 — make-up chlorine, 7 — steel reactor with water jacket, 8 — water inlet, 9 — salt column, 10 — thermometer, 11 — complex-chloride outlet tube, 12 — thermometer, 13 — complex-chloride collector, 14 — cyclone condenser, 15 — water input, 16 — VCl_4-collection, 17 — outgoing gas, 18 — contact thermometer, 19 — indicator, 20 — cooling water outlet, 21 — supplementary chlorine gas cylinder, 22 — raw vanadium charging, 23 — salt charging

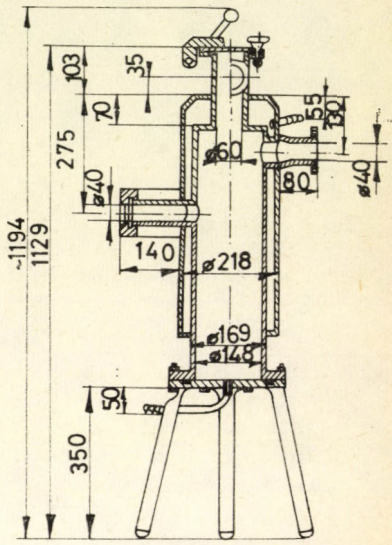

Fig. 5.

Scheme of water cooled steel reactor for the production of vanadium(IV) chloride on a scale of 15 kg/h

The cooled steel reactor is shown in *Fig. 5*.

The productivity of the automatically controlled plant is high: 15 kg/h. The iron and aluminium content of the product is below 20 ppm Due to its readiness to decomposition, vanadium(IV)-chloride has to be protected against light, humidity and heat, and used if possible, within few days.

Preparation of Vanadium(V) Oxide Trichloride (VCl_3O)

A summary of the laboratory processes so far known for the preparation of vanadium(V) oxide trichloride is given in *Table 3*.

Table 3.

Comparison of processes for making vanadium (V) oxide trichloride

Process	Starting materials	Temp. °C	Development stage	Construction material of the reactor	Remarks
Ruff Lickfett 1911	$V_2O_3 + C + Cl_2$	2—300	laboratory tests	quartz	contaminated product
Ruff Lickfett 1911	$V_2O_3 + S_2Cl_2$	2—300	laboratory tests	quartz	contaminated product
Ruff Friedrich 1914	$VCl_4 + O_2$	600	laboratory tests	quartz	uncertain, too much V_2O_5 was formed
Ruff Lickfett 1911	$V_2O_5 + Cl_2$	2—400	laboratory process	quartz	not yet elaborated
Oppermann Gmelin Slawish 1962, 1970	$V_2O_5 + C + Cl_2$	2—400	laboratory process	quartz	contaminated product
Hecht Janden Schappman 1947	$V_2O_5 + SOCl_2$	300	laboratory process	glass	boiled with reflux-cooler, contaminated product
Schelden Tyree 1959	$V_2O_5AlCl_3$	300	laboratory process	unpublished	product contains some Al
Du Pont 1959	$NH_4VO_3 +$ + air + Cl_2	200—400	technical scale operation	unpublished	at first V_2O_5 is produced by the fluidising technique
Ruff Lickfett 1911	$VCl_3 + O_2$	5—600	laboratory tests	quartz	expensive procedure
Roscoe 1868	$VCl_4 + Na$	152	laboratory purification process	glass	risk of explosion. Earlier used for purification
Dynamit-Nobel 1962	$VCl_4 + O_2$	300	technical scale, batch process	unpublished	indirect, slow oxidation, batch process
New FKI[1] process 1970	VCl_4 + air	400—450	technical scale, continuous process	nickel	direct flame reaction continuous

[1] FKI = Fémipari Kutató Intézet (Research Institute for Non-Ferrous Metals) Budapest.

The unsuccessful experiment of RUFF and FRIEDRICH [5] fifty years ago was chosen as the starting point of our method among the existing laboratory processes. The vanadium(IV) chloride was treated with oxygen at red hot temperature and a lot of vanadium-pentoxide was formed in addition to vanadium(V) oxyde-trichloride.

During the kinetic measurements carried out at different temperatures and with different oxygen-nitrogen mixtures in the model unit illustrated in *Fig. 6.*, it was found that the process takes place under a strong flame forma-

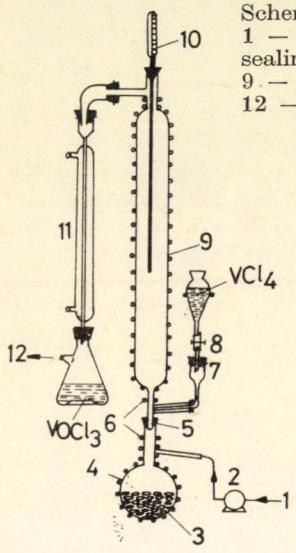

Fig. 6.
Scheme of model reactor
1 — air, 2 — compressor, 3 — VCl_4-boiler, 4 — heating, 5 — sealing, 6 — VCl_4-inlet, 7 — inspection window, 8 — charging, 9 — transparent model-reactor, 10 — thermo- meter, 11 — cooler, 12 — outgoing gas

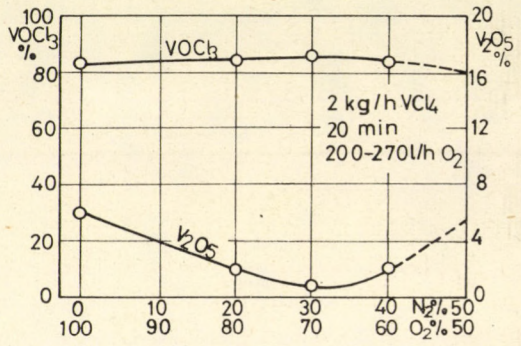

Fig. 7.
Formation of vanadium (V) oxide trichloride and vanadium-pentoxide as a function of VCl_4 temperature

tion at 400° C temperature. The formation of undesirable vanadium pentoxide can be reduced from 15 per.cent to 5 per cent *(Fig. 7.)* by the appropriate setting of the inlet gas temperature and to a neglible value by the use of a suitable nitrogen dilution according to *Fig. 8.*

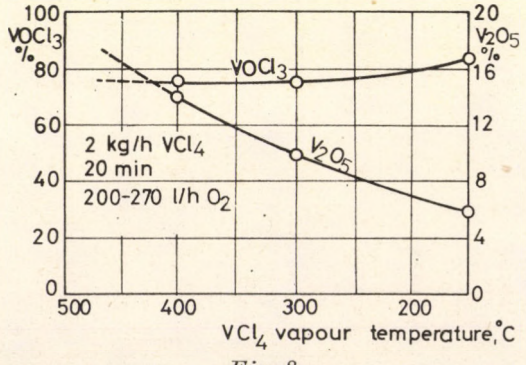

Fig. 8.
Formation of vanadium(V) oxide trichloride and vanadium-pentoxide as a function of the oxygen concentration

Finally, the dilution resulted in a gas mixture corresponding to the composition of air, which also added to the economy of the process.

The product is a clear liquid, golden yellow in colour, it does not decompose, and can be easily purified by destillation. The product is not only used as a catalyst, but also as an important basic material for the manufacture of vanadium-pentoxide of semi-conductor quality.

In *Fig. 9* the flame reactor and in *Fig. 10* the process flowsheet of a laboratory unit of 10 kg/h output can be seen.

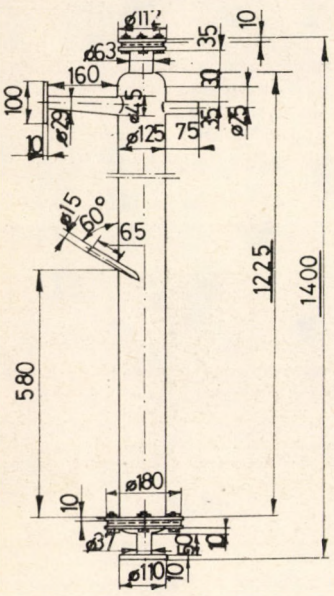

Fig. 9.
Scheme of nickel flame reactor

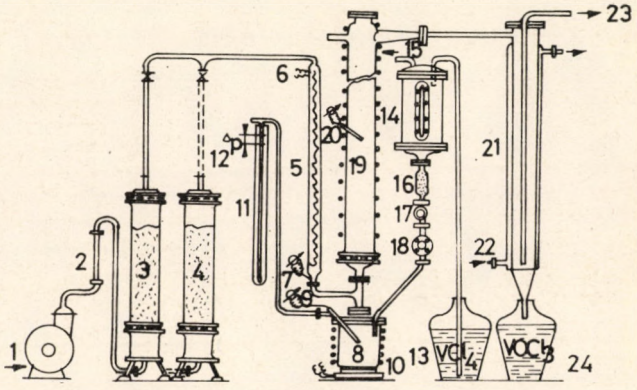

Fig. 10.
Process flow sheet of the manufacture of vanadium (V)-oxide-trichloride on scale of 10 kg/h
1 — turbo-blower, 2 — rotameter, 3—4 — silicagel columns, 5 — air preheater, 6 — current inlets, 7 — thermometer, 8 — flash-distillator, 9 — thermometer, 10 — heater, 11 — pressure gauge, 12 — pressure difference, 13 — VCl_4-bottle, 14 — feeder, 15 — vacuum pump, 16 — filter, 17 — feeding valve, 18 — inspection window, 19 — flame reactor, 20 — thermometer, 21 — cyclone condenser, — 22 cooling water, 23 — outgoing gas, 24 — VCl_3O-collecting bottle

The above processes and equipments are also suitable for the preparation and purification of other metal-chlorides, verified by the production of niobium(V), and tantalum(V) chlorides carried out in this device. Two Hungarian patents cover these methods. [6, 7].

REFERENCES

1. Foley, E. et al.: Extraction and Refining of the Rarer Metals. The Institution of Mining and Metallurgy. London 1957.
2. Iván L., Vitányi I.: A Study-Tour in Freiberg. FKI Ed. 31. p. 1965.
3. Várhegyi Gy., Iván L.: Production of Vanadium tetrachloride. Proc. FKI *9*, 157. p. (1971).
4. Korshunov, B. G., Morozov, I. Sz., Chih-Chin-Fang: „Tsvetnaya Metallurgiya" *7*, No. 3. 114. (1964).
5. Ruff, O., Friedrich, L.: J. Anorg. Chem. *89*, 279. (1914).

6. Hungarian Pat. 162.790. USSR Pat. 1,840.043, UK Pat. Sp. No. 40.137, French Pat. Sp. 72.35722.
7. Hungarian Pat. 161.069, USSR Pat. 1,840.068. UK Pat. Sp. No. 47.549. Franch Pat. Sp. No. 72.36332.

РЕЗЮМЕ

Авторами разработана технология непрерывного получения хлорида ванадия (IV) и трёххлористого окисла ванадия (V), исходным сырьём для которой служит необработанный ванадий, полученный в ходе переработки боксита. На основе результатов, полученных в ходе модельных опытов, были сконструированы необходимые реакторы. Так для хлорирования применяется стальной реактор, а для очистки — солевая колонна, из которой загрязняющие компоненты непрерывно отводятся в виде двойных комплексных солей ($NaAlCl_4$ и $NaFeCl_4$).

Получение трёххлористого окисла ванадия (V) осуществляется путём парциального окисления хлорида ванадия (IV) воздухом, что сопровождается реакцией в пламени.

Изготовление таких реакторов высокой производительности не требует больших затрат. Осуществление этих способов получения сопровождается минимальными энергетическими затратами.

HUNGARIAN JOURNAL
OF INDUSTRIAL CHEMISTRY
VESZPRÉM
Vol. 6. pp. 11–20 (1978)

EFFICIENT CATALYTIC OXIDATION PROCESS FOR AIR POLLUTION ABATEMENT

L. Szepesy, K., Welther and Zs. Sebestyén

(Hungarian Oil and Gas Research Institute, Veszprém)

Received: May 16, 1977

The development and testing of the efficiency of a new metal catalyst for the elimination of air pollutants of different types are described. The new catalyst contains a very small amount of noble metal in a highly dispersed form on a solid support. Due to the unique structure of the catalyst, high efficiency can be achieved at relatively low temperatures.

The effects and the interrelation of the temperature and space velocity are demonstrated by virtue of the conversion curves. The development of catalytic oxidation processes for industrial air pollution problems by using the new catalyst is discussed. Industrial realisation of the process is described and further developments of catalytic reactors are indicated.

Introduction

Various adsorption and absorption processes, thermal and catalytic combustion methods have been developed and introduced for the elimination of harmful and malodorous substances in air and industrial off-gases. The selection of the most suitable method for a given task mainly depends on the quality and concentration of the pollutants. For the elimination of inflammable substances in low concentrations, catalytic oxidation is considered to be the most suitable method from the point of view of its economy and efficiency.

Catalytic oxidation is generally carried out in a temperature range between 350 and 700° C depending on the type of the catalyst used as well as on the quality and concentration of the pollutants involved.

Catalytic oxidation is achieved with catalyst composites containing catalytically active metals or metal compounds on supports. For the elimination of air pollution in the main noble metal catalysts are used.

Development of a New Type of Catalyst

Based on a detailed analysis of literature references and the results of laboratory experiments carried out with self-made catalysts of different compositions, it was found that the efficiency and other characteristics of the catalyst

composite vary considerably, depending on the quantity of the metal component as well as on the operating conditions used in the coating procedure.

On the basis of our experimental results, it was ascertained that by appropriate selection and control of the operating conditions, high efficiency catalysts can be prepared with a very low metal content. By changing the operating conditions, the characteristics of the catalysts can be modified within a certain limit depending on the assignment given [1].

The new catalyst contains about 10^{-6}–10^{-7} g/g palladium calculated to the unit weight of the support used. The metal is very highly and uniformly distributed on the surface of the support, making a fast interaction possible with the pollutants from the air passed through the catalyst bed [2]. Due to the special structure of the catalyst, high efficiency can be achieved. The high activity of the catalyst makes it possible to eliminate pollutants in a low concentration at relatively moderate temperatures and with high space velocities. A very important characteristic of the catalyst is its behaviour in the presence of such compounds which are regarded as catalyst poisons. According to literature, catalysts prepared in the usual way and containing 10^{-2}–10^{-3} g/g platinum metal are very sensitive against sulphur compounds (mercaptans, sulphides) and the activity of such a catalyst rapidly decreases. The activity of our catalyst did not show any decrease when working for a prolonged time with gases containing a considerable amount of sulphur compounds. This catalyst was also successfully applied for the elimination of phosphorus containing air pollutants (insecticides).

The choice of the support depends on the given assignment. Several alumina and ceramic supports of different types and different surfaces areas were used.

With regard to the process, the shape and the size of the support determine the pressure drop in the catalyst bed. During our experiments, supports of various shapes were investigated. In *Table 1.* the main characteristics are given of the catalysts studied.

Table 1.

Characteristics of the catalysts developed

Shape (Material)	Raschig rings (ceramic)	Balls (alumina)	Honeycomb tubes (alumina)
Size, mm	5—25	5—10	43 × 43 × 100
Bulk density, kp l^{-1}	0.8	1.0	0.9
Temperature range, °C	180—450	180—450	180—450
Upper temperature limit, °C	1 000	800	900
Space velocity, h^{-1}	10—50 000	20—100 000	20—200 000

Testing the Efficiency of Catalysts

The efficiency and life duration of catalysts were investigated in reactors coupled with a gas chromatograph. The flow-sheet of the reactor system is shown in *Fig. 1.* The reactor is connected in by-pass to the gas chromatograph and by switching the appropriate valves, samples can be directly introduced into the gas chromatograph from the reactor inlet and outlet, respectively.

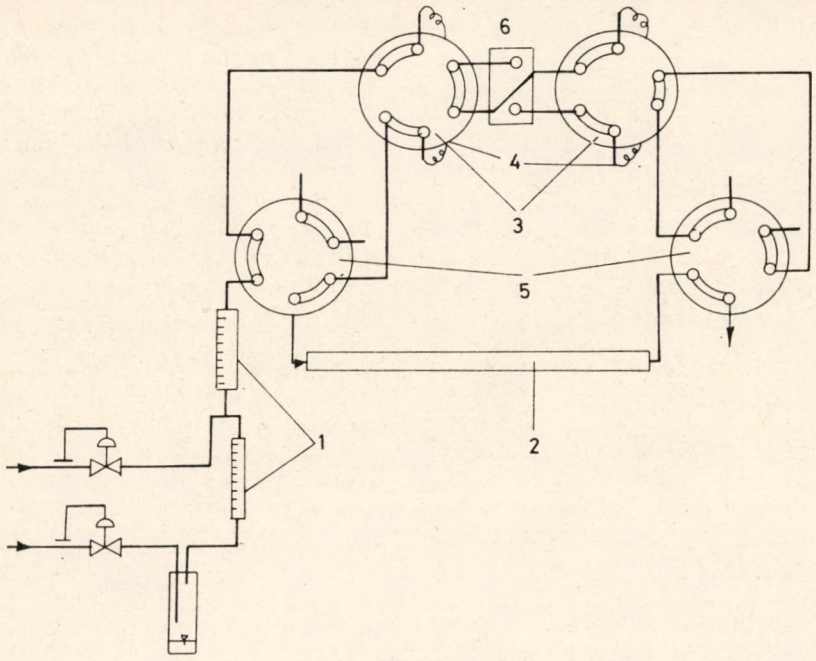

Fig. 1.
Reactor – gas chromatograph system
1 — Flow meter, 2 — Catalytic reactor, 3 — Sampling valve, 4 — Sampling loop, 5 — Switching valve, 6 — Gas chromatograph

Different reactors of 1–100 cm^3 volume were used for these tests.

Some catalysts were also tested for longer periods in separate reactors. The activity of the catalyst after 8,000 stream hours was found to be about 95% of the initial activity.

In laboratory reactors the conversion of a large number of air pollutants were measured as a function of the concentration, temperature and residence time. The compounds investigated are listed in *Table 2*.

Table 2.

Air pollutants investigated

Hydrocarbons		Sulphur compounds	
Methane	2,2,4-Trimethyl pentane	Methylmercaptan	Carbonyl sulphide
Ethane	Benzene	Ethylmercaptan	Dimethyl sulphide
n-Pentane	Toluene	Butylmercaptan	Butyl sulphide
n-Hexane	Xylene	Amylmercaptan	
Cyclohexane	Tetralene		
Oxygen compounds		**Phosphorus compounds**	
Methanol	Acetone	o-ethyl-S,S-dipropyl dithiophosphate	
Ethanol	Ethyl acetate	o,o-diethyl-S-ethylthiomethyl dithiophosphate	
Isopropanol	Formaldehyde	**Solvents**	
Butanol	Formic acid	Shellsol-A	Mavesol DS
		Aromasol	Helux

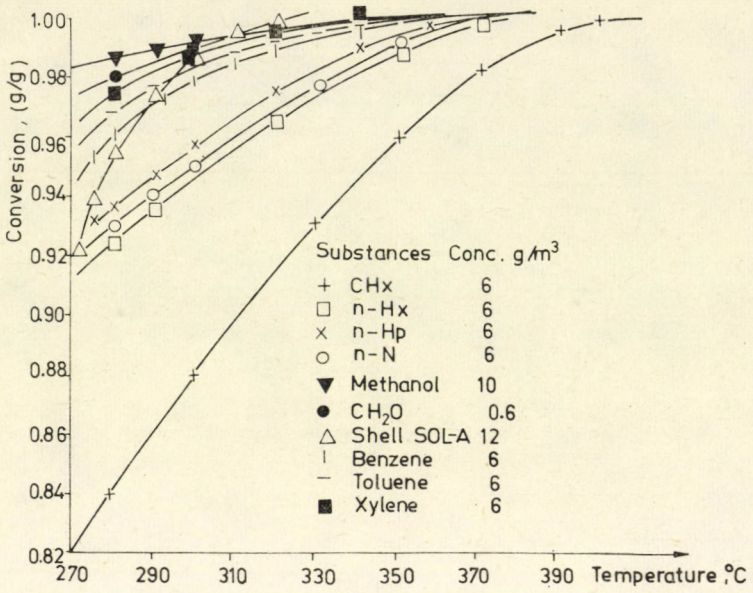

Fig. 2.
Conversion of some model substances vs. temperature
Space velocity: 10,000 h^{-1}

In *Fig. 2* the conversion curves of some of the investigated compounds are shown as a function of the reactor temperature. It can be seen in the figure that for most of the compounds shown an about 95% conversion can be achieved at about 300° C, however, for cyclohexane the same conversion can be achieved only at 350° C.

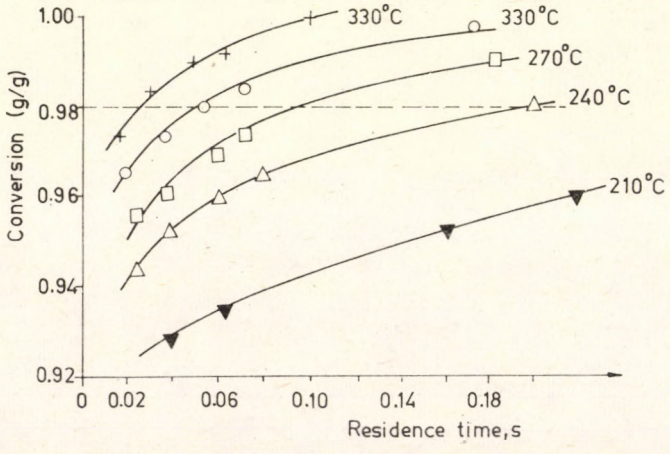

Fig. 3.
Conversion of methanol vs. residence time (4 g/m³ methanol in air)

In *Fig. 3* methanol conversion curves are presented as a function of the residence time measured with air containing 4 g/m³ methanol. As the figure shows, 98% conversion can be achieved at a 300° C temperature with a residence time of 0.05 sec, at 270° C with a residence time of 0.1 sec.

The temperature and the residence time are interrelated in a given conversion range. At a higher temperature, lower residence time is sufficient, that is to say a higher space velocity can be applied in order to achieve a given conversion.

In *Fig. 4* the same types of conversion curves are shown measured with air containing 35 g/m³ methanol.

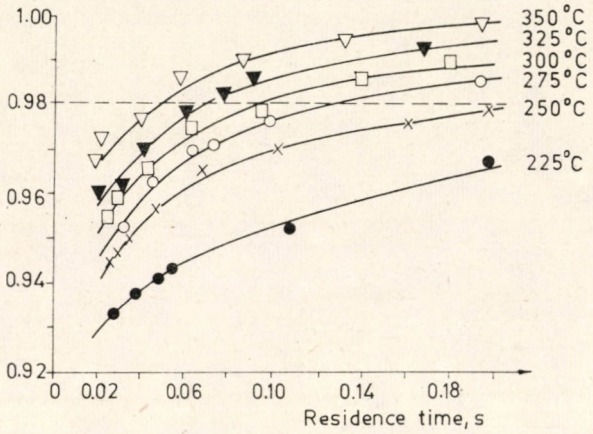

Fig. 4.
Conversion of methanol vs. residence time (35 g/m³ methanol in air)

It can be seen in the figure that the residence time corresponding to 98% conversion is 0.09 sec at 300° C and 0.13 sec at 275° C, respectively. These residence times are somewhat higher than that obtained with air containing 4 g/m³ methanol.

By comparing the conversion curves presented in *Fig. 3* and *4*, it can be seen that the catalyst can efficiently be applied for the elimination of pollutants that are present in a wide concentration range.

The selection of the optimum operating conditions depends on the one hand on the concentration, and on the other hand on the quality of the pollutants.

For demonstration purposes, the relationship between the temperature and the space velocity is shown in *Fig. 5* for the elimination of different pollutants with the same conversion from air containing methanol, toluene and *n*-hexane, respectively.

As the figure shows, the same conversion (98%) of a more refractive, less oxidable compound can be achieved with considerably lower space velocity at a given temperature, or putting this another way, in order to achieve the same space velocity a higher temperature is required.

In some cases the selection of operating conditions is also influenced by other factors. For the elimination of compounds which are harmful or malodorous at very low concentrations (low MAC value or low odour threshold limit) 99–99.99% or even higher conversion should be achieved. As shown in the

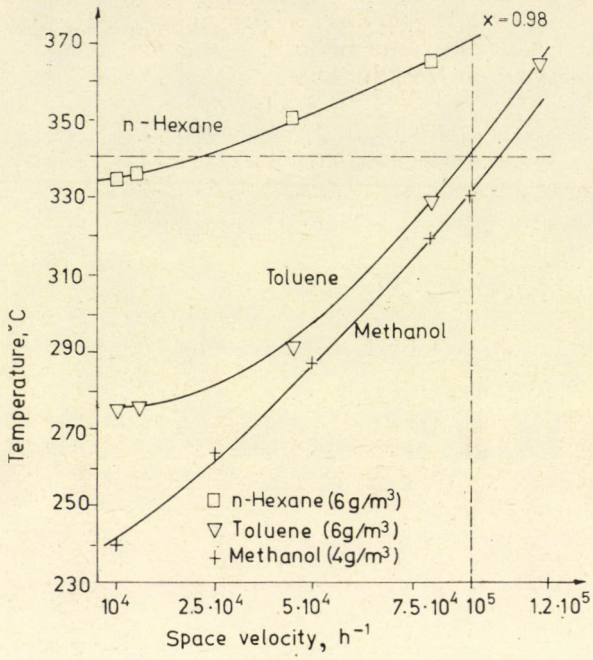

Fig. 5.
Interrelation of temperature and space velocity for the oxidation of some model substances at 98% conversion

figures representing the conversion curves, such a high conversion can be achieved by increasing the temperature and decreasing the space velocity, that is by the appropriate adjustment of these two parameters.

Generally speaking it can be concluded that the optimum conditions of a catalytic oxidation process can be established on the basis of experiments in the knowledge of the concentration and quality of the pollutants to be eliminated and the required purity of the outlet gases.

Development of Catalytic Oxidation Processes

On the basis of industrial requirements, process technologies have been developed for the elimination of harmful substances in air and industrial off-gases [3].

The main steps of this development were as follows:

1. Selection of the appropriate catalyst based on laboratory measurements carried out in the microreactor—gas chromatograph system.
2. Laboratory and bench-scale experiments with model mixtures under different operating conditions.
3. Experiments carried out with a bench-scale unit in a factory to eliminate the pollutants and select the operating conditions.
4. Planning of process technology and furnishing of design data.

For the experiments on a bench-scale and for the industrial measurements, a mobile catalytic oxidation unit furnished with an electrical preheater was built with a capacity of 60 Nm^3/h. The flow-sheet of the equipment is shown in *Fig. 6.*

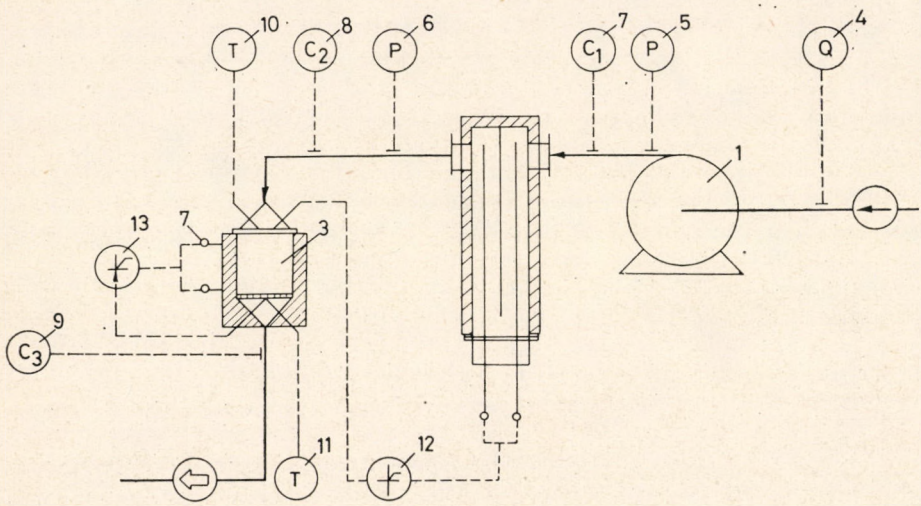

Fig. 6.

Flow diagram of the bench scale reactor system
1 — Fan, 2 — Preheater, 3 — Catalytic reactor, 4 — Flow meter, 5 — Pressure gauge, 7, 8, 9 — Sampling points, 10, 11 — Temperature recorder, 12, 13 — Temperature control

In the following paragraph, some examples show the wide application possibilities of catalytic oxidation.

In plants manufacturing animal proteins, the effluent of some processing units contains malodorous protein fragments in a relatively high concentration (1–2 wt.%), mainly sulphur and nitrogen containing substances causing a critical odour problem in the plant and in the neighbourhood. Deodorization of the effluent gases cannot be solved by the generally used absorption process. Thermal incineration also proved to be inefficient for the complete elimination of the malodorous substances.

On the basis of the laboratory model experiments and measurements carried out in the plant, it was demonstrated that the malodorous substances from the effluents can be completely eliminated by catalytic oxidation. The catalyst selected on the basis of laboratory experiments can be used for a longer period without a decline in activity.

It should be noted that some of the malodorous substances, i.e. mercaptans, have a very low odour threshold value, below 0.1 ppm, which means that very efficient conversion must be achieved in order to eliminate the odour of the effluents.

A process technology was suggested for the deodorization of effluents at a temperature of 250° C.

A similar task emerged in a pharmaceutical factory working with the extraction of active compounds from animal organs, which could also be efficiently solved by catalytic oxidation.

A process was elaborated for the elimination of solvent vapours evolved in the spray painting unit of a machine factory. The concentration of the solvent vapours in air varied between 1 and 10 g/m³. As different types of solvents and solvent mixtures were used, working conditions had to be chosen for the elimination of the most refractive compound. The appropriate working conditions were determined for the removal of at least 98% of the solvent vapours. For the industrial scale unit, a reactor working at 330° C was suggested.

In the manufacture of a pharmaceutical product 90 kg/charge methylmercaptan and some ethylmercaptan are evolved. Due to batchwise production the amount of the mercaptans evolved varies considerably in time by the progress of the reaction. The effluent was diluted with air and passed through the pilot reactor. The mercaptan concentration of the inlet air varied from 0.1 to 5%. On the catalyst selected on the basis of laboratory experiments working at 280° C temperature, the outlet gas contained 0.001% i.e. about 10 ppm mercaptan. Working at 330 °C mercaptan was not detectable by gas chromatography and the outlet gas was odourless.

This example illustrates that catalytic oxidation can be applied for the elimination of pollutants evolved in high concentration and changing in time.

Industrial Application

A catalytic oxidation system was built in a pharmaceutical factory for the deodorization of the effluent evolved in the spray-drying unit of the plant producing B_{12} vitamin. The flow-sheet of the process is shown in *Fig. 7.*

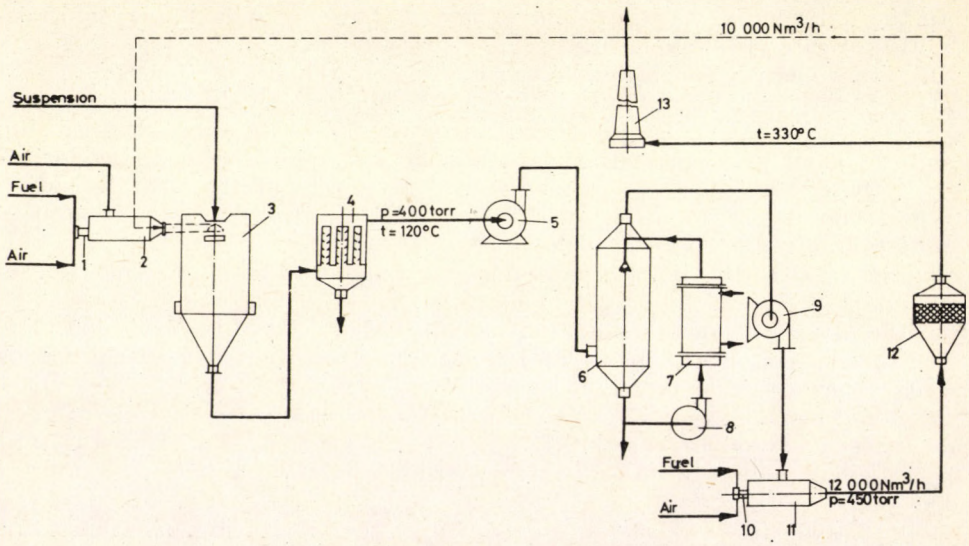

Fig. 7.

Flow sheet of the industrial unit for deodorization of a fermentation product
1, 10 — Burner, 2, 11 — Mixing chamber, 3 — Spray drier, 4 — Bag filters, 5, 9 — Fan, 6 — Scrubber, 7 — Heat exchanger, 8 — Pump, 12 — Catalytic reactor, 13 — Stack

400 kg water containing 15 kg suspended solids is sprayed with 10,000 Nm^3 air at 320° C inlet temperature into the drying unit. From the air stream leaving the drying unit at 130° C the product particles of diameters of a few microns are recovered by bag filters. The effluent passes through a scrubber, the temperature of the outlet gas is 50° C and is saturated with water vapour. This outlet gas is preheated to 320° C and contacted with the catalyst. The reactor effluent leaves the system through the stack or a larger part of the clean gas can be recycled into the drying unit and only a part of it, corresponding to the quantity of the flue gas produced in the burner, will be exhausted.

For the processing of a small amount of polluted air or off-gases, a mobile catalytic oxidation unit was constructed, with a nominal capacity of 1,000 Nm^3/h. The schematic drawing of the reactor is shown in *Fig. 8* which

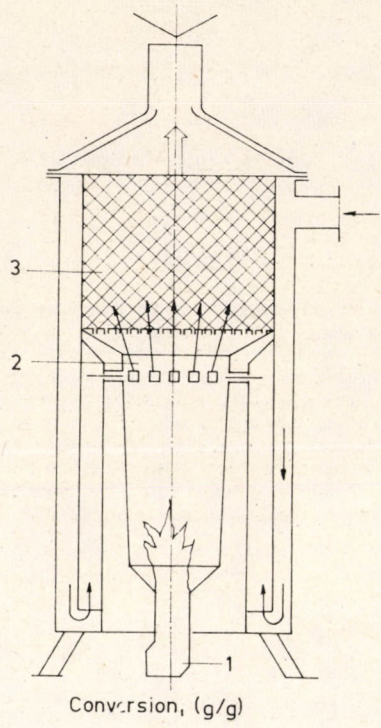

Fig. 8.
Schematic drawing of the 1,000 m^3/h capacity reactor
1 — Burner, 2 — Mixing chamber, 3 — Catalyst

also illustrates the operation of the reactor. A blower feeds the polluted air into the reactor through the casing of the reactor which also serves as a heat insulator. The inlet air is intimately mixed with the hot flue gases in the mixing chamber, then enters the catalyst bed at temperatures between 250 and 400° C, and the clean air leaves the reactor through the stack.

Preheating the air to the reaction temperature is accomplished by the products of combustion from a conventional gas or oil fired burner. The unit shown is equipment with an oil fired burner (100.000 Kcal/h).

The temperature of the catalyst bed is measured at two points by thermoelements, i.e. at the gas inlet and at the middle height of the bed. Preheating of the inlet gas is controlled according to the temperatures measured.

The above reactor system can be used for the processing of 500–1000 Nm^3/h polluted air or off-gas. Another feature of the system is that it can easily be transported and can be used as a pilot reactor for determining design data for larger units.

With the above system, the deodorization of gases evolved in fermentation was investigated and some other applications of the process are under preparation.

In addition to the units described, the development of larger units, equipped with heat recuperation systems, was also started in order to decrease the energy requirement of the process.

REFERENCES

1. Hungarian Patent 167.019.
2. Welther, K. and Szepesy, L.: Dechema-Monographien Nr. 1639–1669. Band 80, Teil 2, 533 (1976).
3. Patent pending.

РЕЗЮМЕ

Авторы знакомят нас с разработкой нового типа металлического катализатора и с изучением его эффективности с точки зрения удаления загрязняющих воздух соединений различного типа. Новый катализатор содержит на носителе очень малое количество благородного металла при высокой его дисперсности. Вследствие специальной структуры катализатора, может быть достигнута высокая его эффективность, а также модифицируются и прочие его качества.

С помощью приведённых кривых конверсии исследуется влияние температуры и объёмной скорости, а также зависимости между ними. При использовании новых катализаторов показана разработка технологий каталитического окисления для решения промышленных задач, связанных с проблемой защиты окружающей среды. Показано также осуществление процесса в промышленности, и направления дальнейшего развития каталитических реакторов.

HUNGARIAN JOURNAL
OF INDUSTRIAL CHEMISTRY
VESZPRÉM
Vol. 6. pp. 21—38 (1978)

GENERAL PROPERTIES OF TECHNOLOGICAL SYSTEMS. I.

F. Mohos

(Budapest Chocolate Factory of the Hungarian Candy Industry)

Received: May 26, 1977

A general technological theory complete with definitions and postullates is advanced. The theory is aimed at selecting technological nonvariants by their use during the examination of the technlogical systems of various materials of biological origin. Raw materials subjected to processing in the technological system were characterized and the hierarchy principle as well as the term technological functional group are presented. Based on the theory developed by Blickle, the internal and external structures of materials were evaluated.

Introduction

A characterization of technological systems based on the central idea of the identification of the technological invariants and their subsequent use is advanced. Blickle developed this method. His publications [1, 2] served as the main basis of this paper. The author is convinced that the examination of technological invariances is extremely important because the evaluative and critical treatment of the vast wealth of experience of the chemical and related industries may lead beyond the particular problems and can result in the recognition of new, general relationships. The theory advanced here, a possible presentation mode of technological theories, is based on definitions and postulates. It should be mentioned at this point that neither the method of presentation nor its content are the sole possible and correct ones, because the particular field where this theory is used is so special that conscious precaution seems advisable.

The primary goal of this paper is the characterization of the technologies used to process raw materials of biological origin, a field closely related to the chemical industries. The author is convinced that by utilizing certain technological invariances, a direct relationship can be established between the technological systems used to process chemical and biological raw materials. Correspondingly, a guide to applying the well advanced results of chemical engineering in bioengineering can be obtained.

1. The Technological System and its Parts

Definition 1*:* The term technological objective is used to denote the artificial production of materials of certain values of use.

Definition 2*:* The term technological system is used to denote a system by which certain initial or raw materials can be turned into products of properties in accordance with the technological objective.

Definition 3*:* The technological system is composed from materials, changes and equipment; materials which are artificially transformed in the technological system; changes which take place in the materials entering the technological system and equipment, which cause or promote these changes of the materials in the technological system or which emerge from the space and time boundaries of these changes.

This definition of the technological system was given by BLICKLE [1]. In fact, this definition is the central core of this theory (see p. 22–94 and p. 39 of [1] for the implicit and explicit definition).

Postulate 1: Various parts of the technlogical system are connected by complex, multilateral relationships. These relationships apply for the various forms of motion, and in a more general sense, for the information flows within the technological system.

Thus, relationships relating to the physical forms of motion (such as energy, force, and momentum), chemical forms of motion (such as the reacting elements, and balance of charges, etc.) and so forth have to be considered.

Postulate 2: The sufficient and necessary condition for completing any technological objective is that all the pertaining relationships relating to actual materials, changes and equipment details are simultaneously fulfilled at any point of the apparatus.

Definition 4*:* The technological system is considered to be in technological equilibrium or technological harmony when all the relationships relating to actual materials, changes and equipment parts are simultaneously fulfilled at each point of the technological system.

Thus, in other words, *Postulate 2* means that the necessary and sufficient condition of the completion of the technological objective is that the technological system should be in technological equilibrium.

At this point, it is important to recognize that the relationships between various forms of motion relate to dynamical relationships, so technological equilibrium itself is also a dynamic condition.

Postulate 3: The technological systems as open systems can interact with each other. In this case, the product of a previous system becomes the raw material of a later system.

Postulate 4*:* Any technological system can be decomposed into a finite number of technological systems functioning as the system of these subsystems.

Postulate 5: Any part of any technological system is a set consisting of a finite number of object-classes as elements and these object-classes can be considered the sets of a finite number of elements.

The relationships between the elements of a technological system are represented by the technological triangle relationship (triangle graph). The points of this graph are the materials, the changes and the equipment as sets

while their arrows are the relationships existing among these sets compounded into a single line. This is shown in *Fig. 1.*

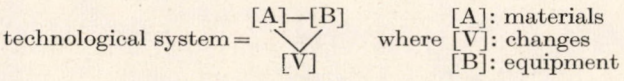

Fig. 1.
Technological triangle relationship

Postulate 6: The triangle relationship of any technological system is the special case of a general technological triangle relationship, it is its particular solution.

It is possible to arrive at the general technological triangle relationship by an examinantion of the elements of the elements (object-classes) of the parts of the technological system materials, changes, and equipment, followed by the detailed examination of the (A)—(V), (A)—(B) and (V)—(B) relationships. Thus all the mathematically possible combinations of all the possible properties of all the materials, changes and equipment have to be taken and reduced by such combinations which, according to undoubtedly correct observations are impossible. These combination-reducing statements are given by BLICKLE (cf. p. 22—28 of [1]) as "Statements of technical chemistry". In my opinion there are a number of statements among them, which due to their widespread acknowledgement can become the axioms of the present technological theory.

Postulate 7: The general technological triangle relationship can be considered the sum of all the mathematically possible relationship-combinations of the parts of the technological system reduced by the technological axioms.

The content of *Postulate* 7 is shown in *Fig. 2.*

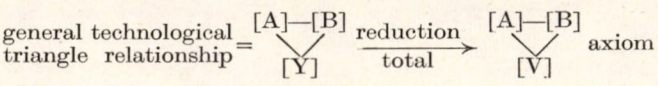

Fig. 2.
The general technological triangle relationship

Statements 1 to 8 of BLICKLE relate to materials, statements 9 to 33 refer to equipment, statements 34 to 64 relate to changes (as algebraic mapping) while statement 65 relates to the relationship of materials and equipment ("operation units"). A few examples are given to demonstrate their axiomatic character.

Statement 34: There is a conservation relationship applying to the elements.
Statement 44: A homogeneous solid-solid system cannot be decomposed into its constituents by any solid material.

Statement 20: Connection in series is feasible only in the continuous operation mode.

How the Terms of the Technological Theory are Derived

The logical path followed so far is shown in *Fig. 3*. As it can be seen, both the technological-material and its value-of-use play central roles in the scheme. A double arrow is due in-between materials and their values-of-use, since the value-of-use is a term entirely different from the term of the technological materials expressed by the object-classes. The value-of-use as a material characteristic is an economic term, while all the other material characteristics (object-classes) are the technical characteristics of the materials. The double arrow represents a specific relationship between value-of-use and technological materials. However, this relationship differs from the conceptual derivation seen in connection with the other terms. This means that the logical path followed is not plagued by circulus vitiosus.

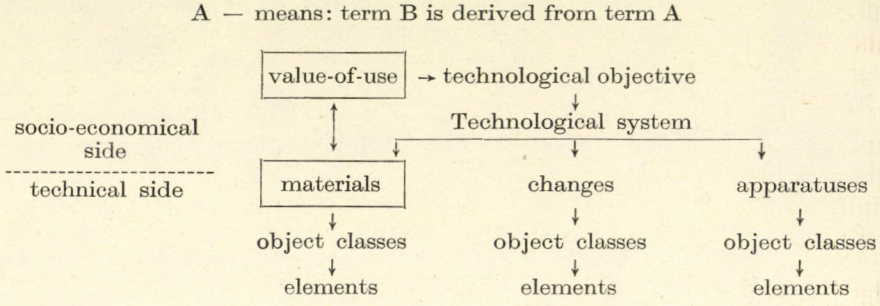

Fig. 3.
Derivation of the terms of the technological theory

The "elements" shown in *Fig. 3* represent the well formulated terms of a given scientific topic — the arrangement of these elements corresponding to the present theory is given below. This definitive importance of the value-of-use of different materials is explicitely expressed in each technological system and the given technological system fulfills its specific social function by it, an apparent form of it is, e.g. the commercial connection, etc.

2. Characterization of the Materials From a Technological Point of View

2.1 *The Hierarchy Levels of Materials Entering the Technological Process*

When a wide range of materials entering the technological system, such as the materials of biological origin are considered and the levels of material organization, the so-called hierarchy levels-at which changes of the characteristics of the materials can take place-are assigned, then the following levels are found:

q_1 = organism
q_2 = part of the organism

q_3 = organ
q_4 = part of the organ
q_5 = tissue
q_6 = part of the tissue
q_7 = cell
q_8 = part of the cell (e.g. organs within a cell)
q_9 = phase systems
q_{10} = phase
q_{11} = component (molecule)
q_{12} = part of the molecule (e.g. radical, functional group, etc.)
q_{13} = atom
q_{14} = part of the atom (e.g. ion, etc.)

The levels of organization in the sphere of materials do not terminate here towards the micro-sphere-side, but for the purpose of the present study these levels are sufficient.

Postulate 8: The materials in a technological system suffer many changes at many hierarchy levels. Nevertheless, there are hierarchy levels in each technological system at which a finite number of changes characteristic to the particular technological system take place.

Definition 5: The elementary material flows of the materials taking part in the characteristic changes of the technological system are the flows of such material groups (the so-called "functional groups") in which the change characterizing the given technological system takes place at and only at one level, the lowest hierarchy level.

According to Definition 5 those groups are called functional groups which

— do take part in the characteristic change of the system
— constantly change only at one level and this is the lowest hierarchy level.

Definition 6: The hierarchy levels assigned to functional groups are called critical hierarchy levels.

In other words, *Definition 5* does indeed assign such "undecomposable" material groups, which act as the atoms of the technological system at any arbitrary hierarchy level range. In the q_{9-14} range this definition is identical to the classical molecule, radical, complex ion and atom or atom-ion terms of chemistry.

Postulate 8 expresses a statement concerning the existence of the characteristic changes of the technological system, but presents no method to determine this characteristic change. Changes which are significant qualitative or quantitative changes are termed characteristic changes.

2.2 Presentation of the Technological Systems on the Basis of the "Hierarchy Principle"

2.21 *The Hierarchy Principle*

Material groups flowing into a technological system represent different levels of materialistic organization and although some of the changes can alter these levels, any technological system can be composed of the flows of such

elementary material groups, the so-called functional groups, which retain their levels of materialistic organization while passing the given technological system.

This principle can be easily demonstrated: the elements, or rather their particular, electrically excited forms remain unchanged in any technological system which means that the changes brought about in a chemical technological system, i.e. the chemical changes cannot alter the chemical elements.

This chemical element principle can well be applied to higher levels of materialistic organization as well (cell, tissue, and organ etc.).

From here on, the term functional group mainly applies to a functional group flow, since these groups as elementary material flows are the constituents of the material flows studied entering and leaving the technological system. This convention—in the author's opinion—is a simple and straightforward one, since technologically there is no real difference in this respect between a flowing or a stagnant system.

According to the above hierarchy principle, the materials flowing into a technological system can be described as the sum of the elementary material flows. Thus, the mathematical treatment-taking the material flows (the systems of elementary material flows) as vectors composed from the elementary material flows as basic vectors-seems justifiable.

It follows that all material flows into a given technological system can be described by equations formed from the elementary material flows of the system. This equation set is characteristic for the given technological system and it is invariant with respect to any states of the given technological system. Accordingly:

a) The material-flow-system set X is a vector space above object T generated by set f of the functional groups as linearily independent basis vectors at critical hierarchy levels determined by the aim of the technological system. The dimensions of X and f are mass/time.

b) Although basic vectors f have an unlimited set of hierarchy levels, they cannot be further decomposed because the critical hierarchy levels are determined.

c) The elements of commutative object T are natural numbers obtained as the ratios of the functional group mass flows and the unit functional group mass flows of the mass-flow-system.

The guideline set by the hierarchy principle is:

$$\text{technological objective} \rightarrow \left[\begin{array}{l}\text{critical hierarchy}\\ \text{levels and appro-}\\ \text{priate changes}\end{array}\right] \rightarrow \text{technological system}$$

The "undecomposibility" of basic vectors f is entirely due to the critical hierarchy levels, because although the materials subjected to technological processing could be further decomposed theoretically towards increasing hierarchy levels, the changes required by the technological objective make this unfeasible.

This means that there is no direct way from the technological objective to the technological system, rather there is a step of theoretical importance in between: the level of materialistic organization at which the technological system in question is required to operate, has to be decided upon.

For example, chemical technological systems are chemical systems because they are created to facilitate changes at the q_{9-14} hierarchy levels. It was experienced that the sets of the material-flow-system in a chemical technological system can always be produced as vector spaces generated by chemical elements, but there is no need in a chemical technological system for deeper decomposition (higher hierarchy level) than that of the ionized element (q_{14}), so $q_{max}=q_{14}$. Occasionally, the basic vectors need not to be elements or their ionized forms, because the changes of the compounds can be described by changes of radicals or complex ions and then the maximal hierarchy level is q_{12}. Of course, this description mode is not the only advantageous one, but in the case of macromolecules, in biochemistry, where the peptide chain is described only by the symbolically noted amino acids and not the chemical elements proper, this representation can be used exclusively. In this case, the functional groups as basic vectors are assigned by describing the q_{12} level as the ciritical level.

The assets of the method outlined above become manifest when it is realized that the usual atomic level cannot be reasonably maintained in the processing of certain materialistic formations, such as plant fragments, and organs, etc., because even the most minute morsel of this material contains an enormous wealth of compounds, and in fact it is not these compounds or at least not all of them, that one has to work with while these materials are processed. Thus, no single hierarchy level or the ξ_{9-14} chemical range can be assigned to this material. It is only the technological objective which specifies the depth of changes to be achieved in the structure of the material.

2.22 *Mathematical Formulation of the Hierarchy Principle*

Let the set of the functional groups in the technological system studied be $[f]$, the set of the critical hierarchial levels corresponging to the functional groups be $[H_{cr}]$ and let the set of the material flow systems of the technological system be $[X]$.

Let set $[\alpha]$ describe the relationships existing between the functional groups and let the elements of the set be:

α_I: there is a relationship between two functional groups

$\alpha_{I,1}$ homogeneous relationship

- $\alpha_{I,11}$ ionic
- $\alpha_{I,12}$ covalent
- $\alpha_{I,13}$ biological
- $\alpha_{I,1}$ other relationship

$\alpha_{I,2}$ heterogeneous relationship

- $\alpha_{I,21}$ coarse suspensions
- $\alpha_{I,22}$ fine suspensions
- $\alpha_{I,23}$ emulsions
- $\alpha_{I,24}$ gels
- $\alpha_{I,25}$ aerosols

α_{II}: there is no relationship between two functional groups.

Then the technological system studied is unambiguously defined by the matrix equation ot the technological system:

$$f \cdot \mathbf{T} = X \quad [H_{cr}] \text{ is set} \tag{1}$$

where: f is the raw matrix describing the functional group set, the set has n elements

$\mathbf{T}$ is an $n \times m$ matrix consisting of natural numbers (ratios)

X is the row matrix describing the material-flow-system set, and the set has m elements.

Since there is n functional groups in the technological system its dimension is n.

The other just as well correct and easy to understand way to determine Eq. 1 is a follows:

- let us examine each material-flow-system of the technological system in such a manner that their hierarchy levels starting from 1 to 14 are noted, and let the material-flow-systems of different hierarchy levels and qualities thus obtained form the columns of a matrix.
- simultaneously let us exmine the hierarchy levels starting from 14 down to 1 searching for those material groups whose quantity remains unchanged in the technological system; let the material groups thus obtained form the rows of the same matrix (in fact, once again flows are concerned here)
- let us fill in the matrix with the ratios of the material-flow-systems and the material group flows
- let us combine the non-independent rows
- the rows obtained during the row elimination process yield the functional groups of the technological system
- the matrix obtained during the row elimination process is matrix **T** of Eq. 1 in which the rows and the columns correspond to f and X, respectively.

Let us complete the quantitative definition of the system by the [α] set of the system. Thus we obtain the (complete) definition of the system.

Thus, the complete definition of the technological system studied becomes:

$$f\mathbf{T} = X \quad [H_{cr}] \text{ and } [\alpha] \text{ are set dimension } n \tag{2}$$

The schematic of this technological system is shown in *Fig. 4.*

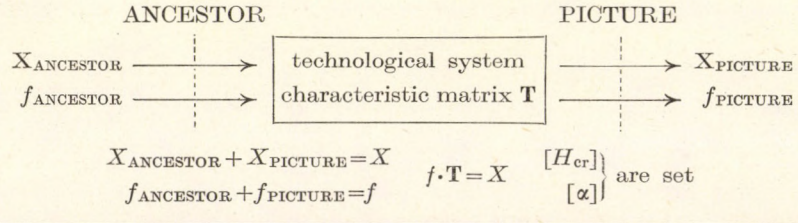

Fig. 4.
The schematic of the technological system

Let us examine an easy to visualize example.

Let the material-flow-systems of the technological system be the flows of the following materials: CO, CO_2, CH_4, HCOOH and C_2H_5OH. Without knowing anything in particular of the technological system proper matrix Eq. 1

can be applied because it is invariant with respect to the changes of the system and only the functional groups have to be known. To select them we have to know that changes of the chemical systems occur at the atomic hierarchy levels (q_{14}). This is shown in *Fig. 5*. It can be seen that the technological sys-

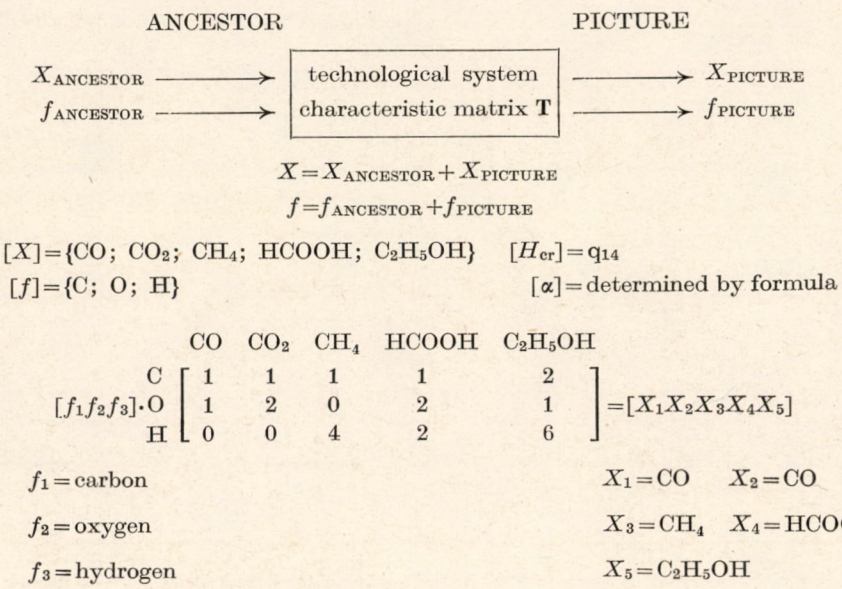

Fig. 5.
Description of a B dimensional technological system

tem has 3 dimensions since it is composed of functional groups C, O and H (elements). It should be noted that the relationships of the functional groups are also known which means that $[\alpha]$ is set.

2.23 *The exact mathematical formulation of the hierarchy principle makes the definition of the linear independence of the functional groups as basic vectors indispensible*

Thus, the linear combination of functional groups f is:

$$\bar{f} = a_1\bar{f}_1 + a_2\bar{f}_2 + \ldots + a_n\bar{f}_n \tag{3}$$

Various material-flow-systems can be composed from the flows of functional groups $\bar{f}_1, \bar{f}_2, \ldots, \bar{f}_n$.

Definition 7: Vector system $\bar{f}_1, \bar{f}_2, \ldots, \bar{f}_n$ is linearly independent then and only then when the expression:

$$a_1\bar{f}_1 + a_2\bar{f}_2 + \ldots + a_n\bar{f}_n = 0 \tag{4}$$

is fulfilled only at $a_1 = a_2 = \ldots = a_n = 0$.

2.24 *It is important to note that Eq. 3 shows how the material flow systems are obtained (at given hierarchy levels), but it does not reveal anything about the connection modes of the functional groups. This is given by set* $[\alpha]$

Set $[\alpha]$ is the set of relationships defined by the Descartes multiple set $[f]\times[f]$ of functional group set $[f]$. If, for example, compound C_2H-OH is examined as shown in *Fig. 6* then it can be seen that the three types of functional

The structural formula of ethanol:

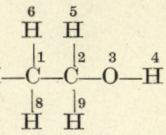

$[\alpha]=\{\alpha_{I,12};\ \alpha_{I,14};\ \alpha_{I,15};\ \alpha_{II}\}$

where

$$[\alpha]=\bigcup_{i=1}^{k} f_l \alpha_i f_m$$

and

$l, m=1, 2, \ldots, n$

if $l=m \Rightarrow \alpha_i \equiv \alpha_{II}$

The $[f]\times[f]$ multiple (following the numbering used on the structural formula):

	1	2	3	4	5	6	7	8	9
1	—	+	—	—	—	+	+	+	—
2	+	—	△	—	+	—	—	—	+
3	—	△	—	◇	—	—	—	—	—
4	—	—	◇	—	—	—	—	—	—
5	—	+	—	—	—	—	—	—	—
6	+	—	—	—	—	—	—	—	—
7	+	—	—	—	—	—	—	—	—
8	+	—	—	—	—	—	—	—	—
9	—	+	—	—	—	—	—	—	—

Symbols

$\alpha_{I,12}$ = covalent = +

α_{II} = −

$\alpha_{I,14}$ = other = △

$\alpha_{I,15}$ = other (2) = ◇

Fig. 6.

The $[\alpha]$ set of the relationships among the functional groups of C_2H_5-OH

groups form a material-flow-system consisting of 9 elements in which set $[\alpha]$ has four relationship elements. This description mode seems complicated and tedious for so simple a compound and indeed it is; the chemical structural formula, a graph representation itself, is much more expressive. Nevertheless, the matrix representation and the structural formula are equivalent. However, there are cases when this graph representation cannot be used, as it can be with chemical compounds. This happens when the possible connection modes are examined during the hierarchy level changes.

Let us now form the Descartes multiple $[q_{1-14}]\times[q_{1-14}]$ over the set of the hierarchy levels and let us examine with respect to each pair, which relationship element of $[\alpha]$ is possible at all. Without claiming completeness these relationships, as I envisage them, are listed here:

$$(q_{1-14})\alpha_{I,11}(q_{9-14})$$

$$(q_{9-14})\alpha_{I,12}(q_{9-14})$$

$$(q_{1-8})\alpha_{I,13}(q_{1-8})$$

$$(q_{1-14})\alpha_{I,2}(q_{1-14}).$$

The heterogenous relationship is not discussed here, it is beyond the scope of this paper. (Relationship α_{II} relates to the "empty" connections.)

It is worthwhile noting that while the relationships obtained during the examination of particular functional groups are symmetrical, the inter-hierarchy level relationships defining the functional groups are not symmetrical with respect to the general possibilities. However, in a particular case, the relationship is symmetrical with respect to both the functional groups and the hierarchy levels defining the functional groups.

2.25 *Determination of the Functional Groups*

Selection of the functional groups is not an easy problem. In principle the method shown below ensures the success in any technological system, but it may require several attempts.

Let us define the union U and section $\cap$ set operations for the functional groups.

Definition 8: The union operation as a set-operation with respect to the functional groups means that the flows of the functional groups are united into a material-flow-system set.

Definition 9: The section operation as a set-operation with respect to the functional groups means that one of the functional groups is hierarchy dependent from another one, i.e. it is not a true functional group; the section operation applied to real functional groups results in an empty set $\{0\}$.

Based on Definition 8, Eq. 3 can be rewritten as:

$$[\bar{f}]=\bigcup_{i=1}^{n}[\bar{f}_i] \tag{5}$$

Based on Definition 9. Eq. 4 can be rewritten as:

$$[\bar{f}_i]\cap[\bar{f}_j]=\{0\},$$

where $i\neq j$ and

$$i, j=1, 2, \ldots, n. \tag{6}$$

Based on Eq. 5 and 6, the functional groups can be selected. Visualized, *Definition 9* means that a non-real functional group contains in fact another real functional group, because one of the characteristic changes of the technological system takes place in it, i.e. it contains a critical hierarchy level which is of a higher level than that characterizing the given group. Let us assume that the set of the material-flow-systems of a given technological system studied is $[X]=\bigcup_{i=1}^{m}[X_i]$. Then let us obtain:

$$\bigcup_{i,j=1}^{m}[X_i]\cap[X_j]\equiv[f], \tag{7}$$

where $i\neq j$

$$[H_{cr}] \text{ is set}$$

and

$$[X_i]\in[X]; \quad [X_j]\in[X].$$

Set $[\bar{f}]$ thus obtained contains the materials from which all the elements of the material-flow-system set $[\bar{X}]$ can be generated. Occasionally Eq. 7 results in an empty set; in these cases $[X_i]$ and $[X_j]$ are relatively linearily indepen-

dent, but from the point of view of the overall system, this only means that they are generated by such functional groups in which there are no identical ones.

If set $[f]$ is successfully selected, then we have to make certain that set $[X]$ can be generated from its elements or not. Generation proceeds as follows:

$$[X_k]=[f_1, f_m, f_n, \ldots] \tag{8/a}$$

$$\overline{X}_k = a_1\bar{f}_1 + a_m\bar{f}_m + a_n\bar{f}_n + \ldots \tag{8/b}$$

Eq. 8a and b, together ensure that the material-flow-system in question can indeed be generated from the selected functional groups.

The situation is more complicated if the section operation according to Eq. 7, allocates f_{1-k} type, i.e. k functional groups to the material-flow-set element $[X_g]$, but the entire material-flow-system cannot be reconstructed from this, only a part of it. This means that the functional groups have to be "completed" by a material fraction $f^{\otimes}$, i.e.

$$[X_g]=\left(\bigcup_{i=1}^{k} f_i\right)\cup f^{\otimes} \tag{9}$$

Then it has to be examined whether material fraction $f^{\otimes}$ results in a non-empty set when its sections are obtained with respect to all the other functional groups of the technological system, i.e. with all the elements of $[f]$. If only empty sets are obtained, then $f^{\otimes}$ is a real functional group and should be added to set $[\bar{f}]$. On the other hand, if the elements of the set:

$$[f_i]\in[f]$$

$$\text{where} \quad i=1, 2, \ldots n$$

$$\left(\bigcup_{i=1}^{n}[\bar{f}_i]\cap[\bar{f}^{\otimes}]\right)=[f_1^{\otimes}, f_2^{\otimes}, \ldots, f_h^{\otimes}] \tag{10}$$

$$[H_{cr}] \text{ is fixed}$$

are not empty sets, then another section operation has to be performed to test the linear independence. This procedure is continued until linearly independent material fractions are obtained at given hierarchy levels.

2.26 *Similarity of Technological Systems*

Definition 10: One of the cases of similarity in technological systems is when their material-flow-systems, i.e. the systems formed from the flows of their functional groups are identical, i.e.

Characteristics of	the first system	the other system
dimensions	n_1	n_2
functional group set	$[f_1]$	$[f_2]$
material-flow-system set	$[X_1]$	$[X_2]$
critical hierarchy level set	$[H_{cr}(1)]$	$[H_{cr}(2)]$
relationship set	$[\alpha_1]$	$[\alpha_2]$

$$1)\ [H_{cr}(1)]=[H_{cr}(2)] \tag{11/a}$$

$$2)\ [f_1]=[f_2]\Rightarrow n_1=n_2 \tag{11/b}$$

$$3)\ [X_1]=[X_2] \tag{11/c}$$

$$4)\ [\alpha_1]=[\alpha_2] \tag{11/d}$$

Definition 10 in fact predicts four cases described by Eq. 11/a–d. If the technological triangle relationship is recalled then this definition of similarity seems justified, since in fact the criterion relating to the set of the hierarchy levels provides limitations on the characteristic technological changes, $[V]$, the most significant part of the set of changes, while the other three criteria relate to the most important properties of material set [A]. The remainder of the characteristics of the technological system, such as the equipment set, [B] contain the differences. However, similarity seems more important in this case than identity, because even the descriptions of similarity contain ambiguities which make identity a theoretical rather than practical category.

2.3. Characterization of Material-Flow-Systems from the Technological Point of View

2.31 *Internal and External Technological Structure*

Definition 11: The internal technological structure of the material-flow-systems characterizes the material-flow-systems by those characteristics which display their effects when they come into contact with each other.

Definition 12: The external technological structure of the material-flow-systems characterizes the material-flow-systems by those characteristics which primarily determine their relationships to the equipment.

2.32 *Description of the Internal Technological Structure of the Material-Flow-Systems*

The object-classes of the characteristic-set of the material-flow-systems are as follows:

1. Chemical structure (c) (if it can be defined)
2. Crystalline structure (k)
3. Form (f)
4. Phase state (h), its elements are: β_1: solid; β_2: liquid; β_3: gas
5. Quantity (G)
6. Temperature (T)
7. Pressure (P)
8. Dispersity, its elemets are:
   N: the number of dispersed particles
   D: the size of dispersed particles
   F: the surface area of dispersed particles.
9. Inhomogeneity, its elemets are:
   I_G: inhomogeneity of quantity
   I_T: inhomogeneity of pressure
   I_N: inhomogeneity of the number of particles
   I_D: inhomogeneity of the size of particles
   I_F: inhomogeneity of the surface area of the particles.

10. Rheological properties, its elements are:
    R_v: viscosus
    R_{pl}: plastic
    R_e: elastic
11. Biological structure (BIO)

The structure graph of the object-classes is shown in *Fig. 7*. The material-

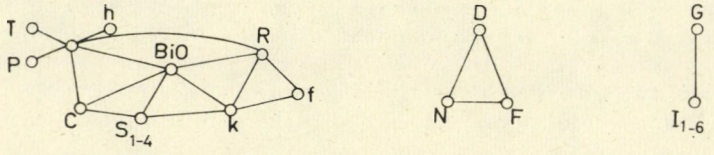

Fig. 7.
The structure graph of the object-classes forming the internal structure of the material flow systems

flow-systems can be adequately characterized from a technological point of view by the above 11 object-classes. However, a given material-flow-system cannot always be characterized in detail by all the object-classes, e.g. non-crystalline material, it has no biological structure, etc. In such cases we have to note that these characteristics are missing.

In the case of jointly flowing material-flow-systems the resultant material-flow-system can be characterized by property α which can assume two values:

$\bar{\alpha}_1$ property: there is a governing material-flow-system. In this case the relationships of the other material-flow-system to the governing materi al-flow-system are depicted by symbols $\Rightarrow$ and $\rightarrow$ in the homogeneous- and heterogeneous cases, respectively, and the arrows point towards the non-governing systems.

$\bar{\alpha}_2$ property: there is no governing material-flow-system. In such cases the relationships between the systems are depicted by symbols $\Leftrightarrow$ and $\leftrightarrow$ in the homogeneous and the heterogeneous cases, respectively.

Obviously, there is a strong relationship between property $\bar{\alpha}$ and relation-ship-properties α existing between the functional groups, it is a macroscopic characteristic, their resultant. Since it characterizes the entire material-flow-system, it plays a major role in shaping the external structure.

The other symbol of the homogeneous relationship is γ_1 which corresponds to $\Rightarrow$ and $\Leftrightarrow$. The other symbol of the heterogeneous relationship is γ_2 which corresponds to $\rightarrow$ and $\leftrightarrow$.

These two symbols can be thought of as the two cases of characteristic γ. Then a general relationship $(q_{1-14})\gamma(q_{1-14})$ can be introduced which shows whether the hierarchy level pairs formed as the Descartes multiples of the set of the hierarchy levels with itself can or cannot be formed according to γ. Without claiming completeness, this relationship set is shown here.

Homogeneous relationship γ_1 corresponds to the dissolution in a chemical sense of covalently bound or ionic materials. Furthermore, the existing biological structure which is the consequence of the coupling of the compounds is also classified.

It should be noted that according to our present knowledge, biological coupling can be decomposed, but cannot in general be created, except perhaps in the case of insuline synthesis, where the formation of a biological connection can be claimed.

Under the heading heterogeneous relationship γ_2 come all the suspensions, emulsions, gels and aerosols.

Thus:

(q_{1-8}) if all the material-flow-systems are biological
(q_{1-14}) γ_1, ion-covalent (q_{9-14}) where
(q_{1-14}) can reflect biological couplings as well
(q_{1-10}) γ_2 (γ_{1-10})

In compounded material-flow-systems, the following object-classes of the separate material-flows-systems have to be considered to describe the resultant characteristics of the resultant material-flow-system:

— chemical structure (c)
— phase state (h)
— crystalline structure (k)
— quantity of material (G)
— inhomogeneity (I)
— sensitivity (S)
— biological structure (BIO)
— dispersity, except in dispersing media of characteristic $\bar{\alpha}_1$.

Thus, based on their internal relationships compounded material-flow-systems can be characterized by the set shown here:

$$[A] = \bigcup_{i=1}^{n} (c, k, h, G, I, \mathrm{BIO})_i ; \bigcup_{i=1}^{n-1} (N, D, F)_i ; f ; P ; T ; R ; \bigcup_{i=1}^{k} \bar{\alpha}_{2,i} \qquad (12)$$

where $1 < k < n-1$

For this relationship it is assumed that

— there is only one material-flow-system of property $\bar{\alpha}_1$ in the system
— the $(n-1)$ material-flow-system of property $\bar{\alpha}_2$ can be reduced to k systems by, e.g. dissolution.

2.33 *Description of the External Technological Structure*

One of the main principles of Blickle's theory is expressed by the following postulate:

Postulate 9: Primarily the structure of the equipment of a technological system is determined by the phase states and the mutual relationships of the material-flow-systems processed in them.

Due to this postulate we have to characterize the material-flow-systems according to both their phase states (h; β_1 = solid; β_2 = liquid and β_3 = gas) and their mutual relationships (γ_1 = homogeneous; γ_2 = heterogeneous).

In this case, the following internal characteristics are neglected:

$$c, k, G, I, S, \mathrm{BIO}, N, D, F, P, T.$$

The description of the external technological structure is shown in *Fig. 8*. It can be seen from Eq. 13 that the mode of contacting (γ) and the characteristic feature ($\bar{\alpha}$) are two interrelated facets of the same phenomenon.

$$b_i = \beta_{1-3} \wedge (\beta_1 \vee \beta_2 \vee \beta_3) \wedge (\gamma_1 \gamma_2)$$

— if there is $\bar{\alpha}_1$ then the characteristic of the govering material-flow-system is entered here	— if there is $\bar{\alpha}_1$ then the phase state of the non-governing material-flow-system is entered here	— if there is $\bar{\alpha}_1$ then the contacting mode of the governing and non-governing material-flow-system is entered here
— if there is $\bar{\alpha}_2$ then the charasteristic representing the phase state of the resultant material-flow-system is entered here	— if there is $\bar{\alpha}_2$ then the phase states occurring (with respect to the resultant material-flow-system) are entered here	— if there is $\bar{\alpha}_2$ then the characteristic contacting modes in the resultant material-flow-system are entered here

Fig. 8.
The description of the external technological system

Based on such considerations, the possible variants of the important-in-practice external technological systems (b_i) are as follows:

$b_1 = \beta_1 \wedge \beta_1 \wedge (\gamma_1 \vee \gamma_2)$	— homogeneous solid phase or mixture of solid powders
$b_2 = \beta_2 \wedge \beta_2 \wedge \gamma_1$	— homogeneous liquid phase
$b_3 = \beta_2 \wedge (\beta_1 \vee \beta_2 \vee \beta_3) \wedge \gamma_2$	— solid, liquid or gas dispersed in liquid medium
$b_4 = \beta_3 \wedge \beta_3 \wedge \gamma_1$	— homogeneous gas phase
$b_5 = \beta_3 \wedge (\beta_1 \vee 2) \wedge \gamma_2$	— solid dispersed in gas or liquid phase.

The following important limiting condition should be noted:

In the case of materials of biological origin the possible phase states according to the hierarchy levels are as follows:

q_{1-5}: solid (β_1)
q_{6-9}: solid (β_1), liquid (β_2)
q_{9-14}: solid (β_1), liquid (β_2), gas (β_3).

The general relationship of the internal and external structures is shown in *Fig. 9*.

The properties of the materials in a technological system can well be described in detail by the terms introduced above. The introduction of the set of changes makes it possible to accentuate in full the significance of the functional groups.

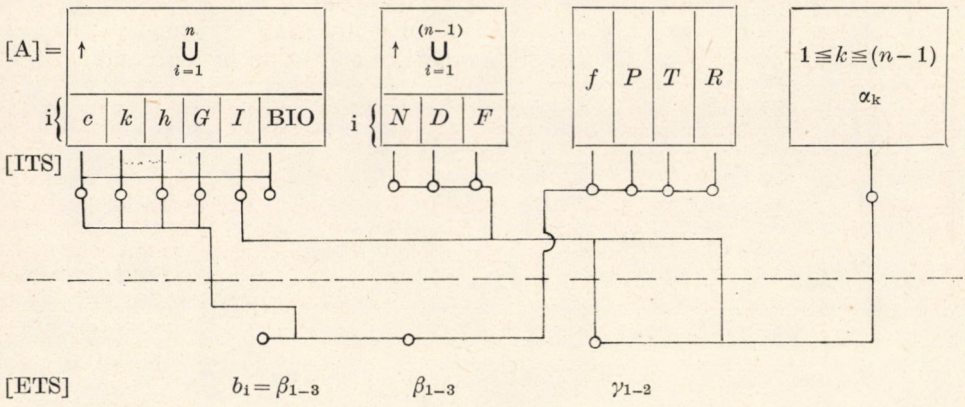

Fig. 9.
The relationship of the external and internal technological structure

REFERENCES

1. T. Blickle and K. Seitz: A modern algebrai módszerek felhasználása a műszaki kémiában. (The Use of Modern Algebraic Methods in Technical Chemistry). Műszaki Könyvkiadó. Budapest, 1975.
2. Műszaki kémiai rendszerek szerkezete. (The Structure of the Systems of Technical Chemistry — in Scientific Results of the MTA MÜKKI series) (Ed.: K. Polinszky), Veszprém, 1974.
3. J. Szendrei: Algebra és számelmélet. (Algebra and Numerical Theory). Tankönyvkiadó. Budapest, 1976.

РЕЗЮМЕ

В I-ой части серии статей автор излагает общую теорию химических технологий, прилагая к ней необходимые определения и постулаты. Целью данной теории является выбор инвариантов и исследование с их помощью технологических систем для материалов в основном биологического происхождения. В интересах описания технологических систем автор приводит характеристики материалов, подвергающихся технологической обработке, знакомит нас с так называемым принципом иерархии и определяет понятие технологической Функциональной группы. Автор, исходя из теории Бликле, истолковывает так называемые внутреннюю и внешнюю технологические системы материалов.

HUNGARIAN JOURNAL
OF INDUSTRIAL CHEMISTRY
VESZPRÉM
Vol. 6. pp. 39–52 (1978)

GENERAL PROPERTIES OF TECHNOLOGICAL SYSTEMS. II.

F. Mohos

(Budapest Chocolate Factory of the Hungarian Candy Trust)

Received: May 26, 1977.

This paper, the second in a series deals with changes occurring in technological systems, presents the L and Z mapping structures describing the changes on the basis of Blickle's theory and finally it discusses the principles and the most important relationships of connection-algebra. Then the application fields of the technological theory advanced are outlined and a general schematic for the design of the system and its subsystems is presented, the latter being the adaptation of Blickle's theory.

3. Changes Taking Place in Technological Systems

3.1 Object-Classes of the Set of the Changes

Definition 13: The general form of a changes is as follows
change $= v \wedge \delta \wedge \tau \equiv \delta \overline{\vee} v \wedge \tau$

where v: is the type of the change
δ: is the characteristic of the change
τ: is the mode of the change.

3.11 *The modes of changes are as follows:*

steady-state:	τ_1
non-steady-state:	τ_2
batchwise:	τ_3

Since the mode of the change is inherently and closely connected to the apparatus of the operation unit, it is advantageously discussed along with the apparatus set.

3.12 *The characteristic of the change* (δ) *can be:*

straight:	δ_1
uniting:	δ_2
decomposing:	δ_3
exchanging:	δ_3

3.13 *The type of change* (v) *can be:*

neutral change:	v_1
change of the standard deviation:	v_2
change of the size:	v_3
change of the form:	v_4
change of temperature:	v_5
change of pressure:	v_6
change of phase state:	v_7
change of the ratio of material-flow-systems:	v_8
change of the connections of the material-flow-systems:	v_9
change of the crystalline structure:	v_{10}
chemical change:	v_{11}
biological change:	v_{12}

v_{12} aims at hierarchy levels q_{1-8}.

3.2 Relationship between the Type of Change (v) end the Internal Technological Structure

This relationship is given on Matrix 1.

ITS \ V	1	2	3	4	5	6	7	8	9	10	11	12
c											+	
k										+		
h							+					
G								+				
I		+										
S					+	+						
BIO												+
N		+										
D			+									
F			+									
P						+						
T					+							
R							+	+	+	+	+	+
$\bar{\alpha}$									+			
f				+								

+ : there is direct connection

empty: there is no direct connection

Fig. 10.
Relationship between the type of change and the inner technological structure (Matrix 1).

3.3 Description of the Technological System by Technological Mappings

3.31 *The definition of technological mapping*

Definition 14: Technological mappings are algebraic mappings which describe the changes occurring in a technological system in such a way that they contain:

- the type (v) and character (δ) of the change and
- the ANCESTOR and the PICTURE of the material-flow-systems involved in the change concerned.

If the changes of the material structure are described by the internal or the external structures then l or z mappings are used, respectively.

3.32 *l-mappings. L-mapping structures*

The general form of l-mapping reads as follows:

$$l_1 = (V \wedge \delta): \begin{bmatrix} A_{\text{ANCESTOR}} \\ A_{\text{PICTURE}} \end{bmatrix} \tag{15}$$

Mappings in which only a single type or character of a change asserts itself are called elementary mapping.

Two important operations can be defined for the l-mappings:

- definitions of operation: let

$$l_1 = (V_k \wedge \delta_m): \begin{bmatrix} a_1 \circ a_2 \circ \ldots \circ a_i \\ a_{i+1} \circ \ldots \circ a_j \end{bmatrix} \tag{16 a}$$

and

$$l_2 = (V \wedge \delta_p): \begin{bmatrix} a_s \circ a_{s+1} \circ \ldots \circ a_t \\ a_n \circ a_{n+1} \circ \ldots \circ a_b \end{bmatrix} \tag{16 b}$$

then

$$l_1 \odot l_2 = (V_k \wedge \delta_m): \begin{bmatrix} (a_1 \circ \ldots \circ a_i) \circ (a_3 \circ \ldots \circ a_t) \\ (a_{i+1} \circ \ldots \circ a_j) \circ (a_4 \circ \ldots \circ a_b) \end{bmatrix} \tag{16 c}$$

In general; if

$$l_1 = (v \wedge \delta)_1: \begin{bmatrix} \text{ANCESTOR}_1 \\ \text{PICTURE}_1 \end{bmatrix}$$

$$l_2 = (v \wedge \delta)_2: \begin{bmatrix} \text{ANCESTOR}_2 \\ \text{PICTURE}_2 \end{bmatrix}$$

then

$$l_1 \circ l_2 = (v \wedge \delta)_1 \cdot (v \wedge \delta)_2: \begin{bmatrix} \text{ANCESTOR}_1 \circ \text{ANCESTOR}_2 \\ \text{PICTURE}_1 \circ \text{PICTURE}_2 \end{bmatrix} \tag{17}$$

Small case letter o is used to "separate" the material-flow-systems and promote comprehension of the notation system.

Operation $\odot$ is used to represent an operation in which the transformation of two material-flow-systems in carried out not separately (in space or time), rather the two material-flow-systems are blended and the changes take place in the resultant material-flow-system in the same space and time element.

Definition of operation $\oplus$:

If

$$l_1=(v\wedge\delta)_1:\begin{bmatrix}\text{ANCESTOR}_1\\ \text{PICTURE}_1\end{bmatrix}$$

$$l_2=(v\wedge\delta)_2:\begin{bmatrix}\text{ANCESTOR}_2\\ \text{PICTURE}_2\end{bmatrix} \tag{18 a}$$

and the condition under which operation $\oplus$ can be carried out is

$$[\text{PICTURE}_1]\cap[\text{ANCESTOR}_2]\equiv K\neq\{\emptyset\} \tag{18 b}$$

at $[H_{cr}]$ being set then

$$l_1\oplus l_2=(v\wedge\delta)_1\cdot(v\wedge\delta)_2:\begin{bmatrix}\text{ANCESTOR}_1\circ[\text{ANCESTOR}_2/K]\\ [\text{PICTURE}_1/K]\circ\text{PICTURE}_2\end{bmatrix} \tag{18 c}$$

For example: let

$$l_1=(v\wedge\delta)_1:\begin{bmatrix}a_1\circ a_2\\ a_3\circ a_4\end{bmatrix};\qquad l_2=(v\wedge\delta)_2:\begin{bmatrix}a_3\circ a_5\\ a_6\circ a_7\end{bmatrix}$$

$$\text{then}\quad [\text{PICTURE}_1]\cap[\text{ANCESTOR}_2]\equiv K=a_3\neq\{\emptyset\}$$

and

$$l_1\oplus l_2=(v\wedge\delta)_1\cdot(v\wedge\delta)_2:\begin{bmatrix}a_1\circ a_2\circ a_5\\ a_4\circ a_6\circ a_7\end{bmatrix}$$

Thus, while operation $\odot$ is to be visualized as the parallel coupling of material-flow-systems, operation $\oplus$ represents the connection in series of material-flow-systems where the connection is ensured by the non-zero-set result of the section operation, in this case material-flow-system a_3. In the course of operation $\oplus$ the critical hierarchy levels should be ensured of because otherwise the section operation cannot be carried out.

Over the set of l-mappings operation $\odot$ and $\oplus$ create the L-mapping structure, $L=(1, \odot, \oplus)$.

These algebraical structures are not treated here in detail, their properties can be very varied according to the chemical conditions.

3.33 *z-mappings, Z-mapping structures*

According to Definition 14 the general form of z-mapping

$$z=(v\wedge\delta):\begin{bmatrix}b_{\text{ANCESTOR}}\\ b_{\text{PICTURE}}\end{bmatrix} \tag{19}$$

Over the set of z-mappings operation $\odot$ and $\oplus$ define the Z-mapping structures (algebraical structures), $Z=(z, \odot, \oplus)$. However, only for the l-mappings can operations $\odot$ and $\oplus$ be carried out directly. The result in the Z-structure can be obtained only after the deduction of the external structure from the internal structure of the material-flow-system formed. This means that a series of relatively complicated steps have to be taken. The practical meaning of Z-structures is that in them the changes become manifest from the point of view of the apparatus since it is the external technological structure which

changes in such cases. These structures have not yet been studied. In my opinion this study is important because once the change-series, $(v \wedge \delta)$ multiples in which the external structure remains unaltered can be identified then the apparatus in which these changes can take place can also be identified.

Thus, while the internal structure changes in the course of operations $\odot$ and $\oplus$—as it is shown by the L-structure—the external structure follows these changes much more "sluggishly", as it is shown by the Z-structure.

The inter-relationship of the two types of mapping is shown in *Fig. 11.*

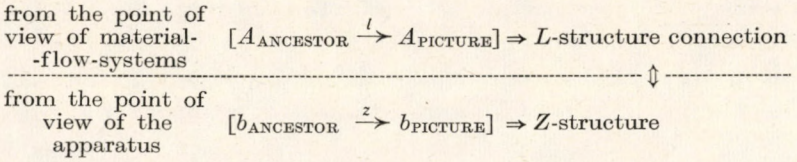

Fig. 11.
Relationship of l- and z-mappings

3.4 Algebraical Stucture "K-connection" Defined Over the Set of the Functioual Groups

So far the relationship between an elementary change, in which only a single V or δ value is changed and another elementary change has been examined. However, if the task is the computation/identification of the intermediary changes and the consideration of all the theoretically possible changes deducible from the known ANCESTOR and PICTURE of a large technological system, then the means developed so far are inadequate.

This problem can be phrased in another way by using the terms defined: why exactly material-flow-systems $(a_3 \circ a_4)$ are formed from material-flow-systems $(a_1 \circ a_2)$ in the course of mapping operation

$$l=(v \wedge \delta): \begin{bmatrix} a_1 \circ a_2 \\ a_3 \circ a_4 \end{bmatrix}.$$

Obviously, if all four material-flow-systems (a_{1-4}) are composed from the flows of the functional groups of the same generator system then other combinations of the functional groups must also be possible and material-flow-systems different from a_3 and a_4 would be founded from a_1 and a_2. Naturally, always the most economical direction of transformation is sought.

The types of the changes can be:

v_9: change of the relationship of material-flow-systems
v_8: change of the ratio of material-flow-systems.

Obviously, v_8 can be considered the special case of v_9, so it is sufficient to concentrate on v_9. So far the types of changes have been related to material-flow-systems and there is no need to change this practice, because if the general definition of a material-flow-system is

$$\bar{f}=a_1\bar{f}_1+a_2\bar{f}_2+\ldots+a_n\bar{f}_n \qquad (3)$$

then

$$\bar{f}_i = 0 \cdot \bar{f}_1 + 0 \cdot \bar{f}_2 + \ldots + 1 \cdot \bar{f}_i + \ldots + 0 \cdot \bar{f}_n \qquad (15)$$

and except for the coefficient of $\bar{f}_i$ all the other coefficients are zero. (In fact, the flows of the functional groups are examined.)

This definition ensures that if change v_9 is applied to the set of the functional groups then in the course of the operation this set is not left i.e. an algebraical structure is formed over the set of the functional groups.

However, connections are not that easily concluded because there are several substeps while a connection becomes established as follows:

Let A and B be functional groups then

— if there is a possibility for connection between A and B then the symbol $(A|B)^\circ$ is used. Symbol | means "contacting". Upper-script o can even be omitted.

— if a homogeneous connection is formed in the case of $(A|B)^\circ$ then

$$(A|B)^\circ \xrightarrow{\Omega(+)} (A|B)^{\Omega(+)}$$

— if a heterogeneous connection is formed in the case of $(A|B)^\circ$ then

$$(A|B)^\circ \xrightarrow{\varepsilon(+)} (A|B)^{\varepsilon(+)}$$

— if homogeneous connection $(A|B)^{\Omega(+)}$ is dissolved then

$$(A|B)^{\Omega(+)} \xrightarrow{\Omega(-)} (A|B)^\circ$$

— if heterogeneous connection $(A|B)^{\varepsilon(+)}$ is dissolved then

$$(A|B)^{\varepsilon(+)} \xrightarrow{\varepsilon(-)} (A|B)^\circ$$

Thus, in general, a connection-algebraical structure is obtained described as $K=(f, |, \Omega, (\pm), \varepsilon(\pm)$, which means that operations, $|$, $\Omega(\pm)$ and $\varepsilon(\pm)$ can be carried out on the functional group set f and the inverse of the last two operations can also be carried out.

The inverse of operation | is also defined, it simply means that two functional groups are separated.

Let us now examine the characteristics of the structure thus obtained.

3.41 *The characteristics of the contacting operation*

At preset $\Omega(\pm)$ and $\varepsilon(\pm)$ the characteristics of the contacting operation, | depend on

— the general properties of the materials contacted
— the maximal hierarchy level of the materials contacted.

Depending on the "degree of decomposition" of the contacted materials the phenomena which can occur are *a*-priori determined.

In contacting operation it is always worthwhile to examine whether the functional groups can form *a* commutative Abel group or not. If they can then the task becomes an exclusively chemical task and the behaviour of the functional groups cannot be determined by algebraical means.

3.42 *Connection-establishing and connection-breaking operations,* $\Omega(\pm)$ and $\varepsilon(\pm)$

The first important statement is that these two operations (and their inverse operations) are the duals of each others, i.e. what holds for one of them holds for the other as well.

The operational axioms are as follows:

$$1.\quad \Omega(\circ)\cdot\Omega(+)=\Omega(+) \qquad \varepsilon(\circ)\cdot\varepsilon(+)=\varepsilon(+) \tag{16a}$$

$$2.\quad \Omega(+)\cdot\Omega(-)=\Omega(-) \qquad \varepsilon(+)\cdot\varepsilon(-)=\varepsilon(-) \tag{16b}$$

$$3.\quad \Omega(\circ)\cdot\Omega(-)=\Omega(\circ) \qquad \varepsilon(\circ)\cdot\varepsilon(-)=\varepsilon(\circ) \tag{16c}$$

Axiom 3 is a convenient convention, not a direct cause of the treatment as the first two. The Cayley operational matrix corresponding to the axioms is shown in *Fig. 12.*

	+	−	0
+	+	0	+
−	0	−	0
0	+	0	0

Fig. 12.
The Cayley matrix of connection-forming and connection-breaking operations (Matrix 2)

The operational characteristics are: non-associative, commutative; idempotent.

3.43 *Characteristics with respect to each other of the operations defined in connection-algebra*

In general, the characteristics with respect to each other of the three operations are determined not by algebraical, rather by chemical laws. Let us see *a* few relationships to demonstrate this principle:

1) $((A|B)^{\Omega}|(C|D)^{\Omega})^{\Omega}$ is not necessarily identical with $(A|B|C|D)^{\Omega}$, because: $NaCl|AgNO_3=AgCl\downarrow|NaNO_3$.

Thus, unexpectedly—unpredictable by algebraical means—a heterogeneous connection does turn up in the system of homogeneous connections.

2) If operation ε is used throughout Example 1, then all the connections on the resultant are not necessarily are heterogeneous, because if any of $A|B$ dissolves any of $C|D$—and there is neither *a* theoretical nor practical objection to it—then a homogeneous connection is established among these functional groups.

3) The transformations shown below cannot be calculated

$$[(A|B)^{\Omega}|(C|D)^{\Omega}]^{\varepsilon}; \qquad [(A|B)^{\varepsilon}|(C|D)^{\varepsilon}]^{\Omega}$$

and

$$[(A|B)^{\Omega}|(C|D)^{\varepsilon}]^{\Omega}; \qquad [(A|B)^{\Omega}|(C|D)^{\varepsilon}]^{\varepsilon}$$

These transformations can be carried out only by allowing for the laws of chemistry, otherwise non-real solutions are obtained.

However, these problems of connection-algebra urge us to consider all the mathematically possible solutions—not only the conventional ones—and exclude those impossible.

This strategy also leads to the correct solution: instead of considering only those few combinations which lead us to the objective, all the mathematically possible combinations are considered and narrowed down as necessary.

Connection algebra is used to trace the trails of functional groups, and the path on which the transformation proceeds. Thus connection algebra yields the trace-graphs of the functional groups.

4. General Characterization and Constuction of the Apparatus of Technological Systems

This chapter is entirely based on Blickle's theory [1], and on his and his coworkers' results. To my best knowledge a more sophisticated version of the theory presented here is in preparation, which can be used to describe the apparatuses of technological systems in more detail and to solve more complicated problems.

4.1 Characteristics-Object-Classes of the Apparatus

b_{1-5}: the esternal technological structure of the material-flow-system
Θ_{1-4} phase-form
t_{1-2}; L_{1-4}: flow-state of the phases
τ_{1-3} run
ξ_{1-2} recirculation
σ_{1-3}: mode of connection
$\zeta_{\text{subscript}}$: order of connection (numerous subscripts)
π_{1-6}: flow conditions
η_{1-3}: energy input
ϑ_{1-z}: type of energy
ε_{1-6}: function of the apparatus element
$\varkappa_{1-7}$: positions and relationships of the apparatus elements
μ_{1-10}: permeability of the material of the apparatus
ν_{1-11}: shape of the apparatus element
λ_{1-6}: motion-possibilities of the apparatus element.

It should be noted that some of these are subsets. The relationships of the object-classes of the apparatus-set (B) and its subsets ($B \times B$) are shown as a graph in *Fig. 3*, p. 47 in [1]. Operations $\vee$ and $\wedge$ on the set ($B \times B$) correspond to the logical disjunction and conjuction operations.

The structure graph of the operation unit is shown in *Fig. 17*, p. 84 in [1]. The following sub-structures can be distinguished on the structure graph:

$R_1 = \{t, \hat{\vartheta}, c, b, \Theta, \xi\}$ types of material-flow-systems or processes
$R_2 = \{\zeta, \zeta^\circ, \varepsilon_5, \sigma, \tau, \gamma, \pi\}$ operation modes
$R_3 = \{\vartheta, \delta, \tau, \gamma, \vartheta\}$ chemical unit operations
$R_4 = \{\hat{\vartheta}, \hat{\eta}, \varepsilon_2, \varepsilon_3\}$ energies
$R_5 = \{\varepsilon, \varkappa, \lambda, \mu, \vartheta\}$ apparatuses.

The graph of the secondary structure of the apparatus-unit is shown in Fig. 18, p. 90 in [1]. To formulate the relationships the decompositions of

τ_{1-3}: run and
b_{1-5}: external technological structure

presented in *Table 4*, p. 91 in [1] or *Table 5*, p. 130 in [2] were used. The relationships of the partial structures are discussed in detail in pp. 114—136 in [2].

The treatment of the structure of the apparatuses by this theory is so complete and extensive that it cannot be presented here in more detail. However, any question can be dealt with after having mastered these two references.

5. Application Fields of the Technological Theory Presented

Two main fields can be identified:

1) General method for the design of complete technological systems ("technology-design")

2) General method for the design of technological subsystems (apparatus units).

5.1 Design of Complete Technological Systems

Design consists of three main types of activity:

1) determination of the set of the functional groups on the basis of the ANCESTOR and PICTURE.

2) Construction of the PICTURE from the ANCESTOR by connection-algebraical means.

3) Construction of the trace-graph of the functional groups and the prescription of the characteristic technological changes.

5.11 *Determination of the set of the functional groups*

This work starts with the assignment of the hierarchy levels and the determination of the characteristic technological changes. Then by section-operation on the sets of the material-flow-systems of the ANCESTOR and PICTURE using Eq. 7 of Part 1, the material fractions which are transfered from one material-flow-system into the other one can be identified. This operation is shown by Matrix 3 in *Fig. 13*. Naturally the "depth of decomposition", the hierarchy level until one can proceed while searching for the material fractions in the section-operation, has to be known.

To help to understand this process better let us select a simple, known example shown in *Fig. 14*.

Otherwise, the search for functional groups is entirely identical with the search for prime numbers (with respect to addition or union operations).

It can be seen that functional group E is not decomposed any further, although it can be written as $C_2H_3\equiv$. However, there is no technological transformation taking place in this technological system which would warrant the

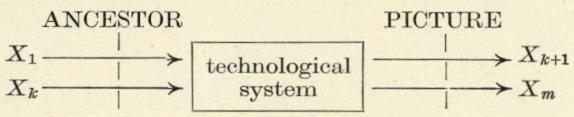

[X] \ [X]	$X_1 \ldots X_j \ldots X_m$
X_1 ⋮ X_i ⋮ X_m	$\langle 1;0 \rangle$

Matrix 3

if $X_i \cap X_j \neq \{\varnothing\} \Rightarrow \langle 1 \rangle$ (at present hierarchy levels)
if $X_i \cap X_j = \{\varnothing\} \Rightarrow \langle 0 \rangle$

The result of the section operation can also be entered in Matrix 3.

$$[X] = [X_{\text{ANCESTOR}}] \cup [X_{\text{PICTURE}}]$$

Fig. 13.
Determination of the functional groups of a technological system

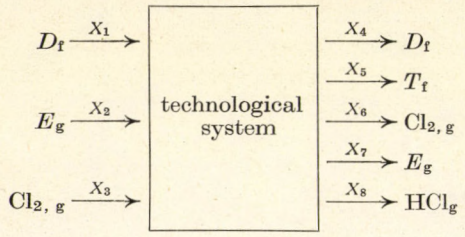

[X] \ [X]	Cl_2	E	D	T	HCl
Cl_2	Cl_2	$\varnothing$	Cl_2	Cl_2	Cl
E	$\varnothing$	E	$(E \cdot H)$	$E\cdot$	$H\cdot$
D	Cl_2	$(E \cdot H)$	D	$(E \cdot Cl_2)$	HCl
T	Cl_2	$E\cdot$	$(E \cdot Cl_2)$	T	(HCl)
HCl	Cl·	H·	(HCl)	(HCl)	(HCl)

D: dichlorethylene
T: trichloroethylene
E: ethylene
g: gas
f: liquid

$X_1 \equiv X_4$; $X_3 \equiv X_6$; $X_2 \equiv X_7$
(Determined by chemical analysis)

Functional groups:

$E\cdot \equiv [C_2H_3 \equiv]$
$H\cdot \equiv [H-]$
$Cl\cdot \equiv [Cl-]$

Construction of the material-flow-system from functional groups:

$(X_1 \equiv X_4) = E\cdot \cup Cl\cdot \cup Cl\cdot$
$(X_2 \equiv X_7) = E\cdot \cup H\cdot (= E)$
$(X_3 \equiv X_6) = Cl\cdot \cup Cl\cdot$
$X_5 = E\cdot \cup Cl\cdot \cup Cl\cdot \cup Cl\cdot (= T)$
$X_8 = Cl\cdot \cup H\cdot (= HCl)$

Fig. 14.
Determination of the functional groups in the case of a particular problem

decomposition of this functional group into atoms, so with respect to the problem to be solved there is no reason to replace the 3 dimensional technological system selected with another generator-system consisting also of 3 basic vectors. It is another question that to ensure uniform handling of the

chemical systems all the technological systems should be described by the linear combination of basic vectors, atoms. In this case atoms C, H and Cl would be the basic vectors.

It is worthwhile noting that if the changes of the technological system discussed are taken as the possible changes then the presence of carbon atoms in group E could not be determined and other changes and further reactions would be necessary to facilitate this determination.

Let us construct according the Eq. 1 the characteristic matrix equation of the technological system.

$$[f_1 f_2 f_3]\cdot \begin{array}{c} \\ f_1 \\ f_2 \\ f_3 \end{array} \begin{array}{c} \begin{array}{cccccccc} D & E & Cl_2 & D & T & Cl_2 & E & HCl \end{array} \\ \begin{bmatrix} 1 & 1 & 0 & 1 & 1 & 0 & 1 & 0 \\ 1 & 3 & 0 & 1 & 0 & 0 & 3 & 1 \\ 2 & 0 & 2 & 2 & 3 & 2 & 0 & 1 \end{bmatrix} \end{array} = [x_1 x_2 x_3 x_4 x_5 x_6 x_7 x_8]$$

where

$D = x_1$ $\quad T = x_5$ $\quad f_1 = C_2H_3$

$E = x_2$ $\quad Cl_2 = x_6$ $\quad f_2 = H^-$

$Cl_2 = x_3$ $\quad E = x_7$

$D = x_4$ $\quad HCl = x_8$ $\quad f_3 = Cl$

and, e.g.

$T = (C_2H_3)_1 (H_-)_0 (Cl_-)_3$

It should be noted that the dimensions of f_i and x_j are mass/time.

5.12 *Derivation of the PICTURE from the ANCESTOR by connection-algebraical means*

The procedure is shown in connection with the previous example.

ANCESTOR:

$$\{\underbrace{(1f_1|1f_2|2f_3)}_{D_f}{}^{\Omega+}|[\underbrace{(2f_3)}_{Cl_2,\,g}{}^{\Omega+}|\underbrace{(1f_1|3f_2)}_{E_g}{}^{\Omega+}]\}^{\varepsilon+} \xrightarrow{\text{step 1}}$$

$$\rightarrow \{\underbrace{(1f_1|1f_2|2f_3)}_{D_f}{}^{\Omega+}|[\underbrace{(2f_3)}_{Cl_2,\,g}{}^{\Omega+}|\underbrace{(1f_1|3f_2)}_{E_f}{}^{\Omega+}]^{\Omega+}|[\text{unaltered ANCESTOR}]\}^{\varepsilon+} \xrightarrow{\text{step 2}}$$

$$\rightarrow \{[\underbrace{(1f_1|1f_2|2f_3)}_{D_f}{}^{\Omega+}|\underbrace{(1f_1|3f_3)}_{T_f}{}^{\Omega+}|\underbrace{(2f_3)}_{Cl_2 f}{}^{\Omega+}|\underbrace{(1f_1|3f_2)}_{E_f}{}^{\Omega+}|\underbrace{(1f_2|1f_3)}_{HCl_f}{}^{\Omega+}]^{\Omega+}|[\underbrace{(2f_3)}_{Cl_2,\,g}{}^{\Omega+}|\underbrace{(1f_1|3f_3)}_{E_g}{}^{\Omega+}]^{\Omega+}\}^{\varepsilon+} \xrightarrow{\text{step 3}}$$

$$\rightarrow \{[\underbrace{(1f_1|1f_2|2f_3)}_{D_f}{}^{\Omega+}|\underbrace{(1f_1|3f_3)}_{T_f}{}^{\Omega+}]^{\Omega+}|[\underbrace{(2f_3)}_{Cl_2,\,g}{}^{\Omega+}|\underbrace{(1f_1|3f_2)}_{E_g}{}^{\Omega+}|\underbrace{(1f_2|1f_3)}_{HCl_g}{}^{\Omega+}]^{\Omega+}\}^{\varepsilon+}$$

PICTURE

The corresponding process-graph is

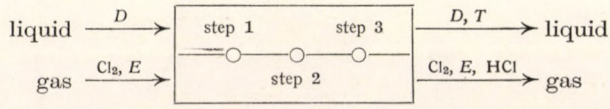

Fig. 15.
Application of connention-algebra

Both liquid D and gaseous Cl_2 and E occur in both the ANCESTOR and the PICTURE, so only their excesses have to be accounted for. Further transformations are shown in *Fig. 15*.

The discussion here is naturally much more complicated than in the case of the conventional method, since the conventional means to discuss chemical technologies are matched to chemical phenomena.

The characteristic changes of the three technological steps are as follows:

Step 1: v_9 occurs
Step 2: v_{11} occurs
Step 3: v_8, v_9 occur

5. 13 *Next those change-types have to be designed which complete the known changes of the three technological steps just mentioned.*

Obviously, the effects of temperature (v_5) and pressure (v_6) have to be identified. It is not impossible that there is a phase-state change (v_7) for one of the components. Common chemical laws and principles should be observed (equilibrium relationships, etc.). Thus, the essential changes necessary to complete the process-graph can be added. However, all changes cannot be selected theoretically, and practical experimental work remains indispensable.

5.2 General Method for the Design of Technological Subsystems

The method discussed here was advanced by BLICKLE and his co-workers and published in pp. 148–149 in [1] and pp. 133–136 in [2]. The most typical and most important forms for practice of the technological subsystems are the apparatus-units. For their design z-mappings relating to apparatus units are required.

— the type (v) and character (δ) of the changes occurring in an apparatus-unit
— changes of the external technological structure (b_i) of the material transformed in the given apparatus unit.

Based on the variables occurring in z-mappings all the variants of the apparatuses performing the changes required can be selected by the help of *Table 4*, p. 91 of [1] and the principle shown in *Fig. 16*.

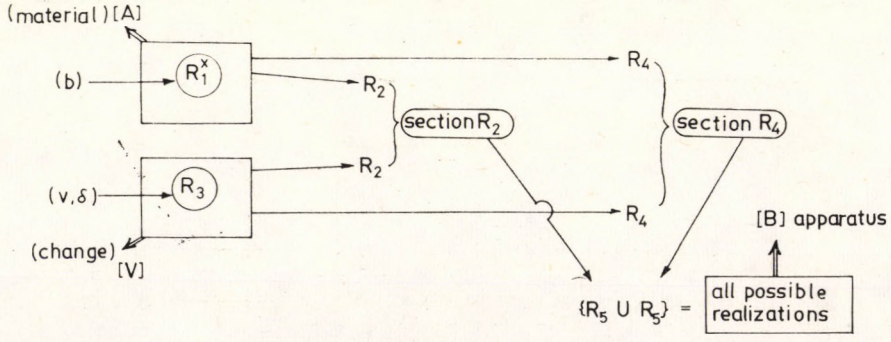

Fig. 16.
Design of an apparatus-unit

— Arrows show the relationships which can be selected from *Table 4.*
— The sets encircled are the common sections of the solutions obtained from "two directions".

The meaning of quantities R are given in the paragraph dealing with the general characterization of the apparatuses, their particular meaning can be found on pp. 85–94 in [1].

It should be noted in *Fig. 16* that the feed of the information on the material-flow-system (b) into R_1^x and the feed of the information on the changes (v, δ) into subsets R_3 mean that the graph shown in *Fig. 16* corresponds to a technological triangle-graph in which R_1^x corresponds to material set A, and R_3 corresponds to the set of changes (V). The remainder rest of the graph (B) is the apparatus-set. This means that the graph shown in *Fig. 16* is one of the possible realization forms of the general technological graph. As far as I know Blickle and his co-workers are working on a more detailed model.

6. Some Problems of the Similarity of Technological Systems

Previously two criteria have been shown which could be used to discuss the similarity of technological systems. One of the main ideas of the theory was given in Part 1, paragraph 2.33 expressed by Postulate 9 as "Primarily the structure of the equipment of a technological system is essentially determined by the phase-states and the mutual relationships of the material-flow-systems processed in them."

This means that the identity based on these features (phase-state and relationship, β and γ) renders the technological systems similar ("identical processes").

This type of "classification" —in my opinion— can be very fruitful, because vastly different technologies dealing with different raw materials in different industries are brought into a similarity relationship. For example any atomization process proves to be similar to the others.

Thus, this similarity criterion works on the bases of the external technological structure of the materials.

However, *Difinition 10* in Part 1, paragraph 2.26 stated another kind of similarity: "One of the cases of similarity in technological systems is ... the flows of their functional groups are identical" — cf. Eqs. 11/a–d.

This approach more appropriately accords with the conventional technological approach which states, e.g. that brewery technologies — in which the raw materials and end products are identical and the materials are decomposed to the same hierarchy level and the characteristic technological changes are identical — are similar. Obviously, the internal technological structure of the materials is called upon in this approach.

In my opinion, these two similarity criteria well demonstrate the two classes of the similarity of technologies. These can be called

— horizontal similarity, which is based on the internal technological structure,
— vertical similarity, which is based on the external technological structure.

Brewing technologies are horizontally similar. Fermentation technologies (independently from the application fields) are vertically similar.

A more exacting definition of similarity reads as follows:

Any technological system can be described as

$$\{A, B, C, D\} \varepsilon E$$

where

A: is the set of material-flow-systems entering the system
B: is the set of material-flow-systems leaving the system
C: is the set of changes
D: is the set of apparatuses
E: is the set of technological systems (to be considered at all for the given problem).

It can be seen that (A, B) C and D form the triangle-graph of the general technological system.

Let us now define a few relationships ϱ_A, ϱ_B, ϱ_C and ϱ_D as follows:

Let e_1 and e_2 be the two technological systems, then if $e_1 \cap A = e_2 \cap A$ then $e_1 \varrho_A e_2$ assumes value 1, in the other case 0.

Similarly, e.g. ϱ_{AB}:

$$e_1 \varrho_{AB} e_2 \Rightarrow \begin{cases} e_1 \varrho_A e_2 \\ e_2 \varrho_B e_2 \end{cases} \quad \text{and}$$

Relationships ϱ_A, ϱ_B, ϱ_C and ϱ_D—used to express the cases of similarity in technological systems—divide set E into disjunct classes, so-called equivalency classes, correspondingly into mappings

$$A \xrightarrow{\varphi_A} E; \qquad B \xrightarrow{\varphi_B} E \quad etc$$

are unambiguous.

Then a value-ordering relationship $\hat{\varrho}_C$ can be defined e.g. in the equivalency class $\varphi_C(C_i) = E(C_i)$ which yields the optimum technology at the element which has the maximum value according to $\hat{\varrho}_C$.

Obviously, the above discussion applies similarily to A, B, C and D as well.

REFERENCES

1. T. Blickle and K. Seitz: A modern algebrai módszerek felhasználása a műszaki kémiában. (The Use of Modern Algebraic Methods in Technical Chemistry) Műszaki Könyvkiadó, Budapest. 1975.
2. Műszaki kémiai rendszerek szerkezete. (The Structure of the Systems of Technical Chemistry; in Scientific Results of the MTA MÜKKI series. Ed. K. Polinszky) Veszprém. 1974.
3. Yu. A. Schreider: Egyenlőség, hasonlóság, rendezés. (Equivalency, Similarity, Ordering) Gondolat Könyvkiadó, Budapest, 1975.

РЕЗЮМЕ

Во II-ой части серии автор уделяет внимание изменениям, происходящим в технологических системах, опираясь на теорию Бликле, приводит структуры отображений L и Z, описывающие эти изменения, а затем обсуждает принцип и взаимозависимости алгебры подключений. Затем автор перечисляет области применения обсуждавшейся ранее теории технологий, приводит общую схему для проектирования технологической системы в целом и её подсистем — это последнее является соответствующей адаптацией теории Бликле.

HUNGARIAN JOURNAL
OF INDUSTRIAL CHEMISTRY
VESZPRÉM
Vol. 6. pp. 53–66 (1978)

THE INHOMOGENEITY PARAMETER AND ITS PROPERTIES. I.
Closed Systems

B. Lakatos and T. Blickle

(Research Institute for Technical Chemistry
of the Hungarian Academy of Sciences, Veszprém)

Received: October 10, 1977

The paper deals with the measures of mixing. The general conditions to be fulfilled by the measure of mixing are scrutinized. It is shown that the appropriately normalized form of the quadratic functional defined for the concentration functions, the so-called inhomogenity parameter is a good measure of mixing which, in agreement with the practical conception, defines a linear ordering relationship between the concentration distributions occurring in reality. In the general case, the exact knowledge of the concentration distribution of the system studied is necessary for the calculation of the inhomogenity parameter. In practice, however, it can be frequently estimated from the discrete form of the distribution derived from measurements of the concentration samples. This is so—among others—in the case of studies of the homogenization processes.

The inhomogeneity parameter is one of the inhomogeneity moments, the second order inhomogeneity moment of the inhomogeneity distribution function defined in this paper. They can be used to approximate the inhomogeneity distribution function to any arbitrary degree of precision.

Introduction

Due to the complexity of the exact equations describing mixing phenomena, these phenomena are frequently characterized by simplified models and so-called qualitative criteria which, no matter what the mechanisms causing the mixing are like, approach the problem via the quality of the distributions obtained. These are called the measures of mixing.

There are several such measures published in literature relating to the mixing of both liquids and solids and these are based on various initial conceptions [1–6].

In the course of the system-theoretical treatment of the processes and apparatuses of technical chemistry, in the so-called structure-theory of the systems of technical chemistry, the need arose for a quantity more in line with the requirements of this theory to characterize the above mentioned distri-

butions, or expressed in a more general way, to approximately characterize the distribution of the continuous object-classes according to their arguments. These requirements were, among others, the following ones: to describe the phenomena of mixing according to the needs of practice; to assign a number to each such state of agitation which can occur in a real process; its structure should not be excessively complex, it could be used to formulate certain optimation problems.

The appropriately modified quadratic functional proved to be such a measure which satisfied most of these requirements. Due to this property, this functional is the most important of the inhomogeneity moments [7]. This paper presents the definition of this measure, described as the inhomogeneity parameter here, and some of its characteristics.

The Range of Concentration Functions and the Measures of Mixing

Let us consider a binary miscible system located in a finite—for the minute being closed—range of space, (its magnitude being constant in time), where the distribution of the miscible component in the carrier is characterized by its concentration.

Let the mathematical representation of the range in space be $\overline{V} \subset R^3$, the compact subset of the three-dimensional Euclidean space R^3, and let $I_2(V)$ be the Hilbert space of the quadratically (Lebesque) integrable functions defined on set V.

If $c = c(x)$ is the concentration of the miscible medium at an $x \in V$ point, then it can be easily shown that the mathematical representation of any practically permitted concentration distribution is the element of the subset of space $L_2(V)$

$$K(V) = \{c \in V \to L_2(V) : \sup_{x \in V} c(x) = \varrho_m \text{ and } \inf_{x \in V} c(x) = 0\} \tag{1}$$

and it is termed the range of the (permitted) concentration functions.

This is the expression of that natural fact that the concentration cannot be negative in any point nor can it ever exceed a positive real number, ϱ_m. The value of ϱ_m depends on the particular problem, but it can always be defined unambiguously.

Any mechanism bringing about a change in the distribution of the miscible component is characterized by abstract function:

$$c : (0, \infty) \to (V) \tag{2}$$

and symbols $c(x)(t)$, $x \in V$, $t \in [0, \infty)$ are used.

Abstract function c(x) (t) defines, according to this formalism, a mixing phenomenon if:

$$\lim_{t \to \infty} c(x)(t) = c_e(x) \tag{3}$$

is true at nearly all the points of set V and $c_e \in K(V)$ is a constant function representing the uniform distribution and where the absolute value of c_e is:

$$|c_e| = \overline{c(t)} = \frac{1}{|V|} \int_V c(x)(t)\, dx \tag{4}$$

where $\bar{c}$ stands for the average value of function $c(x)$ over range V.

Thus, if a functional:

$$f: K(V) \to R \tag{5}$$

can be defined in such a way that it is true for any mixing process $c(x)(t)$ that a $t_2 \in [0, \infty)$, $t_2 > t_1$ minute can be assigned to any given $t_1 \in (0, \infty)$ minute that:

$$f[c(x)](t_2) < f[c(x)](t_1) \tag{6}$$

then functional f can be used to construct the extent of mixing. (Naturally, relationship (6) can point in the opposite direction as well).

This, in practice, means that function f defines such a linear ordering relationship for the elements of the range of concentration functions $K(V)$ which is in agreement with practical experiences.

Naturally, it follows from the above definition that if there is one such t_2 then there are an infinite number of them too and condition 6 is always fulfilled for any $t_2 > t_1$ in the case of fluctuation-free processes.

The Inhomogeneity Parameter

Let us cinseider the "distance-square-density in unit volume" of an arbitrary distribution $c \in K(V)$ from a uniform distribution $c_e \in K(V)$, i.e. the quadratic functional:

$$d_V^2[c] = \frac{1}{|V|} \int_V [c(x) - c_e(x)]^2 \, dx \tag{7}$$

which — since $|c_e| = \bar{c}$ — can be written as:

$$d_V^2[c] = c^2 - (\bar{c})^2$$

Range (KV) is convex, $d_V^2[c]$ is a convex functional over range (V) [8]. The solutions of the problem:

$$\underset{c}{\text{extremum}} \{d_V^2[c] \mid c \in K(V)\} \tag{8}$$

i.e. those distributions which yield the minimum and maximum values of functional $d_V^2[c]$ within the range of the permitted concentration functions are given by the following distributions 1° $d_V^2[c]$ assumes its minimum value in the case of uniform distribution, i.e.

$$c_{\min}(x) = c_2(x) \qquad x \in V \tag{9}$$

and

$$d_V^2[c_{\min}] = 0, \tag{10}$$

2° $d_V^2[c]$ assumes its maximum value in the case of a completely segregated distribution, i.e.

$$c_{\max} = \begin{cases} \varrho_m, & \text{if} \quad x \in V_1 \\ 0, & \text{if} \quad x \in V \mid V_1 \end{cases} \tag{11}$$

where $|V_1| = \bar{c}|V|/\varrho_0$ and

$$d_V^2[c_{\max}] = \bar{c}(\varrho_0 - \bar{c}). \tag{12}$$

The derivation is shown in Appendix 1.

Thus, it can be seen that functional $d_V^2[c]$ determines the distribution of minimum and maximum transmixing in range $K(V)$ in agreement with practice. To establish the relationships among the distributions within these two extreme states let us examine the linear diffusion process described by boundary-value problem:

$$\frac{\partial c(x,t)}{\partial t} = \operatorname{div}[D \operatorname{grad} c(x,t)], \quad x \in V, \quad t > 0 \tag{13}$$

$$c(x,0) = c_0(x) \quad x \in V \tag{14}$$

$$\frac{\partial c(x,t)}{\partial n} = 0 \quad x \in S, \quad t > 0 \tag{15}$$

Let us make the known equivalency relating to the second derivate of the square of the functions, the Gauss theorem and let us carry out a few simple substitutions to arrive at the initial boundary-value problem:

$$\frac{d\{d_V^2[c](t)\}}{dt} = -\frac{2}{|V|}\int_D D\,[\operatorname{grad} c(x,t)]^2\,dx \tag{16}$$

$$d_V^2[c](0) = d_V^2[c_0] \tag{17}$$

It follows that — since $D \geq 0$ and $(\operatorname{grad} c)^2 \geq 0$ — the linear diffusion process becomes manifest via such distributions which result in strictly monotonously decreasing $d_V^2[c](t)$ with increasing time from any arbitrary initial distribution c_0. It is apparent from Eq. 16 that the smaller the rate of decrease, the smaller diffusion coefficient D and $(\operatorname{grad} c)^2$ are. Therefore, it follows that the rate of equalization decreases with decreasing gradients due to equalization.

Since this process can be considered the "most typical" equalization process, it means that the normalized form of functional $d_V^2[c]$

$$I_V^2[c] = \frac{d_V^2[c]}{d_V^2[c_{max}]}, \quad c \in K(V) \tag{18}$$

can be considered a good measure of the extent of mixing.

Let us introduce ordering relationship R_k in set $K(V)$ in such a manner that: $c_1 R_k c_2$ then and only then, if $I_V^2[c_1] \leq I_V^2[c_2]$ (19)

$$c_1, c_2 \in K(V)$$

which means that distribution c_1 represents a state more thoroughly transmixed than c_2. Relationship R_k orders set $K(V)$ in a linear manner, i.e. $c_1 R_k c_2$ or $c_2 R_k c_1$ for any arbitrary $c_1, c_2 \in K(V)$ while the minimum element of $K(V)$ is the uniform distribution c_m determined by Eq. 9 and its maximum element is distribution c_{max} given by Eq. 11.

Elements c_{min}, c_{max}, and an inner element of $K(V)$ in a onedimensional case is shown in *Fig. 1.*

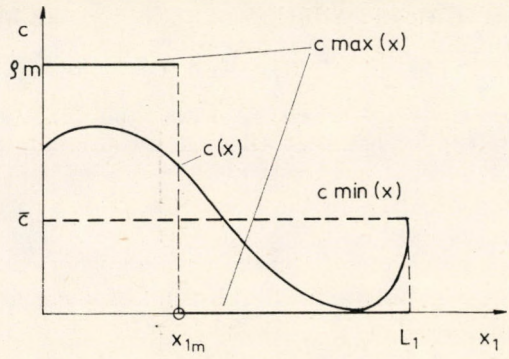

Fig. 1.
Elements $c_{\min}$, $c_{\max}$ of range $K(V)$ along with an arbitrary internal element c

It can be concluded that ordering relation R_k called mixing relation relates the elements of $K(V)$ on the basis of the diffusion process, i.e. if $c_1=c(x, t_1)$ and $c_2=c(x, t_2)$ are the two solutions of initial boundary problem Eq. 16 and 17 and $t_2 \geq t_1$ then $I_V^2[c_2] \leq I_V^2[c_1]$, and correspondingly $c_2 R_k c_1$. Naturally, it can be seen from Eq. 18 that:

$$0 \leq I_V^2[c] \leq 1 \qquad \forall c \in K(V). \tag{20}$$

If $I_V^2[c_1]=I_V^2[c_2]$ then distributions c_1 and c_2 represent states of equal degree of mixing and are not distinguished from the point of view of this study. Thus, the symmetric mirror image with respect to the normal bisector $[0, L]$ as symmetry axis of distribution c shown in *Fig. 1* is equivalent with c. Similarly, any arbitrary distribution obtained from the original one by cutting section $[0, L]$ into finite pieces, followed by the arbitrary mixing of these finite sections along with the function segments belonging to them, is also considered equivalent with c, since these operations do not influence the value of the inhomogeneity parameter. However, this is a rather static kind of equivalency, because as it follows from Eq. 16, dynamic equivalency in any minute requires the identity of $(\text{grad } c)^2$ as well, a requirement most frequently not assumed by these operations, since due to such cutting and mixing operations, new breakage points are formed and the "environment" of the elements is also changed.

Certain Characteristics of the Inhomogeneity Parameter

The discrete form of inhomogeneity parameter I_V^2 defined by Eq. 18 — when it is calculated from a limited number of samples as:

$$I_V^2=\frac{1}{n \cdot d_V^2[c_{\max}]} \sum_{i=1}^{n} [c_i-\bar{c}]^2 \tag{21}$$

where:

$$\bar{c}=\frac{1}{n} \sum_{i=1}^{n} c_i \tag{22}$$

is the average value of n concentration samples — is an appropriate qualitative criterium to study the homogenization process [1,8].

It follows from the definition of I_V^2 that the sampling points are set, i.e. the ith sample $i=\overline{1, n}$ is always taken from the same place, and the n sampling points are distributed in such a way that each represents a space element to be homogenized of equal $|V|/n$ magnitude.

Due to the stochastic nature of the homogenization processes, I_V^2 in general can never reach the zero value, not even when, according to the average value, the system can be considered completely homogeneous.

Let us assume that the adequate description of some homogenization process $c(x)(t)$ is the simplified model known from the theory of turbulent fowl [9] in which stochastic velocity and concentration spaces are accounted for by a constant value and a superpositioned fluctuating component each of a much higher frequency range, e.g., in the case of concentration:

$$c = \langle c \rangle + c' \tag{23}$$

Let us substitute this expression into Eq. 18 and assume that due to the homogenization process, the average value is identical in any point, then the expression:

$$I_V^2[c] = \frac{1}{|V| d_V^2[c_{max}]} \int_V [c'(x)]^2 \, dx \tag{24}$$

is obtained which is proportional with the standard deviation of stochastic process c' and in general, its value is not equal to zero.

Thus, it can be seen that the value of the inhomogeneity parameter decreases to a minimum value given by Eq. 24, but due to the stochastic nature of the mixture it cannot assume a smaller value. If the mixture is a perfect (ideal) one, then $c' = 0$ and the inhomogeneity parameter can also assume zero value.

Let us consider a linear, normal distribution series over range V, characterized by normalized density functions of the form:

$$c(x) = \frac{1}{a} e^{-bx^2} \tag{25}$$

where:

$$a = \int_V e^{-bx^2} \, dx \tag{26}$$

and parameter b is a function monotonously decreasing with the standard deviation of the parameters, σ. In such cases, the inhomogeneity parameter defined in space yields an ordering similar to the standard deviation σ of these distributions, i.e. in the case of two arbitrary distributions of the form of Eq. 25 c_1 and c_2, where the respective standard deviations are σ_1 and σ_2, it is true that:

$$\text{if} \quad \sigma_1 < \sigma_2 \quad \text{then} \quad I_V^2[c_1] > I_V^2[c_2]. \tag{27}$$

The details of the derivation are shown in Appendix 2.

Obviously, this is in agreement with the "measure of mixing" nature of the inhomogeneity parameter, because in the case of "normal distributions", the "flatter" the distribution, the greater is the standard deviation, which means that it is closer to the homogeneous distribution, i.e. the value of the inhomogeneity parameter belonging to it is smaller.

The inhomogeneity parameter, I_V^2 can be generalized for systems containing n components as follows.

Let us introduce concentration vector $c^T=(c_1, c_2, c_3, \ldots, c_n)$ where c_i, $i=\overline{1, n}$ is the concentration of the ith component.

The inhomogeneity parameter characterizing the system is given by:

$$I_V^2[c]=\frac{1}{d_V^2[c_{max}]|V|}\int_V (c-\bar{c})^T(c-\bar{c})\,dx \tag{28}$$

where $d^2[c_{max}]$ reads as:

$$d_V^2[c_{max}]=\sum_{i=1}^{n}\bar{c}_i(\varrho_m^i-\bar{c}_i). \tag{29}$$

Thus, the relationship between the inhomogeneity parameters $I_V^2[c_i]$ of the respective components and the inhomogeneity parameter of the entire system containing n components is given by:

$$I_V^2[c_{max}]=\frac{d_2^V[c_i]}{d_V^2[c_{max}]}I_V^2[c_i] \tag{30}$$

The Inhomogeneity Moments

Let us now consider the permitted concentration function $c\in K(V)$ and let us introduce the function:

$$F(\varrho)=m\{x: c(x)<\varrho\} \tag{31}$$

It can be seen from the definition of $F(\varrho)$ that it is a monotonously non-decreasing and continuous-from-the-left-hand-side function:

$$\lim_{\varrho\to 0}F(\varrho)=0 \quad \text{and} \quad \lim_{\varrho\to\varrho_m}F(\varrho)=|V| \tag{32}$$

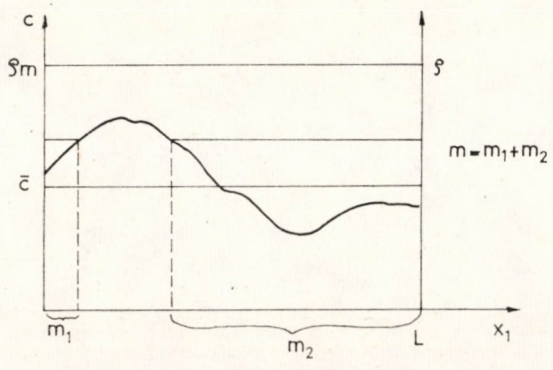

Fig. 2.
Determination of function $F(\varrho)$

The latter, in sum, means that $\psi(\varrho)=F(\varrho)/|\ V\ |$ is a concentrated distribution function over the interval $[0,\ \varrho_m)$ and it is termed the inhomogeneity distribution function of the permitted concentration function, $c\in K(V)$. The determination of function $F(\varrho)$ in the one-dimensional case is shown in *Fig. 2.*

It can be shown [10] that if g is a Lebesque-measurable function over the interval $(0,\ \varrho_m)$ then:

$$\int_0^{\varrho_m} g(\varrho)\,\mathrm{d}\psi(\varrho)=\frac{1}{|V|}\int_V g[c(x)]\,\mathrm{d}x \tag{33}$$

provided any of the integrals shown in the equivalency exist.

Let us substitute function $g(\varrho)=\varrho^i$, $i=1,\ 2\ldots$ into Eq. 33 to obtain

$$\int_0^{\varrho_m} \varrho^i \mathrm{d}\psi(\varrho)=\frac{1}{|V|}\int_V c^i(x)\,\mathrm{d}x \qquad i=1,\ 2,\ \ldots \tag{34}$$

From here it can be easily shown that:

$$\frac{1}{|V|}\int_V [c-\bar{c}]^i\,\mathrm{d}x=\int_0^{\varrho_m}(\varrho-\bar{\varrho})^i\,\mathrm{d}\psi(\varrho), \qquad i=2,\ 3,\ \ldots \tag{35}$$

i.e. the ith inhomogeneity moment at the left-hand-side of Eq. 35 is equal to the ith central moment of the inhomogeneity distribution function $\psi(\varrho)$, i.e. the inhomogeneity moments act as the central moments of a one-dimensional distribution concentrated over the interval $[0,\ \varrho_m)$. Thus, if a distribution $c\in K(V)$ is characterized by its inhomogeneity moments, then a $c\to\psi$ mapping—mainly a fictious one—is carried out and thus there is no need to examine the space dependency of the concentration. This, and another very similar approach [11] as mentioned before, is used primarily to characterize the quality of homogenization processes and batch-wise operations of the chemical industry.

The inhomogeneity distribution functions ψ_{max}, ψ_{min} and ψ corresponding to distributions c_{max}, c_{min}, $c\in K(V)$ shown in *Fig. 1* are shown in *Fig. 3.*

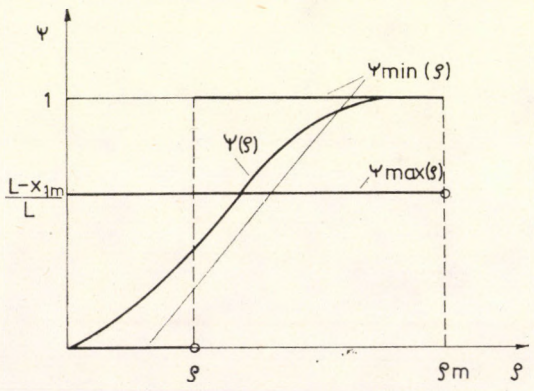

Fig. 3.
The inhomogeneity distribution functions of concentration functions c_{min}, c_{max} and c shown in *Fig. 1.*

It can be seen from Eq. 34 and 35 that the approximations of the moments of inhomogeneity distribution function $\psi(\varrho)$ can be calculated by expressions of the form shown in Eq. 21 constructed for the ith, $i=1, 2, \ldots$ power, i.e. the calculation is based directly on the concentration sample taken at point n.

Distribution function $\psi(\varrho)$ [12] can be calculated as a good approximation by the Bernstein polynomes from these samples, or rather from the moments calculated from these samples. If the $c \to \psi$ mapping is mutually unambiguous, then the original concentration distribution $c \in K(V)$ can also be reconstructed unambiguously.

Final Remarks

In the general case, inhomogeneity parameter I_V^2, as shown by Eq. 16, can be calculated only when the exact concentration distribution of the system is known. For practice, however, it is Eq. 21 which is important, because it ensures that the inhomogeneity parameter can be calculated by the discrete form (Eq. 21) from measured concentration samples — as, e.g. when homogenization processes are examined.

Eq. 16 is a very important and significant result because thus the diffusion process is considered a basic process for the derivations and can be used to classify the respective elements of the $K(V)$ range of the permitted concentration functions.

It can be seen from Eq. 35 that the inhomogeneity parameter is — from the stand-point of probability theory, the standard deviation of the inhomogeneity distribution function $\psi(\varrho)$ defined by Eq. 31, where $\psi(c)$ is the probability of the occurrence of a particle in the system studied at a point where the concentration is smaller than ϱ. It should also be noted that the third momentum informs us about the symmetricity of distribution c, i.e. about the ratio of the areas swept by the function sections above and below the average value.

On the basis of the above discussion, the simplicity of its structure and its frequent use as the qualitative criterion of optimation problems, it can be concluded that the inhomogeneity parameter satisfies all the requirements advanced in the Introduction and thus it can be appropriately used in the structural theory of the systems of technical chemistry.

Although this paper dealt with phenomena connected to components, the results shown can also be applied to heat phenomena, since the equations used to describe heat phenomena in the systems of technical chemistry are similar to the equations dealing with component transport, so the inhomogeneity parameter also applies in their case.

SYMBOLS USED

a — constant, (Eq. 26)
b — constant
c — concentration, (kgm^{-3}); concentration function
c_e — uniform concentration distribution
c_{min} — minimum concentration distribution
c_{max} — maximum concentration distribution
$d_V^2[c]$ — Eq. 7
D — diffusion coefficient, (m^2s^{-1})
f — functional

F — distribution function
g — function
I_V^2 — inhomogeneity parameter, (Eq. 18)
$K(V)$ — the range of the permitted concentration functions
L_1 — the length of the system in direction, α_1, (m)
$L_2(V)$ — the space of the functions quadratically integrable over V
m — measure of the set
n — normal, natural number
R — the set of real numbers
R^3 — three dimensional, Eucledian space
R_k — transmixing relation, (Eq. 19)
S — boundary surface of V
t — time, (sec)
x — space vector
V — set
V_1, V_2, V_3 — sets
ϱ — probability variable
ϱ_m — maximum concentration value
σ — standard deviation
ψ — inhomogeneity distribution function
φ — Lagrange functional
λ_1, λ_2 — Lagrange functions
ν — Lagrange constant
α, α' — constants
γ — function
Θ — empty set

Indices

1, 2 — particular value
0 — initial value

Mathematical operations

$\overline{(\cdot)}$ — average value
$|\cdot|$ — measure of the set, absolute value
$\langle\cdot\rangle$ — probability average
$(\cdot)'$ — fluctuating component
$(\cdot)^T$ — transporation
$\overline{(\cdot)}$ — vector
$\overline{(\cdot)}/(\cdot)$ — difference of sets

REFERENCES

1. Danckwerts, P. V.: Appl. Scient. Res., *A3*, 279 (1953)
2. Hobler, T., Strek, F.: Chemia Stosowana, *3*, 143 (1959)
3. Landau, J. and Prochazka, J.: Coll. Czech. Chem. Comm., *26*, 1976 (1961)
4. Fan, L. T., Chen, S. J. and Watson, C. A.: Ind. Eng. Chem., *62*, 53 (1970)
5. Tőrös, R.: Hung. J. Ind. Chem., *1*. 329 (1973)
6. Tőrös, R.: Hung. J. Ind. Chem., *3*, 227 (1975)
7. Blickle, T. and Bátor, E.: MTA VEAB Monography, *1*, 35 (1975)
8. Lakatos, B.: Inhomogeneity in Technical Chemistry and its Changes. Doctor Thesis, Veszprém, 1975.
9. Slattery, J. C.: Momentum, Energy and Mass Transfer in Continua. McGraw-Hill, New York, 1972
10. Gihman, I. I. and Skorokhod, A. V.: Bevezetés a sztochasztikus folyamatok elméletébe (Introduction to the Theory of the Stochastic Process), Műszaki Könyvkiadó Budapest, 1975
11. Horváth, G.: Hung. J. Ind. Chem, *3*, 467 (1975)
12. Feller, W.: An Introduction to Probability Theory and its Applications. Vol. 2. Wiley, New York, 1966
13. Kulikowski, R.: Sterowanie w wielkich systemach. WNT, Warszawa, 1970

Appendix 1

Solution of Problem (8)

This problem is divided into two: the determination of the minimum and maximum elements. This determination was made with the Lagrange functional method [13].

Determination of the Distribution Yielding the Maximum Value

Since d_V^2 is convex over range $K(V)$ functional $-d_V^2$ is a concave functional and the determination of the distribution resulting in the maximum value is given by the solution of the following problem:

Let us determine element c_{max} minimizing functional:

$$-d_V^2[c] = -\overline{(c-\bar{c})^2} \tag{A.1.1.}$$

under the limiting conditions:

$$\bar{c} = |c_e| \tag{A.1.2.}$$

$$c(x) - \varrho_m \leq 0 \tag{A.1.3.}$$

$$-c(x) \leq 0 \tag{A.1.4.}$$

The Lagrange functional of the problem becomes:

$$\phi(c, \mu, \lambda_1, \lambda_2) = -\overline{(c-\bar{c})^2} + \mu(\bar{c}-c_2) + \int_V \lambda_1(x)[c(x)-\varrho_m]\,dx + \int_V \lambda_2(x)[-c(x)]\,dx \tag{A.1.5.}$$

so the necessary and sufficient conditions become:

$$\operatorname{grad}_c \phi(c, \mu, \lambda_1, \lambda_2) = \frac{2}{|V|}[\bar{c}-c(x)] + \mu + \lambda_1(x) - \lambda_2(x) = 0 \tag{A.1.6.}$$

$$\int_V \lambda_1(x)[c(x)-\varrho_m] = 0; \qquad \int_V \lambda_2(x)[-c(x)] = 0 \tag{A.1.7.}$$

$$\lambda_1(x) \geq 0, \qquad \lambda_2(x) \geq 0 \tag{A.1.8.}$$

and also, conditions A.1.2 to A.1.4.

Let us assume that constraint A.1.3 is active in the range $V_1 \subset V$, A.1.4 in the range $V_2 \subset V$ and there does exist such a set of non-zero-measure $V_3 \subset V$ that none of the constraints is active there. Then, since $V_i \cap V_j = \phi$, i, j $= 1, 2, 3$ and $V_1 \cup V_2 \cup V_3 = V$, Eq. (A.1.6.) can be decomposed as:

$$\frac{2}{|V|}[\bar{c}-c(x)] + \mu + \lambda_1(x) = 0, \quad \text{if} \quad x \in V_1 \tag{A.1.9.}$$

$$\frac{2}{|V|}[\bar{c}-c(x)] + \mu - \lambda_2(x) = 0, \quad \text{if} \quad x \in V_2 \tag{A.1.10.}$$

$$\frac{2}{|V|}[\bar{c}-c(x)] + \mu = 0, \quad \text{if} \quad x \in V_3 \tag{A.1.11.}$$

It follows from (A.1.11) that $c(x)=\bar{c}+\mu(V)/2$ is constant over set V_3 and let this set be α and $0<\alpha<\varrho_m$. Then, however, one can immediately find such a function to which functional $-\mathrm{d}_V^2$ is smaller.

Let us consider *Fig. A.1.1* showing—for the sake of simplicity—the one-dimensional case. Let $\alpha'>\alpha$ and $\alpha'\,|V_3|'=\alpha(V_3)$. The difference of the two

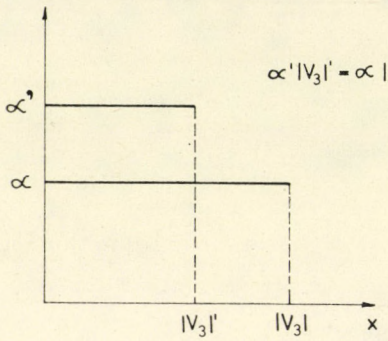

Fig. A.1.1.
Schematic used for the determination of the distribution acting as the maximum element

functionals is given by $\alpha'^2\,|V_3|'-\alpha^2\,|V_3|$. If the above values are substituted here then one obtains:

$$\alpha|V_3|(\alpha'-\alpha)>0 \tag{A.1.12.}$$

If $\alpha'=\varrho_m$ then set V_3 is bisected and the value $c(x)=\varrho_m$ is selected on set V_3'. Let $c(x)=0$ on the set V_3/V_3'. If ranges V_1 and V_2 are completed in such a manner then the value of functional $-(\mathrm{d}^2)$ decreases. Thus, it follows that in the case of the minimum element $|V_3|=0$.

Then let us select $\mu=0$. $\lambda_1(x)=2(\varrho_\mathrm{m}-\bar{c})/|V|$ over range V_1 and $\lambda_2(x)=2\bar{c}/|V|$ over range V_2. Since $\varrho_\mathrm{m}-\bar{c}\geq 0$ for any $c\in K(V)$ it follows from condition (A.1.2) that:

$$c_{\max}(x)=\begin{cases}\varrho_m, & x\in V_1\\ 0, & x\in V_2\end{cases} \tag{A.1.13.}$$

where $|V_1|=\bar{c}\,|V|/\varrho_\mathrm{m}$ and $|V_2|=|V|-|V_1|$.

The determination of the distribution yielding the minimum value is carried out analogous to the previous procedure (and therefore it is not repeated here) under the necessary and sufficient conditions resulting in the uniform distribution:

$$c_{\min}=c_\mathrm{e} \tag{A.1.14.}$$

Appendix 2

Derivation of Eq. (27)

Since the average value is constant it is sufficient to examine the sign of the derivative according to σ of:

$$|V|\overline{c^2}=\frac{1}{a^2}\int_V e^{-2bx^2}\,\mathrm{d}x=a^{-2\gamma},\quad \gamma=\int_V e^{-2bx^2}\,\mathrm{d}x \tag{A.2.1.}$$

The derivative becomes:

$$\frac{\mathrm{d}(a^{-2\gamma})}{\mathrm{d}\sigma} = -2a^{-3}\frac{\mathrm{d}a}{\mathrm{d}\sigma}\gamma + a^{-2}\frac{\mathrm{d}\gamma}{\mathrm{d}\sigma} \tag{A.2.2.}$$

if the derivation rule of definite integrals with respect to parameters is made use of then:

$$\frac{\mathrm{d}a}{\mathrm{d}\sigma} = -\frac{\mathrm{d}b}{\mathrm{d}\sigma}\int_V x^2 e^{-bx^2}\,\mathrm{d}x \tag{A.2.3.}$$

and:

$$\frac{\mathrm{d}\gamma}{\mathrm{d}\sigma} = -2\frac{\mathrm{d}b}{\mathrm{d}\sigma}\int_V x^2 e^{-2bx^2}\,\mathrm{d}x \tag{A.2.4.}$$

If Eq. A.2.3 and A.2.4 are substituted into A.2.2, then after rearrangement one obtains:

$$\frac{\mathrm{d}(a^{-2\gamma})}{\mathrm{d}\sigma} = 2a^{-2}\frac{\mathrm{d}b}{\mathrm{d}\sigma}\left[\int_V e^{-2bx^2}\,\mathrm{d}x\right]\left[\frac{\int_V x^2 e^{-bx^2}\,\mathrm{d}x}{\int_V e^{-bx^2}\,\mathrm{d}x} - \frac{\int_V x^2 e^{-2bx^2}\,\mathrm{d}x}{\int_V e^{-2bx^2}\,\mathrm{d}x}\right] \tag{A.2.5.}$$

It is immediately apparent that the sign of the first derivative of $(a^{-2\gamma})$ with respect to σ depends only on the signs of $\mathrm{d}b/\mathrm{d}\sigma$ and the term in the second parenthesis, because the signs of the other terms are always positive.

However, the first term of the difference in the second parenthesis is the second common moment of a normal distribution of parameter b, while the second term yields the second moment of a distribution of parameter $b' = 2b$. Since $b' < b$ and function $\sigma \to b$ is a monotonously increasing one, i.e. $\sigma(b) > \sigma(2b)$ the difference in the second parenthesis is larger than zero.

Thus, it follows that the sign of the left hand side of Eq. A.2.5 is identical with that of $\mathrm{d}b/\mathrm{d}\sigma$, i.e.

$$\frac{\mathrm{d}(a^{-2\gamma})}{\mathrm{d}\sigma} < 0 \tag{A.2.6.}$$

Eq. 27 directly follows from here.

РЕЗЮМЕ

Темой данной статьи является степень паремешанности. В статье рассматривается, каким общим условиям должна удовлетворять характеристика, применяемая в качестве степени перемешанности. Было доказано, что соответственно нормализованная Форма квадратичного Функционала (т. н. параметра неоднородности), толкуемого на основе Функций концентрации, является чрезвычайно хорошей мерой перемешанности. Этот параметр связывает распределения концентраций, имеющих место в действительности, при помощи линейных реляции, соответствующей практическим представлениям. В общем случае, для расчёта параметра неоднородности необходимо точно знать распределение концентраций в исследуемой системе, однако на практике зачастую — так и при изучении процессов гомогенизации — это может быть определено с помощью дискретной Формы параметра, на основе образцов концентрации, полученных в ходе проведения опытов.

Параметр неоднородности является одним из моментов неоднородности — а именно моментом неоднородности второго порядка, — которые представляют собой не что иное, как моменты Функции распределения неоднородности можно приблизить с любой степенью точности.

HUNGARIAN JOURNAL
OF INDUSTRIAL CHEMISTRY
VESZPRÉM
Vol. 6. pp. 67–80 (1978)

THE INHOMOGENEITY PARAMETER AND ITS PROPERTIES. II.
Open Systems

B. LAKATOS and T. BLICKLE

(Research Institute for Technical Chemistry
of the Hungarian Academy of Sciences, Veszprém)

Received: October 10, 1977

This paper deals with the application of the inhomogeneity parameter used to characterize the steady-state conditions of open systems (concerning mass transport) to compare different states and systems.

Even microscopic mixing can be characterized in continuous flow-through systems by the inhomogeneity parameter—although only as an approximation—resulting in a wealth of useful information.

The relationship of three empirical mixing characteristics—recirculation—and the inhomogeneity parameter are scrutinized.

It is concluded that systems can be easily compared by the inhomogeneity parameter: at first the approximate value of the inhomogenity parameter is calculated from measured data, then the empirical characteristic sought is obtained by the appropriate equations.

Introduction

The term inhomogeneity parameter was defined in Part 1 of this paper [1] and a few of its characteristics were shown in the case of closed systems (no mass transport between the system and its environment whatsoever). It was concluded that the inhomogeneity parameter defined a linear ordering relation among the true concentration distributions obtained in agreement with the practical point of view, so it could be used as the measure of the extent of mixing. In the general case, the concentration distribution of the system studied had to be exactly known to calculate the inhomogeneity parameter. In practice, however, it could frequently be estimated by its discrete form from measured concentration samples as, e.g. in the case of studies relating to homogenization processes.

The application of the inhomogeneity parameter for the characterization of the steady-state conditions of systems, open with respect to mass transport and for the comparison of different states and systems, will be dealt with here.

Micromixing in Continuous Flowing Systems

Let us consider an arbitrary continuous flowing system in which the residence time distribution spectrum relating to the mixed fluid is $F(t)$. This function describes the macroscopic mixing in the system. Once the system arrives at a steady-state condition, the concentration distribution of the fluid mixed becomes uniform in the system and the inhomogeneity parameter characterizing the distribution becomes zero, i.e. $I_V^2[c]=0$. Since in steady-state conditions, this is time for any such system, the form derived for I_V^2 in closed systems cannot tell flowing systems from each other.

However, after an appropriate modification, conclusions can also be drawn with the assistance of the inhomogeneity parameter about the microscopic mixing in continuous flowing systems in their steady-state conditions.

DANCKWERTS [2] introduced the term "fluid point" to describe microscopic mixing. A fluid point is a fluid element of negligible size compared to the entire system, yet it contains enough molecules to allow for the definition of the distributions and average values of certain intensive characteristics.

Any fluid stream entering the system is decomposed into a large number of such elements. During their residence in the system these elements can be transformed and mixed with each other. Yet independently from these changes, the can be considered perfectly mixed at any moment.

Let α be the age of any arbitrary molecule in the system at a given moment and let it be equal to the time that has elapsed since the molecule entered the system [3]. Similarily, let the life expectation of the molecule be λ [3] and let it be equal to the time the molecule will still spend in the system from the given minute on.

Thus, if the residence time of a molecule is t then:

$$t=\alpha+\lambda. \tag{1}$$

Due to the stochastic nature of the phenomenon, the age of all the molecules in the system can obviously be characterized by a distribution function called the age function designated $\Theta(\alpha)$.

Let the age distribution function belonging to the pth point, $p\in P$ and where P is the set of indices used to denote the points, be $\Theta_p(\alpha)$. According to the above definition this can be defined for each point and let its concentration be c_p.

Then the concentration of this "point" due to molecules of an age not greater than α is given by the following expression:

$$c_p(\alpha)=c_p\Theta_p(\alpha) \tag{2}$$

so the inhomogeneity parameter in space given by molecules of an age not greater than α can be expressed as:

$$I_V^2(\alpha)=\frac{1}{d^2[c_{max}]|V|}\int_V\left[c_p\Theta_p(\alpha)-\frac{1}{|V|}\int_V c_p\Theta_p(\alpha)\,dV\right]^2 dV \tag{3}$$

where, for the sake of simplicity, summing the operation according to p is written as the integral according to volume and the second term in the brack-

ets is the average value given by molecules of age not greater than α, i.e.

$$\bar{c}(\alpha)=\frac{1}{|V|}\int_V c_p\Theta_p(\alpha)\,dV \tag{4}$$

In steady-state conditions $c_p=\bar{c}=\text{const.}$, thus:

$$I_V^2(\alpha)=\frac{\bar{c}}{(\varrho_0-\bar{c})|V|}\int_V[\Theta_p(\alpha)-\Theta(\alpha)]^2\,dV \tag{5}$$

where:

$$\Theta(\alpha)=\frac{1}{|V|}\int_V\Theta_p(\alpha)\,dV \tag{6}$$

Thus, it can be seen that $I_V^2(\alpha)$ indeed informs us about the degree of segregation in the system, because the greater the differences between the age distribution functions of the respective points, the greater the value of $I_V^2(\alpha)$.

The distribution of the molecules remaining in the system since a moment between α and $\alpha+d\alpha$ between the "points" is given by the respective density functions formulated according to Eq. 5.

The most interesting case during the examination of $I_V^2(\alpha)$ expressed by Eq. 5 is when $I_V^2(\alpha)=0$, i.e. $\Theta_p(\alpha)=\Theta(\alpha)$ for any $\alpha\in[0,\infty]$ and all $p\in P$, i.e. the age distribution function of all the "points" are identical and equal to the age distribution function of the system.

It will be shown that $I_V^2=0$ if and only if the system is perfectly mixed in both macroscopic and microscopic scale.

It is known from the model given by ZWIETERING [3] for a microscopically perfectly mixed system, characterized by any arbitrary residence time distribution function $F(t)$ that the age distribution function of a "point" of life expection λ_p reads as:

$$\Theta_p(\alpha)=\frac{F(\lambda_p+\alpha)-F(\alpha_p)}{1-F(\lambda_p)} \tag{7}$$

while the same function of the system is calculated by:

$$\Theta(\alpha)=\frac{1}{\tau}\int_0^\alpha[1-F(\alpha)]\,d\alpha' \tag{8}$$

If the residence time function of a macroscopically perfectly mixed system $F(t)=1-\exp(-t/\tau)$ is substituted into Eq. 7 and 8, then the equivalency $\Theta_p(\delta)=\Theta(\alpha)=1-\exp(-\alpha/\tau)$ is obtained proving the first part of the statement.

To prove the reversed statement let us consider the model shown in *Fig. 1.*

The model consists of a long tube of constant cross section S divided into a large number of sections of width Δx moving continuously along the dotted line.

Each section is divided by $(n-1)$ walls into n cells of equal volume along axis y corresponding to the "points" defined earlier.

The system is composed from an appropriate number of cells of the n sections actually found between points $0-L$, i.e. $L=n\Delta x$, according to the fol-

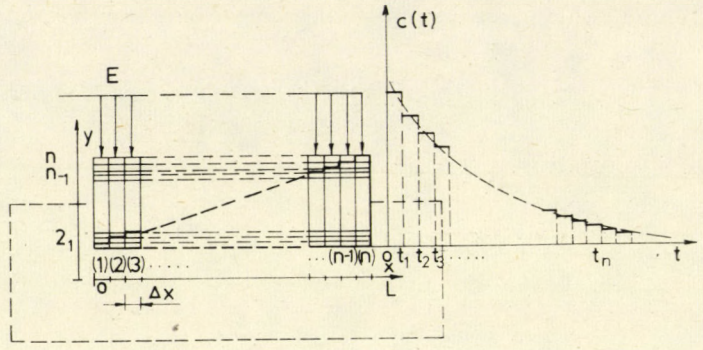

Fig. 1.
Model to study microscopic mixing in a continous flowing system

lowing rule: the first cell of the first section, the first and second cells of the second section, ... the first, second, ... i^{th} cell of the ith section and the first, second, ... n^{th} cells of the nth section, i.e. the system always consists of the enumerated $n(n+1)/2$ cells.

Let us assume that the flow rate of liquid entering the system is $q = \text{const}$. Then the system controlled by an appropriate automatism operates through the following cycles:

1) Distributor E distributes the liquid of volume $q\Delta t$ entering the system during time interval Δt as equal doses into the n sections between points 0 and L in such a manner that liquid dose of volume $q\Delta t/n$ enters the ith cell in section i, $i = \overline{1, n}$.

2) There is a certain transmixing taking place between the section.

These steps are completed in no time or, at least, during a time period much smaller than Δt.

3) Sections move a distance of Δx along the positive x axis at a constant speed w, while the fluid of volume $n(q\Delta t/n) = q\Delta t$ in the cells of the nth, while the last section leaves the system mixed to a degree determined by step 2. As a result of this step the ith section becomes the $(i+1)^{th}$ section $(i = \overline{1, n-1})$ while a previous section of the "continuous elevator" takes the place of the first section.

If the volume of a cell is ΔV then the following relationship is valid:

$$q \cdot \Delta t = n \cdot \Delta V \tag{9}$$

$$w = \frac{q}{S} \tag{10}$$

and:

$$t = \frac{2\tau}{n+1} \tag{11}$$

Let us assume that the model resumed its operation at $t = -\infty$ so at $t = 0$ it is in a steady-state condition and let us trace the trail of volume element $q\Delta t$ entering the system this minute.

Obviously, the system can be considered perfectly mixed microscopically only when the fluid entering the system at $t=0$ during step 2 is uniformly distributed among the cells, i.e. all cells receive "fresh" liquid as volume $(2q\Delta t)/(n+1)$ leaves the system during the interval $(0, t_1)$ in step 3, uniformly distributed during this interval according to velocity $w=\text{const}$.

Let us assume that the concentration of a tracer of the liquid flow entering the system is c_0 then the exit concentration becomes:

$$c(t_0)=\frac{2c_0\,\Delta t}{n+1}=\frac{c_0\,\Delta t}{\tau} \tag{12}$$

The amount of tracer left in the system is $qc_0\Delta t(1-\Delta t/\tau)$, its age becomes $\Delta t=\alpha_1$ and after transmixing it is once again uniformly distributed among all the cells.

It follows that the value of the next concentration pulse is:

$$c(t_1)=\frac{c_0\,\Delta t}{\tau}\left(1-\frac{\Delta t}{\tau}\right) \tag{13}$$

and the amount of tracer left in the system is $qc_0\Delta t(1-\Delta t/\tau)^2$. Its age is $2\Delta t=\alpha_2$.

Let us continue this process. The value of the nth concentration pulse becomes:

$$c(t_n)=\frac{c_0\,\Delta t}{\tau}\left(1-\frac{\Delta t}{\tau}\right)^n \tag{14}$$

and the amount of the tracer left in the system is $qc_0\,\Delta t(1-\Delta t/\tau)^{n+1}$, its age is $(n+1)\Delta t=\alpha_{n+1}$.

Since a similar process takes place for all concentration pulses $c_0\,\Delta t=c_{0(\Delta)}$ entering the system during all further time intervals, it follows that the equivalency $\Theta_p(\alpha)=\Theta(\alpha)$ is valid for any time interval for all $p=\overline{1,\ n(n+1)/2}$.

Let us substitute $t_n=\Delta t\cdot n$ into Eq. 14. According to the binomial formula, the following expression is then obtained:

$$c(t_n)=\frac{c_{0(\Delta)}}{\tau}\left\{1-\frac{t_n}{1!\,\tau}+\frac{t_n^2}{2!\,\tau^2}\left(1-\frac{1}{n}\right)-\frac{t_n^3}{3!\,\tau^3}\left(1-\frac{1}{n}\right)\left(1-\frac{2}{n}\right)+\dots\right.$$
$$\left.\dots+(-1)^n\frac{t_n^n}{n!\,\tau^n}\left(1-\frac{1}{n}\right)\left(1-\frac{2}{n}\right)\dots\left(1-\frac{n-1}{n}\right)\right. \tag{15}$$

Let $t_n=t$ and let us decrease the duration of intervals Δt, i.e. let us obtain the limiting valves $\Delta t\to 0$, $n\to\infty$ while c_0 should change in such a manner that the equivalency $c_0\Delta t=1$ holds for any Δt.

Obviously Eq. 15 then becomes the infinite series:

$$c(t)=\frac{1}{\tau}\left[1-\frac{t}{1!\,\tau}+\frac{t^2}{2!\,\tau^2}-\frac{t^3}{3!\,\tau^3}+\dots+(-1)^n\frac{t^n}{n!\,\tau^n}+\dots\right] \tag{16}$$

from which it is immediately apparent that:

$$c(t)=\frac{1}{\tau}\,e^{-t/\tau} \tag{17}$$

i.e. the density function of the residence time distribution of the system is entirely identical with the density function of the macroscopically perfectly mixed system, quod erat demonstrandum.

Let the system characterized by residence time distribution $F(t)$ now be perfectly segregated microscopically [2, 3]. $I_V^2(\alpha)$ can then easily be obtained in a closed form.

The age distribution function of any $p \in P$ "point" of a perfectly segregated system is a step function, i.e.

$$\Theta_p(\alpha) = \begin{cases} 0, & \text{if} \quad \alpha \leq \alpha_p \\ 1, & \text{if} \quad \alpha > \alpha_p \end{cases} \tag{18}$$

It can be easily shown that now:

$$\Theta(\alpha) = \frac{|V_1|}{|V|} = \frac{1}{\tau} \int_{\alpha}^{\infty} [1 - F(\alpha')] \, d\alpha', \tag{19}$$

where $|V_1|$ is the volume occupied by "points" remaining in the system for a time greater than α.

Let us substitute Eq. 19 into Eq. 5 then:

$$I_V^2(\alpha) = \frac{\bar{c}}{\varrho_0 - \bar{c}} \Theta(\alpha)[1 - \Theta(\alpha)] \tag{20}$$

It is immediately apparent that $I_V^2(\alpha)$ depends only on the residence time distribution function of the system.

The Inhomogeneity Parameter of the Recirculation Model

The recirculation model is used to characterize the mixing rate of the transferred material in steady-state systems during the examinations of transfer processes. Let there be a tube of length L with plug flow in the forward branch into which the material is transported along length co-ordinate x from a surrounding of concentration $c_k = \text{const}$ by transfer coefficient α. The concentration of the material entering and leaving the system is c_0 and c_L, respectively. Thus, the differential equation of the tube with plug flow is:

$$q \frac{dc}{dx} = \alpha K[c_k - c_{(x)}] \tag{21}$$

and the initial condition is:

$$qc_0 + Rqc_L = (1 + R/qc/0] \tag{22}$$

This states that the concentration in the plane at $x = 0$ of the tube is obtained by the appropriate mixing of initial c_L according to mass flow rates q and $q' = Rq$.

The solution of Eq. 21 and 22 is:

$$c(x) = c_k - \frac{c_k - c_0}{1 + R(1 - e^{-\alpha L})} e^{-\gamma x} \tag{23}$$

or if the term:

$$C(x)=\frac{c_k-c(x)}{c_k-c_0} \tag{24}$$

is used then:

$$C(x)=\frac{1}{1+R(1-e^{-\gamma L})}\,e^{-\gamma x} \tag{25}$$

By simple operations one can arrive at:

$$I_V^2[C]=\frac{A}{[1+R(1-e^{-\gamma L})]^2} \tag{26}$$

where:

$$A=\frac{1}{2\gamma^2L^2}[\gamma L(1-e^{-2\gamma L})-2(1-e^{-\gamma L})^2] \tag{27}$$

It is apparent from Eq. 26 relating to the inhomogeneity parameter that function $I_V^2(R)$ is a monotonously decreasing one, i.e. the greater the recirculation ratio R, the smaller the inhomogeneity parameter $I_V^2(R)$ reflecting the natural fact that the faster the mixing rate, the more uniform the concentration distribution in the system.

Let us not that:

$$\lim_{\gamma\to\infty} I_V^2=0 \tag{28}$$

i.e. a uniform concentration distribution is established in the system when the transfer rate in infinitely fast. At the same time:

$$\lim_{\gamma\to 0} I_V^2=\lim_{\gamma\to 0} A \tag{29}$$

where A becomes a $0/0$ undetermined form during the $\gamma\to 0$ limit test. According to l'Hospital's rule:

$$\lim_{\gamma\to 0} A=\lim_{\gamma\to 0} e^{-\gamma L}(1-e^{-\gamma L})=0 \tag{30}$$

i.e.

$$\lim_{\gamma\to 0} I_V^2=0. \tag{31}$$

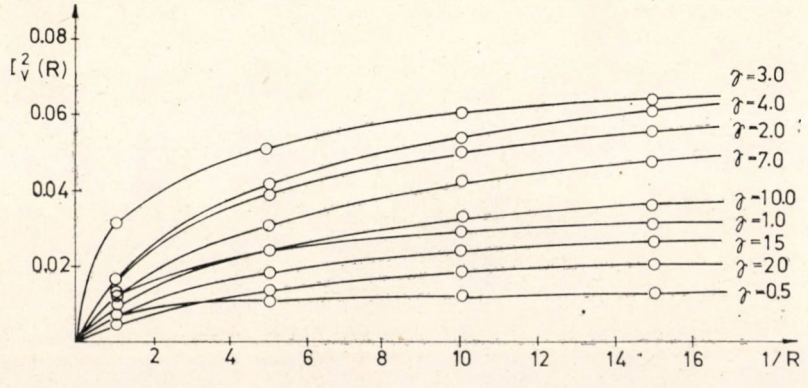

Fig. 2.
The inhomogeneity parameter of the recirculation model plotted against $1/R$ ($L=1$)

Since I_V^2 is a continuous function of γ it passes a maximum value with incerasing γ. This can be seen in *Fig. 2*, where the changes of the inhomogeneity parameter of the recirculation model are plotted against $1/R$ for various γ values. At e.g. $1/R=15$ I_V^2 initially then decreases with increasing γ and $L=1$.

The Inhomogeneity Parameter and the Number of Mixing Units

Another frequently used empiric characteristic of mixing processes is the number of mixing units [4, 5]. In this case the mixing phenomenon occurring in a system is modelled by a cascade series consisting of n perfectly mixed systems and n is termed the number of mixing units. The equation of the ith system in steady-state condition is:

$$q(c_i - c_{i-1}) = \alpha \frac{F}{n}(c_k - c_i) \tag{32}$$

or, if the concentration simplex:

$$C_i = \frac{c_k - c_i}{c_k - c_0} \tag{33}$$

is introduced once again then Eq. 32 becomes:

$$C_i = \left(1 + \frac{\beta}{n}\right)^{-1} \times C_{i-1} \tag{34}$$

from which:

$$C_i = \left(1 + \frac{\beta}{n}\right)^{-i} = \left(\frac{n}{n+\beta}\right)^i \tag{35}$$

because $C_0 = 1$.

If the summation formula of the first n members of a geometric series is used, then the average value becomes:

$$\overline{C} = \frac{1}{\beta}\left[1 - \left(\frac{n}{n+\beta}\right)^n\right] \tag{36}$$

and the square average becomes:

$$\overline{C^2} = \frac{n}{\beta(2n+\beta)}\left[1 - \left(\frac{n}{n+\beta}\right)^{2n}\right] \tag{37}$$

In the case of $n=1$ the inhomogeneity parameter is obtained by simple rearrangements:

$$I_V^2(1) = 0. \tag{38}$$

But since $u^v = \exp(v \ln u)$ and l'HOSPITAL's rule can be used:

$$\lim_{n\to\infty} \overline{C} = \frac{1}{\beta}\left[1 - \lim_{n\to\infty} \exp\left(n \cdot \ln \frac{n}{n+\beta}\right)\right] = \frac{1}{\beta}\left[1 - \lim_{n\to\infty}\left(-\frac{\beta}{1+\frac{1}{\beta}}\right)\right] = \frac{1}{\beta}(1 - e^{-\beta}) \tag{39}$$

and:

$$\lim_{n\to\infty} \overline{C^2} = \lim_{n\to\infty} \frac{1}{\beta\left(2+\frac{\beta}{n}\right)} \cdot \left[1 - \lim_{n\to\infty} \exp\left(2n \cdot \ln \frac{n}{n+\beta}\right)\right] = \frac{1}{2\beta}\left(1 - e^{-2\beta}\right) \tag{40}$$

so:

$$\lim_{n\to\infty} I_V^2(n) = \frac{1}{2\beta}\left(1 - e^{-2\beta}\right) - \frac{1}{\beta 2}\left(1 - e^{-\beta}\right) \tag{41}$$

i.e. lim I_V^2 is a finite positive number when $0 < \beta < \infty$.

Since the general form of the inhomogeneity parameter vs. mixing unit number relationship:

$$I_V^2(n) = \frac{n}{\beta(2n+\beta)}\left[1 - \left(\frac{n}{n+\beta}\right)^{2n}\right] - \frac{1}{\beta^2}\left[1 - \left(\frac{n}{n+\beta}\right)^{n}\right] \tag{42}$$

is too complicated to draw direct conclusions, numerical calculations were carried out.

Function $I_V^2(n)$ is shown in *Fig. 3* for a number of β values. The function

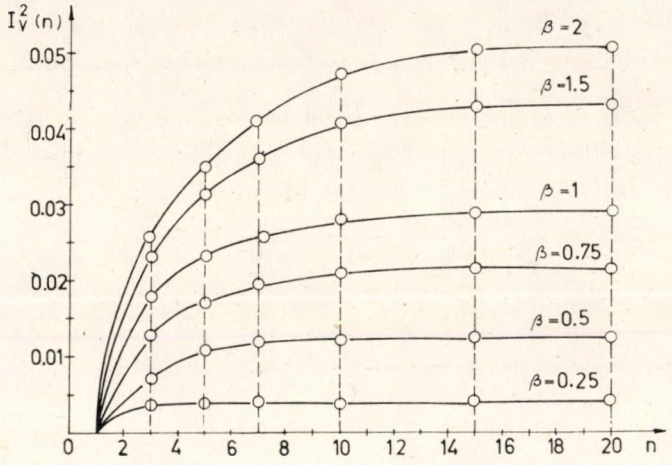

Fig. 3.
The inhomogeneity parameter plotted against the number of mixing units

increases strictly monotonously. When $n = 1$ it is equal to zero, corresponding to the perfectly mixed state of the system, i.e. uniform concentration distribution. $I_V^2(n)$ increases with increasing n, i.e. the smaller the mixing, the "less uniform" the concentration distribution and it reaches its maximum value at $n = \infty$, i.e. when the number of mixing units describing the mixing phenomenon in the system is infinite. It can be seen that this is also equivalent to the plug flow model.

Let us consider the plug flow model described by Eq. 25 and le us multiply both of its sides by length L of the model. Then, after simple rearragements

the differential equation:

$$\frac{dC(z)}{dz} + \beta C(z) = 0 \tag{43}$$

$$C(o) = 1 \tag{44}$$

is obtained.

Let us integrate Eq. 43 over the interval [0, 1] and observe Eq. 44. The average value becomes:

$$\overline{C} = \frac{1 - C(1)}{\beta} \tag{45}$$

which, if the solution of Eq. 43 is noted, is identical with Eq. 39. Similarily, the square average is determined by the expression:

$$\overline{C^2} = \frac{1 - C^2(1)}{2\beta} \tag{46}$$

which is identical with Eq. 40.

It follows that the inhomogeneity parameters are identical, that is the models studied are indeed equivalent.

The Inhomogeneity Parameter of the Axial Dispersion Model

Perhaps the most frequently used model to describe mixing processes is the axial dispersion model. Its boundary conditions depend on the actual problem [7, 8]. It can be written as:

$$\frac{1}{Pe}\frac{d^2c}{dz^2} - \frac{dc}{dz} = \beta_L(c_k - c) \tag{47}$$

and the boundary conditions are:

$$c_0 = c - \frac{1}{Pe}\frac{dc}{dz} \quad z = 0 \tag{48}$$

and:

$$\frac{dc}{dz} = 0 \qquad z = 1 \tag{49a}$$

or:

$$\lim_{z \to \infty} c < \infty \tag{49b}$$

If the boundary conditions are selected and express by Eq. 48 and 49a, then the inhomogeneity parameter becomes:

$$I_V^2[c] = A_1^2\left[\frac{e^{2\lambda_1} - 1}{2\lambda_1} - \frac{(e^{\lambda_1} - 1)^2}{\lambda_1^2}\right] + A_2^2\left[\frac{e^{2\lambda_2} - 1}{2\lambda_2} - \frac{e^{\lambda_2} - 1}{\lambda_2^2}\right] +$$

$$+ 2A_1A_2\left[\frac{e^{\lambda_1 + \lambda_2} - 1}{\lambda_1 + \lambda_2} - \frac{(e^{\lambda_1} - 1)(e^{\lambda_2} - 1)}{\lambda_1\lambda_2}\right] \tag{50}$$

where:

$$A_1 = \frac{c_0}{\left(1-\frac{\lambda_1}{\mathrm{Pe}}\right)-\left(1-\frac{\lambda_2}{\mathrm{Pe}}\right)\frac{\lambda_1}{\lambda_2}\,e^{(\lambda_1-\lambda_2)}}$$

and (51)

$$A_2 = \frac{c_0}{\left(1-\frac{\lambda_2}{\mathrm{Pe}}\right)-\left(1-\frac{\lambda_1}{\mathrm{Pe}}\right)\frac{\lambda_2}{\lambda_1}\,e^{(\lambda_1-\lambda_1)}}$$

and:

$$\lambda_1 = \frac{\mathrm{P}}{2}\left(1+\sqrt{1+\frac{4\beta_L}{\mathrm{Pe}}}\right) \quad \text{and} \quad \lambda_2 = \frac{\mathrm{P}}{2}\left(1-\sqrt{1-\frac{4\beta_L}{\mathrm{Pe}}}\right) \tag{52}$$

If the boundary conditions selected are expressed by Eq. 48 and 49b, then the above expressions are significantly simplified and the inhomogeneity pa-

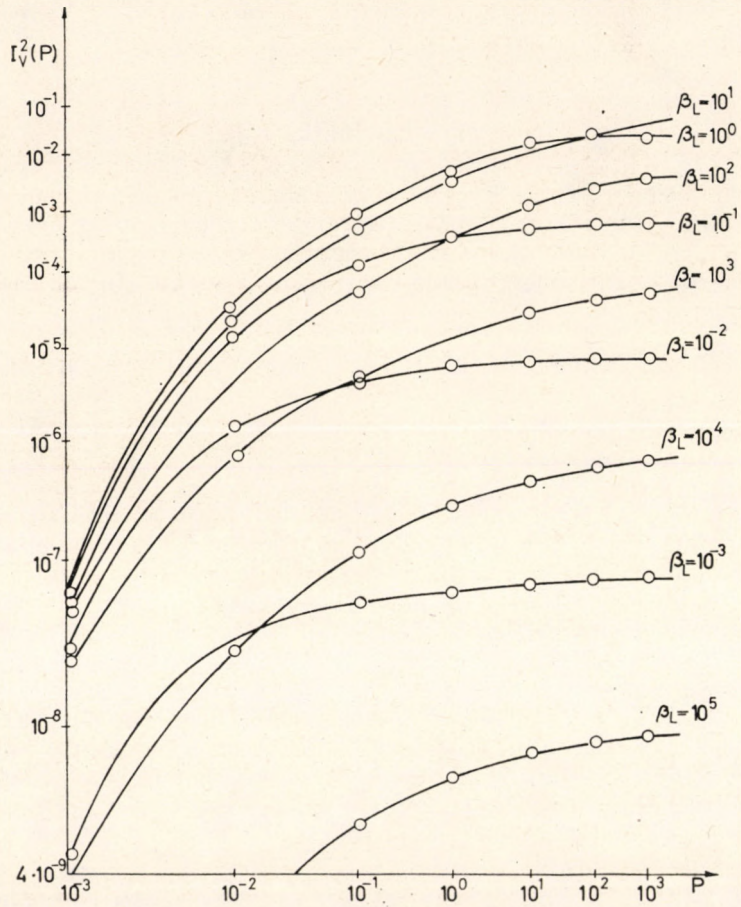

Fig. 4.

The inhomogeneity parameter of the axial dispersion model plotted against the Pe number in the case of boundary conditions expressed by Eq. 48 and 49a

rameter becomes:

$$I_V^2[c]=\frac{e^{\lambda_2}-1}{\left(1-\frac{\lambda_2}{Pe}\right)^2\cdot\lambda_2}\left[\frac{e^{\lambda_2}+1}{2}-\frac{e^{\lambda_2}-1}{\lambda_2}\right] \tag{53}$$

If $Pe\to 0$ then corresponding to perfect mixing $I_V^2\to 0$ in both cases. If $Pe\to\infty$ then both lim Eq. 50 and lim Eq. 51 become:

$$I_V^2[c]=\frac{1-e^{-\beta_L}}{\beta_L}\left(\frac{1+e^{-\beta_L}}{2}-\frac{1-e^{-\beta_L}}{\beta_L}\right) \tag{54}$$

which corresponds to the plug flow model as it can be seen from Eq. 43 to 46.

Between the two limiting values I_V^2 increases monotonously with increasing Pe numbers (cf. *Fig. 4*). This means that there is an unambiguous correspondance between the inhomogeneity parameter and the Peclet number. It should be noted that I_V^2 once again passes a maximum value, while β_L increases from zero to infinity.

Final Remarks

Since the condition $\bar{c}=\text{const}$ is valid in continuous flowing systems in steady-state conditions, the inhomogeneity parameter as determined previously [1] can well be used for these systems. The significance of this application is that thus there is an opportunity to compare various systems. In the case of different systems, equal inhomogeneity parameters mean that concerning this study, the systems behave identically. If the mixing phenomenon in one system is described by the recirculation model and in another one by the number of mixing units, then a relationship can be established between the two directly incomparable quantites by making Eq. 26 and 42 equal. The Peclet number used in the axial dispersion model can be similarily treated.

The determination of the empirical characteristics in question becomes much more simple with Eq. 26, 42, 50 and 53. If the concentration is measured at several points in a system in steady-state conditions, then the approximate value of the inhomogeneity parameter can be calculated by its discrete form. The recirculation ratio belonging to this value can be easily calculated by Eq. 26. The calculation of the number of mixing units or the Peclet number from Eq. 42 and 50 or 53 is more complicated. They can easily be obtained graphically.

Microscopic mixing in a continuous flowing system can be characterized approximately by the inhomogeneity parameter. Nevertheless, even this yields very useful information. It has been shown that for any arbitrary age α the condition $I_V^2=0$ is feasible only for macroscopically perfectly mixed systems. Since $I_V^2\geq 0$ this means that this is the minimum value of the inhomogeneity parameter.

Naturally, although only component mixing was treated here, the results shown can also be directly applied to heat phenomena, since similar equations describe both heat and component transports in the systems of technical chemistry.

Symbols Used

A — constant, Eq. 27
A_1, A_2 — constants, Eq. 51
c — concentration, (mole·m^{-3})
C — concentration simplex
c_k — concentration of the environment, (mole·m^{-3})
c_{max} — concentration distribution resulting in maximum, $d^2[c]=c-c^2$
D — axial dispersion coefficient, (m^{2}s^{-1})
$E(t)$ — residence time distribution density function
$F(t)$ — residence time distribution function
I_V^2 — inhomogeneity parameter
K — circumference
$K(t)$ — residence time distribution density function
L — length, (m)
n — number of mixing units, natural number
Pe — Peclet number ($=wL/D$)
R — recirculation ratio
S — cross section, (m^2)
t — time, (s)
V — volume, (m^3)
w — linear velocity, (ms^{-1})
x — axial co-ordinate
y — co-ordinate perpendicular to x
z — dimensionless axial co-ordinate $\left(=\frac{x}{L}\right)$
u, v — functions
q — flow rate, (m^{3}s^{-1})
α — age of molecules, (s); mass transfer coefficient
β — constant ($=F/q$)
γ — constant ($=K/q$)
λ — life expectation time, (s)
Θ — age distribution function
τ — average residence time, (s)
σ^2 — standard deviation
λ_1, λ_2 — Eq. 52

Indices

p — denotes the "fluid point"
o — input signal
i — ith serial number

REFERENCES

1. Lakatos, B. and Blickle, T.: Hung. J. Ind. Chem.
2. Danckwerts, P. V.: Chem. Eng. Sci., *8*, 93 (1958)
3. Zwieterling, Th. N.: Chem. Eng. Sci., *11*, 1 (1959)
4. Kramers, H. and Alberda, G.: Chem. Eng. Sci., *2*, 172 (1953)
5. Seitz, K. and Tőrös, R.: Acta Chim. Sci. Hung., *62*, 19 (1969)
6. Tőrös, R.: Hung. J. Ind. Chem., *3*, 227 (1975)
7. Levenspiel, O.: Chemical Reaction Engineering. J. Wiley, New York, 1962.
8. Wen, C. Y. and Fan, L. T.: Models for Flow Systems and Chemical Reactors. M. Dekker, New York, 1975

РЕЗЮМЕ

Статья касается применения параметра неоднородности для характеристики стационарных состояний систем, открытых с точки зрения материального оборота, а также для сравнения отдельныхсостояний и систем.

С помощью параметра неоднородности может быть охарактеризовано — хотя лишь приблизительно — микроперемешивание систем с непрерывным потоком, и тем самым — получено значительное количество полезной информации.

В статье рассматривается связь трёх эмпирических характеристик перемешивания — доли рециркуляции, числа единиц перемешивания и коэффициента продольной дисперсии — с параметром неоднородности, и сделан вывод о том, что с помощью параметра неоднородности можно без труда провести сопоставление систем, благодаря тому, что на основе измеренных данных сначала рассчитывается приближённое значение параметра неоднородности, а затем, с помощью соответствующих уравнений — значение искомой эмпирической характеристики.

HUNGARIAN JOURNAL
OF INDUSTRIAL CHEMISTRY
VESZPRÉM
Vol. 6. pp. 81–92 (1978)

HYDRODINAMICAL STUDIES ON FLUIDIZED BEDS. V.
Studies on the Particle Mixing Phenomena in Dual-cell Fluidized Beds Using Isotope Tracer Techniques

T. SZENTMARJAY, B. CSUKÁS and Z. ORMÓS

Research Institute for Technical Chemistry
of the Hungarian Academy of Sciences, Veszprém)

Received: October 21, 1977

The knowledge of the extent of transmixing between the cells in a multicell fluidization apparatus is essential. An experimental technique has been developed to determine the magnitude of the backmixing mass flow rate and the effects of various process and apparatus parameters upon this backmixing mass flow rate.

Experimental results and their evaluation are presented. Relationship were deduced between the backmixing mass flow rate and the process, as well as the apparatus parameters. Experimental results are evaluated by a hypothesis that assumes that pressure fluctuations also result in backmixing.

The experimental apparatus and the evaluation method developed to determine the particle mixing phenomena in multicell fluidized beds were published in a previous paper [1]. An evaluation of the experimental results and relationships mixing mass flow rate and various process and apparatus parameters are also shown.

The Effects of the Size of the Opening Between the Cells and Solid Mass Flow Rate Upon the Magnitude of Backmixing Mass Flow Rate

The effects of the shape and area of the opening at height Y_k between the cells upon a backmixing mass flow rate were examined at various input mass flow rates. The values of backmixing mass flow rate were calculated by Eq. 34 of [1].

From the analysis of the experimental data it could be concluded that the backmixing mass flow rate depended only on the area of the opening, but not on its geometrical parameters, so the values obtained with identical opening areas could be averaged. Averaged values are shown in *Table 1* and *Fig. 1* and 2.

Table 1.

$\overline{G} = 1.95$ kg $\quad Y_k = 2 \times 10^{-2}$ m $\quad U'' = 0.175$ m/s

$\dot{G} \times 10^4$ (kg/s)	$F_b \times 10^4$ (m^2)	$\dot{g} \times 10^4$ (kg/s)
4.17	1.5	12.8
	3.0	21.2
	4.5	40.8
	6.0	52.1
8.33	1.5	11.6
	3.0	22.3
	4.5	32.8
	6.0	43.1
16.7	1.5	9.1
	3.0	18.0
	4.5	27.4
	6.0	32.6
25.0	1.5	6.4
	3.0	12.7
	4.5	22.1
	6.0	26.1

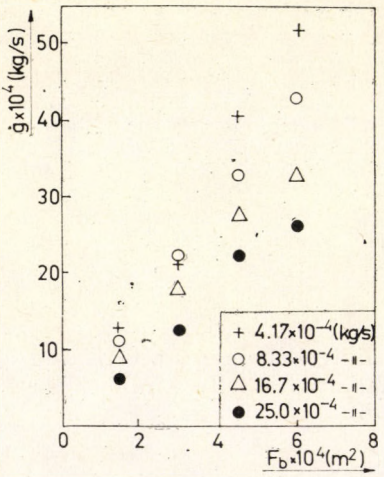

Fig. 1.
Backmixing mass flow rate as a function of the opening area

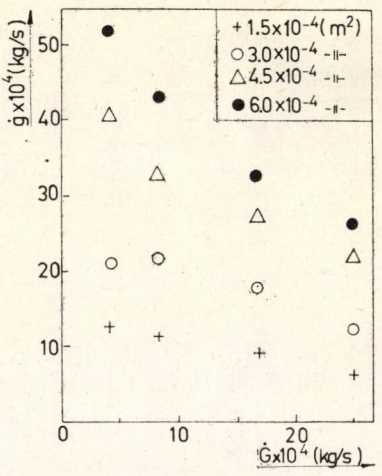

Fig. 2.
Backmixing mass flow rate as a function of solid material mass flow rate

It can be seen that a backmixing mass flow rate increases with the enlarged opening areas. At a given opening area the backmixing mass flow rate decreases with an increasing input solid material mass flow rate.

The relationship between the backmixing mass flow rate $\dot{g}$, the opening area F_b and the input solid material mass flow rate can be described by the following empirical function:

$$\dot{g}=\frac{k_1 F_b}{1+k_2\dot{G}} \tag{1}$$

Obviously, if:

$F_b \to 0$ then $\dot{g}\to 0$ and

$F_b \to F_{b\max}$ $\dot{g}\to \dot{g}_{\max}$ and

$\dot{G}\to\infty$ $\dot{g}\to 0$.

$F_{b_{max}}$ stands for the maximum flow-through cross section obtained without separating baffles between the two cells.

Coefficients in Eq. 1 are obtained from the linearized form of Function 1 as:

$$\frac{F_b}{\dot{g}}=\frac{1}{k_1}+\frac{k_2}{k_1}\dot{G} \tag{2}$$

If the $F_b/\dot{g}$ values calculated at various opening areas are plotted against $\dot{G}$ (cf. *Fig.* 3) then it can be seen that the points define a line. In the case

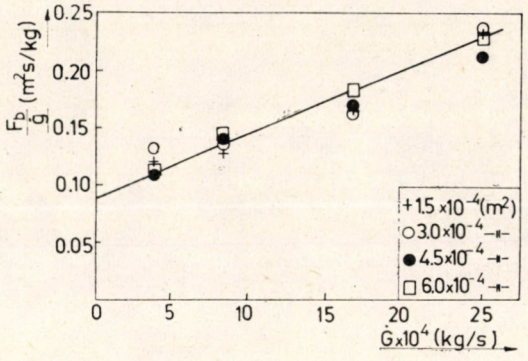

Fig. 3.
Calculated $F_b/\dot{g}$ values relating to various opening areas plotted against input solid material mass flow rate

of the model material used (0.2–0.4 mm sand fraction) coefficients k_1 and k_2 become:

$$k_1 = 10.9 \text{ kg/sm}^2$$

$$k_2 = 597.6 \text{ s/kg}.$$

The Effects of the Height of the Midpoint of the Opening, Linear Gas Velocity and Changing Input Solid Material Mass Flow Rate Upon the Backmixing Mass Flow Rate

The backmixing mass flow rate as a function of the height of the midpoint of the opening was examined at a constant input solid material mass flow rate. Experiments were carried out at four Y_k midpoint height values at a given, constant opening area and input solid material mass flow rate. The calculated backmixing mass flow rate values and experimental parameters are summarized in *Table 2*.

Table 2.

$F_b = 3 \times 10^{-4}$ m^2 $\quad \bar{G} = 1.95$ kg $\quad U'' = 0.175$ m/s

$\dot{G} \times 10^4$ (kg/s)	$Y_k \times 10^2$ (m)	$\dot{g} \times 10^4$ (kg/s)
16.7	0.5	16.5
	2.5	16.4
	4.5	18.3
	6.5	19.0
25.0	0.5	13.8
	2.5	10.8
	4.5	12.5
	6.5	12.2

It can be seen from the figures shown in *Table 2* that the changes of the height of the midpoint of the opening have no significant effects upon the backmixing mass flow rate.

If the backmixing mass flow rates are plotted against the linear gas velocity (cf. *Fig. 4*) then it can be seen that $U''_m = 0.075$ m/s is obtained for the

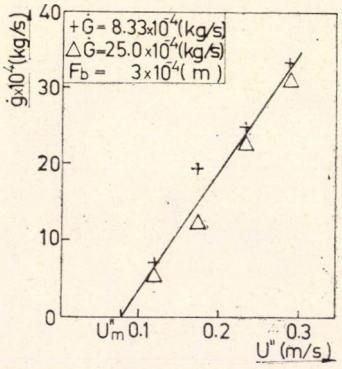

Fig. 4.
Backmixing mass flow rate as a function of linear gas velocity ($U''_m = 0.075$ m/s)

minimum fluidization velocity from the line fitted to the points. It was assumed that only coefficient k_1 depended on the linear gas velocity in Eq. 1. Its value was calculated by the following relationship:

$$k_1 = \dot{g}(1 + k_2\dot{G}) \frac{1}{F_b} \tag{3}$$

and it was found to depend on the linear gas velocity as:

$$k_1 = b_0(U'' - U''_m) \tag{4}$$

If Eq. 4 is substituted into Eq. 1 then it becomes:

$$\dot{g} = (U'' - U''_m) \frac{F_b}{1 + k_2\dot{G}} b_0 \tag{5}$$

The backmixing mass flow rate values ($\dot{g}_s$) were calculated by Eq. 5. These values and those calculated from the moments agreed well, so parameter k_2 was indeed independent of the linear gas velocity (cf. *Table*).

Table 3.

$U''_m = 7.5 \times 10^{-2}$ m/s $\quad \bar{G} = 1.95$ kg $\quad k_2 = 597.6$ s/kg

$\dot{G}\times10^4$ (kg/s)	$(U''-U''_m)\times10^2$ (m/s)	$\dot{g}\times10^4$ (kg/s)	$\dot{g}_s\times10^4$ (kg/s)
8.3	4.2	6.7	7.2
	10.0	21.3	17.8
	15.9	25.4	27.5
	21.5	36.3	37.1
25,0	4.2	5.1	5.9
	10.0	12.3	14.2
	15.9	22.8	22.6
	21.5	32.2	30.6

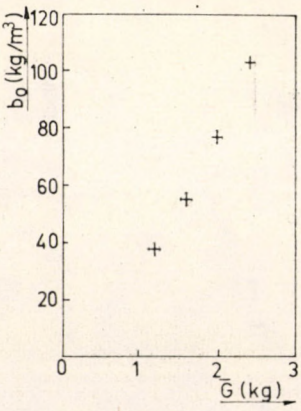

Fig. 5.
Parameter of b_0 as a function of the mass of the fluidized bed

Further experiments proved that parameter k_2 did not depend on the mass of the fluidized bed either. The values of parameter b_0 in Eq. 4 were calculated by parameters k_1 for various amounts loaded into the fluidized bed. It can be seen in *Fig. 5* that parameter b_0 increases approximately linearly with increasing fluidized bed mass.

The Effects of the Parameters of Mechanical Agitation Upon the Backmixing Mass Flow Rate

The effects of two different types of agitators (cf. *Fig. 6*) were tested in the experiments. Measurements were carried out at four different rotation speeds with two identical openings at different heights. In one case the height of

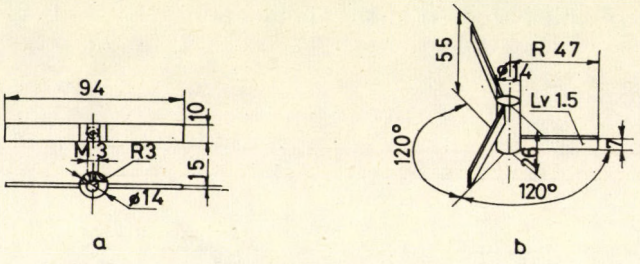

Fig. 6.
Mechanical agitator elements used in the experiments

the midpoint of the opening was in level with the active height of the agitator, in the other case it was different. In the case of the three-wing agitator called b in *Fig. 6*, the active height of the agitator was — by definition — taken as the height of the midpoint of the opening in level with the horizontal wing.

The backmixing mass flow rate is plotted in *Fig. 7* and *8* against the rota-

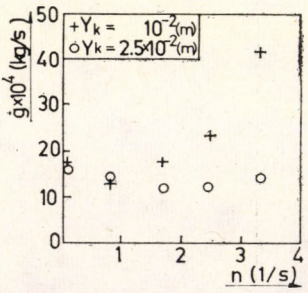

Fig. 7.
Backmixing mass flow rate as a function of rotation speed of the two-wing agitator placed aq the bottom of the fluidized bed

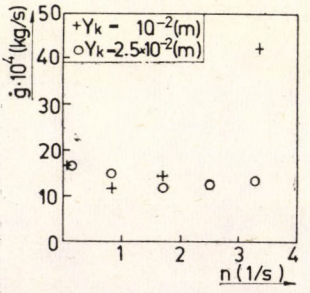

Fig. 8.
Backmixing mass flow rate as a function of the rotation speed of the three-wing agitator

tion speed of the agitator. It can be seen that when the midpoint of the opening is in level with the agitating element, then the backmixing mass flow rate decreases with increasing rotation speed. Beyond a certain value, it increases significantly. When the midpoint of the opening and the agitating element are not in level, then the backmixing mass flow rate is practically independent from the rotation speed.

There is no uniform approach as of how to characterize the intensity of the mechanical agitation used in fluidized beds. The intensity of the agitation depends on the type, size, and rotation speed of the agitating element, and the characteristics of the fluidized bed. Let us consider an agitator of rotation speed n rev/min in a fluidized bed of diameter $2R$ and minimum bed height Y_m (cf. *Fig. 9*). Let the joined lengths of the line pieces in direction z on the

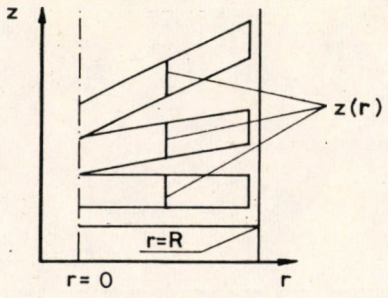

Fig. 9.
Definition of the intensity of mechanical agitation

perpendicularly projected picture of the agitating elements be turned into plane $z-r$ at a given point of radial co-ordinate r be $z(r)$.

Let the circumferential velocity of an elementary part of surface area $z(r)\mathrm{d}r$ of the agitating element at a point of radius r be $2\pi\ r$ n. The volume element in the fluidized bed „swept" by the elementáry part of surface area $z(r)\mathrm{d}r$ in unit time is n $2\pi z(r)\mathrm{d}r$. If the average density of the fluidized bed is ϱ then the mass of the solid material moved by the above elementary part of the agitator is $2r\pi z(r)\mathrm{d}r\varrho n$. Let us assume that the kinetic energy transferred to the particles by the elementary part of the agitator is:

$$E=\frac{1}{2}\,\mathrm{m}v^2=\eta\,\frac{1}{2}\,2r\pi z(r)\,\mathrm{d}r\varrho n(n2\pi r)^2 \tag{6}$$

where η is an efficiency factor. Thus, the kinetic energy transferred to the bed by the agitator can be expressed by the integral of Eq. 6 between limits $r=0$ and $r=R$:

$$\dot{E}=\eta^4\pi^3 n^3\varrho\int_0^R z(r)r^3\,\mathrm{d}r \tag{7}$$

The power transferred to the unit mass in the dense layer of the fluidized

bed becomes:

$$\xi^* = \frac{\dot{E}}{G} = \frac{\eta^4 \pi^3 n^3 \varrho \int_0^R z(r) r^3 \, dr}{R^2 Y_m \pi \varrho} \tag{8}$$

i.e.

$$\xi^* = \frac{\eta^4 \pi^2 n^3 \int_0^R z(r) r^3 \, dr}{R^2 Y_m} \tag{9}$$

Let us introduce the term:

$$\xi = \frac{\xi^*}{\eta^4 \pi^2} \tag{10}$$

and let us characterize the intensity of the agitation by the quantity:

$$\xi = \frac{n^3 \int_0^R z(r) r^3 \, dr}{R^2 Y_m} \tag{11}$$

The characteristic values of ξ indicating the intensity of the agitation in the fluidized bed were calculated for the agitating elements and fluidized bed used in the experiments. Then b_0 was obtained from Eq. 5 as:

$$b_0 = \dot{g} \frac{1 + k_2 \dot{G}}{F_b} \frac{1}{U'' - U''_m} \tag{12}$$

The values of parameter b_0 calculated for the two agitators are plotted against the intensity of agitation (cf. *Fig. 10*). It can be seen that b_0 increases linearly with increasing agitation intensity.

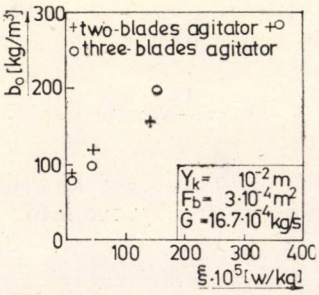

Fig. 10.
A sine component of the pressure drop as a function of the height of the opening

Evaluation of the Experimental Results by the Pressure Fluctuation Hypothesis Causing Backmixing

It was discussed in detail in a previous paper that the driving force of the solid material flow between the cells was the pressure difference, a statistical value between the pressure drop values Δp in the two cells. Backmixing between the cells can be explained by this phenomenon, namely a temporary pressure difference occurs at different points of the opening which forces the solid material to flow back from the second cell into the first one.

Let us consider an opening of small height and assume that pressure is constant at a given minute at both sides, but due to fluidization it fluctuates in time.

Let us examine a sine component of the fluctuating pressure difference:

$$p_1(t) - p_2(t) = \Delta p(t) \tag{13}$$

at the height of the opening (cf. *Fig. 11*).

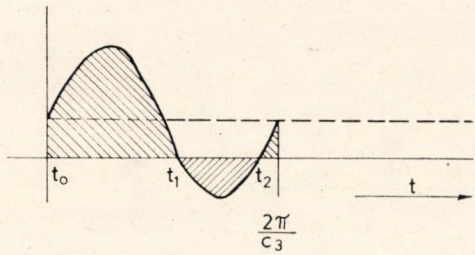

Fig. 11.
How the b_0 parameters change with the mixing intensity

Let us assume that the material flows only in one direction through the opening at a given minute.

Let us consider the changing pressure difference following a sine function:

$$\Delta p(t) = c_1 + c_2 \sin c_3 t \tag{14}$$

to be the driving force of the mass flow. The momentary mass flow between the cells can be described as a mass transfer phenomenon by function:

$$\dot{I}t = kF_b \Delta p(t) \tag{15}$$

The sign of the function is negative when the material flows from the second cell into the first one.

Let us consider a period of sine function $\Delta p(t)$.

Obviously, during a given period there is a backflow only in the (t_1, t_2) interval (cf. *Fig. 11*). Its average over the entire period becomes:

$$-\dot{g} = \frac{c_3}{2\pi} \int_{t_1}^{t_2} kF_b \Delta p(t)\, dt \tag{16}$$

Similarly, the average value of the mass flow transferred from the first cell into the second one during the periods $(0, t_1)$ and $(t_2, c_3/2\pi)$ is given by:

$$\dot{G}+\dot{g}=\frac{c_3}{2\pi}\left[\int_0^{t_1} kF_b\Delta p(t)\,dt+\int_{t_2}^{\frac{2\pi}{c_3}} kF_b\Delta p(t)\,dt\right] \tag{17}$$

After integration and summation, the value of the solid material flow is obtained as:

$$\dot{G}=kF_bc_1 \tag{18}$$

The difference of two functions yields the overall mass flow rate:

$$\dot{G}+2\dot{g}=kF_b\left\{c_1\left[\frac{c_3}{\pi}(t_1-t_2)+1\right]+\frac{c_2}{\pi}(\cos c_3t_2-\cos c_3t_1)\right\} \tag{19}$$

The relationship between the overall mass flow rate and the opening area was tested using the experimental data shown in *Table 1*. It was found that in the case of small openings, the overall mass flow rate is constant and independent of the input solid material mass flow rate $\dot{G}$. However, in the case of large openings, the overall mass flow rate was not independent of $\dot{G}$ (cf. *Fig. 12*).

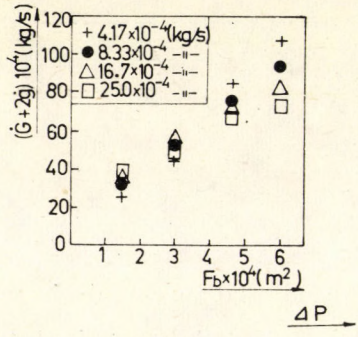

Fig. 12.
Overall mass flow rate as a function of opening area

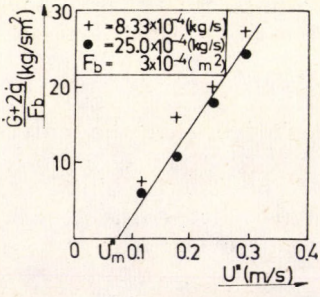

Fig. 13.
Relationship between overall mass flow rate over unit opening area and gas velocity

If a small opening area is selected then it can be seen that the overall mass flow rate over the unit area is proportional to the gas velocity (cf. *Fig. 13*). The backmixing mass flow rate can be obtained by the integration of Eq. 16.

The integration limit t_1 can be determined from the condition:

$$c_1 + c_2 \sin c_3 t_1 = 0 \tag{20}$$

as:

$$t_1 = \frac{1}{c_3} \text{ arc sin } \left(-\frac{c_1}{c_2}\right) \tag{21}$$

Integration limit t_2 then becomes:

$$t_2 = 2\left(\frac{3}{4}\frac{2\pi}{c_3} - t_1\right) + t_1 = \frac{3\pi}{c_3} - t_1 \tag{22}$$

After integration:

$$-\dot{g} = kF_b \left\{c_1 \left[\frac{3}{2} - \frac{1}{\pi} \text{ arc sin } \left(-\frac{c_1}{c_2}\right)\right] + \frac{c_2}{\pi} \cos \text{ arc sin } \left(-\frac{c_1}{c_2}\right)\right\} \tag{23}$$

It can be seen that the function is similar to Eq. 18 and 19, so the backmixing mass flow rate is proportional to the opening area.

Experimental data support the hypothesis that backmixing can be explained by the pressure fluctuation mechanism. In the case of small opening heights, this statement is substantiated by experimental data. The deviation in the case of large opening areas is due to the fact that the pressure difference along the opening depends not only on time, but also on the height of the opening.

SYMBOLS USED

b_0 coefficient of Eq. 4, (kg/m³)
$\dot{E}$ kinetic energy flow, (w/s)
F_b opening area, (m²)
G mass of the fluidized bed, (kg)
$\dot{G}$ input solid material mass flow rate, (kg/s)
$\dot{g}$ backmixing mass flow rate, (kg/s)
k_1 coefficient of Eq. 1, (kg/sm²)
k_2 coefficient of Eq. 1, (s/kg)
n notation speed of the mechanical agitator, (1/s)
R radius of the bed, (m)
U'' linear gas velocity over the entire cross section of the bed, (m/s)
U''_m minimum fluidization velocity, (m/s)
Y_k height of the midpoint of the opening measured from the bed supporting plate, (m)
Y_m minimum fluidized bed height, (m)
Δp pressure drop in the fluidized bed, (kg/ms²)
ξ intensity of mechanical agitation, (w/kg)
ϱ average density of the fluidized bed, (kg/m³)

REFERENCE

1. Szentmarjay, T., Csukás, B. and Ormós, Z.: Hung. J. Ind. Chem., *5* 213 (1977)

РЕЗЮМЕ

При применении способа многоячеечного псевдоожижения очень важно располагать данными перемешивания между ячейками. Авторами статьи разработан метод для определения массового потока обратного перемешивания, исследовалось также влияние, оказываемое параметрами установки и применяемой установки на массовый поток обратного перемешивания.

В данной работе приводятся опытные данные и их оценка. Авторами была установлена зависимость между массовым потоком обратного перемешивания и параметрами способа и установки. Опытные данные истолковываются также и на основе предположения о том, что колебание давления является причиной обратного перемешивания.

HUNGARIAN JOURNAL
OF INDUSTRIAL CHEMISTRY
VESZPRÉM
Vol. 6. pp. 93—104 (1978)

HYDRODYNAMICAL STUDIES ON FLUIDIZED BEDS. VI.
Studies on the Hydrodynamical Properties of Gas Fluidized Beds with Conical Inserts

Mrs E. Horváth, K. Pataki and Z. Ormós

(Research Institute for Technical Chemistry
of the Hungarian Academy of Sciences, Veszprém)

Received: September 12, 1977.

Major hydrodynamical properties of fluidized beds with and without conical inserts are presented here (pressure drop vs. air flow rate, bed expension vs. air flow rate, minimum fluidization velocity, and void volume fraction of the bed vs. bed height). Local void volume fraction values are obtained by a method based on the pressure drop of the fluid phase. Void volume fraction maps based on measured and calculated data are presented for various air flow rates and three conical inserts of different geometrical parameters.

Introduction

Ordered motion of the fluidized particulate material within the fluidized bed can be advantageous for various technological, operational purposes. There are several ways and means which ensure this characteristic vertical forced-circulation in the bed.

This motion can be achieved by the division of the bed holder plate into two concentric sections. If air velocity in the outer ring is higher than in the inner ring, then a reverse geysering motion is obtained [1, 2].

Conical inserts can also modify the flow characteristics causing an ordered motion, vertical recirculation in the bed. This solution is frequently used in practice, e.g. catalytical fluidized reactors with conical inserts are used at du Pont [3] to produce vinyl acetate. The aim of this solution is the drastic decrease of the extent of fragmentation and wear of the catalyst particles. Another characteristic application is the coating of particles in fluidized beds. This process is quite widespread in the pharmaceutical industry, but it can also be important in food processing, pesticide and fertilizer production [2, 4, 5, 6].

When a conical insert is used, then the fluidizing gas enters the bed through a reduced annular area. The velocity of the fluidizing gas decreases with in-

creasing height from the distributing plate according to:

$$u''(z)=\frac{4V''}{\pi}\cdot\frac{1}{-\frac{d_k^2}{Y_k}z^2+\frac{2d_k^2}{Y_k}z+D^2-d_k^2} \tag{1}$$

At the height of the cone, this value becomes equal to the average value relating to the overall cross section. Particles move in a much more orderly fashion than in simple fluidized beds without conical inserts where large particles (>1 mm dia) frequently push each other, hindering free motion.

This paper presents the results of a study carried out to compare the major hydrodynamical characteristics of fluidized beds with and without conical inserts. The bed expansion vs. air velocity, and pressure drop vs. air velocity functions determined are shown together with the changes of the void volume fractions plotted against bed height for various air velocities and insert sizes in fluidized beds with and without conical inserts.

Experimental Methods and Apparatus

The fluidized bed of 10.8 cm diameter and the instruments connected to it are shown schematically in *Fig. 1.*

There are four measuring points at the bottom of the bed immediately above the distributing plate. Probes of 2 mm internal diameter covered with sieve caps were placed at these points. A special probe with side bores was placed above the fluidized layer. These probes were used to determine the pressure drop valve in the bed.

Another probe-pair readily movable vertically and radically in the bed was also used to determine the static pressure drop. Its diameter was similar to that of the particles (2 mm). As it can be seen in *Fig. 1* the probes with side bores were used to measure the pressure drop over a 1 cm section of the bed. A micromanometer filled with alchohol was used for the measurements.

A calibrated rotameter was used to measure the flow rate of the fluidizing air. Temperature and pressure data were also recorded.

Three conical inserts of different shapes were used. The area fractions covered by these inserts were as follows: No. 1 insert: 31%; No. 2 insert: 42%; No. 3 insert: 55%. The inserts were 5 cm high equal to the minimum fluidization bed height ($Y_m=5.4$ cm).

A porous metal plate was used to hold the bed and distribute the fluidizing air. A mm scale fastened to the wall of the bed was used to measure bed height.

Spherical, prilled urea (1.25—1.60 mm dia.) was used as test material. Experiments were carried out with 350 g doses. Prior to runs, the bed was loosened by passing air through it. Air flow rate was slowly, and carefully discontinued to bring the bed to rest again.

The position of the movable probe-pair was changed both vertically and radically in 1 cm increments.

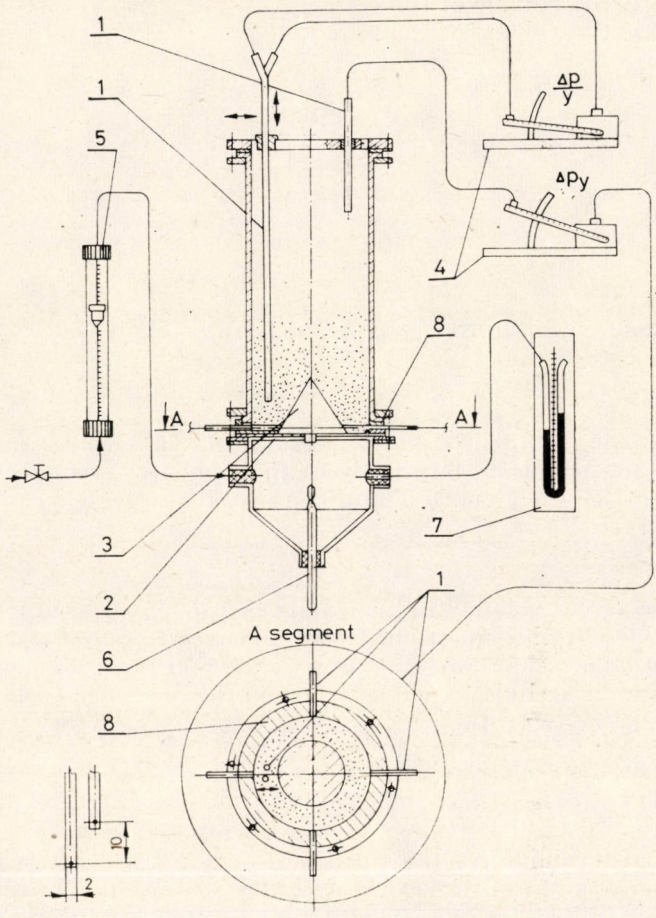

Fig. 1.
Experimental apparatus
A — probes, 2 — air distributor, 3 — conical insert, 4 — micropressure gauge, 5 — flowmeter, 6 — thermometer, 7 — pressure gauge, 8 — ring for probes

Theoretical Foundation of Local Void Volume Fraction Determinations [7]

It is known that the pressure drop of the fluid phase in a fluidized bed is approximately equal to the bed weight over unit cross section area:

$$\Delta p_Y \sim \frac{G}{F} \frac{\varrho - \varrho''}{\varrho} \tag{2}$$

The average void volume fraction was determined as:

$$\varepsilon'' = \frac{V_r - V^*}{V_r} \tag{3}$$

where V_r – is the volume of the bed
V^* – is the volume of the material.

Therefore, it follows that:

$$\bar{\varepsilon}''_Y = \frac{Y - \frac{G}{\varrho g F}}{Y} \tag{4}$$

and:

$$\frac{G}{\varrho g F} = Y(1 - \bar{\varepsilon}'') \tag{5}$$

Thus, the pressure drop in the fluidized bed can be expressed by the following equation:

$$\Delta p_Y \sim Y(1 - \bar{\varepsilon}'')g(\varrho - \varrho'') \tag{6}$$

If a probe-pair suitable for static pressure measurements are placed into the bed close to each other, but displaced in height by a distance (y), then the pressure drop over the given y length of the bed can be determined. According to Eq. 6.

$$\Delta p_y \sim y(1 - \varepsilon'')G(\varrho - \varrho'') \tag{7}$$

In principle a void volume fraction could be calculated from measured pressure drop values by this equation. However, according to experimental evidence, the actual measured pressure drop values and those calculated from bed weight data can differ by as much as $\pm 20\%$ in the case of gas-solid systems [9].

Let us divide Eq. 7 by Eq. 6 to arrive at:

$$1 - \varepsilon'' = \frac{G}{yg\varrho F} \cdot \frac{\Delta p_y}{\Delta p_Y} \tag{8}$$

The local void volume fractions can be calculated accurately enough from measured overall and local (over the height y) ressure drop values by Eq. 8. Thus, the void volume fractions at different points of the bed can be determined by the movable probe-pair.

Result and Discussion

The most important hydrodynamical relationships characterizing the fluidized beds are as follows: pressure drop vs. air velocity, bed expansion vs. air velocity, and void volume fraction vs. vertical and radial position. The effects of conical inserts and their shapes upon these functions had to be determined.

a) Overall Pressure Drop vs. Air Velocity

If the logarithm of the overall pressure drop of the bed is plotted against the logarithm of air velocity then, as it is known, a steeply rising line is obtained for the stationary bed section and an approximately parallel to axis x line is obtained for the fluidized bed section (theoretically). The lines intersect at the so-called minimum fluidization velocity value.

The experimentally determined overall pressure drop vs. air velocity relationships are plotted in a log-log scale in *Fig. 2* for fluidized beds without and with conical inserts (3 inserts of various sizes). To facilitate comparison,

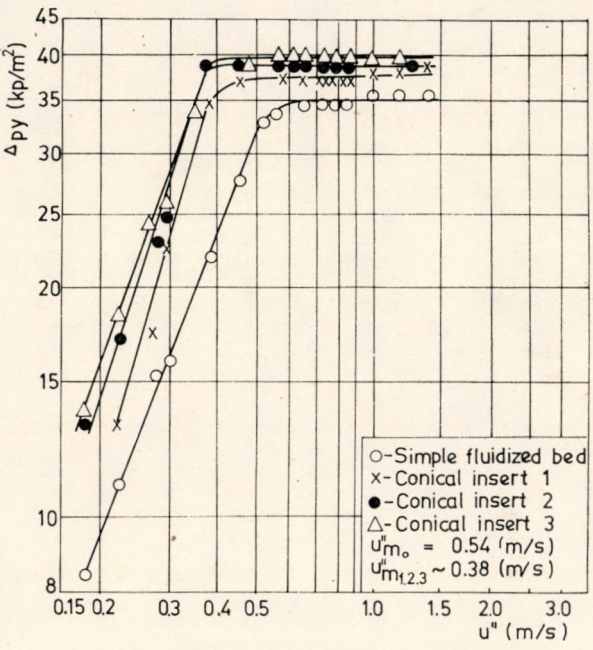

Fig. 2.
Overall pressure drop as a function of air velocity

air velocity values are given with regard to the overall cross section area, even in the case of conical inserts. Experimental data are summarized in *Table 1.*

The minimum fluidization velocity (0.54 m/s) measured in a fluidized bed without a conical insert, or rather taken from the pressure drop versus air velocity plot, agrees well with the value (0.56 m/s) calculated by Ergun's equation (Eq. 9) shown below:

$$u''_m = \sqrt{\frac{42.8\,1-\varepsilon''_m\mu''}{d\varrho''} + \frac{0.57g(\varrho-\varrho'')d}{\varrho''}\cdot\varepsilon''^3_m} - \frac{428(1-\varepsilon''_m)\mu''}{d\varrho''} \qquad (9)$$

In fluidized beds with conical inserts, lower air velocities than in beds without inserts can fluidize the same charge. Obviously, it is due to the fact that the velocity of the fluidizing air is higher at the bottom of the bed, so a special initial momentum is imported to the particles forcing them to move at a lower than usual superficial air velocity. The strange phenomenon occurring in fluidized beds with conical inserts, namely, when there is a shallow smoothly fluidized layer above the distributing plate, but under an otherwise stationary layer is also explained by the above reasoning. (This phenomenon

Table 1.

Overall pressure drop as a function of air velocity
(T = 24° C p ~ 750 Hg mm)

	u'' (m/s)	ΔP_Y (kp/m²)		u'' (m/s)	ΔP_Y (kp/m²)
	0.18	8.4		0.18	13.2
	0.22	11.2		0.22	17.2
	0.27	15.2		0.27	23.2
	0.29	16.0		0.29	24.8
	0.38	22.0		0.38	39.2
	0.44	28.0	Fluidized bed	0.45	39.2
Simple	0.52	33.6	with conical	0.55	39.2
fluidized bed	0.56	34.4	insert in the	0.63	39.2
	0.65	34.8	bottom	0.65	39.2
	0.73	35.2	(2) $\Phi = 42\%$	0.73	39.2
	0.78	35.2		0.78	39.2
	0.85	35.2		0.86	39.2
	0.98	35.6		0.98	39.2
	1.20	36.0		1.16	39.2
	1.40	36.0			
	0.22	13.2		0.18	14.0
	0.27	17.6		0.22	18.4
	0.29	22.8		0.27	24.0
	0.38	34.8		0.29	26.0
	0.45	37.2		0.34	34.4
Fluidized bed	0.58	37.6	Fluidized bed	0.38	39.6
with conical	0.65	38.0	with conical	0.47	39.6
insert in bottom	0.73	38.0	insert in the	0.58	40.0
(1) $\Phi = 31\%$	0.74	38.0	bottom	0.61	40.0
	0.78	38.0	(3) $\Phi = 55\%$	0.65	40.4
	0.84	38.0		0.73	40.4
	0.85	38.0		0.79	40.4
	0.98	38.4		0.87	40.4
	1.2	38.8		0.98	40.4
	1.4	39.2		1.15	40.4

cannot occur in fluidized beds without conical inserts, if they are charged with well fluidizing material.)

In all three fluidized beds with conical inserts, the pressure drop values proved to be higher than those obtained in fluidized beds without inserts, but of equal bed weight. This pressure drop increases with increasing base diameter of the conical insert, both in the stationary and in the fluidized sections. This is caused by the increased flow losses brought about by the decreased free cross section areas.

b) Bed Expansion Versus Air Velocity

Ideally, in the case of large spherical particles, bed expansion (the ratio of the actual and minimum fluidized bed height) increases linearly with increasing air velocities up to a $y/y_m = 2$–2.5 value [8]. However, interestingly enough, in fluidized beds with conical inserts, this linear relationship is broken at a

certain air velocity. Below this air velocity value, the fluidized beds with an insert, above it those without an insert appear more expanded (cf. *Fig. 3* showing all the measured bed expansion versus air velocity curves).

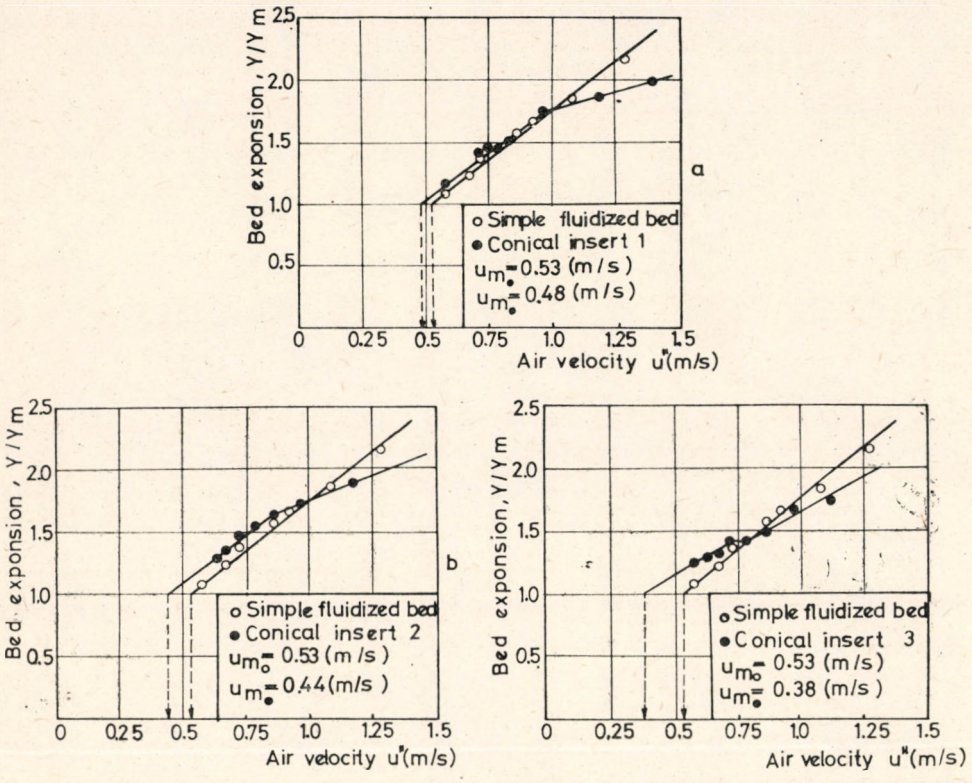

Fig. 3.
Bed expansion as a function of air velocity

The regeysering motion characteristic of fluidized beds with conical inserts becomes fully developed above this air velocity value; the pushing, disordered motion is absent, so the bed appears less expanded and the number of bubbles seen is also smaller. Under the air velocity, corresponding motion is stochastic, nonuninform, and pushing, even in fluidized beds with conical inserts.

According to the experimental bed expansion vs. air velocity curves, the air velocity belonging to the breaking point is twice as high as the minimum fluidizing velocity for all three inserts.

The minimum fluidizing velocity is determined as follows. The line representing the bed expansion vs. air velocity relationship is extended to $Y/Y_m = 1$ and the corresponding air velocity is read from the diagram [9].

The conclusions relating to the minimum fluidization velocity are also partly substantiated by the bed expansion vs. air velocity relationships. The value of the minimum fluidization velocity obtained in a simple fluidized bed

without conical insert agrees rather well, it is 0.53 m/s. According to these measurements, an air velocity 30% less then this figure is sufficient to start the fluidization of the change if 55% the surface of the distributing plate is covered by a conical insert. This difference decreases with decreasing cone-base diameter.

c) Void Fraction vs. Vertical and Radial Position

To demonstrate the accuracy of the method discussed, a test experiment is presented here to help judge the method based on the pressure drop measurements of the fluid phase. The void fraction belonging to the minimum fluidization velocity point in a simple fluidized bed without conical insert is determined by the method shown. Measured data are shown in *Table 2*. In this

Table 2.

Determination of the void volume fraction

Position of probes		ΔP_Y (kp/m²)	$\Delta P/Y$ (kp/m²cm)	ε''_m
Y (cm)	r (cm)			
0.7	5.1	35.2	6.98	0.43
1.7	5.1	35.2	6.9	0.43
2.7	5.1	35.2	6.98	0.43
3.7	5.1	35.2	7.1	0.42
3.7	4.0	34.4	7.1	0.41
2.7	4.0	34.4	7.25	0.40
1.7	4.0	34.8	7.0	0.42
0.7	4.0	34.4	7.0	0.41
0.7	3.0	34.4	7.0	0.41
1.7	3.0	34.8	7.0	0.42
2.7	3.0	34.4	7.2	0.40
3.7	3.0	34.4	7.2	0.40
3.7	2.0	34.4	7.2	0.40
2.7	2.0	34.4	7.1	0.41
1.7	2.0	34.4	7.0	0.41
0.7	2.0	34.4	6.9	0.42
0.7	1.0	34.4	6.9	0.42
1.7	1.0	34.4	6.9	0.42
2.7	1.0	34.4	7.2	0.42
3.7	1.0	34.4	7.2	0.42

$$\bar{\varepsilon}''_m = 0{,}41$$

case, the pressure drop over a 1 cm long section is determined in such a manner that the maximum value is recorded on the differential manometer connected to the probe-pair around the minimum fluidizing velocity point, while the air velocity is continuously increased.

The minimum value of the void fraction of solid, non porous spheres of narrow size distribution, according to literature, is 0.41 and it is independent from the actual diameter of the spheres. In the case of the spherical urea test material of size fraction 1.25–1.60 mm, the same figure was obtained by the method discussed here. This indicates that the local void volume fraction

values, calculated from the pressure drop values over a 1 cm long section of the bed, are real, trustworthy data.

Local pressure drop values in fluidized beds without and with conical inserts (three inserts of different sizes) were measured at three different air velocities at a number of points of different vertical and radical positions.

Void fraction data calculated from measured figures by Eq. 8 are shown as a map in *Fig. 4*. To help visualize this picture, void fractions in the bed

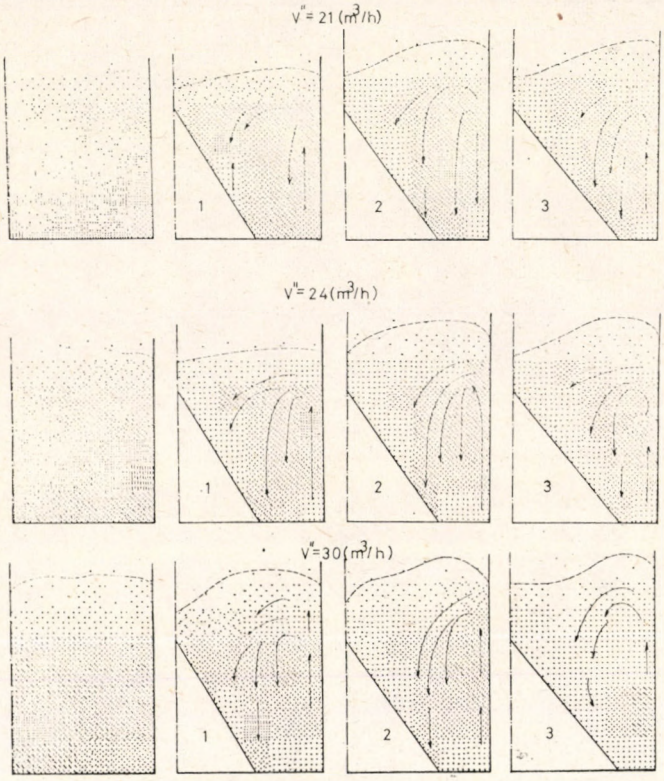

Fig. 4.
Void fraction as a function of radial and axial position
p ~ 750 Hg mm, T = 24° C

are characterized by the number of points in a 10×10 mm square around a given point of the bed drawn to scale as follows.

If $\varepsilon'' = 0.40-0.45$ then, number of points	150
0.45—0.50	100
0.50—0.55	67
0.55—0.60	50
0.60—0.70	25
0.70—0.80	17
0.80—0.90	12
0.90—0.95	3
0.95—0.99	1

The following conclusions can be drawn:

No direct conclusion concerning the particle motion can be drawn from the local void fraction data, because they reflect the relative positions of the particles in the bed, not their velocities. The sharp boundary between the dense and dilute layers found in a fludized bed without conical inserts, disappears in a fluidized bed with an insert when the area covered by the conical insert increases and the bed becomes more dilute. Due to the momentum imparted to the particles by the fluidizing air flowing upward along the wall of the bed, the particles rise up to the top of the cone, then they sink back again.

Nevertheless, the characteristic regeysering motion caused by the conical insert shown in *Fig. 5* can be detected by the void fraction data, because in

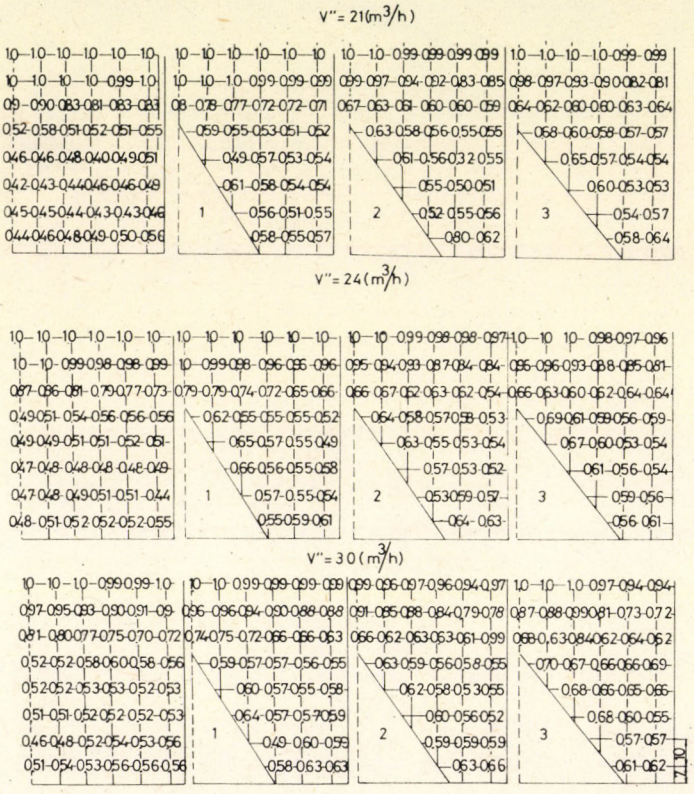

Fig. 5.
Void fraction as a function of radial and axial position

the majority of cases tested the motion is not uniform enough. Only at 30 m³/h and with conical insert No. 3 do the hydrodynamical characteristics become stable enough, ensuring a bubble-free bed and regular particle recirculation. If the void fraction maps are considered, then it can be seen that the height of the bed and along with it, the volume fraction of the particles are the smallest immediately above the cone. At 30 m³/h and insert No. 3, this sharp bed height and particle volume fraction decrease disappear.

This helps to visualize the previous statements about the bed expansion versus air velocity relationships. It can be seen in *Fig. 3* that indeed only at 0.92 m/s air velocity (corresponding to flow rate 30 m^3/h) and at that only with conical insert No. 3 covering the 55% of the area of the distributing plate, is one definitely beyond the critical region around the breaking-point to achieve stable, uniform, developed regeysering movement. This explains why the bed is so extremely homogeneous under these conditions.

CONCLUSIONS

Fluidization was studied in fluidized beds without and with conical inserts. It was found that fluidization started at a much lower air flow rate when there was an insert in the bed. Minimum fluidization velocity decreases with increasing coverage of the area of the distributing plate.

Contrary to findings relating to fluidized beds without conical inserts, the bed expansion versus air velocity relationship is not linear in beds with inserts, rather there is a breaking point at an air velocity twice as high as the minimum fluidizing velocity. Below and above this value, the bed expansion of the fluidized bed with and without inserts respectively is seen to be higher. This is due to the fact that only at $u'' > 2u''_m$ does particle recirculation become stable, and develop regular and uniform layer movement, in contrast to the pushing particle movement, when there is a relatively dense layer with large bubbles and above it a dilute fluidized layer. These findings are substantiated by the local void fraction maps. It can be seen that once the stable regeysering movement has developed, then the layer becomes extremely homogeneous and more dilute than the layer in a fluidized bed without an insert at the same air flow rate.

These findings will be used in the course of the film coating of particles in fluidized beds. The forced circulation of the particles in the layer will ensure a better, more uniform coating of the particles.

SYMBOLS USED

D	diameter of the fluidized bed, (m)
d	particle diameter, (m)
d_k	diameter of the base-plate of the conical insert, (m)
F	cross section of the bed (m^2)
G	weight of the bed, (kp, N)
g	gravity constant, (m/s^2)
Δp_y	overall pressure drop, (kp/m^2, N/m^2)
Δp_Y	pressure drop in the bed over a section of length, y, (kp/m^2, N/m^2)
$\Delta p/y$	pressure drop in the bed over 1 cm, ($kp/m^2 \cdot cm$)
r	radial position of the probe, (cm)
Y/Y_m	bed expansion
Y_k	height of the cone, (m)
y	length element of the bed, (cm)
u''	air velocity, (m/s)
u''_m	minimum fluidization velocity, (m/s)
V''	fluidizing air flow rate, (m^3/s)
z	distance above the distributing plate, (m, cm)
ε''	void fraction
$\bar{\varepsilon}''$	average void fraction

ε''_m minimum void fraction
u'' dynamic viscosity of the fluid phase, (kg/ms)
ϱ density of the solid material, (kg/m³)
ϱ'' density of the fluid phase, (kg/m³)
Φ fraction of the area of the distributing plate covered ny the conical insert, (%)

REFERENCES

1. La Nauze, R. D.: Powder Technology, *15* 117, (1976)
2. Harada, Kauzo, Fujita, Jinshiro: Hitachi Zosen Giho, *36* (3) 149, (1975)
3. Kunii, D. and Levenspiel, O.: Fluidization Engineering, Wiley, New York, 1969.
4. Zeller, H. G.: Die Pharm. Ind., *31* 11, (1969)
5. Kala, M., Dittgen, M. and Moldenhauer, H.: Pharmazie, *26* (11) 664, (1971)
6. Brit. Pat. 1.418.868
7. Blickle, T. and Ormós, Z.: Hung. J. Ind. Chem., *1* 31, (1973)
8. Ginzburg, A. S. and Rechikov, V. A.: Szushke pishevüh produktov v kipjasem sloje. Moskva, 1966.
9. Ormós, Z.: Thesis, University of Chemical Engineering, Veszprém, 1968.

РЕЗЮМЕ

Авторы сопоставили основные гидродинамические характеристики (зависимости типа давление — скорость воздушного потока, объём слоя — скорость воздушного потока, а также минимальную скорость псевдоожижения, изменение свободного объёма в слое в зависимости от локальной координаты местонахождения) простых псевдоожиженных слоёв и слоёв, снабжённых конусным вкладышем. Для определения локальных значений доли свободного объёма был избран метод, основанный на измерении падения давления флюида. Из замеренных и расчётных данных, для различных скоростей воздушного потока и для трёх конусных вкладышей с различной геометрией, были составлены карты.

HUNGARIAN JOURNAL
OF INDUSTRIAL CHEMISTRY
VESZPRÉM
Vol. 6. pp. 105—114 (1978)

PYROLYSE HÖHERSIEDENDER TECHNISCHER ERDÖLFRAKTIONEN

S. Nowak, G. Keil und G. Zimmermann

(Akademie der Wissenschaften der DDR, Zentralinstitut
für Organische Chemie, Berlin — Leipzig)

Eingegangen am 13. Oktober, 1977

Die Pyrolyse von Benzin, Gasöl, hydriertem und entaromatisiertem Gasöl, aus *n*-Heptan sowie zyklischen Kohlenwasserstoffen bestehenden Gemischen, ferner von mono- und polyzyklischen Naphtenen wurde in Labor- und Technikums-einrichtungen untersucht.

Die vorbehandelten (aromatenfreien bzw. aromatenarmen) Mitteldestillate (Gasöle) ergaben bei der Pyrolyse ähnliche Produktausbeuten wie die Benzinpyrolyse und erwiesen sich wesentlich günstiger als die unbehandelten Rohdestillate.

Untersuchungen an verschiedenen zyklischen Kohlenwasserstoffen ergaben einen wesentlichen Einfluß der chemischen Konstitution auf die Ausbeute der Zielprodukte.

Einleitung

Ausgangspunkt dieses Beitrages sollen folgende bekannte Feststellungen sein:

1. Die Pyrolyse von Kohlenwasserstoffen ist seit vielen Jahren Kernstück der Erzeugung organischer Grundstoffe, das heißt von niederen Olefinen und Aromaten.

2. Athylen stellt gegenwärtig den mengenmäßig organishen Grundstoff auf Erdölbasis dar und ist Ausgangsprodukt für ca. 30% aller erzeugten Petrochemikalien und

3. die Olefinerzeugungsanlagen haben hinsichtlich Kapazität und Anzahl ständig zugekommen.

Es ist bekannt, daß der Bedarf an organischen Grundstoffen in den nächsten Jahren stärker steigen wird als die Verarbeitung von Erdöl. Bei Beibehaltung der derzeitigen Struktur der Erdölverarbeitung würde daraus unter anderen eine starke Diskrepanz zwischen dem Aufkommen und dem Bedarf an Benzinkohlenwasserstoffen erwachsen. Dieser sich abzeichnenden Situation könnte prinzipiell auf mehreren Wegen begegnet werden. So z.B.

— durch eine vermehrte Spaltung von Mittel- und Schwerdestillaten zu vorzugweise Benzinkohlenwasserstoffen oder

— durch den Einsatz von Mittel- und Schwerdestillaten anstelle von Benzinen für die Erzeugung organischer Grundstoffe.

Für den ersten Weg ist der Bau von sogenannten „Konversionsanlagen" für Mittel- und Schwerdestillate zur Erhöhung des Aufkommens von Benzinkohlenwasserstoffen sehr kostenaufwendig und stellt nicht von vornherein die technisch-ökonomisch günstigste Variante zur Lösung der volkswirschaftlichen Probleme dar.

Der zweite Weg erfordert nach dem derzeitigen Stand für den Bau von Anlagen zur Erzeugung organischer Grundstoffe durch Pyrolyse von Mitteldestillaten beziehungsweise Gasöl hohe spezifische Investitionskosten, die um ca. 25% über denen von solchen Olefinerzeugungsanlagen liegen, welche auf der Grundlage von straight-run-Benzinen betrieben werden. Dabei muß man allerdings berücksichtigen, daß diese Kostenberechnungen in den meisten Fällen fast ausschließlich auf die niederen Olefine und Diolefine bezogen sind und die zahlreichen anderen entstehenden organischen Grundstoffe bei der Berechnung zu wenig Beachtung finden. Beim Einsatz von Schwerdestillaten in den Pyrolyseprozeß steigen nach der derzeitigen Betrachtungsweise die Investitionskosten weiter an und dürften Mehraufwendungen von nahezu 30% erfordern. Hinzu kommt, daß die Verarbeitungskosten bei der Verarbeitung von Mittel- und Schwerdestillaten auch steigen!

Die bisher gemachten Erfahrungen mit dem Betrieb von Anlagen, die für die wahlweise Verarbeitung von Benzinen und Gasöl ausgelegt sind, führen uns zu der Einschätzung, daß die Verarbeitung von straight-run-Mitteldestillaten zu niederen Olefinen und Aromaten durch Pyrolyse und anschließende Zerlegung des Spaltproduktes durch Tieftemperatur-Mitteldruck-Destillation heute zwar als technisch, nicht aber als ökonomisch und erst recht nicht als wissenschaftlich gelöst angesehen werden kann.

Es wird im allgemeinen eingeschätzt, daß die bei der Verarbeitung von straight-run-Mittel- und straight-run-Swerdestillaten durch Pyrolyse und anschließende Zerlegung der Spaltprodukte auftretenden Schwierigkeiten in erster Linie auf den hohen Anteil an Kohlenwasserstoffen im Einsatzprodukt zurückzuführen sind, denen aromatische Strukturelemente zugrundeliegen. Das sind in der Regel zwischen 20 und 30 Vol.-%. Die daraus resultierenden Schwierigkeiten könnten auf folgenden Wegen überwunden werden:

— durch eine der Pyrolyse vorgeschaltete Abreicherung der aromatischen Kohlenwasserstoffe mit Hilfe physikalischer Trennmethoden (Adsorption; Lösungsmittel-Extraktion; Extraktiv-Destillation) oder

— durch Überführung der aromatischen Kohlenwasserstoffe in Naphthene mittels katalytischer Hydrierung.

Untersuchungen zur Pyrolyse vorbehandelter Mitteldestillate

Über orientierende Untersuchungen zur Vorbehandlung und Pyrolyse von Mitteldestillaten wurde von uns bereits zum letzten Welterdölkongreß in Tokio vorgetragen [1].

Die Ergebnisse haben gezeigt, daß aromatenfreie beziehungsweise aromatenarme Mitteldestillate mit ähnlichem Erfolg der Pyrolyse unterworfen werden

Tabelle 1.

Charakteristische Ausbeuten bei der Pyrolyse technischer Destillatfraktionen aus Romachkino-Erdöl[1]

Spaltprodukte (Ma-%) (bezogen auf Einsatzprodukt)	Roh-Benzin 39—148 °C	Roh-Dieselöl 189—318 °C	hydriertes Dieselöl[2] 142—310 °C	entaromat. Dieselöl[3] 195—320 °C
Spaltgas $\leqq C_4$	70,3	59,1	70,9	68,9
Äthylen	24,5	21,4	28,3	25,4
Propylen	17,0	13,8	15,1	16,5
Butadien	4,9	4,4	6,2	5,5
Pyrolysebenzin < 200 °C	27,6	23,6	22,5	23,3
Benzol	3,4	2,5	5,8	4,0
Pyrolyseöl > 200 °C	2,1	17,2	6,5	7,8

[1] *Spaltbedingungen:*
Austrittstemperatur 830 °C
Verweilzeit 0,22 s
Dampf/Kohlenwasserstoff 0,6 (Gew-Teile)
[2] *Hydrierbedingungen*
Katalysator NiO und WO_3 auf Alumosilikat
Belastung 1,5—5 v/vh
Hydriertemperatur 320—380 °C
H_2-Partialdruck 100—200 at
H_2/KW—Vol.-Verhältnis ~500
[3] Durch Extraktion mit Kattwinkelsäure ($H_2SO_4 + P_2O_5$)

können wie straight-run-Benzine. Der in *Tabelle 1* an wenigen charakteristischen Kenngrößen vorgenommene Vergleich führt zu dem Schluß, daß die Spaltung derartig vorbehandelter Mitteldestillate zu einer mit der Benzinspaltung vegleichbaren Produktausbeute führt und gegenüber der Spaltung von Rohdieselöl wesentliche Vorteile bietet.

Bei der Pyrolyse hydrierter Dieselöle steigen nicht nur die rohstoffspezifischen Ausbeuten an Äthylen und Propylen, sondern überraschenderweise auch die von Butadien und Benzol. Dementsprechend vermindern sich die Ausbeuten an Pyrolyseöl.

Die Entfernung der im Roh-DK vorhandenen Heteroatome Schwefel und Stickstoff mit dem Hydriergas (als H_2S bzw. NH_3) entlastet die Gaswäsche den Trennteil der Pyrolyseanlage und führt zu umweltfreundlicheren Flüssigprodukten (Pyrolysebenzin, Heizöl). Inwieweit die genannten Vorteile allerdings den Bau und den Betrieb der Vorbehandlungsstufen rechtfertigen, kann nur durch eine detaillierte Kosten-Nutzen-Analyse ermittelt werden. Im Falle einer Aromatenentfernung durch Lösungsmittelextraktion erhebt sich die Frage nach einer sinnvollen Weiterverwendung des aromaten- und schwefelreichen Extraktes.

Außer der Siedelage unterscheiden sich die von uns untersuchten Mitteldestillate insbesondere hinsichtlich der Stofftypenzusammensetzung. Aus der Gegenüberstellung in *Tabelle 2* geht unter anderen hervor, daß im Falle der Aromatenabreicherung durch physikalische Stofftrennprozesse, das heißt

Tabelle 2.

Stofftypenzusammensetzung technischer Destillat-fraktionen aus Romaschkino-Erdöl

Stofftyp (Ma-%) (bezogen auf Einsatzprodukt)	Roh-Benzin 39—148 °C	Roh-Dieselöl 189—318 °C	hydriertes Dieselöl* 142—310 °C	entaromat. Dieselöl* 195—320 °C
Paraffine	70,6	37,4	53,6	51,4
Naphthene	19,2	35,3	41,3	48,6
Aromaten	10,1	27,3	5,1	0
davon Alkylbenzin	10,1	4,5	0,2	0

* Siehe Fußnoten *Abbildung 1.*

durch die „ersatzlose" Entfernung der aromatischen Kohlenwasserstoffe, der Gehalt an Paraffinen von 37 auf 51 und der der Naphthene von 35 auf 49 Vol.-% steigt. Bei der katalytischen Hydrierung werden zunächst die kondensierten Aromaten in Cycloalkylaromaten und diese schliesslich zusammen mit den Alkylbenzolen in mehr- u. monocyclische Naphthene umgewandelt *(Abb. 1)*,

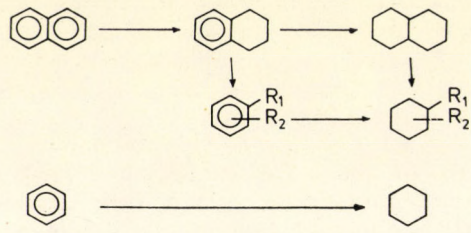

Abb. 1.
Hydrierung der aromatischen Inhaltsstoffe am Ni/Mo-Katalysator bei 350 °C und 200 at

so daß hieraus Einsatzprodukt für die Pyrolyse resultiert, das zu 54% aus Paraffinen und zu 41% aus Naphthenen besteht [2]. Die Naphthenkohlenwasserstoffe haben somit für das Ausbeutespektrum eine nicht mehr zu vernachlässigbare Bedeutung.

Wir haben deshalb die Frage geprüft, welche Produkte man nach dem vorliegenden wissenschaftlichen Erkenntnisstand bei der Verarbeitung solcher Fraktionen unter den Bedingungen der Pyrolyse erwarten kann. Dabei mußten wir feststellen, daß so gut wie keine wissenschaftlich gesicherten Erkenntnisse über das Verhalten von Cycloparaffinen unter den Bedingungen der Pyrolyse vorliegen.

Wir wissen heute im großen und ganzen recht gut Bescheid über die beim thermischen Kracken von Paraffinen ablaufenden Reaktionen und deren Beeinflussung durch die dabei gebildeten Zwischen- und Zielprodukte und wir sind demzufolge in der Lage, die beim thermischen Kracken von Paraffinen ablaufenden Vorgänge zu modellieren. Unsere Kenntnisse über die Vorgänge beim thermischen Kracken von Benzinen sind schon viel unvollständiger.

Die Erfahrung lehrte jedoch, daß diese Kenntnisse zur Auslegung von Pyrolyseanlagen für Benzinfahrweise für praktische Zwecke ausreichen, weil die Auslegung in diesem Falle in der Regel so erfolgt, als würde es sich bei Rohbenzinen um Pseudoparaffinkohlenwasserstoffe handeln. Eine solche Vorgehenweise ist zwar wissenschaftlich in keiner Weise befriedigend, sie läßt sich jedoch aus dem praktischen Erfolg rechtfertigen sowie aus dem Tatbestand, daß die zur Olefinerzeugung eingesetzten Rohbenzine zu etwa 70% aus Paraffinen bestehen.

Für die Spaltung von straight-run-Mittel- oder -Schwerdestillaten ist eine Behanglung als Pseudoparaffin nicht mehr gerechtfertigt, weil der Anteil an cyclischen Verbindungen (Aromaten, Naphthene) bei oberhalb 50% liegt. Wir haben uns deshalb zum Ziel gestzt, die Grundlagen für eine wissenschaftlich gesicherte Auslegung von Pyrolysereaktoren zur Spaltung von Mitteldestillaten mit hohen Naphthengehalten zu erarbeiten. Wir haben unsere Forschungsarbeiten aus diesem Grunde auf die Verarbeitung von straight-run-Mittel- und straight-run-Schwerdestillaten durch katalytische Hydrierung und Pyrolyse der hydrierten Fraktionen orientiert, wobei unser wissenschaftliches Interesse insbesondere auf mechanistische und kinetische Untersuchungen des thermischen Zerfalls der Cycloparaffine gerichtet ist.

Noch 1966 berichteten Purnell und Quinn in einer Monographie [3], daß Cycloparaffine ausschließlich nach einem Radikalkettenmechanismus zerfallen. Inzwischen wissen wir, daß die thermischen Zerfallsreaktionen von Cyclopropan- und Cyclobutankohlenwasserstoffen keinen ausgeprägten Radikalketten-Charakter besitzen [4]. Mechanismus und Kinetik der thermischen Kracken von Cyclopentan und Cyclohexankohlenwasserstoffen wurden bischer nur vereinzelt untesucht. Die Interpretation der meßtechnisch erhaltenen Ergebnisse ist weitgehend spekulatív geblieben.

Neuere und bisher unveröffentlichte Untersuchungen von Kalinenko und Shevelkowa vom Institut für Erdölchemische Synthese der Akademie der Wissenschaften der UdSSR [5] deuten darauf hin, daß die Spaltung von Cyclopentan von molekularen Fragmentierungen begleitet ist, während die Spaltung von Cyclohexan vorwiegend nach einem Radikalkettenmechanismus erfolgt.

Ist über das Spaltverhalten monocyclischer Naphthene wenig bekannt, so liegen über das Reaktionsverhalten mehrcyclischer Naphthene unter Pyrolysebedingungen praktisch keine gesicherten Ergebnisse vor. Es ist deshalb zur Zeit nicht möglich, die mit der Spaltung höhersiedender Erdölfraktionen verbundenen Besonderheiten hinreichend zu deuten. Nachdem es uns zusammen mit Becker und Mitarbeitern aus dem VEB Leuna-Werke „Walter Ulbricht" [6] gelungen ist, die in straight-run-Dieselölen enthaltenen Aromaten an Ni/W- beziehungsweise Ni/Mo-Trägerkatalysatoren bei einer Belastung von 1,5—5 v/vh, einem Gas-Produkt-Verhältnis von 500 und Wasserstoffpartialdrücken zwischen 100 und 200 at bei einem minimalen Hydrospaltanteil von etwa 10% bis zu einem Restgehalt von 2—5 Vol.-% in Naphthene zu überführen, haben wir nunmehr die Aufklärung des Reaktionsverhaltens von Cycloalkylaromaten und Naphthenen unter den Bedingungen des thermischen Krackens in Angriff genommen. Erste Ergebnisse wurden von Zimmermann, Bach und Günschel bereits auf dem Symposium Alken 77 in Böhlen [7] vorgetrangen.

Die in *Abb. 2* zusammengestellten Kohlenwasserstoffe wurden als Modellsubstanzen zur Untersuchung eingesetzt. Sie wurden in reiner Form bezie-

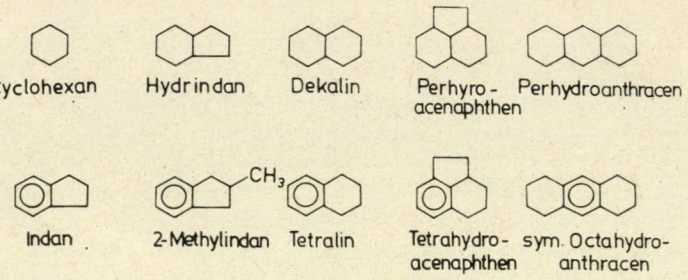

Abb. 2.
Eingesetzte Ringkohlenwasserstoffe

hungsweise zusammen mit *n*-Heptan bei unterschiedlichen Temperaturen in einem Laborreaktor aus Edelstahl (⌀2 mm, Länge 3 m) beziehungsweise einem Technikumsreaktor (⌀8 mm, Länge 18 m) gespalten und die Umsätze sowie die Reaktionsprodukte gaschromatographisch bestimmt. Zur Analyse setzten wir 4 Trennsäulen ein:

– H_2, CH_4 und die C_2-Kohlenwasserstoffe wurden an einer 2 m langen Porapak-N-Säule aufgetrennt,
– die C_2–C_5-Kohlenwasserstoffe analysierten wir an einer 6 m langen Säule mit Oxydipropionitril auf Al_2O_3,
– die im Gasprodukt mitgerissenen C_5-Bestandteile trennten wir an einer 10 m langen Silikongumisäule und
– die Flüssigproduktanalyse erfolgte an einer 120 m langen Glaskapillare mit Carbowax 20 M als Trennflüssigkeit.

Der Parameterraum, in dem die Pyrolyseversuche durchgeführt wurden, ist in *Tabelle 3* zusammengestellt.

Tabelle 3.
Parameterraum der Spaltversuche

Austrittstemperatur	700—830 °C
Austrittsdruck	1,5—26 at
Dampf/Kohlenwasserstoff	0,6—3,0 (Gew.-Teile)
Kohlenwasserstoff	rein bzw. n-C_7/cyclo-KW = 85/15 bis 40/60 (Gew.-Teile)
Verweilzeit	0,3—0,5 sec

Die erhaltenen Ergebnisse und die daraus abgeleiteten Schlußfolgerungen können wie folgt zusammengefaßt werden:

1. Die Zerfallsgeschwindigkeiten der mehrcyclischen Naphthene liegen durchweg höher; die der Cycloalkylaromaten niedriger als die Zerfallsgeschwindigkeit des n-Heptans (vergl. *Abb. 3*).

2. Mono- und mehrcyclische Naphthene führen zu Spaltprodukten mit zum Teil signifikant anderen Zusammensetzungen als wir sie bei der Pyrolyse von *n*-Heptan fanden *(Abb. 4)*.

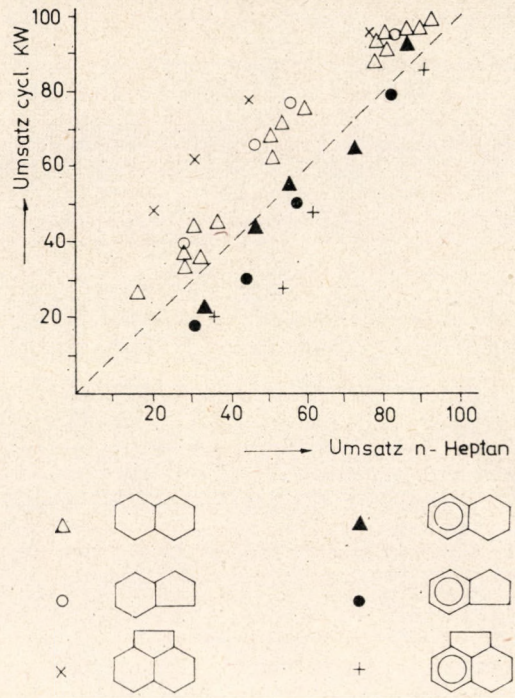

Abb. 3.
Simultaner Umsatz von cyclischen Kohlenwasserstoffen und *n*-Heptan

Spaltgas $C_2 - C_4$	mN	~	P
	p N	<	P
Butadien	mN	>	P
	p N	~	P
Flüssigprodukt $> C_5$	mN	~	P
	p N	>	P
Benzol	mN	~	P
	p N	>>	P

Legende: mN : monocyclische Naphthene
p N : polycyclische Naphthene
P : Paraffine

Abb. 4.
Vergleich der Ausbeuten beim Einsatz von Paraffinen, monocyclischen und polycyclischen Naphthenen

Diese allgemeinen Aussagen sollen durch einen Vergleich des Anfalls wichtiger Inhaltsstoffe des Spaltgases für die Cyclohexan- und Dekalin-Spaltung bei 825 °C belegt werden. Bei diesen Versuchen wurden beide Kohlenwasserstoffe in jeweils reiner Form in Gegenwart von Wasserdampf gespalten *(Tabelle 4)*.

Tabelle 4.

Vergleich der Spaltproduktzusammensetzung bei der Cyclohexan- und Dekalinkrackung

Spaltbedingungen: Spaltrohr (18 m lang, ∅8 mm); t_A=825 °C; τ=0,5—1,0 s; P_A=2,0 at; $m_{H_2O}/m_{Einsatzstoff}$=0,6		
	Cyclohexan	Dekalin
Methan	5	12
Äthylen	31	22,5
Butadien	24,5	4,5
Benzol	4,5	17
Toluol	1	10

(Angaben in Ma-% vom Einsatz)

3. Cycloalkylaromaten werden erwartungsgemäß bevorzugt dehydriert. Aus Tetralin entsteht Naphthalin, daneben als Reaktionsprodukt einer stufenweisen Dehydrierung Dihydronaphthalin und als Isomerisierungsprodukte 2- und 3-Methylindene *(Abb. 5)*.

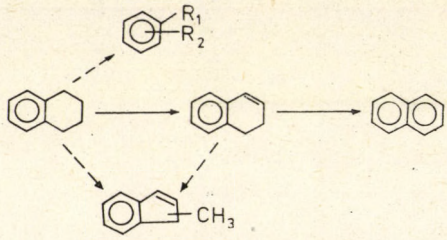

Abb. 5.

Reaktionsprodukte des Tetralins unter Pyrolysebedingungen. Einsatzgemisch: *n*-Heptan/Tetralin; Mengenverhältnis 70:30.
t_A=775 °C; p_A=26 at; p_{H_2}=1,1 at; τ=0,4 s; m_{H_2O}:m_{KW}=2,8

4. Schließlich entstehen aus mehrcyclischen Naphthenen mehr Benzol und Benzolhomologe (C_6—C_9) als aus Cycloalkylaromaten. Zu diesem Ergebnis

Ring-KW in n-Heptan	Spaltgas ≤C_4	Olefine C_2+C_3	flüss. Prod. ≥C_5	Aromaten C_6-C_9
 30 %	45.3	24.6	54.7	2.9
 30 %	52.3	27.7	47.7	14.7
 30 %	40.6	23.1	59.4	2.2
 30 %	60.7	33.2	39.3	12.6

Abb. 6.

Ausbeuten bei vergleichenden Spaltversuchen mit verschiedenen Ring-KW (in Masse-%)

führten Versuche zur vergleichsweisen Spaltung der von uns untersuchten Verbindungen, die unter einem H_2-Partialdruck von ca. 15 atm durchgeführt wurden, um der Dehydrierung etwas entgegenzuwirken *(Abb. 6)*.

Mit diesem Erkenntnisstand müssen wir es vorerst bewenden lassen. Mechanistische Deutungen der hier vorgestellten ersten Ergebnisse sind verfrüht; sie müßten zwangsläufig zu viele Spekulationen enthalten. Weitere Untersuchungen sind im Gange, über deren Ergebnisse wird zu gegebener Zeit berichtet.

Schlußfolgerungen

Wir sind der Meinung, daß der Einsatz von zumindest Mitteldestillaten zur Herstellung organischer Grundstoffe eine Alternative zur Verarbeitung von Benzin darstellt, wenn zwei Probleme durch systematische Arbeit positiv gelöst werden können:

1. Die hydrierende Vorbehandlung von Mittel- und unter Umständen auch Schwerdestillaten zur Überführung der Aromaten in Naphthene unter ökonomisch tragbaren Bedingungen und
2. die Abtrennung und die ökonomische Verwendung aller bei der Pyrolyse anfallenden Grundstoffe für die Ausweitung des Sortiments an organischen Zwischenprodukten als entscheidende Basis für die dynamische Entwicklung der chemischen Industrie.

Nach unserer Meinung ist die Bearbeitung dieser Probleme für die Entwicklung der chemischen Industrie bedeutungsvoll.

Wir möchten an dieser Stelle allen Mitarbeitern Dank sagen, über deren Arbeitsergebnisse hier berichtet wurde. Es sind dies insbesondere Dr. H. Günschel, Dr. R. Rehm, Dr. W. Zychlinski, Dr. G. Bach sowie eine Reihe ungenannter Mitarbeiter, die uns geholfen haben, die zahlreichen, zum Teil recht schwierigen analytischen Probleme zu lösen.

LITERATURVERZEICHNIS

1. S. Nowak, G. Keil, H. Günschel, G. Pechstein: IX. Welterdölkongress, Tokyo 1975, PD 19 (4), S. 145.
2. H. G. Struppe, D. Rennecke, H. Günschel: bisher unveröffentlichte Ergebnisse
3. J. H. Purnell, C. P. Quinn: „Photochemistry and Reaction Kinetics" Cambridge Univ. Press, 1966, S. 330.
4. H. M. Frey, R. Walsh: Chem. Rev. *69* (1969) 103.
5. R. Kalinenko und L. Schevelkowa: persönl. Mitteilung
6. Patentanmeldung DDR WP C10 G/199624
7. G. Zimmermann, G. Bach und H. Günschel: Plenarvortrag „Alken 77", DDR/Böhlen

SUMMARY

Laboratory and pilot plant scale experiments were carried out for the pyrolysis of gasoline, diesel oil, hydrated and dearomatised diesel oil, the mixture of *n*-heptane and cyclic hydrocarbons moreover of mono- and polycyclic naphthenes.

The pyrolysis yield of pretreated (dearomatised) middle fractions (diesel oils) is similar to the same one of the gasoline and this value is more favourable than the yield obtained at the pyrolysis of untreated, crude distillates.

The yield of the desired product is influenced by the chemical structure of the raw materials, this was proved by the data of the experiments carried out with cyclic hydrocarbons.

РЕЗЮМЕ

На лабораторных и пилотных установках исследовались смеси, состоящие из бензина, газойля, гидратированного газойля и газойля, освобождённого от содержания ароматических соединений, из *н*-гептана и циклических углеводородов, а также пиролиз моно- и полициклических нафтенов.

При пиролизе предварительно обработанных (без содержания ароматических соединений или с малым содержанием их) средних дестиллятов, выход их достигается подобно тому, как это наблюдалось при обработке предварительно не обрабатывавшихся, сырых дестиллятов.

Результаты опытов, проведённых с различными циклическими углеводородами, подтверждают тот факт, что химическая структура соединений оказывает значительное влияние на выход целевого продукта.

HUNGARIAN JOURNAL
OF INDUSTRIAL CHEMISTRY
VESZPRÉM
Vol. 6. pp. 115–122 (1978)

VAPOUR PHASE DEHYDRATION OF ETHYL ALCOHOL OVER ALUMINA AND RELATED CATALYSTS

P. K. GUPTA* and M. RAVINDRAM

(Department of Chemical Engineering, Indian Institute of Science,)
BANGALORE–560 012. INDIA

Received: November 2. 1977.

Vapour phase dehydration of ethyl alcohol was studied in a flow reactor under isothermal conditions over heat treated alumina and molecular sieve catalysts, in the 250–350° C temperature range. The validity of a parallel-constructive reaction scheme for the dehydration of ethyl alcohol was demonstrated.

Introduction

Most aliphatic alcohols yield the corresponding ether and olefin on dehydration. The resulting products have a large number of industrial applications. Ethyl alcohol is dehydrated to ether and ethylene, depending on the temperature range and catalysts employed. The texture of the catalyst also significantly influences the product distribution. Reported studies on dehydration of ethyl alcohol were mainly conducted over conventional alumina and silica-alumina catalysts (1–4). In view of their precise pore size characteristics, molecular sieves are now being used as catalysts for the dehydration of alcohols (5–7). Depending on the experimental conditions, various investigators proposed (8, 9) mechanical models for dehydration involving either series or parallel reaction schemes.

The present investigation was made to establish the most probable reaction scheme for the dehydration of ethyl alcohol.

Methods

The experimental set-up given in *Fig. 1* essentially consisted of: (i) an alcohol feeding and metering unit, (ii) a preheater and reactor assembly and (iii) the product collection unit. Suitable controls were provided to obtain isothermal

* Present Address: B.A.R.C., Bombay.

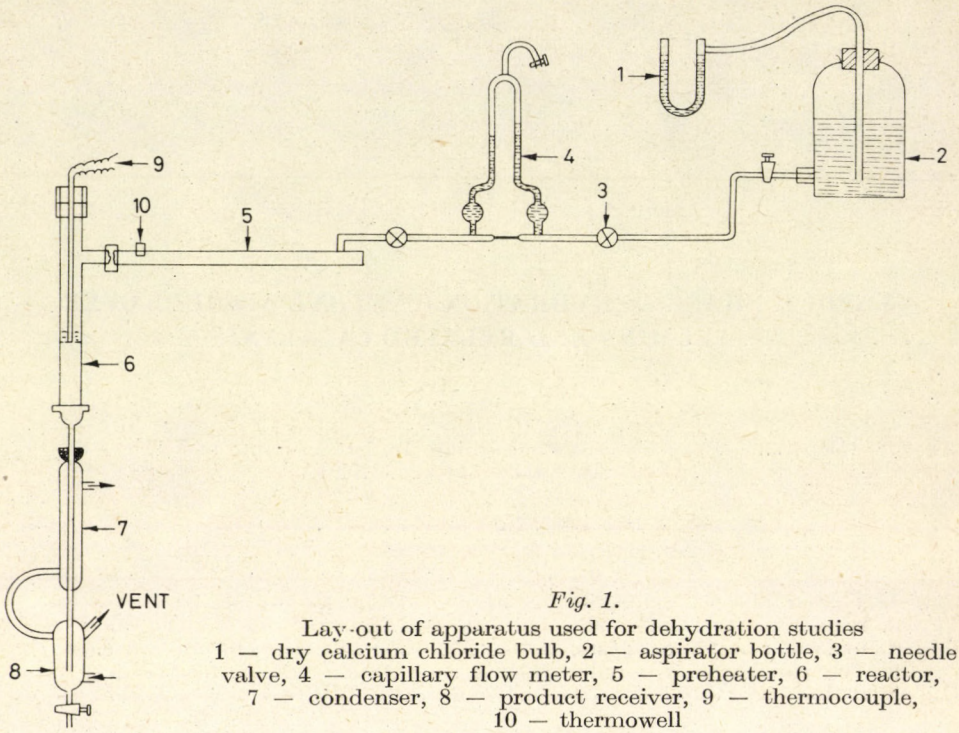

Fig. 1.
Lay-out of apparatus used for dehydration studies
1 — dry calcium chloride bulb, 2 — aspirator bottle, 3 — needle valve, 4 — capillary flow meter, 5 — preheater, 6 — reactor, 7 — condenser, 8 — product receiver, 9 — thermocouple, 10 — thermowell

conditions in the reactor. The liquid product consisting of ether, water and unreacted alcohol was analyzed by vapour phase chromotography, and the product ethylene was analyzed by an Orsat gas analyzer.

An alumina catalyst was prepared by precipitation by the addition of ammonium hydroxide to a solution of aluminium nitrate. The hydroxyde precipitate was thoroughly washed and dried in a oven at 110° C for 24 hours. The texture of the alumina catalyst was changed by subjecting the same to a heat treatment at different temperatures, viz., at 500, 630 and 730° C for 48 hours. A Linde molecular sieve 10*x* supplied by M/s. Union Carbide was used.

The specific surface area of the catalyst was measured by the BET method and the surface acidity by non-aqueous titration using *n*-butyl amine. The catalyst properties are given in *Table 1.*

Table 1

Properties of Heat Treated Alumina

Catalyst	Temperature of heat treatment (°C)	Surface area (sq·m/g)	Acidity (*m* moles/g)
Alumina	500	226.5	0.498
Alumina	630	160.6	0.427
Alumina	730	126.6	0.337
Molecular sieve 10*x*	500	615.5	0.597

Results

Initially conditions were established by following the methods suggested by YOSHIDA et al (10 under which bulk and pore diffusional resistances were at a minimum. Having established these conditions, kinetic data were collected by determining the conversion of ethyl alcohol to ether and ethylene as a function of contact time and reaction temperature.
The following range of variables was employed:

Temperature .. 350—350° C
Contact time W/F .. 0.37—1.87 g. cat. hr/g. mole
(W is the weight of catalyst in g. and
F is the feed rate in g. moles/hr.)

A representative plot is presented in *Fig. 2*. In general, it was found that at

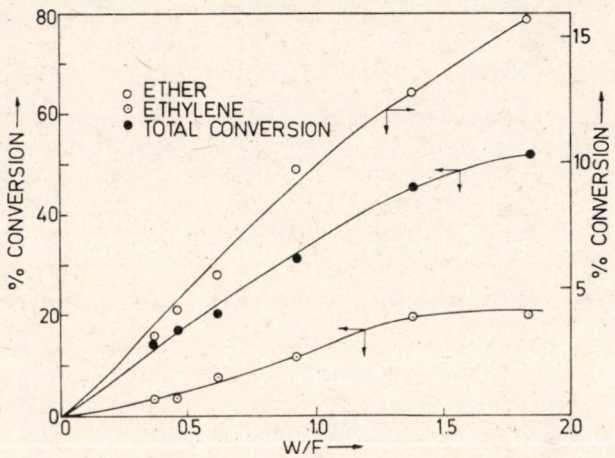

Fig. 2.
Effect ot time factor on conversion
Catalyst: 10 x molecular sieve. Temperature: 300° C

lower temperatures conversion to ethylene and ether increases as a function of contact time. However, at higher temperatures, conversion to ether passes through a maximum as a function of contact time, while the conversion to ethylene increases continuously. This suggests that apart from ethylene formed directly from alcohol, ether which forms first as an intermediate is also subsequently converted to ethylene.

Probable Reaction Schemes

Dehydration of ethyl alchohol can yield ethylene and diethyl ether. In addition the later can also yield ethylene. The reactions can be stoichiometrically represented as:

$$2\,C_2H_5OH \xrightarrow{k_1} (C_2H_5)_2O + H_2O \ldots \quad \text{(i)}$$

$$C_2H_5OH \xrightarrow{k_2} C_2H_4 + H_2O \qquad \text{(ii)}$$

$$(C_2H_5)_2O \xrightarrow{k_3} 2\,C_2H_4 + H_2O \qquad \text{(iii)}$$

In the present investigation, since both diethyl ether and ethylene are found in the products, the possible reaction schemes can be postulated as:

I. *Consecutive Reaction Scheme:*

In this scheme, it is assumed that the direct dehydration of alcohol to ethylene is negligible, and that ethylene is formed only by the dehydration of diethyl ether.

$$\text{Ethyl alcohol} \xrightarrow{k_1} \text{diethyl ether} + \text{water}$$
$$\qquad\qquad\qquad\qquad\qquad\qquad\quad \downarrow k_3$$
$$\qquad\qquad\qquad\qquad\qquad\qquad\quad \text{ethylene} + \text{water}$$

The stoichiometry is given by reactions (i) and (iii).

II. *Parallel Reaction Scheme:*

In this scheme, ethylene is assumed to essentially form by the direct dehydration of alchohol and that the dehydration of ether to ethylene is negligible.

$$\text{Ethyl alcohol} \xrightarrow{k_2} \text{Ethylene} + \text{water}$$
$$\quad \downarrow k_1$$
$$\text{Ether} + \text{water}$$

The stoichiometry is given by reactions (i) and (ii).

III. *Parallel-Consecutive Reaction Scheme:*

In this scheme, it is assumed that ethylene is formed by both the routes, i.e., by the dehydration of alcohol, as well as by the dehydration of ether

$$\text{Ethyl alcohol} \xrightarrow{k_1} \text{Ether} + \text{water}$$
$$\qquad\quad \searrow^{k_2} \qquad \swarrow_{k_3}$$
$$\qquad\quad \text{Ethylene} + \text{water}$$

The stoichiometry is given by reactions (i), (ii) and (iii).

Formulation of Rate Expressions:

Since the parallel and consecutive reaction schemes are special cases of the parallel-consecutive reaction scheme, the derivations of the rate expressions were carried out for the later case alone. However, the rate expressions for the parallel and consecutive reaction schemes can be obtained by a simplification of the equations for the parallel-consecutive scheme.

Preliminary analysis of the data indicated first order kinetics. The same was thus assumed in deriving the rate expressions. In addition, the volume change in reactions (i)–(iii) was neglected, as was done by other investigators [11, 12].

Considering that all the reactions are first order, the rate expressions for the parallel-consecutive reaction scheme can be written as:

For alcohol diappearance:

$$-\frac{dC_A}{d(W/F)}=(k_1+k_2)C_A \tag{1}$$

For ether formation:

$$\frac{dC_B}{d(W/F)}=1/2k_1C_A-k_3C_B \tag{2}$$

For ethylene formation:

$$\frac{dC_C}{d(W/F)}=k_2C_A+2k_3C_B \tag{3}$$

where C_A, C_B and C_C are the concentrations of alcohol, ether and ethylene and k_1, k_2 and k_3 are the specific reaction rate consistants for reactions (i), (ii) and (iii) respectively.

The above equations (1–3) on integration give:

$$C_A=C_{A0}\exp\left[-(k_1+k_2)\,(W/F)\right] \tag{4}$$

$$C_B=\frac{k_1\cdot C_{A0}\{\exp\left[-(k_1+k_2)W/F\right]-\exp\left[-k_3(W/F)\right]\}}{2[k_3-(k_1+k_2)]} \tag{5}$$

$$C_C=C_{A0}\left[1+\frac{k_2-k_3}{k_3-(k_1+k_2)}\exp\left[-(k_1+k_2)W/F\right]+\frac{k_1}{k_3-(k_1+k_2)}\exp\left[-k_3(W/F)\right]\right] \tag{6}$$

where C_{A0} is the initial concentration of ethyl alcohol. Eq. (4) can be rewritten as:

$$\ln\frac{C_{A0}}{C_A}=(k_1+k_2)W/F \tag{7}$$

Determination of rate constants:

According to q. (7) a plot of ln (C_{A0}/C_A) Vs. (W/F) should yield a straight line passing through the origin if the assumption of first order kinetics is correct. In fact such was found to be the case as shown in *Fig. 3 and 4*. From the scopes of these straight lines, the values of (k_1+k_2) were evaluated at all the temperatures studied. Individual values of k_1, k_2 and k_3 were determined making use of eq. (5) and (7), by linear regression analysis. The individual values of k_1, k_2 and k_3 for the different catalysts are given in *Table 2*. The reaction velocity constants are reported, based on the unit surface area of the catalyst in *Table 2*. It can be seen that k_1 and k_2 values are initially higher than k_3 values. However, at higher temperatures the k_3 values increase very sharply. The reaction velocity constants were related to the temperature by means of the ARRHENIUS equation. A representative plot is presented in *Fig. 5*.

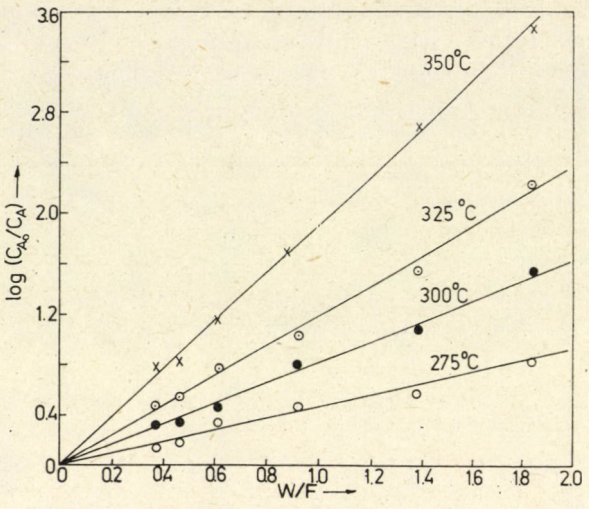

Fig. 3.
Determination of $K_1 + K_2$
Catalyst: 10 x molecular sieve

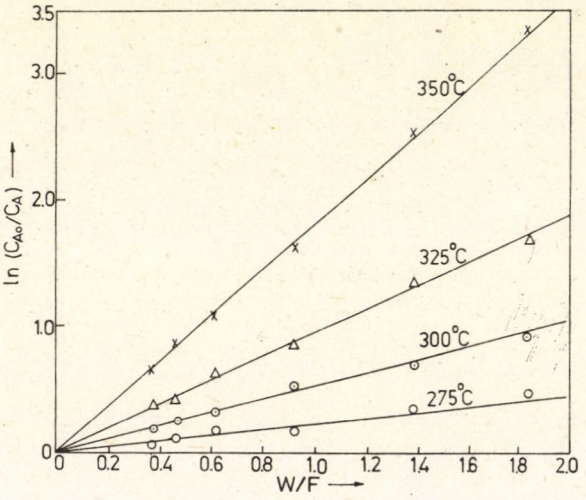

Fig. 4.
Determination of $K_1 + K_2$
Catalyst: Alumina heat treated at 630° C

The calculated values of the activation energy and the frequency factor are reported in *Table 3*. Heat treatment does not appear to have a significant influence on the activity of the catalysts. This may be due to the fact that the intrinsic acidity (acidity per unit surface area) is more or less the same for the different alumina catalysts. The molecular sieve $10x$ was found to be an active catalyst for the dehydration reaction.

Table 2

Reaction velocity constants for the parallel consecutive reaction scheme

Reaction temperature °C	Reaction velocity constant·10^4 (1/sq·cm·hr)	M.S. $10x$	Alumina heat treated at		
			500 °C	630 °C	730 °C
275	k_1	3.47	5.44	8.53	10.04
	k_2	4.19	8.73	5.75	19.22
	k_3	2.32	3.68	5.50	8.55
300	k_1	6.10	12.06	17.93	22.75
	k_2	7.18	16.67	15.46	27.45
	k_3	7.63	14.91	19.17	17.25
325	k_1	8.52	22.37	30.92	43.14
	k_2	10.73	26.54	27.52	36.86
	k_3	15.81	32.24	38.24	40.78
350	k_1	15.00	40.35	53.18	65.88
	k_2	15.97	44.74	59.36	48.63
	k_3	26.62	105.26	123.07	128.63

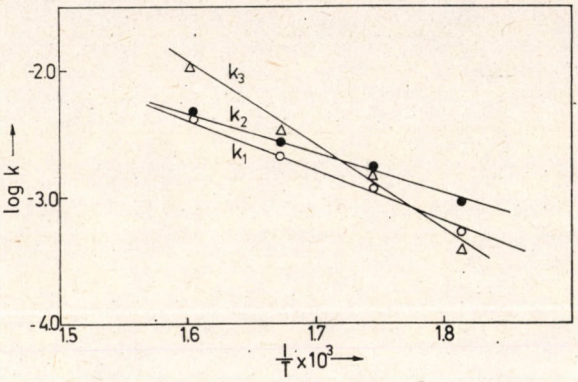

Fig. 5.
Arrhenius plot Catalyst: Alumina heat treated at 500° C

Table 3

Values of the activation energy and frequency factor

Catalyst	Activation energy, E (k cal/g mole)			Frequency factor (1/sq. cm hr.)		
	E_1	E_2	E_3	A_1	A_2	A_3
MS $10x$	10.07	12.81	22.89	3.98	52.48	3.58×10^5
Alumina heat treated at 500° C	17.40	14.65	30.21	4.79×10^3	6.08×10^2	4.21×10^8
Alumina heat treated at 630° C	14.19	16.93	21.98	4.37×10^2	3.80×10^3	3.47×10^5
Alumina heat treated at 730° C	14.64	16.87	18.1	9.33×10^2	1.15×10^3	1.35×10^4

Conclusions

In conclusion, it can be said that the dehydration of ethyl alcohol proceeds by a parallel-consecutive reaction scheme over alumina and related catalysts. The heat treatment of alumina did not significanthy change its activity for the various competing reactions. Synthetic zeolite (molecular sieves) can be used as active catalysts for dehydration reactions.

NOMENCLATURE

C_A, C_B, C_C	Concentrations of alcohol, ether and ethylene respectively moles/litre.
F	Feed rate, g. moles/hr.
k_1, k_2, k_3	Reaction velocity constants, litres/sq. cm. hr.
T	Absulute temperature °C
W	Weight of catalyst, g.

REFERENCES

1. Butt, J. B., Bliss, H. Walker, C. A: A. J. Ch. E. Jl., 8, 42 (1962)
2. Miller, D. N. and Krik, R. S.: A. J. Ch. E. Jl., *8*, 183 (1962)
3. Wade, W. H., Taramishu, S. and Durhan, J. L.: J. Phy. Chem., *69*, 590. (1965)
4. Stauffer, J. E. and Kranich, W. L.: Ind. Engg. Chem. Fundamentals, *1*, 107, (1962)
5. Ralac, M. Coll. Czech. Chem. Commun. *30*, 3411, (1951)
6. Ralac, M. and Grumbnor, O.: International Cong. on Catalysis, 1302, (1964)
7. Sarma, G. S. and Ravindram, M.: Indian J. Technol., *10*, 431, (1932)
8. Inagulyants, C. U. and Balandin, A. A.: Russian J. Phy Chem., *38*, 10, (1914)
9. Padmanabhan, U. R. and Eastburn, F. J.: J. Catalysis, *24*, 88, (1972)
10. Yoshida, F., Ramaswami, O. and Hougen, O. A.: A. I. Ch. E. Jl., *8*, 5, (1962)
11. Reddy, K. A. and Doraiswamy, L. K.: Chem. Engg. Sci., *24*, 1415, (1969)
12. Murthy, M. S. and Rajamani, K.: Chem. Engg. Sci., *29*, 601, (1964)

РЕЗЮМЕ

Парофазная дегидратация этилового спирта изучалась при изотермических условиях, в температурном интервале 250—300 °C, в присутствии термически обработанной окиси алюминия и катализаторов-молекулярных фильтров, при использовании реактора непрерывного действия. Опытные данные показывают, что реакция легидратации этилового спирта имеет параллельно-последовательный характер.

CONTENTS

VÁRHEGYI, Gy., MISKEI, M. and IVÁN, L.: Intensive Methods for the Preparation of Vanadium Chlorides from Bauxite Ore 1
SZEPESY, K., WELTHER, K. and SEBESTYÉN, Zs.: Efficient Catalytic Oxidation Process for Air Pollution Abatement 11
MOHOS, F.: General Properties of Technological Systems. I. 21
MOHOS, F.: General Properties of Technological Systems. II. 39
LAKATOS, B. and BLICKLE, T.: The Inhomogeneity Parameter and its Properties. I. Closed Systems 53
LAKATOS, B. and BLICKLE, T.: The Inhomogeneity Parameter and its Properties. II. Open Systems..... 67
SZENTMARJAY, Z., CSUKÁS, B. and ORMÓS, Z.: Hydrodynamical Studies on Fluidized Beds. V. Determination of the Particle Mixing Characteristics in Dual-Cell Fluidized Beds by Isotope Tracer Technique 81
HORVÁTH, E., PATAKI, K. and ORMÓS, Z.: Hydrodinamical Studies on Fluidized Beds. VI. Studies on the Hydrodynamical Properties of Gas-Fluidized Beds with Concial Inserts 93
NOWAK, S., KEIL, G. and ZIMMERMANN, G.: Zur Pyrolyse höhersiedener technischer Erdölfraktionen. (The Pyrolysis of High Boiling Point Oil Fractions) 105
GUPTA, P. K. and RAVINDRAM, M.: Vapour Phase Dehydration of Ethyl Alcohol over Alumina and Related Catalysts 115

78.2724 Egyetemi Nyomda, Budapest. Felelős vezető: Sümeghi Zoltán igazgató

THE FOLLOWING ARE PLEASED TO ACCEPT SUBSCRIPTIONS TO THIS JOURNAL:

AUSTRALIA

C.B.D. Library and Subscription Service
Box 4886 G.P.O.
Sydney 2000

Cosmos Book and Record Shop
145 Acland Street
St. Kilda 3182

Globe and Co.
694—696 George Street
Sydney 2000

AUSTRIA

Globus (VAZ)
Höchstädtplatz 3
A—1200 Wien XX

BELGIUM

"Du Monde Entier" S. A.
Rue du Midi 162
B—1000 Bruxelles

Office International de Librairie
Avenue Marnix 30
B—1050 Bruxelles

CANADA

Pannonia Books
P.O. Box 1017
Postal Station "B"
Toronto, Ontario M5T 2T8

DENMARK

Munksgaard's Boghandel
Norregade 6
DK—1165 Copenhagen K

FINLAND

Akateeminen Kirjakauppa
Keskuskatu 2, P.O.B. 128
SF—00 100 Helsinki 10

FRANCE

Office International de Documentation et Librairie
48 Rue Gay Lussac
75 Paris 5

GERMAN FEDERAL REPUBLIC

Kubon und Sagner
Pf 68
D—8 München 34
BRD

GREAT BRITAIN

Bailey Bros and Swinfen Ltd.
Warner House, Folkestone
Kent CT 19 6PH England

HOLLAND

Martinus Nijhoff
Periodicals Department
P.O. Box 269
The Hague

Swets and Zeitlinger
Keizersgracht 487
Amsterdam C

ITALY

Licosa
P.O.B. 552, Via Lamarmora 45
50121 Firenze

JAPAN

Igaku Shoin Ltd.
Foreign Department
Tokyo International P.O. Box 5063
Tokyo

Maruzen Co. Ltd.
P.O. Box 5050
Tokyo International 100—31

Nauka Ltd.
Yasutomi Bldg. 5F 2—12 Kanda
Jinbocho, Chiyoda-ku
Tokyo 101

NORWAY

Tanum—Cammermayer
Karl Johangt. 41—43
Oslo 1

SWEDEN

Almqvist and Wiksell Förlag A. B.
Box 2120
S—103 13 Stockholm 2

Wennegren—Williams AB
Subscription Department Fack
S—104 Stockholm 30

SWITZERLAND

Karger Libri A. G.
Petersgraben 31
CH—4011 Basel

USA

Ebsco Subs. Services
1 st Ave North at 13th street
Birmingham, Ala. 35201

HUNGARIAN

Journal of

INDUSTRIAL CHEMISTRY

Edited by

the Hungarian Oil & Gas Research Institute (MÁFKI),
the Research Institute for Heavy Chemical Industries (NEVIKI),
the Research Institute for Technical Chemistry of the
Hungarian Academy of Sciences (MÜKKI),
the Veszprém University of Chemical Engineering (VVE).
Veszprém (Hungary)



Volume 6. 1978 Number 2.

HU ISSN: 0133—0276
CODEN: HJICAI

Editorial Board:

R. CSIKÓS and GY. MÓZES
Hungarian Oil & Gas Research Institute
(MÁFKI Veszprém)

A. SZÁNTÓ and M. NÁDASY
Research Institute for Heavy Chemical Industries
(NEVIKI Veszprém)

T. BLICKLE and O. BORLAI
Research Institute for Technical Chemistry
of the Hungarian Academy of Sciences
(MÜKKI Veszprém)

A. LÁSZLÓ and L. PÉCHY
Veszprém University of Chemical Engineering
(VVE Veszprém)

Editor-in Chief:
E. BODOR

Assistant Editor:
J. DE JONGE

Veszprém University of Chemical Engineering
(VVE Veszprém)

The „Hungarian Journal of Industrial Chemistry" is a joint publication of the Veszprém scientific institutions of the chemical industry that deals with the results of applied and fundamental research in the field of chemical processes, unit operations and chemical engineering. The papers are published in four numbers at irregular intervals in one annual volume, in the English, Russian, French and German languages

Editorial Office:
Veszprémi Vegyipari Egyetem
„Hungarian Journal of Industrial Chemistry"
H—8201 Veszprém, P. O. Box: 28.
Hungary

Subscription price $ 45.— per volume/per year. Orders may be placed with
KULTURA
Foreign Trading Co. for Books and Newspapers
Budapest 62. POB 149
or with its represenatatives abroad, listed on the verso of the cover

FELELŐS SZERKESZTŐ: DR. BODOR ENDRE

KIADJA A LAPKIADÓ VÁLLALAT, 1073 BP. VII., LENIN KRT. 9—11.
TELEFON: 221-285. LEVÉLCÍM: 1906 BP. PF. 223
FELELŐS KIADÓ: SIKLÓSI NORBERT IGAZGATÓ

HUNGARIAN JOURNAL
OF INDUSTRIAL CHEMISTRY
VESZPRÉM
Vol. 6, pp. 125–130 (1978)

SOME LINEAR RELATIONS IN HIERARCHIC MODELLING OF MULTIPHASE REACTORS

J. HOLDERITH

(Eötvös L. University, Laboratory of Chemical Cybernetics, Budapest)

Received: November 2, 1977.

It is shown that in multicomponent mass transfer processes, the locally averaged diffusive fluxes through the unit interfacial area are linear functions of locally averaged concentration of both phases. This relationship can be used for the development of mathematical models with the hierarchic structure of the multiphase reactors.

Introduction

In an earlier paper [1] the basic principles of the hierarchic development of multilevel mathematical models of multiphase chemical reactors were treated in detail. In another paper [2] certain linear relations were investigated in connect with the hierarchic modelling of two-phase reactors of gas-liquid type. Namely, it was shown that if the gas-phase of a two-phase elementary object is well-mixed and in the liquid phase the reactions of first and/or zero order are assumed then the linear relations between the functionals representing the averaged absorption rates and the averaged concentrations of liquid phase are valid.

In the present work, as a generalization of the above mentioned results, a model of a two-phase elementary object in which both (fluid) phases are inhomogeneous is investigated. A special example of this general model is the elementary model type of fluid-porous catalyst.

Theory

Let L be a second-order linear differential operator:

$$Lx = \operatorname{div}[\vec{v}(\vec{r}) \cdot x - \vec{\vec{D}}(\vec{r}) \cdot \operatorname{grad} x]$$

where:

$\vec{v}(\vec{r})$ is a three-dimensional velocity field, i.e. a preset vector function of the three-dimensional vector of the independent variables $\vec{r}$,

$\vec{\vec{D}}(\vec{r})$ is a dispersion field, i.e. a preset tensor function of $\vec{r}$,

x is an operator argument, i.e. a function, a vector of functions or a matrix of functions.

Let us consider a singly connected domain V of the three-dimensional space confined by the surface F divided by a surface F_3 in two parts, i.e. the a-phase and the b-phase. In the following the value of any variable in the a-phase and b-phase will be denoted by indices a and b respectively.

The surface F may be divided in two parts:

$$F = F_1 + F_2$$

on the basis of the velocity field $\vec{v}(\vec{r})$:

$$\text{if} \quad \vec{n}(\vec{r})\cdot\vec{v}(\vec{r}) < 0 \quad \text{then} \quad \vec{r} \in F_1, \quad \text{and}$$
$$\text{if} \quad \vec{n}(\vec{r})\cdot\vec{v}(\vec{r}) \geq 0 \quad \text{then} \quad \vec{r} \in F_2,$$

where $\vec{n}(\vec{r})$ is the normal vector of the surface F. The following equations exist: $F_i = F_{ia} + F_{ib}$ and $F = F_a + F_b$ of course $V = V_a + V_b$. All preset functions constructed on the domain V may have jumped on the surface F_3 with except of the normal component of the velocity field $\vec{v}(\vec{r})$, which is continuous on all point of the surface F_3 and agree with the move velocity of the surface F_3.

Let us consider in the domain V the following system of transport equations with linear sources:

$$Lc = \mathbf{A}\cdot c + b \tag{1}$$

where:

x is an N-dimensional vector of unknown functions of $\vec{r}$ (of the concentrations of components),

$\mathbf{A}$ is an $N \times N$ matrix of the preset functions of $\vec{r}$,

b is an N-dimensional vector of the preset functions of $\vec{r}$,

with the boundary conditions:

$$\vec{r} \in F_{1i} : c = c_j^0 + \mathbf{C}\cdot n_1 \cdot \operatorname{grad} c; \qquad j = a, b \tag{2}$$

$$\vec{r} \in F_2 : \vec{n}_2 \cdot \vec{\vec{D}}(\vec{r}) \cdot \operatorname{grad} c = 0 \tag{3}$$

where:

$\vec{n}_i$, $i = 1, 2$; are the normal vectors of the corresponding surfaces F_i,

$\mathbf{C}$ is a (generally diagonal) $N \times N$ matrix of the preset functions on F_1,

c_j^0, $j = a, b$; are N-dimensional vectors of the preset constants,

0 is an N-dimensional zero vector.

Let us suppose that the diffusive fluxes:

$$\vec{j}_k(\vec{r}) = -\vec{\vec{D}}(\vec{r}) \cdot \operatorname{grad} c_k; \qquad k = 1, \ldots, N$$

are continuous functions of the positional vector $\vec{r}$ inside the domain V, hence also on the surface F_3 and let us consider the following vectors of functionals determined from the solution of problem (1)—(3):

$$J = -\frac{1}{F_3} \int_{F_3} n_3 \cdot \vec{\vec{D}} \cdot \operatorname{grad} c \, \mathrm{d}F_3 \tag{4}$$

$$J_a = \frac{1}{V_a} \int_{V_a} c \, \mathrm{d}V_a \tag{5}$$

$$J_b = \frac{1}{V_b} \int_{V_b} c \, \mathrm{d}V_b \tag{6}$$

Functionals of type (4) can be interpreted as diffusive fluxes through the interfacial area, averaged locally in space (transfer fluxes). On the other hand, functionals of type (5) and (6) can be interpreted as concentrations of the components, averaged locally in space inside the single phases. Below it will be shown that they are linearly related independently of the c° values. For this purpose, it will be necessary to assume the existence of the solution of problem (1)—(3) and of functionals (4)—(6).

Let $\mathbf{U}_1$ and $\mathbf{U}_2$ two $N \times N$ matrices of the functions of $\vec{r}$, and v an N-dimensional vector of the functions of $\vec{r}$ satisfying the following $2N+1$ systems of equations:

$$L\mathbf{U}_i = \mathbf{A}\cdot\mathbf{U}_i, \quad i=1,2; \quad Lv = \mathbf{A}\cdot v + b$$

with the following boundary conditions:

$$\vec{r}\in F_{1a}: \mathbf{U}_1 = \mathbf{E} + \mathbf{C}\cdot\vec{n}_{1a}\cdot\text{grad}\,\mathbf{U}_1; \quad \mathbf{U}_2 = \mathbf{0}; \quad v = 0$$

$$\vec{r}\in F_{1b}: \mathbf{U}_1 = \mathbf{0}; \quad \mathbf{U}_2 = \mathbf{E} + \mathbf{C}\cdot\vec{n}_{1b}\cdot\text{grad}\,\mathbf{U}_2; \quad v = 0$$

$$\vec{r}\in F_2: \vec{n}_2\cdot\vec{\vec{D}}\cdot\text{grad}\,\mathbf{U}_i = \mathbf{0}, \quad i=1,2; \quad \vec{n}_2\cdot\vec{\vec{D}}\cdot\text{grad}\,v = 0$$

where $\mathbf{E}$ is a unit matrix, $\mathbf{0}$ is a zero matrix.

All these systems of partial differential equations are special cases of the original problem (1)—(3), hence the existence of their solutions follows from the assumed existence of the solution of $c = c(\vec{r})$. The same statement is also valid for the corresponding functionals:

$$\mathbf{J}_i = -\frac{1}{F_3}\int_{F_3} \vec{n}_3\cdot\vec{\vec{D}}\cdot\text{grad}\,\mathbf{U}_i\,\mathrm{d}F, \quad i=1,2;$$

$$\mathbf{J}_{ji} = \frac{1}{V_j}\int_{V_j} \mathbf{U}_i\,\mathrm{d}V_j, \quad i=1,2; \quad j=a,b;$$

$$J_v = -\frac{1}{F_3}\int_{F_3} \vec{n}_3\cdot\vec{\vec{D}}\cdot\text{grad}\,v\,\mathrm{d}F_3$$

$$J_{jv} = \frac{1}{V_j}\int_{V_j} v\,\mathrm{d}V_j, \quad j=a,b;$$

It will be shown that the solution of problem (1)—(3) can be represented as:

$$c = \mathbf{U}_1\cdot c_a^0 + \mathbf{U}_2\cdot c_b^0 + v \tag{7}$$

For this purpose it is sufficient to verify that the vector of functions c defined by equation (7) satisfies the system of equations (1) and boundary conditions (2) and (3). The proof will be obtained from the following series of equalities:

1. $Lc = L\mathbf{U}_1\cdot c_a^0 + L\mathbf{U}_2\cdot c_b^0 + Lv = \mathbf{A}\cdot\mathbf{U}_1\cdot c_a^0 + \mathbf{A}\cdot\mathbf{U}_2\cdot c_b^0 + \mathbf{A}\cdot v + b =$
   $= \mathbf{A}\cdot(\mathbf{U}_1\cdot c_a^0 + \mathbf{U}_2\cdot c_b^0 + v) + b = \mathbf{A}\cdot c + b$
2. $\vec{r}\in F_{1a}: c = \mathbf{U}_1\cdot c_a^0 + \mathbf{U}_2\cdot c_b^0 + v = (\mathbf{E} + \mathbf{C}\cdot\vec{n}_{1a}\cdot\text{grad}\,\mathbf{U}_1)\cdot c_a^0 = c_a^0 + \mathbf{C}\cdot\vec{n}_{1a}\cdot\text{grad}\,c$
3. $\vec{r}\in F_{1b}: c = \mathbf{U}_1\cdot c_a^0 + \mathbf{U}_2\cdot c_b^0 + v = (\mathbf{E} + \mathbf{C}\cdot\vec{n}_{1b}\cdot\text{grad}\,\mathbf{U}_2)\cdot c_b^0 = c_b^0 + \mathbf{C}\cdot\vec{n}_{1b}\cdot\text{grad}\,c$
4. $\vec{r}\in F_2: \vec{n}_2\cdot\vec{\vec{D}}\cdot\text{grad}\,c = \mathbf{0}\cdot c_a^0 + \mathbf{0}\cdot c_b^0 + 0 = 0$

From equation (7), and from the linearity of the functionals it follows that:

$$J = \mathbf{J}_1 \cdot c^0 + \mathbf{J}_2 \cdot c^0 + J_v \tag{8}$$

$$J_j = \mathbf{J}_{j1} \cdot c_a^0 + \mathbf{J}_{j2} \cdot c_b^0 + J_{jv}; \quad j = a, b; \tag{9}$$

where by definition, the functionals forming the $N \times N$ matrices $\mathbf{J}_i$ and $\mathbf{J}_{ji}$ ($j = a, b$; $i = 1, 2$) and the N-dimensional vectors J_v and J_{jv} ($j = a, b$) are independent of vectors c_a^0 and c_b^0. On the assumption that the appropriate matrices are non-singular, by elimination of vectors c_a^0 and c_b^0 form the system of equations (8)—(9) one may obtain the required linear relations. For this reason let us introduce the following hypermatrices:

$$c^0 = \begin{bmatrix} c_a^0 \\ c_b^0 \end{bmatrix}, \quad C = \begin{bmatrix} J_a \\ J_b \end{bmatrix}, \quad C_v = \begin{bmatrix} J_{av} \\ J_{bv} \end{bmatrix}, \quad \mathbf{C}_u = \begin{bmatrix} \mathbf{J}_{a1} & \mathbf{J}_{a2} \\ \mathbf{J}_{b1} & \mathbf{J}_{b2} \end{bmatrix}$$

$$\mathbf{J}_3 = [\mathbf{J}_1 \quad \mathbf{J}_2]$$

Then the system of equations (8)—(9) takes a simpler form:

$$J = \mathbf{J}_3 \cdot c^0 + J_v$$

$$C = \mathbf{C}_u \cdot c^0 + C_v$$

whence it can be seen that:

$$J = \mathbf{G} \cdot \mathbf{C} + g \tag{10}$$

where $\mathbf{G} = \mathbf{J}_3 \cdot \mathbf{C}_u^{-1}$ and $g = J_v - \mathbf{J}_3 \cdot \mathbf{C}_u^{-1} \cdot C_v$, supposing that the hypermatrix $\mathbf{C}_u$ is non-singular. Thus the following statement has been proved.

Statement. Let a solution of problem (1)—(3) and functionals (4)—(6) exist. Then linear relationships (8)—(9) presented in parametric form are valid. In addition, if $\det(\mathbf{C}_u) \neq 0$, then the linear relationship (10) exists.

Remarks

1. The hierarchic modelling of multiphase reactors requires the relationship to be given between the composition and the intensities of sources of components. If the right side of the system of equations (1) is denoted by $q = q(c)$ then the required relationship can be represented by functionals:

$$Q_j = \frac{1}{V_j} \int_{V_j} q \, \mathrm{d}V_j; \quad j = a, b; \tag{11}$$

as functions of corresponding functionals J_j. By substituting the right side of eq. (1) into (11), and by use of (5) and (6) immediately it follows that:

$$Q_j = \frac{1}{V_j} \int_{V_j} (\mathbf{A} \cdot c + b) \, \mathrm{d}V_j = \mathbf{A} \cdot J_j + b; \quad j = a, b; \tag{12}$$

A chemical interpretation of the relationship (12) can be written in the form of the next assertion. It results from the existence of zero or/and first order reactions on the kinetic level of the model that zero or/and the first order intraphase sources of the components also exist on the higher level of model. The reverse assertion is generally not valid.

2. It is possible that in the development of a concrete model of an elementary object, a certain co-ordinate component of conductive transport may be neglected and thus the respective second-order derivate is omitted from the transport equation (1). Then the corresponding equation in the boundary conditions of type (3) will be automaticaly omitted. This is the reason for—apparently unnecessary—performing the multiplicator $\vec{\vec{D}}(\vec{r})$. Consequently all the above mentioned statements are also valid for this special model.

3. Results for the two-phase elementary object of gas-liquid type treated in the recent paper [2] can be deduced as special cases of relationships introduced in this work. Namely if one of the phases, say phase "a" is perfect mixed, then the following relationships are valid: $J_a = c_a^0$; and if $\vec{r} \in V_a$ then $c(\vec{r}) = c_a^0$; and what is more, if $\vec{r} \in F_3$ then also $c(\vec{r}) = c_a^0$. Hence in addition to the statement announced in the paper [1] it follows that constant vector g itself is a linear expression:

$$g = \mathbf{G}_1 \cdot c^* + g_1$$

where c^* denotes in the work [2] the value of vector $c(\vec{r})$ on the surface F_3.

4. It is easy to see that if the matrix $\mathbf{A}$ is diagonal and its elements are non-positive and $b = 0$ (for example, if we consider only one equation for transport of a component reacted in a single first order reaction) then the system of differential equations $Lv = \mathbf{A} \cdot v + b$ has only a trivial solution: $v = 0$. Then values of all its functionals are also zero consequently: $C_v = 0$, $J_v = 0$ and $g_1 = 0$, and so the above mentioned linear relationships become significantly simpler.

5. In the case of zero-order reactions, i.e. if $b \neq 0$, the whole original problem has a physical sense as far as solution c is non-negative. But some of the functions generating the c according to (7) may also have negative values.

6. Results introduced here can be easily extended for two following cases:

6.1. Concentrations on the boundary surface of phases have discontinuities, but here both phases are in equilibrium and the distribution ratios are constants.

6.2. Though the distribution ratios are functions of concentrations, they have constant values on the surface F_3 due to concrete circumstances or model assumptions.

REFERENCES

1. Holderith, J.: Magy. Kém. Foly. *83*, 69 (1977)

2. Bykov, V. I., Holderith, J.: Reaction Kinetics and Catalysis Letters *3*, 371 (1975)

РЕЗЮМЕ

В данном сообщении показано, что при многокомпонентных процессах массопереноса с химическими реакциями первого и нулевого порядков, локально осреднённые диффузионные потоки через единицу поверхности раздела фаз являются линейными функциями локально осреднённых концентраций. Такие соотношения могут быть использованы при построении математических моделей многофазных реакторов с иерархической структурой.

HUNGARIAN JOURNAL
OF INDUSTRIAL CHEMISTRY
VESZPRÉM
Vol. 6. pp. 131–144 (1978)

GENERAL PROPERTIES OF TECHNOLOGICAL SYSTEMS. III.

F. Mohos
(Budapest Chocolate Factory of the Hungarian Candy Trust)

Received: September 27, 1977.

The technological system of cocoa processing is reviewed together with the technological processes of cocoa butter, commercial cocoa powder, cocoa paste and indirect chocolate production. The material-flow-systems and functional groups of cocoa processing are described. The latest technological trends in chocolate production are also reviewed. The degrees of freedom of the cocoa processing technological system are determined.

7. Discussion of the Complete Technological Systems of Cocoa Processing

7.1 General Remarks

The technological theory presented in *Parts 1* and *2* was based on Blickle's general theory [1, 2 in *Part 1*]. This theory can be applied to all fields of chemical industries. Some generalizations are discussed here which permit the extension of the theory to non-chemical fields in the strict meaning of the term. Thus, general guidelines are presented for the description of industries processing raw materials of biological origin. These conclusions and guidelines are based on the studies of cocoa processing technologies. Though the significance of cocoa processing is rather limited even in the food processing industries, it seemed a suitable field to attain the set objectives. Cocoa processing takes place on a large scale by automated machinery.

Initially the problem has to be dealt with where only the raw materials (ANCESTOR) are known and the technological system to be designed has to take into account all the real possibilities of realizaton.

Why should all the feasable realization possibilities sought in an industry processing materials of biological origin be bound by strong conventions which exclude the possibilities of new technologies based on entirely new concepts. Since the capacities of conventional technologies cannot meet the increased demands, research projects based on entirely new concepts are unavoidable even in this field. However, a venture such as this requires that the very essence of the technology be understood and the solution is sought deeper than at the

level of formal technological innovations. The essence of any technology is —and this is the main achievement of BLICKLE's theory—the change of materials in the given technological system, i.e. any study has to concentrate on the sets of the structures of the materials (A) and changes (V). Added to this as a more simple task is the selection of the structure of the apparatuses. In an appropriate approach this task can be readily algorithmized. This means that according to BLICKLE's theory, the task of apparatus contruction is a second rate task compared with the determination of the changes occurring in the structure of the materials, the essence of the technological task. This order is essential for the design of any technology.

7.2 Functional Groups of the Cocoa Processing Technological System

Cocoa processing became an industry about 150 years ago, although traces of a few processing principles valid even today were known to and were also practiced by the Aztek Indians. This industrialization process has been accompanied by careful studies of the properties and structure of cocoa bean, i.e. there has also been vigorous analytical activity preparing the soil for improved technologies.

Let us now consider the statements which, without further help, allow for the determination of the functional groups of the technological system of cocoa processing.

Raw materials of cocoa processing (ANCESTOR)

- raw cocoa bean (a_1)
- powdered or crystalline sugar (a_2)
- powdered milk (skimmed or full) (a_3)
- lecithine (a_4)
- alkali (alkali ash, $KHCO_3$, etc.) (a_5)
- water to dissolve alkali (a_6)

End products (and wastes) of cocoa processing (PICTURE)

- cocoa bean shell (a_7)
- cocoa bean germ (a_8)
- roasting wastes and exhaust gases (a_9)
- commercial cocoa powder (a_{10})
- milk chocolate paste (a_{11})
- process vapour (a_{12})
- cocoa butter (a_{13})
- vapours from cocoa powder drying (a_{14})

Technological research concluded that

- roasting exhaust gases (a_9) consist mostly of water vapour, carbon dioxide and volatile acids,
- alkalic digestion is appropriate for commercial cocoa powder production and the end product also contains the neutralization products,
- the MAILLARD reaction taking place between sugar and milk powder used to produce milk chocolate paste (a_{11}) has to be taken into consideration, while the quantitative aspects of polyhydroxy phenol transformation reactions can be neglected,

— considerable vapour formation occurs during the refining and drying processes after the alkalic digestion of the cocoa paste. This vapour mainly consists of water and volatile acids,
— considering the extreme stability of cocoa butter, the saponification effects of alkalic digestion can be neglected.

These findings are shown in *Table 1*. Let us then form the multiple (a_i, ANCESTOR $x\, a_j$, PICTURE) shown by *Matrix 4*. The result of the multiplication is

1, if a_i and a_j contain a material fraction transferred from a_i into a_j
0, if the opposite of the above statement is true.

Only the cases when the result is equal to 1 have to be examined. The material fraction transferred from a_i into a_j is sought.

The problem becomes complicated when the material-flow of the PICTURE is composed from the material flows of several ANCESTORS as, e.g. in the case of a_{101} or a_{111}. The term "several" is justified, because, e.g. the sum of a_{102} and a_{101} is equal to a_{10}. Since in optimum cases a_{102} can be determined, a_{101} can be obtained by increasing the amount of reaction products to a_{10}. There is also a similar case for a_{11}. When the quantitative description of a technological sys-

Table 1

Material-flow-systems of conventional cocoa processing

ANCESTOR

a_1: raw cocoa bean
a_2: sugar (powder or crystalline)
a_3: powder milk (whole or skimmed)
a_4: lecithin or other emulgeater
a_5: alkali (ash, etc.)
a_6: water to dissolve a_5

PICTURE

a_7: cocoa shell
a_8: cocoa germ
a_9: roasting product:
  a_{91}: water vapour
  a_{92}: CO_2
  a_{93}: volatile acids
a_{10}: commercial cocoa powder:
  a_{101}: the rest (multicomponent material)
  a_{102}: reaction product:
    a_{1021}: anion
    a_{1022}: cation
a_{11}: milk chocolate:
  a_{111}: the rest (multicomponent material)
  a_{112}: Maillard-reaction product:
    a_{1121}: aldose
    a_{1122}: protein-amine
a_{12}: refining vapour:
  a_{121}: water vapour
  a_{122}: volatile acids
a_{13}: cocoa butter
a_{14}: process vapours:
  a_{141}: water vapour
  a_{142}: volatile acids

Matrix 4:

Relation of the material-flow-systems of ANCESTOR and PICTURE in the cocoa processing technological system

(a_1) PICTURE / ANCESTOR	a_7	a_8	a_9			a_{10}			a_{11}			a_{12}		a_{13}	a_{14}	
						a_{101}	a_{102}		a_{111}	a_{112}						
			a_{91}	a_{92}	a_{93}		a_{1021}	a_{1022}		a_{1121}	a_{1122}	a_{121}	a_{122}		a_{141}	a_{142}
a_1	1	1	1	1	1	1	1	—	1	—	—	1	1	1	1	1
a_2	—	—	—	—	—	—	—	—	1	1	—	—	—	—	—	—
a_3	—	—	—	—	—	—	—	—	1	—	1	—	—	—	—	—
a_4	—	—	—	—	—	—	—	—	1	—	—	—	—	—	—	—
a_5	—	—	—	—	—	—	—	1	—	—	—	—	—	—	—	—
a_6	—	—	—	—	—	1	—	—	—	—	—	—	—	—	—	—

tem is prepared, then the amounts of materials have to be taken into consideration. This is especially important when the quantitative independency of the material flows of the system or its degrees of freedom are tested.

After *Matrix 4* is filled in the nature of material fractions transferred from a_i into a_j should be determined on the basis of analytical information. These results are shown in *Table 2*.

Table 2

Determination of the elements of the functional group set of the cocoa processing technological system

$a_1 \cap a_7 = R_1$ (cocoa shell)
$a_1 \cap a_8 = R_2$ (cocoa germ)
$a_1 \cap a_{13} = R_3$ (cocoa butter)
$a_1 \cap a_{91} = R_4$ (water content)
$a_1 \cap a_{92} = R_5$ (decomposable C)
$a_1 \cap a_{93} = R_6$ (acid content)
$a_1 \cap a_{101} =$ multicomponent material
$a_1 \cap a_{1021} = R_6$ (acid content)
$a_1 \cap a_{111} =$ multicomponent material
$a_1 \cap a_{121} = R_4$ (water content)
$a_1 \cap a_{122} = R_6$ (acid content)
$a_1 \cap a_{141} = R_4$ (water content)
$a_1 \cap a_{142} = R_6$ (acid content)

According to chemical analysis multicomponent materials

$(a_1 \cap a_{101})$ and $(a_1 \cap a_{111})$ can be expressed as
$(a_1 \cap a_{101})$ and $(a_1 \cap a_{111}) = (R_3 \cup R_7)$

where R_7 is the dry and oil-free cocoa tissue fraction containing no material liberated in the roasting step.

Furthermore:

$a_2 \cap a_{111} = R_8$ (inert saccharose fraction)
$a_2 \cap a_{1121} = R_9$ (reacting aldose fraction of saccharose)
$a_3 \cap a_{111} = R_{10}$ (inert fraction of powder milk)
$a_3 \cap a_{1122} = R_{11}$ (reacting amine fraction of powder milk)

Finally:

$$a_4 = R_{12} \quad a_5 = R_{13} \quad \text{and} \quad a_6 = R_{14}.$$

Construction of material-flow-systems of functional groups:

$a_1 = (R_{1,\,2,\,3,\,4,\,5,\,6,\,7})$ $a_2 = (R_{8,\,9})$
$a_3 = (R_{10,\,11})$ $a_4 = (R_{12})$ $a_5 = (R_{13})$
$a_6 = (R_{14})$ $a_7 = (R_1)$ $a_8 = (R_2)$
$a_9 = (R_{4,\,5,\,6})$ $a_{10} = (R_{3,\,6,\,7,\,13,\,14})$
$a_{11} = (R_{3,\,7,\,8,\,9,\,10,\,11,\,12})$ $a_{13} = (R_{4,\,6})$
$a_{13} = (R_3)$ and $a_{14} = (R_{4,\,6,\,14})$.

The designation used: $(R_i, R_j) = (R_{i,\,j})$.

Let us consider the ratios of the quantities of the functional groups within the respective material flow systems a_i. Then the functional group matrix can be written as:

$$\mathbf{T} = \begin{bmatrix} R_1 \\ \vdots \\ R_{14} \end{bmatrix} [a_1 \ldots a_{14}]$$

If the quantitative composition of the materials in a technological system is thoroughly known, then the fractional contributions of the respective functional groups can be determined.

("Functional groups" R_i are, in fact, functional group flows. Their dimensions, just as those of a_j are mass/time.)

It should be emphasized that information relating to structural changes and critical hierarchy levels previously determined by chemical analytical methods were used to create *Table 1*. Let us now determine the critical hierarchy levels involved in cocoa processing.

Frequently, several q values, so-called critical hierarchy bands have to be assigned to certain functional groups. Changes in the structure of the material take place simultaneously in several directions causing the above problem. However, these joint changes always have a single function.

R_1: cocoa bean hull — part of an organ, q_4
R_2: cocoa bean germ — organ, q_3
R_3: cocoa butter — phase, q_{10}
R_4: water content of cocoa bean — q_{8-11} (naturally the type of water involved in the respective cases cannot be easily identified)
R_5: decomposable carbon content — q_{11-12}
R_6: acid content of the cocoa beans. For the sake of simplicity it is assumed that the amount of volatile acids is equal to the amount of acid that reacts with alkali during the digestion step — q_{11-12}
R_7: roasting wastes contain no components of the cocoa bean tissue, are free of oil and water — part of a cell, q_8
R_8: unreacted saccharose content of the milk chocolate — phase, q_{10}

R_9: saccharose content of the milk chocolate consumed in the Maillard reaction — phase, q_{10}
R_{10}: inert fraction of milk powder in the milk chocolate. Milk powder is assumed to contain no water, this approximation is not valid all the time — phase system, p_9
R_{11}: fraction os milk powder in milk chocolate involved in the Maillard reaction — molecule, q_{11}
R_{12}: lecithin — phase system, q_9
R_{13}: alkaline compounds — molecule, q_{11}
(There is another simplification here. Alkali metals are considered cations, so they cannot enter vapours a_{14}, only the commercial cocoa powder. This, strictly speaking, is not true, but less dimensions lead to the same value, so this is a convenient simplification.)
R_{14}: water used to dissolve the alkaline compounds — molecule, q_{11}.

Material flow systems q_{1-14} as sets consisting of functional groups R_{1-14} are shown in *Table 2*. The critical hierarchy level bands assing the hierarchy level ranges in which changes of the material-flows-systems can take place.

Once **T** is determined the functional matrix equation:

$$R_{1-14} \cdot \mathbf{T} = a_{1-14}$$

is obtained. It is invariant with respect to all states of the technological system examined. This equation describes the entire material transport in the technological systems.

Essential indicators such as, e.g. the cocoa yield number, the leading indicator of the economics of cocoa processing can be calculated from it. Material consumption guidelines for various products produced in the given technological system should also be deduced from matrix **T**. The functional matrix equation is especially valuable when the technological system is connected to other systems, a frequent case in practice (e.g. a cocoa bean processing unit produces intermediates such as, e.g. chocolate mass, cocoa butter, and industrial cocoa powder, etc., for other factories).

The above decomposition into functional groups can be simplified in the case of industrial cocoa powder and dark chocolate mass containing no powder milk.

7.3 Construction of the Technological System of Cocoa Processing by Connection-Algebraical Means

Once the material-flow-systems of ANCESTOR and PICTURE are decomposed into functional groups, the material structure transformation, i.e. functional group transformation technological operations producing the PICTURE sought from the ANCESTOR given can be determined by connection algebraical means. It should be noted that connection-algebra alone is not sufficient to solve this technological problem, the actual properties of the materials transformed also have to be taken into consideration. This means that functional groups can be randomly coupled to each other like letters of the alphabet, but the technological validity of these mathematical operations has to be verified.

These algebraical transformations are shown in *Table 3* for direct and indirect milk chocolate producing technological systems. For the sake of easier comprehension symbol R_{index} is modified and 3 stands for R_3. Roman numbers are used to note the serial number of the algebraica l transformations. Their technological meaning is as follows.

Table 3

Construction of the cocoa processing technological system by connection algebra

ANCESTOR: /1/2/3/4/5/6/7 ∘ /8/9/ ∘ /10/11/ ∘ /12/ ∘ /13/ ∘ /14/
a_1 a_2 a_3 a_4 a_5 a_6

PICTURE: /1/ ∘ /2/ ∘ /4/5/6/ ∘ /3/6/7/13/14/ ∘ /3/7/8/9/10/11/12/ ∘ /4/6/ ∘ /3/ ∘ /4/6/14/
a_7 a_8 a_9 a_{10} a_{11} a_{12} a_{13} a_{14}

Algebraical transformations

/1/2/3/4/5/6/7/ $\xrightarrow{\text{Step 1}}$ /1/ ∘ /2/ ∘ /4/5/6/ ∘ /3/4/6/7/
a_1 a_7 a_8 a_9
ANCESTOR in PICTURE-state (cocoa mass or ground cocoa)

Production of cocoa powder-cocoa butter:

1/a: /3/4/6/7/ ∘ /13/ ∘ /14/ $\xrightarrow{\text{Step 2}}$ /3/6/7/13/14/ ∘ /4/6/14/
a_5 a_6 a_{14}
(PICTURE)

/3/6/7/13/14/ $\xrightarrow{\text{Step 3}}$ /3/6/7/13/14/ ∘ /3/
a_{10} a_{13}
in PICTURE-state

1/b: /3/4/6/7/ $\xrightarrow{\text{Step 4}}$ /3/4/6/7/ ∘ /3/
a_{10} a_{13}
variant in PICTURE-state

Production of milk chocolate mass

/3/4/6/7/ ∘ /3/ ∘ /8/9/10/11/ ∘ /12/ $\xrightarrow{\text{Step 5}}$ /3/4/6/7/8/9/10/11/12/
a_{13} a_2 a_3 a_4
ANCESTOR

$\xrightarrow{\text{Step 6}}$ /3/7/8/9/10/11/12/ ∘ /4/6/
a_{11} a_{12}
in PICTURE-state

Step I: separation of a_7 (cocoa bean hull), a_8 (cocoa bean germ) and roasting wastes a_9 should be separated as soon as possible. This obviously follows from the PICTURE. The material obtained in this process (3/4/6/7) is the ground meat of the cocoa bean, and its fine suspension is called cocoa paste. Besides R_4 and R_6 this material contains functional groups R_3 (cocoa butter) and R_7 (oil-free, inert, dry cocoa bean tissue) found both in cocoa powder and milk chocolate. However, their weight ratio differs in the two products. This, in fact, means that cocoa powder (a_{10}) and milk chocolate (a_{11}) productions represent two different technological approaches. At the same time production of $R_3 = a_{13}$ should also be started.

Cocoa powder (a_{10}) and cocoa butter ($R_3 = a_{13}$) are produced as follows.

Step II: a_5 and a_6 are added to intermediate (3/4/6/7). After evaporation side product a_{14} and another intermediate is formed from which:

Step III: a_{10} and $a_{13} = R_3$ can be produced (by pressing-separation and grinding operations).

As a result of variant 1/b *(Step IV)* industrial cocoa powder $(3/4/6/7) = a_{10(\text{variant})}$ and cocoa butter $a_{13} = R_3$ is formed.

Preparation of milk chocolate paste:

Step V: by adding a_2, a_3, a_4 and a_{13} to (3/4/6/7) an intermediate (chocolate cake) is produced from which in:

Step VI: a_{11} (milk chocolate paste) and a_{12} (byproduct) are obtained.

The operations listed in *Table 3* do not refer to a number of operations which do not effect the technological trail-graph, the connection relations of the materials. Thus, e.g. the difference between direct and indirect milk chocolate production cannot be seen. In the direct process product /3/4/6/7/ obtained in *Step I* is coarsely ground cocoa bean and becomes a fine suspension only in *Steps V* and *VI* when it is finely ground together with the other components. In the indirect process coarsely ground cocoa is reffined into a fine suspension as early as *Step I*. The two technologies differ by the efficiency of grinding, ground cocoa and cocoa paste feed and storage, etc. It should, however, be noted that according to the original Dutch process material /3/4/6/7/ is coarse in *Step II*. Thus, direct chocolate and cocoa powder technology is based on coarsely ground cocoa (Dutch process) while indirect chocolate and cocoa powder technology is based on cocoa mass (German process). Naturally, there are a number of "mixed" technologies, although most modern technologies are based on cocoa mass.

Table 4

New milk chocolate producing technological systems

LSCP process

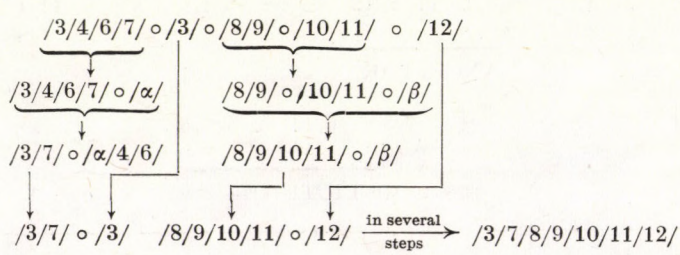

WIENER process

$$/3/4/6/7/ \circ /8/9/ \circ /10/11/ \circ /3/ \circ /L/ \xrightarrow{\text{with reflux}} /3/7/8/9/10/ \circ$$
$$\circ /L/4/6/ \circ /12/ \longrightarrow /3/7/8/9/10/11/12/$$

CADBURY/BAKER—PERKINS process

$$/3/4/6/7/ \circ /8/9/ \circ /10/11/15/ \longrightarrow /3/4/8/9/10/11/ \circ /6/7/15/ \circ /3/4/6/7/ \circ$$
$$\circ /3/ \longrightarrow /3/4/6/7/8/9/10/11/ \circ /4/6/ \circ /12/ \longrightarrow /3/7/8/9/10/11/12/$$

Milk chocolate production proper takes place in *Steps V* and *VI*. The technologies discussed above are conventional technologies. Nevertheless, there are also several modern processes, summarized in *Table 4*. They are variants of *Steps V* and *VI* (algebraical transformations). Since there are many functional groups there can be many variants.

Lindt et Sprüngli Chocolate Process (LSCP for short)

Based on fragmentary—quite obviously—literature references, LSCP can be represented by mentioned method as follows.

Reactants are separated into hydrophylic and hydrophobic materials. The carriers of functional groups 8, 9, 10 and 11 (sugar and powder milk) are hydrophilic, the carrier of functional groups 3, 4, 6 and 7 is hydrophobic (cocoa paste). Hydrophylic components are mixed with material β which promotes the Maillard reaction. Hydrophobic cocoa paste is reacted with material α. During this reaction the acidic components which have unfavourable taste are steam-distilled. From here on, milk chocolate paste is produced by conventional methods.

Wiener process

Functional groups 4/6 are stripped from the system by air (L). Oxygen advantageously effects the cocoa-taste. It can be seen that these processes carry out changes in the material-flow-systems of both the ANCESTOR and the PICTURE. Compared to conventional technology, new materials are antroduced and new byproducts are formed. A characteristic example follows here.

Cadbury/Baker-Perkins Process

Whole milk is substituted for milk powder in this process. Therefore, a further material fraction, R_{15} has to be introduced to account for the material separated during milk powder production. Milk as the material-flow-system can be described by the following set: $a_{\text{milk}} = (R_{10}, R_{11}, R_{15})$. According to *Table 4* cocoa mass, milk and sugar are homogenized, the volatile acids of cocoa mass are distilled out along with the water content of the milk resulting in the so-called milk crumb. Milk crumb then is homogenized with cocoa mass and cocoa butter. The volatile acids of cocoa mass added are stripped in a special refluxing system during continuous grinding.

The so-called Budapest process (Hungarian Candy Trust, Budapest Chocolate Factory) is a variant of the conventional milk chocolate technology resulting in the so-called "crystal-chocolate" which has a special structure.

As can be seen, the trail-graphs of material-flow-systems can be designed by connection-algebraical means. New connections or breaking of existing connections can be planned in advance. This process-graph still has to be completed, because it only contains the connection relations.

7.4 Completion of the Process-Graph of Cocoa Processing: Operations to be Carried Out on the Material-Flow-Systems

The process-graph has to be supplemented by certain technological information. It has to be mentioned at this point that this information is only of indicative value. The limit of the technological theory advanced concerning the design of

the entire technological system lies here. Nevertheless, there are design possibilities concerning the sub-units, i.e. operation units. Therefore, the sequence of the design activity is as follows: the sub-system design from the process-graph, pilot-plant sized sub-systems, and the design of the entire, full-scale technological system. Thus, it is in fact a kind of iterative job, its major and decisive milestones being the pilot-plant-scale experiments. No theory can substitute or render practical experience irrelevant.

Based on *Matrix 4*, *Table 5* contains the relations relating to the connection between the elements of the ANCESTOR and PICTURE. The most character-

Table 5

Completition of the process graph by change-elements of the cocoa processing technological system

$a_{ANCESTOR}$ →	$a_{PICTURE}$	Difference object class $\Delta(a_1)$	Changes causing differences (V_1)	Number of the technological step according to *Table 3*
1	7	D, f, c	3, 11	I.
1	8	D, f, c	3, 11	I.
1	9	h, c, D, f	3, 7, 11	I.
1	10	D, f, c	3, 11	I—II.
1	11	D, f, c	3, 11	I—III., V—VI.
1	12	h, c	3, 7, 11	I—III., V—VI.
1	13	h, d, f, c	3, 7, 11	I—III.
1	14	h, D, f, c	3, 7, 11	I—II.
2	11	D, f, c	3, 11	V—VI.
3	11	D, f, c	3, 11	V—VI.
4	11	—	—	V—VI.
5	10	c, h	7, 11	II—III.
6	10	c, h	7, 11	II—III.
← on the basis of *Matrix 4* →		on the basis of *Matrix 1*		

istic and obvious property changes obtained from the comparison of the materials of the ANCESTOR and PICTURE are listed in the column "difference-object-class".

When the elements of the "difference-object-class" are identified then false information can enter the system and important information can be unconsciously missed. Therefore, theoretical work is based on a rather insecure foundation from this point on.

Based on the "difference-object-class" the change types which bring about these changes can be selected by *Matrix 2*. This selection can introduce further errors, so it is advisable to note the following points:

— auxiliary or complementary changes might be necessary at any type of change, changes of the state variable always have to be anticipated,
— changes establishing or breaking connections are not considered again here, though they may create numerous practical problems,

– certain changes might be called upon more than once, e.g. reflux and the duration of the changes cannot be estimated theoretically either.

Generally, it can be stated that theoretical technology design must cooperate most closely with practice at this point.

Based on *Table 5*, the following conclusions can be made:

$$Step\ I \xrightarrow{v_3, v_7, v_{11}} Step\ III;\ Step\ V \xrightarrow{v_3, v_7, v_{11}} Step\ VI$$

Steps I to *III* correspond to the production of cocoa paste, cocoa butter and cocoa powder. These steps are indeed characterized by size changes, v_3, phase state changes, v_7 and chemical changes, v_{11}.

Steps V and *VI* correspond to the production of milk chocolate and the same changes are characteristic here as well.

7.5 Determination of the Degree Freedom of the Cocoa Processing Technological System Allowing for the Quantity and Quality of the Material-Flow-Systems

14 functional groups and 14 material-flow-systems have been required to describe the technological system discussed. Formally it follows that no material-flow-system (functional group) can be freely selected since there are 14 relationships (equations) for 14 functional groups.

In fact there exist a number of linear relations among the material-flow-systems, and there also should be considered while the degrees of freedom of the material-flow-systems are sought. The following statements can be made:

– a_1 (raw cocoa bean) is linearily independent from any other a_i quantity, so it should be reserved independent, i.e.
  $a_1 = b_1$ where b_i stands for the material-flow-systems during the determination of the degree of freedom
– any two of a_2, a_3 and a_4 automatically determines the third one since their ratio in milk chocolate is constant, i.e.
  $a_2 + a_3 + a_4 = b_2$
– the same applies to a_5 and a_6, i.e.
  $a_5 + a_6 = b_3$
– similarily
  $a_7 + a_8 = b_4$
– $a_9 = b_5$
– $a_{10} = b_6$; $a_{14} = b_7$
– entirely analogously
  $a_{11} + a_{12} = b_8$
– $a_{13} = b_9$

There exist quantitative, but no qualitative relations among the functional groups, i.e. no functional group can be described as the linear combination of others at the critical hierarchy level.

The following condensations can be carried out from a quantitative point of view:

$$R_1 + R_2 = f_1 \qquad R_5 = f_5$$

$$R_3 = f_2 \qquad R_8 + R_9 + R_{10} + R_{11} + R_{12} = f_6$$

$$R_7 = f_3 \qquad R_{13} + R_{14} = f_4$$

$$R_4 + R_6 = f_4$$

The cocoa processing technological system should now be scrutinized, allowing for the fact that it can be decomposed into three subsystems:

Subsystem 1 (it corresponds to *Step III* in *Table 3*)
Production of Cocoa Pate (b^+)
input: b_1 output: b_4, b_5 and b^+

Let us use only the subscripts of functional groups f_i, so

$$b_1 = (1, 2, 3, 4, 5) \quad b_4 = (1) \quad b_5 = (4, 5) \quad \text{and} \quad b^+ = (2, 3, 4)$$

The number of quantities b_i is: $SZF(b) = 4$ but it is decreased by the relationship $b_1 = b_4 + b_5 + b^+$. In fact $SZF(b) = 3$. The number of functional groups is: $SZF(f) = 5$, but since f_2 and f_3 act jointly in this subsystem (they cannot be changed separately) the number is smaller. In fact $SZF(f) = 4$ because f_2 has to be considered as a separate variable only in the entire technological system. Thus $SZF_1 = SZF(f) - SZF(b) = 1$. This means that the quantity of as few as a single functional group unambiguously determines technological *Subsystem 1.*

Subsystem 2 (it corresponds to *Step II* and *III* in *Table 3*)
Production of Cocoa Powder and Cocoa Butter
input: b^+ output: b_6, b_7 and b_9

$SZF(b) = 3$ because it holds that
$b^+ = b_6 + b_7 + b_9$ $b^+ = (2, 3, 4)$ $b_6 = (2, 3, 4, 7)$
$b_7 = (4, 7)$ and $b_9 = (2)$.
Thus $SZF(f) = 4$ and $SZF_2 = 4 - 3 = 1$.

This means that the quantity of as few as a single functional group unambiguously determines technological *Subsystem 2.*

Subsystem 3 (it corresponds to *Step V* and *VI* in *Table 3*)
Production of Milk Chocolate Paste
input: b_2, b^+ and b_9 output: b_8

$SZF(b) = 3$ since $b_2 + b^+ + b_9 = b_8$; $b_2 = (6)$; $b^+ = (2, 3, 4)$;
$b_9 = (2)$ and $b_8 = (2, 3, 4, 6)$, i.e. $SZF(f) = 4$.
Thus $SZF_3 = 4 - 3 = 1$.

This means that the quantity of as few as a single functional group unambigously determines technological *Subsystem 3.*

The Degree of Freedom of the Entire Technological System

The continuity equations constructed for the subsystems have to be supplemented by two further relationships to obtain the mass balance equation and the degrees of freedom of the entire technological system

$$b_1^+ = b_2^+ + b_3^+,$$

i.e. none of b^+ (cocoa paste or ground cocoa) transferred among *Subsystem 1, 2*

and *3* leaves the entire system, so it does not appear either in the ANCESTOR or the PICTURE.

The other relationship is:

$$b_9^3 = b_9^3 + b_9^{\text{PICTURE}}$$

Let us then set $b_9^{\text{PICTURE}} = 0$, i.e. the system is closed with respect to b_i, both cocoa mass and cocoa butter. Then the following modification makes the system determined:

1. Let us set at $\text{SZF}_1 = 1$ of *Subsystem 1* any of the following qualities – since they are quantitatively linearily dependent –
   - cocoa bean (b_1),
   - cocoa shell + cocoa germ (f_1),
   - roasting gases (b_5).

Any of these defines the quantity of cocoa paste (b^+) though there is an independent functional group among them. So, the amount of cocoa powder (b_6) and chocolate (b_8) which can be produced from it can be determined as follows.

Let the amount of cocoa mass required for the chocolate be x, the cocoa butter be c_x and the amount of cocoa powder produced during the production of C_x amount of cocoa butter be K_x then the amount of all the cocoa paste to be used becomes $x + Cx + Kx$, a known value. Since C and K are material norm coefficients a linear equation is obtained for x.

The condition of the solution is that no cocoa butter is removed from the system, all that is formed in the pressing step is used for chocolate production, i.e. $b_9^{\text{PICTURE}} = 0$.

2. The degree of freedom of *Subsystem 2* is $\text{SZF} = 1$. If any of the following quantities is set then *Subsystem 2* becomes determined since these quantities are linearily dependent:
   - cocoa powder (b_6),
   - alkali (f_7),
   - process vapours (b_7).

The amount of cocoa bean (b_1) to be used for cocoa powder production directly follows from the material norms. The amount of cocoa butter produced in the pressing step determines the amount of chocolate (b_8) which can be produced in *Subsystem 3*. The amount of cocoa paste required for chocolate production is added to the amount of cocoa bean determined earlier, so all three subsystems become determined.

3. The degree of freedom of *Subsystem 3* is $\text{SZF} = 1$. Only $f_6 = (\text{sugar} + \text{powder milk} + \text{lecithin})$ appears in the ANCESTOR as an independently dosable and changeable functional group.

If its amount or the amount of milk chocolate mass to be produced, which is proportional to it is set, then the entire technological system becomes determined. The amount of cocoa paste (b^+) and cocoa butter ($f_2 = b_9$) required for milk chocolate (b_8) is determined by mass norms. The amount of cocoa paste determines that of cocoa bean (b_1) while the amount of cocoa butter determines that

of cocoa paste (and correspondingly, cocoa bean) required in the pressing step. This also determines the amount of cocoa powder formed. Thus all three technological subsystems and the entire system become determined.

It can be concluded that the cocoa processing technological system has, with respect to the free selection of the quantities of material flows or material-flow-systems, one degree of freedom, i.e. $SZF = 1$.

It should be noted that when cocoa butter ($b_9^{PICTURE}$) or cocoa paste ($b_{PICTURE}^{+}$) is to be produced or these materials are received from an external system (i.e. these materials show up in the ANCESTOR as well) then the material-flow-systems have to be selected according to the technological objective. The situation is different if cocoa powder or chocolate is to be produced.

РЕЗЮМЕ

В третьей части данной серии статей рассматривается технологическая система переработки какао, определяются системы массовых потоков и функциональные группы переработки какао; описываются далее технологические процессы производства какаовой массы, масла какао и изготовляемого для торговых целей какаового порошка, приводятся также новейшие тенденции в области технологий производства шоколада. И наконец, в статье определяется степень свободы технологической системы по переработке какао.

HUNGARIAN JOURNAL
OF INDUSTRIAL CHEMISTRY
VESZPRÉM
Vol. 6. pp. 145–154 (1978)

GENERAL PROPERTIES OF TECHNOLOGICAL SYSTEMS. IV.

F. MOHOS

(Budapest Chocolate Factory of the Hungarian Candy Trust)

Received: September 27, 1977.

Conventional cocoa processing technology is reviewed and two practical examples are presented to demonstrate the use of the technological representation advanced for the design of operation units in which alkali preparation and the refining of the cocoa mass take place.

7.6 Detailed Description of the Cocoa Processing Technological System

So far only the raw materials, end products and wastes have been assumed to be known in the course of this study on the cocoa processing technological system. This assumption is no longer necessary since all teh statements concerning the entire system have been made. The known technologies of cocoa processing are extremely refined. These technologies are described here by the use of the functional groups presented and finally two special practical problems are solved by BLICKLE's theory.

7.6.1 Production of Cocoa Paste

This description covers all the important relations necessary for the design of the operation units involved. Only the subscripts (numbers) are used for the functional groups, according to *Part 3* (e.g. 3 stands for R_3). The heterogeneous and homogeneous relations symbolized by $\rightarrow$ and $\Rightarrow$ according to BLICKLE'S theory are symbolized by / and // here, for the direction is rarely of any importance now (these are more universal connection algebraical signs). Material flow systems are separated by "$\circ$".

This process is the detailed description of technological

Step I of *Part 3*.

Step I: $/1/2/3/4/5/6/7/ \rightarrow \underset{a_1}{/1/}\ \underset{a_7}{/2/}\ \underset{a_8}{\circ /4/5/6/}\ \underset{a_9}{\circ /3/4/6/7/}$ (cocoa paste)

Operation unit 1:

Roasting of cleaned cocoa beans takes place here.

Mappings: – temperature rise (l_6)
– heterogeneous chemical reaction (roasting) (l_{30})
– temperature decrease (l_6^{-1})

$$l_6 = (v_5 \wedge \delta_2)^{t_0 \to t_m} : \begin{bmatrix} /1/2/3/4/5/6/7/ \\ /1/2/3/4/5/6/7/ \end{bmatrix},$$

where:

t_0: initial temperature
t_m: maximum temperature of roasting

$$l_3 = (v_{11} \wedge \delta_3)^b : \begin{bmatrix} /1/3/4/5/6/7/ \\ /1/2/3/4/6/7/ \circ /4/5/6/ \end{bmatrix},$$

where:

b: the amount of roasting gases

$$1_6^{-1} = (v_5 \wedge \delta_2)^{t_m \to t_2} : \begin{bmatrix} /1/2/3/4/6/7/ \\ /1/2/3/4/6/7/ \end{bmatrix},$$

where: t_2: the temperature at the end of cooling.
Resultant mapping:

$$L_1 = (l_6 \odot l_{30}) \oplus l_6^{-1} \tag{17}$$

Operation unit 2:

Pre-grinding and hulling of roasted and cooled cocoa bean.

Mappings: – grinding (l_2)
– hulling (l_{10})

$$l_2 = (v_3 \wedge \delta_1)^{d_1} : \begin{bmatrix} /1/2/3/4/6/7/ \\ /1/2/3/4/6/7/ \end{bmatrix},$$

where: d_1: characterizes particle size changes

$$l_{10} = (v_3 \wedge \delta_3) : \begin{bmatrix} /1/2/3/4/6/7/ \circ (\text{air}) \\ /4/ \circ /2/ \circ (\text{air}) \circ /3/4/6/7/ \end{bmatrix},$$

For the sake of simplicity ground cocoa is assumed to contain on hull (1) and germ (2), otherwise these should also show up in the simple /3/4/6/7/ notation. This waste fraction is conveniently included in /7/ as a convention. Resultant mapping:

$$L_2 = l_2 \oplus l_{10} \tag{18}$$

(Air used for the separation is not considered here as a functional group, though strictly speaking, it should be.)

Operation unit 3:

Pre-grinding and fine grinding of ground cocoa.

Mappings: — warming up (l_6)
— grinding (l_2)

$$l_6^1 = (v_5 \wedge \delta_2)^{\Delta t_1} : \begin{bmatrix} /3/4/6/7/ \\ /3/4/6/7/ \end{bmatrix},$$

where: Δt_1: temperature rise

$$l_2^1 = (v_3 \wedge \delta_1)^{d_2} : \begin{bmatrix} /3/4/6/7/ \\ /3/4/6/7/ \end{bmatrix},$$

where: d_1: characterizes grinding.

l_6^2 = as l_6^1 but characterized by Δt_2
l_2^2 = as l_2^1 but characterized by d_3.

Resultant mapping:

$$L_3 = (l_6^1 \odot l_2^1) \oplus (l_6^2 \odot l_2^2) \tag{19}$$

7.6.2. Chemical Treatment of Cocoa Paste, Production of Cocoa Butter and Commercial Cocoa Powder

This process corresponds to technological *Step II* and *III* in *Table 3*.
Step II: Only case 1/a is treated here. Case 1/b is similar but simpler:

$$/3/4/6/7/ \circ /13/ \circ /14/ \rightarrow /3/6/7/13/14/ \circ /4/6/14/$$
$$a_5 \quad a_6 \qquad\qquad\qquad a_{14}$$

Operation unit 4:

Chemical treatment of cocoa paste (e.g. by aqueous caustic solution).

Mappings: — warming up (l_6)
— homogenization (l_{22})
— exchange decomposition (l_{30})
— chemical reactions (l_{31})
— steam distillation (l_8)
— pressure venting (l_{17})

$$l_6 = (v_5 \wedge \delta_2)^{\Delta t_3} : \begin{bmatrix} /3/4/6/7/ \\ /3/4/6/7/ \end{bmatrix},$$

where Δt_3: temperature rise.

$$l_{22} = (v_8 \wedge \delta_4) : \begin{bmatrix} /3/4/6/7/ \circ /13/14/ \\ /3/4/6/7/13/14/ \end{bmatrix},$$

$$l_{30} = (v_{11} \wedge \delta_4) : \begin{bmatrix} /3/4/6/7/13/14/ \\ /3/4/6/7/13/14/ \end{bmatrix},$$

reaction of (6) and (13).

$$l_{31} = (v_{11} \wedge \delta_2) : \begin{bmatrix} /3/4/6/7/13/14/ \\ /3/4/6/7/13/14/ \end{bmatrix},$$

e.g. reactions of flavonoids.

$$l_8 = (v_6 \wedge \delta_3): \begin{bmatrix} /3/4/6/7/13/14/ \\ /3/6/7/13/14/ \rightarrow /4//6//14/ \end{bmatrix}$$

$$l_{17} = (v_8 \wedge \delta_3): \begin{bmatrix} /3/6/7/13/14 \rightarrow /4//6//14/ \\ /3/6/7/13/14/ \circ /4//6//14/ \end{bmatrix}$$

Resultant mapping:

$$L_4 = l_6 \oplus (l_{22} \odot l_{30} \odot l_{31}) \oplus (l_8 \odot l_{17}) \tag{20}$$

Step III: Production of cocoa butter

$$/3/6/7/13/14/ \xrightarrow{\text{Step III}} /3/6/7/13/14/ \circ /3/_{a_3}$$

Operation unit 5:

Cooling after alkali digestion, decreasing the butter content of cocoa by pressing.

Mappings: – cooling (l_6^{-1})
– pressure rising (l_8)
– separation (l_{17})

$$l_6^{-1} = (v_5 \wedge \delta_2)^{\Delta t_4}: \begin{bmatrix} /3/6/7/13/14/ \\ /3/6/7/13/14/ \end{bmatrix}$$

where Δt_4: decrease of temperature.

$$l_8 = (v_6 \wedge \delta_2)^{\Delta p}: \begin{bmatrix} /3/6/7/13/14/ \\ /3/6/7/13/14/ \end{bmatrix}$$

where Δp: pressure rise

$$l_{17} = (v_8 \wedge \delta_3)^{q}: \begin{bmatrix} /3/6/7/13/14/ \\ /3/6/7/13/14/ \end{bmatrix}$$

where q: is the percentage of cocoa butter in the pressed cake.

Resultant mapping:

$$L_5 = l_6^{-1} \oplus (l_8 \odot l_{17}) \tag{21}$$

Operation unit 6:

Cooling of pressed cocoa cake, rough and fine grinding, thermostation.

Mappings: – cooling (l_6^{-1})
– grinding (l_2)
– grinding (l_2)
– cooling (l_6^{-1})
– phase state change of cocoa butter (l_9)
– formation of stable (β), crystalline cocoa butter (l_4)

$$l_{6,1}^{-1} = (v_5 \wedge \delta_2)^{\Delta t_4}: \begin{bmatrix} /3/6/7/13/14/ \\ /3/6/7/13/14/ \end{bmatrix}$$

where Δt_5: characterizes cooling

$$l_{2,1} = (v_3 \wedge \delta_1)^{d_3} : \begin{bmatrix} \text{(as above)} \\ \text{(as above)} \end{bmatrix}$$

where d_3: characterizes grinding

$$l_{2,2} = (v_3 \wedge \delta_1)^{d_4} : \begin{bmatrix} \text{(as above)} \\ \text{(as above)} \end{bmatrix}$$

where d_4: characterizes grinding

$$l_{6,2}^{-1} = (v_5 \wedge \delta_2)^{\Delta t_6} : \begin{bmatrix} \text{(as above)} \\ \text{(as above)} \end{bmatrix}$$

where Δt_6: characterizes cooling

$$l_9 = (v_7 \wedge \delta_1) : \begin{bmatrix} \text{(as above)} \\ \text{(as above)} \end{bmatrix}$$

$$l_4 = (v_{11} \wedge \delta_2) : \begin{bmatrix} \text{(as above)} \\ \text{(as above)} \end{bmatrix}$$

where β: stable crystalline cocoa butter

Resultant mapping:

$$L_6 = l_{6,1}^{-1} \oplus l_{2,1} \oplus l_{6,2}^{-1} \oplus (l_{2,2} \odot l_9 \odot l_4) \tag{22}$$

7.6.3 Production of Milk Chocolate

This process is called *Steps V* and *VI* in *Table 3. Steps V* and *VI:* Preparation of milk chocolate paste.

$$/3/4/6/7/ \circ /3/ \circ /8/9/ \circ /10/11/ \circ /12/ \xrightarrow{\text{Step V}} /3/4/6/7/8/9/$$

$$/10/11/12/ \xrightarrow{\text{Step VI}} /3/7/8/9/10/11/12/ \circ /4/6/.$$

Operation unit 7:

Preparation of milk chocolate cake.

Mapping: — homogenization (l_{25})

$$l_{25} = (v_8 \wedge \delta_4) : \begin{bmatrix} /3/4/6/7/ \circ /3/ \circ /8/9/ \circ /10/11/ \\ /3/4/6/7/8/9/10/11/12/ \end{bmatrix}$$

Resultant mapping:

$$L_7 = l_{25} \tag{23}$$

Operation unit 8:

Fine grinding of milk chocolate cake.

Mappings: — grinding (l_2)

$$l_2 = (v_3 \wedge \delta_1)^{d_5} : \begin{bmatrix} /3/4/6/7/8/9/10/11/ \\ /3/4/6/7/8/9/10/11/ \end{bmatrix}$$

where d_5: characterizes grinding.

Resultant mapping:

$$L_8 = l_2 \tag{24}$$

Operation unit 9:

Refining of milk chocolate paste and production of end product *(Step VI)*.

Mappings: – homogenization (l_{25})
– oxidation (l^1_{31})
– Maillard reaction (l^2_{31})
– pressure venting (l_8)
– decomposition (l_{17})
– homogenization (emulgeation) (l_{25})

$$l_{25} = (v_8 \wedge \delta_4): \begin{bmatrix} /3/4/6/7/8/9/10/11/ \circ /3/ \\ /3/4/6/7/8/9/10/11/ \end{bmatrix}$$

$$l^1_{31} = (v_{11} \wedge \delta_2): \begin{bmatrix} /3/4/6/7/8/9/10/11/ \\ /3/4/6/7/8/9/10/11/ \end{bmatrix}$$

aroma-developing step

$$l^2_{31} = (v_{11} \wedge \delta_2): \begin{bmatrix} /3/4/6/7/8/9/ \Rightarrow 11/10/ \\ /3/4/6/7/8/9/ \Rightarrow 11/10/ \end{bmatrix}$$

$$l_8 = (v_6 \wedge \delta_3)^{\Delta P_2}: \begin{bmatrix} (\text{as above}) \\ (\text{as above}) \end{bmatrix}$$

where Δp_2: pressure venting.

$$l_{17} = (v_8 \wedge \delta_3): \begin{bmatrix} /3/4/6/7/8/9 \Rightarrow 11/10/ \\ /3/7/8/9 \Rightarrow 11/10/ \circ /4 \Rightarrow 6/ \end{bmatrix}$$

$$l_{25} = (v_8 \wedge \delta_4): \begin{bmatrix} /3/7/8/9 \Rightarrow 11/10/ \circ /12/ \\ /3/7/8/9 \Rightarrow 11/10/12/ \end{bmatrix}$$

Resultant mapping:

$$L_9 = l_{25} \oplus (l_{31} \odot l^2_{31} \odot l_8 \odot l_{17}) \oplus l_{25} \tag{25}$$

7.6.4 Mapping Series of Cocoa Processing

Let $$\bigcup_{i=1}^{n} L_i = L_1 \oplus L_2 \oplus \ldots \oplus = L_n$$

then the mapping series of

– cocoa paste production (technological *Step I*) is

$$\mathcal{L}_I = \bigcup_{i=1}^{3} L_i \tag{26}$$

– cocoa butter and commercial cocoa powder production (*Steps II* and *III*) is

$$\mathcal{L}_{II-III} = \bigcup_{i=4}^{6} L_i \tag{27}$$

and

$$\mathcal{L}_{\text{I-III}} = \bigcup_{i=1}^{6} L_i \tag{28}$$

— milk chocolate production (*Steps V* and *VI*)

$$\mathcal{L}_{\text{V-VI}} = \bigcup_{i=7}^{9} L_i \tag{29}$$

$$\mathcal{L}_{\text{I, V-VI}} = \left(\bigcup_{i=1}^{3} L_i\right) \oplus \left(\bigcup_{j=7}^{9} L_j\right) \tag{30}$$

7.7 Design of Milk Chocolate Paste Refining Operation Unit According to Blickle's *Theory [1, 2]*

Operation unit 9, a unit used to refine milk chocolate mass and called "conches" (from the Spanish concha) was discussed in Chapter 7.6.3. It is shown here that the description of processes as advanced here allows for the selection of all those apparatus types which can be thought of at all for this purpose. This also obviously indicates the direction apparatus development has to go.

To select the operation unit, the external structure (b) of material flows processed has to be known (cf. Chapters 2.33 and 4 in *Parts 1* and *2*, respectively). The types (v_i) and characteristics (δ_j) of changes expected to take place in the operation unit also have to be known.

Chocolate paste in *Operation unit 9* is viscous, its external structure can be characterized as:

$$b_3 = \beta_2 \wedge [\beta_1 v \beta_2 v \beta_3] \wedge \gamma_2$$

The external technological structure remains practically unchanged during the entire operation.

Apart from the external structure all ($v_i \wedge \delta_j$) coefficients of all the mappings are necessary for the z mappings, so the resultant Z mapping of the operation unit to be designed becomes:

$$Z_{(9)} = (v_8 \wedge \delta_4)^2 (v_{11} \wedge \delta_2)^2 (v_6 \wedge \delta_3)^2 (v_8 \wedge \delta_3)(b_3 \to b_3) \tag{31}$$

From here on all references are made to [1], so the whole process of solution can be followed because due to the excessive volume of the relationships no details can be shown here. Since reference is no longer made to functional groups letter R stands for one of the elements of the apparatus-property-set defined by Blickle [1].

Symbols: in general ${}_{1-3}R_1$ stands for ${}_1R_1$, ${}_2R_1$, ${}_3R_1$, etc. To enable the process to be grasped more easily the steps are numbered.

Step I.: R_1 belonging to external technological structure b_3 is determined (p: 85—86)

$${}_3R_1 \to {}_3R_1^+$$

$${}_{10}R_1 \to {}_9R_1^+$$

Step II.: R_3 belonging to $(v \wedge \delta)$ values is determined (p: 87.)

$$(v_8 \wedge \delta_4) \rightarrow {}_9R_3$$

$$(v_{11} \wedge \delta_2) \rightarrow {}_{12}R_3$$

$$(v_6 \wedge \delta_3) \rightarrow {}_6R_3$$

$$(v_8 \wedge \delta_3) \rightarrow {}_8R_3$$

Exponents of the changes only mean that there are several of the same type of changes taking place, which obviously cause no change in the apparatus.

Step III.: R_2 can be determined after R_3 (p: 91.)

$${}_9R_3 \rightarrow {}_{1,2,3,6,7}R_2$$

$${}_{12}R_3 \rightarrow {}_{1\text{-}9}R_2$$

$${}_6R_3 \rightarrow {}_{1\text{-}9}R_2$$

$${}_8R_3 \rightarrow {}_{2,3,6,7}R_2$$

Step IV.: R_2 can be determined from R_1 (p: 91.)

$${}_3R_1^+ \rightarrow {}_{1\text{-}4}R_2$$

$${}_9R_1^+ \rightarrow {}_{1\text{-}3}R_2$$

Step V.: The section of R_2 values determined in *Steps III* and *IV* is determined, i.e. the common part of ${}_2R_2$ and ${}_3R_2$.

Step VI.: R_4 is determined from R_3 (p: 91.).

$${}_9R_3 \rightarrow {}_{1\text{-}17;\,0}R_4$$

$${}_{12}R_3 \rightarrow {}_{1\text{-}6,\,9\text{-}17;\,0}R_4$$

$${}_6R_3 \rightarrow {}_{1\text{-}3,\,5}R_4$$

$${}_8R_3 \rightarrow {}_{1\text{-}12,\,17}R_4$$

Step VII.: R_4 is determined from R_1^+ (p: 91.)

$${}_3R_1^+ \rightarrow {}_{1,2,3,4,7\text{-}12}R_4$$

$${}_9R_1^+ \rightarrow {}_{1,2,3,5,7\text{-}9}R_4$$

Step VIII.: Determination of the section of R_4 values determined in *Steps VI* and *VII:* ${}_1R_4$ and ${}_3R_4$.

Step IX.: Determination R_5 from R_2 (p: 91.)

$${}_2R_2 \rightarrow {}_{1\text{-}10,\,x}R_5$$

$${}_3R_2 \rightarrow {}_{1\text{-}4,\,9,\,10,\,x}R_5$$

Step X.: Determination of R_5 from R_4 (p: 91.)

$${}_1R_4 \rightarrow {}_{1\text{-}10}R_5$$

$${}_3R_4 \rightarrow {}_{3,4,7,8}R_5$$

Step XI.: Determination of the section of R_5 values calculated in *Steps IX* and *X:*

$$_3R_5 \quad \text{and} \quad _4R_4$$

This is the solution of the problem. It means that refining can be carried out in an operation unit which is characterized as follows:

Processes (material-flow-system characteristics):

$$_3R_1^+ \quad \text{and} \quad _9R_1^+ \quad \text{(cf. p. 86)}$$

Operation modes:

$$_2R_2 \quad \text{and} \quad _3R_2 \quad \text{(cf. p. 87)}$$

Chemical operations:

$$_9R_3, \quad _{12}R_3, \quad _6R_3 \quad \text{and} \quad _8R_3 \quad \text{(cf. p. 87)}$$

Energies:

$$_1R_4 \quad \text{and} \quad _3R_4 \quad \text{(cf. p. 87—88)}$$

Apparatuses:

$$_3R_5 \quad \text{and} \quad _4R_5 \quad \text{(cf. p. 88—89)}$$

All the characteristics of the operation unit designed can be found at the respective places referred to, so there is no need to publish these lengthy items here.

The characteristics thus calculated fully agree with principles followed in the course of practical refining unit development.

7.8 Design of the Operation Unit Used for the Alkali Treatment of Cocoa Mass (No. 4 in Chapter 7.6.2) According to Blickle's Theory

The calculations shown in Chapter 7.7 are applied to *Operation unit 4.* The practical forms of these two operation units apparently followed two separate lines of development. However, the essential similarity of the operations to be carried out in the two units becomes more and more manifest, even to that degree that apparatuses are becoming more similar.

$$Z_{(4)} = (v_8 \wedge \delta_4)(v_{11} \wedge \delta_4)(v_{11} \wedge \delta_2)(v_6 \wedge \delta_3)(v_8 \wedge \delta_3)(b_3 \rightarrow b_3) \tag{32}$$

Omitting the details of the calculations, the result becomes:

Processes:

$$_3R_1^+ \quad \text{and} \quad _9R_1^+$$

Operation modes:

$$_2R_2 \quad \text{and} \quad _3R_2$$

Chemical operations:

$$_{3,6,8,9,5,12}R_3$$

Energies:

$$_1R_4$$

Apparatuses:

$$_{1-4,\,9,\,10}R_5$$

It can be shown with the help of [1] that this result is very similar to that of the refining units.

8. Summary

A technological theory was advanced in *Part 1* and *2* of this series. It is based on BLICKLE and co-workers' results [1, 2], only the presentation mode is different. A uniform treatment was attempted of materials of biological origin. This treatment seems applicable to show the essentials of both chemical and related (e.g. food processing, etc.) technologies.

The treatment makes use of the terms hierarchy level and functional group, and the connection algebra defined for the functional groups. This apparatus seemed indispensable to treat as exactly as possible the most important technological problems of cocoa processing. *Part 3* discusses the technological variants of cocoa processing as results naturally following from connection algebra. The limits of connection algebraical treatment are also carefully presented. Conventional cocoa processing technology is treated in detail in *Part 4*. Two examples demonstrate the use of this technological representation for the design of operation units.

REFERENCES

1. BLICKLE, T. and SEITZ, K.: Modern Algebraical Methods in Technical Chemistry (A modern algebrai módszerek felhasználása a műszaki kémiában.) Műszaki Könyvkiadó, Budapest, 1975.
2. POLINSZKY, K. (ed.): Structure of the Systems of Technical Chemistry. Scientific Results of the Research Institute for Technical Chemistry of the Hungarian Academy of Sciences. *Part 2.*
(Műszaki Kémiai rendszerek szerkezete. MTA MÜKKI tudományos eredményei II. Szerk.: POLINSZKY K.) Veszprém, 1974.

РЕЗЮМЕ

В четвёртой части серии статей даётся подробное изложение традиционной технологии переработки какао, и воспользовавшись двумя примерами, взятыми из практики, освещается возможность применения этого вида технологий для проектирования процессионных единиц щелочной обработки консоля и какаовой массы.

HUNGARIAN JOURNAL
OF INDUSTRIAL CHEMISTRY
VESZPRÉM
Vol. 6. pp. 155–162 (1978)

UNTERSUCHUNGEN DER ZUR DEHYDRIERUNG VON *n*-HEXAN VERWENDETEN KATALYSATOREN

Cs. Csikós und J. Báthory

(Ungarisches Erdöl und Erdgas Forschungsinstitut, Veszprém)

Eingegangen am 2 Dezember, 1977

Monoolefine mit langen geraden Kohlenstoffketten werden neuerdings durch katalytische Dehydrierung von *n*-Paraffinen gewonnen. In unseren Versuchen wurde mit Hilfe der Impulstechnik die Dehydrierung von *n*-Hexan als Modellreaktion und die Wirkungsweise von Katalysatoren untersucht, welche 4 Komponenten, das heißt an γ-Al_2O_3 Trägern Platin (als aktives Metall), Arsen beziehungsweise Wismut (als katalytische Inhibitoren) sowie Lithium (als Promotor) enthielten. Es wurden die günstigste Zusammensetzung der Katalysatoren sowie die zweckmäßigsten Temperaturgebiete der Reaktion ermittelt. Es wurde festgestellt, daß diese Parameter bei verschiedenen Katalysatoren zusammenfielen, die Ausbeute an *n*-Hexanen sowie die Selektivität der Olefinbildung aber gleichzeitig bedeutende Unterschiede aufweisen.

Die Entwicklung der Weltproduktion an *n*-Kohlenwasserstoffen weist eine eindeutig zunehmende Tendenz auf, und hat zwei richtige Bedarfsgebiete: die petrolchemische Industrie und die drängende Lebensmittelnot. *n*-Alkane verschiedener Kohlenstoffatomzahl werden zur Zeit mit Hilfe von zwei Verfahren, durch die Harnstoff-Adduktbildung und das Molsiebverfahren hergestellt, und wie soeben erwähnt teils über Fermentationsverfahren, teils chemisch weiter verarbeitet. Die Entwicklung auf dem Gebiet der *n*-Kohlenwasserstofferzeugung der Welt ist in *Abbildung 1* dargestellt, wo beide Verfahren auch getrennt veranschaulicht wurden. Die Welterzeugung der *n*-Kohlenwasserstoffe erreichte innerhalb eines Jahrzehntes die zwölffache Menge und beträgt zur Zeit 3,4 Millionen Jahrestonnen.

Das Endziel der petrolchemischen Verarbeitung besteht in der Gewinnung von Detergentien, Weichmachern, biologisch abbaufähigen Waschmitteln sowie von einigen nützlichen Intermediären für Synthesen.

Die hierzu meist verwendeten *n*-Monoolefine werden aus *n*-Alkanen wirtschaftlich durch Dehydrierung gewonnen. Darüber berichteten in den letzten Jahren zahlreiche Arbeiten. Sämtliche Verfahren arbeiten mit kurzen Kontaktzeiten bei nahezu atmosphärischem Druck, unter Anwendung einer weitgehenden

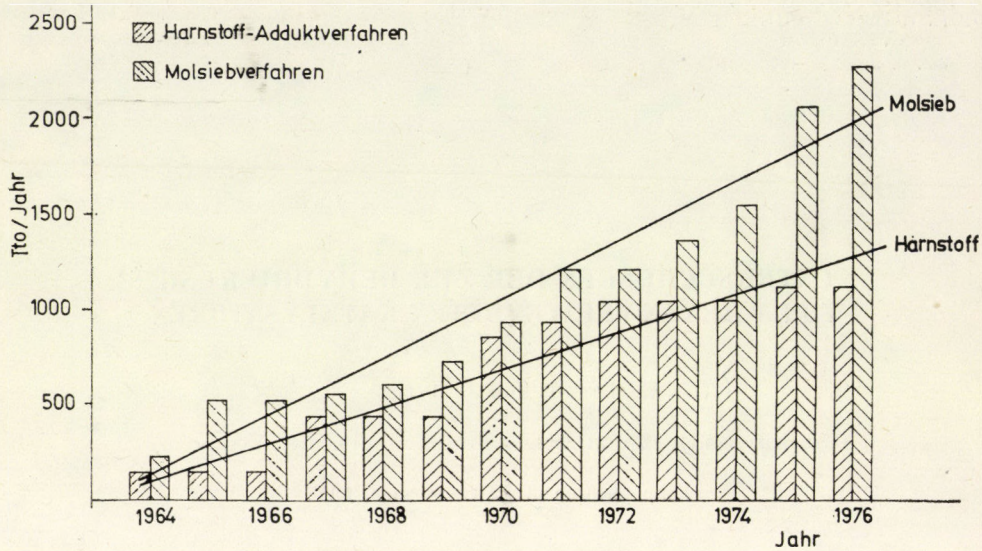

Bild 1.
Entwicklung der *n*-Kohlenwasserstoff-Erzeugung

Verdünnung des Kohlenwasserstoffs mit Wasserstoff und Anwendung eines Mehrkomponenten-Katalysators [1].

Zweck unserer Arbeit bestand in der Untersuchung des Einflusses der Katalysatorzusammensetzung auf die Dehydrierung von *n*-Hexan als Modellsubstanz mit Hilfe der Impulstechnik [2].

Versuchsdurchführung

Die Vierkomponenten-Katalysatoren wurden im Laboratorium durch Imprägnierung hergestellt. Auf einem technischen γ-Al_2O_3-Träger enthielten sie als aktives Metall Platin, als Promotor Lithium und als Inhibitor Arsen oder Wismut. Die Konzentrationsgrenzen lagen bei 0,05—2,0 Gew. % Platin, 0—1,0 Gew. % Lithium und bei einem Inhibitor/Platin-Atomverhältnis von 0—1,0. Das Trägermaterial bestand aus zwei verschiedenen (A und B) Sorten von γ-Al_2O_3.

Die Testuntersuchung der Katalysatoraktivität erfolgte mit Hilfe der Impulstechnik in einem Mikroreaktor von 0,4 cm³ Inhalt und einem dazu gekoppelten Gaschromatograph. Das in den Trägergasstrom zugegebene *n*-Hexan (5 μl) wurde durch den Wasserstoff in den Mikroreaktor gespült, die erhaltenen Produkte wurden als einzelne Komponenten detektiert. Es wurden vier Hauptkomponenten erhalten, und zwar: nicht näher definierbare Krakkprodukte, unreagiertes *n*-Hexan, *n*-Hexengemische und Benzol. Die Aktivität des Katalysators wurde jeweils durch die Konversion, die Hexenausbeute und die Selektivität der Reaktion charakterisiert [3].

Die Reproduzierbarkeit der Messungen war beruhigend, wenn die Untersuchungen mit stets frischen Kontakten wiederholt wurden, sonst waren die Ergebnisse vom Vorleben des Katalysators abhängig.

Versuchsergebnisse

a) Einfluß des Platingehaltes

Der Einfluß des Platingehaltes wurde bei einem durch Vorversuche festgelegten Arsen/Platin beziehungsweise Wismut/Platin-Atomverhältnis von 0,3 und einer Lithiumkonzentration von 0,5% an γ-Al_2O_3 A und B bestimmt. Die Ergebnisse sind in *Abbildung 2* dargestellt.

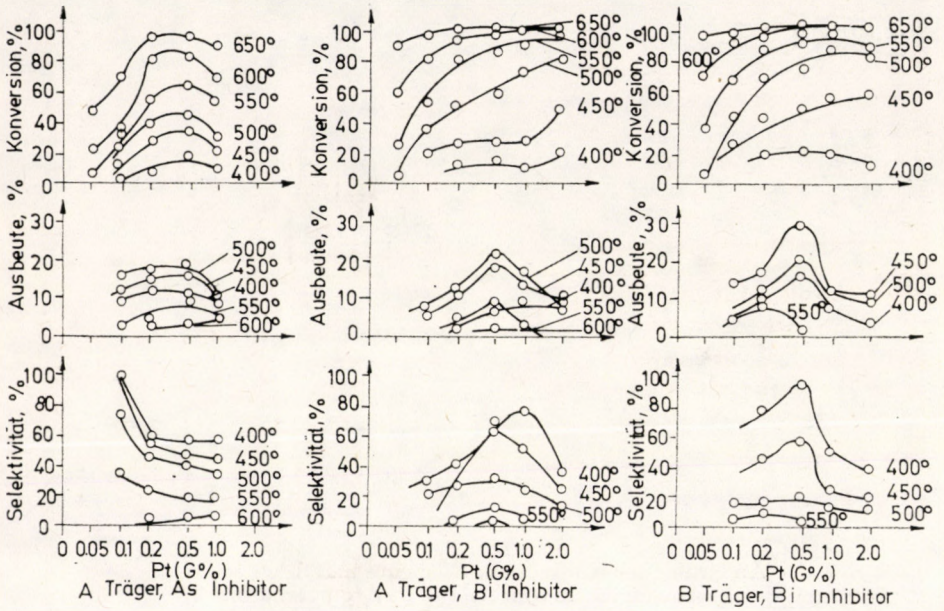

Bild 2.
Änderung der Konversion, Ausbeute und Selektivität in Abhängigkeit vom Pt-Gehalt

Demnach gelangten also zwei Träger und zwei Inhibitoren zur Untersuchung und die Ergebnisse sind in Abhängigkeit vom logarithmisch aufgetragenen Platingehalt bei verschiedenen Temperaturen angegeben. Mit zunehmendem Platingehalt nimmt die Konversion gleichmäßig zu oder besitz bei 0,2—1,0 Gew.% Pt ein flaches Maximum. Die Ausbeutekurven wiesen bei 0,5% Pt ausgeprägte Maximas auf, welche bei 450 und 500 °C oberhalb 20% *n*-Hexen lagen. Der Ablauf der Selektivitätskurven war bei den beiden Inhibitoren verschieden. Mit Wismut wurden auch hier ausgeprägte Maximas erhalten, bei Arsen war

der Verlauf monoton fallend. Unabhängig also vom Träger und vom Inhibitor bestimmen Ausbeute und Selektivität zusammen ein eindeutig optimales Verhalten bei Platingehalten um 0,5%.

b) Einfluß des Inhibitors

Die Wirkung des Inhibitors bei einem Platingehalt von 0,5% und einem Lithiumgehalt von ebenfalls 0,5% ist in *Abbildung 3* für verschiedene Träger und Temperaturen dargestellt. Es ist überraschend, daß unabhängig vom

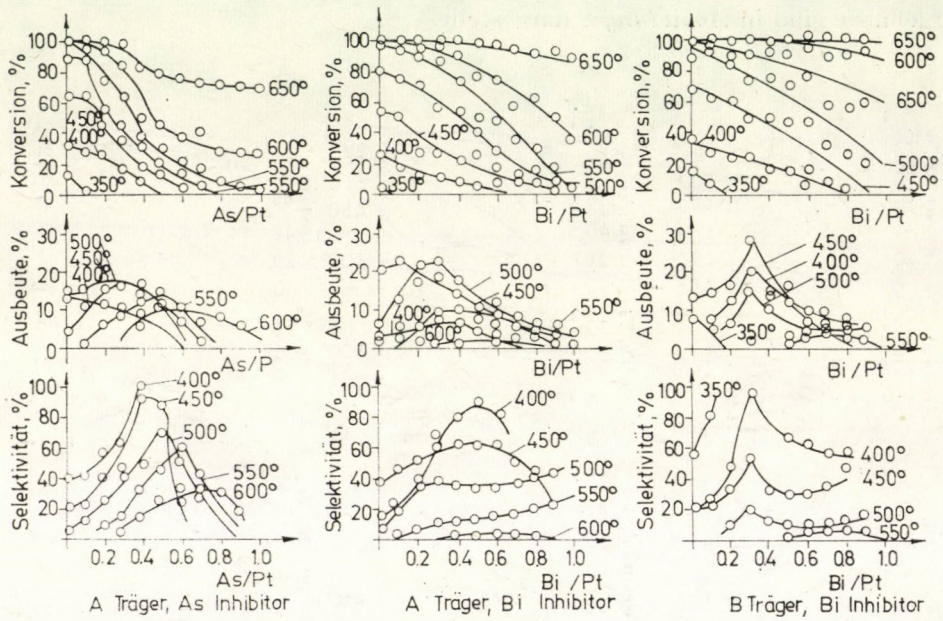

Bild 3.
Änderung der Konversion, Ausbeute und Selektivität in Abhängigkeit vom As(Bi)/Pt Atomverhältnis

Trägermaterial und vom Inhibitor Kurven mit ähnlichem Verlauf erhalten werden. Die Konversionskurven verlaufen bei steigendem Inhibitorgehalt fallend, was auf die Katalysatorgiftwirkung des Arsens und des Wismuts zurückzuführen ist. Gleichzeitig weisen die Ausbeute- und Selektivitätskurven Maximas auf, welche bei der optimal erscheinenden Temperatur im Intervall zwischen 400—500 °C bei einem Atomverhältnis Inhibitor zu Platin von etwa 0,3 auftreten. Aus den Kurven ist auch zu entnehmen, daß durch Änderung des Trägers, der Temperatur sowie des Inhibitors die Maximas der Konversions- und Selektivitätskurven geringfügig verschoben werden könne, wodurch die Möglichkeit besteht die gegenteilige Forderung nach Menge und Reinheit des erzeugten *n*-Olefins einigermaßen zu befriedigen.

c) Wirkung des Lithium-Promotors

Die Wirkung des Lithium-Promotors bei einem Platingehalt von 0,5 Gew. % und einem Arsen-beziehungsweise Wismut/Platin-Atomverhältnis von 0,3 wird in *Abbildung 4* veranschaulicht. Es zeigt sich, daß der Verlauf der Kurven

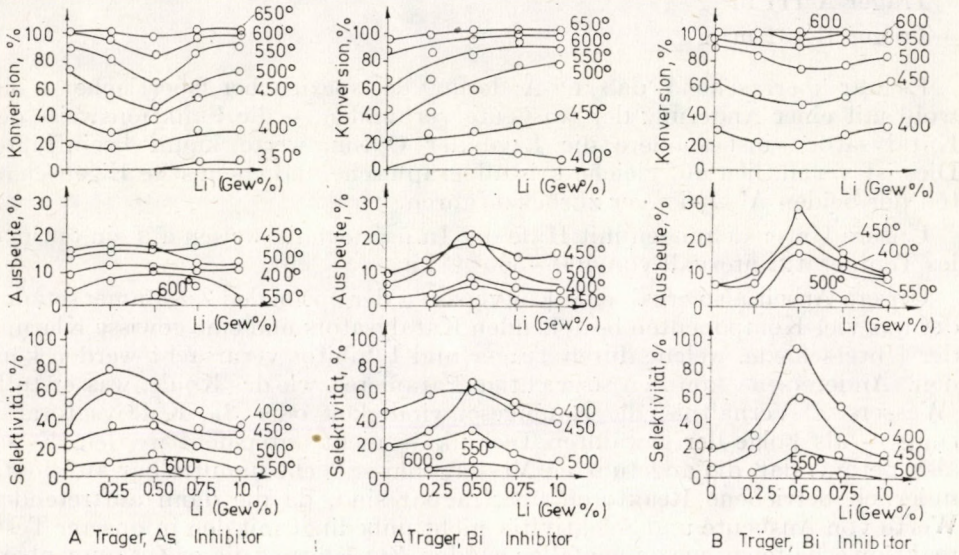

Bild 4.
Änderung der Konversion, Ausbeute und Selektivität in Abhängigkeit vom Li-Gehalt

in Abhängigkeit vom Träger und vom Inhibitor sehr verschieden sein kann. Während die Konversionskurven in Abhängigkeit vom Promotorgehalt im allgemeinen konstante oder flache Minimumwerte zeigen und demnach die Ausbeuten über flache Maximumwerte verfügen, ergibt sich durch Zusammenwirken der beiden Faktoren in den Selektivitätskurven ein ausgeprägtes Maximum bei einem Lithiumgehalt von 0,5%, und zwar unabhängig von der Art des Katalysatorträgers und des Inhibitors.

Diskussion der Ergebnisse

Unsere experimentellen Ergebnisse können wie folgt zusammengefaßt werden. An zwei verschiedenen Trägern wurde festgestellt, daß Katalysatoren mit vier Komponenten bei folgender Zusammensetzung optimales Verhalten zeigen:

Platingehalt 0,5 Gew. %
Lithiumgehalt 0,25 – 0,5 Gew. %
Arsen oder Wismut/Platin-Atomverhältnis 0,2 – 0,4.

Aus einer Analyse der Optimalwerte geht hervor, daß bei etwa gleicher Selektivität eine höhere Ausbeute bei Anwendung des Wismuts als Inhibitor zu erwarten sei, was auf die schwächere Giftwirkung des Wismuts zurückgeführt werden kann. Die Werte des Maximums erscheinen günstiger beim γ-Al_2O_3 vom Typ B als Träger. Die spezifische Oberfläche der beiden Trägersubstanzen betrugen:

Träger A 111 m^2/g
Träger B 161 m^2/g

Es war überraschend, daß die Änderung der spezifischen Oberfläche — obwohl mit einer Änderung der Ausbeute verbunden — die Funktionsweise des Katalysators, insbesondere die Lage der Optimalwerte kaum beeinflußte. Dies ist vermutlich auf gleiche kristallographische und chemische Eigenschaften der beiden Al_2O_3-Träger zurückzuführen.

Unsere Untersuchungen mit Hilfe der Impulstechnik weisen auf ein optimales Temperaturintervall von 400—500 °C hin.

Unsere Arbeit also ergab eine Eingrenzung der optimalen Zusammensetzung des aus vier Komponenten bestehenden Katalysators und eine gewisse Klärung der Unterschiede, welche durch Träger und Inhibitor verursacht werden können. Andererseits konnten so wichtige Parameter, wie das Kohlenwasserstoff/ /Wasserstoff-Verhältnis, die Raumgeschwindigkeit oder die Katalysatoralterung — als Folge der gewählten Technik — nicht untersucht werden. Es sei also betont, daß die angeführten Messergebnisse nicht unmittelbar auf kontinuierlich betriebene Reaktoren übertragbar sind, da die dann auftretenden Werte von Ausbeute und Selektivität nicht unbedingt mit den in unserer Testreaktion erhaltenen zusammenfallen werden. Zur Klärung dieser Zusammenhänge sind weitere Arbeiten im Gange.

LITERATUR

1. N. R. Bursian, S. B. Kogan, A. M. Moroz: Zh. Vses. Khim. O-va, *22*, 68 (1977) Refs.
2. R. J. Kokes, J. Tobin, H. Emett: J. Amer. Chem. Soc., *77*, 5860 (1955)
3. Cs. Csikós, és J. Báthory: Magy. Kém. Lapja (in Vorbereitung)

SUMMARY

Nowadays the dehydrogenation of *n*-paraffins is applied for the production of monoolefins having long hydrocarbon chain structures. In the experiments as model reaction the dehydrogenation of *n*-hexane was studied with the aid of impulse technique, moreover the mechanism of the four component catalysts were examined. These catalysts contain on the gamma aluminium oxide support platinum as active metal, arsenic and/or bismuth as catalytic inhibitors and lithium as promotor. Based on experimental data, there were determined the optimum composition of the catalysts, and the suitable working temperature ranges of the reactions. It was found that the values of these parameters are nearly the same in the case of the examined catalysts but markedly differs in the yield of *n*-hexenes and the selectivity of the olefin formation.

РЕЗЮМЕ

В настоящее время распространилась практика получения моноолефинов с прямой, длинной углеводородной цепью путём дегидрогенизации *н*-парафинов. В ходе проведения экспериментов, проходивших с применением импульсного метода, в качестве модельной реакции исследовалась дегидрогенизация *н*-гексана и изучался механизм действия катализаторов, содержащих четыре компонента: нанесённые на носитель из γ-Al_2O_3 платину (как активный металл), мышьяк и висмут (как каталитические ингибиторы), и литий (как промотор). Был установлен наиболее благоприятный состав катализаторов и наиболее соответствующий температурный интервал реакции. Было выявлено, что эти параметры в случае различных катализаторов совпадают, но выход *н*-гексана и селективность образования олефина при этом дают сильной отличающиеся результаты.

HUNGARIAN JOURNAL
OF INDUSTRIAL CHEMISTRY
VESZPRÉM
Vol. 6. pp. 163—174 (1978)

ENERGETISCHE UND EXERGETISCHE ANALYSE EINER ROHÖLDESTILLATIONSANLAGE

W. Fratzscher und K. Michalek

(Technische Hochschule „Carl Schorlemmer" Leuna-Merseburg, DDR)

Eingegangen am 7 Januar, 1978

Im Beitrag werden die Anfertigung einer energetischen und exergetischen Analyse einer Rohöldestillationsanlage dargestellt und die Ergebnisse diskutiert. Dazu werden das Energie- und Exergieflußbild der Anlage aufgezeigt und Beurteilungsquotienten, wie Güte und Wirkungsgrade, für Anlagenteile und die Gesamtanlage angegeben und miteinander verglichen.

Es zeigt sich, daß die wesentlichen Verluste nicht beim destillativen Trennvorgang, sondern bei der Energiezufuhr in den Röhrenöfen und im System der regenerativen Wärmeübertragung auftreten. Verbesserungsmöglichkeiten liegen in einer Vergrößerung der Wärmeübertragungsfläche und Verringerung der mittleren Temperaturdifferenz im regenerativen Wärmeübertragersystem und in einer Verminderung der notwendigen Energiezufuhr über die Röhrenöfen.

1. Die Bedeutung energetischer Analysen stoffwirtschaftlicher Verfahren

Mit der Entwicklung des wissenschaftlich-technischen Fortschritts nimmt die Bedeutung der Prozeßanalyse zur Rationalisierung und Rekonstruktion bestehender Anlagen als auch zur optimalen Gestaltung von Projekten zu. In der stoffwandelnden Industrie verdient dabei durch die enge Verknüpfung der stoffwandelnden mit energetischen Prozessen die energetische Analyse eine große Beachtung. Durch Preisveränderungen in den letzten Jahren bei den Energieträgern hat deren kostenmäßiges Gewicht relativ zugenommen, so daß energetische Betrachtungen zur Minimierung der Herstellungskosten noch bedeutungsvoller geworden sind.

In [1] und [2] wird darauf hingewiesen, daß wesentliche Aussagen energetischer Analysen nur zu erwarten sind, wenn über die prinzipielle Substitutierbarkeit der verschiedenen Energieformen hinaus die thermodynamischen und technischen Eigenschaften der verschiedenen Energieformen berücksichtigt werden. Dies soll u.a. durch die Benutzung der Exergie, die sowohl 1. als auch 2. Hauptsatz der Thermodynamik widerpsiegelt, erreicht werden.

Auf die Bedeutung energetischer Verbesserungen bei der Erdölaufarbeitung

und dabei auch der Rohöldestillation wird in [3] hingewiesen, wobei festgestellt wird, daß ein überhöhter Energieaufwand durch die Auffassung begünstigt wird, daß benötigte Energie in Form der verarbeiteten Rohstoffe stets zur Verfügung steht und immer auf die energetische Nutzung anfallender minderwertiger Produkte zurückgegriffen werden kann. Immerhin wird bei einer Weltjahresförderung von etwa 2,5 Md t etwa 1% des Energieinhaltes des geförderten Rohöls zu seiner Rektifikation aufgewendet.

Zur energetischen Analyse der Rohöldestillation liegen bisher verschiedene Arbeiten vor. Es sei hier auf RICHTEROVA [4] und BOGNER, MÜHLING u. a. [5] hingewiesen. RICHTEROVA zieht für ihre Bewertung eine Heizwertbilanz heran, wobei Effekte, die mit der Umwandlung thermischer Energien verbunden sind, nicht sichtbar werden. Da die Heizwertbilanz zu ihrer Summe durch die rein physikalischen Prozesse der Rektifikation kaum verändert wird, und 2% des Rohöls zur Energiebereitstellung verbrannt werden (wobei die Heizwerte der Fraktionen relativ wenig voneinander abweichen), ergibt sich ein Wirkungsgrad von 98%. Das unterscheidet sich sehr wesentlich von den Aussagen, die unter Berücksichtigung der thermischen Energien gewonnen werden. Bei Benutzung nur des 1. Hauptsatzes sind außer den Wirkungsgraden von ca. 10% für die Destillation keine besonders aussagekräftigen Ergenbisse zu erhalten. Die hier benutzte exergetische Methode liegt auch den Arbeiten von Bogner und Mühling zugrunde. Diese haben an verschiedenen Anlagen in der Tendenz ähnliche Ergebnisse gewonnen. Auf Grund dieser Arbeiten und eigener Berechnungen sollen nun zusammenfassend die wesentlichen Ergebnisse der Untersuchung einer Rohöldestillationsanlage vorgestellt werden.

2. Beschreibung der Rohöldestillationsanlage

In *Bild 1* ist das allgemeine technologische Schema der untersuchten Rohöldestillationsanlage aufgezeigt, wobei auf Einzelheiten, die für die Analyse keine Bedeutung hatten, verzichtet wurde, wie die Schaltung der zweistufigen Entsalzungsanlage, die Anordnung der Pumpen oder aller Behälter. Um das Schema einfach und übersichtlich zu gestalten, wurden die Wärmeübertrager in die Ströme sowohl für die warme als auch kalte Seite eingezeichnet, wobei die gleiche Bezeichnung darauf hinweist, daß es sich um ein und dieselbe Wärmeübertragergruppe handelt. Das bedeutet, daß die Wärmeübertrager zur regenerativen Aufheizung der im Schema eingezeichneten Ströme zweimal aufgeführt sind, einmal für den wärmeabgebenden und einmal für den wärmeaufnehmenden Strom.

Der Rohölstrom 1, der bei Umgebungstemperatur vorliegt, wird in zwei Strängen durch die Rohrbündelwärmeübertrager $\ddot{U}$ 1 bis $\ddot{U}$ 6 geleitet, regenerativ aufgewärmt und anschließend wieder vereinigt, wobei sich eine Mischtemperatur von 135 °C ergibt, mit der der Rohölstrom der zweistufigen Elektroentsalzungsanlage zugeführt wird. Die regenerative Erwärmung erfolgt durch die Ströme 26 (2. zirkulierender Rücklauf von K 9), 27 (1. Seitenstrom von K 9), 29 (Goudron) und 15 (2. zirkulierender Rücklauf von K2), 16 (3. zirkulierender Rücklauf von K 2). 20 (4. Seitenstrom von K 2, Fraktion 290—350 °C).

Nach der Entsalzung hat sich der Rohölstrom um etwa 10 °C abgekühlt und wird zweisträngig durch die Wärmeübertragergruppen $\ddot{U}$ 7 und $\ddot{U}$ 8 geführt, wobei er nach seiner Vermischung eine Temperatur von 213 °C aufweist, mit der

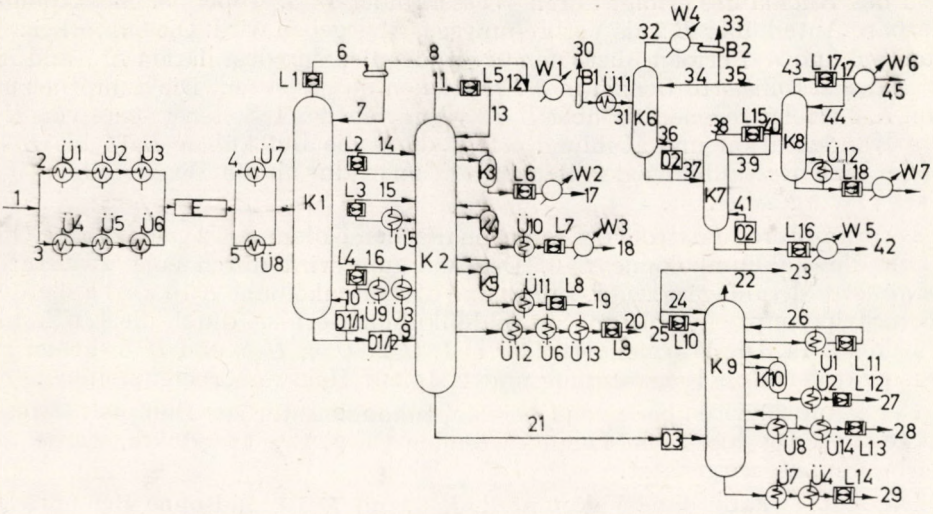

Bild 1.
Technologisches Grobschema einer Rohöldestillationsanlage
K 1 — Vorkollone; K 2 — atmosphärische Kollone; K 3 bis K 5 — Sripkolonnen; K 6 — Stabilisierungskolonne; K 7 und K 8 — Benzinkolonnen; K 9 Vakuumkolonne; K 10 — Stripkolonne; $\ddot{U}$ 1 bis $\ddot{U}$ 14 — Wärmeübertragergruppen des regenerativen Systems, davon $\ddot{U}$ 9, $\ddot{U}$ 10, $\ddot{U}$ 14 — zur Heißwasserbereitstellung und $\ddot{U}$ 13 — zur Heizölvorwärmung; L 1 bis L 18 — Luftkühler; W 1 bis W 7 — Wasserkühler; E — zweistufige Entsalzungsanlage; 01/1 bis 03 — Röhrenöfen; 1 bis 45 — Stoffströme der Anlage, davon 1 bis 5 — Rohöl und der Rest-Fraktionen und Zirkulationen

er in die Vorkolonne K 1 eintritt. In der Vorkolonne wird im Kopf Leichtbenzin mit Flüssiggas abgetrennt, das mit dem Kopfproduktstrom 12 der atmosphärischen Kolonne K 2 gemischt wird. Das getoppte Rohöl wird über den Ofen 01/2 in die Kolonne K 2 geleitet. Die Heizung von K 1 geschieht über den Sumpf durch Ofen 01/1, die Kondensation des Rücklaufes und des Kopfproduktstromes erfolgt über den Luftkühler L 1.

In die atmosphärische Kolonne K 2 und die Seitenstromkolonnen K 3 bis K 5 wird Stripdampf eingeblasen. Zur Verbesserung der Belastungsverhältnisse in K 2 verfügt diese über 3 zirkulierende Rückläufe. Ein großer Teil der Wärmeabfuhr erfolgt über Luftkühler L 2 bis L 9. Zur Erreichung der notwendigen niedrigen Temperaturen der Ströme 12, 17, 18 sind die Wasserkühler W 1 bis W 3 notwendig. Der 2. und 3. zirkulierende Rücklauf und der 4. Seitenstrom werden mit $\ddot{U}$ 5, $\ddot{U}$ 3 und $\ddot{U}$ 6 zur Rohölvorwärmung genutzt. Außerdem wird die Wärmeabfuhr des 3, zirkulierenden Rücklaufes und des 2. und 4. Seitenstromes mit $\ddot{U}$ 9, $\ddot{U}$ 10 und $\ddot{U}$ 13 zur Heißwasserbereitstellung und Heizölvorwärmung verwertet. Mit den heißesten Seitenströmen wird über $\ddot{U}$ 11 und $\ddot{U}$ 12 eine regenerative Erhitzung des Einlaufstromes in die Stabilisierungskolonne K 6 und die Sumpfheizung der Benzinredestillationskolonne K 8 erreicht.

Nachdem die in W 1 nicht kondensierten Anteile der Kopfbenzinströme von K 1 und K 2 aus B 1 in das Netz der Verbrennungsgase abgegeben worden sind, wird Strom 31 in $\ddot{U}$ 11 regenerativ erhitzt und in K 6 bei 11,5 at die Stabilisierung durchgeführt. Die Kondensation des Kopfproduktes „Flüssiggas"

und des Rücklaufes erfolgt durch Wasserkühler W 4, wobei der nichtkondensierbare Anteil über B 2 als Verbrenungsgas abgegeben wird. Die Sumpfheizung von K 6 und K 7 erfolgt über Ofen 02. In der Benzinredestillation K 7 und K 8 wird das stabilisierte Benzin in 3 Fraktionen aufgespalten. Die Sumpfheizung von K 8 erfolgt regenerativ über $\dot{U}$ 12 vermittels des 4. Seitenstromes von K 2. Die Kondensation und Kühlung erfoglt über die Luftkühler L 15 bis L 18, wobei eine Restkühlung der Benzinfraktionen durch die Wasserkühler W 5 bis W 7 vorgesehen ist.

Der Sumpfproduktstrom der atmosphärischen Kolonne K 2 gelangt über Ofen 03 in die Vakuumkolonne L 9. Das Vakuum wird durch eine zweistufige Dampfstrahleranlage erzeugt. In K 9 und die Seitenkolonne K 10 wird außerdem noch Stripdampf eingeblasen. Sie Schlußkühlung erfolgt durch die Luftkühler L 10 bis L 14. Die Wärmeübertrager $\dot{U}$ 1, $\dot{U}$ 2, $\dot{U}$ 4, $\dot{U}$ 7 und $\dot{U}$ 8 dienen zur regenerativen Rohölvorwärmung und $\dot{U}$ 14 zur Heißwasserbereitstellung.

Der Strom 22 wird über einen Oberflächenkondensator zur Dampfstrahlpumpe geleitet. Die hier nicht kondensierenden Gase, Crackprodukte, werden als Verbrennungsgase genutzt.

Die Anlage kann ohne Vakuumteil, K 9 und K 10, und ohne Benzinredesrillationsteil, K 7 und K 8, gefahren werden, wobei die Kolonnen aber für regenerative Zwecke die gleichen Wärmeübertrager umfahren.

3. Ergebnisse der Analyse

Die Berechnung der Enthalpie- und Exergiewerte erfolgte auf Grund von Projektangaben über Menge, Zusammensetzung, Druck und Temperatur und für Romaschkino Erdöl als Einsatzgemisch. Sie wurde mit dem Exergieberechnungsprogramm EX 1 der VEB Leuna-Werke „Walter Ulbricht" durchgeführt. Als Umgebungszustand wurden $p_u = 1$ at und $t_u = 10$ °C als niedrigste Temperatur des Prozesses und die Zusammensetzung des Rohöls als im gehemmten Gleichgewicht mit der Umgebung befindlich festgelegt.

In Übereinstimmung mit den in [6] getroffenen Aussagen wird im Gegensatz zu [4] die chemische Energie des Rohöls nicht mit in die Bilanz einbezogen, da dieser Energieanteil wie ein prozeßfremder Energiestrom in die Bilanzen eingehen und die Bewertungsgrößen in ihrer Aussage verfälschen würde. Eine Ausnahme bildet natürlich die Verbrennung des Rohöls in den Röhrenöfen, bei der die chemische Energie in Form des Heizwertes berücksichtigt werden muß.

In *Bild 2* ist das vereinfachte Energieflußbild und in *Bild 3* das vereinfachte Exergieflußbild dargestellt. Um die Übersichtlichkeit und Aussagefähigkeit zu erhöhen, wurden die Bilanzen einzelner Anlagenteile zusammengefaßt. Der Energiefluß entspricht damit nicht dem Stoff-fluß. Es sind nur die zwischen den Anlagen übertragenen Energiemengen eingezeichnet, wodurch die meisten Umlaufströme wegfallen. So entspricht z.B. die von K 2 bis K 5 an die Luftkühler L 1 bis L 9 abgegebene Energiemenge der Summe der Enthalpieabnahme der in L 2 bis L 9 gekühlten Ströme auf der warmen Seite der Luftkühler. Für das Exergieflußbild wurde analog vorgegangen, so daß die bei der Wärmeübertragung auftretenden Exergieverluste eindeutig den Wärmeübertragern und nicht der Kolonne zugeordnet werden. Die Zufuhr an Elektroenerige,

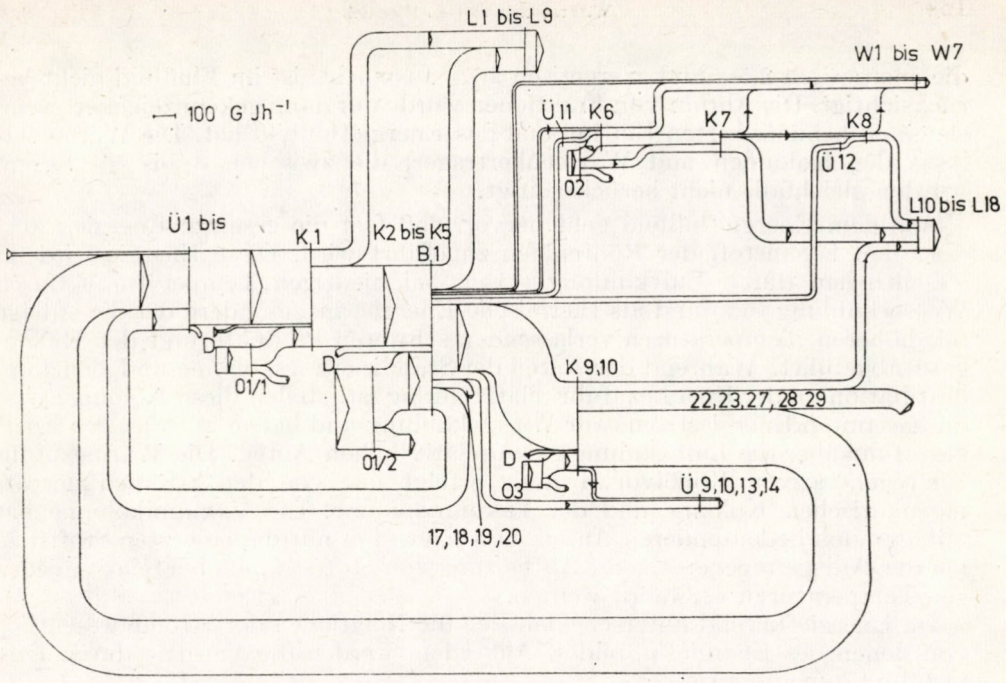

Bild 2.
Vereinfachtes Energieflußbild der Rohöldestillationsanlage

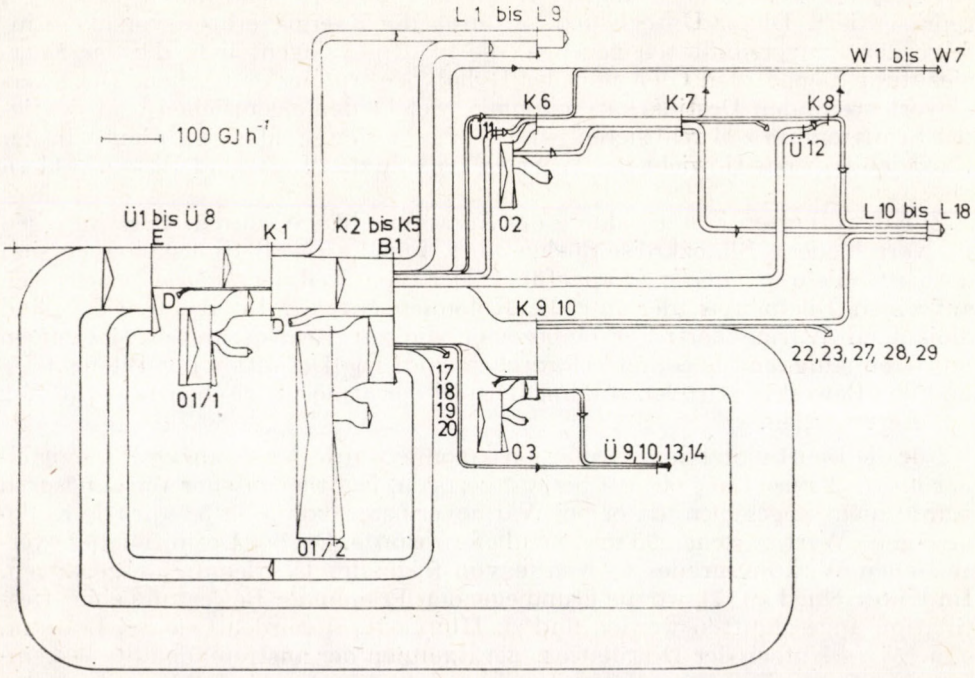

Bild 3.
Vereinfachtes Exergieflußbild der Rohöldestillationsanlage

die energetisch 2,5% und exergetisch 2,7% ausmacht, ist im Flußbild nicht berücksichtigt. Die Abfuhr von Fraktionen wurde nur dann gekennzeichnet, wenn sie einen nennenswerten Einfluß aud das Energieflußbild hat. Die Wärmeverluste der Kolonnen und Wärmeübertrager, die zwischen 3 bis 5% liegen, wurden gleichfalls nicht berücksichtigt.

Aus dem Energieflußbild geht hervor, daß fast die gesamte Energie (90%) über den Brennstoff der Röhrenöfen zugeführt wird. Diese Energie wird im wesentlichen durch Luftkühlung (41%), bei niedrigen Temperaturen durch Wasserkühlung (6%) und als thermische Energie, insbesondere der die Anlage mit höheren, Temperaturen verlassenden schweren Produkte und der Rauchgase abgeführt. Während der Anteil der Stabilisierungskolonne und Benzinredestillation an der Energiezufuhr relativ gering ist, stellen diese Kolonnen fast die gesamten Energieströme zur Wasserkühlung und haben auch an der Energieabfuhr über die Luftkühlung einen relativ hohen Anteil. Die Wärmezufuhr zur regenerativen Rohölvorwärmung erfolgt nur von den Strömen der atmosphärischen Kolonne und der Vakuumkolonne. Die Vakuumkolonne hat mit 70% den bedeutenderen Anteil. Das zeigt, daß nur die heißesten Stoffströme der Anlage regenerativ zur Aufheizung von Stoffströmen bei relativ niedrigen Temperaturen verwandt werden.

Im Exergieflußbild unterscheiden sich die Relationen der Ströme wesentlich von denen des Energieflußbildes. Außerdem werden die Verluste durch Irreversibilitäten ausgewiesen.

Es ist zu erkennen, daß der Unterschied zwischen der Summe der Exergie der abgeführten Ströme und der Summe der zugeführten Exergieströme sehr groß ist. Letztere werden noch deutlicher als im Energieflußbild durch das Heizöl repräsentiert. Dieser Unterschied ist durch die Exergieverluste vor allem infolge der Irreversibilitäten gegeben, die in den Anlagenteilen, die der Energiezufuhr dienen, den Öfen und der Rohölvorwärmung, entstehen. Die Exergieverluste in den Destillationskollonnen, welche den eigentlichen beabsichtigten Stofftrennprozeß realisieren, sind relativ gering. Schließlich nimmt in der Exergiebilanz das Gewicht der Wärmeabgabe in den Luft- und Wasserkühlern ab.

Zur detaillierten Untersuchung der Zusammenhänge wurden Berechnungen für verschiedene Bilanzkreise durhgeführt. Für die Destillationskolonnen sind die Ergebnisse in *Tabelle 1a* angeführt. Der linke Teil der *Tabelle* bezieht sich auf einen Bilanzkreis, der nur die Kolonnen enthält. Im rechten Teil sind diejenigen Wärmeübertrager einbezogen, die zur Realisierung der jeweiligen Stofftrennaufgabe unbedingt erforderlich sind. Die Definition der Bilanzkreise und der Bewertungsgrößen soll am Beispiel der atmosphärischen Kolonne K 2 erläutert werden.

Für die Beurteilung der Destillationskolonne wurde der Bilanzkreis unmittelbar um K 2 einschließlich K 3 bis K 5 gezogen. Ein thermischer Wirkungsgrad wurde nicht angegeben, da er bei Wärmeverlusten von 3 bis 5% für alle Kollonen einen Wert zwischen 95 und 97% liefern würde. Bei der Definition des exergetischen Wirkungsgrades η_{ex} wurde von folgender Überlegung ausgegangen. Im Unterschied zu [7], wo die grundlegenden Fragen der Bewertung einer Destillation angeschnitten werden und zu MÜHLING [5] wurden, wie bei BOGNER, u. a. [5] als Nutzen der Destillation, die Exergien der austretenden Ströme eingesetzt. Damit soll ausgedückt werden, daß die thermische Energie dieser Ströme z.B. über regenerative Schaltungen prinzipiell noch ausnutzbar ist.

Tabelle 1a

Güte- und Wirkungsgrade der Destillationskolonnen

Kolonne	Bilanzgrenze nur um Kolonne gezogen			in Bilanzgrenze zusätzlich einbezogene Apparate zur Energieumwandlung	ohne Berücksichtigung der Verluste bei Energieumwandlung			mit Verlusten bei Energieumwandlung	
	v	η_{ex}	$\eta_{ex,\,mT}$		η_{th}	v	η_{ex}	v	η_{ex}
K 1	0,89	0,86	0,033	01/1, *L* 1	0,83	0,85	0,74	0,52	0,46
K 2, 3, 4, 5	0,83	0,81	0,039	01/2, *L*2, *L*3, *L*4, *L*5, *Ü*3, *Ü*5, *Ü*9	0,79	0,80	0,71	0,44	0,33
K 6	0,90	0,82	0,041	02, *Ü*11, *W* 4	0,56	0,81	0,60	0,38	0,20
K 7	0,90	0,80	0,067	02, *L* 15	0,26	0,80	0,33	0,33	0,12
K 8	0,88	0,76	0,076	*Ü*12, *L*17	0,20	0,76	0,28	0,51	0,22
K 9, 10	0,89	0,87	0,017	03, *Ü*1, *Ü*8, *L*10, *L*11	0,89	0,87	0,82	0,47	0,42
K 2, 3, 4, 5	0,83	0,81	0,039	01/2, *L*2, *L*3, *L*4, *L*5, *L*6, *L*7, *L*8, *L*9, *Ü*3, *Ü*5, *Ü*6, *Ü*9, *Ü*10, *Ü*11, *Ü*12, *Ü*13, *W*2, *W*3	0,71	0,80	0,65	0,41	0,28

Für die Kolonne *K* 2 wurde so als Nutzen die Differenz der Ströme 11 und 13 (da der Rücklauf unbedingt der Kolonne zuzuführen ist), die Ströme 17 bis 21 nach Austritt aus der Kolonne und die Exergieverringerung der zirkulierenden Rückläufe 14 bis 16 angesehen. Für den Aufwand wurde der zugeführte Strom 9 nach 0 1/2 und der Stripdampf eingesetzt. Als Vergleich ist der exergetische Wirkungsgrad bei Bezugnahme auf die minimale Trennarbeit als Nutzen $\eta_{ex_{mT}}$ angegeben. Zur weiteren Illustration ist in der *Tabelle 1b* die minimale Trennar-

Tabelle 1b

Minimale Trennarbeit

Kolonne	Minimale Trennarbeit in GJ/h	Aufteilung der minimalen Trennarbeit in %	Relation des Exergieaufwandes der Kolonnen in %
K 1	3,763	19,1	21,6
K 2, 3, 4, 5	10,328	5,24	42,9
K 6	0,665	3,4	2,6
K 7	1,310	6,6	3,1
K 8	0,745	3,8	1,8
K 9, 10	2,894	14,7	27,9

beit der einzelnen Kolonnen absolut und relativ angegeben. Infolge der unterschiedlichen Exergieverluste korreliert dieser Wert natürlich nicht direkt mit der entsprechenden Exergiezufuhr. Die Bildung des Gütegrades ν ist problemlos und beinhaltet den Quotient der Summe der abgeführten Exergieströme zur Summe der zugeführten Exergieströme und ist somit ein relatives Maß der Irreverisibilitäten. In einem zweiten Bilanzkreis um die atmosphärische Destillation werden, wie in *Tabelle 1* angegeben, die Wärmeübertrager, die in den Rückläufen angebracht sind, und der Ofen mit einbezogen. Damit wird deutlich, ob an diesen Stellen eine vorteilhafte Kopplung mit dem Gesamtsystem vorliegt oder nicht. Als Nutzen werden dabei nur die in den Rückläufen übertragenen Energien und die Summe der an die Produkte gebundenen Energien betrachtet. Aufwand und Gütegrad sind entsprechend den oben angestellten Betrachtungen in einfacher Weise zu definieren.

Wie schon ausgeführt, haben die Kolonnen relativ gute Wirkungs- und Gütegrade. Bei Einbeziehung der Wärmeübertragungseinrichtungen verringert sich die energetische Güte deutlich, da die Verluste der Energiezufuhr hinzukommen. K 1 arbeitet exergetisch noch relativ gut, da der große Sumpfproduktstrom in K 2 genutzt wird. Für K 6 bis K 8 sind die Ergebnisse besonders ungünstig, da die anfallenden Produkte energetisch z.B. zur Regeneration nicht genutzt werden.

In *Tabelle 2* sind die Ergebnisse für die Energiezufuhr, die im wesentlichen

Tabelle 2

Güte- und Wirkungsgrade der Röhrenöfen

Röhrenöfen	aufzuheizende Medien	Enthalpiedifferenz d. aufzuheizenden Ströme in GJ/h	Temperaturbereich der Aufheizung in °C	$\frac{T_m - T_0}{T_m}$	η_{ht}	η_{ex}	ν
01/1	Heizkreislauf K 1	103,7	240—350	0,50	0,73	0,35	0,54
	Dampf	1,4	215—385				
01/2	Erdöl, getoppt	302,6	240—370	0,51	0,73	0,36	0,55
	Dampf	4,4	215—385				
02	Stabilbenzin	41,3	180—230	0,37	0,67	0,24	0,45
	Fraktion 85—130 °C	41,2	144—160				
03	Masut	95,0	340—400	0,56	0,75	0,40	0,71
	Dampf	2,8	215—420				
Komplex		592,4		0,50	0,72	0,35	0,57

über die Röhrenöfen realisiert wird, dargestellt. Detaillierte Untersuchungen über die Ursachen und die Aufgliederung der Verluste sind in [8] veröffentlicht. Als Nutzen werden die Enthalpie- bzw. Exergiedifferenzen der aufzuheizenden Ströme und als Aufwand die Energiezufuhr durch den Brennstoff angesehen. Während die thermischen Verluste durch das Rauchgas bei 25% liegen, betragen die Verluste durch Verbrennung, Abwertung der thermischen Energie und die Exergieverluste durch das Rauchgas ca. 65%, wobei die Exergieverluste durch Abwertung der thermischen Energie im Verhältnis zur gesamten zugeführten Exergie mit 43% ausgewiesen werden. Der hauptsächliche

Verlust im Exergieflußbild kommt demnach durch die Abwertung der im Brennstoff gebundenen Energie auf das Temperaturniveau der abgeführten thermischen Energie zustande. Hierbei sind die Bewertungszahlen für 0 2 mit der niedrigsten Wärmeabfuhrtemperatur an die Stabilisierung und Benzinredestillation besonders gering.

Als weitere wesentliche Quelle von Exergieverlusten sind im Exergieflußbild die Wärmeübertrager zur Rohölvorwärmung erkennbar. Deshalb sind in *Tabelle 3* die Wärmeübertrager, die zu einer regenerativen Ausnutzung der thermischen

Tabelle 3

Güte- und Wirkungsgrade der Wärmeübertrager des regenerativen Systems

Bezeichnung	$T_{k,m}$ in K	ΔT_m in K	ν	η_{ex}
$\dot{U}$ 1	309	94	0,40	0,27
$\dot{U}$ 2	353	80	0,57	0,49
$\dot{U}$ 3	400	77	0,77	0,68
$\dot{U}$ 4	298	125	0,33	0,15
$\dot{U}$ 5	350	70	0,70	0,55
$\dot{U}$ 6	392	11	0,99	0,87
$\dot{U}$ 7	440	91	0,79	0,70
$\dot{U}$ 8	438	80	0,78	0,69
$\dot{U}$ 9	365	39	0,98	0,95
$\dot{U}$ 10	405	24	0,98	0,95
$\dot{U}$ 11	350	70	0,66	0,51
$\dot{U}$ 12	375	112	0,89	0,73
$\dot{U}$ 13	364	23	0,93	0,80
$\dot{U}$ 14	383	38	0,97	0,92

Energie der Rohöldestillation dienen, betrachtet worden. Ein thermischer Wirkungsgrad ist hier uninteressant, da die Wärmeübertrager annähernd adiabat arbeiten. Exergetisch stellt sich der Sachverhalt durch die Abwertung des Arbeitswertes der Wärme beim Wärmeübertragungsvorgang wesentlich anders dar. Die Entstehung der Exergieverluste und ihre Berechnung ist in [9] und die Bewertung in [10] dargestellt. Aus *Tabelle 3* ist zu erkennen, daß der exergetische Wirkungsgrad und der Gütegrad in einem breiten Bereich schwanken. Das erklärt sich daraus, daß die mittlere Temperatur des aufzuheizenden Mediums $T_{K,m}$ und die Triebkraft der Wärmeübertragung ΔT_m stark schwanken und in keinem Verhältnis zueinander stehen, obwohl auf Grund thermoökonomischer Überlegungen nachgewiesen werden kann, daß zwischen diesen beiden Größen eine direkte Proportionalität bestehen sollte [12]. Besonders die Wärmeübertrager der Rohölvorwärmung, mit Ausnahme von $\dot{U}$ 6, im niederen Temperaturbereich und die regenerativen Wärmeübertrager zur Stabilisierung und Benzinredestillation $\dot{U}$ 11 und $\dot{U}$ 12 weisen niedrige Kennzahlen auf. Das bedeutet, daß ein großer Teil der Wärmeenergie mit einem unötig hohen Temperaturniveau zur Verfügung gestellt wird. Die Wärmeübertrager zur Heißwasserbereitstellung und Heizölvorwärmung weisen dagegen sehr günstige

Werte auf. Es ist demnach zu erwarten, daß die regenerative Wärmeausnutzung durch eine Veränderung der Schaltung und Vergrößerung der Wärmeübertragerflächen wesentlich verbessert werden kann. Dies würde außerdem eine Einsparung der in den Öfen zugeführten Energie und damit eine weitere zusätzliche Verringerung der Exergieverluste bedeuten.

Obwohl die Wasser- und die Luftkühler reine Verlustprozesse realisieren, kann die Frage nach einer Bewertung des inneren Verhaltens aufgeworfen

Tabelle 4

Gütegrade der Wasserkühler und -kondensatoren

Bezeichnung	ΔT_m in K	ΔH in GJ h^{-1}	ΔE_w in GJh^{-1}	ν
W 1	11	4,23	0,29	0,99
W 2	12	2,89	0,13	0,99
W 3	9	4,52	0,59	0,85
W 4	26	35,21	1,97	0,96
W 5	22	5,90	1,55	0,96
W 6	16	1,51	0,17	0,96
W 7	10	0,25	0,04	0,99

werden. Für die Waserkühler bzw. -kondensatoren *(Tabelle 4)* können deshalb nur Gütegrade sinnvoll definiert werden. Da Wasserkühlung im Projekt nur für solche Kühlprozesse eingesetzt wird, für die das Temperaturniveau der

Tabelle 5

Energetische und exergetische Leistungskennziffer der Luftkühler und -kondensatoren

Bezeichnung	ΔT_m in K	ΔH_w in GJh^{-1}	ΔE_w in GJh^{-1}	ε	ε_{ex}
L 1	36	85,9	17,6	82,0	16,5
L 2	69	31,9	7,6	96,1	22,9
L 3	55	13,8	1,8	34,2	4,5
L 4	62	5,6	1,2	55,5	11,5
L 5	30	45,7	9,6	45,4	9,5
L 6	53	10,2	1,8	61,5	10,8
L 7	57	11,6	1,6	70,0	9,9
L 8	41	2,5	0,4	6,2	1,1
L 9	52	8,6	1,8	34,2	7,3
L 10	61	31,4	7,9	156,1	39,3
L 11	70	10,0	2,6	49,6	12,8
L 12	34	1,8	0,4	29,2	6,1
L 13	74	8,4	1,6	66,7	13,0
L 14	72	11,5	1,9	45,7	7,7
L 15	27	53,5	7,8	106,1	15,5
L 17	18	41,3	6,9	72,8	12,2
L 16	69	5,9	1,6		
$+L$ 18	69	2,6	0,5	51,5	12,6

Luftkühlung zu niedrig ist, sind die Triebkräfte hierbei klein, so daß sich geringe Exergieverluste und damit gute Gütegrade ergeben. Die abgeführte Energie geht allerdings der Anlage verloren.

Für die Luftkühler *(Tabelle 5)* konnten auf Grund fehlender Angaben zum Luftzustand nur Leistungsziffern ε als Verhältnis von abgeführter Energie zum Elektroenergieaufwand für den Ventilator energetisch bzw. exergetisch gebildet werden. Diese schwanken besonders für das exergetische Verhältnis in einem sehr breiten Bereich, da sich bei geringem Temperaturniveau der Arbeitswert der abzuführenden Wärme verringert, durch die Verringerung der Triebkraft aber gleichzeitig der Aufwand zur Kühlung erhöht wird. Trotzdem läßt der breite Schwankungsbereich die Frage nach einer optimalen Auslegung offen.

In *Tabelle 6* sind Beurteilungsquotienten für ähnliche Anlagen der unter-

Tabelle 6

Wirkungsgrad und Gütegrad verschiedener untersuchter Anlagen

Anlagentyp	η_{ex} in %	ν in %
atmosphärische Rohöldestillation	2,3	17,4
Rohöldestillation, einstufig	4,1	11,1
dreistufige Rektifikation von C_5-Fraktionen	8,3	13,1
integrierte Erdöl- und Rohbenzindestillation	11,4	15,0
untersuchte Anlage	2,0	18,0

suchten Anlage gegenübergestellt [11]. Die geringe energetische Güte der untersuchten Anlage erklärt sich aus der Anzahl der Trennstufen und durch die Tatsache, daß sämtliche Produkte auf Lagertemperatur gekühlt werden, während sie bei den anderen Anlagen mit dem aktuellen Zustand einer Weiterverarbeitung zugeführt werden. Trotz der Einschränkung, die an den Vergleich der hier aufgeführten Beurteilungsquotienten verschiedener Anlagen gemacht werden muß, soll darauf hingewiesen werden, daß der spezifische Energieverbrauch um etwa 50% höher liegt als der in [4] angeführten vergliechbaren Anlage.

4. Zusammenfassung

Eine richtige Aufdeckung der Verluste ist nur durch quantitative und qualitative Bewertung der Energie also z.B. durch exergetische Untersuchungen möglich.

Bei Rohöldestillationsanlagen erweisen sich die Verluste beim destillativen Trennvorgang als relativ gering. Die wesentlichste Verlustquelle ist die Energiezufuhr in den Röhrenöfen. Außerdem treten hohe Verluste im System der regenerativen Wärmeübertragung auf. Als Verbesserungsmöglichkeit bietet sich vor allem eine günstigere Gestaltung des regenerativen Systems, eine größere Einbeziehung warmer Ströme in dieses System und eine Vergrößerung der Wärmeübertragungsflächen verbunden mit einer Verringerung der mitt-

leren Temperaturdifferenzen an. Damit werden gleichzeitig die Exergieverluste im regenerativen System und in den Röhrenöfen gesenkt und eine Verringerung des Energiebedarfs der Anlage erreicht. Dies muß mit einer optimalen Auslegung der Destillationskolonnen zur Verringerung des Energiebedarfs über z.B. eine Verringerung des Rücklaufverhältnisses oder eine Verringerung der Trennstufenzahl verbunden sein.

Die Ergebnisse der Arbeit wurden teilweise im Auftrag und in Zusammenarbeit mit dem VEB MAG Grimma erhalten. Für die dabei gewährte Unterstützung möchten die Autoren dem VEB MAG Grimma Dank sagen.

LITERATUR

1. Fratzscher, W.: Energieanwendung *14*, 282 (1965)
2. Fratzscher, W.: Chem. Techn. *27*, 205 (1975)
3. Schirmer, W. und Harenz, H.: Chem. Techn. *25*, 453 (1973)
4. Richterova, V.: Erdöl und Kohle *24*, 403 (1971)
5. Bogner, H.—J. und Mühling, K. u.a.: Diplomarbeiten, Tech. Hochsch. Chem. „Carl Schorlemmer" Leuna-Merseburg
6. Rant, Z.: Gas Wärme *14*, 28 (1965)
7. Fratzscher, W. und Klöditz, D.: Wiss. Z. Tech. Hochsch Chem. „Carl Schorlemmer" Leuna-Merseburg *10*, 134 (1968)
8. Fratzscher, W. und Elsner, W.: Chem. Techn. *19*, 395 (1967)
9. Gregorig, R.: Chem Ing. Techn. *37*, 108, 524, 956 (1965)
10. Fratzscher, W. und Otte, F.: Wiss. Z. Tech. Hochsch. Chem. „Carl Schorlemmer" Leuna-Merseburg *7*, 88 (1965)
11. Born, G.: Diplomarbeit, Tech. Hochsch. Chem. „Carl Schorlemmer" Leuna-Merseburg
12. Autorenkollektiv: Energiewirtschaft für Verfahrenstechniker, VEB Deutscher Verlag für Grundstoffindustrie, Leipzig 1974

SUMMARY

The paper presents the energetic and exergetic analysis of a crude oil distillation plant and evaluates the results. For this sake the energetic and exergetic flow sheets of the facilities are constructed, and the qualifying numbers related to the single parts and the whole facilities are given and compared to each other. These numbers are the coefficient of efficiencies and the utilities.

It is shown that the essential losses do not occur at the distillative separation processes but at the energy input and at the regenerative heat exchangers. These losses can be lessened if the heat transfer area of the exchangers is increased and the mean temperature differences are decreased, moreover if the needed energy input to the tube still is lessened.

РЕЗЮМЕ

В статье проводится энергетический и эксэнергетический анализ нефтеперегонной установки и оценка полученных результатов. Для этого авторами была снята энергетическая и эксэнергетическая процессионная схема установки, а для отдельных частей установки и для установки в целом задаются и сравниваются друг с другом такие квалификационные отношения, как добротность и к. п. д.

Можно заметить, что основные потери происходят не в процессе разделения перегонкой, а в трубчатых печах во время принятия ими энергии и в регенеративном теплообменнике. Этот недостаток может быть исправлен путём увеличения поверхности теплопередачи, понижения средней разницы температур в регенеративной системе теплообмен ' и понижением количества необходимой принимаемой энергии в трубчатой печи.

HUNGRIAN JOURNAL
OF INDUSTRIAL CHEMISTRY
VESZPRÉM
Vol. 6. pp. 175–186 (1978)

ИССЛЕДОВАНИЕ ПРОЦЕССОВ ПЕРЕНОСА ТЕПЛА И ВЕЩЕСТВА В ТРЕХФАЗНОМ НЕПОДВИЖНОМ СЛОЕ КАТАЛИЗАТОРА

В. А. КИРИЛЛОВ, Б. Л. ОГАРКОВ

Институт катализа СО АН СССР

Поступила в редакцию 2 февраль 1978 г.

Рассмотрены процессы переноса тепла и вещества в 3-х фазном неподвижном слое катализатора при восходящем прямоточном движении фаз. Проведенное экспериментальное исследование на модельной реакции подтвердило справедливость предложенных зависимостей на математической модели процесса.

Каталитические реакторы с прямоточным восходящим движением газа и жидкости через неподвижный зернистый слой находят широкое применение в промышленности органического синтеза и нефтепереработке. Химическое взаимодействие в них осуществляется на поверхности зерен катализатора между газом, растворенным в жидкости и непосредственно компонентами жидкой фазы что может сопровождаться значительными тепловыми эффектами. Последнее обстоятельство приводит при проектировании реакторов к необходимости учета процессов переноса тепла и вещества как между фазами, так и в продольном направлении слоя. Некоторые из этих вопросов будут рассмотрены в настоящей работе.

1. Гидродинамика течения газа и жидкости через зернистый слой

Как показали наши исследования, проведенные с помощью емкостного датчика, в ТНС в зависимости от расходов газа и жидкости, а также геометрической структуры слоя возможно наличие до 5-ти гидродинамических режимов: пузырькового; снарядного в каналах между зернами; поршневого в масштабе слоя; дисперсно кольцевого и капельного *(рис. 1)*. Пузырьковый режим характеризуется движением отдельных изолированных друг от друга пузырей газа, соизмеримых с размерами частиц или величиной капиллярной константы. Как правило он имеет место при небольших (меньше 0,4) газосодержаниях. С увеличением расходов газа расстояние между пузырями уменьшается, они частично сливаются между собой образуя устойчивые длинные пузыри или снаряды.

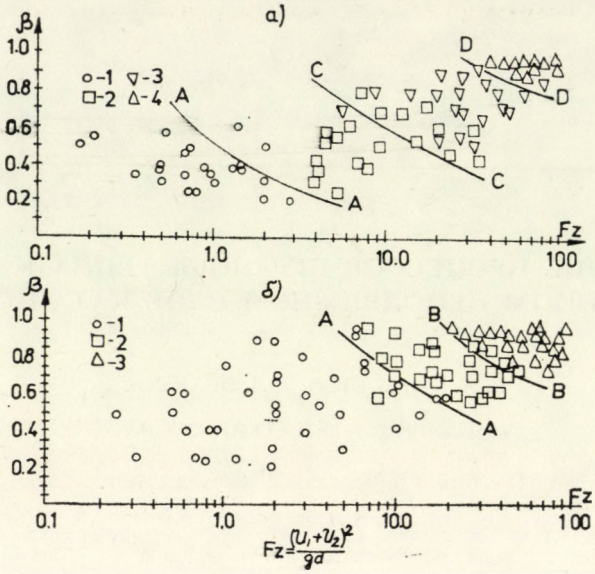

Рис. 1.
Гидродинамические режимы в 3-*х* фазном неподвижном слое.
1 — пузырьковый режим; 2 — снарядный; 3 — поршневой; 4 — дисперсно-кольцевой; A—A, B—B, C—C, D—D — границы режимов;
а) насадка $d=8$ мм; *б)* насадка $d=18$ мм

Дальнейшее увеличение расхода газа приводит к разрушению жидкостных перемычек между снарядами и образованию поршней, диаметр которых соизмерим с размером реактора. Наконец, дальнейшее увеличение расходов приводит к распаду поршней и образованию жидкой пленки на поверхности частиц и капель в ядре несущего газового потока. Это дисперсно-кольцевой и капельный режимы.

Условия течения газа и жидкости в свободном объеме неподвижного зернистого слоя (ТНС) в значительной степени определяют протекание процессов переноса тепла и вещества, а также величину межфазной поверхности и интенсивность обмена между газом и жидкостью. Сложность гидродинамической обстановки в свободном объеме слоя приводит к необходимости исследования профессов переноса в указанных режимах с получением зависимостей справедливых в пределах существования данного гидродинамического режима.

2. Межфазная поверхность и коэффициенты массообмена газ-жидкость

В настоящее время известно всего несколько экспериментальных работ, посвященных определению межфазной поверхности при восходящем прямотоке [1—5]. Исследования проведены при широком варьировании скоростей газа и жидкости, форм насадок и размеров. После обработки приведенных в них данных в [6] оказалось, что наблюдается хорошая корреляция между скоростями газа и жидкости, определяемыми числами Re_1 и Re_2 и межфазной поверх-

ностью, если последнюю представить в виде безразмерного соотношения, определяемого критерием Этвеша. Так при $Re_2<200$

$$E\ddot{o}=0{,}00266E_s^{1{,}8}Re_2^{0{,}36}Re_1^{0{,}45} \tag{1}$$

при

$$Re_2<200$$

$$E\ddot{o}=0{,}234\cdot10^{-4}E_s^{1{,}8}Re_2^{1{,}21}Re_1^{0{,}45} \tag{2}$$

где

$$E\ddot{o}=\frac{\sigma a^2}{\varrho_2 g};\quad E_s=\frac{\sqrt[3]{S}}{\sqrt{V}};\quad Re_1=\frac{u_1 d}{\nu_1};\quad Re_2=\frac{u_2 d}{\nu_2}$$

Приведенные зависимости справедливы в области Re_2 не более 1000 и $Re<500$.

На основании экспериментальных данных, приведенных в [1—4] можно определить коэффициенты массообмена между газом и жидкостью, но отнесенные к единице межфазной поверхности. Так, экспериментальные данные хорошо укладываются в единую корреляционную зависимость если в качестве определяющего размера в числе Шервуда взять капиллярную константу. Влияние геометрии слоя как и раньше может быть учтено через E_s.

Так:

$$Sh=230E_sRe_1^{0{,}18}Re_2^{0{,}33} \tag{3}$$

где

$$Sh=\frac{\beta_{12}}{D}\sqrt{\frac{\sigma}{\varrho_2 g}}$$

Интересно отметить, что в отличие от данных по массообмену одиночных пузырей, где наблюдается зависимость $Sh\sim\sqrt{Re_2Sc}$ в рассмотренном случае получается более низкая степень при Re_2, близкая скорее к твердым телам.

В настоящей работе мы не будем подробно останавливаться на анализе процессов массообмена между жидкостью и твердым телом, поскольку это было сделано несколько ранее в [7] для пузырькового и снарядного режимов. Приведенные в [8] экспериментальные данные, полученные с помощью электрохимической методики, также описываются зависимостью [7]:

$$Sh=3{,}02\left\{0{,}7+0{,}12\left[\frac{u_2(1-\varphi)}{u_2\varphi}\right]^{0{,}62}\right\}Pe^{0{,}33}\left(\frac{d}{m}\right)^{0{,}33} \tag{4}$$

где

$$Sh=\frac{\beta_{23}R}{D}$$

3. Перенос тепла между газо-жидкостной смесью и неподвижной насадкой

Определение коэффициентов теплообмена между зернами неподвижного слоя и газо-жидкостным потоком осуществлялось с помощью известной стационарной методики [9]. Датчик представлял собой полый шар диаметром, равным размеру частиц слоя (18 мм и 8 мм), внутри которого помещался нихромовый нагреватель. Последний подогревался за счет проходящего через него электри-

ческого тока соответствующей мощности. Измерения температур проводились с помощью термопар, одна из которых фиксировала температуру газо-жидкостного потока, а вторая „разнесенная" температуру поверхности датчика. Для записи показаний использовался высокочувствительный цифровой вольтметр. Коэффициенты теплообмена, усредненные по всей поверхности датчика рассчитывались по зависимости

$$\alpha = \frac{J^2 R_0}{S \Delta T} \tag{5}$$

Экспериментальные исследования были проведены при варьировании скоростей газа Re_1=50—3500; скоростей жидкости Re_2=5—300; газосодержаний 0,04—0,85 и размеров частиц d=18 и 8 мм. На *рис. 2* приведены некоторые

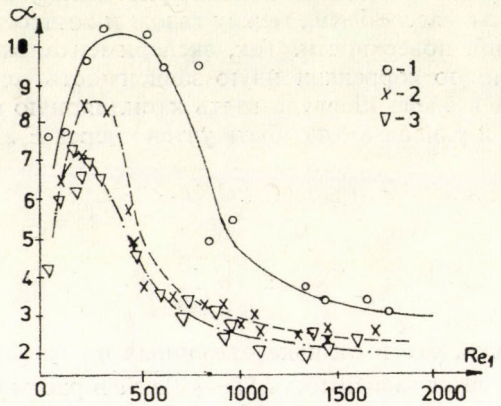

Рис. 2.
Коэффициенты теплообмена в ТНС насадка шарики d=8 мм;
1 — Re_2=70; 2 — Re_2=30; 3 — Re_2=10

из полученных результатов для зернистого слоя, состоящего из шариков d= =8 мм. Из этого рисунка видно, что зависимость коэффициента теплообмена от скоростей газа и жидкости имеет сложный немонотонный характер, что, очевидно, связано с различными гидродинамическими режимами течения газа и жидкости в свободном объеме слоя. Для получения аппроксимационной зависимости оказалось удобным использовать известное теоретическое соотношение для коэффициентов обмена [10]

$$Nu Pe^{0,33} \tag{6}$$

в котором с учетом двухфазности потока физические параметры газожидкостной смеси имели вид:

$$c_p = c_{p_2}\left[1 + \frac{c_{p_1}\varphi}{c_{p_2}(1-\varphi)}\right]; \quad u = u_2\left[1 + \frac{u_1(1-\varphi)}{u_2\varphi}\right]$$

и

$\lambda = \lambda_2 F(\varphi)$, где $F(\varphi)$ — некоторая функция газосодержания, определяемая экспериментально.

На основании (6) оказалось возможным получить аппроксимационные зависимости только для конкретных гидродинамических режимов течения газа и жидкости. Полученные результаты приведены на *рис. 3*.

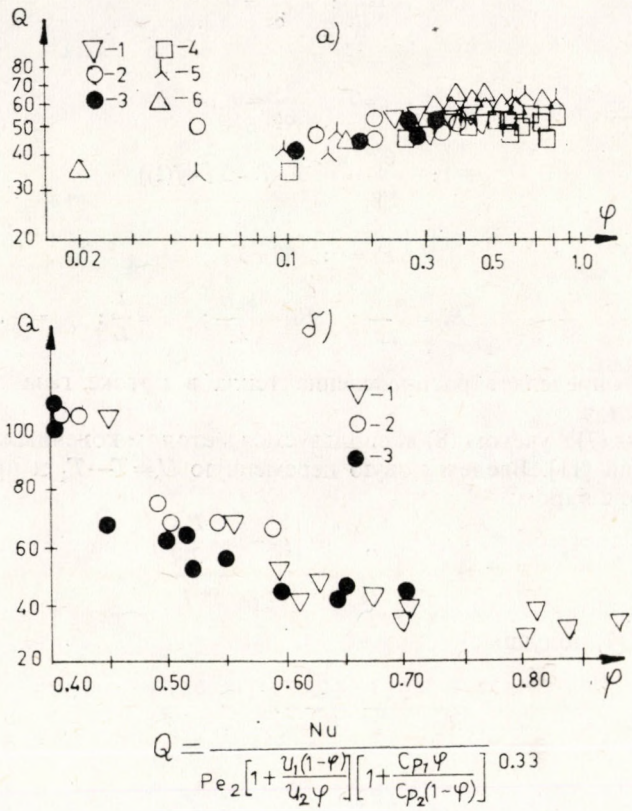

Рис. 3.
Обработка экспериментальных данных по коэффициентам теплообмена:
а) пузырьковый и снарядный режимы; *б)* поршневой и дисперсно-кольцевой режимы, шарики d=8 мм; 1 — Re_2=8,8; 2 — Re_2=72,2; 3 — Re =32,4; шарики d=18,8 мм; 4 — Re_2=48,6; 5 — Re_2=97; 6 — Re_2=250

3.1. Продольная теплопроводность неподвижного слоя

Перенос тепла в продольном направлении слоя осуществляется как с помощью газо-жидкостного потока, так и по зернам катализатора. В настоящей работе мы ограничимся определением вклада в общий перенос тепла только кондуктивной составляющей. Представим зернистый слой в виде системы цилиндров с некоторым эффективным размером R и длиной L. Тогда математическое описание переноса тепла при таких предположениях будет иметь вид:

$$\overline{a}^2 \frac{\partial^2 T}{\partial \xi^2} + \frac{\partial^2 T}{\partial \varrho^2} + \frac{1}{\varrho}\frac{\partial T}{\partial \varrho} = \frac{\partial T}{\partial F_0} \qquad (7)$$

при

$$\xi=0: \quad \frac{\partial T}{\partial \xi}=Bi_1(T-T_1)$$

$$\xi=\frac{L}{R}: \quad \frac{\partial T}{\partial \xi}=0$$

при (8)

$$\varrho=0: \quad \frac{\partial T}{\partial \varrho}=0$$

$$\varrho=1: \quad \frac{\partial T}{\partial \varrho}=-Bi_2[T-T_1-f(\xi)]$$

при

$$F_0=0: \quad T=T_0$$

$$\bar{a}^2=\frac{a_1}{a_2}\frac{R^2}{L^2}; \quad Bi_1=\frac{\alpha_1 R}{\lambda_1}; \quad Bi_2=\frac{\alpha_2 R}{\lambda_2}; \quad \xi=\frac{l}{L}; \quad \varrho=\frac{r}{R}.$$

Функция $f(\xi)$ определяет распределение тепла в потоке газа в продольном направлении слоя.

Для решения (7) с учетом (8) воспользуемся методом конечных интегральных преобразований [11]. Введем новую переменную $U=T-T_1$ и преобразование по координате с ядром:

$$K_n(\xi, \mu_n)=\frac{R}{L}\frac{\cos\left(\mu_n-\mu_n\xi\frac{R}{L}\right)}{\mu_n+\sin\mu_n\cos\mu_n}\cdot 2\mu_n \tag{9}$$

Тогда вместо (7) получим:

$$\frac{\partial^2\tilde{u}_n}{\partial\varrho^2}+\frac{1}{\varrho}\frac{\partial\tilde{u}_n}{\partial\varrho}-\lambda_n^2\tilde{u}_n=\frac{\partial\tilde{u}_n}{\partial F_0} \tag{10}$$

при

$$\varrho=1: \quad \frac{\partial\tilde{u}_n}{\partial\varrho}=-Bi_2[\tilde{u}_n-\tilde{f}(\xi)]$$

$$\varrho=0: \quad \frac{\partial\tilde{u}_n}{\partial\varrho}=0 \tag{11}$$

$$F=0: \tilde{u}_n=(\tilde{T}_0-T_1)$$

где

$$\lambda_n=a\mu_n\frac{R}{L}; \quad (\tilde{T}_0-T_1)=\frac{2(T_0-T_1)\sin\mu_n}{\mu_n+\sin\mu_n\cos\mu_n}$$

$$\tilde{f}(\xi)=\frac{R}{L}\frac{2\mu_n}{\mu_n+\cos\mu_n\sin\mu_n}\int_0^{L/R} f(\xi)\cos\left[\mu_n-\mu_n\xi\frac{R}{L}\right]d\xi=B_n$$

μ_n — корень трансцендентного уравнения

$$\frac{L}{R}Bi_1\operatorname{ctg}\mu_n=\mu_n \tag{12}$$

Введением новой переменной $\tilde{W}_n = \tilde{u}_n - B_n$ система (10—11) приводится к однородным граничным условиям, но неоднородным становится (10).

$$\frac{\partial^2 \tilde{W}_n}{\partial \varrho^2} + \frac{1}{\varrho}\frac{\partial \tilde{W}_n}{\partial \varrho} - \lambda_n^2(\tilde{W}_n + B_n) = \frac{\partial \tilde{W}_n}{\partial F_0} \tag{13}$$

при

$$\varrho = 0: \quad \frac{\partial \tilde{W}_n}{\partial \varrho} = 0$$

$$\varrho = 1: \quad \frac{\partial \tilde{W}_n}{\partial \varrho} = -Bi_2 \tilde{W}_n \tag{14}$$

Решение (13—14), полученное обычными приемами математической физики имеет вид:

$$\tilde{W}_n = \sum_{m=1}^{\infty} \frac{2E_n Bi_2 J_0(q_m \varrho)}{J_0(q_m)[q_m^2 + Bi_2^2]} \exp\left[-(q_m^2 + \lambda_n^2)F_0\right] -$$

$$- \sum_{m=1}^{\infty} \frac{2\lambda_n^2 B_n Bi_2 J_0(q_m \varrho)}{(q_m^2 + Bi_2^2)(q_m^2 + \lambda_n^2) J_0(q_m)} \cdot \{1 - \exp\left[-(q_m^2 + \lambda_n^2)F_0\right]\} \tag{15}$$

где

$$E_n = \frac{2(T_0 - T_1)\sin \mu_n}{\mu_n + \sin \mu_n \cos \mu_n} - B_n;$$

трансцендентного уравнения:

$$Bi_2 J_0(q_m) = q_m J_1(q_m) \tag{16}$$

Возвращаясь к исходным переменным, можно получить решение исходной системы (7—8). Так, имеем:

$$T = T_1 + \sum_{n=1}^{\infty} B_n \cos\left(\mu_n - \mu_n \xi \frac{R}{L}\right) + \sum_{n=1}^{\infty} 2Bi_2 E_n \cos\left(\mu_n - \mu_n \xi \frac{R}{L}\right) \times$$

$$\times \sum_{m=1}^{\infty} \frac{J_0(q_m \varrho)\exp\left[-(q_m^2 + \lambda_n^2)F_0\right]}{(q_m^2 + Bi_2^2) J_0(q_m)} - \sum_{n=1}^{\infty} 2\lambda_n^2 B_n Bi_2 \times$$

$$\times \cos\left(\mu_n - \mu_n \xi \frac{R}{L}\right) \sum_{m=1}^{\infty} \frac{J_0(q_m \varrho)}{(q_m^2 + \lambda_n^2)(q_m^2 + Bi_2^2) J_0(q_m)} \times \{1 - \exp\left[-(q_m^2 + \lambda_n^2)F_0\right]\} \tag{17}$$

Анализ корней трансцендентных уравнений (12, 16) показывает, что они сопоставимы, следовательно для реальных размеров зерен катализатора

$$q_m^2 \gg \left(\mu_n \bar{a} \frac{R}{L}\right)^2 \tag{18}$$

Это означает, что время перехода из одного стационарного состояния в другое определяется радиальным переносом тепла по зерну.

Анализ полученного решения, проведенный численно, при варьировании параметров:

$$\bar{a} = 0{,}0001 \div 1; \quad Bi_1 u Bi_2 = 0{,}1 \div 100; \quad \xi = 0{,}1 \div 1$$

и линейной функции $f(\xi) = T_1 \xi$ показал, что для значений L/R близких к 200 „а" практически не влияет на решение. Погрешность, возникающая при переходе от решения уравнений, учитывающих продольный перенос к решению без учета последнего практически не зависит от Bi_2, но изменяется при варьировании Bi_1 *(рис. 4)*, причем для $L/R = 200$ величина максимальной погрешности не пре-

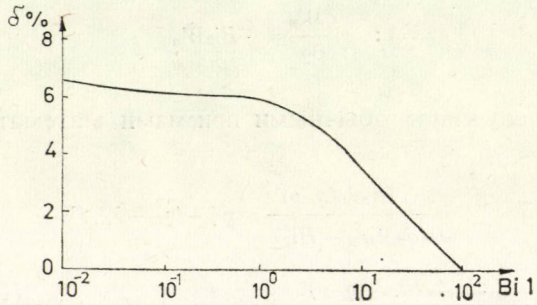

Рис. 4.
Влияние числа Bi_1 на относительную погрешность решения
$\delta = (T|_{Bi_1 \to \infty} - T|_{Bi_1}) T|_{Bi_1 \to \infty}$

вышает 6%. Это означает, что при больших L/R и не слишком крутых значениях $f(\xi)$ влиянием продольного переноса тепла по зернам катализатора можно пренебречь.

4. Экспериментальное исследование процессов переноса на модельной реакции

Рассмотрим, в какой степени ранее приведенные зависимости для расчета коэффициентов справедливы в случае протекания каталитической реакции. Остановимся на реакции гидрирования *н*-гептена в гептан. Кинетические закономерности этой реакции подробно исследованы в [12]. В области малых концентраций *н*-гептена (0,13 моль/литр) эта реакция протекает по первому порядку, а при больших значениях по нулевому. Экспериментальные исследования были проведены на Ni-скелетном катализаторе на экспериментальной установке, приведенной на *рис. 5*. Она состояла из двух сырьевых емкостей *Е*—1 и *Е*—2, поршневого насоса *Н*—1; фильтра *Ф*—1; ротаметров *РС*—5 и *РС*—3 сепараторов *С*—1, *С*—2, *С*—3, компрессора; холодильника *Х*—1; манометров, серии регулирующих и запорных вентелей *В*—1 — *В*—7 и колонны. Последняя была оборудована термостатированной рубашкой, пробоотборниками и сепаратором. Экспериментальные исследования проводились следующим образом. В емкости *Е*—1 и *Е*—2 заливался раствор *н*-гептена 2-*х* различных концентраций. Затем из одной из них с помощью насоса *Н*—1 через колонну устанавливался постоянный расход раствора. В эту же колонну восходящим прямотоком с помощью компрессора *К*—1 подавался водород. Непрореагировавшая часть H_2 через систему сепараторов и холодильников подпитывалась свежим водо-

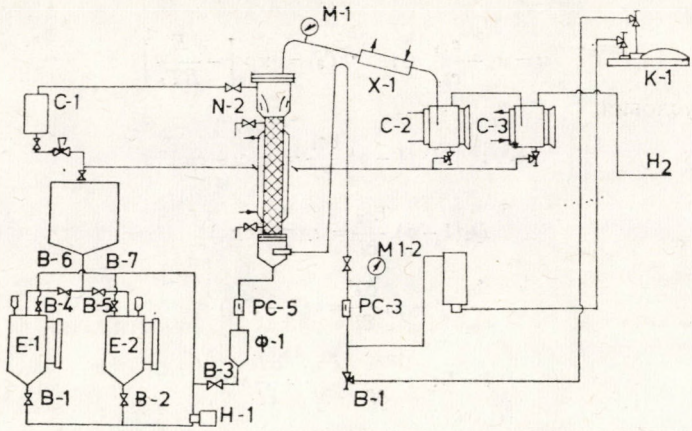

Рис. 5.
Принципиальная схема экспериментальной установки для исследования тепло-массопереноса методом модельной реакции (обозначения в тексте)

родом из баллонов и подавалась опять в реактор. Из колонны с помощью пробоотборников, расположенных внизу и вверху через определенные интервалы времени (~2—5 мин.) производился отбор проб *н*-гептена, концентрация последнего определялась хроматографически. На входе и выходе колонны были установлены термопары, которые фиксировали изменения температуры. После установления стационарного режима с помощью вентилей *B*—1 или *B*—2 проводилось переключение на новую концентрацию гептена и измерения повторялись в течение всего переходного режима.

Экспериментальные исследования были проведены при варьировании скорости газа в расчете на полное сечение в пределах 15,2—30,5 см/сек; скорости жидкости 0,2—0,37 см/сек, давления водорода 1,5—3 ата; концентрации гептена 2—15 объемных процентов. Размер зерен катализатора 2—5 мм, пористость слоя 0,5; диаметр колонны 65 мм, а ее длина 1,2 м.

В виду высокой активности катализатор в ходе эксперимента разбавляется инертным веществом в соотношении близком к 1:1.

5. Обработка экспериментальных данных

Математическое описание процесса гидрирования *н*-гептена в неподвижном слое катализатора может быть представлено в виде:

$$D_1(1-\varphi)\frac{\partial^2 c_1}{\partial l^2} - u_2\frac{\partial c_1}{\partial l} + \beta_{12}\delta_{12}(c_1^* - c_1) - W_1\frac{1-\varepsilon}{\varepsilon}f(\tau) = (1-\varphi)\frac{\partial c_1}{\partial t} \tag{19}$$

$$D_2(1-\varphi)\frac{\partial^2 c_2}{\partial l^2} - u_2\frac{\partial c_2}{\partial l} - W_2\frac{1-\varepsilon}{\varepsilon}f(\tau_3) = (1-\varphi)\frac{\partial c_2}{\partial t} \tag{20}$$

$$\frac{\lambda_2(1-\varphi)}{c_{p_2}}\frac{\partial^2 T}{\partial l^2} - u\frac{\partial T}{\partial l} + \frac{\alpha_{23}S_{23}}{c_{p_2}\varepsilon}(T_3 - T) = (1-\varphi)\frac{\partial T}{\partial t} \tag{21}$$

$$-\frac{\alpha_{23}S_{23}}{c_{p_3}}(T_3 - T) + \frac{W_2 Q(1-\varepsilon)}{c_{p_3}}f(T_3) = (1-\varepsilon)\frac{\partial T_3}{\partial t} \tag{22}$$

где

$$u = u_2 + \frac{c_{p_1}}{c_{p_2}} u_2; \qquad f(T_3) = \exp\left[-\frac{E}{RT_3}\right]$$

Граничные условия:

$$l = 0: \qquad D_1(1-\varphi)\frac{\partial c_1}{\partial l} = u_2(c_1 - c_{1_{b_x}}) \tag{23}$$

$$D_2(1-\varphi)\frac{\partial c_2}{\partial l} = u_2(c_2 - c_{2_{b_x}}) \tag{24}$$

$$\frac{\lambda_2}{c_{p_2}}(1-\varphi)\frac{\partial T}{\partial l} = u(T - T_{b_x}) \tag{25}$$

$$l = L: \qquad \frac{\partial c_1}{\partial l} = \frac{\partial c_2}{\partial l} = \frac{\partial T}{\partial l} = 0 \tag{26}$$

индексы: 1 — водород; 2 — *н*-гептен.

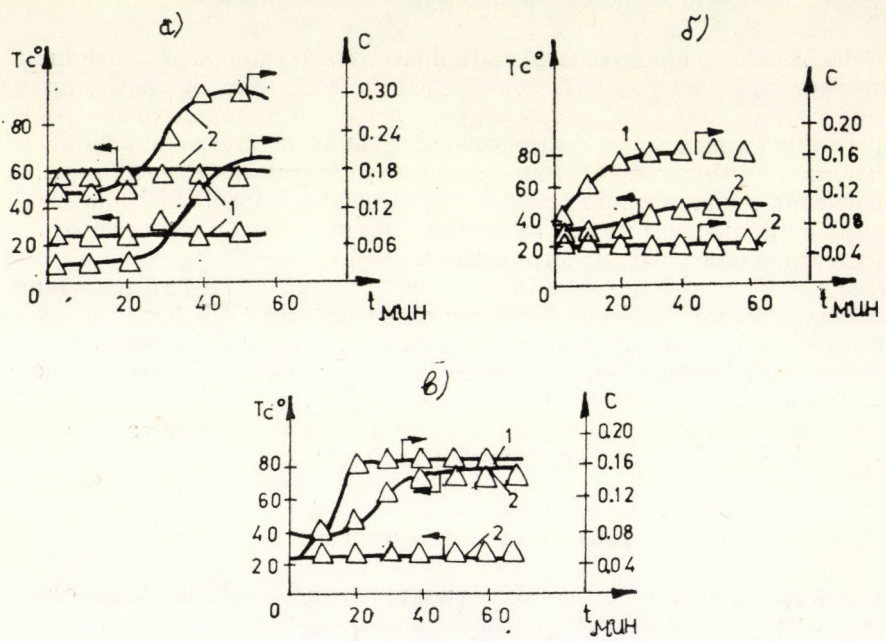

Рис. 6.

Сопоставление расчитанных (сплошные линии) и экспериментальных значений температур и концентрации на выходе из слоя катализатора.

а) давление водорода 1,5 ата; расход газа 1000 л/час; расход жидкости 24 л/час. 1 — пусковой режим; 2 — переходной режим при изменении концентрации гептена на входе в слой с 14,42 до 30,1%

б) давление водорода 3 ата. расход газа 1000 л/час; расход жидкости 24 л/час. Переходной режим при изменении концентрации *н*-гептена с 2% до 19,7%. 1 — изменение концентрации на входе в слой; 2 — изменение концентрации и температуры на выходе из слоя

в) давление водорода 1,5 ата. Расход газа 1000 л/час; расход жидкости 13 л/час. Переходные режимы при изменении концентрации *н*-гептена с 4,4 до 16,5%. 1 — изменение концентрации на входе в слой; 2 — изменение температуры и концентрации на выходе из слоя

Система уравнений (19—26) решалась численно на ЭВМ Минск—32 методом прогонки. При расчетах значения коэффициентов массообмена между газом и жидкостью величина межфазной поверхности рассчитывалась по (1—3). Величина коэффициента продольного перемешивания D_1, D_2 и теплопроводности λ_2, а также газосодержание рассчитывались на основании данных [13].

Можно показать, что реакция гидрирования на зернах 3—5 мм протекает во внешнедиффузионной области. Это означает, что скорость химического превращения определяется интенсивностью внешнего массообмена. При расчетах на основании концентрационных и температурных измерений подбиралась такая величина наблюдаемой константы скорости реакции, которая наилучшим образом описывает экспериментальные данные. Оказалось, что с учетом разбавления катализатора ее величина с точностью $\pm 15\%$ попадает в интервал значений определяемых формулой (4). На *рис. 6* в качестве примера показано сопоставление рассчитанных и экспериментальных значений концентраций и температур во времени на выходе из слоя катализатора. Как следует из этих рисунков результаты расчетов удовлетворительно согласуются с экспериментальными данными, что указывает на достоверность приведенных в этой работе расчетных зависимостей для коэффициентов переноса.

УСЛОВНЫЕ ОБОЗНАЧЕНИЯ

a — межфазная поверхность;
σ — коэффициент поверхностного натяжения;
ϱ_2 — плотность жидкости;
g — ускорение свободного падения;
S — поверхность зерна;
V — объем зерна;
ν_1, ν_2 — киниматические вязкость газа и жидкости;
u_1, u_2 — скорость газа и жидкости на свободное сечение слоя;
d — размер зерна;
β_{12} — коэффициент массообмена газ-жидкость;
D — коэффициент диффузии;
φ — газосодержание;
m — толщина пленки;
α_{23} — коэффициент теплообмена;
c_{p_1}, c_{p_2} — теплоемкость газа и жидкости;
l — координата по длине слоя;
r — координата по радиусу зерна;
a_1, a_2 — коэффициенты температуропроводности в радиальном и продольном направлениях;
λ_1, λ_2 — то же, но коэффициенты теплопроводности;
t — время;
R — радиус зерна;
T — температура;
D_1, D_2 — коэффициенты продольного перемешивания вещества;
λ_2 — то же, но тепла;
$S_{12}=a$;
W_1, W_2 — скорости реакции по компонентам;
C — концентрация;
C^* — равновесная концентрация водорода;
ε — пористость;
S_{23} — удельная поверхность насадки;
E — энергия активации;
T_3 — температура катализатора;
T — температура газо-жидкостного потока;
c_{b_x} — концентрация на входе в слой;
R_0 — сопротивление датчика;
J — сила тока;
ΔT — перепад температур между потоком и поверхностью зерна.

ЛИТЕРАТУРА

1. Voyer R. D., Miller A. I.: Can. J. Chem. Eng.: *46*, 335 (1968)
2. Mashalkar Sharma M. M., Trans. Inst. Chem. Eng.: *48*, 162 (1970)
3. Saada I.: Chimie et Indi Genie Chim.: 105, 20, 1415, (1972)
4. Specchia V., Sicardi S,, Gianetto A.: AIChE J.: *20*, 647 (1974)
5. Böxkes W., Hofmann H.: Verfahrenstechnik, *9*, (3) 112, (1975)
6. В. А. КИРИЛЛОВ, Б. Л. ОГАРКОВ: Второй советско-французский семинар по математическому моделированию каталитических процессов. Новосибирск, 1976, 150.
7. В. А. КИРИЛЛОВ, М. А. КАСАМАНЯН: Hung. J. Ind. Chem.: *3*, 21 (1975)
8. Satoshi M., Tatsuro M.: Chem. Eng. Sci., *25*, 1328 (1974)
9. М. Э. АЭРОВ, О. М. ТОДЕС: Гидравлические и тепловые основы работы аппаратов со стационарным и взвешенным зернистыми слоями. М., Химия, 1968.
10. В. Г. ЛЕВИЧ: Физико-химическая гидродинамика. М., Госиздат, 1959.
11. Н. С. КОШЛАКОВ, Э. В. ГЛИКЕР, М. М. СМИРНОВ: Основные дифференциальные уравнения математической физики. М., Физмат. 1962.
12. Г. К. ЗИГАНШИН, Е. Ф. СТЕФОГЛО, А. ЕРМАКОВА: Кинетика и катализ, *14*, 2 (1973)
13. В. А. КИРИЛЛОВ, М. А. КАСАМАНЯН: ТОХТ, *9*, 870 (1975)

SUMMARY

The heat and mass transfer was investigated in fixed catalyst bed during upwards, co-current phase flow. To the experiments a model reaction was applied, the gained results proved the reliability of the suggested relations and the mathematical model of the process.

HUNGARIAN JUORNAL
OF INDUSTRIAL CHEMISTRY
VESZPRÉM
Vol. 6. pp. 187–194 (1978)

STUDIES ON ETHYLENE DICHLORIDE FORMATION IN A ROTARY FILM REACTOR I.

Kinetical Investigations

SZÉPVÖLGYI, J. and UJHIDY, A.

(Research Institute for Technical Chemistry of the
Hungarian Academy of Sciences, Veszprém)

Received: February 6, 1978.

The present paper which is the first of this series discusses the formation of ethylene dichloride in a rotary film reactor. The suitable conditions of the homogeneous phase reaction were determined from the viewpoint of the reaction kinetics. Conditions for homogeneous kinetical investigations were determined. The measured data are evaluated on the basis of earlier developed formal kinetical treatment.

1. Introduction

In the rotary film procedure that can be regarded as an intensive one, the desired technological step is realized in a thin liquid layer being formed mechanically in the equipment. As a consequence of the forced movement of the liquid film, very favourable heat and mass transfer conditions can be ensured; this equipment can mainly be applied to carry out physical and chemical procedures accompained with heat and mass transfer.

The applicability of rotary film equipment as a reactor has so far only been investigated in the case of liquid-liquid reactions. However, in order to extend the scope of its application, the conditons formed in the given equipment for gas-liquid reactions were studied. The results of this activity are discussed in this series of papers.

The simultaneous absorption and chemical reaction following that of two gases belong to those processes that were so far studied only slightly. The formation of ethylene dichloride was selected as the model.

As it is known from literature, ethylene and chlorine do not react with each other below 150 °C in a gaseous phase, however, if they are absorbed in a common solvent an exotherm chemical reaction of a high rate soon takes place between the absorbed gases at room temperature. The main product of the reaction, of the ethylene dichloride itself was chosen as the solvent.

Having selected the model reaction, the following aims were set:

1. Investigations on the kinetics of the ethylene dichloride formation in a homogeneous phase by the elimination of the mass transfer, in order to determine the kinetical information necessary for the construction of the mathematical model of rotary film equipment, as the reactor.

2. Investigations on the reaction of ethylene and chlorine in equipment ensuring the known transfer surface, in order to determine the effect of the gas-liquid mass transfer. Experiments carried out in this equipment make it possible to select the transfer model and to separately study the source members in the mathematical model.

3. Investigations on the applicability of rotary film equipment to realize the processes of a given type and the control of the mathematical model for the rotary film reactor.

This paper discusses the results of kinetical measurements.

2. Addition of Chlorine on Monoolefines

Most of the carbon-carbon double bonds can easily be halogenized by bromine, chlorine and interhalogen compounds. Addition usually takes place according to electrophil mechanism. The electrophil character of halogen addition was experimentally verified by WILLIAM [1].

According to ROBERTSON et al. [2, 3, 4] the rate equation of chlorination by addition is as follows:

$$-\frac{d[Cl_2]}{dt} = k_2\,[\text{olefine}]\,[Cl_2] \tag{1}$$

where the symbols in the brackets represent concentrations.

In the above papers the authors verified that the transitional state determinig the reaction rate contains both the electrophil and nucleophil part of halogen:

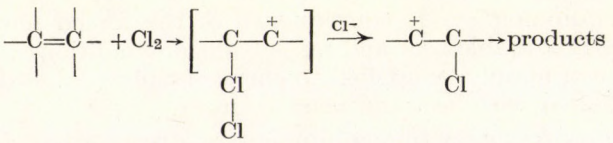

(2)

SHILOV [5] described the special effect of Cl^- breaking off in the 2nd step of the reaction and he recommended the following rate equation:

$$-\frac{d[Cl_2]}{dt} = k_3\,[\text{olefine}]\,[Cl_2]\,[Cl^-] \tag{3}$$

The effects of the materials catalyzing the chlorine addition were investigated in detail. For example, in the case of $FeCl_3$ by HENNE et al. [6] the electrophil complex having a good reactivity is formed as follows:

$$Cl_2 + FeCl_3 \rightleftarrows [Cl^+FeCl_4^-] \tag{4}$$

Investigations on the reaction of ethylene and chlorine were described in

numerious papers [7, 8, 9, 10]. The main goal of the investigations was almost always to clarify the mechanism of the reaction and the kinetics were only slightly studied.

3. Method of Kinetical Measurements

References dealing with ethylene dichloride formation describe it as a fast reaction. CALDIN [11] indicated two basic methods for kinetical investigation of fast reaction:

1. If the conditions of reaction are suitably selected it can be so slow that it is possible to follow it by „traditional" methods.

2. The reacting solutions are mixed as rapidly as possible, but during observation extremely rapid methods are not applied.

Having studied the above possible methods from the viewpoint of the kinetical investigation of ethylene dichloride formation, the application of a quenching method belonging to the second set of possibilities seemed to be expedient. For the removal of the first reagent, viz. chlorine, the reduction by KI that is known in analytical chemistry is applicable. By experimental observations, the reduction is instantaneous, howover, few details are known in literature regarding its rate constant. As a guideline, it is possible to take into consideration the fact that for the rate of iodide oxidation, rate constants of $10^7 - 10^{10}$ order of magnitude are given for different reagents and different solvents.

During kinetical investigations of addition in the liquid phase, the effect of the gas-liquid mass transfer had to be eliminated. For this reason, ethylene and chlorine were bubbled for a given period through ethylene dichloride solvent, and pouring together adequate volumes of the ethylene and chlorine "solutions" so gained the changes in ethylene and chlorine concentration versus time were measured. The experiments were carried out in a thermostated glass apparatus of approximately 100 ml volume and equipped with a stirrer.

Prior to the kinetical investigations, two problems must be studied:

— whether as a consequence of considerable reaction heat, the temperature of the mixture does not rise in the starting moment of the reaction (pouring together the solutions);
— what is the extent of desorption caused by intensive mixing.

The temperature of the reaction mixture was measured by a thermometer immersed in the solution. The measurements did not show in any case a temperature rise higher than 0.5 °C following the start of the reaction; this resulted from the relatively high heat capacity of the system and large circulation rate of the cooling liquid.

Occasional desorption of gases was investigated from 10 to 40 °C. The quantity of desorbed ethylene was verified to have been lower than 5% compared to the solved ethylene at the applied initial concentrations. For chlorine, this value was 4.6%.

During kinetical investigations, the initial ethylene-chlorine molar ratios were 1 and 0.33 respectively. Such selection of concectrations was partly supported by the fact that contradictionary data can be found in literature regarding the excess of any reagent, partly because 0.33 initial molar ratio concentrations of ethylene and chlorine change against the time in such a manner that

the complete ethylene-chlorine molar ratio range, occurring in apparatuses to be studied later, is covered.

Ethylene dichloride without a catalyst and that containing 0.1% $FeCl_3$ were used as the solvent respectively.

The temperature of the reaction mixture varied from 14 to 40 °C.

The reaction was quenched by a 10% KI solution poured into the mixture at a suitable moment. The quantity of reacted chlorine was determined by the titration of iodine of an equivalent amount that was formed in the solution, while the quantity of reacted ethylene was calculated indirectly from the analysis data of the mixture gained after determination of the chlorine content.

The series of concentration vs. time values were gained as a result of the kinetical investigations. As an example, changes of ethylene and chlorine concentrations against the time for a given series of experiments are shown in *Fig. 1.*

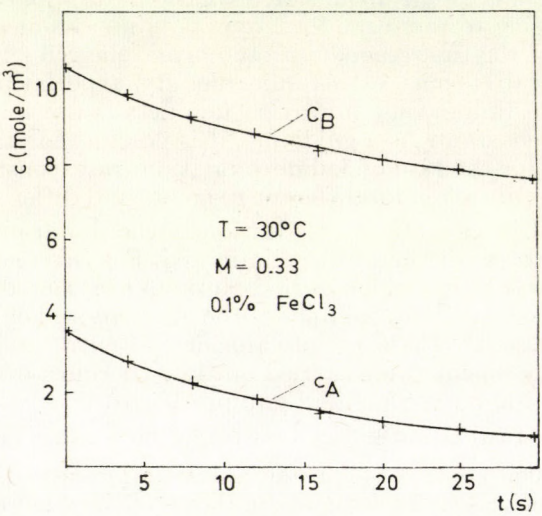

Fig. 1.
Changes of ethylene (c_A) and Chlorine (c_B) concentrations versus time

4. Calculations of Kinetical Characteristics

In the following the rate equation of the studied reaction gained from the data of the kinetical investigations is given. A general method to find the rate equations of chemical reactions is unknown. In practice correlations describing the measured data with the best fitting are usually determined on the basis of certain assumptions relating to stoichiometrics and the mechanism of the reaction by a trial and error method.

Starting from the consideration of theoretical systems, a method was developed to give stoichiometric and rate equations of homogeneous reactions.

The elaborated method described earlier [12—15] can be favourably used partly to construct a programme of kinetical measurements and partly to evaluate experimental results.

Applying the above method for the studied system, the occurrence of the following two reactions were verified, similarly to the results of the kinetical measurements:

$$C_2H_4 + Cl_2 = C_2H_4Cl_2 \tag{5}$$

$$C_2H_4 + 2Cl_2 = C_2H_3Cl_3 + HCl \tag{6}$$

Describing the formal kinetical correlations for reactions (5) and (6):

$$r_1 = -\frac{dc_B}{dt} = k_1 c_A c_B \tag{7}$$

$$r_2 = -\frac{1}{2}\frac{dc_B}{dt} = k_2 c_A c_B^2 \tag{8}$$

Based on Eq. (7) and (8) assuming that for sufficiently small Δt $\frac{dc}{dt} \approx \frac{\Delta c}{\Delta t}$ the rate constants can be calculated as follows:

$$k_1 = \frac{\Delta c_B - 2\Delta c_A}{c_A \cdot c_B \cdot \Delta t} \tag{9}$$

$$k_2 = \frac{\Delta c_A - \Delta c_B}{c_A \cdot c_B^2 \cdot \Delta t} \tag{10}$$

where:

k_1 is the rate constant of Eq. (5) while k_2 is that of Eq (6), c_A concentration of ethylene, c_B that of chlorine, t time.

Having calculated values of k_1 from Eq. (9) and k_2 from Eq. (10) on the basis of measured concentration vs. time values, the gained rate constants can be regarded as constant ones with good approximation, and do not show a change

Table 1.

Kinetical characteristics of reactions taking place between ethylene and chlorine in liquid phase

$FeCl_3$ (%)	T (°C)	$10^3\ k_1$ ($m^3\ mole^{-1}\ s^{-1}$)	$10^7\ k_2$ ($m^6\ mole^{-2}\ s^{-1}$)	ΔH_1	ΔH_2
				(kcal $mole^{-1}$)	
0	14	0.48	0.70	23.41	24.33
	20	1.11	1.69		
	25	2.19	3.40		
	30	4.24	6.73		
	35	7.93	13.02		
	40	14.58	24.50		
0.1	14	0.71	0.73	23.14	24.10
	20	1.62	1.73		
	25	3.18	3.47		
	30	6.00	6.90		
	35	11.34	13.06		
	40	20.69	24.43		

of tendency character in the function of any parameter. This fact refers to the applicability of the formal kinetical treatment for the description of the system.

The mean values of rate constants and activation enthalpies calculated from ARRHENIUS' equation are summarized in *Table 1.*

5. Conclusions

Based on *Table 1,* the following conslusions can be drawn:

1. The addition (formation of ethylene dichloride) can be regarded as a fast reaction in accordance with terminology of [11].

2. On the effect of the $FeCl_3$ catalyst, the rate constant of the addition is increased by up to 40—50%, while that of the substitution (ethylene trichloride formation) practically does not change. Taking into account the main goal of the realization of the reaction, i.e. the formation of as much ethylene dichloride as possible, further investigations will be carried out in solutions containing a $FeCl_3$ catalyst.

3. Between the studied temperature limits, the activation enthalpies of addition and substitution are approximately equal. Both reactions are those of moderate activation enthalpy.

SYMBOLS

c concentration in the bulk of liguid phase, mole m^{-3};
Δc concentration difference, mole m^{-3};
ΔH activation enthalpy, kcal $mole^{-1}$;
k_1 rate constant of addition, m^3 $mole^{-1}$ s^{-1};
k_2 rate constant of substitution, m^6 $mole^{-2}$ s^{-1};
M ethylene-chlorine molar ratio in liquid phase, mole/mole;
r reaction rate, mole m^{-3} s^{-1};
T temperature, °C;
t time, s;

Indices

A ethylene
B chlorine

REFERENCES

1. WILLIAMS, G.: Trans. Far. Soc. *37*, 749 (1941)
2. ROBERTSON, P. W., CHLORE, N. T., MCNAUGHT, K. J. PAUL, C. W.: J. Chem. Soc. 335 (1937)
3. DELAMARE, P. B. D., ROBERTSON, P. W.: J. Chem. Soc. 888 (1945)
4. HARTMAN, I., ROBERTSON, P. W.: J. Chem. Soc. 891 (1945)
5. SHILOV, E. A.: Bull. Soc. Chim. France 2903 (1963)
6. HENNE, A. L., HEPPARD, J. W., YOUNG, E. J.: J. Am. Chem. Soc. *72*, 3577 (1950)
7. GALITZENSTEIN, E., WOOLF, G.: J. S. C. I. *69*, 289 (1950)
8. GALITZENSTEIN, E., WOOLF, G.: ibid. *69*, 294 (1950)
9. BALASUBRAMANIAN, S. N., RIHAMI, D. N.,DORAISWAMY, L. K.: Ind. Eng. Chem. Fundam. *5* ,184 (1966)
10. VOLITOV, R. B., PRUSZENKO, B. E., GARIFJANOV, G. G., MOROZOV, JU. D., PANCSENKOV G. M.:, Neftekhim. *16*, 606 (1976)
11. GALDIN, E. F.: Fast Reactions in Solution. Blackwell, Oxford, 1964.
12. BLICKLE, T., SEITZ, K.: A modern algebrai módszerek felhasználása a műszaki kémiában (The Application of Modern Algebraic Methods in Technical Chemistry) Műszaki Könyvkiadó, Budapest, 1975. p. 101.

13. Blickle, T., Szépvölgyi, J.:Hung. J. Ind. Chem. *4*, Suppl. 79 (1976)
14. Szépvölgyi, J.: MTA MÜKKI Tudományos Eredményei IV. Veszprém, 1976. Vol. II. p. 313.
15. Blickle, T., Szépvölgyi, J., Novák, B.: Számítógépi algoritmus adott vegyületekből felépíthető sztochiometriai egyenletek előállítására (Computer Algorithm for the Contruction of Stoichiometric Equations from Given Compounds) Műszaki Kémiai Rendszerek '77 Konferencia, Keszthely, 1977.

РЕЗЮМЕ

В статье, являющейся первой частью серии статей, речь идёт о кинетическом исследовании реакции образования 1,2-дихлор-этана, которая была выбрана в целях изучения ротационного плёночного аппарата, как газо-жидкостного реактора.

Были установлены условия проведения кинетических исследований в гомогенной фазе. Полученные экспериментальные данные были оценены с помощью применения разработанного ранее формального кинетического метода обработки.

HUNGARIAN JOURNAL
OF INDUSTRIAL CHEMISTRY
VESZPRÉM
Vol. 6. pp. 195–210 (1978)

STUDIES ON ETHYLENE DICHLORIDE FORMATION IN A ROTARY FILM REACTOR II.

Investigations in a Reactor of Known Transfer Surface

SZÉPVÖLGYI, J.

(Research Institute for Technical Chemistry of the Hungarian Academy of Sciences, Veszprém)

Received: February 6, 1978

Ethylene dichloride formation as a model reaction absorption with chemical reaction was studied in a reactor of given, constant gas-liquid contact surface. The values of the operational parameters that ensure the production of as much ethylene dichloride as possible in the given reactor were determined. These data formed the basis for the planning of experiments aimed at studying a rotary film reactor.

A unidimensional diffusion model was constructed to describe the studied system and qualitatively evaluate the mass transfer conditions. Based on the model, the existence of both liquid and gas side mass transfer resistances was verified and those are comparable.

1. Introduction

In accordance with the goal described in the previous paper [1], the determination of rate constants of the formation of ethylene dichloride in an apparatus of known, constant gas-liquid contact surface described in Ref. [2], was investigated.

As a consequence of the bad solubility of reacting gases, and because of the rapid addition reaction between absorbed ethylene and chlorine, the gross rate of the process is probably determined by mass transfer. However, taking into account the change of the gas-liquid transfer surface as a function of operational parameters in rotary film equipment, that can be measured only with difficulty, it seemed more favourable to study the operational parameters in equipment ensuring a known and constant gas-liquid transfer surface.

Experiments carried out in this equipment partly provided data to study the effect of the mass transfer, and hence the changes in quantity and the composition of the product against the operational parameters, and the applicability of the physical-mathematical model of the system could also be investigated.

2. The Experimental Assembly and Technique

The experiments were carried out in an assembly *(Fig. 1)* constructed according to Ref. [2]. During the operation a constant liquid level has to be maintained in the reactor *1* within the limits of ± 1 mm.

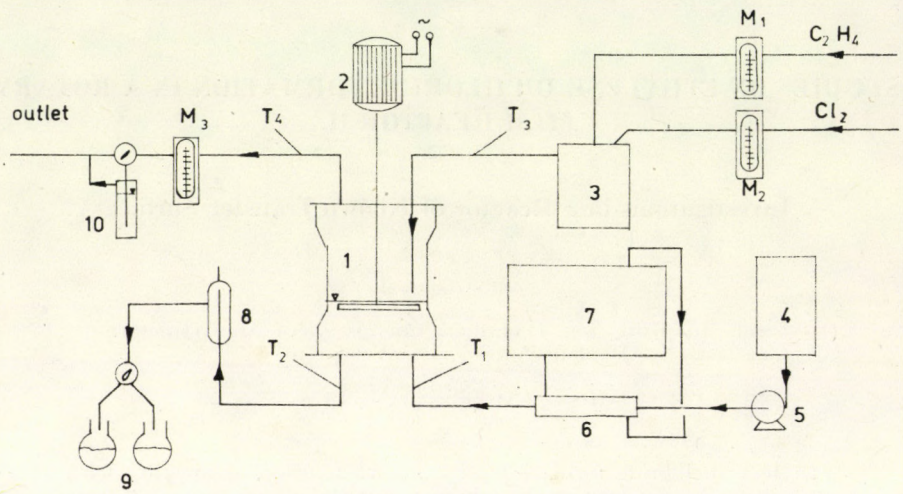

Fig. 1.
Experimental assembly ensuring known gas-liquid contact surface
1 — chlorinating reactor; 2 — driving motor; 3 — gas mixer; 4 — ethylene dichloride tank; 5 — peristaltic pump; 6 — cooler; 7 — thermostat; 8 — level regulator; 9 — collecting bottles; 10 — gas scrubber; M_1, M_2, M_3 — differential manometers; T_1—T_4 — thermometers

The actual gas-liquid contact surface in apparatus *1* was 7.70×10^{-3} m^2, while the transfer surface related to the volume of the liquid phase was 24.31 m^{-1}.

The feed rate of the solvent (ethylene dichloride) varied from 3.85 to $4.10 \cdot 10^{-7}$ m^3 s^{-1}, so the mean residence time of the solvent in the chlorinating reactor was 768—826 s.

The solvent was fed by peristaltic pumps, while the gases were taken from cylinders. The mean residence time of the gas phase in the reactor *1* varied from 17 to 70 s depending on the gas feed rate and composition.

The mixture leaving the reactor was collected in bottle *9* as can be seen in *Fig. 1*. The experimental assembly was constructed so that the liquid reached the bottle for a period corresponding to 1% of the mean liquid residence time in the reactor.

The bottles contained the 10% KI solution (to determine the dissolved but unreacted chlorine) and KAUFMANN'S solutions (to determine the solved, but unreacted ethylene) so the reaction was quenched there.

The determination of ethylene on the basis of KAUFMANN'S iodine-bromine number is disturbed by the chlorine dissolved in the liquid phase, because the latter reacts with KBr in KAUFMANN'S solution. For this reason, the amount of bromine, formed by the expected chlorine concentrations in the reaction of

Cl_2 and KBr, was determined. A calibration curve was constructed from these measured data and the quantity of dissolved ethylene was calculated, taking this calibration into account.

The composition of the fed gas mixture was calculated from the viewpoint of the purity and mixing ratio of the gases. The fed and discharged liquid phase (after suitable preparation) were analyzed by gas-chromatograph.

For the experimental assembly shown on *Fig. 1*, the transfer conditions within the reactor are determined by the following factors:

- temperature of the system;
- mixing conditions within the liquid phase;
- feed rate of the gas mixture;
- composition of the gas mixture.

The temperature of the reaction mixture varied from 14 to 40 °C, while the r.p.m. of the stirrer was constant, viz. 160.2. Above this rpm value, the gas side resistance hardly decreases with increased rpm, and at the above value a flat gas-liquid contact surface was gained that was free of waves.

The ethylene feed rate related to the gas-liquid contact surface was 2.667 — 8.935 mole $m^{-2}\,s^{-1}$, and the ethylene-chlorine molar ratio in the gas phase changed between 0.9 and 1.4.

With the solubility measurements, chlorine is dissolved in ethylene dichloride 13 times better compared to ethylene. For this reason the ethylene was regarded as a suitable basic component in the studied system.

On the basis of the analysis data conversion, the yield and selectivity values relating to the ethylene as a basic component were calculated as follows:

$$X = \frac{\text{reacted ethylene (mole)}}{\text{fed ethylene (mole)}} \tag{1}$$

$$K = \frac{\text{formed ethylene dichloride (mole)}}{\text{reacted ethylene (mole)}} \tag{2}$$

$$H = X \cdot K$$

where X conversion, K selectivity, H yield.

3. The Experimental Results

The primary realization aim of the studied model reaction is that as large a part of the fed ethylene (and chlorine) as possible must be dissolved and reacted, and the reaction between the dissolved gases must take place so that the product is mainly ethylene dichloride. The quantity of the formed product is given by $B'_A \cdot X$ (where B'_A is the ethylene feed rate relating to the gas-liquid contact surface) while the selectivity gives information about the composition of the product. The main goal is to ensure the largest possible value of $B'_A \cdot X \cdot K = B'_A \cdot H$ in the given equipment.

The yield values measured at different operational parameters are summarizzed in *Tables 1* and *2*.

If the amount of ethylene dichloride formed on the unit of the gas-liquid contact surface for unit time is plotted against the temperature *(Fig. 2.)* a slight increase of $B'_A \cdot H$ can be seen between 14—30 °C and a slight decrease

Table 1.

Measured yield values in the equipment of known transfer surface I.

$10^2 B'_A$ (mole $m^{-2}s^{-1}$)	T (°C)	M' (mole/mole)	H (%)	M' (mole/mole)	H (%)
2.667	30	0.90	27.5	0.99	53.1
	35		21.9		29.7
	40		14.1		26.6
3.650	30	0.90	50.0	0.98	51.0
	35		43.1		47.7
	40		21.6		42.2
4.430	14	0.90	39.9	1.01	40.8
	20		42.0		43.0
	25		44.2		46.4
	30		49.3		51.1
	35		41.2		50.4
	40		30.7		41.0
5.868	30	0.90	42.2	0.99	49.8
	35		34.9		46.8
	40		25.9		38.5
7.290	30	0.90	35.6	0.99	40.9
	35		29.4		38.9
	40		21.3		33.9
8.935	30	0.90	30.3	1.00	35.0
	35		25.0		32.9
	40		18.5		28.5

above 30 °C with increased T. Some characteristic series of experiments are shown in *Fig. 1*, however, for all the studied B'_A values a similar tendency can be observed.

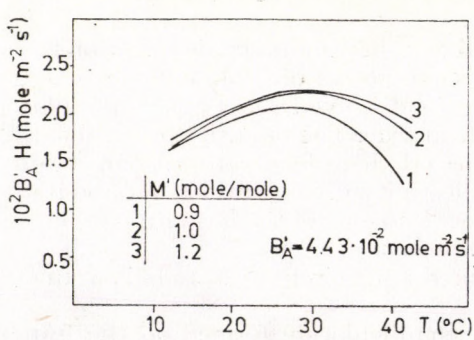

Fig. 2.
Quantity of formed ethylene dichloride as plotted against the temperature

Table 2.

Measured yield values in the equipment of known transfer surface II.

$10^2\ B'_A$ (mole $m^{-2}s^{-1}$)	T (°C)	M' (mole/mole)	H (%)	M' (mole/mole)	H (%)
2.667	30	1.19	37.8	1.38	38.6
	35		33.2		34.4
	40		29.8		29.8
3.650	30	1.21	53 5	1.41	52.3
	35		50.4		48.9
	40		44.5		45.2
4.430	14	1.19	41.9	1.38	41.8
	10		45.2		43.2
	25		47.8		45.4
	30		51.3		48.0
	35		48.6		42.9
	40		44.6		38.0
5.868	30	1.20	41.5	1.40	47.2
	35		47.9		44.9
	40		42.5		40.8
7.290	30	1.22	43.6	1.38	46.1
	35		40.8		39.5
	40		35.4		37.6
8.935	30	1.20	36.5	1.41	40.3
	35		34.5		34.4
	40		31.5		33.1

In the investigated range, the $B'_A \cdot H$ value increases with the increased gas load of the reactor *(Fig. 3)*, however, to a constantly decreasing extent.

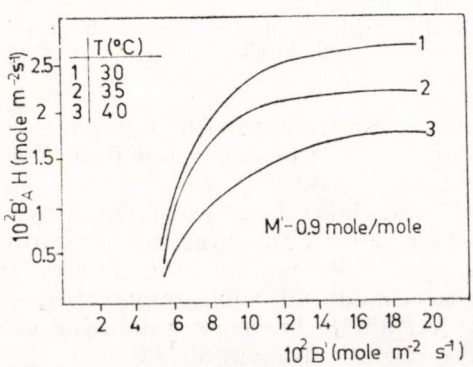

Fig. 3.
Quantity of formed ethylene dichloride as plotted against gas feed rate

The amount of ethylene dichloride formed is also increased with the increased ethylene-chlorine molar ratio (*Figs. 4* and *5*), so a slight ethylene excess seems to be favourably ensured. However, during the development of the programme

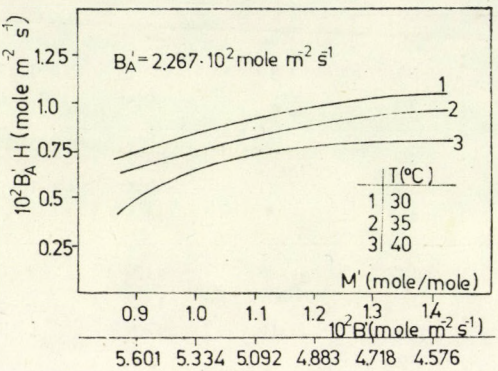

Fig. 4.
Quantity of formed ethylene dichloride as plotted against the ethyalene-chlorine molar ratio I.

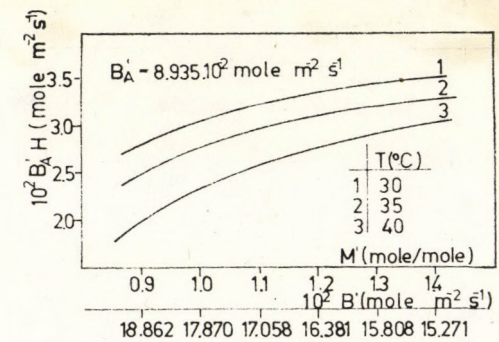

Fig. 5.
Quantity of formed ethylene dichloride as plotted against the ethylene-chlorine molar ratio II.

of measurements to be carried out in rotary film equipment consideration has to be given to the fact that the effect of the change in M' exactly in the $0.9 \leq \leq M' \leq 1$ range is the most expressed.

Based on experimental data, the reaction can favourably be realized in the temperature range from 14 to 30 °C. However, taking into consideration the strongly exothermic character of the reaction and the heat transfer problems caused by this fact, the reaction advisably has to be carried out at about 30 °C. It should be noted that certain technologies producing ethylene dichloride below its boiling point also operate at about 30 °C.

In the given equipment as it could be seen, the quantity of formed ethylene dichloride was increased with increased B'_A. However, if based on *Tables 1* and

2, the changes of yield is investigated as a function of B'_A, the yield values are the highest in the $3.650 \times 10^{-2} \leq B'_A \leq 5.868 \times 10^{-2}$ mole $m^{-2}s^{-1}$ range. Following from the above mentioned, the suitable value of the ethylene feed rate is 5.10^{-2} mole $m^{-2}s^{-1}$.

4. The Applied Model

Relatively few papers have discussed the process studied here, viz. the simultaneous absorption of two gases and their chemical reaction with each other following absorption [3–9], is not to be found in a model applicable to describe the above investigated system.

In order to evaluate quantitatively the measured data, the elaboration of a suitable model became necessary.

The following assumptions can be made during the construction of the model:

- the system is isothermal and of a steady-state;
- both the liquid and gas phase are homogenous in the bulk;
- along the contact surface of the phases, a boundary film is formed both on the gas and the liquid side, and the flow and concentration conditions in these films vary in a different manner than in the main masses of the phases;
- a chemical reaction occurs only in the liquid phase;
- the concentration does not change either in the gas or in the liquid phase in the direction being parallel to the gas-liquid contact surface.

Based on the above physical model, the system is described by a unidimensional diffusion model. The balance equations of the ethylene and chlorine are given for the boundary films by phases.

The liquid side balance equation of ethylene that takes into account the results of the kinetical investigations [1]:

$$-D_A \frac{d^2\hat{c}_A}{dx^2} + k_1\hat{c}_A\hat{c}_B + k_2\hat{c}_A\hat{c}_B^2 = 0 \tag{4}$$

The boundary conditions for Eq. (4)

$$\begin{aligned} &\hat{c}_A(0) = c_A^* = H'_A c'_A(0) \\ &\hat{c}_A(Z) = c_A \\ &\hat{c}_B(0) = \hat{c}_B(Z) = c_B \end{aligned} \tag{5}$$

In connection with the above boundary conditions, it can be remarked that the chlorine concentration in the liquid side boundary film must be (and may be) regarded as a constant one, only in the sense that during the solution of the mathematical model calculation can be made with a pseudo-first order reaction.

Solution of Eq. (4) taking into account Eq. (5):

$$c_A = \frac{\frac{1}{\omega_1} c_A^* - c_A}{\frac{1}{\omega_1} - \omega_1} \exp(\lambda x) + \frac{c_A - \omega_1 c_A^*}{\frac{1}{\omega_1} - \omega_1} \exp(-\lambda x) \tag{6}$$

where:

$$\lambda = \sqrt{\frac{k_1 c_B + k_2 c_B^2}{D_A}} \tag{7}$$

$$\omega_1 = \exp(\lambda Z) \tag{8}$$

The gas side balance equation of ethylene (for the boundary layer):

$$-D'_A \frac{d^2 c'_A}{dx^2} = 0 \tag{9}$$

The boundary conditions:

$$c'_A(0) = \frac{c^*_A}{H'_A} \tag{10}$$

$$c'_A(Z') = c'_A$$

In the description of Eq. (9) it was tacitly taken into consideration that in the gas phase, ethylene dichloride vapour is also present, in addition to ethylene and chlorine, and the ratio of the ethylene and chlorine feed rates is not equal to the ratio of absorption rates.

The solution of Eq. (9—10) is as follows:

$$c'_A = \frac{\frac{c^*_A}{H'_A} - c'_A}{Z'} x + \frac{c^*_A}{H'_A} \tag{11}$$

The connecting condition for gas and liquid phases:

$$\overline{R}_A = \overline{R}'_A \tag{12}$$

The absorption rates are the following:

$$\overline{R}_A = -D_A \left(\frac{dc_A}{dx}\right) x = 0 \tag{13}$$

$$\overline{R}'_A = -D'_A \left(\frac{dc'_A}{dx}\right) x = 0 \tag{14}$$

Let Eq. (6) be replaced into Eq. (13):

$$\overline{R}_A = -D_A \lambda \frac{\frac{1}{\omega_1} c^*_A - c_A}{\frac{1}{\omega_1} - \omega_1} + D_A \lambda \frac{c_A - \omega_1 c^*_A}{\frac{1}{\omega_1} - \omega_1} \tag{15}$$

Now let Eq. (11) be replaced into Eq. (14):

$$\overline{R}_A = -D'_A \frac{\frac{c^*_A}{H'_A} c'_A}{Z'} \tag{16}$$

Following from Eq. (12), (15) and (16):

$$\bar{k}_A \left[\frac{1}{2\omega_1}+\frac{\omega_1}{2}\,(c_A^*-c_A)\right]=\bar{k}'_A\left(\frac{c_A^*}{H'_A}-c'_A\right) \tag{17}$$

where:

$$\bar{k}_A=-\frac{2D_A\lambda}{\frac{1}{\omega_1}-\omega_1} \tag{18}$$

$$\bar{k}'_A=\frac{D'_A}{Z'} \tag{19}$$

In Eq. (17) the driving force of the mass transfer contains the c_A^* surface concentration. Now let the driving force be expressed by the bulk concentrations. If we express c_A^* from Eq. (17) and replace it to Eq. (16) after suitable transformations, the following equation is gained:

$$\bar{R}'_A=\frac{1}{\frac{H'_A ch Y}{\bar{k}'_A}+\frac{\mathrm{sh}\,Y}{D_A\lambda}}[(H'_A \mathrm{ch}\,Y/c'_A-c_A] \tag{20}$$

where:

$$Y=\lambda Z$$

and

$$\frac{\mathrm{sh}\,Y}{D_A}=\frac{1}{\bar{k}_A} \tag{21}$$

The complete component transfer coefficient for ethylene:

$$\bar{k}_{A\,(\mathrm{comp.})}=\frac{1}{\frac{H'_A \mathrm{ch}\,Y}{\bar{k}'_A}+\frac{1}{\bar{k}_A}} \tag{22}$$

The complete component transfer coefficient for chlorine follows from the assumption made during the model construction:

$$\bar{k}_{B\,(\mathrm{comp.})}=\frac{1}{\frac{H'_B}{\bar{k}'_B}+\frac{1}{\bar{k}_B}} \tag{23}$$

So the absorption rate for chlorine:

$$\bar{R}_B=\frac{1}{\frac{H'_B}{\bar{k}'_B}+\frac{1}{\bar{k}_B}}\,(H'_B c'_B-c_B) \tag{24}$$

The gas side component transfer coefficient of ethylene is the following:

$$\bar{k}'_A=\frac{D'_A}{D'_B}\,\bar{k}'_B \tag{25}$$

In order to calculate the component transfer coefficients, the value of Y has to be known. After suitable replacements and transformations, the following expression is gained:

$$\frac{D_A D'_B H'_A}{D_B D'_A H'_B} Y - \frac{\lambda D_A D'_B H'_A (H'_B c'_B - c_B)}{D'_A H'_B \overline{R}_B} + \frac{\lambda D_A H'_A c'_A}{\overline{R}_A} = \text{th } Y + \frac{\lambda D_A c_A}{\overline{R}_A} \text{ ch } Y \tag{26}$$

From Eq. (26) the value of Y can soon be calculated at the given operational parameters, if the absorption rates, the concentration in the bulk of phases and the material constants are known. Then the transfer coefficients can be calculated as follows:

$$\overline{k}_A = \frac{\sqrt{D_A (k_1 c_B + k_2 c_B^2)}}{\text{sh } Y} \tag{27}$$

$$\overline{k}_B = \frac{D_B}{Y} \sqrt{\frac{k_1 c_B + k_2 c_B^2}{D_A}} \tag{18}$$

$$\overline{k}'_B = \frac{H'_B R'_B}{H'_B c'_B - c_B - \dfrac{\overline{R}'_B}{k_B}} \tag{29}$$

The gas side mass transfer coefficient for ethylene can be calculated from Eq. (25) and (29).

5. Evaluation of the Experiments

During the evaluation of the experiments carried out in the equipment of constant, known transfer surface values of component transfer, the coefficients were calculated from the measured data (*Tables 3* and *4*).

A comparison of adequate liquid and gas side component transfer coefficients show that they are of equal order, altough the liquid side transfer coefficients are slightly larger. So for the given equipment, there is mass transfer resistance both on the liquid and gas side.

The $\overline{k}_A$ and $\overline{k}_B$ values summarized in *Table 3*, do not show definite changes either against gas composition (M′) or temperature. However, if the calculated $\overline{k}_A$ (and $\overline{k}_B$) values are plotted against the total gas feed rate, taking into account common changes of B'_A and M', an ascending series of points is gained *(Fig. 6)*.

Starting from the tendency shown on *Fig. 6*, an empirical correlation was given between the component transfer coefficient and the gas feed rate. The adequate correlations are of the following form:

$$\overline{k} = A_1 B'^3 + A_2 B'^2 + A_3 B' + A_4 \tag{30}$$

The coefficients of Eq. (30) are given in *Table 5*.

In order to control the interpolation formula given by Eq. (30), the component transfer coefficients were calculated by Eq. (30), then with these coefficients the absorption rates of ethylene and chlorine were determined *(Table 6)*.

Table 3. Calculated liquid side component transfer coefficients

$10^2 B'_A$ (mole $m^{-2} s^{-1}$)	T (°C)	$M'=0.9$		$M'=1.0$		$M'=1.2$		$M'=1.4$	
		$10^3 \bar{k}_A$	$10^3 \bar{k}_B$	$10^3 \bar{k}_A$	$10^3 \bar{k}_B$	$10^3 \bar{k}_A$	$10^3 \bar{k}_B$	$10^3 \bar{k}_A$	$10^3 \bar{k}_B$
		(m s^{-1})							
2.667	30	1.00	1.09	1.00	1.10	0.96	1.05	0.96	1.09
	35	0.96	1.02	1.09	1.14	1.02	1.08	0.99	1.04
	40	1.03	1.13	1.12	1.19	1.12	1.18	1.00	1.06
3.650	30	2.35	2.74	2.40	2.66	2.30	2.62	2.42	2.71
	35	2.20	2.66	2.30	2.76	2.37	2.71	2.48	2.79
	40	2.64	2.73	2.89	3.05	2.89	3.05	2.69	2.92
4.430	30	3.32	3.73	3.63	3.98	3.33	3.71	3.21	3.62
	35	3.33	3.74	3.73	4.06	3.43	3.72	3.39	3.71
	40	3.68	3.89	3.70	3.91	3.79	4.00	3.52	3.94
5.868	30	4.52	4.96	4.76	5.03	4.66	4.95	4.48	4.79
	35	4.49	4.96	4.70	5.02	4.58	4.81	4.58	4.85
	40	4.48	5.08	4.85	5.12	4.60	4.86	4.72	5.07
7.290	30	4.57	5.10	4.67	5.15	4.74	5.24	4.52	4.96
	35	4.89	5.23	5.01	5.31	4.84	5.30	4.68	4.98
	40	5.03	5.50	4.97	5.48	5.02	5.31	4.87	5.29
8.935	30	4.95	5.50	5.15	5.76	5.28	5.69	5.10	5.48
	35	5.13	6.16	5.31	5.89	5.34	5.83	5.28	5.69
	40	5.22	6.20	5.56	5.97	5.52	6.17	5.39	5.82

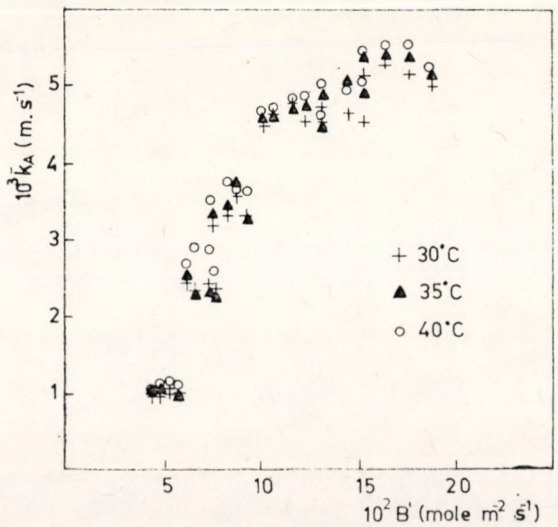

Fig. 6.
Liquid side component transfer coefficient for ethylene as plotted against the gas feed rate

Table 4.

Calculated gas side component transfer coefficients

$10^2 B'_A$ (mole $m^{-2}s^{-1}$)	T (°C)	$M'=0.9$	$M'=1.0$	$M'=1.2$	$M'=1.4$
		$10^3 \overline{k}'_B$ ($m\,s^{-1}$)			
2.667	30	1.18	1.19	1.18	1.13
	35	1.03	1.10	1.11	1.08
	40	1.05	1.00	1.06	1.12
3.650	30	1.66	1.78	1.67	1.56
	35	1.45	1.67	1.65	1.56
	40	1.62	1.71	1.58	1.64
4.430	30	2.10	2.19	1.99	1.91
	35	1.79	2.15	1.97	1.77
	40	1.78	2.19	1.96	1.76
5.868	30	2.33	2.76	2.64	2.52
	35	2.47	2.66	2.58	2.52
	40	2.42	2.67	2.60	2.56
7.290	30	2.39	2.84	2.86	2.92
	35	2.34	2.71	2.81	2.86
	40	2.28	2.86	2.66	2.85
8.935	30	2.46	2.96	3.00	2.94
	35	2.41	2.80	2.91	3.01
	40	2.37	2.94	2.82	2.95

Table 5.

Coefficients of Eq. (30)

Transfer coefficient	A_1	A_2	A_3	A_4
$\overline{k}_A$	2.022	−1.047	0.184	−0.0059
$\overline{k}_B$	1.914	−1.006	0.182	−0.0056
$\overline{k}_B$	−0.358	−0.015	0.032	−0.0004

The differences of the calculated and measured absorption rates were calculated as follows:

$$\Delta = \frac{(\overline{R})_S - \overline{R}}{\overline{R}} \cdot 100 \tag{31}$$

The calculated Δ values are to be found in *Table 7*.

The Δ values for $M'=0.9$ and for lower gas feed rates are relatively high, however, even in this cases they are within limits of errors generally accepted in literature that deals with absorption.

Table 6.

Calculated absorption rate values

$10^2\ B'_A$ (mole $m^{-2}\,s^{-1}$)	T (°C)	$M'=0.9$		$M'=1.0$		$M'=1.2$		$M'=1.4$	
		$10^2(\overline{R}_A)_s$	$10^2(\overline{R}_B)_s$	$10^2(\overline{R}_A)_s$	$10^2(\overline{R}_B)_s$	$10^2(\overline{R}_A)_s$	$10^2(\overline{R}_B)_s$	$10^2(\overline{R}_A)_s$	$10^2(\overline{R}_B)_s$
		(mole $m^{-2}\,s^{-1}$)							
2.667	30	1.494	2.711	1.538	2.462	1.618	1.987	1.405	1.685
	35	1.268	2.728	1.468	2.453	1.509	1.981	1.288	1.675
	40	0.915	2.373	1.373	2.245	1.408	1.971	1.180	1.662
3.650	30	2.760	3.808	2.771	3.484	2.695	2.842	2.399	2.735
	35	2.667	3.816	2.672	3.478	2.599	2.846	2.327	2.711
	40	1.483	2.598	2.561	3.184	2.484	2.838	2.412	2.430
4.430	30	3.378	4.606	3.371	4.182	3.438	3.537	2.975	3.390
	35	3.272	4.609	3.260	4.177	3.326	3.534	2.749	3.185
	40	2.505	3.655	3.131	3.831	3.914	3.527	2.570	2.712
5.868	30	4.192	5.713	4.165	5.148	4.333	4.415	3.761	4.504
	35	4.070	5.725	4.056	5.158	4.182	4.411	3.759	4.548
	40	3.029	4.680	3.890	4.734	4.022	4.397	3.548	4.345
7.290	30	4.386	5.977	4.558	5.649	4.863	4.984	4.843	5.639
	35	4.258	5.993	4.435	5.678	4.708	4.976	4.432	5.224
	40	2.850	4.593	4.250	5.204	4.536	4.969	4.177	4.993
8.935	30	4.458	6.013	4.612	5.823	5.056	5.172	4.984	5.176
	35	4.322	6.007	4.538	5.792	4.905	5.177	4.612	5.129
	40	3.375	5.147	4.329	5.418	4.728	5.167	4.491	5.268

The data of *Table 7* show the applicability of the given model for the description of absorption accompained with chemical reaction in equipment of known transfer surface. In addition, the acceptability of qualitative conclusions taken during the determination of the suitable values for operational parameters can be found. Following from definitions of conversion and yield:

$$\overline{R}_A = B'_A X + B_{ki} c_A \tag{32}$$

$$\overline{R}_B = B'_A (2X - H) + B_{ki} c_B \tag{33}$$

From Eq. (32) and (33):

$$B'_A H = 2\overline{R}_A - \overline{R}_B + B_{ki}(c_B - 2c_A) \tag{34}$$

Eq. (34) is naturally also valid for the replacement of the calculated absorption rate values. Regarding the similar changes of the calculated and measured absorption rates against the operational paramaters, and the equality of $B_{ki}(c_B - 2c_A)$ both for the calculation of $B'_A H$ and $(B'_A H)_s$, the calculated and measured quantities of ethylene dichloride also vary similarly.

Table 7.

Δ values calculated from Eq. (31)

$10^2 B'_A$ (mole $m^{-2} s^{-1}$)	T (°C)	$M'=0.9$		$M'=1.0$		$M'=1.2$		$M'=1.4$	
		Δ_A	Δ_B	Δ_A	Δ_B	Δ_A	Δ_B	Δ_A	Δ_B
		(%)							
2.667	30	28.5	11.1	24.3	3.6	22.1	−6.3	4.4	−10.8
	35	30.6	26.9	30.7	12.1	25.8	−0.9	3.7	−6.3
	40	22.7	32.8	29.3	22.7	26.4	3.8	2.3	−3.5
3.650	30	25.1	8.6	18.0	−2.7	15.0	−7.0	5.2	3.7
	35	38.9	24.4	20.8	3.2	12.1	−5.8	4.8	2.9
	40	30.4	18.6	25.1	0.5	15.9	−1.9	13.4	−5.9
4.430	30	17.4	3.8	13.2	−5.7	18.8	−5.0	11.3	4.7
	35	34.2	21.5	10.9	−3.9	18.4	−2.4	12.4	5.8
	40	28.2	13.3	20.2	−5.3	17.9	−1.8	15.6	−2.7
5.868	30	28.8	15.6	8.9	−7.5	11.4	−9.1	6.7	5.2
	35	48.3	36.3	10.5	−3.9	13.3	−7,0	8.6	6.3
	40	38.2	31.9	18.9	−4.2	16.4	−7.4	10.3	7.5
7.290	30	29.9	18.2	16.3	−1.2	18.5	−5.0	12.4	6.9
	35	48.0	38.0	17.1	3.4	20.4	−3.3	15.1	8.0
	40	28.5	29.3	19.9	−2.0	26.3	1.8	10.7	3.8
8.935	30	27.6	15.4	12.5	−2.3	19.1	−5.9	8.6	−2.7
	35	44.3	33.5	15.6	−2.1	20.4	−3.1	13.1	−0.5
	40	43.9	39.1	18.5	−0.7	22.4	−0.2	12.0	3.2

Acknowledgement

The author is very grateful to Dr. T. Blickle for his valuable advice.

SYMBOLS

$A_1 - A_4$ coefficients; Eq. (30);
B' gas feed rate relating to the surface unit, mole $m^{-2} s^{-1}$;
c concentration in the bulk of the liquid, mole m^{-3};
c' concentration in the bulk of the gas, mole m^{-3};
c^* surface concentration in the liquid phase, mole m^{-3};
$\hat{c}$ concentration in the boundary film formed along the gas-liquid contact surface, mole m^{-3};
D diffusivity, $m^2 s^{-1}$;
H {yield, %; Henry' constant, mole m^{-3} at^{-1};
$H' = HRT$ reduced Henry' constant;
K selectivity, %;
k_1 rate constant of addition, m^3 $mole^{-1}$ s^{-1}:
k_2 rate constant of substitution, m^6 $mole^{-2}$ s^{-1};

k liquid side mass transfer coefficient, m s^{-1};
k' gas side mass transfer coefficient, m s^{-1};
M' ethylene-chlorine molar ratio in gas phase, mole/mole;
R gas constant, m^3 at K^{-1} $mole^{-1}$; absorption rate, mole m^{-2} s^{-1};
T temperature, °C and K;
X conversion, %;
x co-ordinate, m;
Y see Eq. (21);
Δ difference of calculated and measured values, %;
λ see Eq. (7);
ω see Eq. (8);

Indices

A ethylene
B chlorine
ki output value
s calculated value

Other signs

' value relating to the gas phase
— mean value

REFERENCES

1. Szépvölgyi, J., Ujhidy A.: Hung. J. Ind. Chem. *6*, 187 (1978)
2. Danckwerts, P. V., Gillham, A. J.: Trans. Inst. Chem. Eng. *44*, T/42 (1966)
3. Roper, G. H., Hatch, T. F., Pigford, R. L.: Ind. Eng. Chem. Fundam. *1*, 144 (1962)
4. Abselrod, Yu, V., Dilman, V. V.: Tr. Nauch.-Issled. Proekt Inst. Azotn. Prom. Prod. Org. Sin. 1971. No. 10, p. Ref. Zh. Him. *1972*, 11 0 14.
5. Huang, T. C., Tsai, F. N.: J. Chin. Inst. Chem. Eng. *2*, 119 (1971)
6. Ramachandran, P. A., Sharma, M. M.: Trans. Inst. Chem. Eng. *49*, 253 (1971)
7. Balasubramamian, S. N., Rihani, D. N., Doraiswamy, L. K.: Ind. Eng. Chem. Fundam. *5*, 184 (1966)
8. Chua, Y. H., Ratcliffe, J. S.: Mech. Chem. Eng. Trans. *7*, 6, 11, 17 (1971)
9. Sasvári, Gy., Tőrös, R.: Magy. Kém. Lapja *27*, 577 (1972)

РЕЗЮМЕ

В известной на основе литературных данных установке с постоянной поверхностью соприкосновения газа и жидкости, была исследована абсорбция, сопровождаемая химической реакцией, образованием 1,2-дихлор-этана, являющейся в данном случае модельной реакцией. Были установлены те значения параметров процесса, при которых в данной установке может быть получено наибольшее количество 1,2-дихлор-этана. Эти данные представляют собой основу для разработки программы проведения серии экспериментов, целью которых является исследование ротационного плёночного аппарата, взятого в качестве реактора.

Для описания исследуемой системы и для количественной оценки условий процесса передачи компонентов, была разработана одномерная диффузионная модель. На основе этой модели было установлено, что в данной установке как со стороны газа, так и со стороны жидкости имеются сопротивления, препятствующие массопередаче, и величины этих сопротивлений сравнимы.

HUNGARIAN JOURNAL
OF INDUSTRIAL CHEMISTRY
VESZPRÉM
Vol. 6. pp. 211–224 (1978)

STUDIES ON ETHYLENE DICHLORIDE FORMATION IN A ROTARY FILM REAKTOR III.

Investigation of Rotary Film Equipment as a Reactor

SZÉPVÖLGYI, J. and UJHIDY, A.

(Research Institute for Technical Chemistry of the Hungarian Academy of Sciences, Veszprém)

Received: February 6, 1978

The applicability of rotary film equipment as a reactor to carry out chemical reaction accompained by gas-liquid mass transfer was investigated. Values of operational parameters to produce as much ethylene dichloride as possible in the given equipment were determined. On the basis of experimental data, rotary film equipment was compared with other laboratory equipment and the advantages of rotary film equipment to carry out the given model reaction were proved.

The application of the earlier developed mathematical model was investigated to describe processes taking place in rotary film equipment. Semiempirical correlations were given using the values calculated by the model. By these correlations, the yield characterizing the operation of rotary film equipment as a reactor can be calculated in the knowledge of gas feed rate, peripheral speed of the blade and reaction temperature.

1. Introduction

Rotary film equipment ensuring relatively short mean liquid residence time can usually be applied to carry out reactions having a high enough reaction rate in order to reach the desired conversion for residence time of second magnitude. However, the residence time can be regulated within certain limits, changing the lenght and form of the reactor and type of rotor, and in order to increase the extent of conversion, partial recirculation can also be applied.

An important condition to apply film equipment as a reactor is to construct separated reaction zones on the heated surface of evaporator. This construction makes it possible to heat or cool the different zones of the reactor in a different manner, if reactions with considerable heat effects are realized. At the same time, during the construction of film reactors, the requirements that originate from the changed purpose have to be taken into consideration.

With regard to the reactions that can be realized in rotary film equipment reference is made to [1].

Surveying the numerous references to be found in literature, it can be seen that the investigation of the reactions realized in a film reactor [2—5] is in a relatively initial state. For this reason, the aim was to invastigate the conditons formed in rotary film equipment in the case of a model reaction of industrial and theoretical importance, viz. ethylene dichloride formation.

2. Experimental Assembly and Technique

The experiments were carried out in laboratory scale rotary film equipment of 0.05 m^2 active surface. The reactor itself was a cylinder of 50.7 mm inner diameter and 0.413 m length, and equipped on both sides with stubs for thermometers and feeding. The cylinder was covered with a cooling jacket.

Based on earlier experimental data, the gas and liquid phases flowed concurrently through the reactor. The rotor consisted of 5 segments with 4 narrowing plates of 50.4 mm and was equipped with wiping blades.

The experimental assembly was described in Ref. [2].

For the given experimental assembly, in the case of the given model reaction, the transfer and hydrodynamical conditions within the reactor are influenced by the following parameters:

1. temperature of reaction;
2. peripheral speed of the blades;
3. quantity of the solvent fed in time unit;
4. quality and concentration of the catalyst in the solvent;
5. ethylene feed rate;
6. ethylene-chlorine molar ratio.

The temperature of the reaction was maintained at a constant value, viz. 30 °C on the basis of experiments carried out in equipment of known transfer surface [6], because the aim was primarily to study the effects of those parameters characterizing the operation of rotary film equipment.

The peripheral speed of the blades varied from 0.99 to 5.83 m s^{-1}. For the given rotary film equipment this peripheral speed corresponds to r.p.m. values of 370 and 2,200 respectively. The lower value is the smallest one necessary to form an uniform liquid film, while the upper one is the highest possible r.p.m. that can be applied because of construction reasons.

The feed rate of the solvent was approximately constant. The peripheral liquid load varied from $6.49 \cdot 10^{-3}$ to $6.59 \cdot 10^{-3}$ kg $m^{-1}s^{-1}$.

As a catalyst, 0.1% $FeCl_3$ previously dissolved in ethylene dichloride was used in accordance with the results of kinetical investigations. The quantity of ethylene fed in unit time varied from $3.766 \cdot 10^{-2}$ to $11.434 \cdot 10^{-2}$ mole m^{-2} s^{-1} relating to the active surface of film equipment, partly on the basis of the results described in [6], and partly that of preliminary experiments.

The ethylene-chlorine molar ratio in the gas mixture varied between 0.9—1.1.

During the realization of the given model the reaction volume of liquid being present in the equipment at a given moment—per definition of the hold up—can be regarded as the active volume of the rotary film equipment. For this reason, prior to the actual experimental activity, the hold up values were determined and from these, the values of mean residence time at different peripheral liquid loads were calculated *(Table 1)*.

Table 1.

Measured holp up and mean residence time values for ethylene dichloride in rotary film equipment of 0.05 m^2 active surface

10^5 B (m^3 $m^{-2}s^{-1}$)	10^3 Γ ($kg\,m^{-1}s^{-1}$)	v ($m\,s^{-1}$)	10^6 V (m^3)	$\bar{t}$ (s)
1.634	6.444	1.08	7.3	8.9
		1.83	7.6	9.3
		2.67	7.8	9.5
		3.67	8.3	10.2
		4.75	8.7	10.6
		5.83	8.9	10.9
1.890	7.454	1.08	7.7	8.1
		1.83	8.0	8.5
		2.67	8.4	8.9
		3.67	8.9	9.4
		4.75	9.3	9.8
		5.83	9.6	10.2
2.100	8.282	1.08	7.8	7.4
		1.83	8.2	7.8
		2.67	8.6	8.2
		3.67	9.1	9.7
		4.75	9.6	9.1
		5.83	10.0	9.5

The experiments were carried out as follows: after setting suitable values of parameters we waited 20 minutes until the steady-state operation was reached and then measurements were made for 5 minutes. Three parallel experiments were carried out at every set of parameters.

3. Experimental Results

Using the data of the experiments in rotary film equipment, the conversion, yield and selectivity values were calculated for ethylene as the basic component in a manner given in [6]. In *Table 2*, the values measured at some ethylene feed rates and peripheral speeds of the blades in the case of equimolar gas mixture feeding are summarized.

If the effect of the different operational parameters are investigated, the following conclusions can be drawn: increased peripheral speed for all investigated molar ratios and for all feed rates increases the quantity of formed ethylene dichloride; obviously this is connected with increased intensity of gas-liquid mass transfer *(Fig. 1.* and *2)*.

The amount of formed ethylene dichloride also increases with the increased gas feed rate in all initial gas compositions *(Fig. 3)*.

Table 2.

Data of experiments carried out in rotary film equipment

$M' = 1.0$ mole/mole

$10^2 B'_A$ (mole $m^{-2} s^{-1}$)	v ($m s^{-1}$)	X (%)	K (%)	H (%)
4.534	1.59	43.4	93.1	40.4
	3.14	48.1	93.2	44.8
	4.83	52.4	93.1	48.8
	5.91	53.7	93.3	50.1
6.400	1.58	42.9	93.1	39.9
	3.14	48.2	93.0	44.8
	4.81	52.8	93.1	49.2
	5.82	54.3	93.2	50.6
9.034	1.58	36.3	92.9	33.7
	3.18	40.6	92.9	37.7
	4.85	42.6	93.1	38.7
	5.84	43.2	93.1	40.2
11.434	1.56	31.8	92.1	29.3
	3.18	32.7	92.7	30.3
	4.75	34.3	92.8	31.8
	5.82	35.0	92.9	32.5

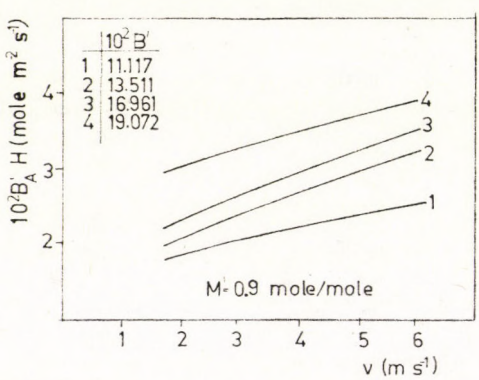

Fig. 1.
Quantity of formed ethylene dichloride as plotted against the peripheral speed of blades I.

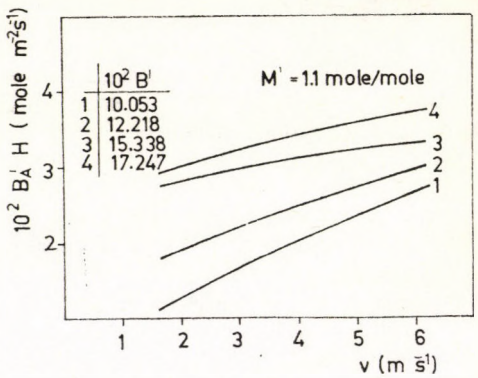

Fig. 2.
Quantity of formed ethylene dichloride as plotted against the peripheral speed of blades II.

However, the quantity of ethylene dichloride slightly changes with increased ethylene-chlorine molar ratio *(Fig. 4)*.

Following from the above mentioned, the gas mixture fed to reactor must be equimolar or so. This statement is in contradiction, e.g. with that described by

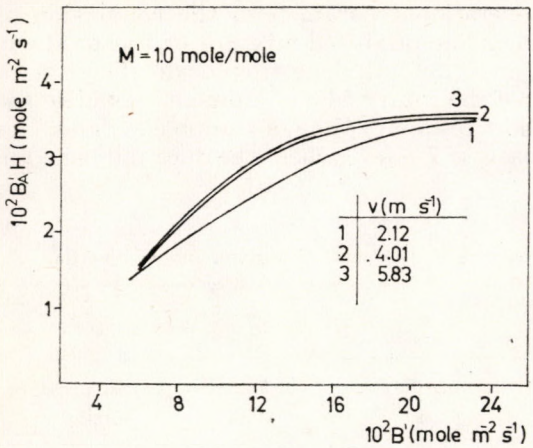

Fig. 3.
Quantity of formed ethylene dichloride as plotted against the ethylene feed rate

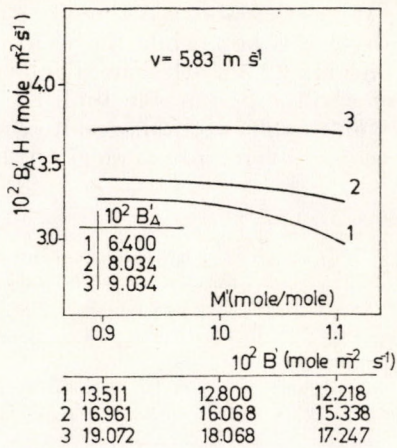

Fig. 4.
Quantity of formed ethylene dichloride as plotted against ethylene-chlorine molar ratio

GALITZENSTEIN [8], who aimed to make a complete absorption of ethylene and thus the conversion by ensuring chlorine excess in the gas mixture. However, in a rotary film reactor having more favourable transfer conditions, compared to equipment ensuring less intensive contact, even absorption of ethylene is more intensive and so it is less affected by the chlorine excess.

Following from $B'_A \cdot H$ vs. v curves the most favourable value for the peripheral speed of blades is 5.83 m s^{-1} corresponding to 37 r.p.m.

During the selection of the appropriate value of the gas load, there is insufficient to study the changes of $B'_A \cdot H$ against B'. In *Fig. 5*, the value of the yield decreases with the increased gas feed rate. Comparing *Fig. 3* and *5* the suitable

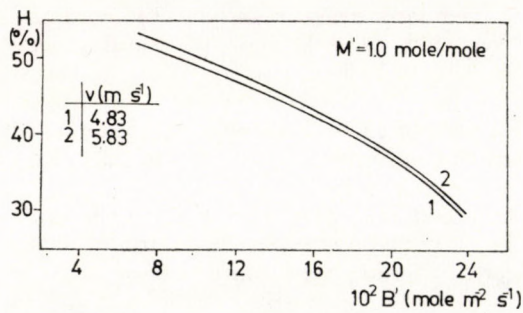

Fig. 5.
The yield as plotted against ethylene feed rate

value of B' in the given equipment is approximately $14 \cdot 10^{-2}$ mole m^{-2} s^{-1}, because at this value the amount of ethylene dichloride still increases with the increased B' and even the value of the yield is also acceptable.

With the above values of the operational parameters, the conversion of ethylene is 50% while the yield is 45%. The produced mixture of the products contains 92.5% ethylene dichloride and 7.5% ethylene trichloride. These data refer to the favourable applicability of the rotary film equipment to realize the given model reaction, despite the short residence time of the phases. This fact becomes even more evident on the basis of *Table 3*, where the data published in

Table 3.

Comparison of different laboratory reactors in the case of a given model reaction

Type of equipment	Volume (m^3)	Ethylene feed		T (°C)	X (%)	Reference	Note
		(mole s^{-1})	(mole $m^{-3} s^{-1}$)				
Cont. stirred tank	$3.50 \cdot 10^{-4}$*	$0.136 \cdot 10^{-3}$ $0.542 \cdot 10^{-3}$	0.389 1.549	32	73.5 45.4	[9]	in presence of light
Cont. stirred tank	$1.10 \cdot 10^{-4}$*	$0.878 \cdot 10^{-3}$ $1.438 \cdot 10^{-3}$	7.981 13.072	55	39.0 33.7	[10]	in presence of light
Bubble column	$1.88 \cdot 10^{-4}$*	$0.416 \cdot 10^{-3}$ $1.210 \cdot 10^{-3}$	2.212 6.436	55	41.9 35.4	[11]	in presence of light
Rotary film equipment	$6.34 \cdot 10^{-4}$** $9.5 \cdot 10^{-6}$*	$2.633 \cdot 10^{-3}$ $4.517 \cdot 10^{-3}$ $5.717 \cdot 10^{-3}$	4.153 7.125 9.017	30	52.7 43.2 38.2		in darkness, 0.1% $FeCl_3$

* volume of liquid phase
** actual volume of equipment

different papers for laboratory equipment and some conversion values measured by us at the highest investigated peripheral speed of the blades are summarized. The fed gas mixture was always equimolar.

For continuous stirred tank reactor and bubble column, the volume of the liquid phase was regarded as the basis of comparison—for both types of equipment it is approximately equal to 70—80% of the total volume of the equipment—while for rotary film equipment, the actual volume calculated from the geometrical sizes of the equipment was taken as the basis of comparison. As it can be seen this volume is equal only to 1.5% for the total equipment volume.

The higher ethylene feed rate values relating to the unit of volume and the higher conversions in rotary film equipment at similar feed rates unambigously prove the advantages of the latter equipment.

4. Evaluation of Experimental Results

For the series of experiments carried out in rotary film equipment, quantities of dissolved, but unreacted gases in a liquid phase leaving the reactor were determined in some cases. The concentration of dissolved unreacted ethylene varied from 4 to 8 mole m^{-3}, while that of chlorine from 10 to 15 mole m^{-3}. In the

knowledge of above values, we could calculate the values of $\overline{R}_A \cdot a$ and $\overline{R}_B \cdot a$ in the rotary film equipment. However, in order to study the applicability of the model described in [6] for rotary film equipment, we would also know directly the $\overline{R}_A$ and $\overline{R}_B$ values.

As it is known, in rotary film equipment the gas-liquid contact surface changes depending on the values of the operational parameters and in most cases can be determined only with difficulty. For rotary film equipment having rotors with wiping blades, KOVÁCS [12] determined the surface with a sulphite oxidation method, and by the data for peripheral liquid loads and peripheral speed of blades applied in our experiments, the actual gas-liquid contact surface is 1.08 – 1.12 times greater compared to the active geometrical surface of the equipment. The relatively low factor can be attributed to the surface decreasing effect of the bow wave formed by a rotor with wiping blades.

In accordance with the above value and taking into account the hold up values summarized in *Table 1* for the studied rotary film equipment the value of a varies from 5.5×10^{-3} to 7.3×10^{-3} $m^2 m^{-3}$. The absorption rates determined by these a values are shown in *Table 4.*

Table 4.

Absorption rates measured in rotary film equipment

$10^2 B'_A$ (mole $m^{-2} s^{-1}$)	v ($m s^{-1}$)	$M'=0.9$		$M'=1.0$		$M'=1.1$	
		$10^2 \overline{R}_A$	$10^2 \overline{R}_B$	$10^2 \overline{R}_A$	$10^2 \overline{R}_B$	$10^2 \overline{R}_A$	$10^2 \overline{R}_B$
		(mole $m^{-2} s^{-1}$)					
3.766				2.158	2.301		
4.534				2.434	2.598		
5.266		2.691	2.891	2.775	2.959	2.517	2.665
6.400	5.85	3.520	3.784	3.475	3.712	3.187	3.386
8.034		3.663	3.945	3.615	3.864	3.503	3.736
9.034		4.074	4.391	3.902	4.173	4.047	4.318
10.334				3.947	4.227		
11.434				4.002	4.288		
	2.17	2.458	2.643	3.069	3.286	3.045	3.254
	3.17	3.189	3.390	3.246	3.471	3.141	3.350
8.034	4.00	3.422	3.655	3.390	3.615	3.262	3.479
	4.83	3.535	3.800	3.454	3.688	3.431	3.655

Following from the consideration relating to the operation of rotary film equipment as a reactor, the film model of [6] cannot be applied to describe the transfer process in rotary film equipment in an analogous manner as in equipment of known mass transfer surface, because in the former equipment the concentration not only changes in an x direction, being perpendicular to the gas-liquid contact surface, but also along the longitudinal axis of the equipment (y co-ordinate).

The mean values of the ethylene and chlorine concentrations, necessary to calculate the mass transfer coefficients, were determined using the results of the kinetical investigations [7] and definitions of conversions and yields [6]. Expressing the quantities of ethylene dichloride and ethylene trichloride formed in a

unit of time, in the basis of above mentioned, the following equations are gained:

$$B'_A FH - Vk_1 c_A c_B \quad (1)$$

$$B'_A F(X-H) = Vk_2 c_A c_B^2 \quad (2)$$

The component transfer coefficients were determined according to model [6] using c_A and c_B values calculated on the basis of Eq. (1) and (2) *(Tables 5* and *6)*.

Table 5.

Liquid side component transfer coefficients calculated for rotary film equipment

$10^2\ B'_A$ (mole $m^{-2} s^{-1}$)	v ($m\ s^{-1}$)	$M'=0.9$		$M'=1.0$		$M'=1.1$	
		$10^3\ \bar{k}_A$	$10^3\ \bar{k}_B$	$10^3\ \bar{k}_A$	$10^3\ \bar{k}_B$	$10^3\ \bar{k}_A$	$10^3\ \bar{k}_B$
		($m\ s^{-1}$)					
3.766				2.05	2.25		
4.534				2.86	3.13		
5.266		4.28	4.69	4.30	4.71	4.47	4.90
6.400		10.88	12.45	12.41	13.59	11.30	12.37
8.034	5.85	14.00	15.34	15.68	17.17	14.10	15.44
9.034		16.58	18.16	17.25	18.89	16.02	17.52
10.334				19.76	21.64		
11.434				20.13	22.03		
8.034	2.17	8.17	8.94	8.43	9.23	8.73	9.56
	3.17	8.89	9.74	9.69	10.62	9.58	10.49
	4.00	11.89	13.03	12.76	13.97	12.58	13.77
	4.83	13.07	14.32	14.64	16.03	13.30	14.57

Table 6.

Gas side component transfer coefficients calculated for rotary film equipment

$10^2\ B'_A$ (mole $m^{-2} s^{-1}$)	v ($m\ s^{-1}$)	0.9	1.0	1.1
		$10^3\ \bar{k}'_B$ ($m\ s^{-1}$)		
3.766			11.49	
4.534			12.29	
5.266		15.41	14.51	13.37
6.400	5.85	20.95	21.60	18.17
8.034		22.96	23.05	21.48
9.034		27.14	27.69	26.09
10.334			31.56	
11.434			33.67	
8.034	2.17	12.63	13.79	13.45
	3.17	15.12	15.60	16.04
	4.00	17.56	18.04	17.09
	4.83	19.73	20.49	20.04

From these *Tables* becomes evident that:

a) both the liquid and gas side component transfer coefficients can be regarded as indipendent of the gas phase composition.

b) The component transfer coefficients increase with the gas load and peripheral speed of blades.

c) The liquid side component transfer coefficient of the chlorine generally is higher by 10% compared to the value calculated for ethylene.

d) If the gas and liquid side coefficients are compered it can be seen that in rotary film equipment the gas side component transfer coefficients are 1.5—5.6 higher compared to the liquid side ones. This means the existence of both liquid and gas side resistances against the mass transfer, however, the liquid side resistance is more considerable.

The comparison of component transfer coefficients determined in equipment of known transfer surface [6] and for rotary film equipment at approximately similar gas loads *(Tables 5* and *6)* shows that in rotary film equipment the adequate liquid side coefficients are 1.2—3 times higher, while the adequate gas side coefficients are 5—10 times higher. This means that in rotary film equipment the intensity of the mass transfer partly increases as a consequence of decreased liquid side resistance, and primarily as a consequence of decreased gas side resistance.

The following empirical correlation can be given for the component transfer coefficients summarized in *Tables 5* and *6*, for the gas load and peripheral speed of blades:

$$\overline{k} = (A_1 B'^3 + A_2 B'^2 + A_4) v^{0,55} \tag{3}$$

Coefficients of Eq. (3) are summarized in *Table 7*.

Table 7.

Coefficients of Eq. (3).

Transfer coefficient	A_1	A_2	A_3	A_4
$\overline{k}_A$	−1.947	0.639	−0.004	−0.002
$\overline{k}_B$	−2.009	0.637	0.005	−0.003
$\overline{k}'_B$	1.357	0.580	0.136	−0.004

The changes of component transfer coefficients calculated from Eq. (3) against the peripheral speed of the blades and the gas load are shown on *Fig. 6—9*. Both the liquid and gas side component transfer coefficients are increased with the increased peripheral speed of the blades at a given constant gas load *(Fig. 6* and *7)* so the rotary film equipment really must be operated at the highest peripheral speed that can be ensured by the given construction.

An increase in the gas feed rate, as a consequence of the increased turbulency of gas phase, also increases the values of the component transfer coefficients *(Fig. 8* and *9)*.

It becomes evident from the above mentioned that for the studied rotary film equipment in the case a given model reaction, the peripheral speed of the blades

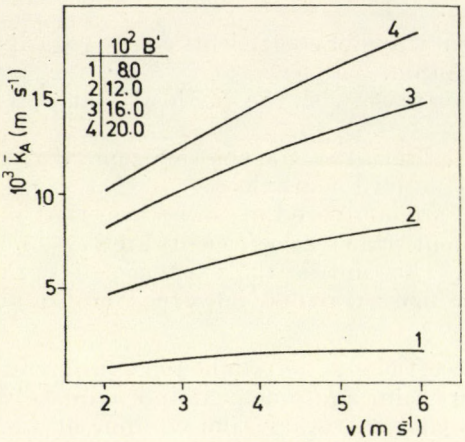

Fig. 6.
Liquid side mass transfer coefficient for ethylene as plotted against peripheral speed of blades

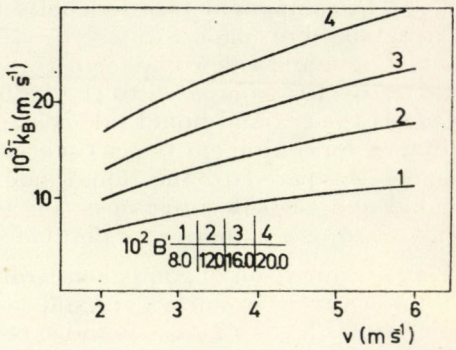

Fig. 7.
Gas side component transfer coefficient as plotted against peripheral speed of blades

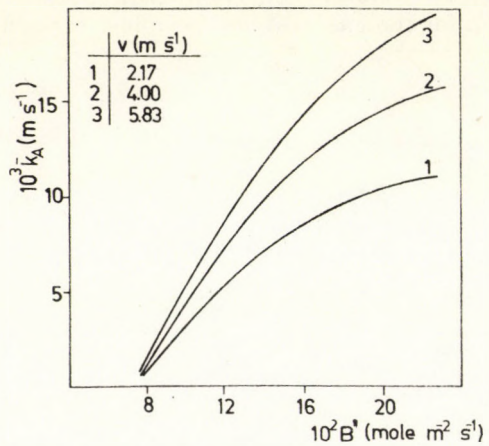

Fig. 8.
Liquid side component transfer coefficient for ethylene as plotted against the gas load

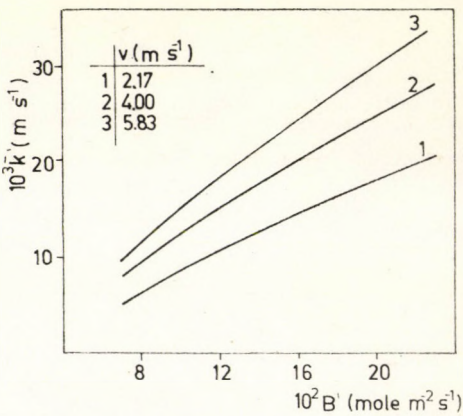

Fig. 9.
Gas side component transfer coefficient as plotted against gas load

and the gas feed rate are the two operational parameters that primarily have an effect on the mass transfer conditions. For this reason it would be expedient for even the driving force of mass transfer to be expressed as a function of these parameters. In this manner, the transfer process would be described by semi-empirical correlations, however, this fact is not in contradiction with the purpose of our activity. We did not consider it our task to elaborate a completely exact model—in our opinion it would be very difficult as a consequence of the

complexity of the given system and the mathematical problems originated from the complexity—but we aimed to give correlations so that the transfer parameters can be calculated with sufficient accuracy.

The mean gas concentrations in a liquid phase that are calculated by Eq. (1) and (2) can be given by the following empirical correlations:

$$C_A = v^{0.05}(A_1 B'^2 + A_3) H'_A c'_A \tag{4}$$

and:

$$c_B = v^{0.05}(E_1 B' + E_2) H'_B c'_B \tag{5}$$

Coefficients of Eq. (4) and (5) are to be found in *Table 8*.

Table 8.

Coefficients of Eq. (4) and (5)

A_1	−10.398
A_2	4.386
A_3	0.365
E_1	0.222
E_2	0.803

The driving force of the mass transfer follows from Eq. (4) and (5):

$$\Delta c_A = H'_A c'_A [1 - v^{0.05}(A_1 B'^2 = A_2 B' + A_3)] \tag{6}$$

$$\Delta c_B = H'_B c'_B [1 - v^{0.05}(E_1 B' + E_2)] \tag{7}$$

On the basis of Eq. (3) and (6)—(7) the absorption rate can soon be calculated in the knowledge of the reaction temperature gas feed rate, and peripherical speed of the blades, and using the absorption rate—assuming the quantity of dissolved but uncreated gases at the outlet point of reactor to be negligibile—the yield from the

$$B'_A H = 2\overline{R}_A - \overline{R}_B \tag{8}$$

correlation gained by the modification of Eq. (34) in [6]. Differences between the calculated and measured yield values were calculated as follows:

$$\Delta = \frac{H_S - H}{H} \cdot 100 \tag{9}$$

The results summarized in *Table 9* show that the yield values can be given by the applied semiempirical correlations with very good accuracy. The applicability of these correlations seems to be possible even for planning, however, it must be verified by informative measurements carried out in film equipment of a larger size.

Table 9.

Calculated absorption rate and yield values in rotary film equipment

$10^2\ B'_A$ (mole $m^{-2}s^{-1}$)	v ($m\,s^{-1}$)	$10^2\ (\overline{R}_A)_s$ (mole $m^{-2}s^{-1}$)	$10^2\ (\overline{R}_B)_s$ (mole $m^{-2}s^{-1}$)	H_s (%)	Δ (%)
3.766	2.17	1.390	1.417	36.2	−22.6
	4.00	1.795	1.865	45.8	−9.3
	4.83	1.884	1.987	47.3	−8.9
	5.83	1.986	2.087	50.1	−6.4
4.534	2.17	1.842	2.055	35.9	−15.9
	4.00	2.381	2.622	47.2	−6.4
	4.83	2.426	2.644	48.7	−0.2
	5.83	2.534	2.812	49.8	−0.6
5.266	2.17	2.396	2.451	44.5	5.2
	4.00	2.825	3.071	48.9	3.8
	4.83	2.907	3.223	49.2	2.3
	5.83	2.993	3.566	49.7	1.0
6.400	2.17	2.791	2.942	41.2	−0.7
	4.00	3.298	3.492	48.5	3.0
	4.83	3.413	3.716	48.6	−1.2
	5.83	3.527	3.963	48.3	−4.5
8.034	2.17	2.916	3.165	33.2	−5.7
	4.00	3.484	3.935	37.8	−4.1
	4.83	3.627	4.048	39.9	−0.5
	5.83	3.715	4.069	41.8	−0.2
9.034	2.17	3.178	3.284	34.0	−3.4
	4.00	3.520	3.761	36.3	−7.6
	4.83	3.641	3.849	38.0	−4.3
	5.83	3.837	4.115	39.4	−2.0s
10.334	2.17	3.372	3.427	32.1	−4.2
	4.00	3.623	3.836	33.0	−4.9
	4.83	3.710	3.989	33.2	−4.3
	5.83	4.039	4.627	33.4	−5.9
11.434	2.17	3.484	3.709	28.5	−4.0
	4.00	3.690	4.064	29.0	−6.5
	4.83	3.783	4.170	29.7	−6.6
	5.83	4.165	4.877	30.2	−7.1

SYMBOLS

$A_1 - A_4$ coefficients;
a specific transfer surface, $m^2\ m^{-3}$;
B liquid feed rate, $m^3\ m^{-2}\ s^{-1}$;
B' gas feed rate relating to surface unit, mole $m^{-2}\ s^{-1}$;
c concentration in the bulk of liquid, mole m^{-3};
c' concentration in the bulk of gas, mole m^{-3};
Δc driving force of transfer, mole m^{-3};
$E_1 - E_2$ coefficients;
F surface, m^2;
H yield,
H' reduced HENRY's constant;
K selectivity, %;
k_1 rate constant of addition, $m^3\ mole^{-1}\ s^{-1}$;
k_2 rate constant of substitution, $m^6\ mole^{-2}\ s^{-1}$;
k liquid side component transfer coefficient, $m\ s^{-1}$;
k' gas side component transfer coefficient, $m\ s^{-1}$;
M' ethylene-chorine molar ratio in gas phase, mole/mole;
R absorption rate, mole $m^{-2}\ s^{-1}$;
T temperature, °C or K;
$\bar{t}$ mean residence time, s;
v peripheral speed of blades, $m\ s^{-1}$;
V hold up, m^3;
X conversion, %;
x, y co-ordinates, m;

Greek letters

Γ peripheral liquid load, $kg\ m^{-1}\ s^{-1}$;
Δ difference of calculated and measured values, %;

Indices

A ethylene
B chlorine
S calculated value

Other signs

′ value relating to the gas phase
— mean value

REFERENCES

1. UJHIDY, A., BABOS, B.: Filmbepárlók, filmreaktorok. (Film Evaporators, Film Reactors) Műszaki Könyvkiadó, Budapest, 1967.
2. UJHIDY, A., SZÉPVÖLGYI, J.: Chem. Tehn. (Leipzig) *25*, 731 (1973).
3. SZÉPVÖLGYI, J., MAGYAR, M., UJHIDY, A.: Chem. Techn. (Leipzig) *26*, 21 (1974).
4. UJHIDY, A., BERKES, R.: Magy. Kém. Lapja *31*, 70 (1976).
5. UJHIDY, A., BERKES, R.: Magy. Kém. Lapja *31*, 140 (1976).
6. SZÉPVÖLGYI, J.: Hung. J. Ind. Chem. *6*, 211 (1978).
7. SZÉPVÖLGYI, J., UJHIDY, A.: Hung. J. Ind. Chem. *6*, 187 (1978).
8. GALITZENSTEIN, E., WOOLF, C.: J. S. C. I. *69*, 289 (1950).
9. BALASUBRAMANIAN, S. N., RIHANI, D. N., DORAISWAMY, L. K.: Ind. Eng. Chem. Fundam. *5*, 184 (1966).
10. CHUA, Y. H., RATCLIFFE, J. S.: Mech. Chem. Eng. Trans. *7*, 11 (1971).
11. CHUA, Y. H., RATCLIFFE, J. S.: ibid. *7*, 17 (1971).
12. KOVÁCS, S.: Témabeszámoló (Report) MTA MŰKKI, Veszprém, 1976.

РЕЗЮМЕ

Авторами была изучена применимость ротационного плёночного аппарата, как реактора, в целях проведения химической реакции, сопровождаемой массопередачей в системе газ-жидкость. Были определены те значения параметров процесса, при которых в данной установке может быть получено максимально возможное количество дихлор-этана, в расчёте на единицу времени и единицу поверхности. На основе полученных экспериментальных данных было проделано сравнение ротационного плёночного аппарата с другими установками лабораторного размера, в результате чего оказалось, что плёночный аппарат обладает большими преимуществами с точки зрения проведения данной моделируемой реакции.

Исследовалась также применяемость разработанной ранее математической модели для описания процессов, происходящих в ротационной плёночной установке. С помощью применения значений, рассчитанных на основе модели, авторами были определены полуэмпирические зависимости, с помощью которых при известной скорости газоввода скорости лопатки по периметру и температуре реакции, можно рассчитать величину выхода, как величину, характеризующую работу плёночного ротационного аппарата, рассматриваемого в качестве реактора.

CONTENTS

HOLDERITH, J.: Some Linear Relations in Hierarchic Modelling of Multiphase Reactors 125
MOHOS, F.: General Properties of Technological Systems. III. 131
MOHOS, F.: General Properties of Technological Systems. IV. 145
CSIKÓS, Cs. und BÁTHORY, J.: Untersuchungen der zur Dehydrierung von n-Hexan verwendeten Katalysatoren (The Examination of Catalysts Used for Dehydrogenation of n-Hexane) 155
FRATZSCHER, W. und MICHALEK, K.: Energetische und exergetische Analyse einer Rohöldestillationsanlage (Energetic and Exergetic Examination of Crude Oil Distillation Plant) 163
KIRILLOV, V. A. and OGARKOV, B. L.: The Examination of Heat and Mass Transfer in a Three Phase, Fixed Catalyst Bed (in the Russian) 175
SZÉPVÖLGYI, J. and UJHIDY, A.: Studies on Ethylene Dichloride Formation in a Rotary Film Reactor I. Kinetical Investigations 187
SZÉPVÖLGYI, J.: Studies on Ethylene Dichloride Formation in a Rotary Film Reactor II. Investigations in a Reactor of Known Transfer Surface 195
SZÉPVÖLGYI, J. and UJHIDY, A.: Studies on Ethylene Dichloride Formation in a Rotary Film Reactor III. Investigation of Rotary Film Equipment as a Reactor 211

78.2920 Egyetemi Nyomda, Budapest. Felelős vezető: Sümeghi Zoltán igazgató

THE FOLLOWING ARE PLEASED TO ACCEPT SUBSCRIPTIONS TO THIS JOURNAL:

AUSTRALIA

C.B.D. Library and Subscription Service
Box 4886 G.P.O.
Sydney 2000

Cosmos Book and Record Shop
145 Acland Street
St. Kilda 3182

Globe and Co.
694—696 George Street
Sydney 2000

AUSTRIA

Globus (VAZ)
Höchstädtplatz 3
A—1200 Wien XX

BELGIUM

"Du Monde Entier" S. A.
Rue du Midi 162
B—1000 Bruxelles

Office International de Librairie
Avenue Marnix 30
B—1050 Bruxelles

CANADA

Pannonia Books
P.O. Box 1017
Postal Station "B"
Toronto, Ontario M5T 2T8

DENMARK

Munksgaard's Boghandel
Norregade 6
DK—1165 Copenhagen K

FINLAND

Akateeminen Kirjakauppa
Keskuskatu 2, P.O.B. 128
SF—00 100 Helsinki 10

FRANCE

Office International de Documentation et Librairie
48 Rue Gay Lussac
75 Paris 5

GERMAN FEDERAL REPUBLIC

Kubon und Sagner
Pf 68
D—8 München 34
BRD

GREAT BRITAIN

Bailey Bros and Swinfen Ltd.
Warner House, Folkestone
Kent CT 19 6PH England

HOLLAND

Martinus Nijhoff
Periodicals Department
P.O. Box 269
The Hague

Swets and Zeitlinger
Keizersgracht 487
Amsterdam C

ITALY

Licosa
P.O.B. 552, Via Lamarmora 45
50121 Firenze

JAPAN

Igaku Shoin Ltd.
Foreign Department
Tokyo International P.O. Box 5063
Tokyo

Maruzen Co. Ltd.
P.O. Box 5050
Tokyo International 100—31

Nauka Ltd.
Yasutomi Bldg. 5F 2—12 Kanda
Jinbocho, Chiyoda-ku
Tokyo 101

NORWAY

Tanum—Cammermayer
Karl Johangt. 41—43
Oslo 1

SWEDEN

Almqvist and Wiksell Förlag A. B.
Box 2120
S—103 13 Stockholm 2

Wennegren—Williams AB
Subscription Department Fack
S—104 Stockholm 30

SWITZERLAND

Karger Libri A. G.
Petersgraben 31
CH—4011 Basel

USA

Ebsco Subs. Services
1 st Ave North at 13th street
Birmingham, Ala. 35201

HUNGARIAN

Journal of

INDUSTRIAL CHEMISTRY

Edited by

the Hungarian Oil & Gas Research Institute (MÁFKI),
the Research Institute for Heavy Chemical Industries (NEVIKI),
the Research Institute for Technical Chemistry of the
Hungarian Academy of Sciences (MÜKKI),
the Veszprém University of Chemical Engineering (VVE).
Veszprém (Hungary)



Volume 6. 1978 Number 3.

HU ISSN: 0133—0276
CODEN: HJICAI

Editorial Board:

R. CSIKÓS and GY. MÓZES
Hungarian Oil & Gas Research Institute
(MÁFKI Veszprém)

A. SZÁNTÓ and M. NÁDASY
Research Institute for Heavy Chemical Industries
(NEVIKI Veszprém)

T. BLICKLE and O. BORLAI
Research Institute for Technical Chemistry
of the Hungarian Academy of Sciences
(MÜKKI Veszprém)

A. LÁSZLÓ and L. PÉCHY
Veszprém University of Chemical Engineering
(VVE Veszprém)

Editor-in Chief:
E. BODOR

Assistant Editor:
J. DE JONGE

Veszprém University of Chemical Engineering
(VVE Veszprém)

The „Hungarian Journal of Industrial Chemistry" is a joint publication of the Veszprém scientific institutions of the chemical industry that deals with the results of applied and fundamental research in the field of chemical processes, unit operations and chemical engineering. The papers are published in four numbers at irregular intervals in one annual volume, in the English, Russian, French and German languages

Editorial Office:
Veszprémi Vegyipari Egyetem
„Hungarian Journal of Industrial Chemistry"
H–8201 Veszprém, P. O. Box: 28.
Hungary

Subscription price $ 45. — per volume/year Orders may be placed with
KULTURA
Foreign Trading Co. for Books and Newspapers
Budapest, 62. POB 149
or with its representatives abroad, listed on the verso of the cover

FELELŐS SZERKESZTŐ: DR. BODOR ENDRE

KIADJA A LAPKIADÓ VÁLLALAT, 1073 BP. VII., LENIN KRT. 9—11.
TELEFON: 221-285. LEVÉLCÍM: 1906 BP. PF. 223
FELELŐS KIADÓ: SIKLÓSI NORBERT IGAZGATÓ

HUNGARIAN JOURNAL
OF INDUSTRIAL CHEMISTRY
VESZPRÉM
Vol. 6. pp. 225–242 (1978)

STUDIES ON PARTICLE COATING. I.
FILM-COATING OF UREA PARTICLES IN FLUIDIZED BED

Mrs. E. Horváth, K. Pataki and Z. Ormós

(Research Institute for Technical Chemistry
of the Hungarian Academy of Sciences, Veszprém, Hungary)

Received: October 18, 1977

The fluidization-atomization film-coating process, its applications and results of film-coating experiments are presented. The effects of various technological parameters upon the physical properties of the coated particles and the quality of the film formed on the particles were studied. Spherical urea and a water-insoluble film forming plastic resin were used as test materials. Experiments were carried out in a batch-operated laboratory scale fluidization apparatus equipped with a conical flow-modifying insert.

Introduction

"Film-coating" is an operation in which solid particulate material (so-called core) is coated with appropriate agent(s) without altering the phase state of the bulk of the solid particle (core). Coating can be commenced for a number of purposes by a vast range of technical chemistry processes.

For the purpose of the operation, particle coating can be film-coating and grain-size increasing coating (shaping). Theoretically, any process in which there is an intense movement of the particles with respect to each other and the wall of the apparatus can be used to carry out the operation.

In film-coating the so-called film-forming agents (cellulose derivatives, high molecular weight polyethylene glycols, acryl and metacryl resins and their copolymers, etc.) are applied as solutions (or melts) onto the particles by an appropriate manner (drying, freezing, and chemical reaction, etc.) to form a solid film coating the particle.

The most obvious advantage of the film composition using the above mentioned resins is the application possibility of fast and easy-to-automate coating processes. It is a further advantage that by the selection of appropriate polymers the properties of the film can be easily controlled. Films covering a relatively wide range of dissolution rates can be obtained by simply changing the ratio of two ingredients [1]. Harada and Fujita [2] while studying film-coating materials concluded that the resistance of the coating material

against dissolution accounts for some 90% of the total resistance and so it becomes the dissolution rate controlling factor. The dissolution rate is an important factor effecting the physical properties of the coated particles during use. Though the above figure determined from laboratory experiments modelling the dissolution of coated fertilizers may appear somewhat exaggerated it well demonstrates the importance of selecting the appropriate film forming agent. This basic fact should not be overlooked when film-formation is studied from an operational point of view and the optimum conditions of film-coating are determined.

So far film-coating has primarily been used in the pharmaceutical industry. Perhaps this is why, even today, the literature dealing with film-coating is pharmaceutically oriented. Apart from the pharmaceutical industry, film-coating could be of interest in the agricultural and food processing industry to prepare fertilizers, pesticides, animal food grain and feed mixtures.

The aim of special coatings on medicines is to protect the solid preparates (crystals, tablets, and granules) from external damage, decrease the irritating effects upon oral administration and ensure direct absorption by the organism. A new form of administering medicines is that of microcapsules. Instead of raw or coated tablets of standard size the appropriate amount of the granulated medicine coated with one or several films is placed into a gelatine capsule. In certain cases microcapsules are definitely advantageous as regards stability and dosage [3].

In order to increase the effective action time of fertilizers, they are given a thin plastic coating [4] which, at the same time, disposes of their unwanted hygroscopic properties. The advantages of the retarded action fertilizers are as follows [2]:

- the availability rate of the fertilizer can be modified as required by the given plant so the utilization rate of the fertilizer is considerably enhanced,
- component losses by drainage are decreased,
- the cost of fertilizing is decreased,
- the danger of excessive fertilizer application and its accumulation is decreased,
- the harmful effects caused by fertilizers washed into lakes and streams are decreased.

Controlled rates of release and decreased dermal toxicity are envisioned when pesticides applied onto inert supports are granulated and coated by thin films.

There is another possibility to be utilized both in the pharmaceutical, pesticide or animal feed industries, namely finely distributed minute amounts of an active ingredient can be applied onto the surface of particulate (granulated) filler or support materials [5].

The aim of thin protective coatings on grains is to kill the bacteria of diseases carried over on the grains and thus control their spread, in fact, to replace conventional steeping.

The characteristic steps of the processes used to carry out film-coating as an operation are as follows:

- intensive motioning of the particles,
- the application of the coating material (and its conditions).

According to the forces called upon to keep the particles in motion there are processes using:

— mechanical energies and,
— the kinetic energies of flowing gases.

In the latter case, gas has a double role since it keeps the particles in motion and increases the rate of film formation.

With regard to coating the tumbling-layer (rolling-drum or rolling-plate) and the fluidization processes are important from point of view the mechanically and the flowing gas agitated processes, respectively. There are a few references in literature mentioning the use of other processes for coating, but their significance is negligible.

According to literature, the main advantages of the fluidization-atomization process are as follows: simplicity, versatility, speed and homogeneous end product [2, 6]. The coating formed in a fluidized bed is more uniform than that formed in a tumbling layer [5]. It has been proved experimentally that the quality of the coating formed is best when it is produced in a fluidized bed (the degree of porosity is the lowest) [7].

WURSTER was the first to describe the use of the fluidization-atomization operation to coat particles [8, 9]. Following his publications, there was a universal interest in the operation as shown by the number of patents and papers relating to coating by fluidization-atomization, the modification of his apparatus, the design of laboratory and pilot plant scale apparatuses for the same purpose and the production of film coated particles therein [1, 2, 6, 7, 10—15].

Essentially, in fluidization-atomization film-coating, the particles to be coated are fluidized by hot air and the film-coating material in liquid form (solution or melt) is atomized into the bed, whereupon the coating liquid is uniformly distributed onto the surface of the intensly mixed particles, and due to the evaporation of the solvent (the freezing of the melt or the completion of the chemical reaction) a solid film, a pellicular layer is formed on the particles.

There is a general consensus that the success of any film-coating operation apart from the surface characteristics and the mechanical properties of the particles (rigidity) is ensured by a specific motion of the particles induced in a bed. This motion is envisaged as the ordered, uniform, vertical recirculation of the particles in a fluidized bed. This vertical forced convection is controlled by the design of the section in which the coating takes place and the optional application of a flow modifying insert. It can also be brought about by the division of the air distributing support plate into two concentric annuli and applying a higher air flow rate to the outer annulus forcing the particles into a circulating motion [2, 6].

The conical insert of the GLATT film-coating apparatus serves the same purpose [7]. The high velocity air rising at the perimeter of the distributing plate lifts the particles until, due to the loss of momentum caused by the increasing flow section, the particles slide back along the conical insert—which also transmits air sufficiently frequently and re-enter the circulation at some point.

The most important physical features of the coated particles are as follows:

— particle-size distribution,
— rolling features,
— wear resistance,
— release rate of the active ingredients.

These features, and the most important one particularly from the point of view of application, the rate at which active ingredients are relaesed, depend upon the quality of the film formed on the particles. The basic factors influencing the quality of the film are as follows:

— physical characteristics dependent upon the type of the material of the coherent film,
— the porosity of the film,
— the thickness of the film,
— the uniformity of the film.

A number of methods have been published in literature concerning the rate of the quality of the films formed [7—16].

In one case, the sample of the phenolphthalein-containing coated particles is placed into a sodium carbonate solution. Colour changes due to the indicator incorporated into the particles are followed. The solution is sampled at appropriate intervals and extinction readings are taken at 550 nm.

Film-coating of NPK fertilizer particles was studied by Japanese researchers [2]. In order the assess the quality of the product and the efficiency of the fertilizer, a special method was developed. The dissolution rate ratio, r_d was measured as a function of time, defined as the ratio of the material dissolved from coated to that of non-coated fertilizers in distilled water.

These researchers studied, among others, the mechanism of dissolution of the fertilizer components. The rate equation and the solid material balance based on their model shown in *Fig. 1* and postulations not detailed here are as follows [2]:

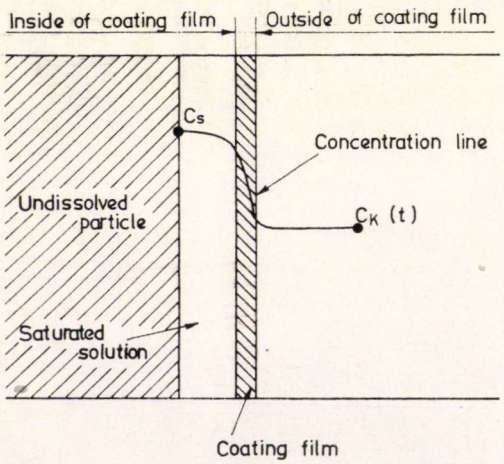

Fig. 1
Model of the dissolution mechanism

$$\frac{dc_k(t)}{dt} = K[c_b(t) - c_k(t)] \qquad (1)$$

$$V_b c_b(0) = V_b c_b(z) + V_k c_k(t) = V c_\infty \qquad (2)$$

Under the conditions $t = 0$ and $c_k(t) = 0$ the solution becomes:

$$1 - \frac{c_k(t)}{c_\infty} = \exp\left[-K\,\frac{c_b(0)}{c_\infty}\right] \qquad (3)$$

This equation will be dealt with later on in detail.

In the paragraphs below, the results of a project aimed at the determination of the effects of the technological parameters (process, operation and apparatus) upon the quality of the product and the film-coating itself will be shown. It is not the absolute value, but the trend of these changes which is of interest. The assessment of the influence of the various parameters and the selection of the primary operational controlling variables were the main goals sought here.

Experimental

The schematics of the batch-operated laboratory-scale fluidization-atomization system (diameter: 10.5 cm) is shown in *Fig. 2*. As an interesting feature, there is a solid cone covering some 32% of the air distributing and supporting plate placed in it. Its height is 5 cm which is approximately equal to the minimum fluidization height. The atomizer is located centrally above the layer.

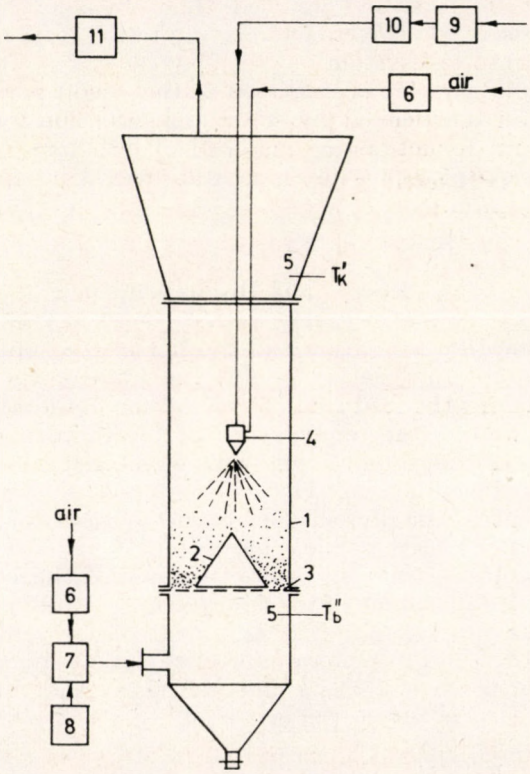

Fig. 2
Schematics of the experimental apparatus
1 — coating chamber; *2* — conical insert; *3* — air distributor; *4* — pneumatic atomizer; *5* — thermometer; *6* — flowmeter; *7* — air preheater; *8* — auto transformer; *9* — mixed liquid tank; *10* — pump; *11* — cyclone

The main point governing its location is to keep as big a cross section wetted as possible without sprinkling the coating material onto the walls.

Spherical urea fraction of narrow particle size distribution and an acrylic resin dissolved in isopropyl alcohol were used as model materials. A colour paint and fine talc powder were also added to the coating liquid.

An appropriate characteristic and a method to measure it were required to sensitively monitor the changes of the quality of the film as a function of various technological parameters. In the so-called dissolution-test, the time required to dissolve a given amount of test material under standardized conditions was determined. The amount dissolved from the coated particles was related to the amount of the overall material and expressed as a percentage ($\overline{S\ \%}$). It was due to this test that a water soluble basic material and water insoluble coating were selected.

For further rating of the product, the efficiency of the coating application and the degree of agglomeration were also determined.

The efficiency of the coating-application was determined as follows. A given amount of water soluble particles coated with a water-insoluble film was charged into distilled water and the basic material was dissolved. The coating left over was washed, dried and weighed. The efficiency of the coating application was expressed as a percentage relating to the total amount of coating material atomized into the system.

The degree of agglomeration is expressed as the weight percentage of a given particle size fraction determined by sieve analysis. These fractions were as follows: over 1.6 mm for a starting material of 0.8—1.25 mm; over 2.0 mm for a starting material of 1.25—1.60 mm and over 3.15 mm for a starting material of 1.6—2.0 mm.

Results and Discussion

The effects upon the film formation and quality of the solid ingredients content (concentration) of the coating liquid, the ratio of the amounts of talc and film forming agent, the feed rate of the coating liquid and its atomization characteristics, as well as the temperature of the fluidizing air entering the system were studied. Film-upbuilding was monitored via the three rating characteristics mentioned above. The effects upon product quality of the design of the apparatus, the presence or absence of inserts (conical, and sieve, etc.), bringing about ordered particle movement were also studied.

The average dissolution rate and the efficiency of the coating-application as a function of the talc content of the film forming liquid are shown in *Fig. 3* and *4*. Experiments proved that it is advantageous to add finely powdered talc to the liquid for it resulted in an improved coating quality. The optimum amount was 30% w/w. No additional amount above that limit had apparent quality improving effects, while the efficiency of the application did in fact significantly decrease.

At a constant talc-solid material content ratio ($c_t = 30$ % w/w) the effects of changing the solid material concentration (g/l) upon the quality of the coating were studied. As it is shown in *Fig. 5* this concentration had an optimum point with respect to the dissolution rate indicating the quality of the coating. If the same amount of coating material was applied either from more

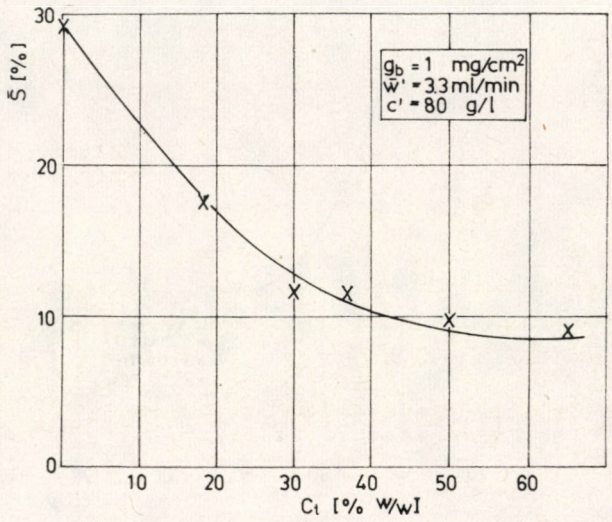

Fig. 3
Average dissolution rate as a function of talc concentration

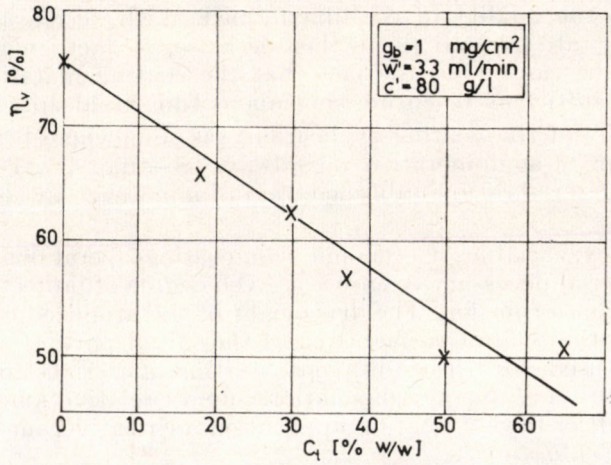

Fig. 4
Efficiency of coating application as a function of talc concentration

dilute or concentrated solutions, inferior results were obtained. As a resultant of the two effects, a film of minimum dissolution rate is obtained at a certain liquid concentration. The degree of dispersity of the liquid improved with decreasing concentration since the size of the droplets decreased and the distribution of the coating material in the surface became more uniform. Accordingly, the dissolution rate, as the indicator of the quality of the film coating decreased. Under a certain concentration, however, dilution became

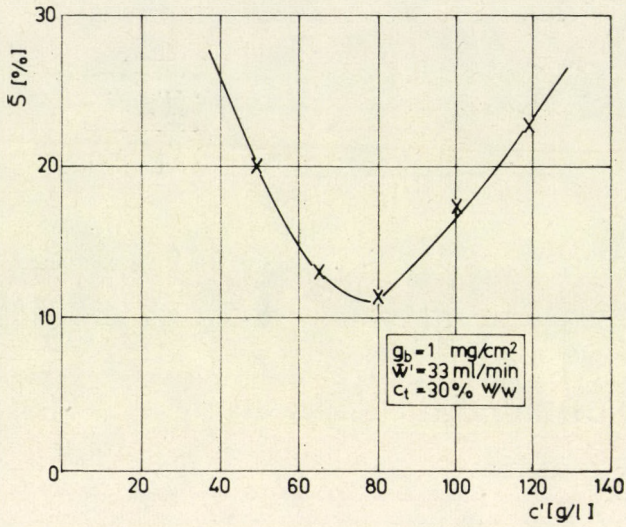

Fig. 5
Average dissolution rate as a function of the concentration of the coating liquid

detrimental to the quality of the film formed. With decreasing droplet size, the dissolution rate showed no further decrease, in fact, it increased. This is believed to be caused by the fact that the coating material in a droplet was no longer sufficient to ensure continuous film build-up.

The efficiency of the coating-application was somewhere between 60—65% and the amount of agglomeration was always less than 1%. This proved that the talc-solid material ratio established was optimum over a wide concentration range.

The other key variable of economic film-coating operations is the amount of coating material necessary to ensure a given degree of protective action—i.e. good quality film formation. The dry-weight of the atomized coating material was related to the overall surface area of the initial particle charge and this quantity was used for three different starting materials to monitor film build-up. Results, i.e. average dissolution rate vs relative amount of coating material and efficiency of coating application vs relative amount of coating are shown in *Fig. 6* and *7*.

For all three starting materials, the dissolution rates steeply decreased with increasing amounts of coating material on the unit surface area and the dissolution rates corresponding to coatings of 1 mg/cm² indicated the very best film qualities attainable in the given experiment. Above this value, the dissolution rate was once again increased and it levelled off at a certain value. This means that below a certain value, the amount of the coating material applied onto the particle is not sufficient to render complete protection, while overdoses do not improve the quality of the coating either. The reason for the second finding is believed to be the agglomerization that becomes effective above 1 mg/cm² coating loadings. This is more pronounced at the smallest and medium particle size fractions. The measured value for the

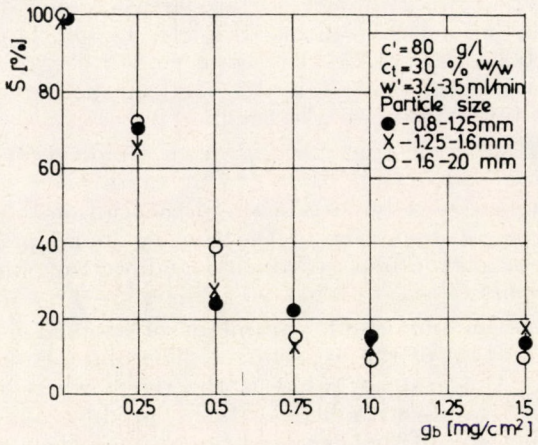

Fig. 6
Average dissolution rate as a function of the relative amount of coating material in three batches of different initial particle size

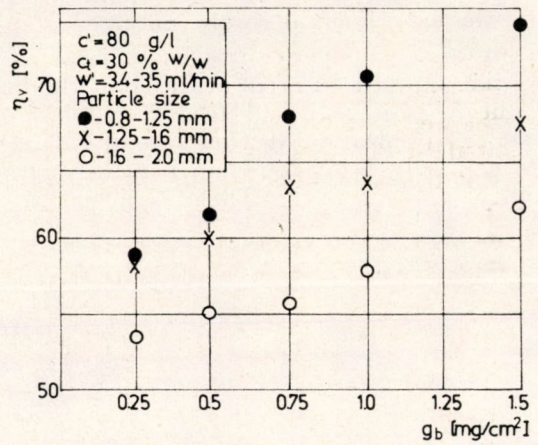

Fig. 7
Efficiency of coating application as a function of the relative amount of coating material in three batches of different particle size

intermediate fraction (1.25—1.60 mm) proved to be 0.5—0.7 % w/w. However, the extent of agglomerization is greater than that. Bridges between the particles are weak, correspondingly they are easily broken at the air velocities applied. Coating is damaged at these points of breakage as witnessed by photomicrographs. Most of the bridges formed remain intact in the case of the smallest size fraction (0.8—1.25 mm) and measured agglomerization becomes as high as 30 % w/w compared to the 1 % w/w value (max.) found in the other cases. The efficiency of the coating material application visibly increases. However, with decreasing initial particle size, the efficiency of the coating application decreases. This phenomenon can be explained, on the one

hand, by the ever growing impact surface area created by the decreasing particle size available for the atomized droplets: 15,900, 11,000 and 8,750 cm^2 for the fraction 0.8—1.25; 1.25—1.60 mm and 1.6—2.0 mm, respectively. On the other hand, mechanical (abrasive) effects acting upon the particles and droplet-carry-out effects are also smaller.

The two main steps of film formation in fluidization-atomization film-coating are wetting and drying. Here drying takes place not only after, but also with the wetting, so it imparts a significant influencing affect. The feed rate and the degree of dispersity of the coating liquid might have a strong effect upon the complex process of drying and wetting under the given experimental conditions.

The feed rate is an important parameter of economic operation since it determines the duration of the experiment. There are a number of questions to be answered in this respect: what is the range where it can be changed to satisfy economic needs without sacrificing product quality? What is the effect of the droplet size of the atomized liquid upon the structure of the film and the physical characteristics of the coated particles? Can the feed rate be increased at decreased droplet size? Does the decrease of the droplet size not influence the rate of the coating material losses due to the carry-out? Answers to these and similar questions are sought in the following paragraphs that discuss the experimental results obtained.

First of all let us examine—under conditions otherwise constant—the effects of the changing coating liquid feed rates at different fluidizing air flow rates. The average dissolution rate vs liquid feed rate relationship is shown as Curve 1 in *Fig. 8* at an atomization air flow rate of 0.35 m^3/h. It can be seen that the feed rate can only be changed in a rather narrow range without impairing the quality of the coating. The dissolution rate also displays an

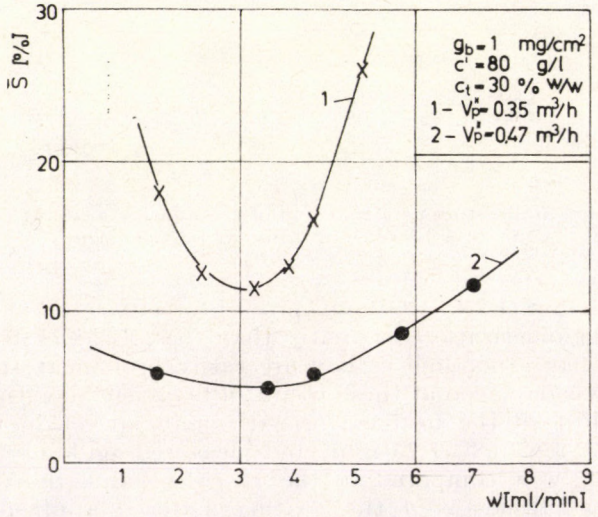

Fig. 8
Average dissolution rate as a function of coating liquid feed rate

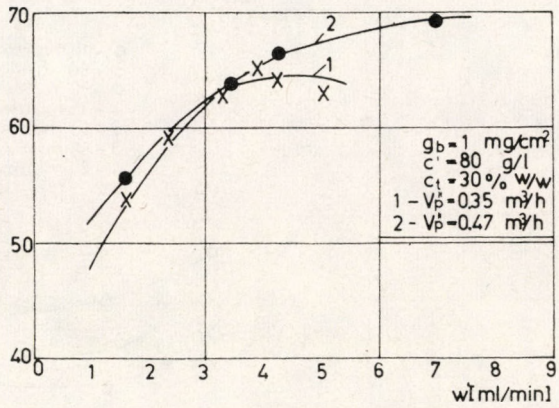

Fig. 9
Efficiency of coating application as a function of coating liquid feed rate

optimum as a function of this parameter. At low feed rates the efficiency of the application decreases (cf. *Fig. 9*). Probably wetting of the particles is not complete. Droplets atomized into the system "overdry" before contacting the particles, film build-up is not sufficiently uniform and there is a significant abrasive action in the bed. At higher feed rates, the formation of bridges as discussed above can be assumed to take place which, as time passes, break up in the bed. It is believed that these are the main causes of film defects.

It should be emphasized that the moisture content of the charge in the bed is extremely low. The relative isopropanol content of the air leaving the system changed in the range studied only between 0.2—1%. At an optimum feed rate its value was 0.5%. Thus local overwetting on the surface of the particle, and not that of the entire charge has to be combated, since temporary local overwetting is entirely sufficient to cause bridging. With decreased droplet size, the frequency of the occurrence of the above phenomenon can be decreased.

This is substantiated by Curve 2 in *Fig. 8* describing the average dissolution rate vs feed rate relationship at a higher atomizing air flow rate (0.47 m^3/h). The curve is similar, but the dissolution rates at any feed rate are lower (cf. *Fig. 9*) and the efficiencies of the coating applications are higher than those at the 0.35 m^3/h atomization flow rate. This is due to the better fine-structure and more appropriate drying rate caused by the finer droplet size of the coating liquid.

Changes of the dissolution rate as a function of the atomizing air flow rate (pressure) are shown in *Fig. 10* from the optimum feed rate upward. The dissolution rate approaches a lower limiting value as a function of this parameter for any feed rate. For increasing liquid feed rates, in turn, this almost constant dissolution rate increases.

The average size of the atomized coating liquid droplets as a function of atomizing air flow rate has also been determined (cf. *Fig. 11*) at a given liquid feed rate (4.3 ml/min). The magnesia method of May was selected

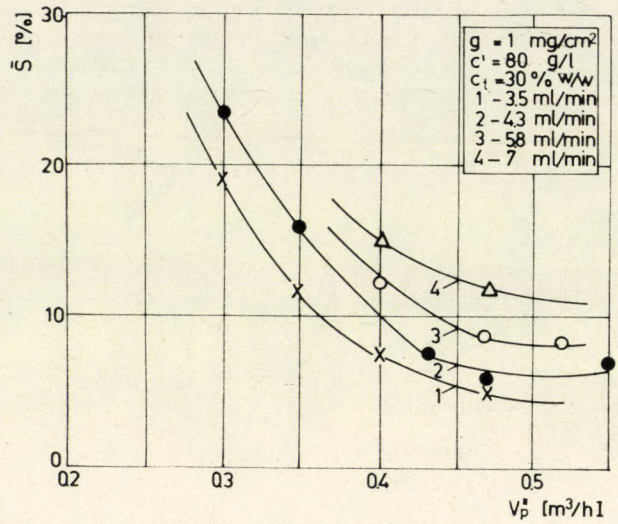

Fig. 10
Average dissolution rate as a function of atomizing air flow rate at different coating liquid feed rates

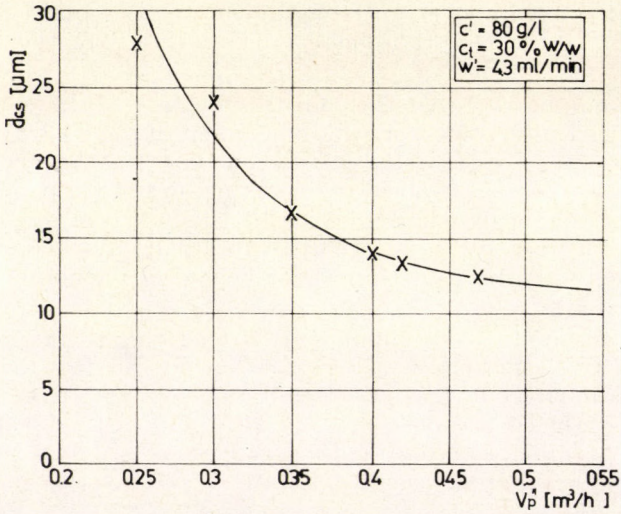

Fig. 11
Average size of atomized droplets as a function of atomizing air flow rate

to determine the droplet size distribution. With increasing atomizing air flow rate the droplet size is continuously decreasing, yet smaller than a given limit droplet size cannot be achieved at a given liquid feed rate, liquid concentration and atomizer orifice.

The dissolution rate—the indicator of coating quality—linearly decreases with decreasing average droplet size at a given liquid concentration and feed rate (cf. *Fig. 12*).

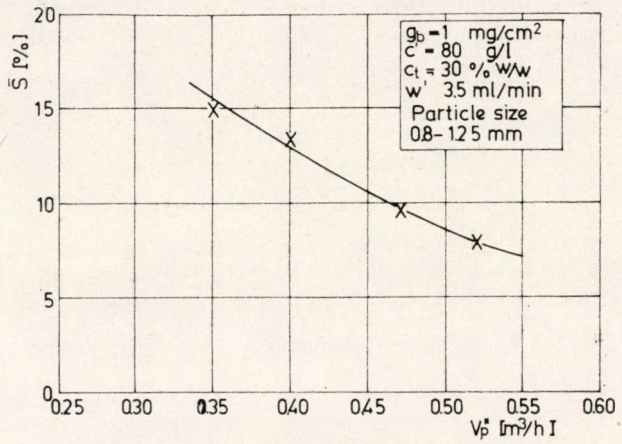

Fig. 12
Average dissolution rate as a function of the average droplet size of the atomized coating liquid

Not only the average size, but also the size distribution of the droplets is advantageously influenced by increasing atomizing air flow rates. The more homogeneous the droplet size distribution of the coating liquid, the more efficient the utilization and the more uniform the product distribution becomes, which most probably also plays a significant role in the increased product quality.

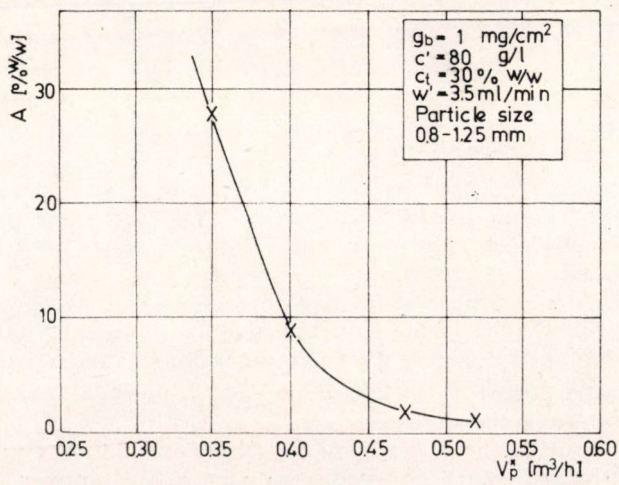

Fig. 13
The extent of agglomerization as a function of atomizing air flow rate

As shown in *Fig. 13*, it can be concluded that the excessive agglomeration witnessed in small initial particle size batches can be controlled by the appropriate selection of the average droplet size and size distribution of the coating liquid, and from 50% w/w it can be decreased to as little as 1% w/w. With an increased atomizing air flow rate—i.e. with decreasing droplet size—the dissolution rate also decreases (cf. *Fig. 14*). Thus, regardless of the erratic

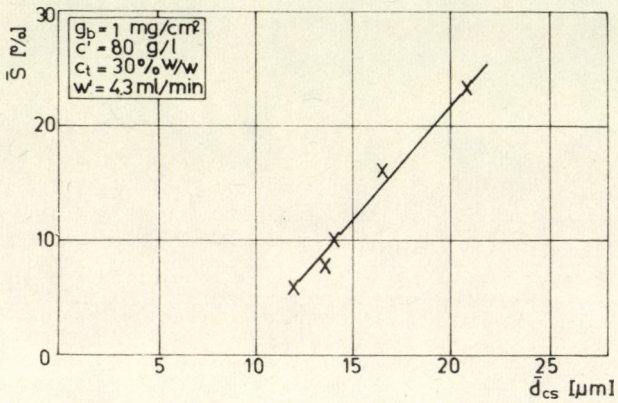

Fig. 14
Average dissolution rate as a function of atomizing air flow rate

behaviour of the efficiency of the coating application, the quality of the coating is undoubtly improved which can be attributed only to a decrease in the number of film deficiences caused by a reduction in the number of particle bridges which can break off.

The aim of the next experimental series was to study the effects of the conditions of drying upon the structure of the film. Drying conditions can most easily be influenced by changing the temperature of the air entering the unit. The input air temperature was changed in the 20—70 °C range. Results are shown in *Fig. 15*.

If the particles are fluidized by 25 °C air instead of 50 °C then a significant change is brought about in the film quality. The increased dissolution rate cannot be correlated with changes in the efficiency of the coating application for the efficiencies are approximately equal in both cases. The sole reason for deteriorated film quality is that the drying rate set by the 25 °C air flow rate is too low. The film formed on the particles remains wet for too long a period, it is damaged during collisions and becomes deformed.

Once the temperature of the fluidizing air is increased above 50—60 °C the film quality again becomes impaired. According to calculations carried out in connection with these experiments, the isopropanol content of the air can change in the 0.1—3.0% range depending on the temperature of the air entering the system. The experimentally established optimum temperature is 50—60 °C corresponding to a relative isopropanol content of 0.4—0.5%.

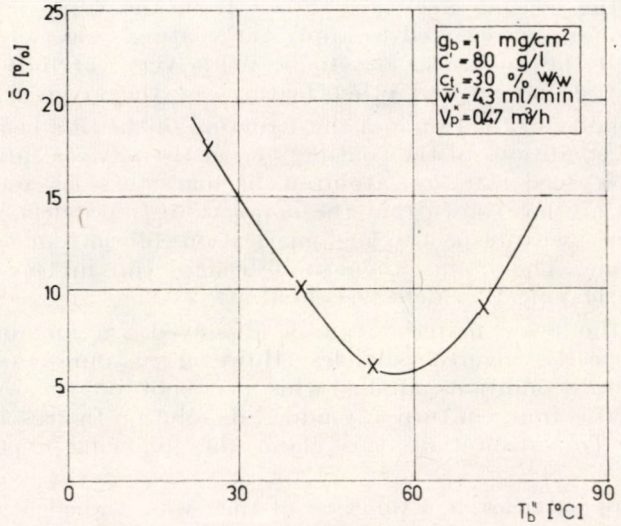

Fig. 16
Average dissolution rate as a function of input fluidizing air temperature

Based on this criterion an optimum feed rate can be assigned to a given input air temperature and vice versa.

Comparative film coating experiments were carried out in apparatuses of different designs. The results are summarized in *Table 1*. As regards product quality there is no significant difference between simple fluidization apparatuses and those with conical, sieve-drum inserts or mechanical agitators. The authors are convinced that with particles agitated at an appropriately intense rate, the primary factors influencing the characteristics of the coated

Table 1

Starting material: urea fraction, 1.25—1.60 mm

$g_b = 1.0$ mg/l	$w' = 4.3$ ml/min	$Y_m = 5.4$ cm	$T_k'' = 50—53$ °C
$c' = 80$ g/l	$V_p'' = 0.47$ m³/h	$Y/Y_m = 1.7—2.5$	$T_b'' = 45—47$ °C
$c_t = 30\%$ w/w	$Y_p = 13.5$ cm		

Method of keeping the particles in motion	G_1 g	V'' m³/h	$\bar{S}$ %	η_v %	Particle size distribution, A % w/w			
					less than 1.25	1.25—1.60	1.6—2.0	above 2.0
Simple fluidized bed	390	35—51	9.5	58.8	2.7	37.3	59.8	0.2
Fluidized bed with sieve drum insert	370	35—46	7.45	59.8	3.2	44.9	51.7	0.2
Fluidized bed with conical insert	350	30—46	6.0	66.4	1.5	33.5	64.5	0.5
Mechanically agitated fluidized bed	370	30—43	5.8	64.5	4.2	32.9	61.2	1.7

particles and the coating itself are—apart from the types of materials involved—the conditions selected to apply the coating. Selection of the appropriate design of the apparatus has to be made very carefully, after having analyzed many economic and other features of the given individual case.

Thus, the quality of the film and the structure of the film coating primarily depend on the conditions of the coating, i.e. on the physical properties of the coating solution, feed rate and atomization characteristics and temperature values. Experience has shown that the majority of film defects can be traced back to efficiency with respect to agglomerization collisions in the bed at some appropriate time. The liquid, then solid bridges can in turn with passing time break up leaving film defects behind.

Obviously, the basic material can be dissolved via membrane diffusion even from perfectly covered particles. However, in our assessment, under the experimental conditions applied this does not on the average exceed 3—5%. Above this limit, in turn any added dissolution figures are due to film imperfections. To substantiate this claim the following experiments were carried out.

Dissolution of particles as a function of time was studied at a given liquid concentration, feed rate and atomization air flow rates of 0.35 and 0.47 m^3/h. Results shown in *Fig. 16* have been processed according to the model of HARADA and FUJITA [2] developed to discuss the mechanism of fertilizer dissolution from coated particles.

Results obtained with the coated particles considered having a good quality coating substantiate this model (cf. *Fig. 16*, Curve 1). On the other hand,

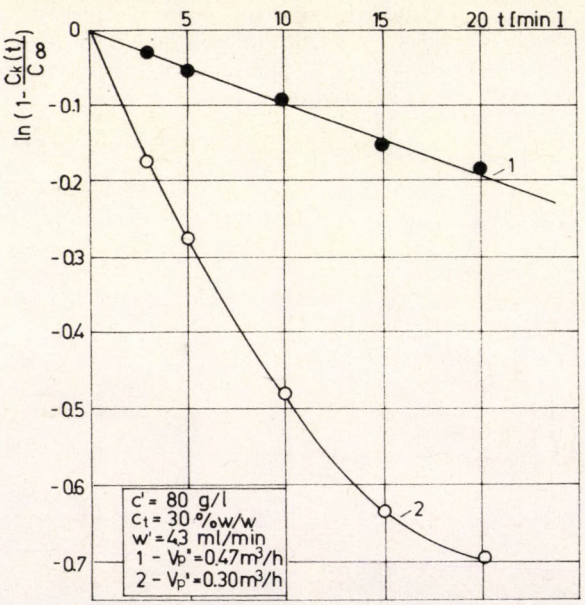

Fig. 16
Kinetical studies on the dissolution rate

when coatings are prepared under unfavourable conditions—in this case due to a coating liquid not dispersed finely enough—the mechanism of the dissolution differs (cf. Curve 2). Obviously, this is also due to film defects.

Thus dissolution form reasonably intact film-coated particles can be considered a first order process, the rate of which is determined by the material qualities of the basic material and coating, and the conditions of dissolution tests. On the other hand, a different kinetics is seen in the case of particles with a defective coating.

SYMBOLS

A — the extent of agglomerization, % w/w
$c_b(t)$ — concentration of the dissolved component inside the film coating, g/cm³
$c_k(t)$ — concentration of the dissolved component outside the film coating, g/cm³
c_∞ — eventual concentration of the dissolved component outside the film coating, g/cm³
c_s — saturation concentration of the dissolved component, g/cm³
c_t — talc concentration in the coating, % w/w
c' — dry material content of coating liquid, g/l
$\bar{d}_{cs}$ — average droplet size of coating liquid, m
G_1 — initial weight of particle charge to be coated, g
g_b — relative amount of coating material on unit particle surface area, mg/cm²
K — overall reaction rate constant of dissolution, 1/h
$\bar{S}$ — average dissolution, %
T''_b — input fluidizing air temperature, °C
T''_k — output fluidizing air temperature, °C
t — time, min, hr
Y_m — minimum fluidization bed height, cm
Y/Y_m — bed expansion
Y_p — distance of atomizing orifice from distributor plate, cm
V_b — volume of the solution at the inner part, cm³
V_k — volume of the solution at the outer part, cm³
V — V_k+V_b, cm³
V'' — flow rate of fluidizing air, m³/h
V''_p — flow rate of atomizing air, m³/h
w' — feed rate of coating liquid, ml/min
η_v — efficiency of coating application, %

REFERENCES

1. Coletta, V., Rubin, H.: J. Pharm. Sci. *53*, 957 (1964).
2. Harada, Kazuo; Fujita, Jinshiro: Hitachi Zosen Giho *36* (3), 149 (1975).
3. Doelker, E., Buri, P.: Pharma. Acta Helv. *50* (4), 73 (1975).
4. Off. Plast. Caoutsch, *18* (27), 266 (1971).
5. Dittgen, M., Kala, H., Moldenhauer, H.: Pharmazie *25*, 349 (1970).
6. Wolkhoff, H. N., Pinchuk, G., Shapiro, P.: J. Pharm. Sci. *57* (2), 317 (1968).
7. Zeller, H. G.: Pharm. Ind. *31*, 11 (1969).
8. Wurster, D. E.: US Patent 2,648,609 (1953).
9. Wurster, D. E.: J. Am. Pharm. Ass. Sci. Ed. *48*, 451 (1959).
10. Caldwell, H. C., Rosen, E.: J. Pharm. Sci. *53*, 1387 (1964).
11. Kala, H., Dittgen, M., Holdenhauer, H.: Pharmazie *26* (11), 664 (1971).
12. Singiser, R. E., Lowenthal, W.: J. Pharm. Sci. *50*, 168 (1961).
13. Cordes, G.: Pharm. Ind. *31*, 566 (1969).
14. Dittgen, M., Hoffmann, G.: Pharmazie *28* (12), 781 (1973).
15. Zsitomirszkij, Z. Sz., Naumcsik, G. N., Roscsin, N. I.: Khim.-Farm. Zh. *8* (7), 46 (1973).
16. Feigenbaum, L.: Labo-Pharma Probl. Tech. *19* (198), 68 (1971).

РЕЗЮМЕ

Авторы приводят метод плёночного покрывания путём распылительного псевдоожижения, возможности его применения, и далее — знакомят с результатами плёночного покрывания. В ходе этих опытов изучалось влияние, оказываемое различными технологическими характеристиками плёночного покрывания на физические свойства гранул и на качество плёночного покрытия, образующегося на поверхности гранул. В качестве модельных материалов применялись шарообразные гранулы мочевины и образующая плёнку, нерастворимая в воде искусственная смола. Опыты проводились в лабораторной псевдоожижающей установке периодического действия, снабжённой конусной вставкой для изменения направления потока.

HUNGARIAN JOURNAL
OF INDUSTRIAL CHEMISTRY
VESZPRÉM
Vol. 6. pp. 243–250 (1978)

PREDICTION OF CATALYTIC REFORMER YIELD BY CHEMICAL EQUILIBRIUM (COMMERCIAL RESULTS)

J. KRAMARZ and M. RADOSZ

(Instytut Chemii i Technologii Organicznej
Politechnika Krakowska, Kraków, Poland)

Received: February 10, 1978.

Commercial reformate compositions were compared with equilibrium compositions. The equilibrium aromatic content and the equilibrium aromatic to paraffin molar ratio were good estimates of the corresponding values for a commercial reformate. The effects of hydrocracking reactions on commercial reformate composition were examined. In order to make the equilibrium composition a better estimation of the composition of the commercial reformate, a correction accounting for the hydrocracking reactions was introduced.

Introduction

C_6-C_9 hydrocarbons and hydrogen are the main components of catalytic reforming mixtures. Chemical reactions bringing about no change in the carbon number of the molecule, e.g. paraffin dehydrocyclisation, naphthene dehydrogenation, and any isomerization [1], are more or less limited by the chemical equilibrium. Since thermodynamically reforming conditions are very favourable for cracking reactions these are a priori excluded from the calculations. This allows for a basic assumption, namely that in chemical equilibrium the "class composition" (C_6 mole%, C_7 mole%, C_8 mole%, C_9 mole%) is constant, e.g. it is the same as that of the class composition of the feed.

Due to the large number of components and the possible chemical reactions, simultaneous chemical equilibria of catalytic reforming have to be calculated via the *minimisation* of the Gibbs' free energy [2, 3, 4]. Equilibrium calculations for a mixture of 103 C_6-C_9 hydrocarbons and hydrogen were made with the Sequential Unconstrained Minimisation Technique (SUMT) of FIACCO-MCCROMIK [5]. Calculations were carried out at constant pressure and temperature. The chemical thermodynamics of catalytic reforming itself was the subject of several papers [6, 7, 8, 9].

The differences between the states prevailing in chemical equilibrium and in a commercial cat reformer might result from the following factors:

1. In the real process hydrocracking of paraffins, and to a minor extent of naphthenes, occurs so the class composition of the reformate is changed compared to that of the feed.
2. The real process is neither isothermic (there is some temperature gradient of several centigrades along the reactor) nor isobaric (pressure is slightly different in the successive different reactors, but almost constant in one reactor).

Commercial experiments

Feed and reformate samples were taken from a commercial reformer with periodically regenerated catalyst (0.35 % w/w Pt/Al_2O_3). The samples corresponded to four runs as different as possible in a commercial plant. The last run was made four weeks after the first one, so during such a short period the activity of the catalyst could be regarded as constant for our purposes. The catalyst was regenerated twice, the last time being about half a year before the experiments. The hydrogen to hydrocarbon molar ratio in the feed

Table 1.

Properties and composition of the commercial feedstock
A, P, and N stand for aromatics, paraffins and naphthenes

RUN No.		1	2	3	4
Density (g/cm³)		0.726	0.734	0.731	0.743
Boiling point range					
— lower end		75	78	76	74
(°C) — upper end		167	166	175	163
Average molar weight		104.5	105.4	105.3	105.1
COMPOSITION, MOLE %					
C_6	A	0.3	0.1	0.1	0.3
	P	18.3	16.5	17.7	18.9
	N	6.4	6.4	5.8	6.2
C_7	A	2.0	2.4	1.9	1.8
	P	17.0	17.7	17.5	16.6
	N	10.6	9.8	10.7	9.9
C_8	A	3.6	3.6	3.5	3.3
	P	19.3	18.4	17.3	17.8
	N	6.1	5.8	5.9	5.3
C_9	A	2.4	2.5	2.6	2.7
	P	12.2	14.6	15.1	15.1
	N	1.8	2.1	1.9	2.1
TOTAL	A	8.3	8.7	8.1	8.1
	P	66.8	67.2	67.6	68.4
	N	24.9	24.1	24.3	23.5

was about 7 to 8. The average pressure was constant (32 at) for all the cases described. Average temperature levels for the four runs did not differ too much, and were:

787 786 784 779 K respectively.

Catalyst loads and feed flow rates were as follows, respectively:

1.2	1.3	1.3	1.3	kg/kg·h
42,100	44,000	44,200	44,600	kg/h.

The conditions described were typical for the given plant.

Samples were analyzed by capillary gas chromatography.

Properties and compositions of the feed and reformate flows for the four runs of the commercial reformer are presented in *Tables 1* and *2* (mole %, C_6-C_9 hydrocarbons total 100 mole %). Though there are only small temperature differences a regular decrease of the aromatic content of the reformate could be seen. The difference between the two extreme cases is 6 mole %.

Hydrocracking reactions resulted in a change of the reformate class com-

Table 2.

Properties and composition of the commercial reformates
A, P, and N stand for aromatics, paraffins and naphthenes

RUN No.		1	2	3	4
Density (g/cm³)		0.760	0.766	0.747	0.756
Boiling point range					
	— lower end	48	58	44	50
(°C)	— upper end	186	188	186	184
RON*		92	90	90	86
COMPOSITION, MOLE %					
C_6	A	6.2	5.9	5.5	5.3
	P	21.9	21.1	22.9	24.1
	N	1.5	1.9	1.7	2.3
C_7	A	18.0	17.7	16.1	14.9
	P	11.4	13.8	13.4	14.7
	N	1.3	1.7	1.5	1.9
C_8	A	19.5	18.7	18.0	17.4
	P	5.4	5.6	6.5	4.4
	N	1.1	0.4	0.6	0.6
C_9	A	11.0	10.7	11.6	11.1
	P	2.4	2.5	2.1	3.1
	N	0.3	—	—	0.1
TOTAL	A	54.7	53.0	51.2	48.7
	P	41.1	43.0	44.9	46.3
	N	4.2	4.0	3.8	4.9

* Research octane number

position (C_6 mole %, C_7 mole %, C_8 mole %, C_9 mole %) compared with that of the feed *(Table 3)*. The C_6 and C_7 hydrocarbon content increased while the C_8 and C_9 hydrocarbon content decreased.

Table 3.

Class composition of the commercial feeds and reformates

	RUN No. / CLASS	1	2	3	4
FEED, Mole %	C_6	23.7	25.0	23.0	25.4
	C_7	30.1	29.6	29.9	28.3
	C_8	27.7	29.1	27.8	26.4
	C_9	18.5	16.3	19.3	19.9
REFORMATE, Mole %	C_6	29.0	29.6	28.9	31.7
	C_7	31.1	30.8	33.1	31.5
	C_8	25.3	26.0	24.8	22.5
	C_9	14.6	13.6	13.2	14.3

The comparison of equilibrium and commercial results

Equilibrium calculations did not include cracking reactions. This is why calculations were carried out twice for each run—once for the feed class composition and the second time for the reformate class composition.

The aromatic content and the corresponding aromatic to paraffin molar ratios in the reformates and in the equilibrium mixtures are presented in *Table 4.* Calculated and experimental results agree very well. Calculated

Table 4.

Aromatics content A and aromatic to paraffin A/P molar ratio in the commercial reformates and in the equilibrium mixture:
I — feed class composition
II — reformate class composition. P = 32 at.

RUN No.		1	2	3	4
T (°K)		787	786	784	779
CATALYST LOAD		1.2	1.3	1.3	1.3
COMMERCIAL REFORMATE	A, mole %	54.7	53.0	51.2	48.7
	A/P	1.3	1.2	1.1	1.0
EQUILIBRIUM MIXTURE I	A, mole %	58.8	60.2	58.7	55.5
	A/P	1.5	1.6	1.5	1.3
EQUILIBRIUM MIXTURE II	A, mole %	54.3	53.6	52.5	48.3
	A/P	1.2	1.2	1.1	1.0

reformate class composition resulted in aromatic content rather close to the corresponding experimental values. Differences between the corresponding aromatic content (A mole %) and aromatic to paraffin ratios (A/P) did not exceed the 1.5 mole % and 0.1 values, respectively.

If the experimental and equilibrium aromatic content of each hydrocarbon class are compared *(Table 5)* then an interesting difference can be seen between

Table 5.

C_6—C_9 aromatic content in the commercial reformates and in the chemical equilibrium composition mole %
P = 32 at.

	RUN No	1	2	3	4
C_6	COMMERCIAL	6.2	5.9	5.5	5.3
	EQUILIBRIUM	1.7	1.6	1.5	1.3
C_7	COMMERCIAL	18.0	17.7	16.1	14.9
	EQUILIBRIUM	15.7	16.6	14.9	13.5
C_8	COMMERCIAL	19.5	18.7	18.0	17.4
	EQUILIBRIUM	23.8	22.7	22.9	19.9
C_9	COMMERCIAL	11.0	10.7	11.6	11.1
	EQUILIBRIUM	13.2	12.8	13.2	13.7

the C_6, C_7 and C_8, C_9 hydrocarbon groups. The differences between experimental and equilibrium aromatic content are shown below:

— in class C_6 it was higher by about 4 mole %
— in class C_7 it was higher by about 1—2 mole %
— in class C_8 it was lower by about 2.5—5 mole %
— in class C_9 it was lower by about 2 mole %.

The comparison of the experimental and equilibrium results is a good basis to explain the significance and the effects of the hydrocracking reaction. These reactions resulted in the following changes of reformate class compositions compared to the feed class composition:

— C_6 content increased by about 5 mole % (+)
— C_7 content increased by about 2 mole % (+)
— C_8 content decreased by about 2 mole % (−)
— C_9 content decreased by about 5 mole % (−)

The numbers given above are average, and at the same time, typical content changes of the respective carbon number classes.

Paraffins and naphthenes of all carbon number classes were cracked under reforming conditions, but the extent of the cracking depended on the actual carbon number. A higher carbon number meant a relatively higher cracking conversion under identical conditions. The relative increase of the C_6—C_7 content in the C_8—C_9 mixture might be explained by the generation of C_6—C_7 hydrocarbons resulting from the cracked heavier components. On the other

hand, the predispositions to hydrocracking did not depend only on the carbon number. They also depended on the relative naphthene and especially the paraffin content of any class of a given carbon number. On that basis, the C_6 and C_7 classes were favourable. If the global paraffin content of a reformate equalled 40—50 mole %, then the C_6—C_7 paraffin content was the same 30—40 mole % and the C_8—C_9 paraffin content was only 10 mole % and C_6—C_9 hydrocarbons totalling 100 mole %, cf. Table 2. So irrespective of the increase of the C_6—C_7 content the hydrocracking of C_6—C_7 hydrocarbons was also considerable.

Hydrocracking reactions decreased the relative paraffin (and to a minor extent, the naphthene) content differently for each carbon number fraction. This hampered the endeavour to achieve chemical equilibrium. Consequently, if the concentration of the components subject to hydrocracking (paraffins and naphthenes) in any carbon number class (mostly C_6 and C_7) was high, then the relative extent of hydrocracking was high compared to that of the aromatization. It resulted in a relative increase, beyond equilibrium levels, of the aromatic content of these classes *(Table 5)*.

Isoparaffin to n-paraffin molar ratios ($i-P/n-P$) in commercial reformates were almost always constant, amounting to same 2.5—2.7, while the value in equilibrium mixtures was 3.4 *(Table 6)*. The $i-P/n-P$ ratios determined

Table 6.

Average molar ratios $i-P/n-P$

	FEED	REFORMATE	EQUILIBRIUM
C_6	1.0	1.9	2.8
C_7	1.1	2.8	4.5
C_8	1.8	4.5	4.5
C_9	3.0	7.5	9.5
TOTAL	1.4—1.7	2.5—2.7	3.4

gaschromatographically are subject to some error because of the division of two small numbers. However, commercial $i-P/n-P$ ratios were lower than equilibrium ratio. In the case of the C_8 class, the equilibrium and commercial $i-P/n-P$ values did agree.

Individual C_8 aromatics were present in the reformate in equilibrium proportions. If the C_8 aromatic content (moles) was taken as 100, then the relative and average molar proportions of *m*-xylene/*o*-xylene/*p*-xylene/ethylbenzene for the commercial reformate and the corresponding equilibrium mixture, were as follows:

42 / 23 / 20 / 15 (commercial)
45 / 23 / 21 / 11 (equilibrium).

Despite some differences between global C_8 aromatic content in commercial and equilibrium mixtures *(Table 5)*, the hierarchies of the relative individual C_8 aromatic proportions were very similar. The coincidence of the equilibrium and commercial data were even more evident when the corresponding

$\frac{o-x+p-x}{m-x}$ ratios were compared. They were important from the commercial point of view. For the four successive commercial runs these ratios were: 1.01; 0.95; 0.89 and 0.91. For the calculations they were taken equal to 0.95.

It would be rather difficult to compare the individual compositions of commercial and equilibrium mixtures by the present analytical techniques applied. The composition of a C_7 mixture in a commercial reformate and in equilibrium are shown here as an example of comparison. The data presented in *Table 7* were obtained in run "1".

Table 7.

The individual hydrocarbon composition of the C_7 fraction in a commercial reformate and in the equilibrium mixture w/w in relation to the C_6—C_9 fractions

COMPOUND	COMMERCIAL REFORMATE	EQUILIBRIUM MIXTURE
1. toluene	16.6	14.60
2. n-heptane	2.9	2.60
3. 2-methylhexane	2.8	3.01
4. 3-methylhexane	3.5	3.31
5. 3-ethylpentane	0.4	0.49
6. 2,2-dimethylpentane	0.5	0.65
7. 2,3-dimethylpentane	—	2.84
8. 2,4-dimethylpentane	0.4	0.54
9. 3,3-dimethylpentane	0.5	0.73
10. 2,2,3-trimethylbutane	0.2	0.18
11. methylcyclohexane	0.2	0.18
12. ethylcyclopentane	0.1	0.14
13. 1,1-dimethylcyclopentane	—	0.08
14. 1,2-dimethylcyclopentane, cis	0.0	0.05
15. 1,2-dimethylcyclopentane, trans	0.1	0.16
16. 1,3-dimethylcyclopentane, cis	0.1	0.14
17. 1,3-dimethylcyclopentane, trans	0.1	0.10

Conclusions

1. Calculated equilibrium aromatic content and aromatic to paraffin molar ratio are good estimates of the corresponding values for commercial reformates.
2. Hydrocracking reactions are responsible for the differences between commercial cat reformate and chemical equilibrium compositions. Hydrocracking changes the class composition (C_6 mole %, C_7 mole %, C_8 mole %, C_9 mole %) of reformates in relation to the feed. There is a relative increase in the C_6 and C_7 and a decrease in the C_8 and C_9 content.
3. In order to improve the match between equilibrium and commercial reformate compositions, a correction has to be introduced into the calculations. This is a correction of the class composition of the feed. In the absence of experimental results the original input data can be changed

as follows: C_6 (+5 mole %), C_7 (+2 mole %), C_8 (−2 mole %), C_9 (−5 mole %). Chemical equilibrium compositions calculated with corrected feed data fit the commercial results very well.

ACKNOWLEDGEMENT

This report is a part of an extensive study on catalytic reforming. Interest in and financing of the programme by the Institute of Petroleum Processing (ITN), Kraków, Poland is acknowledged.

REFERENCES

1. Henningsen, J., Bungaard-Nielson, B.: Brit. Chem. Eng., *15*, 1433 (1970).
2. Van Zeggeren, F., Storey, S. H.: The computation of chemical equilibria. Cambridge Univ. Press, 1970.
3. Zeleznik, F. J., Gordon, S.: Ind. Eng. Chem., *60* (6), 27 (1968).
4. Holub, R.: Chem. Listy, *62*, 87 (1968).
5. Radosz, M., Kramarz, J.: Die Anwendung der Methode der schrittweisen Minimalisierungen zur Berechnung der Gleichgewichtzusammensetzung des Reformates, Chem. Techn., to be published.
6. Kugelman, A. M.: Hydrocarbon Process., *55*, 95 (1976).
7. Wermann, J., Lucas, K.: Chem. Techn., *16*, 342 (1964).
8. Krane, H. G., Groh, A. B., Schulman, B. L., Sinfelt, J. H.: Fifth World Petroleum Congress, Sec. III, 39, New York, 1959.
9. Żorow, J. M., Panczenkow, G. M., Zelcer, S. P., Tirakjan, J. A.: Chimia Techn. Topliv Masel, 1, 12 (1965).

РЕЗЮМЕ

Состав продукта, полученного в установке реформинга бензина, сравнивался с составом, рассчитанным на основе данных химического равновесия. Было установлено, что содержание ароматических соединений в продукте, а также молярное соотношение ароматических и парафинных соединений в нём хорошо совпадали с расчётными значениями. Исследовалось также влияние реакций гидрокрекинга на состав продукта реформинга (реформат). При выполнении расчётов целесообразно воспользоваться корректирующим фактором, при помощи которого принимается во внимание влияние реакций гидрокрекинга.

HUNGARIAN JOURNAL
OF INDUSTRIAL CHEMISTRY
VESZPRÉM
Vol. 6. pp. 251—258 (1978)

STUDY ON THE EFFECT OF A DETERGENT ADDITIVE, AND TEST SEVERITY ON MOTOR OIL TEST RESULTS

K. A. A. Hakim, A. Zalai, A. Lechner and A. Tóth

(Hungarian Oil and Gas Research Institute)

Received: February 18, 1978.

The paper contains a study on some effects of a detergent additive, and engine test severity on motor oil test results. Bench tests, model-wear tests and field tests were carried out for this purpose by using Ba-alkylbenzol sulphonate + Ba-thiophosphonate detergent additive.

Increasing the concentration of the detergent additive caused significant improvement in the merit rating and in the wear reduction of the test engine parts.

1. Introduction

Developments in the construction of the internal combustion engines places ever increasing requirements on motor oils. Motor oils are therefore commonly blended with anti-oxidants, detergents, and anti-wear, etc., additivies. This paper deals with a study on some effects of a detergent additive, and engine test severity on motor oil test results. The "Ba-alkylbenzol sulphonate + Ba--thiophosphonate" detergent additive, which is also produced in Hungary, was selected for this study. Bench tests, model-wear tests and field tests were carried out for this purpose.

2. Methods and materials

2.1 *Bench Tests*

These were carried out on a Petter AV-1 laboratory type, single cylinder, 4-stroke, pre-combustion chamber, kerosene cooled Diesel engine [1, 2]. Some tests were carried out for 120 hours according to the standard IP 175/69 oil test method [2, 3]. Other tests were more severe and for longer operating periods than the standard method. The main operating conditions of the bench tests are shown in *Table 1.*

Table 1.

Main operating conditions of the bench tests

Bench test number	1	2	3			4		
Test duration, hours	120	120	120	160	200	120	160	200
Characteristic of test severity	normal	normal	more severe			normal		
duration	normal	normal	more longer			more longer		
Detergent additive content, %	2.7	7.0	7.0	7.0	7.0	7.0	7.0	7.0
Oil designation	B	A	A			A		
Load, HP	5.3	5.3	5.2	5.2	5.2	5.3	5.3	5.2
Inlet air temperature, °C	21	24	29	29	29	29	27	30
Exhaust gas temperature, °C	377	388	430	430	430	383	373	379
Smoke content, Bosch	1.1	1.9	2.2	2.1	2.1	1.8	1.4	1.5
Lube oil consumption, g/hr	9.6	7.7	8.7	8.9	9.4	6.9	10.1	11.3
Fuel consumption, g/hr	1086	1087	1092	1092	1092	1081	1076	1076

2.2 *Model-Wear Test*

The standard Reichert method was used for determining the anti-wear properties of the oils used. The method is shown diagramatically in *Fig. 1*, the details of which are given in reference 4 and 5.

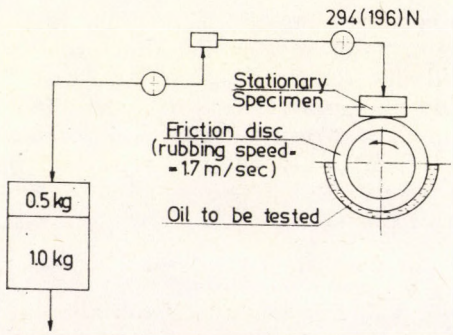

Fig. 1

2.3 *Field Tests*

Two lorries were used in a field test procedure. The lorries were used under severe conditions for carrying road building materials. The main technical data of both lorries are shown in *Table 2*.

Table 2.

Data of engines

Engine	Vehicle I	Vehicle II
Cycle	4-stroke Diesel	4-stroke Diesel
Number of cylinders	6	8
Position of cylinders	V/90°	V/90°
Bore, mm	130	130
Stroke, mm	140	140
Swept volume, litre	11.16	14.86
Compression ratio	16.5	16.5
Maximum power, bhp	180	240
at speed, r.p.m.	2100	2100
Maximum torque, kp.m	67	90
at speed, r.p.m.	1500	1500
Lubrication mode	pressure	
Coolant	water	
Oil capacity	24	32
Injection type	direct injection	

2.4 *Characteristics of Motor Oils*

In the bench tests, Supplement-1 and HD oils were used. The base oil was SAE-30, refined oil made from Soviet crude oil. The oxidation inhibitor was Zn-dithiophosphat and the concentration was kept unchanged in all tests.

Table 3.

Characteristic ranges of the lubricating oils used by the different tests

Designation No.	A	B	C
Oil quality*	Suppl.-1	HD	Base oil
SAE grade	30	30	30
Specific weight, g/ml	0.900	0.896	0.892
Flash point, °C	245	240	231
Pour point, °C	−30	−28	−17
Viscosity at 50 °C, cSt	64.88 67.78	58.13	56.87
at 100 °C, cSt	11.12—11.69	10.16—10.27	10.12
Viscosity index	89—92	85—87	84
Conradson carbon, %	1.15—1.41	0.60—0.67	0.1
Ash content, %	0.91—1.18	0.44—0.52	0.003
SO_4 ash content, %	0.99—1.26	0.48—0.56	—
Acid No.	0.67—0.89	0.66—0.87	0.03
Colour, ASTM	6.0—7.0	4.0—5.5	3.5
Bench tests	×	×	not
Field tests	×	not	not
Model-wear tests	×	×	×

* Suppl.-1 = Supplement-1
HD = Heavy duty

The detergent additive was "Ba-alkylbenzol sulphonate + Ba-thiophosphonate" in a ratio of 4:3. It was used in two concentration levels, i.e. 7% in oil "A", Supplement-1 oil, and 2.7% in oil "B" HD oil.

In the model-wear tests, SAE-30 base oil, designated as oil "C", HD oil and Supplement-1 oil were used.

In the field tests, only Supplement-1 oil was used, but in different SAE viscosity categories depending on the season, during which the lorries were used.

The general characteristics of the oils used in all tests are shown in *Table 3.*

3. Results and discussion

3.1 *Bench Tests*

According to the IP 175/69 oil test method, two tests were carried out using oil "A" test 2, and oil "B" test 1.

Oil "A" was then examined in two longer tests than the standard, i.e. for 120, 160 and 200 hrs. One of these tests, test 3 was more severe than the other test 4.

The results obtained from these bench tests are shown in *Table 4.*

Table 4.

Merit rating and wear figures of engine components for the bench tests

Bench test number	1	2	3*			4		
Test duration, hr	120	120	120	160	200	120	160	200
Detergent additive concentration, %	2.7	7.0	7.0	7.0	7.0	7.0	7.0	7.0
Oil designation	B	A	A	A	A	A	A	A
MERIT RATING**								
Ring sticking	10	10	10	9.5*	9.4+	10	10	10
Piston skirt inside	10	10	10	10	10	10	10	10
Piston crown deposits, inside	8.4	9.0	8.0	7.1	6.2	8.7	8.0	7.1
Piston skirt outside	10	10	10	10	10	10	10	10
Oil scraper ring deposits	10	10	10	11	10	10	10	10
1—4 groove deposits, average	3.3	8.3	5.6	2.9	0.9	7.8	4.6	3.0
1—3 land deposits, average	6.2	8.7	8.4	4.4	1.6	8.8	6.0	5.4
Groove + Land, average	4.8	8.5	7.0	3.7	1.3	8.3	5.3	4.2
Overall rating/100	82.7	94.3	87.9	76.3	68.0	93.3	83.7	79.3
WEAR DATA								
First ring weight loss, mg	169.3	109.8	—	—	152.4	86.9	118.2	152.4
1—4 ring weight loss, mg	222.2	165.8	—	—	265.5	150.6	202.9	250.1
Liner wear, mg	6	4	—	—	—	—	—	—

* More severe than the standard
** 10 = clean, 0 = completely covered with deposits

* Cold ring sticking
\+ Hot sing sticking

3.1.1 *Influence of the "Ba-sulphonate + Ba-phosphonate" Detergent Additive Concentration on the Test Results*

Raising the detergent additive concentration from 2.7% to 7.0% caused the merit rating of the piston zones to be improved significantly, e.g. the average merit rating of the ring grooves increased from 3.3 to 8.3 and that of the land from 6.2 to 8.7 out of 10, while the total merit rating of the whole piston improved from 82.7% to 94.3%. On the other hand, this increase in the detergent additive concentration caused significant reduction in the wear of the first compression ring and of the liner by more than 30%.

3.1.2 *Influence of Test Severity and Lengthening the Test Duration on the Results*

Comparing the results of test 3 and test 4, shown in *Table 4*, the merit rating values tended to fall-off by lengthening the duration of tests from 120 to 160 and to 200 hours. The severity of test 3, caused them to became lower, which resulted in accumulation of insolubles in the oil accompained by "cold" sticking of the first and second rings over 45° at 160 hours; while "hot" sticking of the first ring and "cold" of the second ring over 80° occurred during the 200 hours test period. The Conradson carbon and the coagulated gasoline insoluble content of the used oil tended in both tests to increase by extending the test period, while the severity of test 3 caused a more sharp increase, particularly from 160 to 200 hours, as shown in *Table 5*.

Table 5.

Analysis of the used oils after the bench tests

Bench test number	1	2	3			4		
Detergent additive content, %	2.7	7.0	7.0					
Oil designation	B	A	A					
Test durations, hours	120	120	120	160	200	120	160	200
Conradson number, %	1.42	2.68	2.53	3.19	4.71	2.42	2.76	3.09
Ash content, %	0.50	1.25	1.26	1.41	1.54	1.20	1.29	1.38
Coagulated gasoline insolubles, %	1.65	1.50	1.40	2.40	4.30	1.25	1.60	1.85

3.2 *Model-Wear Tests*

The Reichert method used, briefly consisted in determining the wear scar area that occurred on the test specimen Fig. 1. The smaller area indicates better anti-wear property of the oil.

In the same test, the friction path during which friction noise could be heard was measured. The smaller this path is, the better the anti-wear property of the oil.

Five parallel tests must be made when examining an oil. The first and the fifth are made by using a reference oil, between which three tests are carried

out using the oil under test. The results of the first and the fifth test must be approximately the same.

The results obtained from tests on oil "A", "B" and "C" are shown in *Table 6*. The wear scar area and the noisy friction path also decrease by in-

Table 6.

Standard Reichert test results under load of 30 kp, friction path of 100 m and room temperature

Oil designation	Wear scar area, mm²					Noisy friction path, m				
	Reference oil	Oil to be tested			Reference oil	Reference oil	Oil to be tested			Reference oil
"C" 0.0% detergents	22.5	14.3	15.0	15.6	22.5	24.0	8	10	10	24
"B" 2.7% detergents	22.5	9.2	9.5	10.3	22.5	24.0	5	6	7	24
"A" 7.0% detergents	22.8	7	4.5	2.8	23.7	25	4	4	3	24

creasing the additive concentration. Oil "B" caused a decrease in the wear scar area and the noisy friction path compared to oil "C" by 33%, while oil "A", compared to oil "B", caused a reduction of 35—50%. These results indicate the benefit of the detergent additive under study in reducing wear and also confirms those results obtained from the bench tests. The influence of increasing the detergent additive concentration on reducing the wear scar area and the noisy friction path is shown on *Fig. 2*.

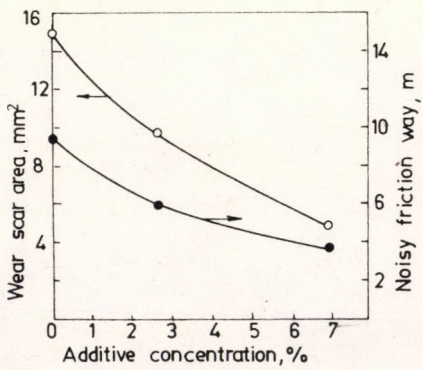

Fig. 2

3.3 *Field Test*

In this test, the vehicles ran an average of 42,000 km. Oil "A" was used and changed after different intervals, i.e. after 3,000, 4,000, 5,000, 6,000 and 7,000 km. The results showed the following:

— After an average of 42,000 km running, the mean of the overall deposit merit rating of the pistons was 71.5% which is equal approximately to 190—200 hours severe bench test on the Petter AV-1 engine.

— No ring sticking occurred and the insoluble content in the used oil samples did not exceed 2% oil change after 7,000 km running.

4. Conclusions

1. Increasing the concentration of the "Ba-sulphonate + Ba-phosphonate" detergent additive from 2.7% to 7.0%, caused significant improvement in the merit rating values of the Petter AV-1 engine parts. Increasing the severity and extending the period of the tests worsened the piston deposit rating values and caused ring sticking.

2. Both the bench—and model wear tests showed that increasing the concentration of the above mentioned detergent additive caused a significant reduction in wear figures.

3. The field test showed that oil "A" can be used with an oil change period of more than 7,000 km without problems appearing such as ring sticking.

REFERENCES

1. Towle, A. and Vaile P. E. B.: J. Inst. Pet. London, *39*, 581 (1953).
2. Schilling, A.: Motor Oils and Engine Lubrication. Scientific Publications G. B. Ltd. 1968.
3. IP Standards for Petroleum and its Products. Part III., London, 1969.
4. Zalai, A.: Kenőanyagok gépi vizsgálata (The Engine Test of Lubricants). Tankönyvkiadó, Budapest, 1970.
5. Reichert, H.: Reibverschleisswage nach Reichert. Schmierstoff-Messmaschine, DBGM 1 749 267.

РЕЗЮМЕ

Данная статья занимается вопросом влияния, оказываемого присутствием детергентных присадок и условиями испытаний, на результаты испытаний моторных масел. С этой целью на испытательном стенде и на встроенных автомобильных двигателях изучалось влияние детергентных присадок алкил-бензол-сульфонат бария + тиобензол-фосфонат бария.

Увеличение концентрации детергентных присадок оказало положительное действие на мощность моторов и снижало изнашиваемость деталей мотора.

HUNGARIAN JOURNAL
OF INDUSTRIAL CHEMISTRY
VESZPRÉM
Vol. 6. pp. 259–274 (1978)

THE SOLUBILITY OF MICRONUTRIENTS IN AMMONIUM POLYPHOSPHATE SOLUTIONS

S. Gór-Nagy*, P. Káldi**, Mrs. J. Bésán*** and A. Szántó***

(* Committee of National Technical Development, Budapest;
** Department of Chemical Technology,
Veszprém University of Chemical Engineering, Veszprém;
*** Research Institute for Heavy Chemical Industries, Veszprém)

Received: April 2, 1978.

Experiments were carried out to determine the solubilities of micronutrients [Fe(III), B, Zn, Cu, Mn, Co, Mo] in 10–34–0 ammonium polyphosphate solution. As a result a method was elaborated which, in the case of polyphosphate solutions containing three of the above mentioned micronutrients, enables the calculation of concentration relationships without the knowledge of the composition and stability coefficients of the formed complex compounds. This method can be extended to the description of fertilizer solutions containing more than three micronutrients.

1. Introduction and Literature

Those elements are termed micronutrients which take part in the structure of a plant's organism and which are present there in a concentration of less than 10^{-2} wt. per cent. These elements, although their amount is more or less negligible, play an important role in the life of a plant. The most important micronutrients are: iron, boron, zinc, copper, manganese, cobalt and molybdenum.

In a modern rural economy which applies industrial monocultural production methods, the need for micronutrients increases every day. The applied production technologies consume steadily growing amounts of NPK fertilizers and, as a consequence the amount of harvested products of a given region, constantly increases. The result of experiments, carried out with different types of fertilizers, show that a further increase of macronutrients results in a lower increase of products from a soil properly supplied with nitrogen, phosphorous and potassium, but with the rise in the micronutrient concentration of the land, the result is a marked growth of the harvested product. Therefore in countries with a developed agriculture a demand arises for supplying the micronutrient deficiency of the soils in addition to and together with fertilization of different nitrogen, phosphorous and potassium compounds.

Based on the data that has appeared in literature, the supplement of micronutrients can easily be solved with the aid of liquid fertilizers, among these the polyphosphate solutions have the advantage that they dissolve the inorganic salts until a degree determined by their original polyphosphate concentration [1a]—[14].

In *Table 1*, the solubility data of micronutrients are presented, related to NP solution containing 8-24-0 (ortophosphate solution); 10-34-0 (40—45 wt.

Table 1.

The solubility of inorganic salts—micronutrients—in ammonium polyphosphate solutions
[1a], [3], [4], [7]—[14]

Dissolved salt	Solubility (%) of (Zn, Cu, Fe, Mn, B, Mo) in		
	8=24=0	10=34=0 solutions	11=37=0
ZnO	0.05	2.25	3.0
$ZnSO_4 \cdot H_2O$	0.05	1.50	2.0
$ZnCO_3$	0.05	2.25	3.0
CuO	0.03	0.53	0.7
$CuSO_4 \cdot 5\ H_2O$	0.13	1.13	1.5
$Fe_2(SO_4)_3 \cdot 9\ H_2O$	0.08	0.80	1.0
Mn_3O_4	< 0.02	0.15	0.2
MnO	< 0.02	—	0.2+
$MnSO_4 \cdot H_2O$	< 0.02	—	0.2+
$Na_2MoO_4 \cdot 2\ H_2O$	0.5++	0.38++	0.5++
$Na_2B_4O_7 \cdot 10\ H_2O$	0.90	0.90	0.9

Note:
+ precipitate formed after several days
++ highest concentration examined

per cent polyphosphate solution) and 11-37-0 (60—70 wt. per cent polyphosphate solution) macronutrient ratios and having only one micronutrient compound. The numbers given above indicate the $N\text{-}P_2O_5\text{-}K_2O$ concentration of the fertilizer solution, in wt. per cent [1a], [3], [4], [7]—[14].

The inorganic compounds of zinc, manganese, copper and iron are almost insoluble in ortophosphate solutions (their solubility is less than 0.1 wt. per cent) due to the formation of metal ammonium ortophosphates.

The relatively higher solubility of metal salts in solutions containing polyphosphates can be explained by the sequestering properties of the condensed phosphates. If a polyphosphate solution is poured progressively into a solution of multivalent metal ions, at first a precipitate forms which dissolves later in the presence of excess polyphosphate. All the condensed phosphates form insoluble salts with multivalent metal ions which transform into a soluble complex compound in the excess of polyphosphate. This phenomenon is termed sequestering property [15]. The sequestering property of the ammonium polyphosphate solution used for fertilizers is attributed to their dipolyphosphate and tripolyphosphate content.

The concentration of micronutrients dissolved in polyphosphate base fertilizer solutions is influenced by the solubility relationships of the other compounds present in the system. *In a system which is in equilibrium, the actual values of the metal ion concentrations are the results of the stability coefficients of complex forming reactions and the solubility relationships of the final products* [1b].

The structure of most of the complexes formed in polyphosphate solutions is unknown, only a few of them were examined thoroughly. Neither the numerical values of the stability coefficients nor the solubility products of these known complexes can be used for the determination of the maximum allowable metal concentration of polyphosphate solutions. These data were determined in pure systems, in dilute electrolytes and hence they cannot be related to the complex mixtures of fertilizer solutions.

In concentrated polyphosphate solutions, the concentration of micronutrient can be higher or lower compared to the previously mentioned data, due to the unknown equilibrium processes. A further complication arises that the form and the composition of the solid phases assumed by the solubility relationships are not always equal due to the crystal dimorphism and isomorph substitution, which have significant effects on the solubility. Adding mixtures of micronutrients to fertilizers, the isomorph substitution occurs more frequently in reaction products.

The large number of components made the generally used solubility diagrams inapplicable for the determination of solubility data and for the identification of solid phases [16]. The liquid polyphosphate solutions are too complicated systems to investigate or represent with simple phase diagrams.

The result of the mentioned difficulties is that the published data on micronutrient solubility in polyphosphate solutions are extremely rare and insufficient, up to now the concentration data of the single micronutrients in polyphosphate solutions are available, but the data concerning cobalt are missing.

Hitherto only two brief references were found dealing with multicomponent systems:

- FORMAINI stated [11] that the concentration of copper, zinc and manganese in a polyphosphate solution can be calculated with the weighted average of the single solubility data,
- based on MORTVEDT's publication the micronutrient concentration limit of 3 wt. per cent cannot be exceeded and the storage time of liquid fertilizers containing various nutrients is shorter than those which contain only a single one [1a].

2. The Method Used for the Determination of Micronutrient Solubility

For the solution of the questions outlined above, a method was elaborated which can be applied for the determination of the solubility of micronutrient mixtures in polyphosphate solutions without the knowledge of the processes taking place during the dissolution and of the composition of the compounds formed.

In the following a method is discussed which can be applied in the case of solutions containing three micronutrients. The principle of the method

can be extended to polyphosphate solutions containing more than three micronutrients, but in these cases the depiction in four, five or more dimensions is impossible. This method was elaborated for the determination of micronutrient solubility in ammonium polyphosphate fertilizers. It is conceivable that similar problems can be successfully if this method is applied.

As the first step, *the solubility data of the single micronutrient* was determined. The examined metal salt was poured into 100 g. of well mixed ammonium polyphosphate solution, at room temperature until an insoluble precipitate was formed. Then the solution was stirred for 24 hours and the precipitate was separated from the solution with an ultracentrifuge (5,000 to 6,000 rpm), and the micronutrient concentration of the clear solution was determined by an atomabsorption spectrometer. If the p_H value of the solution decreased during the dissolution of the salt, ammonia gas was bubbled into the solution.

The metal concentration value of the clear solution being in equilibrium with the formed precipitate was taken as the solubility of the examined salt.

Knowing the solubility data of the examined micronutrient salts, in the second step the *solubilities of micronutrient pairs* were determined. A series of solutions were prepared which contained 25, 50, 75 and 100 per cent of the soluble amount of the given salt and into these well mixed solutions was added the second salt, at room temperature, until the formation of an insoluble precipitate. Then, if necessary, the p_H value of the solutions was adjusted to 5.85. The following procedures were similar as described above.

The metal concentrations of polyphosphate solutions containing two micronutrients were presented with the help of a rectangular co-ordinate system, the solubilities of the single micronutrients were plotted on the axes in (g metal/100 g ammonium polyphosphate) [APP] units. The concentration values of the solution containing two micronutrients form a plane limited by the axes, this means that all points of this figure represent stable fertilizer solutions. The border curves of the plain figure were approximated by straight lines. This neglection could be done because the examined concentration range is very narrow and as a consequence, the curvature is negligible.

The following method was used for *the determination of the concentration relationships of polyphosphate solutions containing three micronutrients:*

The solubility relationships of three micronutrients can be represented by a figure having three dimensions i.e. by a solid. The construction of this solid is described below:

The plane figures determined by micronutrient pairs was placed into a space co-ordinate system. Here, the solubilities of the single micronutrients are given on the x, y and z axes as point values, and the planes formed by the axes represent the solubilities of micronutrient pairs. This is shown in *Fig. 1.*

Marking the tips of the solid with letters:

P_2 (a, 0, 0)
P_3 (0, b, 0)
P_4 (0, 0, c)
P_5 (A, B, 0)
P_6 (C, 0, D)
P_7 (0, E, F)

(It is to be noted that the origin, formed by the axes is meaningless!)

The co-ordinates of the points being in brackets, represent the solubilities of the individual metals or micronutrient pairs: P_2, P_3 and P_4 give information

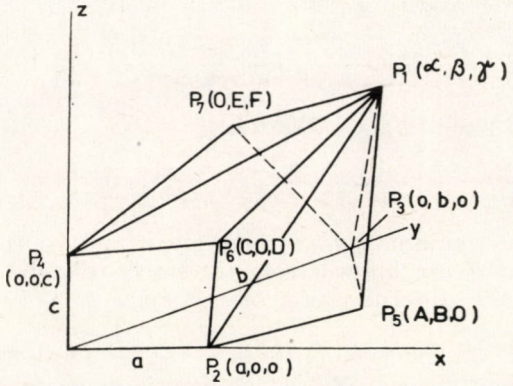

Fig. 1
The Solubility of Micronutrient Triad in General Case
a, b, c = the maximum metal concentration (g metal/100 g APP) of the system containing single micronutrient
A, B, C, D, E, F = the maximum metal concentration (g metal/100 g APP) of the system containing micronutrient pairs
α, β, γ = the maximum metal concentration (g metal/100 g APP) of the system containing micronutrient triad

about the concentration of the micronutrient, while points P_5, P_6 and P_7 represent the solubility relationships of micronutrient pairs. Marking an optional $P_1(\alpha, \beta, \beta)$ point—here α, β and γ give the solubility data of three micronutrients being present in the solution—and let us connect this together with the points P_2, P_3, P_4, P_5, P_6 and P_7. These latter points are carriers of certain information. Now, a plane can be placed on P_1 and on both the points being in neighbourhood of P_1; six such planes can be placed. In this way a solid can be formed which is bordered by planes representing the solubilities of the examined micronutrients. For the mathematical description of this solid the equation of a plane represented by three points can be used. Taking the symbols given in *Fig. 1:*

For the plain represented by P_1, P_2 and P_5:

$$\frac{x}{a}+\frac{y}{b}\left(1-\frac{A}{a}\right)+\frac{z}{\gamma}\left(1-\frac{\alpha}{a}-\frac{\beta}{B}+\frac{A}{a}\cdot\frac{\beta}{B}\right)=1$$

For the plain represented by P_1, P_3 and P_5:

$$\frac{x}{A}\left(1-\frac{B}{b}\right)+\frac{y}{b}+\frac{z}{\gamma}\left(1-\frac{\alpha}{A}-\frac{\beta}{b}+\frac{B}{b}\cdot\frac{\alpha}{A}\right)=1$$

For the plain represented by P_1, P_2 and P_6:

$$\frac{x}{a}+\frac{y}{\beta}\left(1-\frac{\alpha}{a}-\frac{\gamma}{D}+\frac{C}{a}\cdot\frac{\gamma}{D}\right)+\frac{z}{D}\left(1-\frac{C}{a}\right)=1$$

For the plain represented by P_1, P_4 and P_6:

$$\frac{x}{C}\left(1-\frac{D}{c}\right)+\frac{y}{\beta}\left(1-\frac{\alpha}{C}-\frac{\gamma}{c}+\frac{\alpha}{C}\cdot\frac{D}{c}\right)+\frac{z}{c}=1$$

For the plain represented by P_1, P_4 and P_7:

$$\frac{x}{\alpha}\left(1-\frac{\beta}{E}-\frac{\gamma}{c}+\frac{\beta}{E}\cdot\frac{F}{c}\right)+\frac{y}{E}\left(1-\frac{F}{c}\right)+\frac{z}{c}=1$$

For the plain represented by P_1, P_3 and P_7:

$$\frac{x}{\alpha}\left(1-\frac{\beta}{b}-\frac{\gamma}{F}+\frac{\alpha}{F}\cdot\frac{E}{b}\right)+\frac{y}{b}+\frac{z}{F}\left(1-\frac{E}{b}\right)=1$$

Dealing with the examination of three given metals, the values of a, b, c, A, B, C, D, E and F are known from the previously discussed experiments. The task is now the determination of the place of point P_1. Knowing the solubility relationships of the given micronutrient pairs, the form of the solid is generally simpler as it is depicted in *Fig. 1*. During the determination of the data representing the solid which describes the concentration relationships of three micronutrients, the aim is to prove that those solutions are stable which can be characterized by the concentration values being "inside" the solid.

For clarity *Fig. 2* shows the photograph of the solid fabricated from wire.

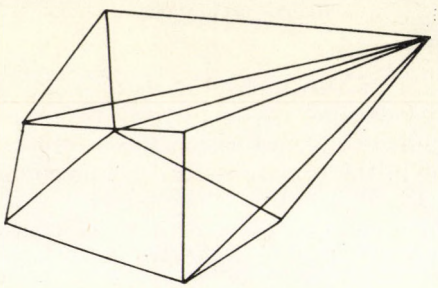

Fig. 2
The Solid Representing the Solubility Relationships of Micronutrient Triad

3. Experimental Results

The application of the method discussed above is shown by the solubility determination of micronutrients in 10-34-0 ammonium polyphosphate solution.

The 10-34-0 polyphosphate solution was prepared in the laboratory. Its analysis data are as follows:

N = 9.58 wt. per cent

P_2O_5 = 34.00 wt. per cent

The distribution of the total P_2O_5:

ortophosphate	52.3 per cent
diphosphate	41.9 per cent
triphosphate	5.7 per cent

Density = 1.3488 g/cm³

p_H = 5.85

The used inorganic compounds—or micronutrients—and their metal concentrations are listed in *Table 2.*

Table 2.

Compounds used as micronutrient source

Micronutrient	Compound		
	name	formula	metal content %
Boron	Borax	$Na_2B_4O_7 \cdot 10\ H_2O$	11.40
Molybdenum	Ammonium Molybdenate tetrahydrate	$(NH_4)_6Mo_7O_{24} \cdot 4\ H_2O$	54.40
Zinc	Zinc Sulphate heptahydrate	$ZnSO_4 \cdot 7\ H_2O$	22.85
	Zinc Oxide	ZnO	80.85
Copper	Copper Sulphate pentahydrate	$CuSO_4 \cdot 5\ H_2O$	25.50
Manganese	Manganous Sulphate monohydrate	$MnSO_4 \cdot H_2O$	32.50
Cobalt	Cobaltous Nitrate monohydrate	$Co(NO_3)_2 \cdot H_2O$	31.08
Iron	Ferric Ammonium Sulphate	$Fe(NH_4)(SO_4) \cdot 12\ H_2O$	11.6

The solubilities of the single micronutrients are presented by the numerical values of a and b, in *Table 3.*

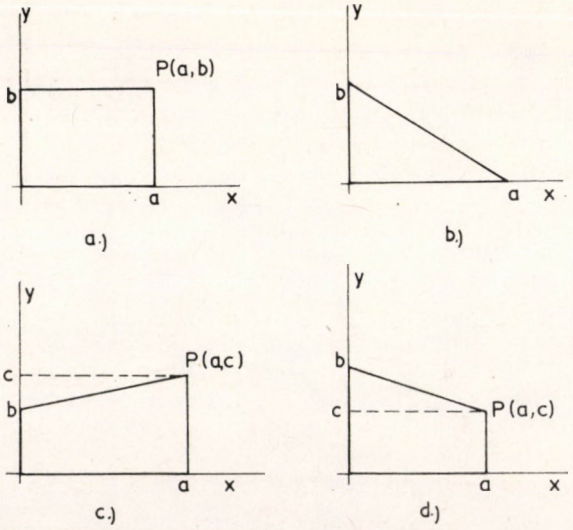

Fig. 3
Diagrams Describing the Concentration Relationships of Micronutrient Pairs in 10=34=0 Ammonium Polyphosphate Solution

Table 3.

The solubility of micronutrient pairs in 10=34=0 ammonium polyphosphate solution (see *Fig. 3*)

Micronutrient pair	Type of diagram	Solubility g metal/100 g APP. Symbols used in *Fig. 3*		
		a	b	c
B-Mo	3a	1.75	1.00	—
B-Zn	3a	1.75	2.08	—
B-Cu	3a	1.75	1.30	—
B-Fe	3c	1.75	2.70	3.66
B-Co	3c	1.75	0.34	1.00
B-Mn	3d	1.75	0.07	0.03
Mo-Zn	3a	1.00	2.08	—
Mo-Cu	3a	1.00	1.30	—
Mo-Fe	3a	1.00	2.70	—
Mo-Co	3a	1.00	0.34	—
Mo-Mn	3a	1.00	0.07	—
Cu-Zn	3b	1.30	2.08	—
Cu-Mn	3b	1.30	0.07	—
Cu-Co	3c	1.30	0.34	0.67
Zn-Mn	3b	2.08	0.07	—
Zn-Co	3b	2.08	0.34	—
Fe-Cu	3a	2.70	1.30	—
Fe-Zn	3b	2.70	2.08	—
Fe-Mn	3a	2.70	0.07	—
Fe-Co	3c	2.70	0.34	0.67
Co-Mn	3b	0.34	0.07	—

Table 3 and *Fig. 3* show the solubility relationships of micronutrient pairs. As micronutrients Fe(III), B, Zn, Cu, Mn, Co and Mo were selected and the solubility of the given micronutrient pairs, determined by the method described above, can be presented by one of the diagrams given in *Fig. 3*.

The solubility data of the micronutrient pairs were substituted into the general equation system of the solid depicted in *Fig. 1* and as a result the configuration given in *Fig. 4* was gained which describes the *solubility relationships of the micronutrient triad.*

Knowing these solids the method was selected, using this it could be proved with relatively few experiments that the solutions characterized by the component concentrations which are "inside" the constructed solid are stable and no precipitate forms. In the case of solutions by which the concentration data of the micronutrient components are "outside" the body, a precipitate forms.

The method used was as follows:

In the cases of *a*, *b*, *c*, *d*, *e* and *f* of *Fig. 4/1*, the component concentrations were increased along the body diagonal, connecting together the point *P* and the origin. The aim was to reach the point *P*. If in this case the solution was

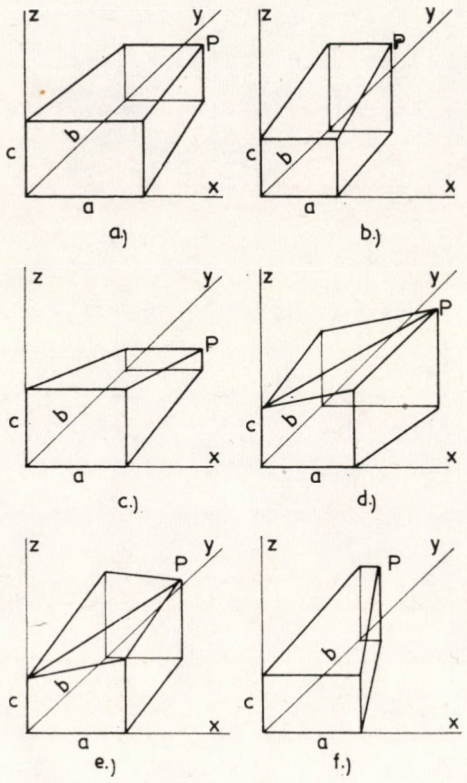

Fig. 4/1
Special Cases of the Solubility of Micronutrient Triads in 10=34=0 Ammonium Polyphosphate Solutions

stable, an attempt was made to "step out" from the formation i.e. more inorganic salts were added into the solution. If this experiment resulted in a precipitate formation, this verified the soundness of the presumption.

In the case of the triangle base prism shown in *Fig. 4/2* g, the increase of component concentration was carried out along the arrow which lies on the boundary plane, and a further increase of the concentration was attempted.

In the cases of *h*, *i*, *j*, *k*, *l* and *m* of *Fig. 4/2* the concentrations were similarly altered, the directions marked with arrows, until the point *P* was reached, taking the formations of *h*, *i* and *j* the samples characterized by A were also prepared.

If the p_H value of the solutions decreased due to the dissolution of the micronutrients, it was readjusted again with ammonia gas until the value of 5.85.

The numerical data of the solubility values of micronutrient triads are listed in *Table 4*. The representation of the micronutrient concentration on the *x*, *y* and *z* axes was carried out in the sequence given in the first column of the *Table*, i.e. the α co-ordinate of point *P* gives the first, β the second and γ the

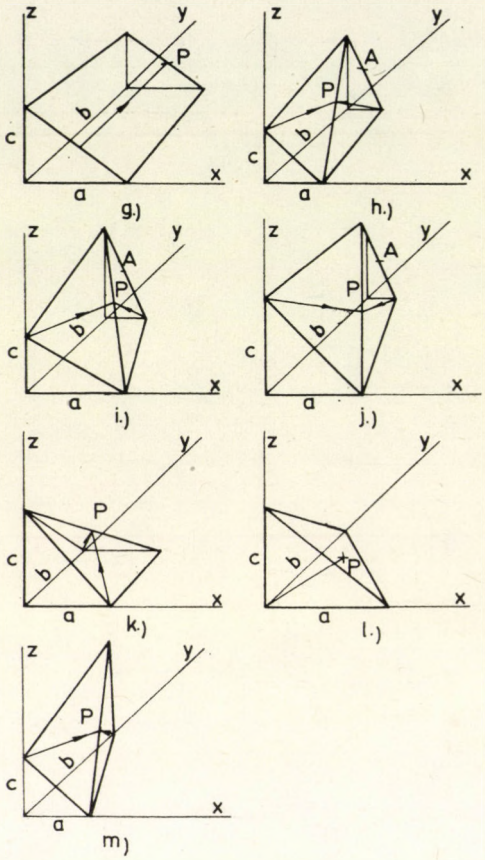

Fig. 4/2
Special Cases of the Solubility of Micronutrient Triads in 10=34=0 Ammonium Polyphosphate Solutions

third element concentration existing in the fertilizer solution characterized by point P. The section of the three axes (a, b, c) is the solubility of the given metal salt, and the three planes of the spatial co-ordinate system being perpendicular to each other, the figures take place which describe the solubility of 2−2 micronutrients. The values of these were presented above and with their help the sizes of the solid can be calculated.

In the cases illustrated with *Figure 4/1 a−f*, the numerical values of the α, β and γ co-ordinates of point P are also presented in *Table 4* on the one hand, the cause of this is the prevention of uncertainties caused by the deforming effect of the drawings, and on the other hand the co-ordinates of the point marked with + symbol do not follow unequivocally from the solubility data of micronutrient pairs. In the cases of *Fig. 4/2 g−m*, the point P moves along one of the edges or on the surface of the solid, therefore their co-ordinates are not presented in *Table 4*.

Table 4.

The solubility relationships of micronutrient triads in 10=34=0 ammonium polyphosphate solution (See *Fig. 4*)

Micronutrient triad	Type of solid	The co-ordinates of point *P* g metal/100 g APP		
		α	β	γ
B-Mo-Zn	4*a*	1.75	1.00	2.08
B-Mo-Cu	4*a*	1.75	1.00	1.30
Fe-Mo-Mn	4*a*	2.70	1.00	0.07
Fe-Mo-Cu	4*a*	2.70	1.00	1.30
Cu-Fe-Cu	4*e*	1.30	2.70	0.67
Mo-Fe-Co	4*b*	1.00	2.70	0.67
Cu-B-Co	4*e*+	1.30	1.75	0.67
Mo-B-Co	4*b*	1.00	1.75	1.00
Cu-B-Fe	4*b*	1.30	1.75	3.66
Mo-B-Fe	4*b*	1.00	1.75	3.66
Fe-B-Co	4*d*+	3.66	1.75	1.00
Fe-Mo-Zn	4*g*	—	—	—
Zn-Mo-Cu	4*g*	—	—	—
Zn-Mo-Co	4*g*	—	—	—
Mn-Fe-Cu	4*g*	—	—	—
Zn-B-Cu	4*g*	—	—	—
Cu-Mo-Mn	4*g*	—	—	—
Co-Mo-Mn	4*g*	—	—	—
Zn-Mo-Mn	4*g*	—	—	—
Mo-Cu-Co	4*b*++	1.00	1.30	0.45
Mn-Fe-Co	4*h*	—	—	—
Mn-B-Zn	4*j*	—	—	—
Mn-B-Cu	4*j*	—	—	—
Zn-B-Co	4*h*	—	—	—
Mn-B-Co	4*i*	—	—	—
Mo-B-Mn	4*c*++	1.00	1.75	0.07
Mn-B-Fe	4*f*	0.03	1.75	3.66
Zn-B-Fe	4*h*	—	—	—
Cu-Fe-Zn	4*k*	—	—	—
Zn-Fe-Mn	4*k*	—	—	—
Cu-Mn-Zn	4*l*	—	—	—
Zn-Co-Mn	4*l*	—	—	—
Zn-Fe-Co	4*m*	—	—	—
Mn-Cu-Co	4*m*	—	—	—
Zn-Cu-Co	4*m*	—	—	—

Notes

+ The co-ordinates of point *P* cannot be given from the solubility data of micronutrient pairs.

++ Irregularities:

1. The solubility of Co is 0.45 g/100 g APP instead of the expected 0.67 g/100 g APP in the Mo-Cu-Co system.
2. Based on the elaborated theory the Mo-B-Mn system could be represented by the solid depicted on *Fig. 4/1 c*. In practice the solid given in *Fig. 4/1 a*. represents the system, i.e. the solubility of manganese is 0.07 g/100 g APP instead of the expected 0.03 g/100 g APP value.

4. The Practical Application of the Method

In possession of the data presented in Chapter 3, it is feasible to meet the claims of rural economists and to decide whether is it possible to prepare the required solution of micronutrients from a 10-34-0 ammonium polyphosphate solution or not.

For systems containing two micronutrients the equations of lines bordering the plain figures can be set up using the symbols presented in *Fig. 3*. If the required concentrations of micronutrients are a_1 and b_1, the following conditions have to be fulfilled for the preparation of a precipitate free fertilizer solution:

In the case of 3.a:

The equations of the bordering straight lines are:

$$x=a \quad \text{and} \quad y=b.$$

The solution is stable, if $a_1 \leq a$ and $b_1 \leq b$.

In the case of 3.b:

The equation of the bordering straight line is:

$$\frac{x}{a}+\frac{y}{b}=1.$$

The solution is precipitate free, if:

$$\frac{a_1}{a}+\frac{b_1}{b} \leq 1.$$

In the case of 3.c:

The equations of bordering straight lines are:

$$x=a \quad \text{and} \quad y=\frac{c-b}{a}x+b.$$

The solution is precipitate free, if

$$a_1 \leq a \quad \text{and} \quad b_1 \leq \frac{c-b}{a} \cdot a_1+b.$$

In the case of 3.d:

The equations of the bordering straight lines are:

$$x=a \quad \text{and} \quad y=-\frac{b-c}{a}x+b.$$

The solution is precipitate free, if:

$$a_1 \leq a \quad \text{and} \quad b_1 \leq -\frac{b-c}{a}a_1+b.$$

For fertilizer solutions *containing three micronutrients* the construction of limiting conditions is similar, the difference is that in this case the equation systems are set up which describe the bordering planes of the spatial figure. The magnitude of the micronutrient concentrations a_1, b_1 and c_1 of the produced solution have to fulfil the demands prescribed by the equation system for the production of a precipitate free, micronutrient triad containing fertilizer solution.

The equation systems describing the solids depicted in *Fig. 4* (using the symbols of *Fig. 1* and *Fig. 4*) are as follows:

In case of 4.a:

$$\frac{x}{a} \leq 1; \quad \frac{y}{b} \leq 1; \quad \frac{z}{c} \leq 1.$$

It is to be seen that the solution will be precipitate free, if:

$$a_1 \leq a: \quad b_1 \leq b; \quad c_1 \leq c.$$

In the case of 4.b:

$$\frac{x}{a} \leq 1; \quad \frac{y}{b} \leq 1; \quad \frac{y}{b}\left(1-\frac{d}{c}\right)+\frac{z}{c} \leq 1.$$

Clear solution can be produced, if:

$$a_1 \leq a; \quad b_1 \leq b; \quad c_1 \leq \frac{1}{c}-\frac{b_1}{cb}\left(1-\frac{d}{c}\right).$$

In the case of 4.c:

$$\frac{x}{a} \leq 1; \quad \frac{y}{b} \leq 1; \quad \frac{y}{b}\left(1-\frac{d}{c}\right)+\frac{z}{c} \leq 1.$$

The conditions of the production of clear solution are:

$$a_1 \leq a; \quad b_1 \leq b; \quad c_1 \leq \frac{1}{c}-\frac{b_1}{cb}\left(1-\frac{d}{c}\right).$$

In the case of 4.d:

$$\frac{x}{a}+\frac{y}{b}\left(1-\frac{e}{a}\right) \leq 1; \quad \frac{y}{b} \leq 1;$$

$$\frac{x}{a}\left(1-\frac{f}{c}\right)+\frac{y}{b}\left(1-\frac{e}{a}-\frac{d}{c}+\frac{e}{a}\cdot\frac{f}{c}\right)+\frac{z}{c} \leq 1;$$

$$\frac{y}{b}\left(1-\frac{d}{c}\right)+\frac{z}{c} \leq 1.$$

The condition of the preparation of the precipitate free solution is that the values of a_1, b_1 and c_1 have to be the roots of the above equation system.

In the case of 4.e:

$$\frac{x}{a} \leq 1; \quad \frac{y}{b} \leq 1;$$

$$\frac{x}{a}\left(1-\frac{e}{c}\right)+\frac{z}{c} \leq 1;$$

$$\frac{x}{a}\cdot\frac{d-e}{c}+\frac{y}{b}\left(1-\frac{d}{c}\right)+\frac{z}{c} \leq 1.$$

The conditions regarding values a_1, b_1 and c_1 are the same as given in the case of 4.d.

In the case of 4.f:

$$\frac{x}{a}+\frac{y}{b}\left(1-\frac{e}{a}\right) \leq 1;$$

$$\frac{y}{b} \leq 1;$$

$$\frac{y}{b}\left(1-\frac{d}{c}\right)+\frac{z}{c} \leq 1.$$

The conditions regarding values a_1, b_1 and c_1 are the same as given in the case of 4.d.

In the case of 4.g:

$$\frac{y}{b} \leq 1;$$

$$\frac{x}{a}+\frac{z}{c} \leq 1;$$

The solution is precipitate free, if:

$$b_1 \leq b \quad \text{and} \quad \frac{a_1}{a}+\frac{c_1}{c} \leq 1.$$

In the case of 4.h:

$$\frac{x}{a}+\frac{z}{d} \leq 1;$$

$$\frac{y}{b} \leq 1;$$

$$\frac{x}{a}+\frac{y}{b}\left(1-\frac{d}{c}\right)+\frac{z}{c} \leq 1.$$

The conditions regarding values a_1, b_1 and c_1 are the same as given in case of 4.d.

In the case of 4.i:

$$\frac{x}{a}+\frac{y}{b}\left(1-\frac{e}{a}\right)+\frac{e}{a}\cdot\frac{z}{d} \leq 1;$$

$$\frac{y}{b} \leq 1;$$

$$\frac{x}{a}+\frac{y}{b}\left(1-\frac{d}{c}\right)+\frac{z}{c} \leq 1.$$

The conditions regarding values a_1, b_1 and c_1 are the same as given in the case of 4.d.

In the case of 4.j:

$$\frac{x}{a}+\frac{y}{b}\left(1-\frac{e}{a}\right)+\frac{z}{c}\cdot\frac{e}{a} \leq 1;$$

$$\frac{y}{b} \leq 1;$$

$$\frac{x}{a}+\frac{z}{c} \leq 1$$

The conditions regarding values a_1, b_1 and c_1 are the same as given in the case of 4.d.

In the case of 4.k:

$$\frac{x}{a}+\frac{z}{c}\leq 1;$$

$$\frac{y}{b}+\frac{z}{c}\leq 1;$$

The solution is precipitate free, if:

$$\frac{a_1}{a}+\frac{c_1}{c}\leq 1 \quad \text{and} \quad \frac{b_1}{b}+\frac{c_1}{c}\leq 1.$$

In the case of 4.l:

$$\frac{x}{a}+\frac{y}{b}+\frac{z}{c}\leq 1;$$

The solution remains precipitate free, if:

$$\frac{a_1}{a}+\frac{b_1}{b}+\frac{c_1}{c}\leq 1$$

In the case of 4.m:

$$\frac{x}{a}+\frac{y}{b}\leq 1;$$

$$\frac{x}{a}+\frac{y}{b}\left(1-\frac{d}{c}\right)+\frac{z}{c}\leq 1.$$

The solution remains precipitate free, if:

$$\frac{a_1}{a}+\frac{b_1}{b}\leq 1;$$

$$\frac{a_1}{a}+\frac{b_1}{b}\left(1-\frac{d}{c}\right)+\frac{c_1}{c}\leq 1$$

ACKNOWLEDGEMENT

The authors are indebted to Miss J. Markos for her help in the solution of mathematical problems.

REFERENCES

1. Mortvedt, J. J. et al.: Micronutrients in Agriculture. Madison, Wisa, USA. Soil Sci. Soc. of America. 1972. a.: pp. 450., b.: pp. 464.
2. Mortvedt, J. J.: Proc. Nat. Fert. Solutions Assoc. Round-Up. 23. *1973.*
3. Achorn, F. P.: Proc. Nat. Fert. Solutions Assoc. Round-Up. 5. *1969.*
4. Hignett, T. P.: Proc. 16th Ann. Fert. Conf. Pac. North-West, Salt Lake City. 1965. pp. 5.
5. Chesnin, L.: Fert. Solutions *13* (1), 23 (1969).
6. Mortvedt, J. J. and Giordano, P. M.: Fert. Solutions *14* (4), 22 (1970).
7. Slack, A. V., Potts, J. M. and Shaffer, H. B.: J. Agr. Food Chem. *13*, 165 (1965).
8. Production of Liquid Fertilizers from Liquid Base 11=37=0. Alabama, National Fertilizer Development Center, Muscle Shoals, 1967.
9. Nabiev, M. N.: Uzb. Khim. Zh. *13* (2), 12 (1969).
10. Forbes, M. R.: Fert. Solutions *18* (6), 98 (1974).

11. Formaini, R. E.: Proc. Fert. Ind. Round Table, Wash. D. C. *18*, 135 (1968).
12. Young, R. D.: Farm. Chem. *132* (8), 52 (1969).
13. Slack, A. V.: Fert. Soc. Proc. *133*, 34 (1973).
14. Farm. Chem. *130* (2), 68 (1967).
15. van Wazer, J. R.: Industrial Chemistry and Technology of Phosphorous and Phosphorous Compounds, A. Encyclopedia of Chemical Technology, 2nd Ed. Interscience Publ. New York. 1969. pp. 255.
16. Káldi, P., Tamás, F. and Pál, L.: Vizes oldatok fázisegyensúlyai (The Phase Equilibrium in Aqueous Solutions). Tankönyvkiadó. Budapest. 1976.

РЕЗЮМЕ

В ходе работы, направленной на определение растворимости в 10-34-0-ом растворе полифосфата аммиака семи наиболее важных микроэлементов — Fe(III), B, Zn, Cu, Mn, Co, Mo —, авторами был разработан такой метод, с помощью которого могут быть заданы соотношения концентраций металлов в растворе полифосфата аммиака, содержащего в себе три микроэлемента, при неизвестном составе и неизвестной константе устойчивости образующихся в растворе комплексов. Данный метод может быть математически распространён и на растворы удобрений, содержащие более трёх элементов.

HUNGARIAN JOURNAL
OF INDUSTRIAL CHEMISTRY
VESZPRÉM
Vol. 6. pp. 275–282 (1978)

RELIABILITY ANALYSIS OF CHEMICAL PLANTS BY MEANS OF MARKOW PROCESSES

G. GRUHN, W. NEUMANN and H. HEINING

(Technical University "Carl Schorlemmer"
Leuna-Merseburg, GDR)

Received: April 12, 1978.

An alternative for using BOOLEAN models for reliability analysis of chemical plants is the application of MARKOW models. Therefore a programme system for reliability analysis of complex plants was developed which allows the application of BOOLEAN or MARKOW models.

By means of this programme system several chemical plants were investigated, among them a distillation plant engaged in a petrochemical work. For this example the method and the numerical results are presented.

Various possibilities for raising the reliability of chemical plants are used in practice. These are organizational as well as technological measures which are derived from corresponding qualitative and quantitative analyses. In this field is it most useful to combine both analysis methods for using their different advantages and possibilities of application in conformity with various industrial demands. The reasons for these various industrial demands are

- the differences in the technological structure and behaviour of the plants being investigated, especially their different complexity,
- the differences in information concerning the reliability behaviour of applied equipment,
- and the differences in knowledge which is necessary for the various stages in the planning of chemical plants.

Quantitative methods gain primary importance for reliability analyses, because they are necessary for the solution of such problems as the synthesis of optimal plant structures, the estimation of technical and economic risks, and the planning of optimal maintenance strategies, etc.

1. Characterization of Markow models

The calculation of the reliability behaviour of technical objects is based on the mathematical theory of stochastic processes caused by the accidental nature of equipment failures. The modellization of the reliability behaviour can on principle be carried out by means of binary or nonbinary models. Binary models, which at present are mainly used, allow the determination

of two states, which are as a rule the state of unrestrained function and the state of total failure. All states between these boundary states are ascribed to them. This simplification is possible for the reliability description of elements, the more so as other states cannot be exactly distinguished from one another. The restraints of BOOLEAN models are more disadvantageous for the description of the reliability behaviour of complex systems. For instance, BOOLEAN models are not suitable to consider statistic dependences in the case of hot redundance (power dependence of reliability). The calculation of reliability data of special redundance groups (subsystems) in considering renewal processes is also impossible, because different function states have to be regarded simoultaneously, as a state of function, state of failure, state of reserve, and a state of repair.

The use of BOOLEAN models is also problematical for the reliability analysis of parallel systems with a split capacity. A reduction of their behaviour to only two states would be an unjustified simplification.

An alternative is the application of MARKOW models using failure rates and maintenance rates as primary dates. The limitation of the number of system states depends on technological aspects and on the capacity of the computers which are available.

Properties of the MARKOW model are:

(1) Each possible state is of accidental nature. The quantity Z of all states is an accidental process $\zeta[Z_j(t),\ t \in T]$. For each state the future behaviour is independent of the past (MARKOW property).

(2) The conditioned probability for an event in the time interval $[t,\ t+\mathrm{d}t]$ is given by:

$$p_{ji}(t+\mathrm{d}t,\ t) = P(Z(t+\mathrm{d}t) = Z_j / Z(t) = Z_i) \tag{1}$$

and by this equation the change-over rate:

$$a_{ji}(t) = \frac{p_{ji}(t+\mathrm{d}t,\ t)}{\mathrm{d}t} \tag{2}$$

In this way the failure rates and renewal rates, obtained by the primary dates on the failure behaviour, can be easily used for quantitative analysis in connection with distribution functions.

(3) The occurrence probabilities of the different states $p_i(t=0)$ must be known. They characterize in each case the starting points of the failure process.

(4) The probability for the occurrence of two events within the time interval $[t,\ t+\mathrm{d}t]$ is zero.

The state probability for the time $t+\mathrm{d}t$ in relation to the state probability for the time t is then given by:

$$p_j(t+\mathrm{d}t) = p_j(t)\Big[1 - \sum_{\substack{\forall \\ i \\ i \neq j}} a_{ij}(t)\,\mathrm{d}t\Big] + \sum_{\substack{\forall \\ i \\ i \neq j}} p_i(t) a_{ji}(t)\,\mathrm{d}t \tag{3}$$

$$p_j(t+\mathrm{d}t) = p_j(t) - p_j(t) \sum_{\substack{\forall \\ i \\ i \neq j}} a_{ij}(t)\,\mathrm{d}t + \sum_{\substack{\forall \\ i \\ i \neq j}} p_i(t) a_{ji}(t)\,\mathrm{d}t$$

$$p_j(t+\mathrm{d}t) - p_j(t) = -p_j(t) \sum_{\substack{\forall \\ i \\ i \neq j}} a_{ij}(t)\,\mathrm{d}t + \sum_{\substack{\forall \\ i \\ i \neq j}} p_i(t) a_{ji}(t)\,\mathrm{d}t \tag{4}$$

By using:

$$a_{ii}(t) = -\sum_{\substack{\forall \\ i}} a_{ij}(t) \qquad i \neq j \tag{5}$$

the sum of the state probabilities (in connection with the start conditions) becomes one, and therefore:

$$p_j(t+\mathrm{d}t) - p_j(t) = p_j(t) a_{ii}(t)\,\mathrm{d}t + \sum_{\substack{\forall \\ i \\ i \neq j}} p_i(t) a_{ji}(t)\,\mathrm{d}t$$

and:

$$\frac{p_j(t+\mathrm{d}t) - p_j(t)}{\mathrm{d}t} = \sum_{\substack{\forall \\ i}} a_{ji}(t) p_i(t) \tag{6}$$

With $\mathrm{d}t \to 0$ the mathematical model is given by a system of ordinary differential equations of 1. order with a dimension corresponding to the number of function states.

Because [according to the property of the BOOLE model noted under (3)] the probabilities of the start states must be known, an initial value problem is given by:

$$\dot{p}(t) = A(t) p(t)$$
$$p(t=0) = \{p_i\} \tag{7}$$

which can be solved without difficulties numerically, and in some special cases also analytically.

2. Reliability Analysis of a Destillation System

By means of BOOLEAN models and MARKOW models a system for the destillative separation of a multicomponent mixture was investigated in order to determine the distribution function of the survival probability. This investigation is a part of a more complex reliability analysis. The technological scheme of this system is shown in *Fig 1.* It consists of 2 distillation columns, heat exchangers and pumps. The heat exchanger E 5a is in cold redundancy to the heat exchanger E 5, but also usable in form of glide redundancy for the heat exchangers E 4 and E 6.

Therefore, the heat exchanger system (E 4, E 5, E 5a, E 6) has 10 possible function states as given in *Table 1.* The states Z_1 to Z_4 are states of functionality, the states Z_5 to Z_{10} are failure states. This relatively high number of states requires an analysis of the reliability behaviour by means of MARKOW processes.

The column C 1, the heat exchangers E 1, E 2, E 3, the tank T 1 and the pumps P 1, P 2, P 3, form a series system (in the sense of reliability logic), which can be analyzed without difficulties in the case of statistical independencies of these elements. *(Fig. 2.)*

Therefore, the main subject of the reliability analysis is the investigation of the heat exchanger system (E 4, E 5, E 5a, E 6) by means of MARKOW processes.

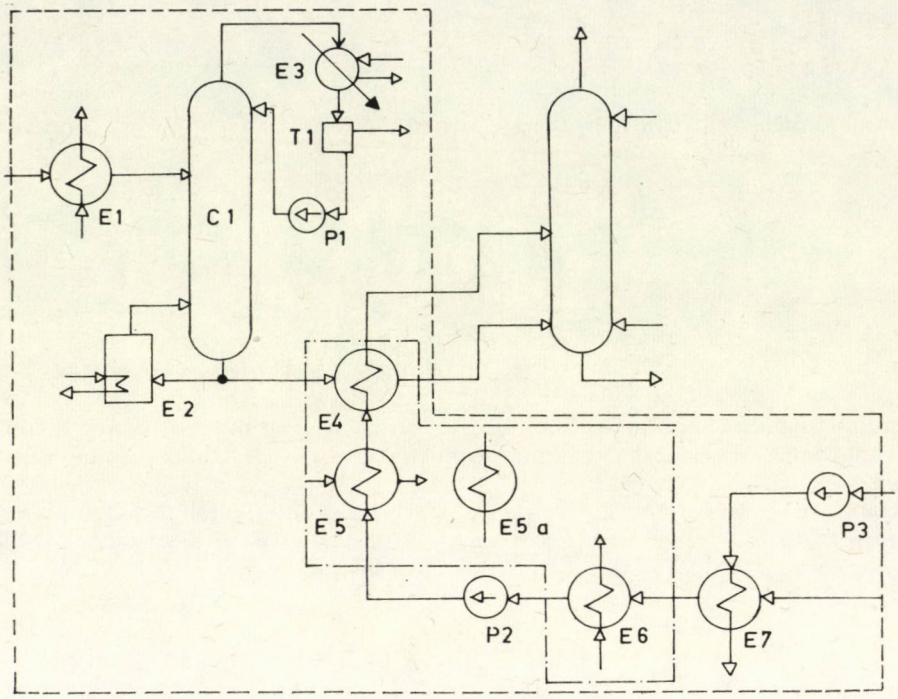

Fig. 1
Technological scheme of the separation system

Table 1.

State scheme of the heat exchanger system

State number	Z_1	Z_2	Z_3	Z_4	Z_5	Z_6	Z_7	Z_8	Z_9	Z_{10}
Element Broken down	—	*E*4	*E*5	*E*6	*E*4 *E*5	*E*4 *E*5*a*	*E*4 *E*6	*E*5 *E*5*a*	*E*5 *E*6	*E*6 *E*5*a*

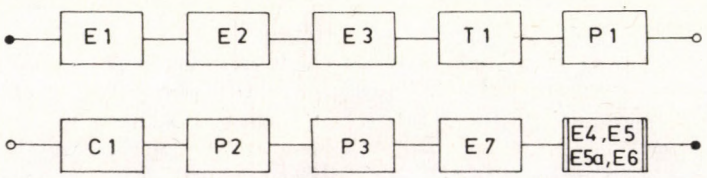

Fig. 2
Aggregated reliability structure of the separation system

Event sequences for systems with many different states are usefully demonstrated with state graphs, especially for deriving the change-over rates. For the heat exchanger system, this state graph is given in *Fig. 3*. The events (failures of the elements) are noted at the arcs of the graph. Considering

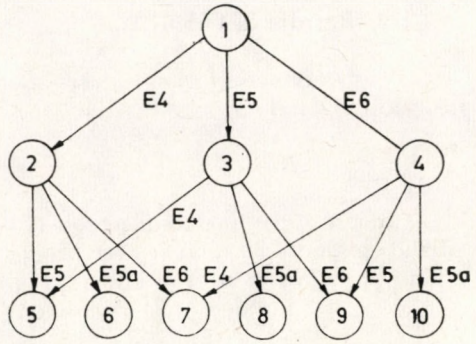

Fig. 3
State graph of the heat exchanger system (regarding the failure behaviour)

these comments, the following differential equation system is given for the heat exchanger system:

$$\frac{dp_j(t)}{dt} = \sum_{i=1}^{10} a_{ji}(t)p_i(t) \qquad \begin{array}{l} j,\ i=1(1)10 \\ p_1(t=0)=1.0 \\ p_i(t=0)=0 \quad \forall\, i \neq 1 \end{array} \tag{8}$$

By simplifying the problem, the matrix $A^*=\{a_{ji}\}$ can be divided into submatrices, because only the state probabilities of the states Z_1 to Z_4 are of interest for the determination of the survival probability. The special structure of the differential equation system allows such a decoupling.

$$A^* = \left(\begin{array}{c|c} B & C \\ \hline A & D \end{array}\right) \tag{9}$$

The matrix A contains the charge-over rates for the failure states of the system, and the matrix B encloses the charge-over rates between function states. The matrices C and D are zero matrices.

$$B = \begin{pmatrix} -(a_{W4}+a_{W5}+a_{W6}) & 0 & 0 & 0 \\ a_{W4} & -(a_{W5}+a_{W5a}+a_{W6}) & 0 & 0 \\ a_{W5} & 0 & -(a_{W4}+a_{W5a}+a_{W6}) & 0 \\ a_{W6} & 0 & 0 & -(a_{W5}+a_{W5a}+a_{W4}) \end{pmatrix}$$

$$A = \begin{pmatrix} 0 & a_{W5} & a_{W4} & 0 \\ 0 & a_{W5a} & 0 & 0 \\ 0 & a_{W6} & 0 & a_{W4} \\ 0 & 0 & a_{W5a} & 0 \\ 0 & 0 & a_{W6} & a_{W5} \\ 0 & 0 & 0 & a_{W5a} \end{pmatrix}$$

For determining the survival probability of the heat exchanger system it is therefore sufficient to use the reduced differential equation system:

$$\dot{p}_B = Bp_B. \tag{10}$$

The 4 function states which are of interest are then described by:

$$R_{TS}(t) = \sum_{i=1}^{4} p_i(t) \tag{11}$$

3. Results of Calculation

For describing the time dependence of the survival probability of the elements the WEIBULL function is used:

$$R(t) = e^{-\lambda t^{\alpha}} \tag{11}$$

The parameters α and λ were determined on the basis of primary dates for the failure behaviour of the elements by a computer programme [3]. The results are given in *Table 2*. The calculation of the survival probability of the investigated separation system was carried out by means of a computer programme demonstrated in *Fig. 4* in its simplified structure.

Table 2.

Parameters of the WIBULL function for the survival probability of the elements

Element	λ in d^{-1}	α
*C*1	$0.926 \cdot 10^{-4}$	1.2
*E*1	$0.128 \cdot 10^{-4}$	1.69
*E*2	$0.137 \cdot 10^{-4}$	1.69
*E*3	$0.116 \cdot 10^{-3}$	1.44
*E*4	$0.185 \cdot 10^{-4}$	1.91
*E*5/*E*5*a*	$0.159 \cdot 10^{-4}$	1.85
*E*6	$0.185 \cdot 10^{-4}$	1.91
*E*7	$0.12 \cdot 10^{-3}$	1.37
*P*1	$0.56 \cdot 10^{-4}$	1.21
*P*2/*P*3	$0.25 \cdot 10^{-4}$	1.43
*T*7	$0.235 \cdot 10^{-5}$	1.0

The survival probability and the availability of subsystems (redundance groups) respectively can be determined by special subprogrammes. By the aggregation of these subsystems, a simplified structure of the superordinate systems is obtained and analized in the following step. This procedure can be repeated. The corresponding programme system was worked out for the R 21 computer in Fortran IV. The structure of this programme system permits the application of different reliability models.

This programme system was used for determining the time dependence of the survival probability of the investigated separation system. The quantitative results are given in *Table 3*. The values of the survival probability are approximatable by the function:

$$R(t) = e^{-\left(\frac{t}{175}\right)^{1.59}} \tag{12}$$

The analysis of these results showed the primary influence of the elements *E* 3, *E* 7 and of the subsystems (*E* 4, *E* 5, *E* 5*a*, *E* 6) caused by the polymerization of the products in these elements.

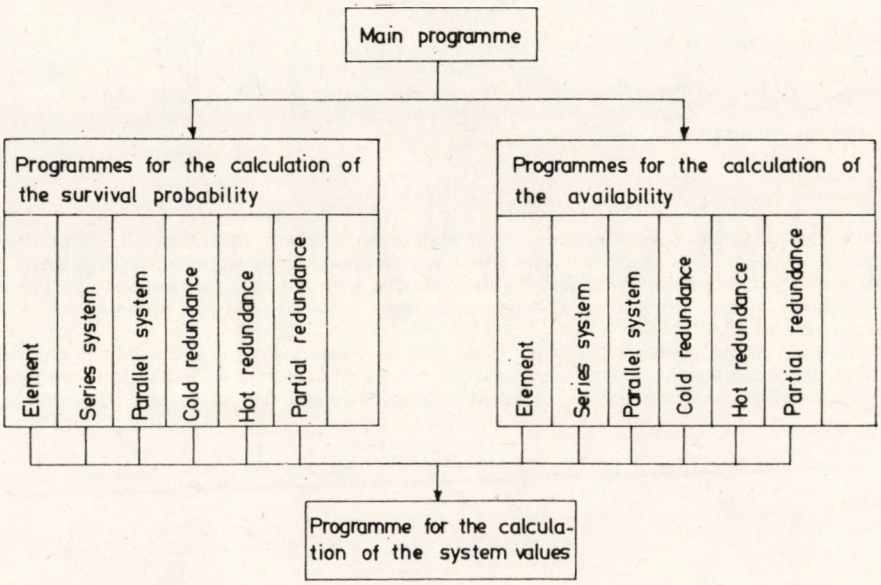

Fig. 4
Simplified structure of the programme system for reliability analyses of technological systems

Table 3.

Time dependence of the survival probability of the investigated system

t in d	40	80	120	160	200
$R(t)$	0.92339	0.79499	0.63547	0.46494	0.30837

SYMBOLS

A, A^*, B, C, D	change-over matrices
a_{ji}	change-over rate
i, j	state indices
p	probability
p_i, p_j	state probability
p_{ji}	change-over probability (from state Z_i to state Z_j)
$R(t)$	survival probability
t	time
Z	state
α	shape parameter of the WEIBULL function
λ	parameter of the WEIBULL function
λ_{ji}	failure rate
μ_{ji}	renewal rate

REFERENCES

1. Reinschke, K.: Zuverlässigkeit von Systemen, Bd. I, VEB Verlag Technik, Berlin 1973.
2. Rosanow, H. A.: Stochastische Prozesse, Akademie Verlag, Berlin 1975.
3. Ermittlung von Zuverlässigkeitsgrößen per EDV, Standardisierung und Qualität, 22 (1972) 2, S. 82—85.

РЕЗЮМЕ

Одной из возможностей исследования надёжности химических предприятий, выполняемого с помощью модели Boolean -а, может послужить применение модели МАРКОВА. С этой целью, в интересах выполнения анализа надёжности комплексных химических предприятий, была создана система программ, которая открывает возможности для применения моделей Booelan -а или МАРКОВА.

С помощью разработанной системы программ было исследовано несколько предприятий, так среди них и цех возгонки петрохимического завода. В статье с помощью данного примера показан способ применения данного метода, а также полученные расчётные результаты.

HUNGARIAN JOURNAL
OF INDUSTRIAL CHEMISTRY
VESZPRÉM
Vol. 6. pp. 283–292 (1978)

THE NATURE OF THE REACTION OF PROPAN-2-OL ON A Zn:Cr:Fe CATALYST

M. SUBRAHMANYAM and J. C. KURIACOSE

(Department of Chemistry
Indian Institute of Technology Madras 600036, India)

Received: April 17, 1978.

Propan-2-ol undergoes normal dehydrogenation and oxidative dehydrogenation on a Zn:Cr:Fe catalyst.

At low partial pressures, oxygen has a beneficial effect on the dehydrogenation activity of the catalyst while at high partial pressures complete oxidation of the alcohol takes place. In addition to the surface reaction, there is also a homogeneous gas phase reaction giving rise to the same product acetone. The results suggest that different forms of oxygen are available for the mild oxidation of propan-2-ol to acetone.

Introduction

Since the early 1960s there has been considerable interest in the oxidative dehydrogenation and ammoxidation of monoolefins to diolefins, aldehydes and nitriles [1–3]. For practical reasons most work to date has been carried out with oxygen added to the feed. Bismuth molybdate catalysts are able to oxidize alkenes selectively even in the absence of molecular oxygen [4, 5] though the high selectivity is maintained only for a shorter time when oxygen is absent. A few studies on the catalytic activity and selectivity of various oxidation catalysts for the decomposition of propan-2-ol have been reported recently [6, 7]. To obtain a high selectivity, the oxidation level of the catalyst must be maintained. This may be achieved by incorporating oxygen in the feed. RENNARD and KEHL [8] reported that a Zn:Cr:Fe catalyst system is a good oxidative dehydrogenation catalyst for butene. The present study is an attempt to understand the role of various oxygen species for the selective oxidation of propan-2-ol to acetone on a catalyst containing Zn, Cr and Fe.

Experimental

The reactions were studied at atmospheric pressure using a flow type reactor, mercury being used to displace the reactant into the reactor [9]. All the chemicals were Analar grade BDH reagents and were used as received.

Because simple precipitation methods often produce ill defined catalysts, the Zn:Cr:Fe catalyst was prepared by the slurry method described by BATIST [10]. The following chemicals were used as starting materials. For iron and chromium, the respective nitrates were used, while ZnO was used in the case of zinc. $Fe(OH)_3$ and $Cr(OH)_3$ were obtained by precipitation from nitrate solutions by the slow addition of Analar ammonia (BHD) keeping the system stirred. A zinc oxide paste made with distilled water was added to the mixture of freshly precipitated, thoroughly washed $Fe(OH)_3$ and $Cr(OH)_3$ and heated for 10 hours on a water bath keeping the total mass stirred vigorously. After reaction the solids were filtered, dried overnight at 110 °C and calcined at 550 °C for 5 hr.

Propan-2-ol and acetone (BDH., AR chemicals) found to be chromatographically pure were used without further purification. Research grade oxygen, hydrogen and nitrogen were used directly from cylinders after passing through gas-towers containing sodalime; fused calcium chloride and concentrated sulphuric acid for the removal of CO_2 and moisture respectively. N_2 was found to be inert on the catalyst by comparing its behaviour with He. Carbon dioxide from the cylinder was passed only through fused calcium chloride and conc. H_2SO_4 before use. Duplicate runs were made at each set of conditions to ensure reproducibility.

Activation was ensured by passing dry air over the catalyst maintained at 450 °C for 20 minutes. The liquid products were analyzed by gas chromatography using a carbowax column at 75 °C and the gaseous products were analyzed using an Orsat's apparatus [9].

Results and Discussion

Catalysts of various compositions of zinc, chromium and iron were prepared and tested for the decomposition of propan-2-ol. Both dehydrogenation and dehydration take place on all catalysts except the one of composition 1:1:1 (atom ratio) on which only dehydrogenation takes place. The experimental results considered here, were all obtained on a 1:1:1 catalyst. The activity of a sample of catalyst for the dehydrogenation of propan-2-ol decreases with time and finally reaches a very low stable value. The decrease in activity with time is shown in *Fig. 1*. When the aged catalyst was regenerated the activity was found to be slightly less than that of a fresh catalyst. After about five runs the activity of the regenerated catalyst was found to have stabilised. Even a stabilised catalyst loses its activity with the time of reaction as shown in *Fig. 1*. The catalyst can be regenerated any number of times indicating that the deactivation is reversible and oxidation restores activity. During regeneration qualitative tests of the exit gas showed that there was no CO_2, proving that there is no coke formation on the catalyst. Acetone and water were found to be the main products of reaction. The gaseous products do not contain propylene, showing that the water formed could only have been due to oxidative dehydrogenation of the alcohol. The gaseous product is hydrogen from the normal dehydrogenation of the alcohol. The alcohol undergoes both normal dehydrogenation and oxidative dehydrogenation, up to about an hour of the duration of the run. Subsequently only normal dehydrogenation takes place as revealed by the absence of water in the liquid products.

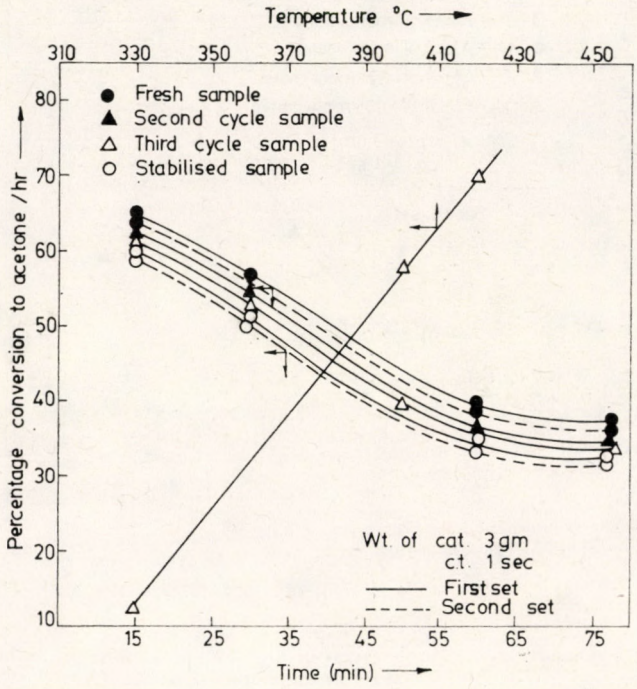

Fig. 1
Effect of a) time at 400 °C and b) temperature on conversion of propan-2-ol

The mechanism in the initial stages appears to be similar to that suggested by MARS and VAN KREVELEN [11] with an initial reduction of the catalyst by the alcohol.

Use of various mole ratios of oxygen and alcohol *(Fig. 2)* leads to a considerable enhancement in the formation of acetone, with a maximum for a mole ratio of oxygen to alcohol of 0.2 at 400 °C. The products are acetone, water and carbon dioxide. For a partial pressure of oxygen of 0.2, the formation of acetone is a maximum at 410 °C *(Fig. 2)*. The variation of the formation of acetone with temperature for various oxygen/alcohol mole ratios is represented in *Fig. 3*. The results show that the oxygen content in the feed and the temperature must be an optimum to obtain the maximum amount of acetone.

The oxygen in the feed can generally play a dual role in the reaction, viz. a) maintain the active form of the catalyst, and b) prevent any coke formation. The latter role appears to be unimportant since there is no evidence for coke formation on the catalyst in the absence of oxygen. The oxidizing species in the system during oxidation may be the oxide ions of the catalyst or adsorbed oxygen. In addition to the heterogeneous reaction there could be a homogeneous reaction with oxygen. If the oxygen from the catalyst, adsorbed or chemically combined, is participating in the reaction, gas phase oxygen may replace the adsorbed oxygen or replenish the anion-vacancies created by reduction of the catalyst surface during the reaction.

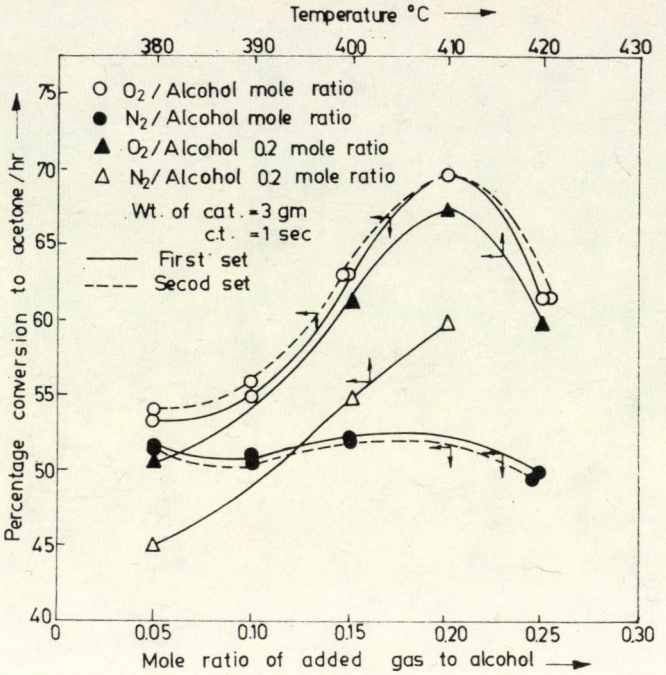

Fig. 2
Effect of a) the variation in the mole ratio of O_2/alcohol at 400 °C and b) temperature on conversion of propan-2-ol

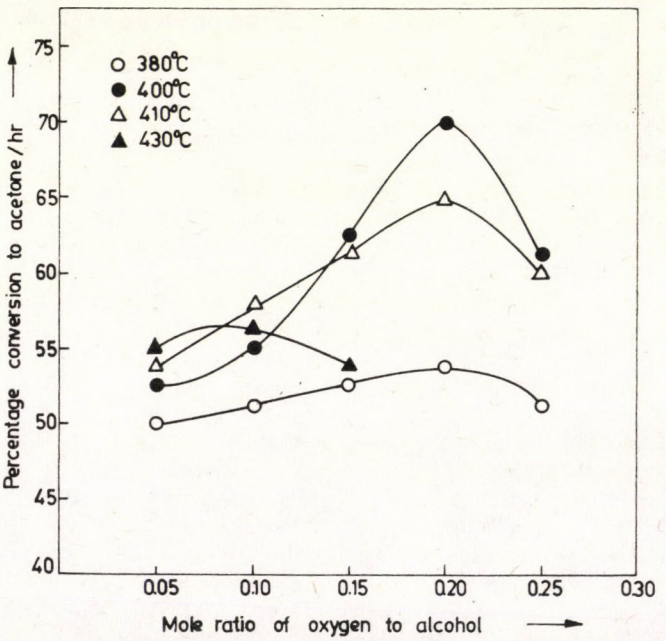

Fig. 3
Effect of temperature on conversion of propan-2-ol with the variation in the mole ratio of O_2/alcohol

The amount of acetone decreases with time even when there is oxygen in the feed *(Fig. 4)*. This decrease in activity may be due to i) the progressive reduction of the catalyst and the inability of the oxygen to oxidize simultaneously the reduced form, or (ii) due to inhibition of the reaction by the accumulation of products.

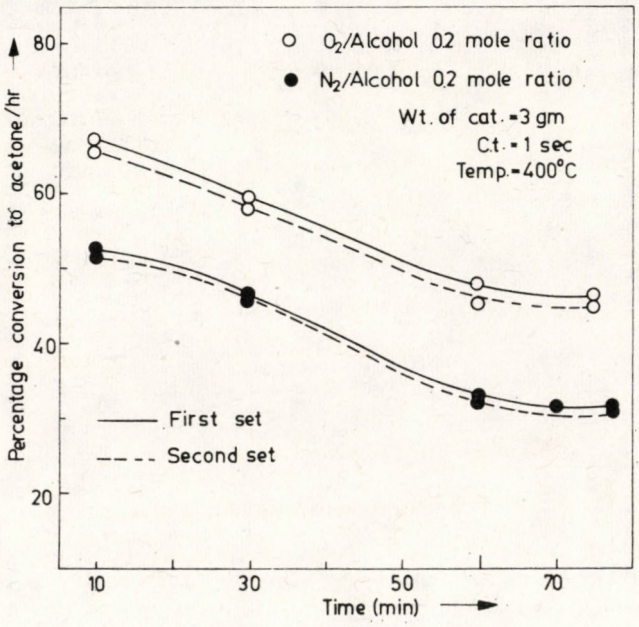

Fig. 4
Effect of time on conversion of propan-2-ol

The catalytic activity of the catalyst pretreated with CO_2 as well as the oxidation of alcohol in the presence of CO_2 *(Fig. 5)* have shown that there is no change in activity. So, it can be said that CO_2 is not an inhibitor causing the decrease in dehydrogenation activity with the time of reaction.

The reaction of secondary alcohols are particularly sensitive to retardation by water. Here, the presence of water during oxidation of the alcohol has caused a small decrease in the formation of acetone *(Fig. 5)*.

When propan-2-ol is fed along with oxygen, carbon dioxide may be formed directly by combustion of alcohol (parallel) or by oxidation of acetone (consecutive) or by both paths (parallel and consecutive).

$$>\mathrm{CHOH} \begin{cases} \xrightarrow[(0)]{\text{i}} >\mathrm{C{=}O} + \mathrm{H_2O} \\ \xrightarrow[(0)]{\text{iii}} \mathrm{CO} + \mathrm{CO_2} + \mathrm{H_2O} \end{cases} \qquad \text{ii} \downarrow (0) \qquad (1)$$

In the case of most catalysts with a high selectivity the products of complete oxidation are largely formed through sequential oxidation of the target product obtained by partial oxidation [12].

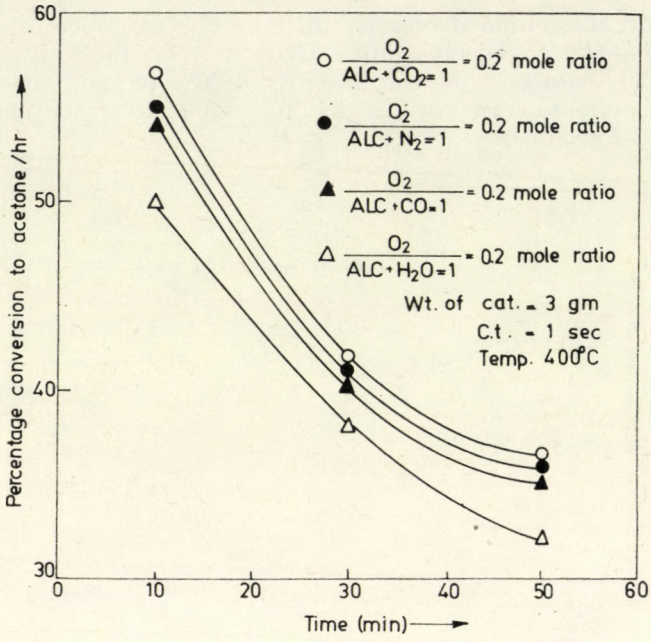

Fig. 5
Effect of products on the reaction

Many catalytic oxidation processes considered recently as purely heterogeneous appear to proceed by the simultaneous operation of both heterogeneous and homogeneous mechanisms [13].

In order to find out whether the carbon dioxide is formed in the gas phase reaction or on the catalyst surface, blank runs were performed in an empty glass reactor as well as one filled with glass chips of uniform size. First, various mole ratios of oxygen and alcohol were passed through the empty reactor. Acetone, water and carbon dioxide were formed. The conversion of alcohol to acetone was maximum (14 percent) at a mole ratio of oxygen to alcohol of 0.15 as shown in *Fig. 6*. The decomposition of the alcohol to acetone is negligible in the presence of N_2. So, there is a significant interaction of oxygen with alcohol in a homogeneous reaction. The formation of acetone was maximum at 420 °C and a further increase in temperature leads to the oxidation of acetone. In contrast to propan-2-ol, methanol undergoes no homogeneous reaction even after several hours at 460 °C if no catalyst is present [14].

The oxidation of acetone seems to be more sensitive to the partial pressure of oxygen than the oxidation of alcohol. This can be seen from the constant amount of alcohol converted in the two runs, i.e. i). at 0.15 mole ratio of oxygen-alcohol, and ii). at 0.18 mole ratio of oxygen-alcohol, while the acetone in the products is considerably reduced in the latter.

It is open to question whether the decomposition reaction

$$>CHOH + O \xrightarrow[\text{lattice}]{} >C{=}O + H_2O \qquad (2)$$

is an oxidative process or dehydrogenation with subsequent oxidation of

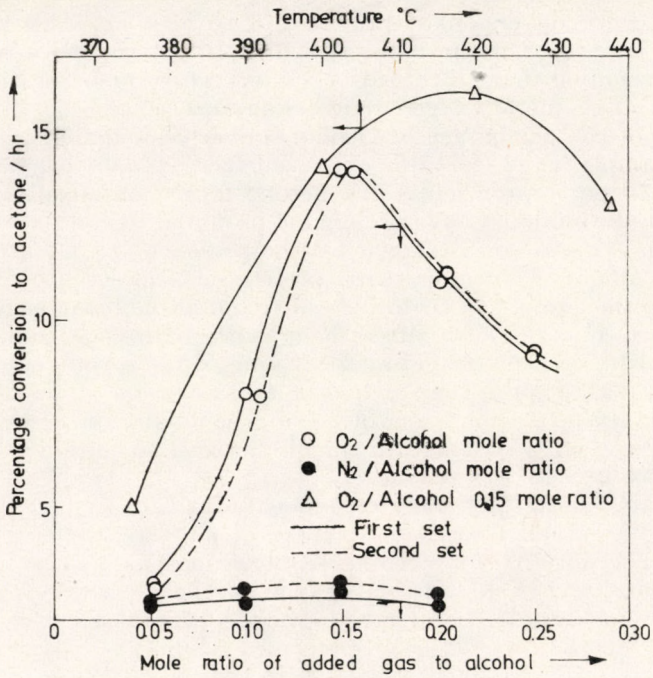

Fig. 6
Effect of a) the variation in the mole ratio of O_2/alcohol at 400 °C and b) temperature on the homogeneous conversion of propan-2-ol

hydrogen. It has been suggested that if there is any oxidative dehydrogenation of a hydrocarbon, hydrogen should be completely absent in the product. It is also required that hydrogen should not reduce these catalysts under these experimental conditions [3].

The catalyst, subjected to pretreatment by hydrogen at various periods of time, showed a decrease in catalytic activity for propan-2-ol decomposition *(Table 1)*. For the fresh sample, the initial catalytic activity corresponds

Table 1.

Decomposition of propan-2-ol on catalysts pretreated with hydrogen
Temp. 400 °C Contact time: 1 second
Times at which samples are collected: 0—5 minutes

Catalyst	Per cent acetone/hr	Per cent carbon dioxide/hr	Per cent alcohol converted/hr
Fresh sample	50	18	70
Sample reduced 20 minutes	60	—	63
Sample reduced 60 minutes	48	—	50
Sample reduced 180 minutes	40	—	40

to a 50 per cent conversion of propan-2-ol to acetone. This may involve the adsorbed oxygen. On the catalyst which is reduced with hydrogen for 20 minutes, assuming that all the adsorbed oxygen is removed, the activity is due only to active metal-oxygen oxidizer groups as can be surmised from a comparison of the percentage of alcohol converted and the yield of ketone. For a fresh sample which contains excess surface oxygen [15] the conversion of alcohol is 70 per cent whereas the ketone formation is only 50 per cent. 20 per cent of alcohol must have undergone profound oxidation by the loosely bound oxygen. This is so, as shown by the presence of CO_2 in the exit gas in the initial stages. The other three pretreated samples are free adsorbed oxygen and so the amount of acetone formed and alcohol converted are almost equal. Increase in time of pretreatment with hydrogen causes increased extent of the reduction corresponding to stripping off of several layers of oxygen from the solid with a consequent reduction in conversion of alcohol to ketone. Hence the catalyst oxygen is involved in the oxidation process. But the attainment of a steady activity with time indicates that pure dehydrogenation also takes place.

An aged catalyst, i.e. a catalyst reduced with alcohol was treated with steam for several hours. There was no gas evolved while treating the catalyst with steam. The activity for decomposition of propan-2-ol was checked on the treated catalyst. There was no change in the activity of the catalyst. It shows that the catalyst could not decompose steam, because if the steam could be decomposed, the oxygen so formed could be expected to oxidize the catalyst.

These observations lead to the conclusion that the decomposition and oxidation of alcohol is taking place in several ways as suggested below. The oxidation reaction may show a complex character due to the occurrence of numerous simultaneous, consecutive and parallel reactions as shown below.

$$\frac{1}{2}\,O_2 + {>}CHOH \rightarrow {>}C{=}O + H_2O \quad \text{(gas phase)} \tag{3}$$

$$4\,{>}CHOH + 6\,O_2 \rightarrow 3\,{>}C{=}O + 3\,CO_2 + 7\,H_2O \quad \text{(gas phase)} \tag{4}$$

$${>}CHOH \rightarrow {>}C{=}O + H_2 \quad \text{dehydrogenation (negligible amount)}$$

$$H_2 + (O)_{\text{lattice}} \rightarrow H_2O \tag{6}$$

$${>}CHOH + (O)_{\text{latttice}} \rightarrow {>}C{=}O + H_2O \tag{7}$$

$${>}CHOH \rightarrow {>}C{=}O + H_2 \quad \text{(surface)}$$

The amount of acetone formed when oxygen and alcohol are fed is always (even after one hour of the duration of run) greater than the amount formed when the alcohol is fed alone because of the parallel homogeneous reaction in the gas phase.

The qualitative test for carbon dioxide during the treatment of a fresh catalyst with CO showed that CO_2 is formed only in the initial stages i.e. up to about 5 minutes. This clearly shows that the Zn:Cr:Fe cannot oxidize CO with lattice oxygen at 400 °C. The initial formation of CO_2 must be due to oxygen adsorbed on the catalyst in the process of preparing and calcining the specimen in air. In contrast to CO treatment, hydrogen pretreatment over the catalyst gives a definite degree of reduction corresponding to stripping off of several layers of oxygen.

The present investigation supports the following conclusions. There are four types of oxygen available for the oxidation of propan-2-ol; a) excess surface oxygen which is used up in the first few minutes of the oxidation during the experiment, b) easily removable lattice oxygen which is available for about an hour of the duration of the experiment, c) non-removable oxygen which may be promoting the normal dehydrogenation, and d) gas phase oxygen for the homogeneous reaction. In the presence of oxygen in the feed it was found that there is always a greater formation of acetone than when there is no oxygen in the feed. This is because of the parallel gas phase homogeneous reaction. The decrease in the amount of acetone with time, even when there is oxygen in the feed is due to the reduction of the catalyst and the inability of the oxygen to simultaneously oxidize the reduced form.

REFERENCES

1. Sampson, R. J., Shooter, D.: Oxid. Comb. Rev. *1*, 223 (1965)
2. Voge, H. H., Adams, C. R.: Adv. Catal. *17*, 151 (1967)
3. Skarchenko, V. K.: Russ. Chem. Rev. *37*, 1 (1965)
4. Batist, Ph. A., Kapteijns, B. C., Schuit, G. C. A.: J. Catal. *7*, 33 (1967)
5. Peacock, J. M., Parker, P. C., Ashmore, P. G.: J. Catal. *15*, 398 (1969)
6. Daniel, C., Subrahmanyam, M., Kuriacose, J. C.: Indian J. Chem. *13*, 419 (1975)
7. Subrahmanyam, M., Kuriacose, J. C.: Indian J. Chem. *15A*, 586 (1977)
8. Rennard, R. J., Kehl, W. L.: J. Catal. *21*, 282 (1971)
9. Kuriacose, J. C., Daniel, C., Swaminathan, R.: Indian J. Chem. *7*, 367 (1969)
10. Batist, Ph. D., Der Kinderen, A. H. W. M.: J. Catal. *12*, 45 (1968)
11. Mars, P., Van Krevelen, D. W.: Chem. Eng. Sci. Suppl. *3*, 41 (1954)
12. Margolis, L. Ya.: Adv. Catal. *14*, 429 (1963)
13. Brown, D. M., Trimn, D. L.: Proc. R. Soc. London. Ser. A, *326*, 215 (1972)
14. mann, R. S., Hahn, K. W.: J. Catal. *15*, 329 (1969)
15. Subrahmanyam, M.: Ph. D. Thesis, I.I.T., Madras, India, 1976, p. 84.

РЕЗЮМЕ

На Zn:Cr:Fe-ом катализаторе Пропан-2-ол претерпевает нормальное и окислительное дегидрогенизирование.

Поскольку парциальное давление имеющегося в наличии кислорода весьма мало, то этот факт оказывает благоприятное действие на дегидрогенизирующую активность катализатора, ведь большое парциальное давление кислорода ведёт к полному окислению спирта. Помимо реакций, происходящих на поверхности катализатора, здесь имеют место и гомогенные газофазовые реакции, в результате которых образуются продукты типа ацетона. Результаты доказывают по-видимому факт того, что при слабом окислении пропан-2-ола в ацетон кислород присутствует в различных состояниях.

HUNGARIAN JOURNAL
OF INDUSTRIAL CHEMISTRY
VESZPRÉM
Vol. 6. pp. 293–300 (1978)

REACTIONS OF BENZYL ALCOHOL ON U-V IRRADIATED ZINC OXIDE

E. P. YESODHARAN, V. RAMAKRISHNAN and J. C. KURIACOSE

(Department of Chemistry
Indian Institute of Technology Madras 600036, India)

Received: April 17, 1978.

Under the influence of ultraviolet irradiation benzyl alcohol undergoes dehydrogenation on zinc oxide to give benzaldehyde, hydrogen peroxide and toluene. Oxygen in the adsorbed state as well as in solution is essential for the reaction which proceeds through free radicals generated at the zinc oxide surface. The rate of the reaction and the behaviour of various products depend on the nature of the solvent. A mechanism consistent with the findings is proposed.

Introduction

The mechanism of photocatalysed reactions of alcohols on an irradiated catalyst is not well understood. The photooxidation of secondary alcohols such as isopropyl alcohol [1, 2] and benzhydrol [3] in the presence of ZnO has been studied earlier, the products being identified as the corresponding ketone and H_2O_2. SCHWAB [4] attributed the photocatalytic effect of ZnO to its n-type semiconductivity. Illumination will promote electrons from the valence band to the conduction band which are subsequently taken up by the adsorbed oxygen to form O_2^-, the active species. The present paper reports some of the results of a study of the interaction of benzyl alcohol with zinc oxide under ultraviolet irradiation.

Experimental

The light source used in all the experiments is a Hanovia high pressure quartz mercury arc. Radiations above 3800 Å are not absorbed by ZnO as is revealed by its reflectance spectrum. The lamp provided with an aluminium foil shade to reflect light downwards is mounted horizontally above a mechanical shaker. The reaction vessel consists of a pyrex tube with an opening for introducing the solids and liquids and a small sidetube for bubbling gases. Through the outer jacket of the reactor, water at the desired temperature can be circulated. 0.35 gm of the catalyst and 30 ml of the liquid under investigation are taken in the reaction vessel which is then closed and clamped

to the platform of the mechanical shaker directly below the lamp and shaken throughout the experiments. Samples are removed through the side-tubes at various intervals and analysed.

The estimation of peroxide was carried out by iodometry [5, 6]. Benzaldehyde and toluene were determined by gas chromatography.

The ZnO sample used was supplied by MAY and BAKER (England). Benzyl alcohol and the solvents were purified by standard methods.

Results and Discussion

The products of the photocatalysed reaction of benzyl alcohol on ZnO are benzaldehyde, H_2O_2 and toluene. The yield increases with the increase in weight of the catalyst to reach a steady value. This may be because with an increase in weight of the catalyst, the amount of light absorbed also will increase until enough ZnO is present to spread completely and uniformly in the reaction vessel to absorb the maximum amount of light. Further addition of zinc oxide may increase only its depth and since light does not reach the interior of the catalyst bulk it is not effective. This is further confirmed by the observation that the bigger the reaction vessel, the higher the limiting amount of the catalyst. The reaction proceeds very slowly in a solution deoxygenated with N_2 as well as on ZnO pretreated with N_2 to remove adsorbed oxygen. Hence both dissolved and adsorbed oxygen are essential for the process.

Fig. 1 illustrates the influence of the concentration of the alcohol on the

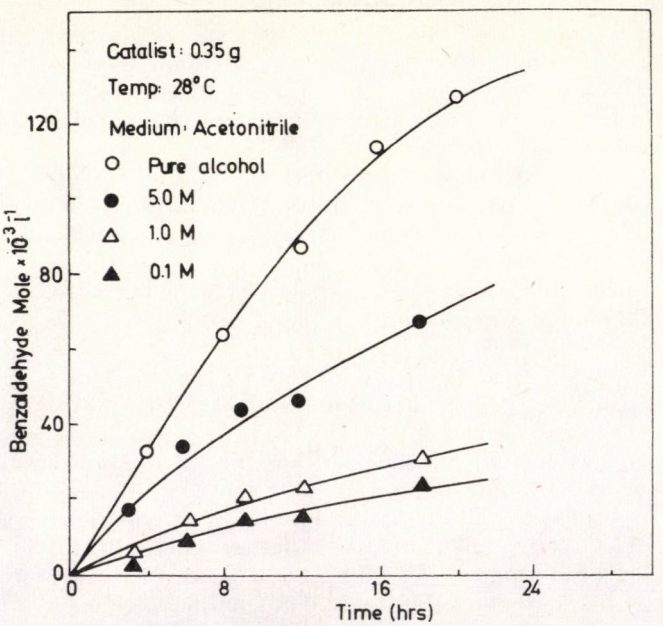

Fig. 1
Influence of concentration of benzyl alcohol on the formation of benzaldehyde

formation of benzaldehyde when acetonitrile is used as a solvent. In a non-polar solvent like cyclohexane, at lower concentrations of the alcohol, the amount of peroxide formed reaches a maximum, then decreases, again goes to a maximum and then decreases as the reaction time is increased *(Fig. 2)*.

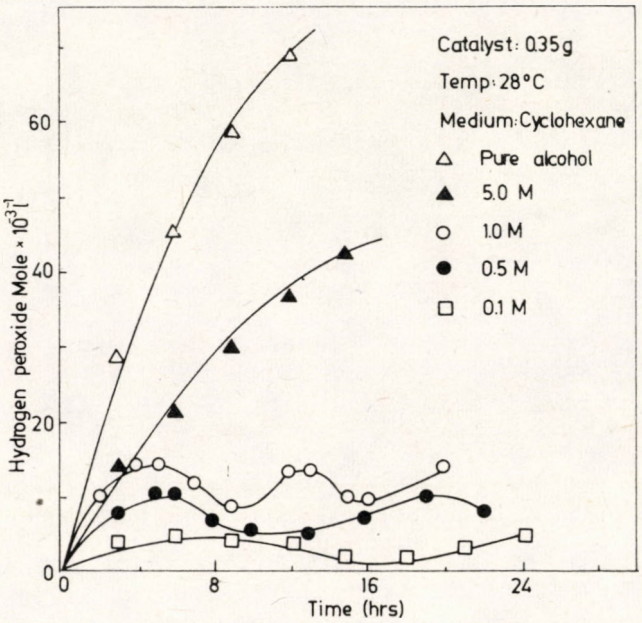

Fig. 2
Influence of concentration of benzyl alcohol on the formation of H_2O_2

This oscillation in the concentration of peroxide is observed in the case of all substrates undergoing dehydrogenation in cyclohexane suggesting this to be a process depending on the solvent and not on the substrate. The phenomenon is dealt with in detail elsewhere [7] and is hence not discussed here. The oscillation is observed only for peroxide, while the other two products, viz. benzaldehyde and toluene show a normal increase with an increase in time as in acetonitrile.

The reaction is comparatively slow in water. But in this case the concentration of toluene passes through a maximum *(Fig. 3)*. Further studies revealed that toluene itself, when irradiated with ZnO in aqueous suspension forms peroxide and phenol. The other product, possibly carbon dioxide, could not be detected since its concentration is very small. The rate of formation of toluene from benzyl alcohol, as well as the disappearance of toluene when it is taken in aqueous suspension of ZnO is shown in *Fig. 4*. The former decreases, while the latter increases with time of irradiation, resulting in a maximum at the point where the two become equal.

The reaction proceeds very slowly in water compared to acetonitrile and cyclohexane. This may be due to the fact that water itself, unlike the other

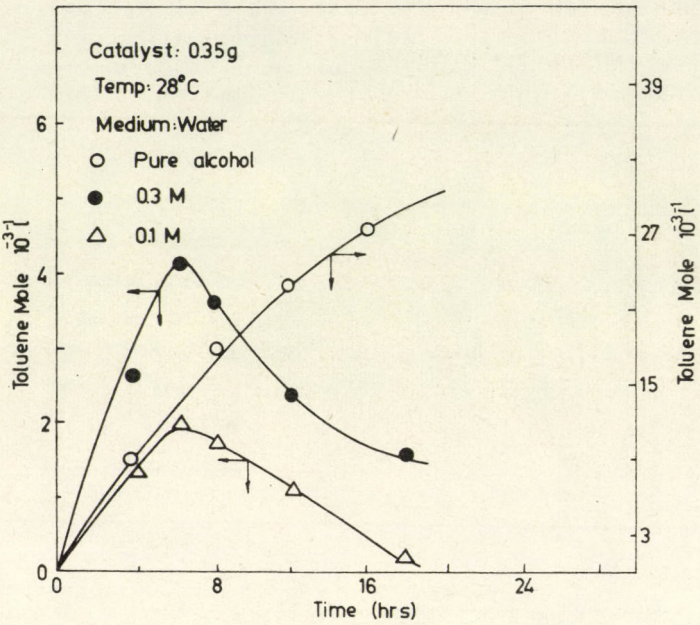

Fig. 3
Influence of concentration of benzyl alcohol on the formation of toluene

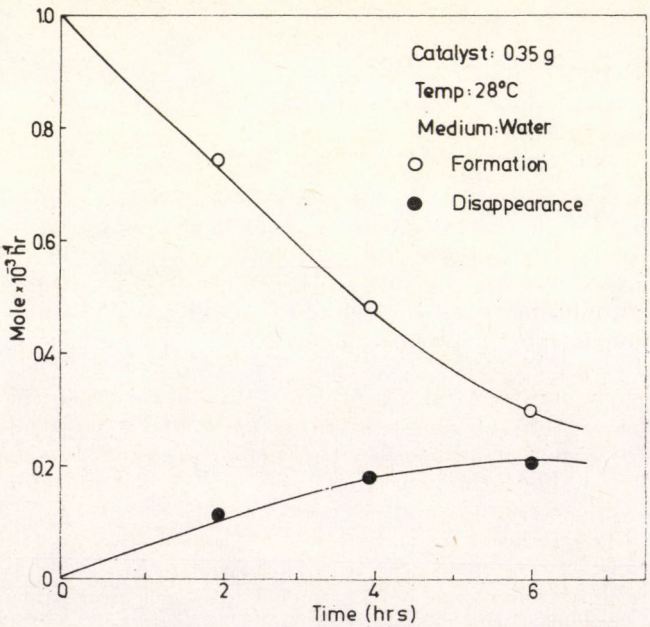

Fig. 4
Rate of formation and disappearance of toluene

solvents competes with the alcohol for the same adsorption sites [3], causing a lowering in the reactivity of the alcohol.

Benzaldehyde and toluene, initially added to the reaction mixture do not affect the rate. But H_2O_2 initially added decomposes readily in water to reach a minimum after which its concentration increases slowly *(Fig. 5)*.

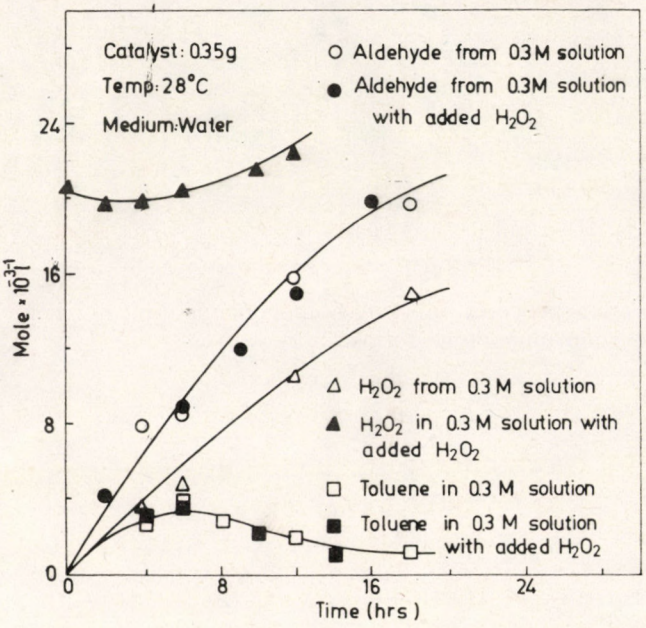

Fig. 5
Influence of initially added hydrogen peroxide on the formation of benzaldehyde and toluene from benzyl alcohol

These studies prove that H_2O_2 is not formed through any secondary reaction involving other products. In addition the decomposition of H_2O_2 in water is not due to its interaction with aldehyde or toluene in the system.

The formation of peroxide at irradiated zinc oxide surfaces involves the reduction of molecular oxygen [1]. This creates electron deficient sites on the catalyst at which the alcohol gets dehydrogenated. Thus the formation of peroxide on irradiated ZnO is an acceptor reaction while the decomposition can proceed both by donor and acceptor type mechanisms. Hence there is competition between the alcohol and peroxide for donor sites, which may be the reason for the suppression of the decomposition of peroxide in the presence of the alcohol.

Since the reaction does not proceed in the dark or on irradiation in the absence of oxygen both light and oxygen are essential for the process. Of the several species of oxygen such as O_2, O_2^-, O^-, O^{2-} etc. O_2^- is the most probable species under our experimental conditions. This suggestion is supported by Kuriacose and Markham [1] and also by Garten and Eppinger [8]. O_2^- is

formed by the transfer of electrons from the conduction band of ZnO to the adsorbed oxygen. The organic reactant gets adsorbed by transferring electrons to the electron deficient ZnO and subsequently reacts.

But, oxygen dissolved in the system is also necessary for a facile reaction. This is confirmed by the observation that the reaction is very slow in a solution deoxygenated with N_2. In the light of these observations a mechanism can be proposed for the reaction.

$$ZnO \xrightarrow{h\nu} (ZnO)^+ + e$$

$$O_2\,(ads) + e \longrightarrow O_2^-\,(ads)$$

$$C_6H_5CH_2OH\,(ads) + O_2^-\,(ads) \longrightarrow C_6H_5\dot{C}HOH\,(ads) + HO_2^-\,(ads)$$

$$C_6H_5\dot{C}HOH\,(ads) \longrightarrow C_6H_5CHO + \dot{H}\,(ads)$$

$$HO_2^-\,(ads) + \dot{H}\,(ads) \longrightarrow H_2O_2 + e$$

$$(ZnO)^+ + e \longrightarrow ZnO$$

The reaction that proceeds in the homogeneous phase with the assistance of dissolved oxygen may be as follows:

$$H^{\cdot} + O_2 \longrightarrow HO_2^{\cdot}$$

$$HO_2^{\cdot} + HO_2^{\cdot} \longrightarrow H_2O_2 + O_2$$

$$HO_2^{\cdot} + C_6H_5\dot{C}HOH \longrightarrow C_6H_5CHO + H_2O_2$$

or

$$C_6H_5\dot{C}HOH + O_2 \longrightarrow C_6H_5CH(OH)O_2^{\cdot}$$

$$C_6H_5CH(OH)O_2^{\cdot} + C_6H_5CH_2OH \longrightarrow C_6H_5CH(OH)O_2H + C_6H_5\dot{C}HOH$$

$$C_6H_5CH(OH)O_2H \longrightarrow C_6H_5CHO + H_2O_2$$

That the photocatalysed reaction of alcohols on ZnO proceed through free radicals has already been established by the use of free radical quenchers [9].

The study reveals that the photocatalysed reactions of benzylalcohol on zinc oxide proceed through free radicals generated at the surface of the catalyst. These radicals can subsequently propagate the reaction in the solution phase as well as on the surface of the catalyst. The function of light is to promote electrons from the valence band of ZnO to the conduction band and make them available for the adsorbed oxygen to form O_2^-, the active species.

ACKNOWLEDGEMENT

We are grateful to the National Science Foundation for financial assistance.

REFERENCES

1. Kuriacose, J. C. and Markham, M. C.: J. Catal. *1*, 498 (1962)
2. Fujita, Y. and Kwan, T.: Bull. Chem. Soc., Japan, *31*, 379 (1958)
3. Yesodharan, E. P., Ramakrishnan, V. and Kuriacose, J. C.: Proc. V. Ibero American Symp. on Catalysis, Lisbon, 1976 (in press)

4. Schwab, G. M.: Adv. Catal. *9*, 229 (1957)
5. Markham, M. C. and Laidler, K. J.: J. Phys. Chem. *57*, 363 (1953)
6. Chari, C. N. and Quereshi, M.: J. Indian Chem. Soc. *21*, 97 (1944)
7. Yesodharan, E. P., Ramakrishnan, V. and Kuriacose, J. C.: Indian J. Chem. (in press)
8. Garten, U. A. and Eppinger, K.: Solar Energy *5*, 77 (1961)
9. Yesodharan, E. P., Ramakrishnan, V. and Kuriacose, J. C.: Indian J. Chem. *15A*, 875 (1977)

РЕЗЮМЕ

Бензиловый спирт под действием ультрафиолетового света и в присутствии окиси цинка дегидрогенизируется, и при этом образуется бензальдегид, перекись водорода и толуол. С точки зрения хода реакции очень важно как количество адсорбированной, так и количество находящейся в растворе окиси цинка. Сама же реакция протекает через посредство свободного радикала, образующегося на поверхности окиси цинка, и который является как бы промежуточным соединением. Скорость реакции и свойства образующегося продукта зависят от количества растворителя. В статье делается предположение относительно возможного механизма реакции.

HUNGARIAN JOURNAL
OF INDUSTRIAL CHEMISTRY
VESZPRÉM
Vol. 6. pp. 301–312 (1978)

PARTICLE FORMATION FROM SOLUTION IN GAS FLUIDIZED BED I.

ESTABLISHMENT OF STEADY STATE CONDITIONS BY SOLID MATERIAL FEED-IN

B. Dencs and Z. Ormós

(Research Institute for Technical Chemistry
of the Hungarian Academy of Sciences, Veszprém, Hungary)

Received: May 3, 1978.

The main results of a project—still under way—dealing with little known and little studied aspects of fluidization are presented. The mechanism of particle formation in a fluidized bed, from solutions, the knowledge relating to particle size changes and the bringing about of steady state conditions are presented in *Part 1*. The experimental apparatus and method are shown, followed by the results obtained with different model materials with and without solid material addition. It is proved that steady state conditions can be created—irrespective of the model material used—by adding solid material to the system.

Introduction

The amount of solid intermediate or end products produced as granules is ever increasing both in the chemical and related industries since it is, in most cases, the most appropriate form for most modern uses. If the material to be formulated is a priori in solid state, i.e. it is a powder, then only a single operation, granulation is called for. The situation is different when initially the material is in a liquid form. There are a number of methods to be used to produce solid particles from the solid material content of solutions such as classical operations (e.g. crystallization-filtration-drying and optionally granulation; evaporation-atomization-drying-granulation, etc.) and particle formation in gas fluidized bed (from here on termed direct particle formation). In contrast to other operations there is only a single step involved in the formation of solid particles from solutions and it can be carried out in a continuously operated fluidized bed. Therefore, direct particle formation can be considered an intensive operation used to substitute classical multistep operations.

Description of the Process

Direct particle formation from solutions takes place as described below. In an appropriately designed continuous fluidization apparatus, a particle change mode of the same material as the solid ingredient in the liquid is fluidized by hot air. The solution to be processed is atomized onto the top (or into the layer itself) of the fluidized change. The droplets of the atomized solution are deposited on the surface of the fluidized particles and due to the effect of hot air keeping the particles in motion, they eventually dry up. Solvent vapours leave the system with the fluidizing air, while the solid material content of the liquid is retained in the bed. A flow of solid particles, its mass corresponding to that of the solid material content of the liquid fed in is continuously taken off from the apparatus.

It should be noted that this process is suitable not only for the extraction of the solid material content of any liquid, but according to literature references it has also been successfully applied to process melts, two component high temperature liquids, suspensions and pastes.

Direct particle formation consists of a number of consecutive and competitive elementary steps. The elementary steps are as follows: mixing of the particles, dispersion (atomization) of the liquid, partial evaporation of the solvent from the particles, wetting of the particles, agglomerization of the particles, desintegration of the particles (and also of the agglomerates) and drying. The most important elementary steps with respect to steady state operation conditions (or the bringing about of it) are the steps leading to changes in the particle size [1].

Particle growth can take place according to two mechanisms [2]: by surface deposition (layering) or subparticle agglomerization. In the case of surface deposition, solvent from the surface of the liquid wetted particles is evaporated, leaving behind its solid material content on the surface of the particle. This mechanism brings about a relatively slow but steady and uniform growth of the particle size. Particle formation from elementary subparticles takes place when fluidized wet particles collide and consequently stick together forming liquid-bridge-held agglomerates. Upon the evaporation of the solvent, solid bridges are left behind and agglomerates become stabilized. This mechanism results in the rapid growth of the particle size and a parallel rapid decline in the number of particles in the fluidized bed. Particle growth in direct particle formation carried out in fluidized beds can occur together by both mechanisms.

Particle degradation is the result of the mechanical wear and surface temperature changes of the particles in the fluidized bed. Particles moving according to a disordered pattern, collide with each other and the wall. If there is sufficient kinetic energy involved in the collisions, minute particles can break off from the surface of the particles already formed [1]. The surface temperature of the particles in the fluidized bed depends on the location of the given particle in the fluidized bed, whether it is in the vincinity of the atomization process or farther away towards the wall where drying takes place. Thus there are a number of temperature changes taking place on the particle while it is in the fluidized bed. It is not surprising that a time and place dependent thermal field is created leading to internal stresses that create radial cracks and eventual falling apart of the particle [3].

It is essential for the succesful completion of the process that steady state conditions, and particularly, steady state particle size distributions be achieved. Steady state conditions in the fluidized bed can be brought about by meeting the following requirements [4].

- the amount of heat entering the system in the hot air should be sufficient to ensure the evaporation of the coating liquid, while in the fluidized state
- the mass of the fluidized particle change be kept constant
- the number of particles in the fluidized bed should be kept constant.

The amount of heat required to evaporate a given amount of solvent introduced into the apparatus can be deduced from the heat balance equation allowing for the rate of heat and mass transfer processes. The mass of the particles charged into the fluidized remains constant if the input and output mass flow rates are kept equal. The number of particles in the fluidized bed decreases due to agglomerization and product offtake. When the number of particles formed in unit time due to particle degradation is greater than the number of particles "consumed" for agglomerization, then steady state conditions can be brought about. If the number of particles formed in unit time due to particle degradation is equal to or smaller than the number of particles consumed in the agglomerization process, then no steady state condition can be arrived at. In such cases, external means are required to increase the rate of degradation sufficiently enough or a solid material flow of appropriate particle size and mass flow rate has to be called upon to establish the steady state conditions.

It should be noted that both literature references and the experience gained in this laboratory indicate that with the majority of materials steady state conditions can only be brought about by external means.

Experimental — Apparatus and Method

Experiments were carried out in a continuous single-cell fluidization apparatus shown schematically in *Fig. 1.*

The main element of the system is a 0.3 m high glass cylinder (diameter 0.105 m) which, along with the air distributing base plate forms the fluidization space. The distributing plate is a perforated stainless steel plate covered with a stainless steel screen (screen opening $4 \cdot 10^{-5}$ m).

Fluidizing air from a central air distributing line enters the system via an oil filter, flow meter and electrical heater. Air passes through the distributing plate, fluidized bed and leaves the system at the top of the glass element. Cyclons are used to trap the particles carried out by the fluidizing air. Input and output air flow temperatures are monitored by resistance thermometers. Input air flow temperature is controlled by a setpoint controller.

The solution to be processed is stored in a thermostated reservoir and is pumped by a dual head calibrated piston metering pump into the pneumatic atomizer where atomizing air is introduced via oil filters and flowmeter.

Solid material feed-in is accomplished by a vibrating feeder. The delivery tube of the feeder is placed close to the top of the fluidized layer, but outside of the spraying cone of the atomizer.

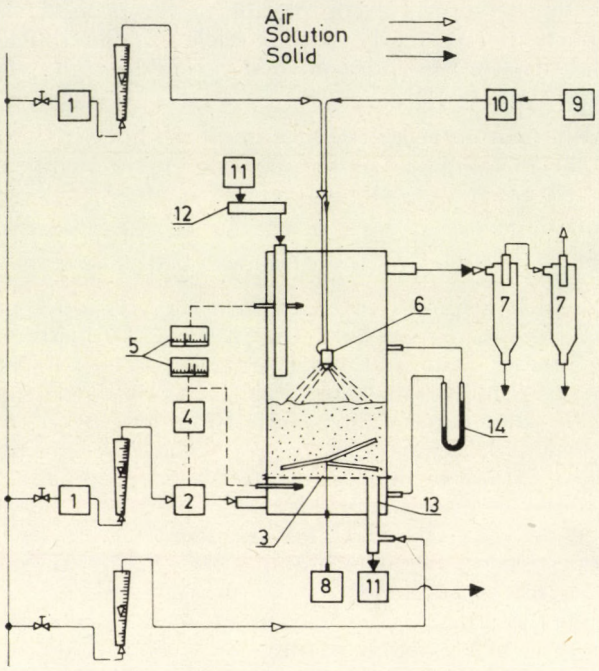

Fig. 1

1 — oil filter
2 — electric air heater
3 — under plate
4 — temperature controller
5 — temperature measuring instruments
6 — pneumatic atomizer
7 — cyclone
8 — motor
9 — thermostated tank
10 — pump
11 — tank
12 — vibration feeder
13 — pneumatic discharge pipe
14 — manometer

Pneumatic offtake is used to take off continuously solid material from the fluidized layer. Offtake air flow rate—a dependent variable—is controlled by a valve and using a flow meter its value is set to maintain the mass flow rate of product granules at a constant value determined by the input mass flow rate. Particles leaving the system via the offtake opening are collected in a product bin.

In order to eliminate fluidization irregularities, mechanical agitation is used as an auxiliary measure. The mixing head is formed of three slanting blades located at 120° each. The mixing element is located immediately above the distributing plate, in the bottom layer of the bed. It is powered by a variable speed electromotor.

Experiments were conducted as follows:

A given amount of solid material of given particle size distribution is charged into the fluidization apparatus. The particles are made of the same material which is dissolved in the solution. At a bed expansion of 1.3 the particles are preheated by hot air to the required temperature. Once this temperature level is reached the mechanical agitation of the layer is initiated at a bed expansion

of 1.7. Then the atomization of the liquid thermostated at 70 °C, the feed of the solid material and the offtake of the product are resumed.

The product leaving the system is periodically sampled and the physical properties of the particles are determined [5]. Experiments are continued until definite steady state or non-steady state conditions become established.

Results

The model materials used to study direct particle formation were as follows: urea, potassium carbonate (hydrated), potassium phosphate, sodium dichromate, sodium nitrate and ammonium nitrate.

Fluidizing and drying air temperatures, layer expansion, initial particle size, solution concentration, atomization rate, geometrical ratio characterizing the bed, and mixer rotation speed were as follows:

$$T'_{in} = 100\ °C,$$
$$Y/Y_m = 1.6-1.8,$$
$$d_0 = 0.63-0.8\cdot10^{-3}\ m,$$
$$\bar{d}_0 = 0.72\cdot10^{-3}\ m,$$
$$c' = 500\ kg/m^3,$$
$$w' = 3.5-3.7\cdot10^{-4}\ m^3/h,$$
$$Y_m/D = 0.75,$$
$$n = 80\ min^{-1}.$$

Unless specified otherwise, these conditions were used throughout the experiments.

a) *Direct Particle Formation Under Non-Steady State Conditions*

Due to particle size changes during direct particle formation in fluidized beds, the physical properties of the particles in the bed are time dependent. When no steady state conditions can be established this change extends through the entire run.

Changes of the physical properties of the particles as a function of time in the fluidized bed could not be directly determined. Therefore, time dependent changes of the physical properties of the product granules taken off from the bed were caused by the changes of the physical properties of the particles in the fluidized bed.

Steady state conditions cannot be achieved with the model materials studied alone. To illustrate this point, the time dependence of the average particle size *(Fig. 2)* and particle size distribution *(Fig. 3)* of the product taken off is shown with urea as model material. Dimensionless time, the ratio of actual time and average residence time of the solid material is plotted on the figures. Apart from a short initial section, average particle size increases linearily with increasing time. Accordingly, distribution curves (cumulated "less than" curves) are successively shifted towards higher values.

Time dependent changes of various particle size fractions of the product formed in a non-steady state process were studied. Time dependent changes of the relative amounts of the various urea fractions are shown in *Fig. 4.*

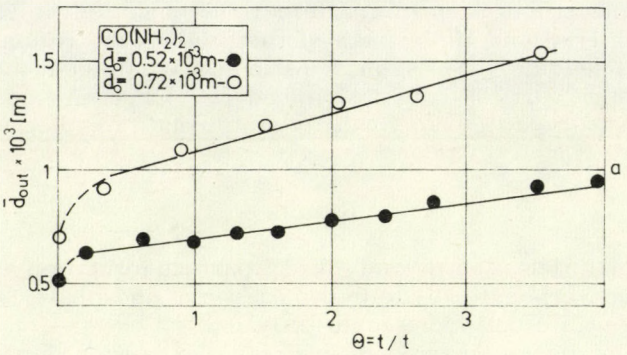

Fig. 2

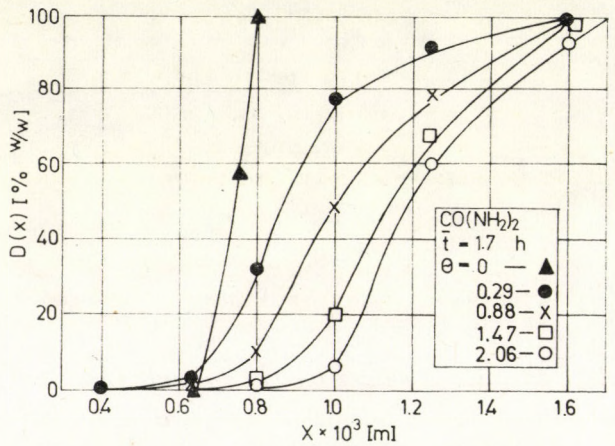

Fig. 3

It should be noted that similar changes were observed with potassium carbonate and sodium nitrate model materials. The amount of the successive size fractions at a given moment and their time dependent changes can be used to make conclusions about the mechanism of particle growth. At a time $\Theta = 0$ the initial urea fraction $0.4 - 0.63 \cdot 10^{-3}$ m is in the fluidized bed. As particle growth proceeds the amount of particles in the above range decreases. At the same time the amount of particles in the $0.63 - 0.8 \cdot 10^{-3}$ m fraction, initially zero, increases. The agglomerization of three or more particles of $0.4 \cdot 10^{-3}$ m size results in a particle bigger than $0.8 \cdot 10^{-3}$ m. At the same time, the amount of particles smaller than $0.4 \cdot 10^{-3}$ m in the bed becomes negligible, so it is obvious that the $(0.63 - 0.8) \cdot 10^{-3}$ m fraction is formed by surface deposition mechanism. Along with the increase of the amount of fraction $(0.63 - 0.8) \cdot 10^{-3}$ the next fraction: $(0.8 - 1.0) \cdot 10^{-3}$ m also sets out, but its rate is smaller. When the amount of particles in the $(0.63 - 0.8) \cdot 10^{-3}$ m range is close to its maximum, the growth rate of particles in the $(0.8 - 1.0) \cdot 10^{-3}$ m

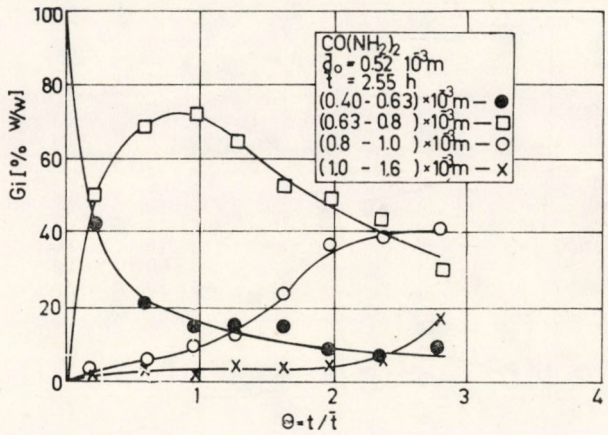

Fig. 4

range is suddenly increased. Then as the amount of particles in the $(0.63-0.8)\cdot10^{-3}$ m range starts to decrease the amount of particles in the $(0.8-1.0)\cdot10^{-3}$ m range shows a steep increase and approaches its maximum. By that time the amount of the next fraction, $(1.0-1.6)\cdot10^{-3}$ m also becomes significant.

Microscopical observations revealed that only single particles can be found in the $(0.4-0.63)$; $(0.63-0.8)$; $(0.8-1.0)\cdot10^{-3}$ m fractions. A small amount of agglomerates, 1—3% can be found in the fraction $(1.0-1.6)\cdot10^{-3}$ m.

It can be seen from *Fig. 4* and the microscopic studies that for the urea model, material particle growth primarily takes place by surface deposition and the role of agglomerization in particle growth is negligible. These same conclusions held for potassium carbonate and sodium nitrate as well.

Changes of the relative amounts of the fractions of potassium phosphate are shown in *Fig. 5*. The amount of particles in the $(0.63-1.0)\cdot10^{-3}$ m range formed by surface deposition, while the relative amount of particles is the $(0.40-0.63)\cdot10^{-3}$ m initial fraction is decreased, is very small and practically unchanged. At the same time, even at the begining of the experiments, $\Theta \ll 1$ the amount of particles in the $(2-4)$; $(4-5)\cdot10^{-3}$ m big particle size ranges is significant. The five to tenfold increase in the particle size during so short a time is possible only as a result of agglomerization. Microscopic observations clearly indicated that particles bigger than $2\cdot10^{-3}$ m were practically all agglomerates. Accordingly, it can be stated that with potassium phosphate the primary growth mechanism is agglomerization. The significance of surface deposition with respect to particle growth is negligible. These same conclusions hold for ammonium nitrate and sodium dichromate as well.

It can be concluded from the experimental results shown that the number of particles formed by degradation processes under the above conditions is not sufficient to bring about steady-state particle size distribution. At the same time, based on the changes of the relative amounts of the various size fractions, the mechanism of particle growth can be clearly established.

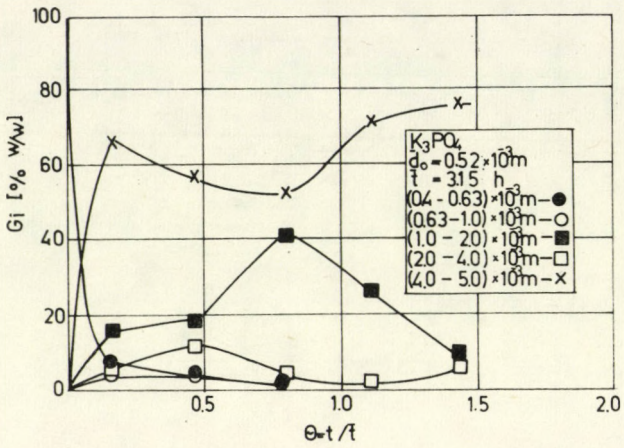

Fig. 5

b) *Direct Particle Formation Under Steady State Conditions*

In order to establish steady state conditions, i.e. steady state particle size distribution, solid material of a given amount and particle size distribution was introduced in the bed.

The feed rate ratio of the solid material was calculated as:

$$B = \frac{\dot{G}_{in}}{\dot{G}_{in} + c'w'} \, 100\% \tag{1}$$

Solid material feed-in brought about, in all cases, steady state conditions ($B = 9 - 25\%$).

Time dependent changes of the physical properties of the granules formed in steady state conditions were studied along with the values found at the early part of the process and its variations after steady state conditions were also achieved. Based on these studies, conclusions could be made as to the time required to achieve steady state conditions and the stability of steady state conditions.

Particle size distribution curves obtained at various time intervals for urea are shown in *Fig. 6*. Particle size distribution in the early, non-steady state section is shifted towards bigger particles and its standard deviation is also increased. In the experiments reviewed here, steady state conditions were achieved at about $\Theta = 2$.

More than 40 experiments with steady state sections were studied in this respect and it was found that steady state conditions did indeed occur in most cases at $1.5 < \Theta < 3$. In a few exceptional cases, however, as much as $3 - 4$ times the average residence time had to elapse before steady state conditions became established. The value of Θ^* is influenced by operational and process parameters, most sensitively by the ratio of solid material feed rate. With increasing solid material ratio, the time required to achieve steady state conditions decreased.

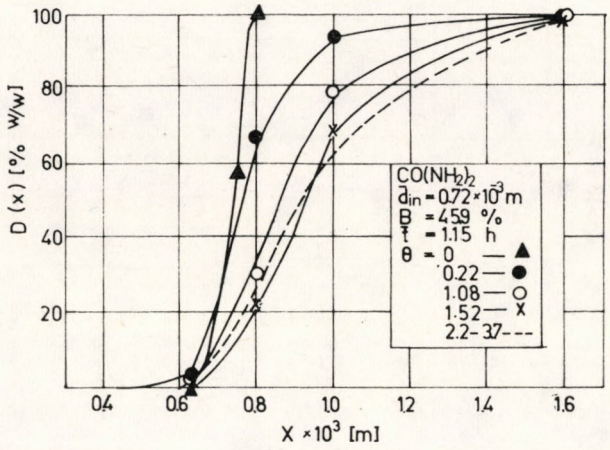

Fig. 6

When the curves describing the time dependent changes of the amounts of the fractions are studied (cf. *Fig. 7*) it can be seen that in the initial phase of particle formation they are similar to those obtained in the non-steady state processes (cf. *Fig. 4*). Thus, the deduced conclusions are also valid in the case of the first phase of steady state particle formation. The time required to achieve steady state conditions $\Theta^* \approx 2$ can also be deduced from *Fig. 7*.

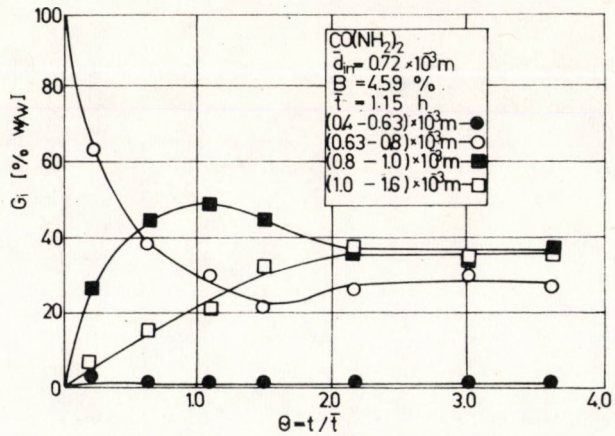

Fig. 7

Time dependent changes of the average particle size in the early phase of particle formation can take place in two ways. The most frequent case is that steady state conditions are achieved by continuosly slowing down particle growth (curves 1 and 2 in *Fig. 8* and *Fig. 9*). However, it can also occur that average particle size changes follow a maximum curve (curve 3

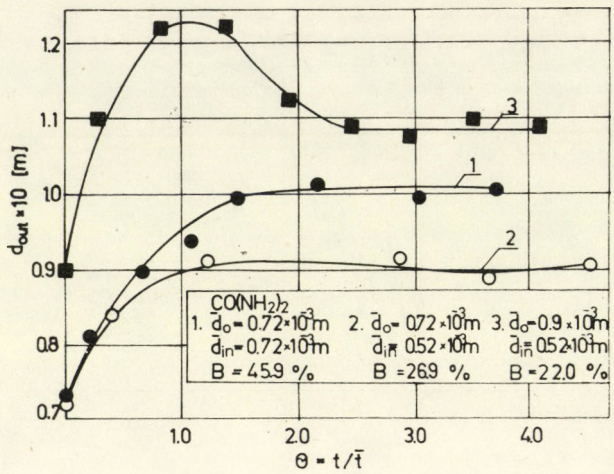

Fig. 8

in *Fig. 8*). This is the case when added particle size is much smaller (about twofold) than that of the initial particle size.

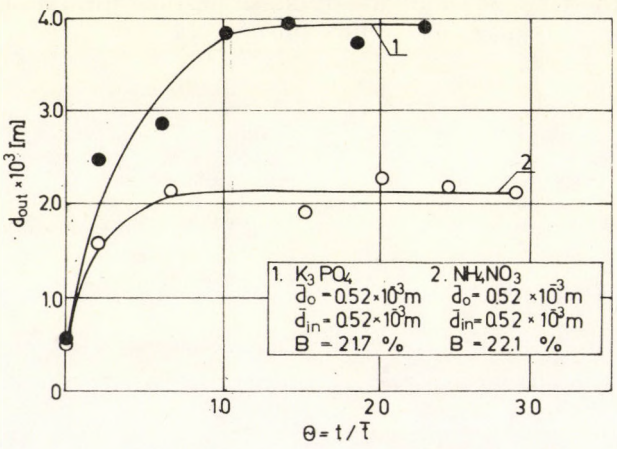

Fig. 9

Physical characteristics of the granules leaving the system in steady state conditions change around an average value. It is due to the statistical nature of processes occurring in the fluidized bed (interparticle collision, collision with liquid particles, etc.). The stability of the steady state section is characterized by the magnitude of changes taking place in the amounts of the various size fractions leaving the system. It can be seen in *Fig. 7* that changes of the relative amounts of the various fractions in the product leaving the system are minor in steady state conditions. From the analysis of the results of over

40 steady state experiments it was concluded that the relative amounts of the various fraction change no more than $\pm 5\%$.

To summarize it can be concluded that irrespective of the growth mechanism and material properties of the components in the solution, steady state conditions could be brought about by adding extra solid material. This leads to a steady state particle size distribution of the product.

SYMBOLS

B solid material feed ratio, %
c' solution concentration, kg/m³
d particle size, m
D diameter of the apparatus bed, m
$D(x)$ relative amount of particles passing a sieve of opening x, % w/w
G_i relative amount of particle fraction i, % w/w
$\dot{G}$ mass flow rate of solid material, kg/h
n rotation speed of mechanical agitator, min^{-1}
t time, h
$\bar{t}$ average residence time of solid material, h
T'' temperature of air, °C
x opening size of the sieve, m
Y height of the fluidized layer, m
Y_m minimum height of the fluidized layer, m
w' feed (atomization) rate of the solution, m³/h
Θ dimensionless time co-ordinate, $\Theta = t/\bar{t}$
Θ^* the time required to achieve steady state conditions, dimensionless

SUBSCRIPTS

o initial value
b input
k output
– average value

REFERENCES

1. Dencs, B., Ormós, Z.: International Congress of Chemical Engineering, Chemical Equipment Design and Automation, CHISA '75, Prague (1975)
2. Volkov, V. F. et alii: Him. Prom. *43*, 452 (1967)
3. Todes, O. M. et alii: Tr. Vses. Nauch. Issled. Proekt. Inst. Gal. *55*, 168 (1971)
4. Todes, O. M. et alii: Gidrodin, Teplo-Massoobmen 69 (1974)
5. Ormós, Z.: Hung. J. Ind. Chem. *1*, 207 (1973)

РЕЗЮМЕ

В данном цикле статей приводятся наиболее важные результаты исследований, ведущихся и в настоящее время, и связанных с этой малоизвестной и неисследованной областью применения метода псевдоожижения. В первой части данного цикла показан процесс образования гранул из раствора в псевдоожиженном слое, процессы изменения размера гранул, а также даётся информация относительно установления стационарного режима. Вслед за ознакомлением опытной установки и метода, производится обощение результатов опытов, выполненных с различными модельными материалами при подаче твёрдого материала и без его подачи. На основе этих результатов было установлено, что независимо от материальных особенностей находящихся в растворе компонентов, при помощи подачи твёрдого материала имеется возможность для установления стационарного режима.

HUNGARIAN JOURNAL
OF INDUSTRIAL CHEMISTRY
VESZPRÉM
Vol 6. pp. 313—322 (1978)

PARTICLE FORMATION FROM SOLUTIONS IN GAS FLUIDIZED BED. II.

THE EFFECTS OF THE CHARACTERISTICS OF THE SOLID MATERIAL AND SOLUCTION FED-IN UPON THE PHYSICAL PROPERTIES OF THE PARTICLES FORMED

B. DENCS and Z. ORMÓS

(Research Institute for Technical Chemistry
of the Hungarian Academy of Sciences, Veszprém, Hungary)

Received: May 3, 1978.

Physical characteristics of the granules (particles) formed in a steady state gas fluidized bed from solutions depend on the values of the independent variables (parameters). Therefore, it is indispensable for the practical embodiment of the process that the trends or functional relationships between the physical properties of the product granules should be known together with their parameters. The independent parameters of the process, and the results of experiments investigating the effects of solid material feed ratio, particle size of the initial solid material, concentration of the solution and feed (atomization) rate of the solution are presented here. From the analysis of the experimental results, the effects of the parameters studied upon the main physical characteristics (particle size, porosity, wear resistance, rolling properties, and moisture content) were determined.

The Parameters of the Process

In practice it is essential that the physical characteristics of the particulate solid material produced from solutions in a steady state gas fluidized bed should meet the requirements of the user or the given application. The physical characteristics of the particulate material can be influenced by changing the values of the independent parameters of the process. Therefore, it is essential that the functional relationship between the physical characteristics of the particulate solid material and the independent variables should be known.

The physical properties of the particulate solid material produced from solutions in a gas fluidized bed depend on the following independent variables:

Operational parameters

- the characteristics of the solid material,
- the concentration of the solution.

Process parameters

- the size distribution of the particles fed in,
- the ratio of the mass flow rates of the solid material fed into the particulate material leaving the system,
- the feed (atomization) rate of the solution,
- the degree of dispersity of the solution fed in,
- the moisture content and temperature of the air fed in,
- the ratio of the minimum bed height to the bed diameter,
- the extent of bed expansion.

Apparatus characteristics

- the shape and characteristics of the fluidization space,
- the quality of the air distributing base-plate,
- the distance of the atomizers from the base-plate and their direction,
- the location and means of solid material offtake,
- the characteristics of the elements of the auxiliary process equipment (e.g. size, shape and rotation speed of the mechanical agitator, etc.).

The linear velocity of the fluidizing air is a dependent variable and its value depends on the particle size distribution and the extent of expansion of the fluidized bed.

Results

Experiments were carried out in the apparatus described in Part 1 [1] following the technique detailed there. Urea was used as a model material to establish the relationships between the physical characteristics of the solid particles formed in steady state conditions and the major independent process variables [2]. The temperature of the fluidizing and drying air, the extent of bed expansion, the initial particle size, the concentration of the solution, the atomization rate, the characteristic geometrical ratio of the bed and the rotation speed of the mechanical agitator were as follows (unless otherwise specified):

$T''_{in} = 100$ °C, $c' = 500$ kg/m^3,
$Y/Y_m = 1.6-1.8$, $w' = 3.4-3.7\cdot10^{-4}$ m^3/h,
$d_0 = (0.63-0.8)\cdot10^{-3}$ m, $Y_m/D = 0.75$,
$\bar{d}_0 = 0.72\cdot10^{-3}$ m, $n = 80$ min^{-1}

a. *The Effects of the Particle Size and Mass Flow Rate of the Solid Material*

Steady state conditions can be achieved by introducing a solid particulate material of appropriate particle size and mass flow rate into the continuously fluidized layer. To characterize the amount of solid material fed in, the so-called solid material feed ratio was defined [1]:

$$B = \frac{\dot{G}_{in}}{\dot{G}_{in} + c'w'} 100 \ (\%) \qquad (1)$$

The effects of solid material feed ratio were examined in the 9.2 — 54% range. The solid material fed in was urea of two narrow particle size ranges [d_{in} = $= (0.4 - 0.63) \cdot 10^{-3}$ m and $(0.63 - 0.8) \cdot 10^{-3}$ m]. Steady state conditions were achieved in both cases. The physical properties of the particulate material formed in steady state conditions were also examined. The cumulated "fall-though" curves of sieve analysis were used to characterize the particle size distribution. The cumulated distribution curves are shown in *Fig. 1* and *2*.

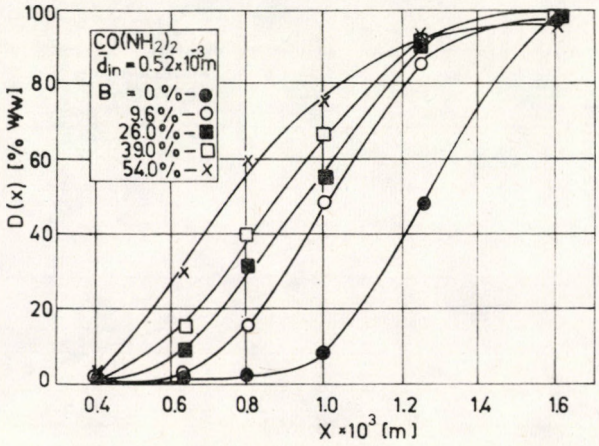

Fig. 1

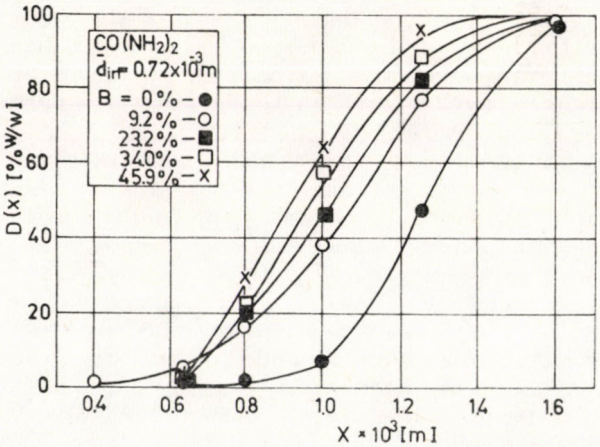

Fig. 2

For the sake of comparison, the distribution curve belonging to $\Theta = 2$ of a non-steady state experiment, i.e. without added solid material is also shown. It can be seen that the particle size distribution of the product is significantly different from the distribution obtained in the non-steady-state case, soon

after the addition of even minute amounts of solid material. With increasing solid material feed ratio, the distribution curves are shifted towards smaller particle size ranges.

With increasing solid material feed ratio, the average particle size of the product formed linearily decreases after an initial, presumably non-linear, steeply decreasing section. Similar behaviour was also found with different particle sizes *(Fig. 3)*.

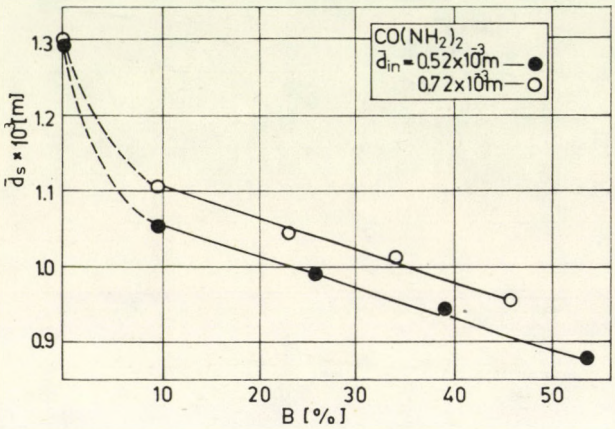

Fig. 3

The position of the lines depends on the size of the particles fed in. For smaller particles, the lines run lower, i.e. decreasing initial particle size results in decreased average product particle size. Thus, a considerably smaller solid material feed rate is required to produce the same average particle size if smaller particles are fed in as seed crystals.

Experiments were carried out with a smaller size fraction [$d_{in} = (0.2 - 0.4) \cdot 10^{-3}$ m] but the results did not unequivocally support the trends obtained previously. Presumably, the main reason for this failure was that fluidizing air carried out most of the fine particles as dust. Therefore, the actual solid material feed rate was considerably smaller than intended.

It was concluded that particle size could be changed only in a well defined range. The lower limit of this range was determined by the flow rate of the fluidizing air, while the upper limit depended on both the growth rate and the average residence time of the particles.

No characteristic trend in the average porosity, average density and bulk density of the product could be observed when the solid material feed ratio was changed. It is worthwhile noting that both the wear resistance and the rolling properties of the granules were extremely favourable, in the 80—90% and 0.35—0.5 ranges, respectively.

b. *The Effect of the Concentration of the Solution*

The concentration of the solution to be processed is one of the most widely changed parameters in the practice of direct particle formation in fluidized beds. The relationship between the properties of the granules produced and the concentration of the solution was examined experimentally. Regarding the concentration of the model solution, the amount of urea was changed in the 300—600 kg/m³ range.

It was found that with increasing concentration, the particle size distribution curves were shifted toward bigger particle sizes *(Fig. 4)*. For example, with

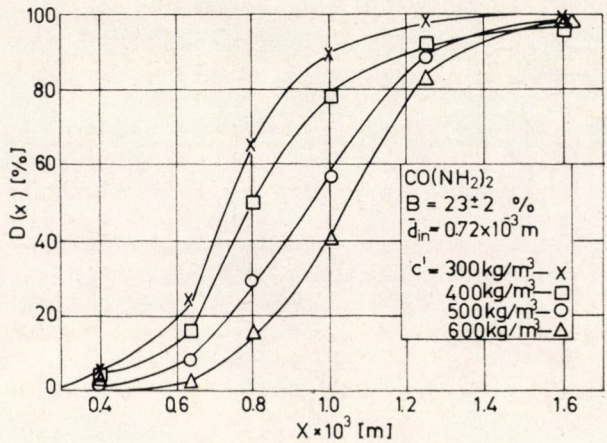

Fig. 4

300 kg/m³ solutions the amount of particles bigger than $1 \cdot 10^{-3}$ m was less than 10% while with a concentration of 600 kg/m³ this value was as high as 60%. Accordingly, the average particle size of the product was also increased 1.6 times *(Fig. 5)*. The relationship between the average particle size and

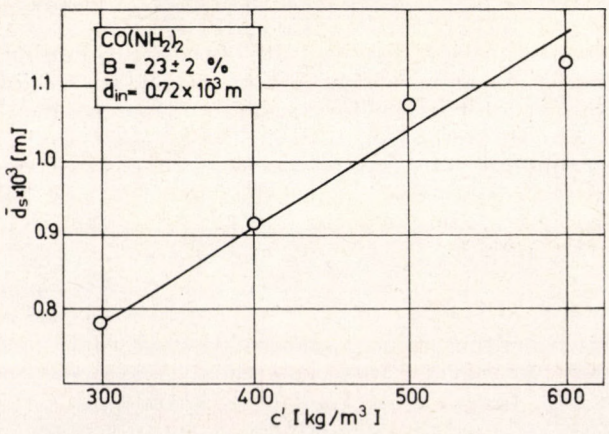

Fig. 5

the concentration of the solution could be approximated by a straight line in the range studied.

The increase of particle size induced by increased concentration is related to the rate of crystallization taking place on the surface of the particle. The driving force of nucleation and crystal growth is the difference between supersaturated and equilibrium concentration values. In this case, supersaturation was caused by the evaporation of the solvent. Starting with higher solvent concentrations the degree of supersaturation achieved during a given period was higher, so the driving force was also higher and the rate of the crystallization was increased. Correspondingly, the probability of stabilization of the aggregates held together by liquid bridges was increased, resulting in an increase of the average particle size.

There was no unequivocal change either in the porosity, the wear resistance or the rolling characteristics of the granules produced from increasingly concentrated solutions. On average porosity was about 15—20% v/v, wear resistance about 80—90% and the coefficient of rolling characteristics was between 0.43—0.48.

The average moisture content of the product, equal to that of the fluidized bed decreased from 1% *w/w* to 0.2% *w/w* in the concentration range studied. Presumably, this was due to two reasons. The first reason was that at a constant evaporation rate the amount of solvent to be evaporated decreased with increasing concentration. The second reason was that with increasing particle size the flow rate of fluidizing air required to achieve a given bed expansion value (identical fluidization motion) increased. Therefore, the flow rate of the fluidizing air had to be increased, resulting in a decreased average bed moisture content.

No limiting value of technological origin, restricting the concentration range of the solutions to be processed in the gas fluidized bed, was found. The energy consumption per unit mass of the product increased with decreasing concentration, so there are economical limits relating to the lowest solvent concentration limits which can be processed.

c. *The Effects of the Feed Rate of the Solution*

At a constant concentration, the feed rate of the solution directly determines the productivity of the particle formation operation, so it is one of the most important parameters of particle formation. An urea solution of 500 kg/m^3 concentration at five different feed rates in the $2.4-4.8\cdot10^{-4}$ m^3/h range was used in the experiments. This range was calculated from the heat balance equation using preliminary experimental data and the heat loss figure of the apparatus.

Experimental results proved that the size of the particles taken off from the bed increased with the increasing feed rate. This conclusion was valid as long as the moisture content of the fluidized bed was below the so-called critical bed moisture content value, a material characteristic. Once the moisture content of the bed was beyond this value then the stabilization of the loose, weak aggregates held together by liquid bridges could not proceed via drying and the formation of solid bridges. If the moisture content was increased beyond the critical one, then there was a sudden decrease in the particle size,

later there were fluidization disturbances of ever increasing severity, while eventually the entire fluidization process collapsed.

In the experiment, shown in *Fig. 6* and carried out at an atomization rate of $4.8 \cdot 10^{-4}$ m³/h the moisture content of the bed was beyond the critical value.

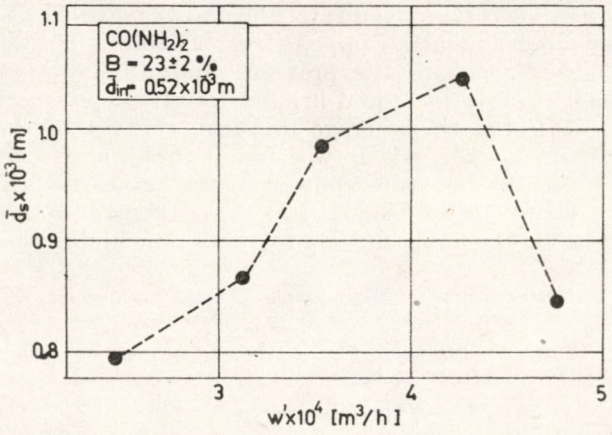

Fig. 6

The aim of this experiment was the determination of the consequences of a slight overwetting in the bed. Apart from that the size increasing effects of the increased atomization rate were also apparent. The average particle size of the product increased by some 30% in the $2.4-4.3 \cdot 10^{-4}$ m³/h feed rate range due to an increase in the extent of agglomerization.

The theoretically possible particle size growth under the experimental conditions used was calculated for the case of particle growth via ideal surface layering. Starting with an average particle size of $\bar{d}_0 = 0.72 \cdot 10^{-3}$ m the product granules could grow as big as ($\bar{d}_{out} = 1.0-1.3 \cdot 10^{-3}$ m, depending on the magni-

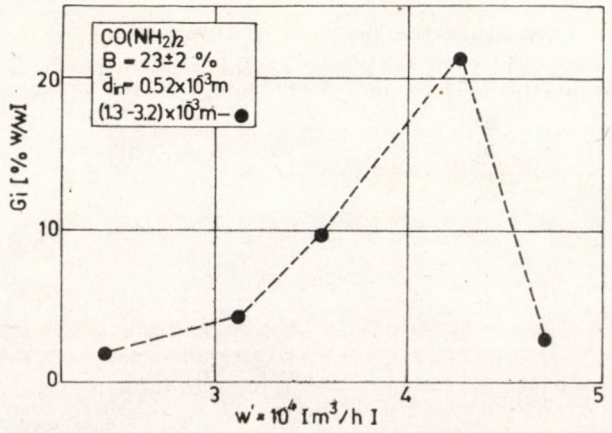

Fig. 7

tude of the average residence time. It was concluded from these and other microscopic results that particles formed and grown via the agglomerization mechanism could be found with a high enough probability only among the big particles, above $1.3 \cdot 10^{-3}$ m. The effects of the feed rate upon the amounts of particles bigger than $1.3 \cdot 10^{-3}$ m were also examined. It was found that the amount of particles bigger than $1.3 \cdot 10^{-3}$ m greatly increased (from 2 to 22% *w/w*) with an increasing feed rate. Beyond the critical moisture content of the bed, this value suddenly dropped (from 22 to 3 *w/w*) *(Fig. 7)*.

This was in agreement with the previous findings, i.e. loosely structured agglomerates held together by liquid bridges could not be stabilized.

Feed rate also effected the average moisture content of the bed, i.e. the product taken off from the bed. It was found that there was a slight, then a sudden increase in the moisture content of the product with an increasing feed rate in the $2.4 - 4.3 \cdot 10^{-4}$ m³/h and $4.3 - 4.8 \cdot 10^{-4}$ m³/h ranges, respectively. Above $4.8 \cdot 10^{-4}$ m³/h the moisture content became higher than the critical one *(Fig. 8)*.

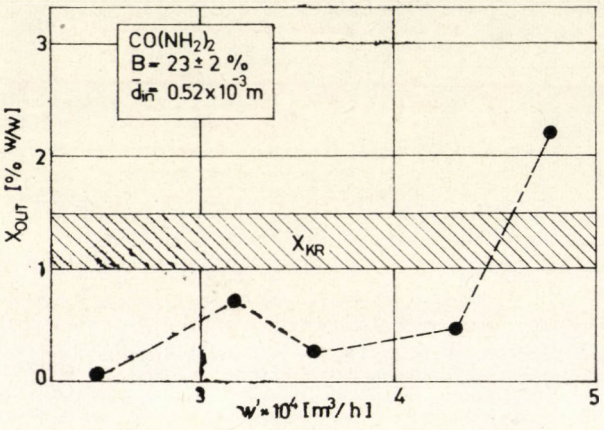

Fig. 8

With increasing feed rate the porosity of the product was increased in the 15 — 25% *w/w* range, the wear resistance was between 80 — 85% while the coefficient of the rolling properties decreased from 0.55 to 0.4.

SYMBOLS

B	solid material feed ratio, %
c'	concentration of the feed solution, kg/m³
d	particle size, m
D	inner diameter of the bed, m
$D(x)$	the relative amount of particles passing the sieve of opening x, % *w/w*
G_i	the relative amount of the ith particle size fraction, % *w/w*
$\dot{G}$	solid material mass flow rate, kg/h
n	rotation speed of the mechanical agitator, min^{-1}
t	time, h
$\bar{t}$	average residence time of the solid material, h
T''	temperature of the fluidizing air, °C

x opening of the sieve, m
X moisture content relating to the dry material, % w/w
X_{KR} critical moisture content, % w/w
Y height of the fluidized bed, m
Y_m minimum height of the fluidized bed, m
w' feed (atomization) rate of the solution, m^3/h
Θ dimensionless time co-ordinate, $\Theta = t/\bar{t}$

Indices

o initial value
in input value
out output value
— average value
s steady state value

REFERENCES

1. Dencs, B. and Ormós, Z.: Hung. J. Ind. Chem., *6*, 301 (1978)
2. Ormós, Z.: Hung. J. Ind. Chem., *1*, 207 (1973)

РЕЗЮМЕ

Физические свойства гранулятов (зёрен), полученных при стационарных условиях из раствора в псевдоожиженном слое, определяются величинами независимо изменяющихся параметров процесса. Поэтому в ходе практического осуществления процесса совершенно необходимо знать тенденции взаимозависимостей между упомянутыми параметрами и физическими свойствами гранулятного продукта. В данной статье приводятся независимо изменяющиеся параметры процесса, а также результаты опытов, целью которых являлосьисследование влияния, оказываемого долей подачи твёрдого вещества, размером введённых зёрен, концентрацией раствора и скоростью ввода (распыления) раствора. На основе полученных результатов было установлено влияние, оказываемое изменением величин исследованных параметров на основные физические свойства зёрен (размер зёрен, пористость, твёрдость на износ, способность к качению, влагосодержание).

HUNGARIAN JOURNAL
OF INDUSTRIAL CHEMISTRY
VESZPRÉM
Vol. 6. pp. 323—332 (1978)

PARTICLE FORMATION FROM SOLUTIONS IN GAS FLUIDIZED BED. III.

THE EFFECTS OF BED GEOMETRY, MECHANICAL AGITATION AND MATERIAL PROPERTIES UPON THE PHYSICAL CHARACTERISTICS OF THE PARTICLES FORMED

B. Dencs and Z. Ormós

(Research Institute for Technical Chemistry
of the Hungarian Academy of Sciences, Veszprém, Hungary)

Received: May 3, 1978.

The physical characteristics of the particles (granules) formed from solutions in steady-state gas-fluidized beds can be effected, among others, by the geometrical ratio of the stationary bed and the rotation speed of the mechanical agitator in the bed. The effects of the above parameters upon the physical characteristics of the product granules were tested on urea as a model compound. The results obtained in this study are presented here. Experiments were also carried out with other model compounds. It can be concluded that the physical characteristics of the particles basically differ, first of all, according to the various growth mechanisms. The particle growth mechanism is governed, on the other hand, primarily by the quality (chemical and physical characteristics) of the dissolved component.

Introduction

The physical characteristics of the particles produced from solutions in gas fluidized beds can primarily be effected by changing the settings of the operational parameters. The independent operational parameters were classified in *Part 2* of this series [1]. The effects of changing the minimum bed height-bed diameter ratio upon the physical characteristics of the granules formed were studied and extensively reported on in literature. However, the conclusions are contradictory for both decreasing [2, 3] and increasing [4, 5] particle size reported with increasing geometrical ratio. To our best knowledge there is no report on the use of mechanical agitation in fluidized beds to improve particle formation from solutions. There are also no references in literature about the effects of mechanical agitation (and rotation speed in the case of a given agitator geometry) upon the physical characteristics of the particles formed. In addition, no data could be found relating to the effects of the physi-

cal or chemical characteristics of the dissolved material upon the physical characteristics of the particles formed. Therefore, recent research activity, the results of which are presented here, was concentrated on the investigation of the effects of the above mentioned independent parameters.

Experimental

Urea, potash, sodium nitrate, ammonium nitrate, tri-potassium phosphate and sodium dichromate model compounds were used to carry out experiments in the apparatus described in *Part 1* [1]. The same experimental technique was followed. The temperature of the fluidizing/drying air flow, bed expansion, initial particle size, concentration and atomization rate of the solution, and the characteristics of the geometrical ratio and agitator speed were as follows (unless otherwise specified).

T''_{in} $=100$ °C
$Y/Y_m = 1.6-1.8$
d_0 $=0.4-0.63\cdot10^{-3}$ m
$\bar{d}_0$ $=0.52\cdot10^{-3}$ m
c' $=500$ kg/m³
w' $=3.5-3.7\cdot10^{-4}$ m³/h
$Y_m/D = 0.75$
n $=80$ min^{-1}.

Steady state conditions—i.e. steady state particle size distribution—were achieved by initial solid particle introduction. Solid material feed rate was 20—26% (B) while average particle size and size range were $\bar{d}_{in}=0.52\cdot10^{-3}$ m and $d_{in}=(0.4-0.63)\cdot10^{-3}$ m.

Results

a. *Effects of the Minimum Bed Height/Bed Diameter Ratio*

Appropriate selection of the so-called geometrical ratio, the ratio of the stationary bed height to the bed diameter (Y_m/D) is very important for any fluidized bed operation and this is also true in the case of particle formation from solutions in fluidized beds. This ratio not only effects the flow and mixing phenomena of the fluidized bed, but the physical characteristics of the granules formed. The geometrical ratio characterizing the stationary bed is the minimum bed height to the bed diameter ratio. Experiments were carried out to determine the relationships between the product characteristics and the geometrical ratio.

The minimum bed height to bed diameter ratio Y_m/D was varied in the 0.5—1.6 range using urea as a model compound. The bed diameter was kept constant and the bed height (mass of the bed) successively increased. It could be concluded that initially the average particle size incresaes with the increasing ratio, then, depending on the material in question (mechanical stability of the particles), it approaches a limiting value or passes a maximum, as shown in *Fig. 1.*

The above change of the average particle size is the result of two counteracting factors. With increasing bed height the average residence time increases

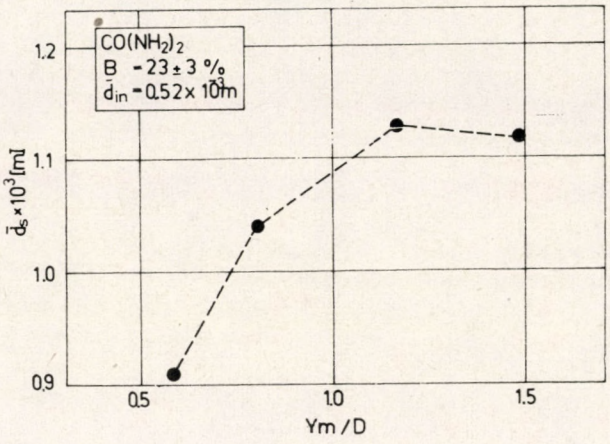

Fig. 1

resulting in increased average particle size. At the same time, increasing bed height means an increased bed mass, resulting in increased mechanical stress. Correspondingly mechanical wear fracturing is also increased, which after a certain point, overtakes the particle size and also increases the effects of the increased residence time.

The point where the maximum of the average particle size vs. Y_m/D ratio is depends on the material in question. There are materials with better and poorer mechanical characteristics (crystal structure, and wear resistance, etc.) than the urea selected for these studies. Correspondingly, disintegration caused by mechanical effects can occur and overtake the size time, both at higher and lower Y_m/D ratios. Thus, the maximum place of the function can be shifted either way. If the experiments are carried out at Y_m/D values lower than that corresponding to the maximum place, then average particle size increases with increasing Y_m/D and the opposite is true if the initial Y_m/D value is beyond that of the maximum point. This is the explanation for the contradictory reports found in literature.

With regard to the other physical characteristics of the products, the porosity increases from 17 to 25% v/v in the range studied, wear resistance is 80—90%, and the rolling coefficient is in the 0.4—0.5 range. The moisture content is decreased from 1.1% to 0.1% with increasing Y_m/D ratio. The decreased moisture content is due to the increased residence time.

b. *The Effects of Mechanical Agitation*

Mechanical agitation can be advantageously used in fluidized beds as an auxiliary means to control fluidization irregularities. In addition, mechanical agitation also effects flow and mixing conditions in the fluidized bed and the physical characteristics of the particles therein.

The relationship between the physical characteristics of the granules formed and the rotation speed was examined using a given mechanical agitator design

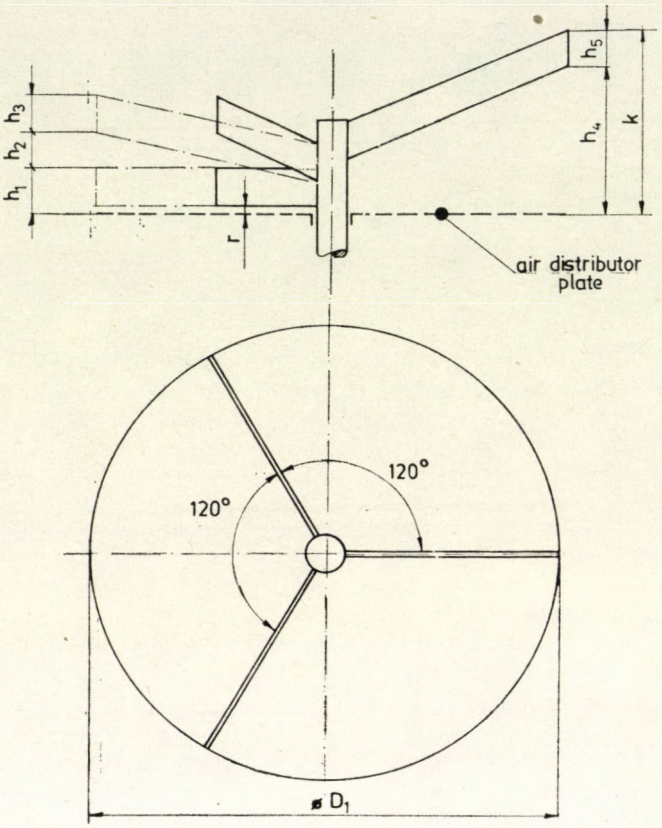
h5
h4
k
h3
h2
h1
r
air distributor plate
120°
120°
ø D1

Fig. 2

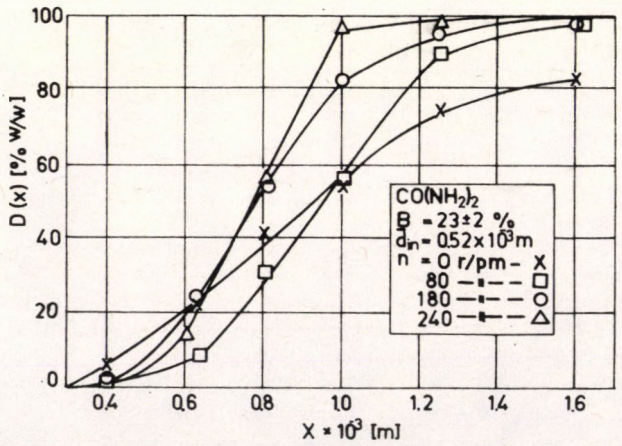
100
80
60
40
20
0
D (x) [% w/w]
0.4
0.6
0.8
1.0
1.2
1.4
1.6
X × 10³ [m]
CO(NH2)2
B = 23±2 %
dm = 0.52x10³m
n = 0 r/pm - X
80 - □
180 - ○
240 - △

Fig. 3

and urea as a model compound. The design of the agitator is shown schematically in *Fig. 2*. The rotation speed was varied in the 0—240 rpm range.

It was found that an increased rotation speed resulted in shifts towards decreased average particle size and also in more narrow size distribution (cf. *Fig. 3*). Correspondingly, extremely narrow particle size distributions could be achieved at high rotation speeds. For example at 240 rpm about 95% *w/w* of the granules fall in the $0.4-1.0 \cdot 10^{-3}$ m range, while at 0 rpm only 50% is within this range.

The average particle size of the granules formed decreases with increasing rotation speed (cf. *Fig. 4*). There is a quasi linear section in the 0—180 rpm

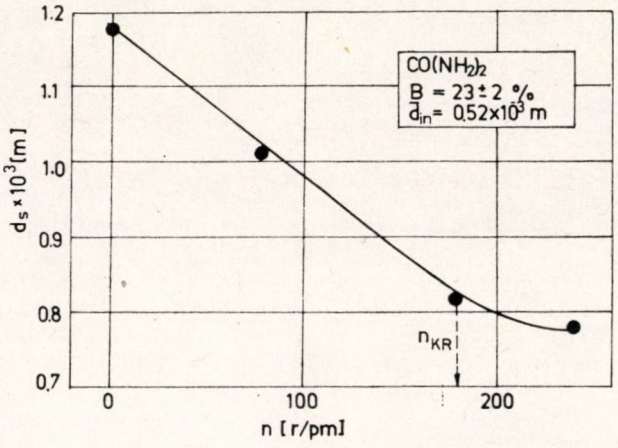

Fig. 4

range. At even higher rotation speeds, the particle size decreases at a lower rate and eventually approaches a limiting value. The rpm value found at the end of the quasi linear relationship is termed the critical rpm value.

Apart from the quality of the material in question the value of the critical rpm primarily depends on the design of the agitator element. The particle size decreasing effect of increased rotation speed is readily explained by the fact that agitation decreases the number of aggregates held together by wet bridges before they could be stabilized. This reasoning is substantiated by the observation that the amount of aggregates, particles above $1.3 \cdot 10^{-3}$ m [6], is decreased with increasing rotation speed (cf. *Fig. 5*). This amount decreased from 25% to 1% in the range studied.

Particle flow and mixing conditions in the fluidized bed change above a certain rotation speed. There is a shift from the completely mixed state towards a sort of ordered state. This phenomenon is brought about by the centrifugal action of the mechanical agitator. With certain agitator element design, fluidization disappears and a rotating layer of circular cross section is formed along the inner wall of the apparatus. In this case, the above phenomenon was observed to occur at about 300 rpm. In our view, the limiting value of average particle size obtained with increasing rotation speed is due, among

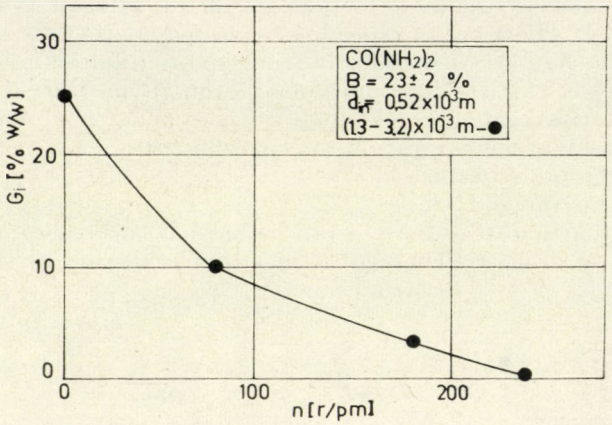

Fig. 5

others, to the above described phenomenon, i.e. changes in the flow and mixing conditions in the fluidized bed.

Upon increasing the rotation speed of the agitator, average particle porosity is decreased from 22% to 8%, while the wear resistance, rolling coefficient and moisture content values lie in the 85—90%, 0.46—0.51 and 0.13—0.52% *w/w* ranges, respectively.

c. *The Effects of the Material Proper*

Experiments were carried out with various materials, such as urea, sodium nitrate, potash, sodium bichromate, ammonium nitrate, tris potassium phosphate, with and without initial solid material feed. One of the objects of the experiments was to determine if steady state conditions could be brought about without initial solid material feed. The other object was to determine if material quality proper had any effect on the growth mechanism and physical properties of the granules formed.

Steady state conditions with the materials studied could not be achieved without initial solid material feed. This can be seen when the major physical characteristics are examined for there is always a definite time trend. The most obvious is the change of average particle size with time (cf. *Fig. 6*). There is a definite growing tendency when average particle size is plotted against dimensionless time. At the beginning of the range studied, there is a section of fast increase followed by a more moderate, quasi-linear growth.

These same experiments were repeated by continuously introducting $d_{in} = 0.52 \cdot 10^{-3}$ m particles into the fluidized bed to bring about steady state conditions. Solid material feed rate was maintained at $24 \pm 2\%$. From the examination of the major physical characteristics, it could be concluded that steady state conditions were indeed achieved with all model materials. After a time, amounting to about twice the average residence time, had passed the particle size distribution, average particle size, average porosity and all other size dependent physical characteristics became constant. For the sake

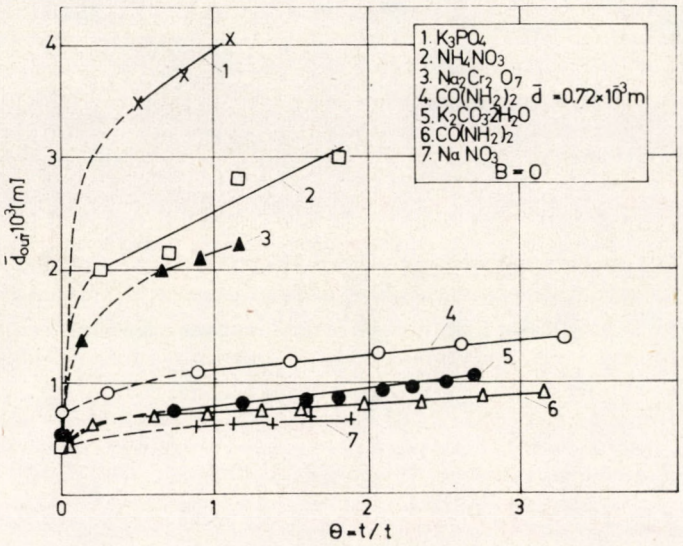

Fig. 6

of comparison, the time dependence of the average particle size is once again shown here (cf. *Fig. 7*).

Conclusions relating to the growth mechanism concerned can be drawn from the slopes and intercepts of the lines shown in *Fig. 6* and *7*. In the case of urea, sodium nitrate and potash (potassium carbonate dihydrate) with initial solid material feed of $\bar{d}_{in} = 0.52 \cdot 10^{-3}$ m lines are in the small particle

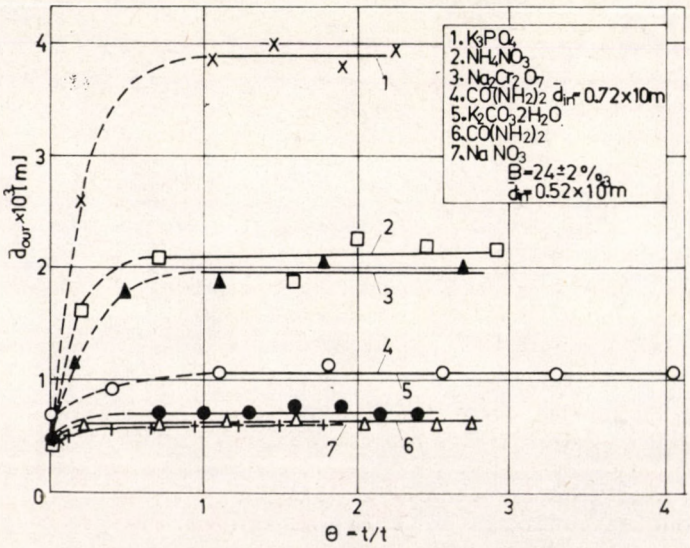

Fig. 7

size range with nearly identical slopes. Thus, it can be concluded that the same growth mechanism is effective. Their particle size indicates that growth takes place by surface layer formation.

Starting with initial urea particles of $\bar{d}_0 = 0.72 \cdot 10^{-3}$ m there is practically no change in the growth mechanism, and the slopes are by and large the same as previously. However, there are larger intercepts due to higher average particle size.

In the case of sodium dichromate, ammonium nitrate and tris potassium phosphate, the lines are in the higher particle size ranges and the slopes are also larger.

Both values indicate that particle growth takes place mainly via particle agglomeration. Calculations indicated that surface layering could result in growth amounting only to a maximum of $0.3-0.4 \cdot 10^{-3}$ m. Thus, after the appropriate residence time has possed the initial particle of $\bar{d}_{in} = 0.52 \cdot 10^{-3}$ m could not be any bigger than $1 \cdot 10^{-3}$ m. However, with the above materials a severalfold increase in the average particle size could be witnessed as early as a fraction of the average residence time. This proved unequivocally that the governing growth mechanism was agglomerization. Naturally, it is also accompanied, by growth via surface layering, but its role is negligible.

The physical characteristics of the steady state products formed from the six test materials were compared. Since experiments were carried out under identical conditions, differences necessarily reflect the effects of material quality.

Depending on the model material in question, the steady state particle size distributions can be very different (cf. *Fig. 8*). The particle size range,

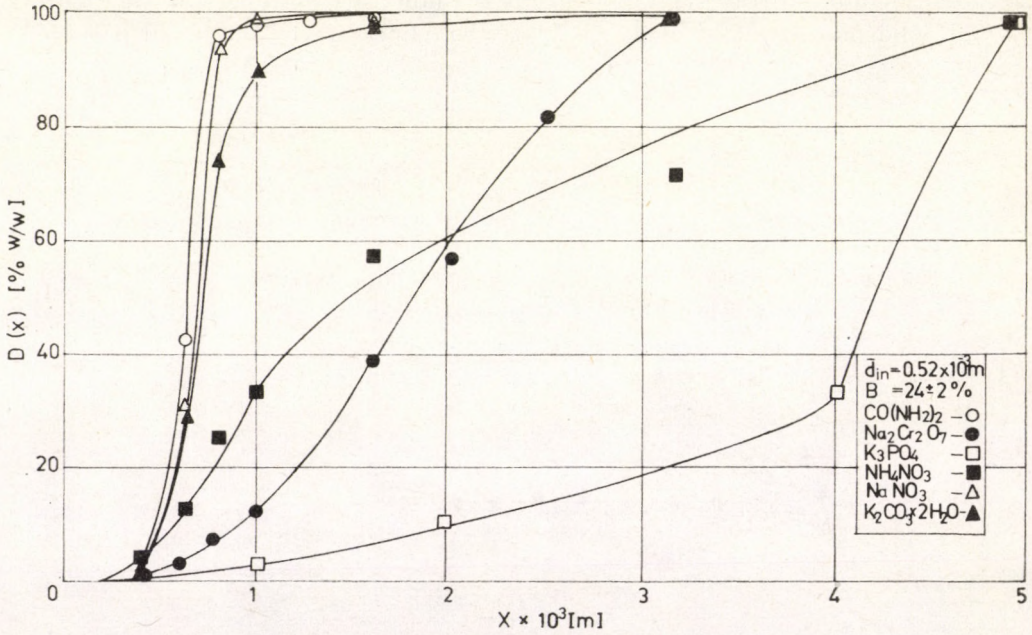

Fig. 8

the shape and correspondingly the particle size distributions can be very different. In the case of urea, sodium nitrate and potassium carbonate dihydrate which grow primarily via surface layering, curves lie in the $0.4-1.6\cdot10^{-3}$ m range and their shapes are very similar. Sodium dichromate, ammonium nitrate and tris potassium phosphate grow primarily by agglomerization and the resulting particle size range is much wider: $0.2-3.2\cdot10^{-3}$ and $0.2-5\cdot10^{-3}$ m. Curves are of widely different shapes depending on the rate of agglomerization. They also differ from the curves obtained by surface layering growth mechanism.

The other major characteristics of the products are summarized in *Table 1.*

Table 1.

Major physical characteristics of the product granules

Test substance	$\bar{d}_s\cdot10^3$ (m)	$\bar{\varepsilon}$ % *v/v'*	$\bar{K}$ (%)	Φ (–)	$\bar{X}$ % *w/w*
growth via surface layering					
$CO(NH_2)_2$	0.64	6.8	85.7	0.5	1.03
$NaNO_3$	0.66	8.8	84.7	0.56	0.03
$K_2CO_3\cdot2\,H_2O$	0.77	9.2	72.4	0.52	7.6
growth via agglomerization					
$Na_2Cr_2O_7$	1.91	27.5	91.3	0.42	0.01
NH_4NO_3	2.20	30	92.3	—	1.8
K_3PO_4	3.86	22.3	96.6	0.40	2.4

The physical properties of the granules formed not only differ among various model substances, but also according to the growth mechanisms involved. In the case of agglomerated particles, the average particle size and porosity are 3–5 and 3–4 times higher respectively, than in the case of growth via surface layering. At the same time, there is also a systematic difference between the wear resistance and rolling coefficients.

These observations are emphasized because they allow for the determination of the particle growth mechanism from the study of a few carefully chosen physical characteristics of the product.

To summarize it can be concluded that the material quality profoundly influences the particle growth mechanism which, in turn, determines the physical characteristics of the products.

SYMBOLS

B initial solid material feed rate, %
c' concentration of the solution, kg/m³
d particle size, m
D bed diameter, m
$D(x)$ relative amount of particles passing the sieve of opening x, % *w/w*
G_i relative amount of ith particle fraction, % *w/w*

K wear resistance, %
n rotation speed of the mechanical agitator, r.p.m.
t time, h
$\bar{t}$ average residence time of the solid material, h
T'' air temperature, °C
x sieve opening size, m
X moisture content relating to dry material, % w/w
Y height of the fluidized bed, m
Y_{r} minimum bed height, m
w' atomization rate of the solution, m^3/h
Θ dimensionless time co-ordinate, $\Theta = t/\bar{t}$
ε_{p} porosity, % v/v
Φ rolling coefficient, (−)

Subscripts

o initial value
in input value
out output value
− average value
s steady state value

REFERENCES

1. Dencs, B. and Ormós, Z.: Hung. J. Ind. Chem. *6*, 313 (1978)
2. Kozlovszkij, V. V. et al: Khim. Prom. *46*, 42 (1970)
3. Nalimov, Sz. P. et al: Zh. Prikl. Khim., *43*, 581 (1970)
4. Todes, O. M. et al: Zh. Prikl. Khim., *44*, 1984 (1971)
5. Todes, O. M. et al: Teor. Osn. Khim. Tekhnol., *7*, 126 (1973)
6. Dencs, B. and Ormós, Z.: Hung. J. Ind. Chem. *6*, 301 (1978)

РЕЗЮМЕ

На физические свойства гранулятов (зёрен), получаемых в стационарных условиях из раствора в псевдоожиженном газом слое, можно повлиять например благодаря изменению геометрических пропорций неподвижного слоя и числа оборотов механической мешалки, расположенной в слое. Влияние, оказываемое изменением указанных параметров на физические свойства гранулятов продукта, исследовалось на модельном материале — мочев ине. При одних и тех же условиях авторами были проделаны эксперименты с модельными веществами различного химического состава. На основании полученных данных было установлено, что физические характеристики образовавшихся зёрен в зависимости от механизма роста зёрен имеют резко различные значения. А механизм роста зёрен определяется в первую очередь качеством материала (физическими и химическими характеристиками растворённого компонента).

CONTENTS

Mrs. HORVÁTH, E., PATAKI, K. and ORMÓS, Z.: Studies on Particle Coating. I. Film-Coating of Urea Particles in Fluidized Bed 225

KRAMARZ, J. and RADOSZ, M.: Prediction of Catalytic Reformer Yield by Chemical Equilibrium (Commercial Results) 243

HAKIM, K. A. A., ZALAI, A., LECHNER, A. and TÓTH, A.: Study on the Effect of a Detergent Additive, and Test Severity on Motor Oil Test Results 251

GÓR-NAGY, S., KÁLDI, P., Mrs. BÉSÁN, J. and SZÁNTÓ, A.: The Solubility of Micronutrients in Ammonium Polyphosphate Solutions 259

GRUHN, G., NEUMANN, W. and HEINING, H.: Reliability Analysis of Chemical Plants by Means of Markow Processes 275

SUBRAHMANYAM, M. and KURIACOSE, J. C.: The Nature of the Reaction of Propan-2-ol on a Zn:Cr:Fe Catalyst 283

YESODHARAN, E. P., RAMAKRISHNAN, V. and KURIACOSE, J. C.: Reactions of Benzyl Alcohol on U-V Irradiated Zinc Oxide 293

DENCS, B. and ORMÓS, Z.: Particle Formation from Solutions in Gas Fluidized Bed. I. Establishment of Steady State Conditions by Solid Material Feed-in 301

DENCS, B. and ORMÓS, Z.: Particle Formation from Solutions in Gas Fluidized Bed. II. The Effects of the Characteristics of the Solid Material and Solution Fed—in upon the Physical Properties of the Particles Formed 313

DENCS, B. and ORMÓS, Z.: Particle Formation from Solutions in Gas Fluidized Bed. III. The Effects of Bed Geometry, Mechanical Agitation and Material Properties upon the Physical Characteristics of the Particles Formed 323

Egyetemi Nyomda — 78.3106 Budapest, 1978. Felelős vezető: Sümeghi Zoltán igazgató

THE FOLLOWING ARE PLEASED TO ACCEPT SUBSCRIPTIONS TO THIS JOURNAL:

AUSTRALIA

C.B.D. Library and Subscription Service
Box 4886 G.P.O.
Sydney 2000

Cosmos Book and Record Shop
145 Acland Street
St. Kilda 3182

Globe and Co.
694—696 George Street
Sydney 2000

AUSTRIA

Globus (VAZ)
Höchstädtplatz 3
A—1200 Wien XX

BELGIUM

"Du Monde Entier" S. A.
Rue du Midi 162
B—1000 Bruxelles

Office International de Librairie
Avenue Marnix 30
B—1050 Bruxelles

CANADA

Pannonia Books
P.O. Box 1017
Postal Station "B"
Toronto, Ontario M5T 2T8

DENMARK

Munksgaard's Boghandel
Norregade 6
DK—1165 Copenhagen K

FINLAND

Akateeminen Kirjakauppa
Keskuskatu 2, P.O.B. 128
SF—00 100 Helsinki 10

FRANCE

Office International de Documentation et Librairie
48 Rue Gay Lussac
75 Paris 5

GERMAN FEDERAL REPUBLIC

Kubon und Sagner
Pf 68
D—8 München 34
BRD

GREAT BRITAIN

Bailey Bros and Swinfen Ltd.
Warner House, Folkestone
Kent CT 19 6PH England

HOLLAND

Martinus Nijhoff
Periodicals Department
P.O. Box 269
The Hague

Swets and Zeitlinger
Keizersgracht 487
Amsterdam C

ITALY

Licosa
P.O.B. 552, Via Lamarmora 45
50121 Firenze

JAPAN

Igaku Shoin Ltd.
Foreign Department
Tokyo International P.O. Box 5063
Tokyo

Maruzen Co. Ltd.
P.O. Box 5050
Tokyo International 100—31

Nauka Ltd.
Yasutomi Bldg. 5F 2—12 Kanda Jinbocho, Chiyoda-ku
Tokyo 101

NORWAY

Tanum—Cammermayer
Karl Johangt. 41—43
Oslo 1

SWEDEN

Almqvist and Wiksell Förlag A. B.
Box 2120
S—103 13 Stockholm 2

Wennegren—Williams AB
Subscription Department Fack
S—104 Stockholm 30

SWITZERLAND

Karger Libri A. G.
Petersgraben 31
CH—4011 Basel

USA

Ebsco Subs. Services
1 st Ave North at 13th street
Birmingham, Ala. 35201

HUNGARIAN

Journal of

INDUSTRIAL CHEMISTRY

Edited by

the Hungarian Oil & Gas Research Institute (MÁFKI),
the Research Institute for Heavy Chemical Industries (NEVIKI),
the Research Institute for Technical Chemistry of the
Hungarian Academy of Sciences (MÜKKI),
the Veszprém University of Chemical Engineering (VVE).
Veszprém (Hungary)



Volume 6. 1978 Number 4.

HU ISSN: 0133—0276
CODEN: HJICAI

Editorial Board:

R. CSIKÓS and GY. MÓZES
Hungarian Oil & Gas Research Institute
(MÁFKI Veszprém)

A. SZÁNTÓ and M. NÁDASY
Research Institute for Heavy Chemical Industries
(NEVIKI Veszprém)

T. BLICKLE and O. BORLAI
Research Institute for Technical Chemistry
of the Hungarian Academy of Sciences
(MÜKKI Veszprém)

A. LÁSZLÓ and L. PÉCHY
Veszprém University of Chemical Engineering
(VVE Veszprém)

Editor-in Chief:
E. BODOR

Assistant Editor:
J. DE JONGE

Veszprém University of Chemical Engineering
(VVE Veszprém)

The „Hungarian Journal of Industrial Chemistry" is a joint publication of the Veszprém scientific institutions of the chemical industry that deals with the results of applied and fundamental research in the field of chemical processes, unit operations and chemical engineering. The papers are published in four numbers at irregular intervals in one annual volume, in the English, Russian, French and German languages

Editorial Office:
Veszprémi Vegyipari Egyetem
„Hungarian Journal of Industrial Chemistry"
H—8201 Veszprém, P. O. Box: 28.
Hungary

Subscription price $ 45.—per volume/per year. Orders may be placed with
KULTURA
Foreign Trading Co. for Books and Newspapers
Budapest 62. POB 149
or with its represenatives abroad, listed on the verso of the cover

FELELŐS SZERKESZTŐ: DR. BODOR ENDRE

KIADJA A LAPKIADÓ VÁLLALAT, 1073 BP. VII., LENIN KRT. 9—11.
TELEFON: 221-285. LEVÉLCÍM: 1906 BP. PF. 223
FELELŐS KIADÓ: SIKLÓSI NORBERT IGAZGATÓ

HUNGARIAN JOURNAL
OF INDUSTRIAL CHEMISTRY
VESZPRÉM
Vol. 6. pp. 333–342 (1978)

TRANSPORT PROCESSES IN PACKED BEDS

M. PARTI

(Department of Chemical Machinery and Agricultural Industries, Technical University, Budapest, Hungary)

Received: April 27, 1978.

According to experimental experiences, it is known that real geometrical conditions appear to be too simplified in the CARMAN capillary model of packed beds, therefore, its application concerning momentum transfer also seems to be impossible. A new hydrodynamic model with varying cross-sections was developed, based upon experimental experiences. Characteristic geometrical dimensions of the model were defined on the basis of the measurement results of momentum transport, and then the correlations accepted for the calculation of transfer coefficients occurring in empty tubes, were applied for the geometrical model. The transport mechanism of packed beds is rather well characterized by the formulas obtained in this way, which can be applied for the calculation of the transport coefficients of these beds with appropriate security.

Introduction

Packed beds play a rather significant role in the different technologies applied in the chemical industry, although the transport processes occurring therein are not yet theoretically sufficiently clarified. Recently a number of papers were published, and with the elaboration of the experimental data an effort was made to give correlations of general validity for the determination of the heat and mass transfer factors [1, 2, 3, 4, 5, 6].

In spite of this, no criterial equations of general validity exist at the moment, which would enable the definition of the heat transfer and mass transfer factors, for every—or nearly every—case, such as for instance, the SIEDER—TATE equations do, for the case of internal flow occurring in empty tubes.

According to literature, the friction factor of packed beds is well characterized by the ERGUN equation [7]. The CARMAN model set up for packed beds gives a lower value for the friction factor than the ERGUN equation.

Therefore, the possibility of setting up a new model with the modification of the CARMAN model, is self apparent, a model being equivalent to packed beds, concerning the pressure losses. In all probability, this model will ap-

proximate the better transport process occurring in packed beds concerning other transport processes.

The suggested new model is set up on the basis of hydrodynamic considerations, the criteria of its validity being the adequate description of the experimental data. In the following, the new model is described and in addition, its characteristics are described and its heat transfer properties are also analyzed.

Hydrodynamic Examination of Packed Beds

CARMAN was the first who endeavoured to convert the hydrodynamic conditions of packed beds to flow conditions occurring in empty tubes, substituting the given irregular pore volume for flow by parallel and straight capillary tubes. These capillary tubes are characterized by the hydraulic equivalent diameter:

$$D_H = 4\frac{F_w}{A_w} = 4\frac{V_p}{F_s}. \tag{1}$$

In the case of the validity of the substitutive model, the pressure loss of the packed beds for given flow conditions can be obtained from the correlation for empty tubes, as:

$$\Delta p = 2\varrho v_p^2 \frac{L}{D_H} f, \tag{2}$$

since the tube friction coefficient for laminar flow [8] is:

$$f = \frac{16}{Re} = \frac{16}{\frac{v_q D_H \varrho}{\eta}}, \tag{3}$$

and its substitution into (2), gives:

$$\Delta p = 32\frac{L}{D_H^2} v_p \eta. \tag{4}$$

The hydraulic equivalent diameter can be further written by the characterization of the particles by a ball diameter, having the same volume as the particles:

$$D_H = \frac{2}{3} D_p \frac{\varepsilon\psi}{1-\varepsilon}. \tag{5}$$

Calculating with the superficial velocity, instead of the real flow velocity arising in the pores:

$$v = \varepsilon v_p. \tag{6}$$

Substituting Equations (5) and (6) into (4), gives:

$$\Delta p = 72\frac{(1-\varepsilon)^2}{\varepsilon^3\psi} \frac{v\eta L}{D_p^2}. \tag{7}$$

According to experimental examinations, the pressure loss of packed beds is rather underestimated by (7). Therefore, the substitutive capillary tube system elaborated by CARMAN, describes the hydrodynamic properties of the packed beds rather unexactly. Experimental results have shown that the constant

of Eq. (7) has to be increased to the ratio 25/12, consequently the pressure loss of the bed will be:

$$\Delta p_B = 150 \frac{(1-\varepsilon)^2}{\varepsilon^3 \psi} \frac{v \eta L}{D_p^2}, \tag{8}$$

which represents the well known BLAKE—KOZENY formula [8]. The quotient of these two terms yields:

$$k = \frac{\Delta p}{\Delta p_B} = \frac{72}{150} = 0.48. \tag{9}$$

The pressure loss of the substitutive model is 48% of the one of packed beds. For the coefficient of Eq. (8) different authors obtained diverse values [8, 9], but the most frequently used one is the BLAKE—KOZENY equation. So at equal velocity, the pressure loss of the packed bed will surpass that of the substitutive model by 110%.

The deviation can be attributed to the following causes:

- the channels in packed beds have no circular cross-section;
- the length of the channels of the packed beds is larger than its height (tortuosity);
- the cross-section of the channels does not remain constant, but expanding and constricting sections follow each other.

However, in our opinion constant changes in the size of the cross-sections have a more significant effect, and can be the cause of the rather considerable portion of the occurring pressure loss and proceeding kinetic energy loss without exception. It seems reasonable, therefore, to substitute the channels of constant cross-sections in the substitutive model by CARMAN, by periodically changing channels—although kept constant by sections. The CARMAN model and the new substitutive model are demonstrated together with the effective bed in *Fig. 1.*

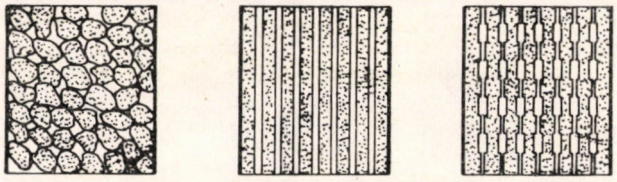

Fig. 1.
Packed beds and its substitutive models

The substitutive system is set up considering the following conditions:

- the narrower and wider sections (diameters: D_1 and D_2, resp.) repeat periodically and have equal length, i.e.:

$$D_1 < D_H = D_0 < D_2 \tag{10.a}$$

and

$$L_1 = L_2 = \frac{L}{2}; \tag{10.b}$$

— the volume of the substitutive system with changing cross-sections is equal to the volume of the substitutive system of the constant cross-section (i.e.: to the volume of the pores). Hence:

$$2D_0^2 = D_1^2 + D_2^2. \tag{11}$$

In order to determine both diameters, the following requirements have to be prescribed:

— the pressure loss of the substitutive system, having varying cross-sections, should correspond to the pressure loss of the packed bed (i.e. to the pressure loss of the system of constant cross section), namely:

$$\Delta p_0 = \Delta p_1 + \Delta p_2$$

and applying Eq. (4), resp.,

$$2\frac{v_{p0}}{D_0^2} = \frac{v_1}{D_1^2} + \frac{v_2}{D_2^2} \tag{12}$$

will be obtained.

— the superficial velocity of the new substitutive system should correspond to that one of the packed bed, or rather:

$$v_1 D_1^2 = v_2 D_2^2 = k v_{p0} D_0^2. \tag{13}$$

The equation (11) must be solved, applying the prescriptions of Equations (12) and (13). The solution is the function of the constant k, referred to Eq. (9):

$$\begin{aligned} D_i &= c_i D_0, \\ c_1 &= 0.72, \\ c_2 &= 1.22. \end{aligned} \tag{14}$$

Summarizing the foregoing, it can be seen that the physical model substituting the packed bed, can be considered as a tube bundle of circular cross-section, the average diameter of which can be obtained by Eq. (5), although the tube diameter is not constant, but, it can be assumed that the half length of the tube sections have diameter D_1, while the other half length has diameter D_2. The intercorrelation of the characteristic diameters is expressed by Eq. (14).

With the knowledge of the dimensions of the geometric model the pressure loss of the system can be defined. This pressure loss consists of two portions: the pressure loss of the straight tube sections and that one of the sudden changes of the cross-sections. The pressure loss of the straight tube sections, according to Eq. (2) can be written as:

$$\Delta p_1 = 2\varrho v_1^2 \frac{L_1}{D_1} f_1 + 2\varrho v_2^2 \frac{L_2}{D_2} f_2. \tag{15}$$

With the application of continuity, the effective velocity and effective friction coefficient can be defined and following Leva [9], we can write:

$$f_i = a Re_i^{n-2}$$

this yields:

$$\Delta p_1 = 2 v_e^2 \varrho \frac{L}{D_0} f_e \frac{c_1^{-3-n} + c_2^{-3-n}}{2} \tag{16.a}$$

and in shorter form:

$$\Delta p_1 = 2\varrho v_e^2 \frac{L}{D_0} f_e \frac{E}{2}, \tag{16.b}$$

where:

$$E = c_1^{-3-n} + c_2^{-3-n}. \tag{17}$$

For laminar flow and introducing the particle REYNOLDS number:

$$\Delta p_1 = 2\varrho v_e \frac{L}{D_0}\left[12E \frac{1-\varepsilon}{\psi Re_p}\right], \tag{18}$$

where:

$$Re_p = \frac{D_p v \varrho}{\eta}. \tag{19}$$

The pressure loss, due to the sudden changes of the cross sections, consists of two portions: the pressure loss at the sudden expansion and at the sudden restriction of the tube, respectively. Its first term can be written as a BORDA — CARNOT loss, while the second one can be expressed by the usual loss coefficient, namely:

$$\Delta p_2 = \beta\left[\frac{\varrho}{2}(v_1 - v_2)^2 + \frac{\varrho}{2} v_1^2 \xi\right] \tag{20.a}$$

and it can be assumed, that:

$$\beta \cong \frac{L}{D_0},$$

therefore:

$$\Delta p_2 = \frac{\varrho}{2} v_e^2 \frac{L}{D_0} F, \tag{20.b}$$

where:

$$F = \frac{1}{c_1^4}\left[\left(1 - \frac{c_1^2}{c_2^2}\right)^2 + \xi\right]. \tag{21}$$

The total pressure loss of the packed bed is the sum of Equation (18) and (20) as:

$$\Delta p = 2\varrho v_e^2 \frac{L}{D_0}\left(12E \frac{1-\varepsilon}{\psi Re_p} + \frac{F}{4}\right). \tag{22}$$

If Eq. (22) is compared with Eq. (2), the friction coefficient of the packed bed:

$$f = \frac{50(1-\varepsilon)}{Re_p} + 0.67. \tag{23}$$

For the friction coefficient defined by Eq. (2). ERGUN [7] obtained a correlation, the structure of wich completely corresponded to Eq. (23) (the additive term is 0.583 instead of 0.67).

Thus the developed geometric model describes the packed bed correctly, concerning pressure losses. It can be expected that with the application of this model further transport processes can also be described. In the following, examinations will be carried out for heat transfer.

Heat Transfer in Packed Beds

In the last thirty to forty years, significant experimental work was carried out to examine the heat transfer conditions of packed beds, of wich an excellent summarization is presented by BARKER [6]. According to experimental measurements, two authors tried to set up criterial equations of general validity. GUPTA et al. [2] stated that the heat transfer factor is inversely proportional to the porosity of the bed, and in their opinion the experimental results can be described by the following correlation:

$$\varepsilon j_H = \frac{2.876}{Re_p} + \frac{0.3023}{Re_p^{0.35}} \tag{24}$$

which can be applied in the following range:

$$10 < Re_p < 10{,}000.$$

WHITAKER [1] obtained the following correlation:

$$\varepsilon j_H = \left[0.4 \left(\frac{1-\varepsilon}{Re_p}\right)^{1/2} + 0.2 \left(\frac{1-\varepsilon}{Re_p}\right)^{1/3}\right] Pr^{0.07}. \tag{25}$$

The applicability ranges are:

$$3.7 \leqq \frac{Re_p}{1-\varepsilon} \leqq 8{,}000,$$

$$Pr \cong 0.7,$$

$$0.34 \leqq \varepsilon \leqq 0.74.$$

The difference between Eq. (24) and Eq. (25) can be seen at the first glance, appearing in the exponent of the REYNOLDS number and in the dependency on porosity. Numerically Eq. (25) will always produce a smaller value for the heat transfer factor than Eq. (24) does. The deviation with the small REYNOLDS numbers may also attain 60%. Instead of continuing the analysis of the experimental data, the heat transfer coefficient and the heat transfer factor will be defined for the model, developed in the foregoing chapter, taking into consideration the following conditions:

- in the tube of diameter D_1 the flow is laminar, its velocity is v_1;
- the fluid enters the tube of diameter D_2 practically with diameter D_1 (and therefore having velocity v_1), but due to the sudden change of the cross-section the flow turns turbulent, forming eddies in the ring of width $(D_2 - D_1)$;
- in the above mentioned ring, no temperature gradient exists (i.e. the temperature gradient can be neglected due to the intensive eddies), thus heat transfer essentially occurs at the wall of diameter D_2.

For the determination of the heat transfer coefficient in the laminar region, the SIEDER—TATE correlation can be applied based upon the GRAETZ solution [10], which describes the experimental results with an accuracy of $\pm 12\%$, except water, i.e.:

$$Nu = 1.86 \left(RePr \frac{D}{L}\right)^{1/3} \varphi^{0.14} \tag{26}$$

if:

$$\left(RePr\frac{D_1}{L}\right)^{1/3} < 2.$$

For turbulent flow, the adequate SIEDER—TATE correlation is again applied [10], which can be used with an accuracy of +15% and −10%, respectively, i.e.:

$$Nu = 0.027 Re^{0.8} Pr^{1/3} \varphi^{0.14} K. \tag{27}$$

According to publications, the latter correlation can also be rather safely applied to the transition region, where the flow conditions are unstable.

For the application of Eqs (26) and (27), the REYNOLDS number and NUSSELT number must be modified, using the packed bed characteristics. Thus:

$$Re_1 = \frac{v_1 D_1 \varrho}{\eta} = \frac{v_0 D_0 \varrho}{\eta} \frac{v_1 D_1}{v_0 D_0} = \frac{2}{3} \frac{\psi}{1-\varepsilon} \frac{Re_p}{c_1} \tag{28.a}$$

and:

$$Nu_1 = \frac{\alpha_1 D_1}{\lambda} = \frac{2}{3} \frac{\varepsilon\psi}{1-\varepsilon} c_1 Nu_{p1}, \tag{28.b}$$

where:

$$Nu_{p1} = \frac{\alpha_1 D_p}{\lambda}. \tag{29}$$

The characteristic simplex is:

$$\frac{D_1}{L_1} = \frac{D_0}{L_1} \frac{D_1}{D_0} = c_1 \frac{2}{3} \frac{\varepsilon\psi}{1-\varepsilon} \frac{D_p}{L_1}.$$

Let:

$$\beta = \frac{L_1}{D_p} \tag{30}$$

then:

$$\frac{D_1}{L_1} = \frac{2}{3} \frac{\varepsilon\psi}{1-\varepsilon} \frac{1}{\beta} c_1. \tag{31}$$

Substituting Equations (28), (29) and (31), and Eq. (26) can be written as:

$$Nu_{p1} = \frac{1.86}{c_1} \frac{1.5^{1/3}}{\beta^{1/3}} \left(\frac{1-\varepsilon}{\varepsilon^2\varphi}\right)^{1/3} Re_p^{1/3} Pr^{1/3} \varphi^{0.14}. \tag{32}$$

If the transformation is also similarly carried out for the turbulent region, applying the former conditions, Eq. (27) becomes:

$$Nu_{p2} = \frac{0.027K}{c_1^{1.8}} 1.5^{0.2} \left(\frac{1-\varepsilon}{\psi}\right)^{0.2} \frac{1}{\varepsilon} Re_p^{0.8} Pr^{1/3} \varphi^{0.14}. \tag{33}$$

The constant K in Equations (27) and (32), resp., takes into consideration the SIEDER—TATE formula related to a developed flow pattern, but due to the short length of the channel this cannot be relied upon. According to the preconditions, the halflength of the channel bears diameter D_1, while for the other half length the diameter is D_2. If it is assumed that the length of the channels corresponds to the particle diameter, then:

$$L_1 = L_2 = D_p/2 \quad \text{and} \quad \beta = 0.5.$$

Thus, the coefficient considering the unsettled nature of the flow pattern is $K = 1.9$, based upon reference [11]. If the heat transfer coefficient and the NUSSELT number, resp., of both sections are averaged for the total channel length, we obtain:

$$Nu_p = \frac{c_1 \beta Nu_{p1} + c_2(1-\beta) Nu_{p2}}{c_1 \beta + c_2(1-\beta)} \tag{34.a}$$

and with substitution of the constants:

$$Nu_p = 0.36 Nu_{p1} + 0.64 Nu_{p2} \tag{34.b}$$

Substituting Equations (32) and (33) into Eq. (34)

$$Nu_p = \left[1.4 \left(\frac{1-\varepsilon}{\psi \varepsilon^2} Re_p\right)^{1/3} + 0.068 \frac{1}{\varepsilon} \left(\frac{1-\varepsilon}{\psi}\right)^{0.2} Re_p^{0.8}\right] Pr^{1/3} \varphi^{0.14} \tag{35}$$

is obtained.

The heat transfer factor:

$$j_H = 1.4 \left(\frac{1-\varepsilon}{\psi \varepsilon^2}\right)^{1/3} Re_p^{-2/3} + 0.068 \frac{1}{\varepsilon} \left(\frac{1-\varepsilon}{\psi}\right)^{0.2} Re_p^{-0.2} \tag{36}$$

where for gas systems: $\varphi^{0.14} \simeq 1$ has been assumed.

Transformation of Eq. (36) yields:

$$j_H \varepsilon = \frac{1.4[\varepsilon(1-\varepsilon)]^{1/3}}{Re_p^{2/3}} + \frac{0.068(1-\varepsilon)^{0.2}}{Re_p^{0.2}}. \tag{37}$$

For the comparison of Equations (24), (25) and (37) with the experimental results, calculations were carried out. *Fig. 2* shows the curves obtained for

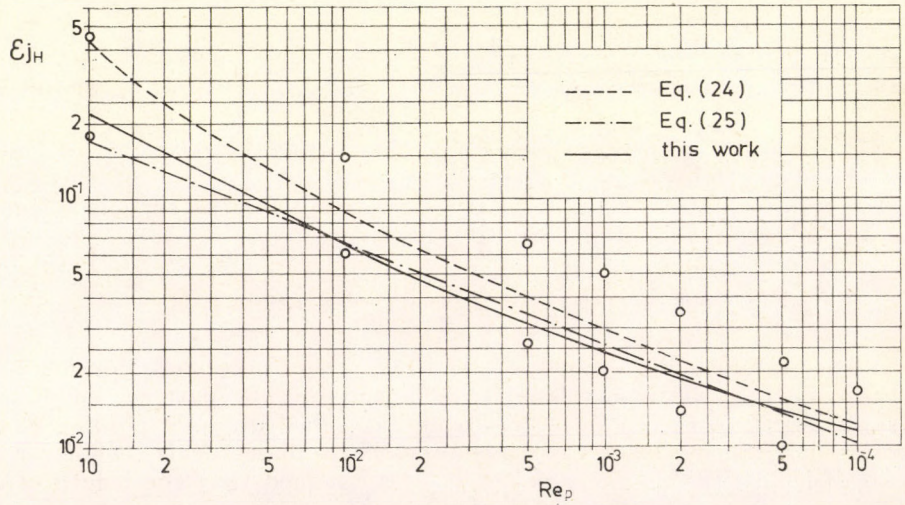

Fig. 2.
Product of heat transfer factor and porosity vs. REYNOLDS number

the porosity value $\varepsilon = 0.4$, denoting the scattering range of measurements. On the basis of the comparison, it is evident that by means of the developed geometric model, packed beds can be very well characterized, also regarding the heat transfer.

Finally, summarizing the foregoing, it can be stated that although the developed new model contains many presumptions (the majority of which are natural presumptions based upon experience), but considering the momentum transfer as well as the heat transfer, the transport mechanism of packed beds can be rather well characterized by it (at least in the case of the most general solid-gas systems), and Eq. (37) may be applied for the calculation of the heat transfer factor in the following range:

$$10 < \mathrm{Rep} < 10{,}000.$$

SYMBOLS

A = surface area, m^2;
a = surface area per unit volume, m^2/m^3;
c = coefficient;
D = diameter, m;
E = constant;
F = constant;
F = cross-section, m^2;
f = FANNING friction coefficient;
j_H = heat transfer factor;
K = coefficient;
k = constant;
L = length, m;
P = periphery, m;
p = pressure, N/m^2;
V = volume, m^3;
v = velocity, m/s;
α = heat transfer coefficient, W/m^2K;
β = geometrical simplex;
Δ = difference;
ε = porosity;
η = dynamic viscosity, kg/ms;
λ = thermal conductivity, W/mK;
ϱ = mass density, kg/m^3;
φ = viscosity number;
ψ = sphericity.

Dimensionless numbers

Nu = NUSSELT number;
Pr = PRANDTL number;
Re = REYNOLDS numbers.

Indices

0, 1, 2 = serial indices;
B = calculated by the BLAKE formula;
e = effective;
H — hydraulic;
i = serial index;
p = referring to pore and solid particle, respectively;
s = referring to solid media;
w = wetted.

REFERENCES

1. Whitaker, S.: Elementary Heat Transfer Analysis, Pergamon press, New York, 1976.
2. Gupta, S. N., Chsube, R. B. and Upadhyay, S. N.: Chem. Eng. Sci., *29*, 839 (1974).
3. Ergun, S.: Chem. Eng. Prog., *48*, 227 (1952).
4. Kumar, S., Upadhyay, S. N. and Mathur, V. K.: Ind. Eng. Chem., Process Des. Dev., *16*, 1 (1977).
5. Dwivedi, P. N. and Upadhyay, S. N.: Ind. Eng. Chem., Process Des. Dev., *16*, 157 (1977).
6. Barker, J. J.: Ind. Eng. Chem., *57*, 43 (1965).
7. Ergun, S.: Chem. Eng. Prog., *48*, 89 (1952).
8. Bird, R. B., Stewart, W. E. and Lightfoot, E. N. Transport Phenomena, Wiley, New York, 1960.
9. Leva, M.: Fluidization, McGraw Hill, New York, 1959.
10. Kern, D. Q.: Process Heat Transfer, McGraw Hill, New York, 1950.
11. Bennet, C. O. and Myers, J. E.: Momentum, Heat and Mass Transfer, McGraw Hill Book Co., New York, 1974.

РЕЗЮМЕ

На основе результатов экспериментов известно, что капиллярная модель Кармана для насадочных слоёв слишком упрощает действительные геометрические соотношения, поэтому её применение для передачи импульса невозможно. Исходя из экспериментальных наблюдений, авторами была составлена новая гидродинамическая модель с изменяющимся разрезом. Характерные геометрические размеры модели были установлены на основе измерений переноса импульса, а затем к этой геометрической модели прикладывались зависимости, общепринятые для расчёта коэффициентов переноса процессов, происходящих в пустых трубах. Полученные таким образом зависимости очень хорошо характеризуют механизм переноса во множествах с насадкой, и с достаточной надёжностью могут быть использованы для расчёта коэффициентов переноса указанных множеств.

HUNGARIAN JOURNAL
OF INDUSTRIAL CHEMISTRY
VESZPRÉM
Vol. 6. pp. 343–350 (1978)

PARTICLE FORMATION FROM SOLUTIONS IN GAS FLUIDIZED BEDS. IV.

DETERMINATION OF AVERAGE PARTICLE SIZE AND SOLID MATERIAL FEED RATIO

B. Dencs and Z. Ormós

(Research Institute for Technical Chemistry
of the Hungarian Academy of Sciences, Veszprém, Hungary)

Received: May 3, 1978.

Two calculations methods used in practice are presented. Both in research and industrial practice, there are frequent calls for the calculation of average steady particle size from known operation and process parameters. The calculation method presented here can be used for this purpose if the primary growth mechanism in surface layering. In our opinion the accuracy of the method is sufficient. In general, the average particle size desired is predetermined for the various industrial products. Therefore, the second calculation method shown here permits the determination of the initial solid material feed ratio ensuring the average particle size desired.

Calculation of the Average Particle Size

One of the most important physical characteristics of granules produced from solutions in gas fluidized beds is the average particle size. In *Part 3* of this series [1] it was shown that the particle size range of various materials was approximately the same when particle growth took place mainly via surface layering. At the same time, the distribution curves were also similar. If the above particle size range is known and the average particle size can, somehow, be calculated, then it can be determined whether the product granules fulfil the requirements, at least as far as the average particle size is concerned.

The solid material mass balance equation of particle formation from solutions in gas fluidized beds (direct particle formation, for short) was modified to allow for the preliminary estimation of product average particle size in those cases where the primary growth mechanism is surface layering.

The mass balance equation of direct particle formation reads:

$$\dot{G}_{\text{in}} + c'w' = \dot{G}_{\text{out}} + \dot{K}. \tag{1}$$

The mass flow of the solid material leaving the system in steady state conditions can be written as:

$$\dot{G}_{out} = \frac{\overline{d}_{out}^3 \pi}{6} \overline{\varrho}_{s_{out}} \dot{N}_{out}. \tag{2}$$

In the case of ideal surface layering, neither agglomerization nor disintegration take place in the fluidized bed. Correspondingly, the number of particles introduced into and taken out of the bed is equal in steady state conditions. In practice, as it was demonstrated in *Parts 1* to 3 of this series [1–3], agglomerization and disintegration always accompany surface layering. In this case, the values of the input and output numerous flows are slightly different as given by the following relationship:

$$\dot{N}_{out} = b\dot{N}_{in}. \tag{3}$$

If $b<1$ then agglomerization, if $b>1$ then disintegration takes place in the fluidized bed.

The numerous flow of particles entering the system is:

$$\dot{N}_{in} = \frac{6\dot{G}_{in}}{\overline{d}_{in}^3 \overline{\varrho}_{s_{in}}}. \tag{4}$$

Solid material feed ratio is defined as:

$$B = \frac{\dot{G}_{in}}{\dot{G}_{in} + c'w'} \tag{5}$$

from which the mass flow rate of the solid material fed into the system can be expressed as:

$$\dot{G}_{in} = \frac{Bc'w'}{1-B}. \tag{6}$$

Let us substitute Equations (2), (3), (4) and (6) into Equation (1). The average particle size of the solid material leaving the system in steady state conditions can be obtained after substitution and rearrangement as:

$$\overline{d}_{out} = \overline{d}_{in} \left[\frac{1}{bB} \left(1 - \frac{\dot{K}(1-B)}{c'w'} \right) \frac{\overline{\varrho}_{s_{in}}}{\overline{\varrho}_{s_{out}}} \right]^{1/3}. \tag{7}$$

Experiments were carried out with particulate, solid material of $\bar{\varepsilon}_p < 0.05$, correspondingly the actual and particle densities were approximately equal [1–3]:

$$\overline{\varrho}_{s_{in}} \approx \varrho. \tag{8}$$

The average particle density of the solid material leaving the system in steady state conditions can be approximated as [4]:

$$\overline{\varrho}_{s_{out}} = \varrho(1 - \bar{\varepsilon}_{p_{out}}). \tag{9}$$

The relationship used to calculate the average particle size of the solid material leaving the system in steady state conditions can be obtained after

substitution of Equations (8) and (9) into Equation (7) and rearrangement:

$$\bar{d}_{\text{out}} = \bar{d}_{\text{in}} \left[\frac{1}{bB(1-\bar{\varepsilon}_{p_{\text{out}}})} \left(1 - \frac{\dot{K}(1-B)}{c'w'} \right) \right]^{1/3}. \tag{10}$$

The solid material feed ratio, B; average input particle size, $\bar{d}_{\text{in}}$; solution concentration, c' and atomization rate w' are the independent parameters in the above equation. The average porosity of the solid material leaving the system $\bar{\varepsilon}_{p_{\text{out}}}$ and the mass flow rate of fine dust carried out ($\dot{K}$) were obtained from the results of the experiments. The results obtained can also be used as good approximating values under different experimental conditions.

In the case of particles grown by surface layering it can be assumed that $b \approx 1$, i.e. changes of the numerousness of the particles in the bed due to agglomerization or disintegration are negligible, or rather their effects are complimentary. The average particle size of the product obtained in steady state conditions was calculated using Equation (10) and compared with the results of sieve analysis (cf. *Fig. 1*). It was found that the difference between

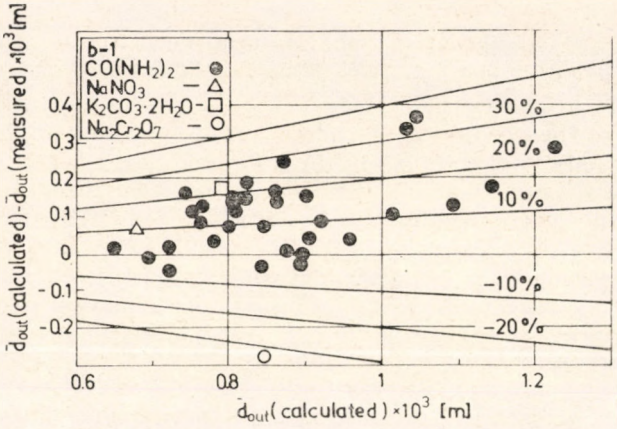

Fig. 1

the calculated and measured average particle size was less than 20% for at least 78% of the experimental runs.

Numerical values of b were also obtained for all experiments. It was found that in the case of surface layering growth mechanism $0.7 < b < 1$, 4, the most frequent value was close to 1. At the same time, it could not be proved unequivocally that changing the operation and process parameters effected the value of b. In the case of particle growth via agglomerization b values significantly different from 1 were obtained ($Na_2Cr_2O_7$:0.21; K_3PO_4:0.03). Using then known b values and Equation 10, the average particle size was recalculated and compared with measured values (cf. *Fig. 2*). In the case of $b \neq 1$ the difference between calculated and measured values did considerably decrease, being less than 20% in all cases and less than 15% in 84% of the cases.

It can be concluded from these results that in the case of particle growth taking place via surface layering the average particle size of the solid material leaving the fluidized bed in steady state conditions can be estimated by Equation 10.

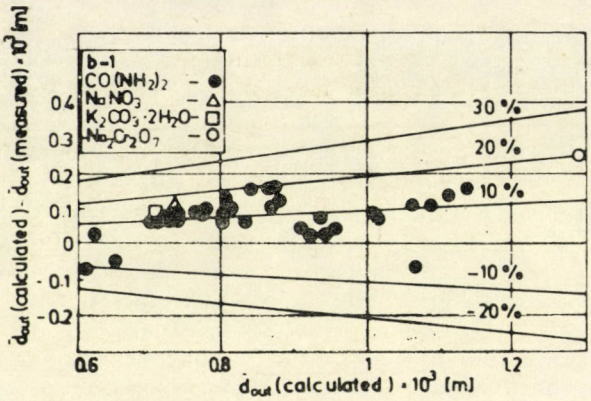

Fig. 2

Calculation of Solid Material Feed Ratio

In practical direct particle formation it is very important that physical characteristics of the product meet certain preset requirements. These requirements vary widely, depending on the intended use of the product. Most frequently, the average particle size and the particle size range of a given major percentage of the product are specified (e.g. in the case of pelletizing machines).

Attempts were made to calculate the solid material feed ratio required to ensure a given average particle size. The balance equation of direct particle formation expressed by numerous flows was used in the calculations:

$$\dot{N}_{\text{in}} + \dot{Q}(t) - \dot{N}_{\text{out}}(t) = \frac{dN_{\text{R}}(t)}{dt}. \tag{11}$$

The following relationships were substituted into Equation (11):

$$\dot{N}_{\text{in}} = n_{\text{in}}\dot{G}_{\text{in}},$$

$$\dot{N}_{\text{out}} = n_{\text{out}}\dot{G}_{\text{out}},$$

$$N_{\text{R}} = n_{\text{R}}G_{\text{R}},$$

$$\dot{Q} = qG_{\text{R}}.$$

Thus, numerous flows were expressed by specific numerousness and source terms were made independent from the mass of the fluidized bed. The equation thus obtained can be rearranged by using the solid material balance equation of direct particle formation [Equation (1)] and the definition equation of solid material feed rate ratio [Equation (5)] can be read as:

$$\frac{Bc'w'}{(1-B)G_{\text{R}}} n_{\text{in}} + q(t) - \frac{c'w'}{(1-B)G_{\text{R}}} n_{\text{out}}(t) = \frac{dn_{\text{R}}(t)}{dt}. \tag{12}$$

It is noted that the mass flow rate of dust precipitated in the cyclone is also present in the solid material balance equation. Calculations would become extremely involved by attempts to account for this flow as well. Since it is only a fraction of the overall mass flow rate it can be neglected without introducing significant errors.

Based on experimental results, the $q(t)$ relationship was examined in steady state conditions. It was concluded that $q(t)$ approached a limiting value irrespective of the values of the solid material feed rate ratio and average initial particle size (cf. *Fig. 3*). In the case of urea the limiting value is:

$$q_\infty = 0.3 \times 10^6 \text{ particle/kgh.}$$

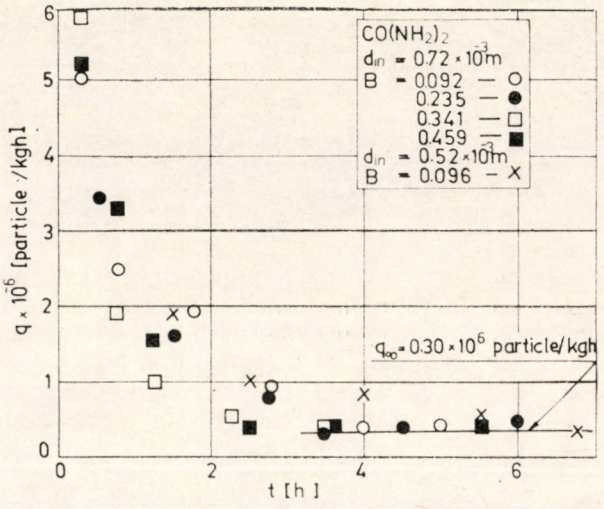

Fig. 3

Equation (12) reads in steady state conditions as:

$$\frac{Bc'w'}{(1-B)G_R} n_{in} + q_\infty - \frac{c'w'}{(1-B)G_R} n_{out} = 0. \tag{13}$$

If Equation (13) is rearranged for the solid material feed, rate ratio (B) and the relationships describing input and output numerousness values are substituted as:

$$n_{in} = \frac{1}{\frac{\overline{d_{in}^3}\pi}{6} \varrho_{s_{in}}},$$

$$n_{out} = \frac{1}{\frac{\overline{d_{out}^3}\pi}{6} \varrho_{s_{out}}}$$

then the following equation is obtained:

$$B=\frac{c'w'\dfrac{6}{\bar{d}_{\text{out}}^3\pi\bar{\varrho}_{s_{\text{out}}}}-q_\infty G_R}{c'w'\dfrac{6}{\bar{d}_{\text{in}}^3\pi\bar{\varrho}_{s_{\text{in}}}}-q_\infty G_R}. \tag{14}$$

Solid material feed rate ratios required to produce granules of various average particle size were calculated with Equation (14). The parameters of the equation were selected to represent the effective values of the parameters used in the actual experiments aimed at determining the effects of solid material feed rate ratio [2]. Thus calculated and measured values could be compared.

The following parameter values were used for the calculations:

$$\begin{aligned} c' &= 500 \text{ kg/m}^3, \\ w' &= 3.8\times10^{-4} \text{ m}^3/\text{h}, \\ q_\infty &= 0.3\times10^6 \text{ particle/kgh}, \\ G_R &= 0.44 \text{ kg}, \\ \bar{d}_{\text{in}} &= 0.72\times10^{-3} \text{ m}, \\ \bar{\varrho}_{s_{\text{in}}} &= 1270 \text{ kg/m}^3, \\ \bar{\varrho}_{s_{\text{out}}} &= 1100 \text{ kg/m}^3. \end{aligned}$$

Values of the $B(\bar{d}_{\text{out}})$ function, calculated using the above parameters and Equation (14), are plotted in *Fig. 4* along with the experimental values.

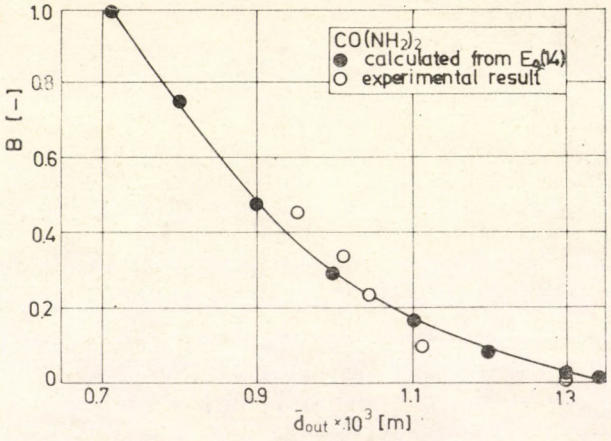

Fig. 4

According to the tendency obtained from Equation (14), average particle size decreases with the increasing solid material feed rate ratio. The agreement between calculated and measured values over the range studied is satisfactory. The calculation method was checked against experimental results obtained with sodium nitrate, potassium carbonate, sodium dichromate, ammonium nitrate and tris potassium phosphate, and also those of reference [1]. The

difference between calculated and measured values for the above test substances was less than 25%.

The test-substance-depending parameters required for the calculations ($\overline{\varrho}_{s_{out}}$, q_∞) can be obtained from a single experiment. The calculation method shown here can be used equally well for surface layering and agglomerization particle growth mechanisms to obtain the solid material feed rate ratio which ensures a product of predetermined average particle size.

SYMBOLS

b: proportionality coefficient characterizing changes of the numerousness, (−);
B: solid material feed rate ratio, (−);
c': concentration of the solution, kg/m³;
d: particle size, m;
G: mass of the solid material, kg;
$\dot{G}$: solid material mass flow rate, kg/h;
$\dot{K}$: flying dust mass flow rate, kg/h;
n: specific numerousness, kg⁻¹;
N: numerousness, particle;
$\dot{N}$: numerous flow, h⁻¹;
q: specific particle source in the fluidized bed, kg⁻¹ h⁻¹;
$\dot{Q}$: particle source in the fluidized bed, h⁻¹;
t: time, h;
w': atomization rate, m³/h;
ϱ: actual density of the solid material, kg/m³;
ϱ_s: particle density, kg/m³;
ε_p: void volume fraction, (−).

Subscripts

in: input value:
out: output value;
$^-$: average value;
R: value relating to the fluidized bed;
∞: limiting value at $t \to \infty$.

REFERENCES

1. Dencs B. and Ormós Z.: Hung. J. Ind. Chem., *6*, 323 (1978).
2. Dencs B. and Ormós Z.: Hung. J. Ind. Chem., *6*, 301 (1978).
3. Dencs B. and Ormós Z.: Hung. J. Ind. Chem., *6*, 313 (1978).
4. Ormós Z.: Hung. J. Ind. Chem., *1*, 207 (1973).

РЕЗЮМЕ

В данной статье приводятся два расчётных метода, применимых на практике. В производственной практике и в ходе проведения исследований часто может возникнуть необходимость в заблаговременном определении среднего размера частиц твёрдого материала на выходе, в случае стационарного режима и известных процессионных и режимных характеристик. Для этой цели пригоден показанный расчётный метод в том случае, если частицы основного материала увеличиваются в первую очередь путём поверхонстного наслоения. По мнению авторов точность данного метода можно считать удовлетворительной. в ходе осуществления каждого конкретного задания обычно предписывается каков должен быть средний размер производимого продукта. Другой расчётный метод даёт возможность для приближённого расчёта пропорции вводимого твёрдого материала, необходимого для производства продукта с заданным наперёд средним размером гранул.

HUNGARIAN JOURNAL
OF INDUSTRIAL CHEMISTRY
VESZPRÉM
Vol. 6. pp. 351–360 (1978)

ZUR GLEICHGEWICHTSBERECHNUNG UND BEWERTUNG GASFÖRMIGER ENERGIETRÄGER BEI HOCHTEMPERATURPOZESSEN

FRATZSCHER, W., HEBECKER, D. und GAFFKE, H.

(Technische Hochschule „Carl Schorlemmer" Leuna-Merseburg,
Sektion Verfahrenstechnik)

Eingegangen am 20. July, 1978

In der Arbeit wurden Gase, bei deren Dissoziation komplexe Stoffsysteme entstehen, hinsichtlich ihrer Eigenschaften als Energieträger im Temperaturintervall $(1-6)\times 10^3 K$ bei einem Druck von 1 bar untersucht. Dabei eignen sich (von den betrachteten Gasen) in energetischer Hinsicht besonders H_2O, NH_3 und H_2S, während eine exergetische Analyse die relativ großen Verluste, die bei der Verwendung von NH_3 als Energieträger in Kauf genommen werden müssen, deutlich aufgezeigt.

Hochtemperaturprozesse haben u. a. im Rahmen der angewandten Plasmachemie große Bedeutung erlangt und sind in verschiedenen Wirtschaftszweigen vom großen Interesse (z. B. chemische, metallurgische, elektronische Industrie). Gründe für die Realisierung derartiger Prozesse sind insbesondere:

- Verschiebung der Gleichgewichtslage auf die Seite erwünschter Produkte,
- wachsende Reaktionsgeschwindigkeiten mit ansteigender Temperatur und daraus resultierende Miniaturisierung der geometrischen Abmessungen chemischer Reaktoren,
- Möglichkeit zur Verwirklichung hoher Reinheitsförderungen und Qualitätsverbesserung von Produkten.

Eine wesentliche Voraussetzung für die Realisierung plasmachemischer Prozesse stellt die geeignete Bereitstellung der Energie dar, die zur zielgerichteten Umwandlung von Rohstoffen in Produkte notwendig ist. Daher ist der Untersuchung der Eigenschaften von Energieträgern, insbesondere in energetischer Hinsicht, bereits Aufnerksamkeit gewidmet worden [1, 2]. In [1] erfolgte die Analyse des energetischen und exergetischen Verhaltens einfacher, molekularer gasförmiger Substanzen (F_2, Cl_2, S_2, O_2, N_2, H_2). Im weiteren soll die Diskussion auf komplexere Stoffsysteme ausgedehnt werden, wobei vor allem wieder der Wert der transportierbaren spezifischen Energie und die Temperatur, bei der diese bereitgestellt wird, von Interesse ist.

Im für Stoffwandlungsprozesse (unter dem hier betrachteten Aspekt) nutzbaren Temperaturbereich von etwa $(1-5)\times 10^3 K$ und bei mittleren Drücken (<50 bar) wird eine Reihe von Gasen teilweiser oder nahezu vollständiger Dissoziation unterworfen, während Ionisation im allgemeinen keine signifikante Rolle spielt. Es ist daher das Vorhandensein komplexer Stoffsysteme zu erwarten, die vorwiegend aus Molekülen, Atomen und Radikalen der als Energieträger eingesetzten Substanz bestehen.

Unter der Voraussetzung, daß sich das reagierende Stoffgemisch im Zustand des thermodynamischen Gleichgewichtes befindet, kann bei fixierten Werten von Druck und Temperatur die Zusammensetzung eindeutig bestimmt werden, wenn die Mengenrelationen des Gemisches im Anfangszustand ebenfalls bekannt sind. Bei gegebener Zusammensetzung lassen sich Enthalpie- und Entropiewerte des Stoffsystems nach einfachen thermodynamischen Beziehungen ermitteln.

Bestimmung der Gleichgewichtszusammensetzung chemisch reagierender gasförmiger Systeme

Bekanntlich ist eine explizite Formulierung der Bedingungen des thermodynamischen Gleichgewichtes für die verschiedensten Spezialfälle auf rein mathematischen Wegen aus der allgemeinen Gibbs'schen Relation ableitbar. Man gewinnt dabei letztlich die Aussage, daß alle thermodynamischen Potentiale im stabilen Gleichgewicht einen minimalen Wert annehmen [3]. Wird zweckmäßiger Weise auf die Formulierung für die freie Enthalpie zurückgegriffen, folgt für eine chemische Reaktion l zwischen den Konstituenten $\bar{l}$ (bei realisiertem thermischen und mechanischen Gleichgewicht) die Bedingung

$$\sum \nu_{li}\mu_l = 0 \tag{1}$$

wobei μ_l — chemisches Potential des Species l,
ν_{li} — stöchiometrischer Koeffizient des l-ten Species in der i-ten Reaktion.

Es soll nun ein aus n Species (Y_i) bestehendes, reagierendes System idealer Gase (eine Voraussetzung, die im angegebenen Bereich der intensiven Parameter anwendbar ist) betrachtet werden, die sämtlich als nach der Beziehung

$$Y_i = \sum_l^m \Phi_{li} X^{(l)} \tag{2}$$

(Φ_{li} — Anzahl der Atome l im Bestandteil i) in ihre m Elemente $x(l)$ zerfallend gedacht werden können. Die Y_i setzen sich aus den Elementen gemäß

$$Y_i = X_{\Phi_{1i}}^{(1)} X_{\Phi_{2i}}^{(2)} \ldots X_{\Phi_{mi}}^{(m)} \tag{3}$$

zusammen. Wegen (1) muß daher gelten (für ideale Gase), daß

$$\sum_l^m \Phi_{li}\left[\mu_l^0(T, p^\circ) + RT \ln\left(\frac{p}{p^\circ}\right) + RT \ln x_l\right] - \mu_i^0(T, p^\circ) - RT\left[\ln\left(\frac{p}{p^\circ} + \ln x_i\right]\right] = 0, \tag{4}$$

bzw.

$$\sum_{l}^{m} \Phi_{li} \ln x_l - \ln x_i = \left[\mu_i^0 - \sum_{l}^{m} \Phi_{li} \mu_l^0 \right] \frac{1}{RT} + \left(1 - \sum_{l}^{m} \Phi_{li} \right) \ln \left(\frac{p}{p^\circ} \right)$$

($^\circ$ — Referenzzustand, x — Molanteil.)

Man erhält $(n-m)$ Bedingungen (4) für alle Species i, die nicht atomar vorliegen. Weiterhin steht die Normierungsbeziehung

$$\sum_{i=1}^{n} X_i = 1$$

oder

$$\ln \left(\sum_{i}^{n} x_i \right) = 0 \tag{5}$$

zur Verfügung. Die restlichen $(m-1)$ Relationen zur eindeutigen Bestimmung der x_i, $i=1$ (1) n, können aus Massenbilanzen oder, hier zweickmäßiger, aus der Bilanzierung der Atome gewonnen werden. Dafür läßt sich angeben, daß

$$\sum_{i}^{n} \Phi_{li} n_i = b_l n_R \qquad l = 1(l)m$$

rsp.

$$\sum_{i}^{n} \Phi_{li} x_i = b_l \frac{n_R}{n} \tag{6}$$

gelten muß [n_R — Molzahl einer fiktiven Anfangssubstanz, n_i — Molzahl des Species i im Gemisch, b_l — charakterisiert die Zusammensetzung der Anfangssubstanz analog Beziehung (3)].

Da nur $(m-1)$ Relationen erforderlich sind, kann eine relative Darstellung mit Bezug auf z. B. Basiskomponente $l=1$ gewählt werden, wofür (6) zu

$$\frac{\sum_{i}^{n} \Phi_{li} x_i}{\sum_{i}^{n} \Phi_{1i} x_i} = \frac{b_l}{b_1} = V_{l-1} \qquad l = 2(1)m \tag{7}$$

wird (V_{l-1} — Anzahl der Atome des Elementes l zu der des Elementes 1).

Die Beziehungen (4), (5) und, aus (7),

$$\ln \left(\sum_{i}^{n} \Phi_{li} x_i \right) - \ln \left(\sum_{i}^{n} \Phi_{1i} x_i \right) - \ln V_{l-1} = 0 \tag{8}$$

bilden das zu lösende Gleichungssystem, das bei Anwendung eines modifizierten Newtonschen Verfahrens mit analytischer Ableitungsbildung auf m lineare Gleichungen ($\equiv$ Anzahl der Basiskomponenten, hier Elemente) reduziert werden kann. Für vorgegebene Atomverhältnisse V bestimmte Werte von Druck p und Temperatur T läßt sich ausgehend von geeigneten Startwerten x° iterativ der Lösungsvektor der Molanteile x eindeutig (mit vorzugebender Genauigkeit) bestimmen, der den angegebenen Bedingungen genügt.

Ermittlung von Enthalpie, Entropie und spezifischer Wärmekapazittät von Idealgasgemischen

Nach den bekannten Beziehungen der Thermodynamik folgt die spezifische Enthalpie des betrachteten Stoffsystems aus

$$h = \sum_{i}^{n} \frac{x_i \bar{h}_i}{\sum_{i}^{n} x_i M_i}, \tag{9}$$

die spezifische Entropie aus

$$s = \sum_{i}^{n} \frac{x_i \left[\bar{s}_i^0 - R \left(\ln x_i + \ln \frac{p}{p^0} \right) \right]}{\sum_{i}^{n} x_i M_i}, \tag{10}$$

und die spezifische Exergieänderung des Stoffgemisches vom Referenzzustand (p^0) zum Zustand, der durch die intensiven Größen p und T gekennzeichnet wird (Zusammensetzung jeweils aus der Gleichgewichtsbedingung), ist schließlich

$$\Delta e = \Delta h - T_0 \Delta s \tag{11}$$

mit $\Delta h = h - h^0$ (Energieinhalt des Stoffgemisches bezogen auf den Ausgangszustand, der dem Bezugzustand ^{0} entsprechen soll) und $\Delta s = s - s^0$.

Die molaren Größen sind demäß

$$\bar{h} = \sum_{i}^{n} x_i \bar{h}_i \tag{12}$$

$$\bar{s} = \sum_{i}^{n} x_i \left[\bar{s}_i^0 - R \left(\ln x_i + \ln \frac{p}{p^0} \right) \right] \tag{13}$$

und

$$\Delta \bar{e} = \Delta \bar{h} - T_0 \Delta \bar{s} \tag{14}$$

zu ermitteln. Die spezifische Wärmekapazität des reagierenden Gemisches bei konstantem Druck erhält man wegen

$$c_{pR} = \left(\frac{\partial h}{\partial T} \right)_p \tag{15}$$

durch numerische Ableitungsbildung. Die Werte für h_i, $\bar{s}_i^0(T)$ wurden (4) entnommen.

Diskussion einiger Ergebnisse

Es wurde das Verhalten folgender Gase untersucht ($p = 1$ bar):

1. SO_2 } als komplexes Gemisch aus S, O, S_2, O_2, S_2O, SO, SO_2, SO_3;
2. SO_3 }
3. NH_3 mit N, H, N_2, H_2, NH, NH_2, NH_3;
4. NF_3 mit N, F, N_2, F_2, NF, NF_2, NF_3;

5. HCl mit H, Cl, H_2, Cl_2, HCl;
6. H_2O mit H, O, H_2, O_2, OH, H_2O;
7. CO_2 mit C, O, C_2, C_3, O_2, CO, CO_2;
8. CO
9. H_2S mit H, S, H_2, S_2, HS, H_2S.

Auf den *Bild 1* und *2* ist die Gleichgewichtszusammensetzung der oben angegebenen Stoffsysteme 1, 3, 4 über der Temperatur aufgetragen. Es wird

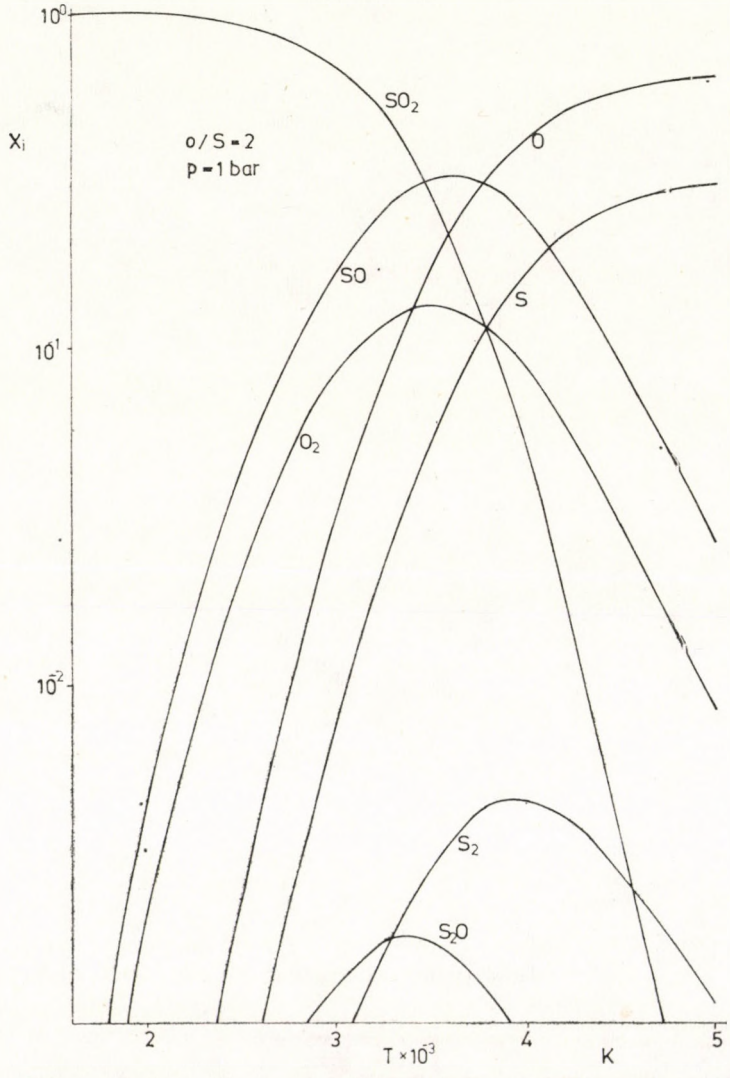

Bild 1.
Gleichgewichtszusammensetzung des durch Dissoziation von Schwefeldioxyd entstehenden Stoffsystems in Abhängigkeit von der Temperatur

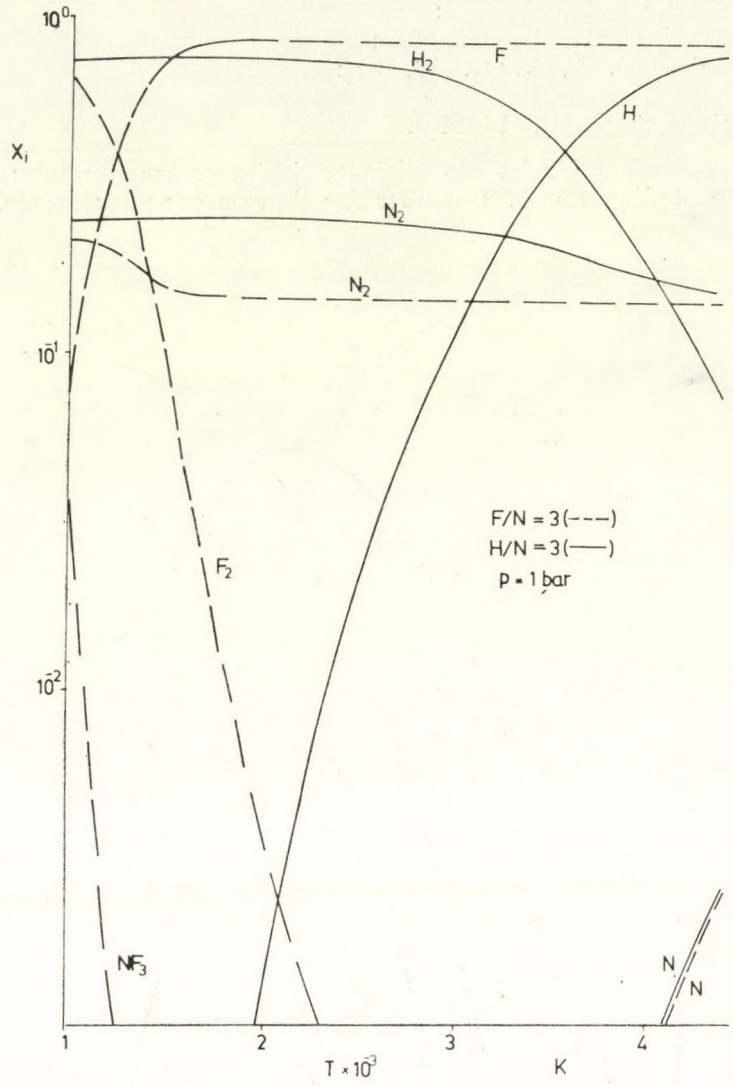

Bild 2.

Gleichgewichtszusammensetzung der durch Dissoziation von NH_3 und NF_3 entstehenden Stoffsysteme in Abhängigkeit von der Temperatur

deutlich, daß für das Gemisch 1 im Bereich $T \leq 2000\ K$ im wesentlichen nur SO_2 existiert und die instabile Verbindung SO bei ca. 3600 K maximale Konzentrationen erreicht, während NH_3 und NF_3 nahezu im gesamten betrachteten Temperaturbereich dissoziiert vorliegen.

Analog erkennt man aus der Darstellung *3*, daß die Verbindungen, die bereits im Bereich relativ niedriger Temperaturen dissoziieren, vergleichsweise große Energiemengen beinhalten, wobei die Breite des Temperaturintervalls, in dem wesentliche Zerfallprozesse ablaufen, den Anstieg der Funktionen

$\Delta\bar{h}(T)$ bestimmt. Die außerordentlich stabile Verbindung CO zeigt daher erst ab ca. 5000 K merkliche Dissoziation.

Für die absolute Größe des Energieinhaltes des Stoffsystems ist hauptsächlich die aufzuwendende Dissoziationsenthalpie verantwortlich, die bei der Rekombination der Zerfallsprodukte wieder frei gesetzt und für andere Zwecke, z. B. Stoffwandlungsprozesse, verfügbar wird. Damit deutet sich

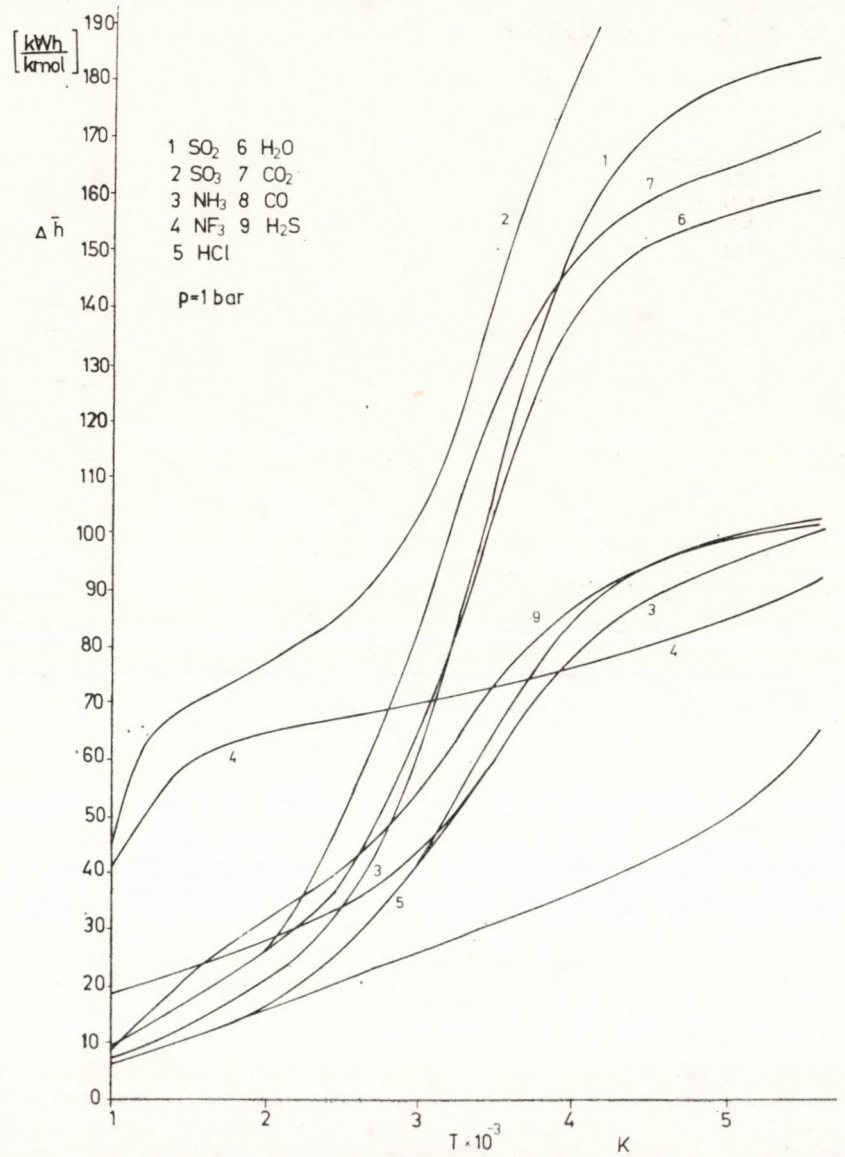

Bild 3.
Molarer Energieinhalt dissoziierender Verbindungen in Abhängigkeit von der Temperatur

gleichzeitig an, daß die chemischen Eigenschaften der Energieträger die Durchführung der beabsichtigten Stoffwandlung beeinflussen können (d. h., die Auswahl eines Energieträgers sollte nicht nur unter Berücksichtigung seiner energetischen Eigenschaften erfolgen).

Da die Molzahl des Stoffsystems mit steigender Temperatur zunimmt (also variabel ist), wurde der spezifische Energieinhalt (analog zu *Bild 3*) auf *Bild 4* dargestellt. Man erhält hierbei die Aussage, daß H_2O und NH_3 bei $T \geq 3000\ K$, bzw. NH_3 und NF_3 im verbleibenden Temperaturbereich, die vergleichweise höchsten spezifischen Energien bereitstellen können.

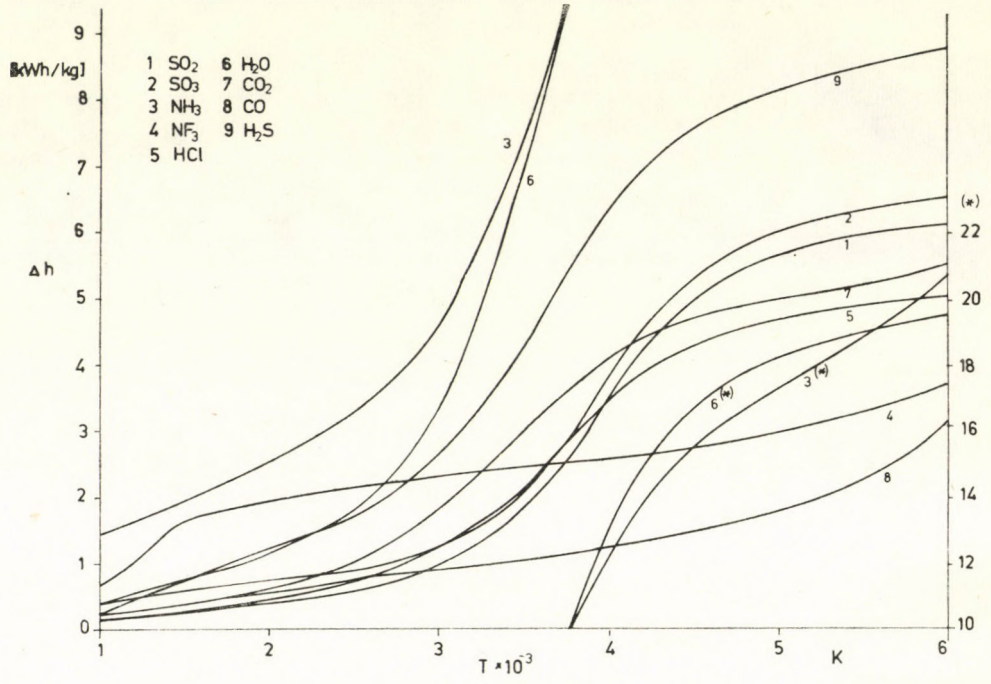

Bild 4.
Spezifischer Energieinhalt dissoziierender Verbindungen in Abhängigkeit von der Temperatur

Das Verhältnis von aus einem Stoffstrom bei reversibler Prozeßführung maximal gewinnbarer Arbeit zu der für die Aufheizung des Systems notwendigen elektrischen Energie (die nur aus Exergie besteht) stellt einen exergetischen Wirkungsgrad dar, der auf *Bild 5* in Abhängigkeit von der Temperatur aufgetragen wurde. Daraus ergeben sich für die im oberen Temperaturbereich energetisch etwa gleichwertigen Gase H_2O und NH_3 ganz offensichtliche Differenzen, die auf den unterschiedlichen Entropietermen beruhen. Vergleichsweise geringe Verluste können für H_2S über einen weitern Temperaturbereich konstatiert werden. SO_2 zeigt zu HCl bzw. CO_2 analoges Verhalten und wurde der Übersichtlichkeit halber nicht eingezeichnet. Zum Vergleich mit nichtdissoziierenden Gasen ist der Carnotfaktor (mit logaritmischer Mitteltempera-

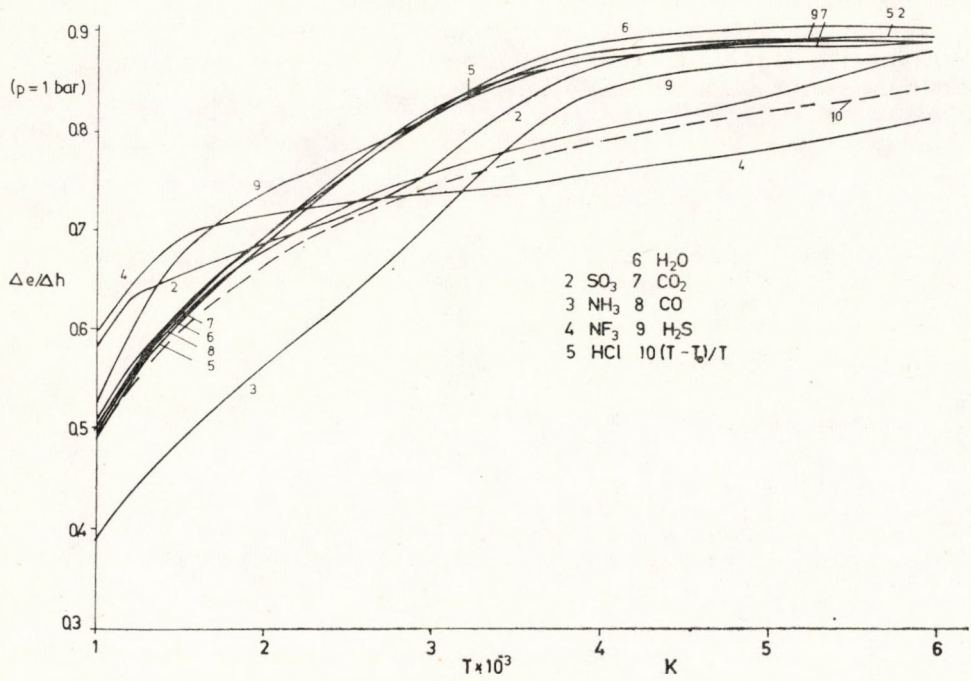

Bild 5.

Exergetischer Wirkungsgrad für die Aufheizung dissoziierender Verbindungen in Abhängigkeit von der Temperatur

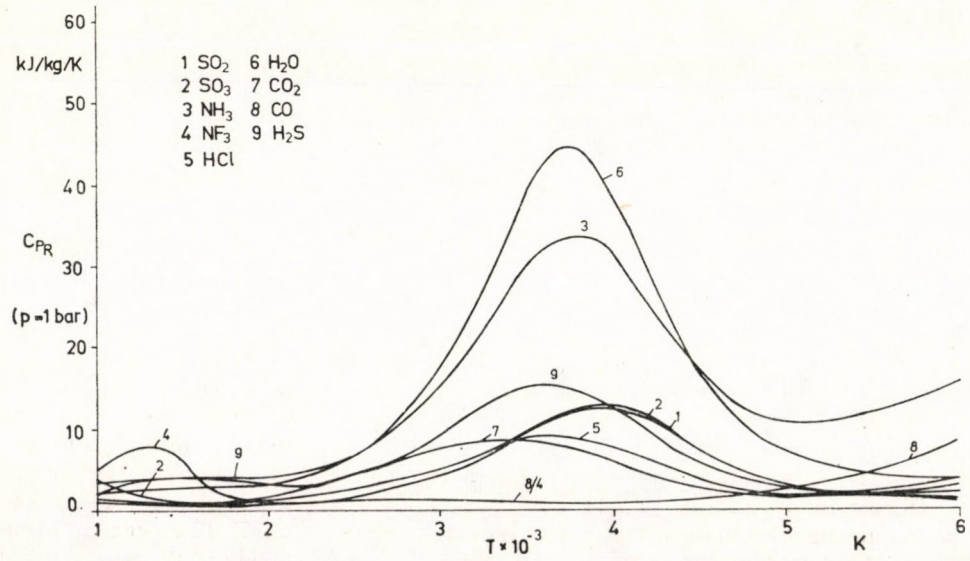

Bild 6.

Spezifische Wärmekapazität dissoziierender Verbindungen in Abhängigkeit von der Temperatur

tur) als unterbrochene Linie eingetragen worden. Eine sehr illustrative Kennzeichnung der Dissoziationsbereiche der unterschiedlichen reagierenden Stoffsysteme ist mit der Darstellung deren spezifischer Wärmekapazität über der Temperatur möglich *(Bild 6)*, die als ergänzung der Aussagen von *Bild 4* dienen kann.

SYMBOLVERZEICHNIS

b — Größe zur Kennzeichnung der Zusammensetzung der Ausgangssubstanz;
c_{pR} — spezifische Wärmekapazität des reagirenden Gemisches bei $p = \text{const.}$;
e — spezifische Exergie;
h — spezifische Enthalpie;
$\bar{h}$ — molare Enthalpie;
m — Anzahl der Basiskomponenten (Elemente);
M — Molmasse;
n — Anzahl der Species;
n — Mozahl;
p — Druck;
R — universelle Gaskonstante;
s — spezifische Entropie;
$\bar{s}$ — molare Entropie;
T — abs. Temperatur;
V — Atomverhältnis;
x — Molanteil;
X — Basiskomponente (Element);
Y — Species des betrachteten komplexen Gemisches;
μ — chemisches Potential;
ν — stöchiometrischer Koeffizient;
Φ — Größe zur Kennzeichnung der Zusammensetzung eines Species Y aus den Elementen X.

LITERATUR

1. Fratzscher/Hebecker/Honscha Hung. J. Ind. Chem., *3*, 115 (1975).
2. Сурис (Асланян) Шорин Химия высокис энергий 8 (1974) с. 392—394
3. Münster Chemische Thermodynamik, Akad. Verl., Berlin, 1969.
4. Глушко (ред.) Термодинамические свойства индивидуальных веществ, Москва 1962, т. 2

SUMMARY

In the article some properties of complex gaseous systems in the range from 1,000 to 6,000 K at a pressure of 1 bar were investigated. These properties are such ones, that give the possibility to characterize the applicability of those systems as a carrier of energy for several technological processes.

Energetic consideration leads to the conclusion, that the H_2O-, NH_3- and H_2S-systems seem to have the best behaviour, while exergetic investigation allows to estimate the energy losses appearing in the NH_3-system.

РЕЗЮМЕ

В работе исследуются термодинамические свойства газовэнергоносителей, образующих при диссоциации в температурном интервале 1000—6000 K при давлении 1 бар комплексные реагирующие системы. В энергетическом отношении особый интерес представляет применение H_2O, NH_3, H_2S. При эксергетическом анализе исследуемых газов выявляются сравнительно большие потери при применении NH_3 в качестве энергоносителя.

HUNGARIAN JOURNAL
OF INDUSTRIAL CHEMISTRY
VESZPRÉM
Vol. 6. pp. 361—368 (1978)

МАССОПЕРЕДАЧА ПРИ НАЛИЧИИ СЛОЖНОЙ ХИМИЧЕСКОЙ РЕАКЦИИ В СИСТЕМЕ „ГАЗ-ЖИДКОСТЬ". II.

ПОСЛЕДОВАТЕЛЬНАЯ ХИМИЧЕСКАЯ РЕАКЦИЯ, ОПИСЫВАЕМАЯ НЕЛИНЕЙНЫМ КИНЕТИЧЕСКИМ УРАВНЕНИЕМ

Гарцман А. Н., Черкашин В. В., Рассадникова Н. И.

(Институт катализа СО АН СССР, Новосибирск 630090, СССР)

Поступила в редакцию 8 Август 1978 г.

В работе рассмотрены вопросы, связанные с протеканием в объеме жидкой фазы последовательной химической реакции

$$A_г \rightarrow A_ж \xrightarrow{\text{катализатор}} B + A_ж \xrightarrow{\text{катализатор}} C.$$

Изучены зависимости среднего диффузионного потока, средних концентраций веществ и избирательности процесса от параметров модели.

Полученные результаты сравниваются с результатами предыдущей работы [1].

В предыдущей работе [1] обсуждались вопросы, связанные с протеканием в объеме жидкой фазы последовательной реакции первого порядка. Наряду с рассмотренными, существует целый ряд промышленно важных процессов, в которых разложение целевого продукта происходит с участием компонента газовой фазы по реакции второго порядка:

$$A_г \rightarrow A_ж \xrightarrow{\text{катализатор}} B + A \xrightarrow{\text{катализатор}} C.$$

По такой схеме протекают процессы парциального окисления и хлорирования парафинов [2—5].

Используя модель массопередачи, предложенную в работе [6], и сохраняя справедливость всех допущений работы [1], за исключением предположения о протекании обеих реакций по первому порядку, получим следующие уравнения математического описания рассматриваемой системы:

$$PeW(y)\frac{\partial C_A}{\partial x} = \frac{\partial}{\partial y}\left(D(y)\frac{\partial C_A}{\partial y}\right) - \Phi_A^2 C_A - \Phi_B^2 C_A C_B \qquad (1)$$

$$PeW(y)\frac{\partial C_B}{\partial x} = \frac{\partial}{\partial y}\left(D(y)\frac{\partial C_B}{\partial y}\right) + \Phi_A^2 C_A - \Phi_B^2 C_A C_B \qquad (2)$$

с начальными и граничными условиями

$$0 \le y \le 1; \qquad x = 0; \qquad C_A = C_{A0}; \quad C_B = C_{B0};$$
$$y = 1; \qquad 0 < x \le 1; \qquad \frac{\partial C_A}{\partial y} = 0; \quad \frac{\partial C_B}{\partial y} = 0; \tag{3}$$
$$y = 0; \qquad 0 < x \le 1; \qquad C_A = 1; \quad \frac{\partial C_B}{\partial y} = 0.$$

Предполагалось, что

$$D(y) = D_0 + (1 - D_0)y^2 \tag{4}$$
$$10^{-3} \le D_0 \le 1.$$

а зависимость $W(y)$ задавалась как в [6].

Уравнения (1)—(3) с учетом (4) были решены численно на ЭВМ с использованием матричной прогонки и разностной схемы Кранка-Никольсона. Вычислялись значения среднего безразмерного диффузионного потока вещества А

$$У = -\int_0^1 D(y) \left.\frac{\partial C_A}{\partial y}\right|_{y=0} dx \tag{5}$$

средних концентраций веществ А и В

$$\overline{C}_A = \int_0^1 \int_0^1 C_A(x, y)\, dx\, dy \tag{6}$$

$$\overline{C}_B = \int_0^1 \int_0^1 C_B(x, y)\, dx\, dy \tag{7}$$

и избирательности по веществу В

$$\Theta = \frac{\varphi_A^2 \overline{C}_A - \varphi_B^2 \overline{C}_A \overline{C}_B}{\varphi_A^2 \overline{C}_A + \varphi_B^2 \overline{C}_A \overline{C}_B}. \tag{8}$$

Результаты расчетов представлены в *таблицах 1—4* и на *рис. 1* и *2*. Данные *таблицы 1* позволяют сравнить полученные значения среднего безразмерного диффузионного потока вещества А с данными работы [6], в которой предполагалось протекание в объеме жидкой фазы одной реакции первого порядка. Из этой таблицы следует, что существенные различия в значениях y для двух указанных задач наблюдаются, если одновременно выполняются соотношения $\varphi_B^2/Pe > 0{,}5$ и $\varphi_A^2/Pe > 0{,}1$. В противном случае значения диффузионного потока и средней концентрации вещества А, полученные при решении уравнений (1)—(3), с удовлетворительной точностью совпадают с результатами расчетов по модели (6).

Данные *таблицы 2* свидетельствуют, что при таких же соотношениях параметров $\varphi_B^2/Pe > 0{,}5$ и $\varphi_A^2/Pe > 0{,}1$ наблюдается зависимость значений $\overline{C}_B$ от вида кинетической функции в уравнениях (1)—(2).

Таким образом, для рассматриваемой модели область „медленных“ реакций, которая в данном случае характеризуется независимостью среднего диф-

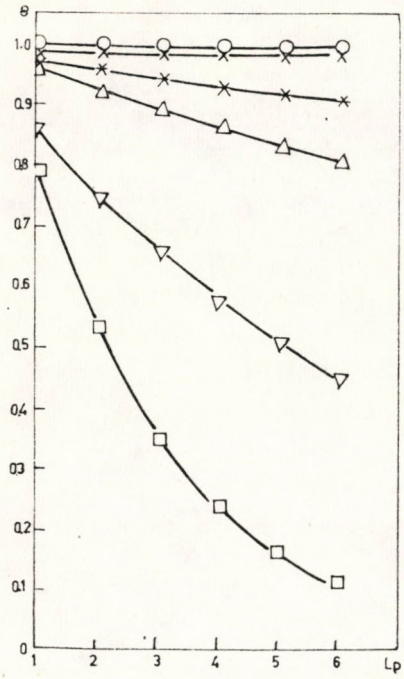

Рис. 1.

Изменение значений избирательности по длине реактора.

$D_0=0{,}01$; $\Phi_B^2=10$.

Обозначения	Φ_A^2	Pe
O	400	1000
X	2,0	100
✳	10,0	10,0
□	1,0	0,5
▽	5,0	
△	400	

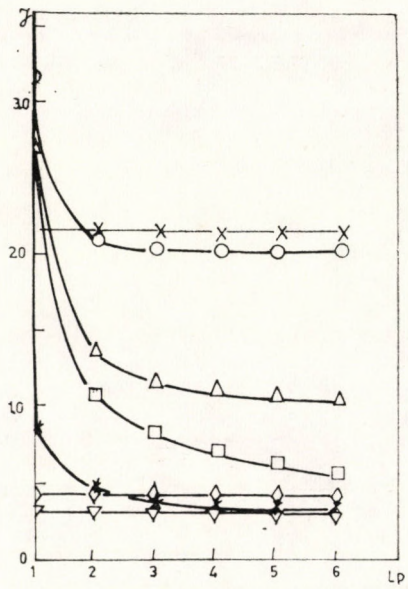

Рис. 2.

Изменение значийен среднего диффузионного потока по длине реактора.

$D_0=0{,}01$; $\Phi_B^2=10$.

Обозначения	Φ_A^2	Pe
O	400	1000
△	100	
□	5,0	
✳	10,0	100
X	400	30
◇	10,0	1,0
▽	5,0	0,5

фузионного потока и средних концентраций веществ от вида кинетической функции, существует при $\varphi_B^2/Pe \leq 0{,}5$ и $\varphi_A^2/Pe \leq 0{,}1$. В этой области для расчета значений $\overline{C}_A$ и $\overline{C}_B$ можно достаточно надежно пользоваться аналитическими зависимостями, которые были получены в работе (1).

Особо следует отметить тот факт, что для данной системы, в общем, не удалось получить область „быстрых" реакций, отличительной особенностью которой является независимость среднего диффузионного потока и средних концентраций веществ от параметров модели, характеризующих гидродинамическое состояние системы.

Таблица 1. Сравнение рассчитанных значений среднего диффузионного потока вещества A с данными работы [6].

Pe	φ_A^2	φ_B^2	Диффузионный поток y	
			настоящая работа	по данным [6]
0,5	0,01	0,01	0,093	0,093
		100	0,093	
	0,1	0,01	0,097	0,097
		1,0	0,101	
		100	0,102	
	100	0,01	1,006	1,007
		0,1	1,011	
		10,0	1,211	
		100,0	1,383	
1,0	1,0	0,1	0,148	0,147
		1,0	0,153	
		10,0	0,169	
		100,0	0,176	
10,0	0,1	0,01	0,275	0,275
		100	0,276	
	100	0,01	1,031	1,030
		0,1	1,032	
		10,0	1,209	
		100	1,329	
1000	10	0,01	2,565	2,566
		100	2,566	
	100	10	2,713	2,712
		100	2,719	
	400	10	3,172	3,169
		30	3,176	
		100	3,192	

Таблица 2. Сравнение рассчитанных значений средних концентраций вещества →B с результатами работы [1] при $D_0=0{,}01$; $\overline{C}_{B0}=0$

Pe	φ_A^2	φ_B^2	$\overline{C}_B$	
			по данным [1]	настоящая работа
0,5	0,01	0,01	0,001	0,001
		100	10^{-5}	10^{-5}
	0,1	0,01	0,009	0,009
		10	0,001	0,003
		100	10^{-4}	10^{-4}
	100	0,01	0,326	0,329
		0,1	0,298	0,322
		10,0	0,021	0,107
		100,0	0,002	0,019
1,0	1,0	0,1	0,033	0,034
		1,0	0,022	0,030
		10	0,004	0,013
	100,0	100	10^{-4}	0,003
300	100,0	10	0,001	0,001
		100	0,001	0,001
	400	10	0,004	0,005
		30	0,004	0,004
		100	0,003	0,004

Действительно, при небольших значениях φ_B ($\varphi_B^2 \leq 10$) такая область имеет место для значений y и $\overline{C}_A$ при $\varphi_A^2/Pe \geq 10$, однако значения $\overline{C}_B$ сильно зависят от величины параметра Pe, как это можно видеть из *таблицы 3*. При больших же

Таблица 3.

Зависимость значений среднего диффузионного потока и средних концентраций веществ от параметра *Pe* при $\varphi_A^2=10$; $\varphi_B^2=1{,}0$; $D_0=0{,}01$

Pe	*y*	$\overline{C}_A$	$\overline{C}_B$
0,1	0,355	0,02962	0,84
0,5	0,355	0,030	0,27
1,0	0,353	0,030	0,16
10,0	0,411	0,023	0,016
30,0	0,544	0,016	0,004
100,0	0,667	0,010	0,001
300,0	1,432	0,006	10^{-4}
1000	2,566	0,003	10^{-5}

значениях φ_B в силу того, что вторая реакция идет со значительной скоростью и y и $\overline{C}_A$ уже не остаются постоянными при $\varphi_B^2/Pe \geq 10$.

Зависимость избирательности Θ от параметров *Pe*, φ_A и φ_B представлена *в таблице 4*.

Таблица 4.

Зависимость избирательности Θ от параметров модели при $D_0=0.01$ и $\overline{C}_{A0}=\overline{C}_{B0}=0$.

φ_A^2	φ_B^2	*Pe*				
		0,5	1,0	10,0	100,0	1000,0
0,1	0,01	0,999	0,999	1,0	1,0	1,0
	1,0	0,932	0,967	0,998	1,0	1,0
	10,0	0,745	0,856	0,984	1,0	1,0
	100,0	0,471	0,703	0,946	0,994	0,99
1,0	1,0	0,944	0,970	0,998	1,0	1,0
	10,0	0,792	0,872	0,984	0,999	1,0
	100,0	0,567	0,738	0,947	0,994	1,0
10,0	1,0	0,973	0,984	0,998	1,0	1,0
	10,0	0,893	0,925	0,987	0,999	1,0
	100,0	0,811	0,857	0,953	0,994	1,0
100,0	10	0,945	0,964	0,993	1,0	1,0
	100	0,887	0,916	0,972	0,995	1,0

Приведенные в этой таблице данные позволяют сделать вывод о существовании тех же областей „высокой“ и „низкой“ избирательности, наличие которых было отмечено в работе (1).

Область „высокой“ избирательности имеет место при $\varphi_B^2/Pe < 0{,}1$ и характеризуется тем, что значения Θ в этой области практически не зависят ни от *Pe*, ни от φ_A. Область „низкой“ избирательности существует при $\varphi_B^2/Pe > 10$ и ха-

рактеризуется резким ростом Θ при увеличении значений φ_A или Pe. Промежуточная область определяется соотношением $0{,}1 \leq \varphi_B^2/Pe \leq 10$.

На *рис. 1* и *2* представлено изменение избирательности и среднего диффузионного потока по длине реактора при всплывании серии одиночных пузырей.

Как видно из этих рисунков, при $\varphi_B^2/Pe \leq 0{,}1$ и любых значениях φ_A величина Θ постоянна и близка к единице. При $\varphi_B^2/Pe > 0{,}1$ значение Θ уменьшается по длине реактора тем сильнее, чем меньше φ_A^2/Pe. При достаточно больших φ_A^2/Pe стационарные значения Θ и $\overline{C}_A$ достигаются на более коротком участке реактора.

Значения безразмерного диффузионного потока при всех рассмотренных значениях φ_B оставались практически постоянными по длине реактора, если выполнялось неравенство $\varphi_A^2/Pe \geq 10$. В противном случае величина y резко уменьшалась на начальном участке реактора, а затем, стремилась к стационару тем быстрее, чем больше было значение φ_A.

В заключение отметим, что все описанные выше закономерности позволяют понять явления, происходящие при протекании в объеме жидкой фазы реакции рассматриваемого типа и, исходя из стратегических соображений, выбрать оптимальную тактику ведения процесса в целом. Например, если необходимо получать целевой продукт с минимальным количеством примесей, то процесс следует вести в области „высокой" избирательности. Однако, при этом концентрация продукта в растворе будет невысока. С другой стороны, существуют процессы, в которых побочные продукты реакции являются также полезными, либо легко превращаются в таковые, или хорошо отделяются от целевого продукта. В то же время, по технологическим соображениям, необходима достаточно высокая концентрация целевого продукта. При таких условиях процесс выгодно вести в области „низкой" избирательности или в промежуточной области. Таким образом, конкретный выбор оптимального гидродинамического режима ведения процесса с учетом изложенных в данной работе результатов и технологических требований позволит добиться желаемого результата.

ОБОЗНАЧЕНИЯ

C_A — безразмерная концентрация вещества А;
C_B — то же для вещества В;
$\overline{C}_A$, $\overline{C}_B$ — средние значения концентраций C_A и C_B;
C_{A0}, C_{B0} — начальные значения концентраций веществ А и В;
$\overline{C}_{A0}$, $\overline{C}_{B0}$ — средние значения концентраций C_{A0} и C_{B0};
$D(y)$ — безразмерный коэффициент кондуктивного переноса по координате y;
D_∞ — коэффициент турбулентной диффузии в ядре потока;
f_1, f_2 — скорости первой и второй реакций в кинетической области, соответственно;
K_1, K_2 — константы скоростей первой и второй реакций, соответственно;
L_x, L_y — характерный линейный размер по координатам x и y, соответственно;

$$Pe = \frac{W_\infty L_x}{D_\infty}\left(\frac{L_y}{L_x}\right)^2$$

W_∞ — скорость течения в ядре потока;
W — безразмерная скорость течения потока;
x, y — координаты;

$$\varphi_A = L_y\sqrt{\frac{f_1}{C_A^* D_\infty}}; \quad \varphi_B = L_y\sqrt{\frac{f_2}{C_A^* D_\infty}}$$

Θ — селективность;

индексы

1 — первая реакция;
2 — вторая реакция;
∞ — значение величины, определяемое в ядре потока;
✳ — значение величины, определяемое на поверхности раздела фаз.

ЛИТЕРАТУРА

1. Гарцман А. Н., Черкашин В. В.: Hung. J. Ind. Chem., *5*, 295 (1977).
2. Inoe H. and Kobayashi T.: Chem. React. Eng. Proc. Enz. Symp. 4—th., 1968, p. 147 (1968).
3. Van de Vusse, J. G.: Chem. Eng. Sci., *21*, 631, 645, 1239 (1966).
4. Ramage M. P. and Eckert R. E.: Ind. Eng. Chem. Process Des. Develop., *12*. (3) 248 (1973).
5. Окисление углеводородов в жидкой фазе, Сб. статей под ред. Н. М. Эмануэля, М. Изд. АН СССР, 1959.
6. Гарцман А. Н., Ермакова А., Рассадникова Н. И., Hung. J. Ind. Chem., *4*, 109. (1976).

CHEMICAL REACTION ACCOMPANIED BY MASS TRANSFER IN LIQUID-GAS SYSTEM II.
Consecutive First and Second Order Chemical Reactions

A. N. Gartsman, V. V. Cherkashin, N. I. Rassadnikova

The authors deal with the consecutive reactions

$$A_{gas} \longrightarrow A_{liqu.} \xrightarrow{catalyst} B + A_{liqu.} \xrightarrow{catalyst} C$$

taking place in liquid phase. The relationships existing between the parameters of the model and the mean diffusion flux, the mean concentrations and the selectivity of the process are studied. The results are compared with the data presented in the previous paper [1].

HUNGARIAN JOURNAL
OF INDUSTRIAL CHEMISTRY
VESZPRÉM
Vol. 6. pp. 369–382 (1978)

THE THROUGHPUT AVAILABILITY OF A CAPACITY-DIVIDED PARALLEL CONNECTION WITH INTERNAL CAPACITY RESERVE

J. Biehounek

(Ingenieurhochschule Köthen, the GDR)

Received: August 17, 1978.

The throughput availability of a parallel connection divided as to its capacity was examined by applying the queuing theory. It became obvious that the substitution of a large plant by small plants could bring about an increase in the availability, provided the partial plants possess a capacity reserve. This reserve must, however, exceed a minimum value. There exists an optimum number of partial plants. It is essentially determined by the efficiency of the repair shop.

Introduction

In the chemical industry many production processes are chains of successive transformations of materials leading from the raw material to the final product. Thus it is possible to introduce a rank order of process engineering systems. In most cases a distinction is made—proceeding from the simple to the composed—between the process group, the process stage, and the process, etc. [1]. That means that a process stage involves several process groups. Here, we are interested in the process stages, wich are composed of similar process groups in parallel connection that function independent of each other. They are referred to as parallel connections divided as to their capacity. Such connections are widely used. In individual cases, more than one hundred process groups are operated parallelly. Therefore, it is of some practical importance to examine the reliability of a parallel connection divided as to its capacity.

Most often the throughput availability:

$$V_D = \frac{q_r}{q_i} \tag{1}$$

is used as a parameter in expressing the reliability [2], [3]. In this connection q_r means the actual quantity of production produced during a certain period

and q_i the quantity of production which could be produced in ideal circumstances during the same period of time.

Different methods are known by which V_D can be calculated. Recently it was proposed that the results of the queueing theory should be used for the calculation [4]. In this way, connections can be established with a modern and much developed mathematical dispicline. After BIEHOUNEK [4] had concentrated on representing the mathematical fundamentals, we shall now deal with the question, in which the circumstances the division of one process stage into several similar process groups will bring about an increased availability.

Let $n_a \in \{0, 1, \ldots, m\}$ be the number of process groups which are intact at a certain instant. Defective groups are repaired. On the other hand, disturbances occur on groups which so far had been functioning well. Hence, n_a is time-dependent. One of the peculiar features of this function is its range of values: it is a discrete set, i.e. $n_a(\tau_i)$ possesses a constant value during certain time intervals $[t_{i-1}; t_i]$ $(\tau_i \in [t_{i-1}; t_i])$. Such functions are referred to as step functions (primitive functions). The capacitiy $\dot{q}_G$ of a process group is also conceived as a step function. It is to be constant during the same intervals as is n_a.

The capacity $\dot{q}_S$ of the process stage is calculated from n_a and $\dot{q}_G$ according to:

$$\dot{q}_S(\tau_i) = n_a(\tau_i)\dot{q}_G(\tau_i). \tag{2}$$

Its mean value during interval $I = (t_0; t_0 + t)$ is:

$$[\dot{q}_S(\tau)]_t = \frac{1}{t}\sum_{i=1}^{s} n_a(\tau_i)\dot{q}_G(\tau_i)\Delta t_i, \qquad \Delta t_i = t_i - t_{i-1}, \qquad \sum_{i=1}^{s}\Delta t_i = t. \tag{3}$$

If $\dot{q}_{GN}$ is the (constant) capacity of o process group, by means of which the m groups produce the quantity of production planned in ideal circumstances and during the time interval I, Eq. (3) will, together with Eq. (1), result in the throughput availability of:

$$V_D = \frac{[\dot{q}_G(\tau_i)]_t t}{m\dot{q}_{GN} t} = \frac{\frac{1}{t}\sum_{i=1}^{s} n_a(\tau_i)\dot{q}_G(\tau_i)\Delta t_i}{m\dot{q}_{GN}}. \tag{4}$$

Fundamentals of the Queueing Theory

First of all we shall consider the special case $\dot{q}_G(\tau) = \dot{q}_{GN} = \text{const.}$ dealt with in [4]. Eq. (4) will then come up to:

$$V_{D0} = \frac{\frac{1}{t}\sum_{i=1}^{s} n_a(\tau_i)\Delta t_i}{m} = \frac{[n_a(\tau_i)]_t}{m}. \tag{5}$$

The average number $[n_a(\tau_i)]_t$ of the intact machines is attributable to two factors: the reliability of the process groups and the efficiency of the repair shop. In our connection, the reliability can quantitatively be characterized by means of the average defect-free time of running $ET_r = \lambda_G^{-1}$. The efficiency of the repair shop is determined *a)* by the average time needed for the repair μ_G^{-1} (it also comprises the skills of the mechanics and such organizational questions as availability of spare parts, etc.), and *b)* by the number 1 of

repair units (mechanics or work teams working independent of each other). The last mentioned factor is rarely considered when calculating the availability of a parallel connection which is divided as to its capacity. However, it is important in dealing with our problem. One can see it when considering a process group breaks down at an instant when all the repair units are engaged. This group must wait until the repair work can be started. The result is a mutual interference between the process groups. It brings about an additional decrease of the mean value $[n_a(\tau_i)]_t$. Another argument which may be used in substantiating that the average repair time is insufficient in order to express the efficiency of the repair shop is the fact which has been established by experience that μ_G^{-1} cannot be reduced at will, but will be maintained at a value of $\mu_G^{-1} \geq \mu_{min}^{-1} > 0$ even if the repair technology is perfect.

Rather, the duration of the defect-free time of running of a process group and the duration of the repair work are largely determined by laws of probability. Hence, the figure $n_a(\tau)$ depends on uncontrollable variables and may be conceived as a realization of the stochastic process:

$$N_{aT} = \{N_a(\tau),\ \tau \in T\}. \tag{6a}$$

The same also applies to $n_d(\tau)$, the number of defective process groups. The relevant process is described with:

$$N_{dT} = \{N_d(\tau),\ \tau \in T\}. \tag{6b}$$

The relationship between the processes is expressed as:

$$N_a(\tau) + N_d(\tau) = m. \tag{7}$$

For stationary ergodic processes the mean value $[n_a(\tau)]_t$ can be approximated through the expected value EN_a. Eq. (5) is transformed into:

$$V_{D0} = \frac{EN_a}{m} = 1 - \frac{EN_d}{m}. \tag{8}$$

The introduction of the expected value EN_d establishes the connection with the queuing theory, where the number of defective process groups is generally described as the number of demands made on the service system.

The service system consists of a waiting room and the service shop, where $1 \leq m$ independent service units work m parallel. The special system considered here is characterized by the fact that only a finite number of sources of the flow of demands exists (the in process groups) and that once a defect has been repaired any group may be in need of repair again later on. It is described as a complete service system [5], [7]. Moreover, it is a pure waiting system. Such systems were investigated for the first time by PALM [6], [8] who proceeded from the following basis (see also [7], [9]):

a) all process groups are similar regarding the average number of defects (related to the unit of productive time) and the average expenditure on repairs,

b) all service units are equivalent,

c) the defect-free time of running and the duration of repairs are distributed exponentially with the densities:

$$f_r(t) = \begin{cases} \lambda_G e^{-\lambda_G t} & \\ 0 & \end{cases} \quad \text{or} \quad f_s(t) = \begin{cases} \mu_G e^{-\mu_G t} & t \geq 0 \\ 0 & t < 0 \end{cases}; \tag{9}$$

d) the process groups function independent of each other. Breakdowns occur by chance, they are not attributable to systematic causes equally effective in all groups (shortage of raw and auxiliary materials, and energy etc.),

e) the service system is in the state of the statistic equilibrium.

The probability function $p_1(i, \tau) = P[N_d(\tau) = i]$, i.e. the probability that i demadns are made at instant τ on the service system, will then be expressed by:

$$p_1(\mathrm{i}) = \begin{cases} \binom{m}{\mathrm{i}} \varrho_G^{\mathrm{i}} p_1(0) & 0 \leq \mathrm{i} \leq l \\ \dfrac{\mathrm{i}!}{l! l^{i-l}} \binom{m}{\mathrm{i}} \varrho_G^{\mathrm{i}} p_1(0) & l \leq \mathrm{i} \leq m \end{cases}; \tag{10}$$

[7]. In Eq. (10) $\varrho_G = \dfrac{\lambda_G}{\mu_G}$, and $p_1(0)$ is calculated as follows:

$$[p_1(0)]^{-1} = \sum_{\mathrm{i}=0}^{l} \binom{m}{\mathrm{i}} \varrho_G^{\mathrm{i}} + \sum_{\mathrm{i}=l+1}^{\mathrm{m}} \frac{\mathrm{i}!}{l! l^{i-l}} \binom{m}{\mathrm{i}} \varrho_G^{\mathrm{i}}. \tag{11}$$

We explain the usage of the equations for $m = l$. In this case a service unit is available for each process group, and Eq. (11) can be simplified to yield:

$$[p_1(0)]^{-1} = \sum_{\mathrm{i}=0}^{\mathrm{m}} \binom{m}{\mathrm{i}} \varrho_G^{\mathrm{i}} = (1 + \varrho_G)^m. \tag{12}$$

The expected value EN_d is:

$$EN_d = \sum_{\mathrm{i}=0}^{\mathrm{m}} \mathrm{i} p_1(\mathrm{i}) = \sum_{\mathrm{i}=0}^{\mathrm{m}} \binom{m}{\mathrm{i}} \mathrm{i} \varrho_G^{\mathrm{i}} p_1(0) = \varrho_G m p_1(0) \sum_{i=1}^{\mathrm{m}} \binom{m-1}{i-1} \varrho_G^{\mathrm{i}-1} \tag{13}$$

and, eventually, after the index has been shifted:

$$EN_d = \varrho_G m (1 + \varrho_G)^{m-1} p_1(0). \tag{14}$$

With (12) and (14), Eq. (8) results in:

$$V_{D0} = \frac{1}{1 + \varrho_G} = \frac{\mu_G}{\mu_G + \lambda_G}. \tag{15}$$

If a service unit is available for each process group, the throughput availability of the process stage is identical with the availability $(1 + \varrho_G)^{-1}$ of the individual process groups. This result is understandable intuitively.

As opposed to the situation in the case of open waiting systems, it is impossible for the system considered here to generally express the availability as a function of ϱ_G, m and l. First the probabilities for each special pair of numbers (m, l) must be calculated according to the Eqs. (10) and (11), and then EN_d must be determined. So the application of the equations is rather troublesome.

However, EN_d yields in a simple way other parameters of the system, for example, the average number:

$$EN_w = (1 + \varrho_G) EN_d - \varrho_G m \tag{16}$$

of process groups waiting for repair, and the average number:

$$EN_s = \varrho_G(m - EN_d) \tag{17}$$

of the groups being repaired, etc. (see e.g. [7]). The behaviour of the service system can then be conceived in greater detail. Among others, one may discuss the influence of machine interference. Using the equation $EN_d = EN_w + EN_s$, the deviation $NV_0 = 1 - V_{D0}$ of the throughput availability from the ideal value (i.e. the non-availability) can be split up into the shares $NV_{0s} = \frac{1}{m}\varrho_G(m - EN_d)$ and $NV_{0w} = \frac{1}{m}(1 + \varrho_G)EN_d - \varrho_G$. The expression NV_0 expresses the decline of production for process groups which have just been serviced, whereas NV_{0w} takes the machine interference into consideration. In *Fig. 1* both shares are contrasted with each other for $l = 1$ in order to illustrate

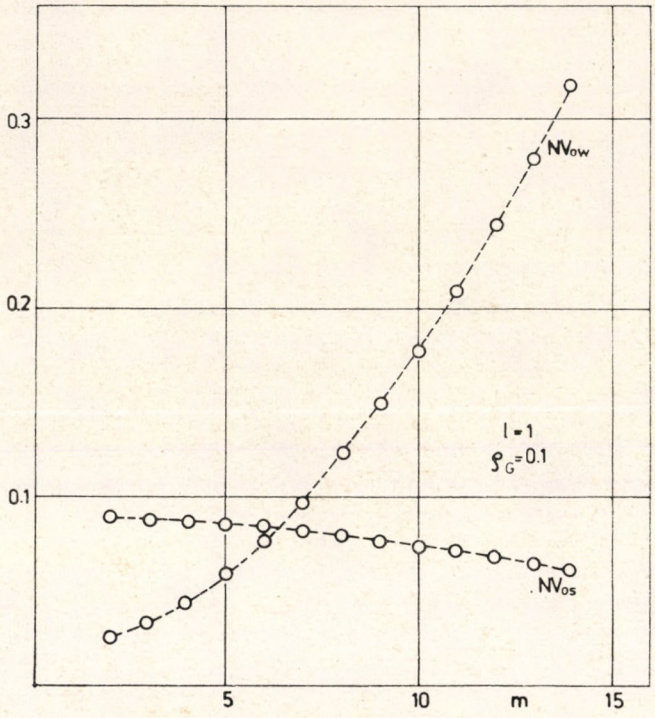

Fig. 1.
Splitting up of the non-availability into the shares NV_s and NV_w for $l = 1$ and $\varrho_G = 0.1$

their proportions. If m increases, the significance of NV_{0w} will also increase. Since the length of the queue is dependent upon the number of service units, it can be expected that l exerts a decisive influence on the throughput availability. *Fig. 2* confirms this assumption.

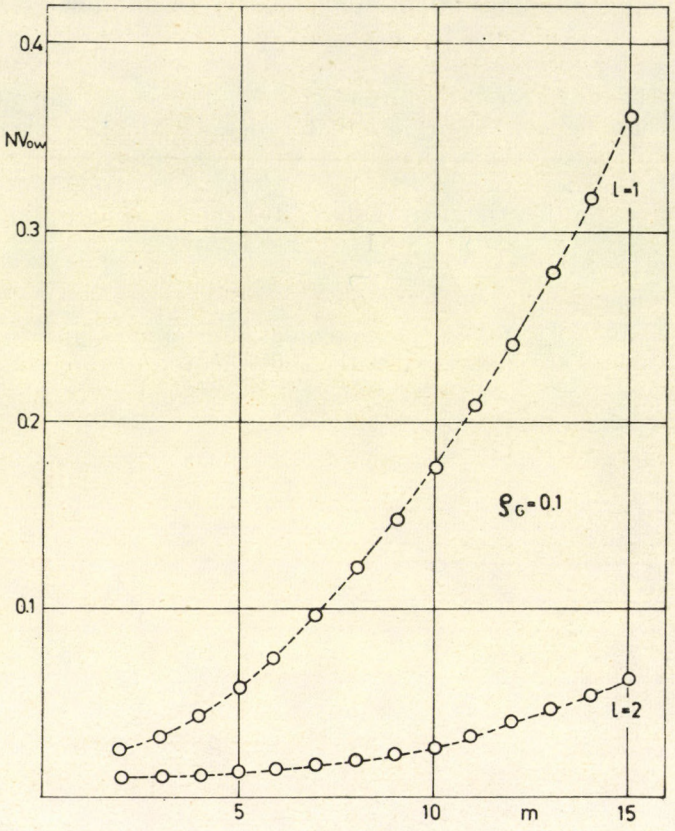

Fig. 2.
The dependence of the expression NV_w on l

As a whole, it becomes apparent that the throughput availability decreases with the growing numbers of process groups [4]. This result is in contradiction with the real behaviour of the throughput availability in the case of divided capacities. When searching for the causes of this discrepancy, an error in the basic mathematical considerations can be ruled out. PALM's model is widely used in practice and generally accepted. Rather, it must be assumed that the suppositions used by us do not fully correspond with the conditions prevailing in practice.

The internal capacity reserve

Up to this point, the calculation was based on the specialization of Eq. (4) by assuming that the capacity of a process group possessed the constant value $\dot{q}_{GN}=\frac{1}{m}\dot{q}_S$ ($\dot{q}_S$ meaning the capacity of the process stage). In general, plants of the chemical industry may, however, be adapted to a certain extent

to changing their service conditions. If necessary, it is possible to increase the output. The nominal capacity $\dot{q}_{GN}$ should, for this reason, be conceived only as the minimum admissible value of the capacity of a group, which, otherwise, varies in the interval $\dot{q}_{GN}=\dot{q}_{G\min}\leq\dot{q}_G\leq q_{G\max}$. Thus a capacity reserve is produced, which can be considered as being a special form of manifestation of the hot redundancy [3]. It is used in the case of breakdowns of individual process groups, in order to wholly or partially compensate for any decline in production and, eventually, finds its expression in an increase of the throughput availability. Hence, the supposition $\dot{q}_G=\dot{q}_{GN}=\text{const.}$ means a considerable limitation. It shall be eliminated in the following. For this purpose, we introduce the internal capacity reserve r_m of a process group corresponding to:

$$r_m=\frac{\dot{q}_{G\max}-\dot{q}_{G\min}}{\dot{q}_{G\min}}\geq 0, \qquad \dot{q}_{G\min}=\dot{q}_{GN}. \tag{19}$$

If, at a certain instant, the share r with $0\leq r\leq r_m$ is used, one process group will possess the capacity:

$$\dot{q}_G(\tau)=\dot{q}_{GN}[1+r(\tau)]. \tag{20}$$

The value of r depends on the number n_a of intact process groups. Hence, r is a indirect function $r=r[n_a(\tau)]$ of τ, the fundamental course of which is shown in *Fig. 3*. The transition form $r(\tau)$ to $r(n_{ai})$ is based on the assumption

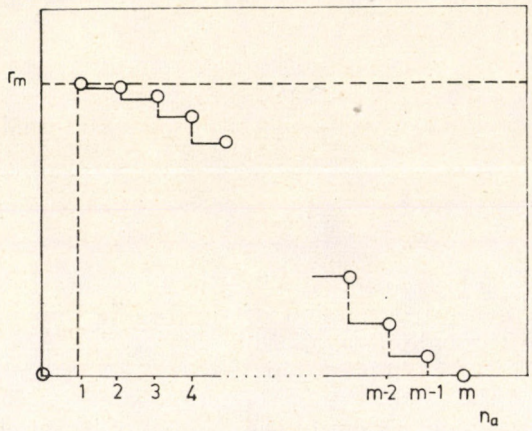

Fig. 3.
Fundamental course of the function $r=r(n_{ai})$

that the change of output was possible without any delay. Moreover, the capacity reserve should be equal for all process groups.

Eq. (3) with Eq. (20) yields as the mean capacity of the process stage in the interval $I=(t_0;\ t_0+t)$:

$$[\dot{q}_S(\tau)]_t=\frac{1}{t}\,\dot{q}_{GN}\sum_{i=1}^{s}n_{ai}[1+r(n_{ai})]\Delta t_i=\dot{q}_{GN}[n_{ae}(\tau)]_t. \tag{21}$$

To shorten the formula, equation:

$$[n_{ae}(\tau)]_t = \frac{1}{t} \sum_{i=1}^{n} n_{ai}[1 + r(n_{ai})] \tag{22}$$

introduces the effective number of elements being intact in the interval I:

$$V_D = \frac{\dot{q}_{GN}[n_{ae}(\tau)]_t t}{\dot{q}_{GN} m t} = \frac{[n_{ae}(\tau)]_t}{m} \tag{23a}$$

follows therefrom as the throughput availability.

The function $n_{ae}(\tau)$ means the realization of the stochastic process $N_{aeT} = \{N_{ae}(\tau),\ \tau \in T\}$, and $[n_{ae}(\tau)]_t$ is the mean value of this realization within the period t. It may be approximated again by the expected value, provided—and this is assumed here—the necessary conditions are fulfilled. One obtains:

$$V_D = \frac{E N_{ae}(\tau)}{m} . \tag{23b}$$

According to Eq. (22) $N_{ae}(\tau) = N_a(\tau)[1 + r(N_a(\tau))]$. Apart from that, N_a may be expressed by N_d by means of Eq. (7), yielding:

$$V_D = 1 - \frac{E N_d}{m} + \frac{E(m - N_d) r}{m} = V_{D0} + \frac{E(m - N_d) r}{m} . \tag{24}$$

V_{D0} is the throughput availability without the internal capacity reserve. Because of $N_d(\tau) \leq m$, the expression $E(m - N_d)r$ is not negative, so that:

$$\Delta V_D = V_D - V_{D0} = \frac{E(m - N_d) r}{m} \geq 0 \tag{25}$$

means the increase in the availability by utilizing an internal capacity reserve.

Results

The difficulties arising in connection with the representation of the expression for $p_1(0)$ render a general discussion of the results impossible, so that the dependence of the throughput availability on ϱ_G, m, r and l can only be illustrated by means of examples. This requires an assumption as to $r(n_{ai})$. r is selected so that the quantity of production comes as close to the desired value as possible, and independent of the number of intact elements, however, without exceeding this desired values. So, the capacity reserve should only be utilized if at least on element has broken down. The dependence:

$$r(n_{ai}) = \begin{cases} \dfrac{m}{n_{ai}} - 1 & n_{ai} \geq \dfrac{m}{r_m + 1} \\ r_m & n_{ai} < \dfrac{m}{r_m + 1} \\ 0 & n_{ai} = 0 \end{cases} \tag{26}$$

meets this necessity.

Fig. 4 illustrates the influence exerted by the capacity reserve on the effective number of process groups. It shows that this number increases if the reserve is utilized, and resulting therefrom is the increase in the throughput availability.

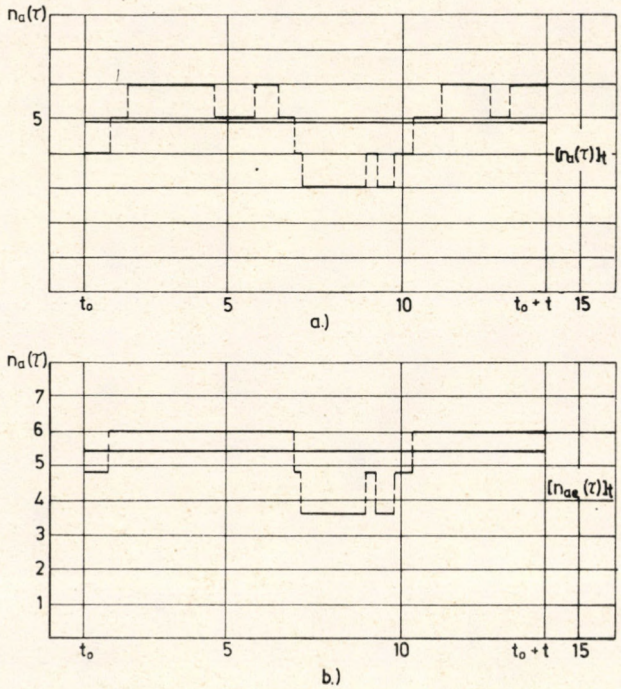

Fig. 4.
Real (*Fig. 4*a) and effective (*Fig. 4*b) number of intact elements (calculated for $r_m = 0.2$)

Fig. 5 shows V_D as a function of m for different values of the parameter r and for the fixed values 1 and 0.05 for l and ϱ_G respectively. First of all, it becomes obvious that if m is fixed, the throughput availability increases with r. This behaviour can easily be explained. On the other hand, attention must be attached to the course of V_D if m increases. In this case, and provided r_m possesses a certain minimum value, an optimum number of partial plants is achieved. In this respect, there is a difference with regard to other calculation methods (see e.g. [3]). *Fig 6* illustrating the correlation $V_D = V_D(\varrho_G, m)$ with m as a parameter explains this difference in detail. For $\varrho_G \to 0$, $V_D \to 1$ does, however, develop like a (relating to parameter m) monotonously increasing function. That means that, in general, $V_D(\varrho_G, m_1) > V_D(\varrho_G, m_2)$ is not valid for $m_1 > m_2$ and for all ϱ_G. Rather, there exist such values of m, for which in certain intervals of the variable $\varrho_G V_D$ is characterized by a more favourable course. *Fig. 6* also shows that for large values of ϱ_G the division of capacities will not entail any advantages. As a whole one can say that the division of the total capacity into m partial capacities does not lead to better results

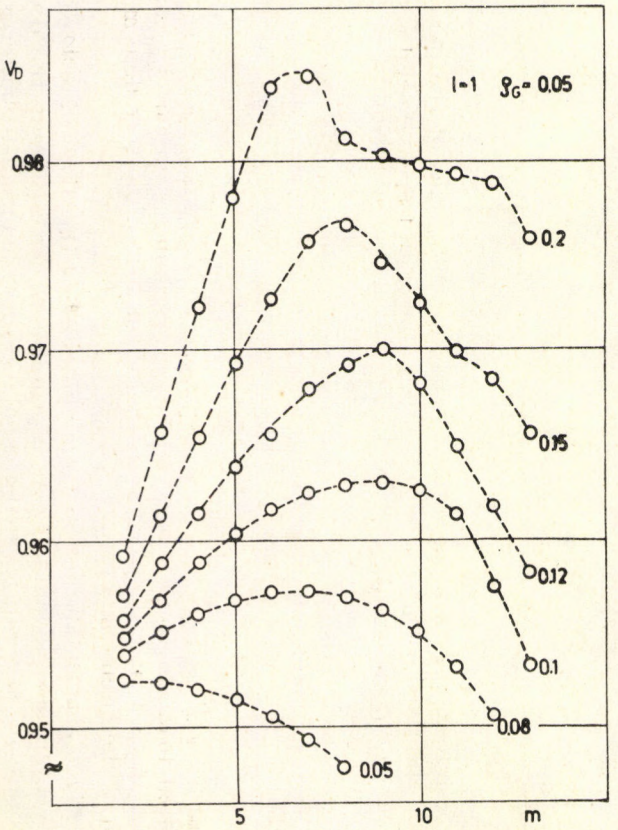

Fig. 5.
Throughput availability for $l=1$ and $\varrho_G=0.05$ as a function of m. Parameter: r_m

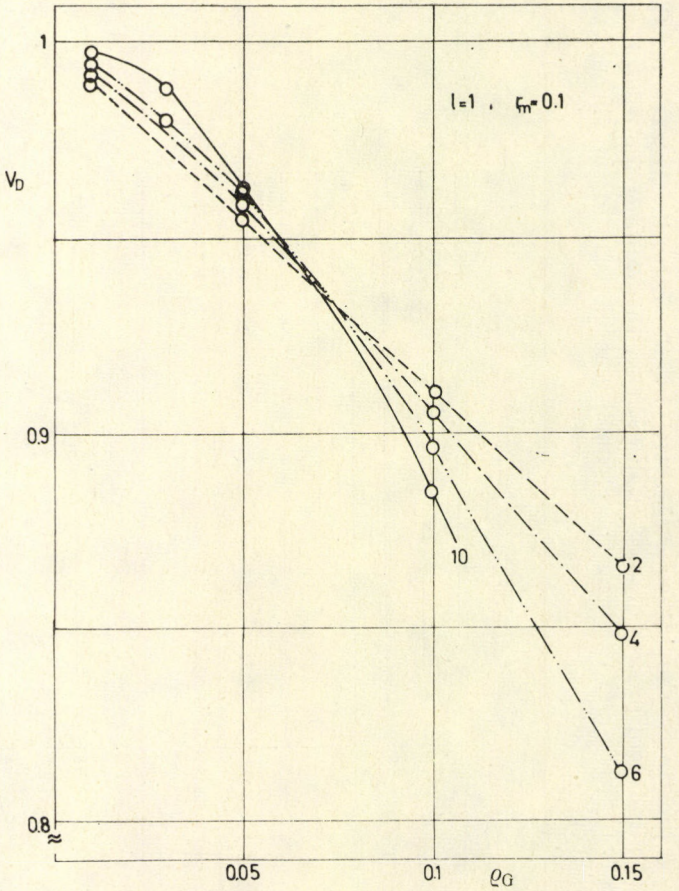

Fig. 6.
Throughput availability for $l=1$ and $r_m=0.1$ as a function of ϱ_G. Parameter: m

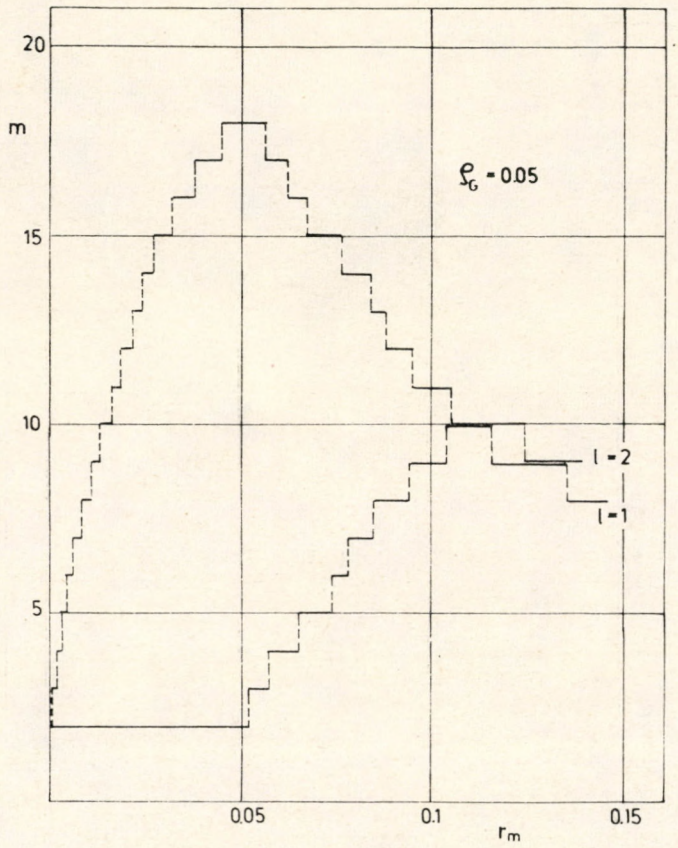

Fig. 7.
Optimum number of partial plants as a function of r_m for $\varrho_G = 0.05$. Parameter: l

if m is increasing. On taking into consideration the limited repair capacity and that with increasing m also the number of the defective partial plants will increase, this result seems to be meaningful.

With increasing r_m the optimum number of the partial plants will, at first, increase. Later on, the extremum will again be shifted towards smaller values (*Figs. 5* and *7*). This effect will, however, become apparent only if the value of r_m is large enough, so that it should be of a very great practical significance.

The number l of the repair units exerts a considerable influence. This is shown if comparing *Figs. 5* and *9*. With increasing l the optimum of partial plants is shifted towards larger values, and the maximum value of V_D increases. All this shows that the efficiency of the repair shop decisively determines the design of the circuit and its availability.

Finally, a comparsion of *Figs. 8* and *9* illustrates the effect of a change of ϱ_G.

Acknowledgement: thanks are expressed to Prof. SCHULTZ-PISZACHICH for his critical review of the manuscript and his suggestions for improvements.

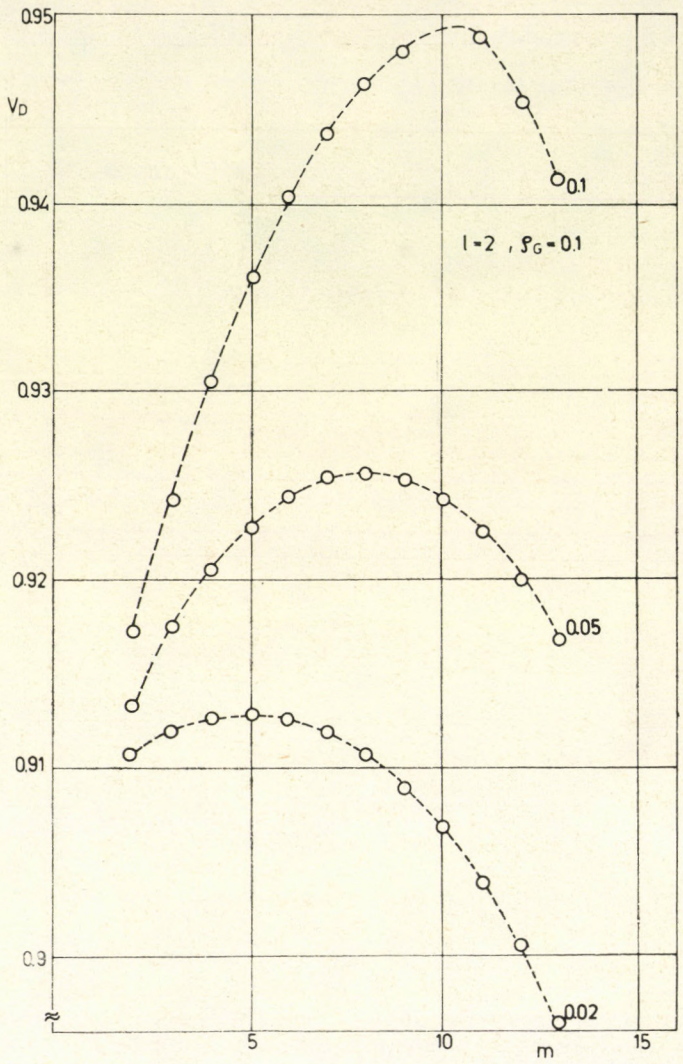

Fig. 8.
V_D as a function of m for $l=2$ and $\varrho_G=0.1$. Parameter: r_m

REFERENCES

1. Gruhn, G.: Systemverfahrenstechnik I. VEB Deutscher Verlag für Grundstoffindustrie, Leipzig, 1976.
2. Kardos, J. und Vondran, J.: CHISA-Vortrag 1975. L 2.4.
3. Vondran, J. und Kardos, J.: Hung. J. Ind. Chem. *3*, 565 (1975).
4. Biehounek, J.: Hung. J. Ind. Chem. *5*, 283 (1977).
5. König, D. und Stoyan, D.: Methoden der Bedienungstheorie. Akademie-Verlag, Berlin, 1976.
6. Palm, C.: Ind. Norden *75*, 75, 90, 119 (1947).

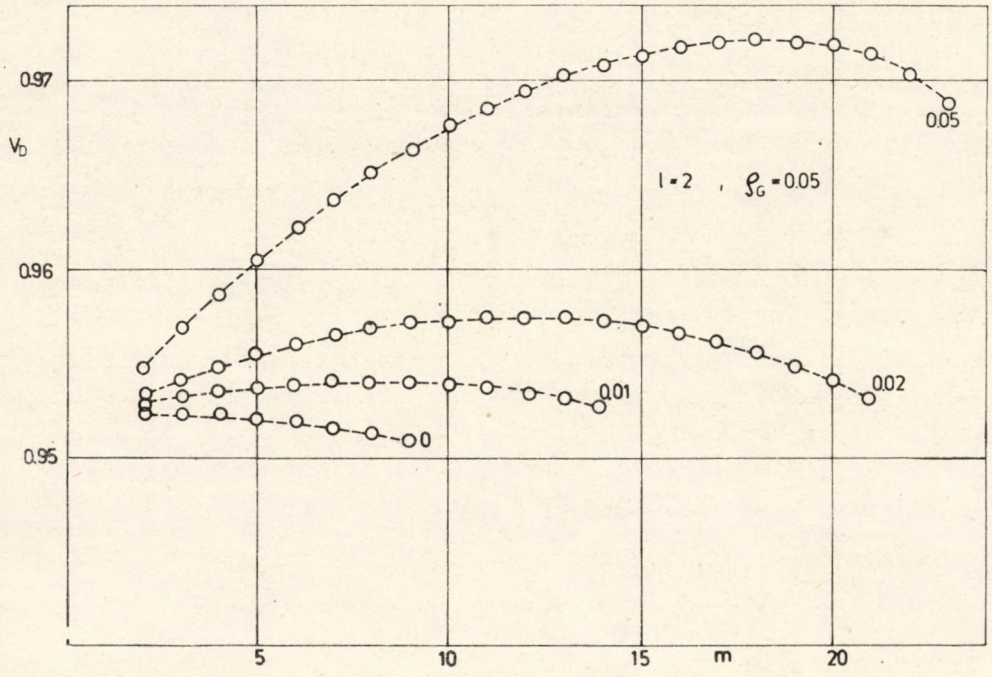

Fig. 9.
V_D as a function of m for $l=2$ and $\varrho_G=0.05$. Parameter: r_m

7. Krampe, H., Kubat, J. und Runge, W.: Bedienungsmodelle. Verlag die Wirtschaft, Berlin, 1974.
8. Palm, C.: Ablauf- und Planungsforschung *6*, 119 (1965).
9. Bharucha-Reid, A. T.: Elements of the Theory of Markov Processes and their Applications. McGraw-Hill, New York—Toronto—London, 1960.

РЕЗЮМЕ

Исследовалась пропускная способность параллельного включения с разделенной мощностью при использовании вспомогательных средств теории массового обслуживания. При этом становится ясным, что замена одной мощной установки на т установок малой мощности может привести к повышению пропускной способности, если, конечно, отдельные установки имеют резервы мощности. Эти резервы мощности все-таки должны превысить минимальное значение. Имеется оптимальное количество отдельных установок. В основном оно определяется производительностью ремонтных мастерских,

HUNGARIAN JOURNAL
OF INDUSTRIAL CHEMISTRY
VESZPRÉM
Vol. 6. pp. 383–394 (1978)

STUDIES ON THE LIQUID-PHASE HYDRODYNAMICS IN BUBBLE AND SIEVE-PLATE COLUMNS EQUIPPED WITH SELECTIVE PARTITIONS I.

LIQUID MIXING PROCESSES IN THE CONNECTING TUBES AND ON THE SELECTIVE PARTITIONS INSTALLED BETWEEN PAIRS OF BUBBLE OR SIEVE-PLATE COLUMNS

L. Balla and Cs. Sisak

(Research Institute for Technical Chemistry of the Hungarian Academy of Sciences, Veszprém, Hungary)

Received: August 30, 1978.

Bubble and sieve-plate column cascades equipped with selective partitions can be considered pairs of columns connected by connecting tubes or selective partitions. Liquid mixing processes, taking place in these connecting tubes or on these partitions, seriously influence the liquid-phase hydrodynamics in these systems. The mixing characteristics presented here have been designed to model these processes. The relationships between the mixing characteristics and the major bubble and sieve-plate column operating parameters were determined. Similarities in the mixing processes, occurring in the connecting tubes and on the selective partitions, were identified.

Introduction

One of the gas-liquid systems used in chemical technology is the dynamic foam system generated by the passage through a liquid layer of an equally distributed flow of gas of 0.5 m/s minimum gas velocity (relating to the overall empty cross section of the apparatus) [1, 2]. At gas velocities below 0.5 m/s, the commonly known bubble system is obtained. Apparently, the two systems are distinguished only by the different gas velocities. However, there is also a qualitative difference, as essentially separate bubbles exist below 0.5 m/s, while above this value, as implied by the name of the technique, a dynamic foam structure is obtained.

Over the past decade, new and specific types of sieve-plate columns were developed at the Research Institute for Technical Chemistry of the Hungarian Academy of Sciences, Veszprém, sieve-plate columns with selective partitions [3, 4, 5]. As described earlier, the fundamental characteristic of the apparatuses

equipped with selective partitions is the intense mass transfer process taking place across the rigid permeable partition (e.g. sieve mesh), installed vertically (in general) between the columns. Mass transfer is due to the pulsating movement, a characteristic feature of the system. The partition is a selective one, i.e. there is no mass transfer with respect to the gas phase [5].

The basic unit of the process consists of two bubble or sieve-plate columns, separated by areas of stainless steel gauze, installed vertically between the columns. Cascade systems are generally arranged horizontally and can be created by connecting sequences of the basic column-partition-column units. The most frequently used system is the counter-current sieve-plate cascade with selective partition [5, 6].

Due to the cascade system the flow structure of the liquid phase is obviously rather complex. Apparently different flow conditions exist in the columns, the connecting tubes (between the columns) and on the gauze partitions. Essentially, the units of the apparatus can be considered single-layer bubble or sieve-plate columns with transversal flows. Mixing in bubble columns was extensively studied. Most papers consider these units to be partially mixed [7, 8, 9]. On the contrary, previous investigations by the present authors proved that systems consisting of cascades with selective partitions were almost perfectly mixed, a fact explained by their special design and method of operation [4, 10].

In the course of further studies on the hydrodynamics of these cascades, emphasis was placed on the investigation of backmixing in the connecting tubes and transmixing through the partitions. Since cascade systems are composed of pairs of bubble and sieve-plate columns, connected by connecting tubes and partitions, such pairs have to be studied first. The effects of major apparatus design and operation parameters upon transmixing through the partition and backmixing in the connecting tube were investigated.

Fundamentals

The same model was applied to both the transmixing and backmixing column pairs. The one-dimensional model is shown in *Fig. 1.*

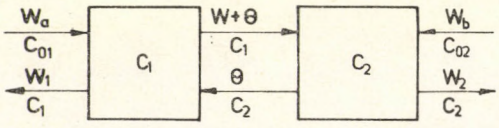

Fig. 1.
Schematics of the column-pair model

The major assumptions of the model are as follows:

- $w_a - w_1 = w_2 - w_b = w$,
- the units are perfectly mixed,
- Θ flow rates are equal in both directions.

In steady-state conditions, a balance equation system describing the model can be constructed as:

$$w_a c_{01} + \Theta c_2 = w_1 c_1 + w c_1 \tag{1}$$

$$w_b c_{02} + \Theta c_1 = w_2 c_2 + \Theta c_2 \tag{2}$$

Let:

$$\Theta = w^* \tag{3}$$

when the model is applied to the column pair with connecting tube, where w^* is the backmixing flow rate. It can easily be shown that the backmixing flow rate thus defined is identical with the parameter of the non-dimensionless form of the internal-recirculation model [11].

$$\Theta = w^{**} \tag{4}$$

in the case of a column pair with partition, where w^{**} is the transmixing flow rate. The transmixing flow rate is analogous to the multiple βA, the parameter of the transfer model developed for columns with partitions [5] (cf. *Fig. 2*).

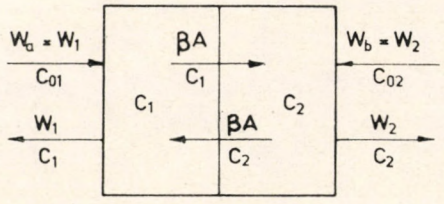

Fig. 2.
Schematics of the "transfer" model

Mixing flow rates can be calculated, in both cases, from the balance equations of both units.

Experimental

There were two methods available for the study of mixing processes in pairs of columns:

a) The first method was based on the residence time distributions of the apparatuses.

b) The second method could be used only in steady-state conditions [4, 10]. In short, the mixing characteristics in steady-state conditions can be calculated from the material balance equations constructed for the phase in question, in each unit of the multi-unit system, if the following conditions are met:
- with respect to the phase in question, the units can be considered perfectly mixed, i.e. the mixing characteristics of material flows of given directions can be assigned to "contact surface areas" between neighbouring units,
- mixing processes do not change if a steady-state flow of a suitable tracer is introduced into the system, while a flow of equal magnitude is taken off from the phase in question.

After careful comparison, the second method was selected. The experimental setup is shown in *Fig. 3.*

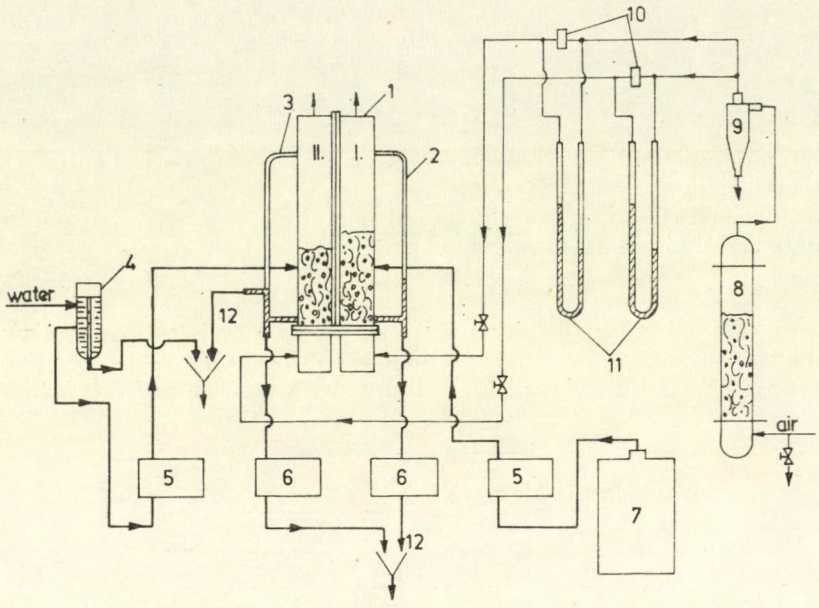

Fig. 3.
Schematics of the experimental set-up

The apparatus (1), made of Persplex, is a pair of columns with either back- or transmixing. The units are 60 cm high, with a cross section area of 50 cm². In the case of the column pair with backmixing, a horizontal tube is installed in the wall separating the columns. The length, diameter and height of the tube can be changed. In the case of a column pair with transmixing, a given portion of the separating wall between the columns is covered with fine mesh gauze (perforated plate), and the area and the diameter of the holes on it can be changed.

Brine, used as tracer, is fed from a container (7). Tap water is introduced via the overflow unit (4) by pumps (5). Liquid is taken off via openings (2) and (3) by pumps (6). Part of the liquid in *Column 1* flows through the partition wall or connecting tube into *Column 2*. The amount of the flowing liquid is controlled by regulating the offtake rates. Part of the liquid from *Column 2* is taken off via an overflow unit. The liquid level in the system can be maintained by changing the vertical position, H_0 of the overflow unit. Air obtained from a compressed air network is introduced into the saturating column (8) after an appropriate relief branch. Saturated air enters the columns via the cyclone (9) and measuring orifice (10). The air flow rate, kept equal in both columns, is regulated by chokes. Brine flows leaving the column are periodically sampled at sampling locations (12). Concentrations are determined conductometrically. Sampling is resumed a few minutes after the run is initiated and it is repeated on a minute basis until steady-state conditions are achieved.

The parameters that varied during the examination of backmixing are as follows:

— the amount of liquid flowing through the connecting tube (w),

- linear gas velocity with respect to the empty cross section area (v'),
- level of the liquid leaving the system at the secondary side (H_0),
- height of the connecting tube measured from the sieve-plate bottom (y_0),
- length of the connecting tube (l),
- cross section area of the connecting tube (q).

The parameters that varied during the examination of transmixing processes are as follows:

- the amount of liquid flowing through the partition (w_F),
- gas velocity calculated with respect to the empty cross section area (v'),
- concentrations of the liquid flows entering *Columns 1* and *2* (c_{01} and c_{02}),
- height of the level of the liquid leaving *Column 2* (H_0),
- opening size of the partition (d_p),
- surface area of the partition (A).

Results and Discussion

Changes of the backmixing flow rate, w^* as a function of the liquid flow rate, w are shown in *Fig. 4*. A constant decrease can be observed on the w^* vs w curves corresponding to the fact that a higher flow rate in the connecting tube

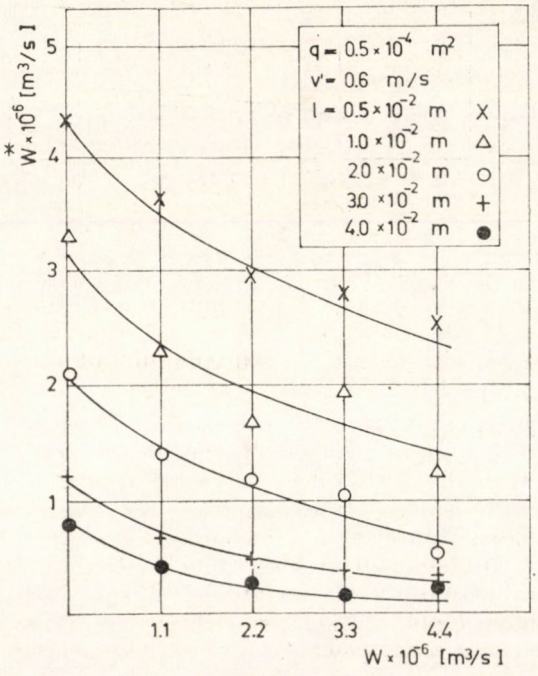

Fig. 4.
Changes of the backmixing flow rate through the connecting tube as a function of the liquid flow rate

increasingly prevents the mixing back of liquid elements from *Column 2* into *Column 1*. Due to the limitations imposed by the physical dimensions of the apparatus, no flow rate could be achieved beyond the 4.4×10^{-6} m^3/s value. However, it seems reasonable to assume that practically no backmixing can occur at sufficiently high liquid flow rates, i.e. w^* approaches zero.

The effect of the gas velocity upon backmixing is shown in *Fig. 5*. There is

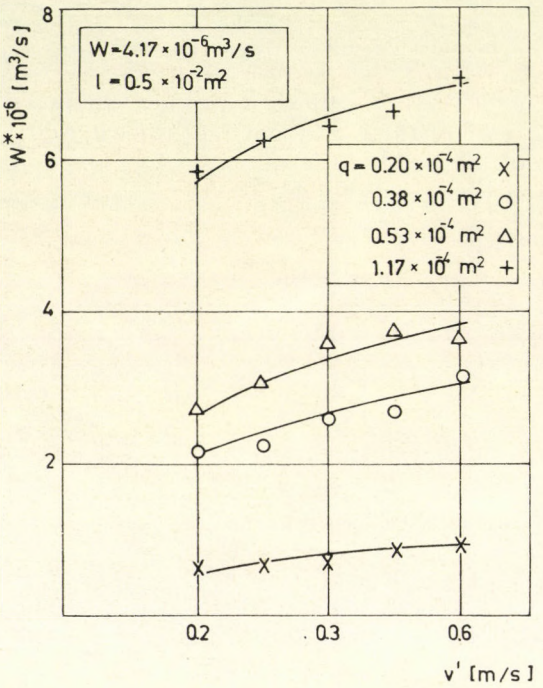

Fig. 5.
Backmixing flow rate as a function of gas velocity

a slight increase in w^* with increasing gas velocity, a fact caused by increased pulsations brought about by the higher gas velocity [5, 6].

It can be concluded from the w^* *vs* l relationship (length of the connecting tube) that there is an almost linear decrease in the value of w^* up to $l<2\times10^{-2}$ m, while with longer tubes w^* approaches a constant value (cf. *Fig. 6*). There is a possible explanation for this characteristic shape, which is as follows. The amplitude of the pulsation characterizing the system at the gas velocity applied (0.6 m/s) is some 2×10^{-2} m [6], i.e. backmixing at $l<2\times10^{-2}$ m is due, mainly, to pulsation, while at $l>2\times10^{-2}$ m it is due, primarily, to turbulent axial diffusion.

Changes of the backmixing flow rate as a function of the connecting tube cross section area are shown in *Fig. 7*. The relationship becomes unequivocally linear only above a tube cross section area of 5×10^{-5} m^2, as in narrower tubes there is practically no chance for backmixing due to bubble movement [6].

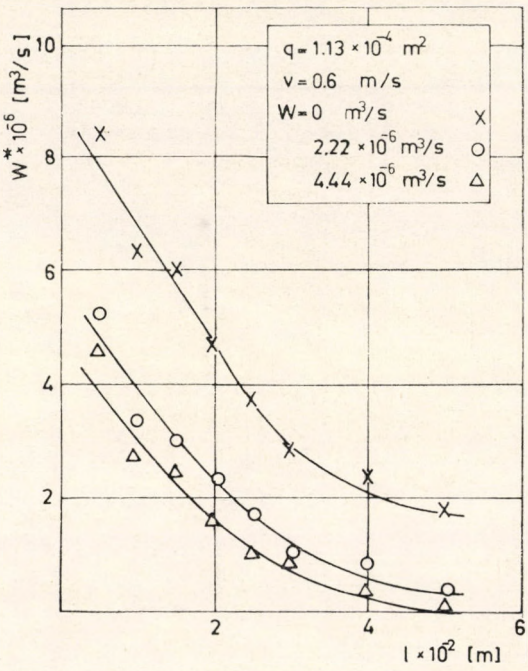

Fig. 6. Backmixing flow rate as a function of the length of the connecting tube

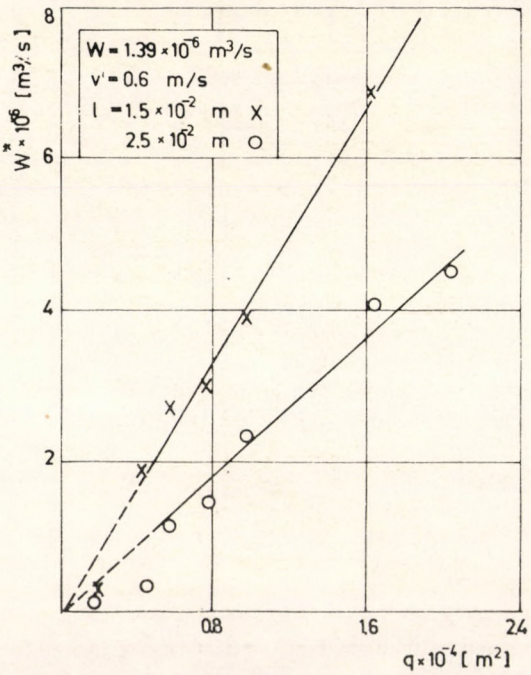

Fig. 7.
Backmixing flow rate as a function of the cross section area of the connecting tube

The liquid level height in *Column 2* H_0, and foam height proportional to H_0 are also linearily proportional to the backmixing flow rate, w^* (cf. *Fig. 8*).

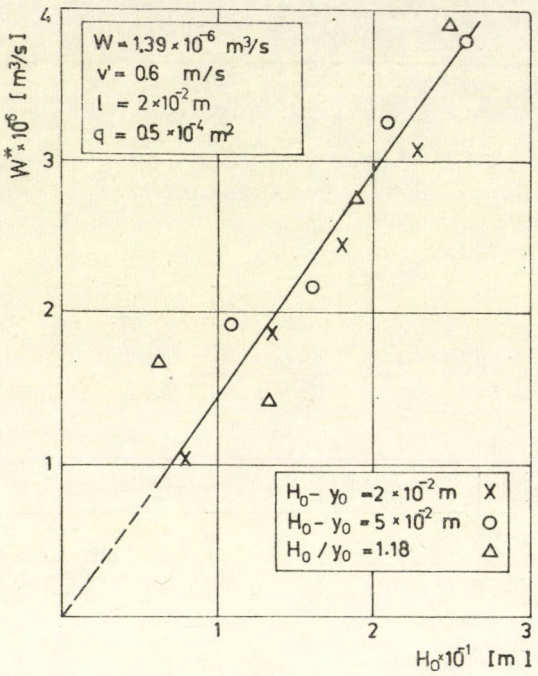

Fig. 8.
Backmixing flow rate as a function of the height of the overflow opening

This change of w^* can probably be explained by the observation that the amplitude of the pulsing movement increases with the increasing liquid level, while its frequency does not decrease proportionally. It is also apparent from the figure that the height of the connecting tube, measured from the sieve base plate y_0, has practically no effect upon the magnitude of the backmixing.

Changes of the transmixing flow rate, w^{**} as a function of the liquid flow rate, w_F are shown in *Fig. 9*. The curves are similar to those shown in *Fig. 4* (w^* *vs* w curves). Apparently the higher H_0 the greater w^{**} becomes.

As shown in *Fig. 10* the transmixing flow rate increases with increasing gas velocity. This increase is steeper in the bubble-range ($v < 0.5$ m/s), it is more moderate in the dynamic foam range and, in fact, approaches a limiting value with fine mesh partitions (25×10^{-6} m, 45×10^{-6} m). This is in agreement with the earlier results obtained with fine mesh gauze partitions [4]. It can also be seen in *Fig. 10* that w^{**} increases with increasing opening size d_p though the free surface areas of the partitions with different openings are maintained equal. This phenomena is probably due to phase boundary effects.

It is apparent from *Fig. 11* that the transmixing flow rate is practically independent from the input liquid concentrations and changes linearily with the increasing partition surface area, A. These results are in agreement with earlier findings at $w_F = 0$ [4, 10].

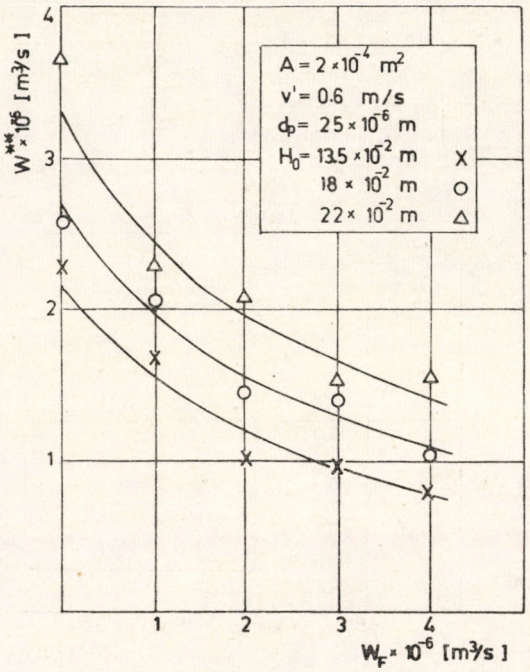

Fig. 9. Transmixing flow rate as a function of the liquid flow rate through the partition

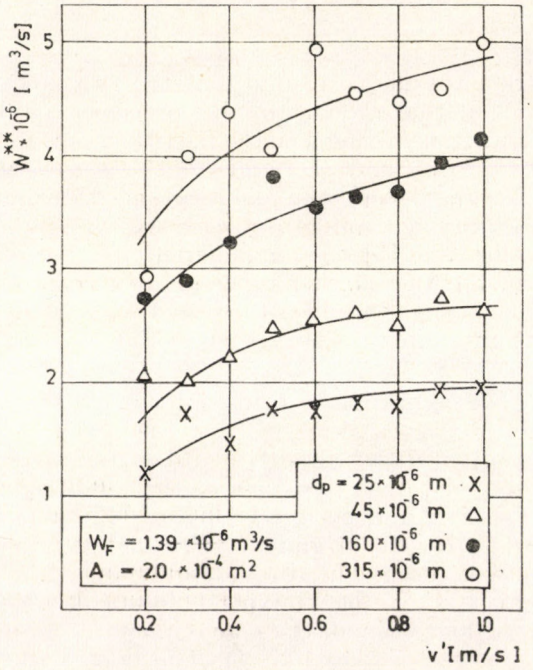

Fig. 10. Transmixing flow rate as a function of the gas velocity

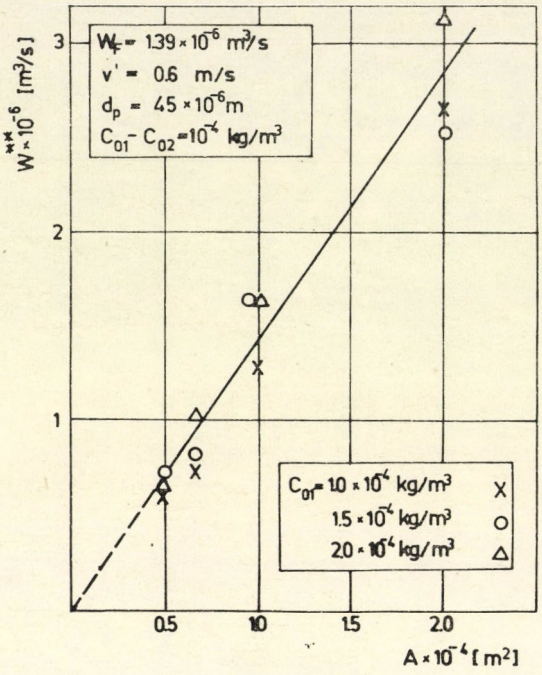

Fig. 11.
Transmixing flow rate as a function of the surface area of partition wall

It is apparent from the above results that the two mixing parameters are not only analogous, but that the two mixing processes, i.e. backmixing in the connecting tubes and transmixing via the partitions are in close relationship as substantiated by *Figs. 4* and *3*, *5* and *10* as well as *7* and *11*. The reason of the similarity is, no doubt, the identical mechanism underlying these processes. Both backmixing and transmixing are brought about by pressure —drop—induced pulsations [5], the characteristic feature of the operation [6]. Differences between the two mixing processes can be attributed to the fact that there a gas transfer takes place through the connecting tube, while no such process exists through the selective partition constructed of fine mesh gauze.

It was assumed that a continuous transition could be achieved—at least—with respect to transmixing (backmixing) between a fine mesh gauze partition of free surface area A_{sz} and a connecting tube of cross section $q = A_{sz}$, the length of which is equal to the thickness of the mesh gauze. Standard mesh gauzes up to 3.5×10^{-6} m and perforated plates of a thickness of 4×10^{-4} m with openings of (1, 2, 3, 4, 5.5 and 8)$\times 10^{-3}$ m with free surface areas of 0.5×10^{-4} m^2 both, were used. The results are presented in *Fig. 12*. It can be seen that the transmixing (backmixing) flow rate does indeed change continuously with the logarithm of the bore diameter. Curves pass a maximum point at a bore diameter of 2.5×10^{-3} m. The bore diameter corresponding to this maximum can be considered, in all probability, a diameter above

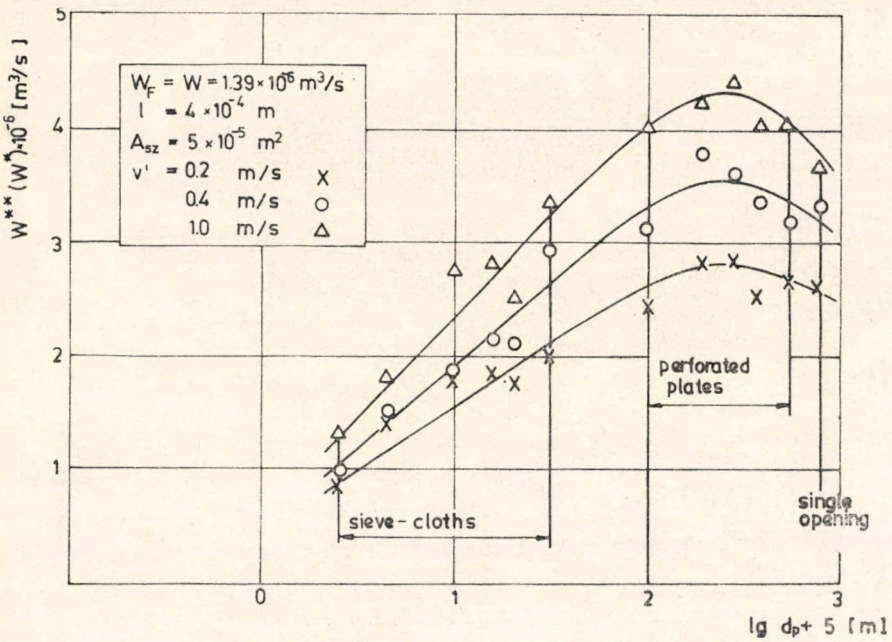

Fig. 12.
Transmixing (backmixing) flow rate as a function of the logarithm of the diameter of the opering

which gas transmixing also takes place, i.e. the free surface area available for the liquid phase is decreased. The curve series shown in the figure also substantiates the analogy between the transmixing and backmixing processes.

SYMBOLS

A — surface area of the selective partition, m²;
A_{sz} — free surface area of the selective partition, m²;
c_1, c_2 — steady state liquid concentrations in *Column 1* and *2*, kg/m³;
c_{01}, c_{02} — input liquid concentrations in *Column 1* and *2*, respectively, kg/m³;
d_p — diameter of the opening of the selective partition, m;
H_0 — height of the overflow opening in *Column 2*, m;
l — length of the connecting tube, m;
q — cross section area of the connecting tube, m²;
v' — gas velocity with respect to the empty cross section, m/s;
w — flow rate of the liquid through the connecting tube, m³/s;
w_a, w_b — liquid feed rate into *Column 1* and *2*, respectively, m³/s;
w_F — flow rate of liquid flowing through the selective partition, m³/s;
w_1, w_2 — liquid offtake rate from *Column 1* and *2*, respectively, m³/s;
w^* — backmixing flow rate, m³/s;
w^{**} — transmixing flow rate, m³/s;
y_0 — height of the connecting tube from distributing bottom sieve plate, m;
β — mass transfer coefficient characterizing mass flow rate through the selective partition, m/s;
Θ — flow rate between elements of the column pair in both directions, m³/s.

REFERENCES

1. Pozin, M. E. et al.: Pennüj Sposob obrabotki gazov i zhidkostiei. Goshimizdat. Leningrad, 1955.
2. Káldi, P. és Blickle, T.: Veszprémi Vegyipari Egyetem Közleményei, *6*, 251 (1962).
3. Apparatus and Process for the Intensification of Gas and Liquid Phase Operations.

Hung. Pat.	157,288	U. S. Pat.	3 796,788
British Pat.	1,243,646	Austrian Pat.	305,958
French Pat.	1,583,578	GDR Pat.	70,562
Soviet Pat.	1,291,389	Italian Pat.	853,742
Soviet Pat.	1,263,248	Czechoslovak Pat.	5,601
U. S. Pat.	3,607,104	GFR Pat.	1,792,156

4. Balla, L.: Studies on the Mass Transfer through Selective Partitions between Dynamic Foam Systems. Thesis, Univ. Chem. Engng, Veszprém, 1969 (in the Hungarian).
5. Blickle, T. und Balla, L.: Chem. Anlagen + Verfahren, *1974* (9), 57, 61.
6. Sisak, Cs.: Studies on the Liquid Phase Mixing Process in Sieve-plate Column Cascades with Selective Partitions. Thesis, Univ. Chem. Engng., Veszprém, 1977 (in the Hungarian).
7. Káldi, P. és Blickle, T.: Veszprémi Vegyipari Egyetem Közleményei, *6*, 273 (1962).
8. Deckwer, W., Graeser, U., Langemann, H. and Serpemen, Y.: Chem. Eng. Sci., *28*, 1223 (1973).
9. Kafarov, V. V., Kruglik, A. E., Trofimov, V. J.: Zh. Prikl. Khim. (Leningrad), *46*, 1712 (1973).
10. Nagy, E.: Studies on the Mass Transfer Processes in Bubble Columns. Thesis, Univ. Chem. Engng., Veszprém, 1974 (in the Hungarian).
11. Haddad, A. H. and Wolf, D.: Can. J. Chem. Eng., *45*, 100 (1967).

РЕЗЮМЕ

Каскады барботажных и пенных колонн селективными переборками могут рассматриваться как комплекты таких колонных пар, которые либо соединены переходной трубой, либо разделены селективной переборкой. На гидродинамику жидкой фазы каскадных установок значительное влияние оказывают процессы перемешивания жидкости, происходящие в упомянутых трубах и на селективных переборках. В целях моделирования, авторами были составлены характеристики перемешивания, а затем рассматривались зависимости между параметрами перемешивания и наиболее важными параметрами, влияющими на работу барботажных и пенных колонн. На основании полученных результатов были выявлены сходные черты между процессами перемешивания, характерными для переходных труб и для селективных перегородок.

HUNGARIAN JOURNAL
OF INDUSTRIAL CHEMISTRY
VESZPRÉM
Vol. 6. pp. 395–408 (1978)

STUDIES ON THE LIQUID PHASE HYDRODYNAMICS IN BUBBLE AND SIEVE-PLATE COLUMNS EQUIPPED WITH SELECTIVE PARTITIONS II.

MODELLING OF THE FLOW CONDITIONS IN COUNTER-CURRENT CASCADES

L. Balla and Cs. Sisak

(Research Institute for Technical Chemistry of the Hungarian Academy of Sciences, Veszprém, Hungary)

Received: August 30, 1978.

The authors established that the so-called counter-current bubble and sieve-plate columns equipped with selective partitions cannot be considered completely countercurrent units, rather a complex convective flow structure is formed in them. A calculation method based on the principle of minimum energy was developed to determine the magnitude of the flow through the connecting tube and the selective partition, respectively. A cascade model was created to describe the flow conditions in the liquid phase. The steady-state concentration characteristics in the cascade system could be calculated by the method presented here using the results described in *Part 1* relating to pairs of sieve-plate columns. Calculated and measured values agreed well.

Introduction

As mentioned in *Part 1* studies on pairs of bubble and sieve-plate columns are necessery to describe the hydrodynamical conditions of cascade systems. The cascade, in fact, consists of the pairs of columns studied. However, only a part of the necessary information could be obtained from the investigation of the mixing processes in the column pairs. A closer examination of convective flow system of the cascade reveals (cf. *Fig. 1*) that the results presented in *Part 1* describe the magnitude of backmixing in the connecting tubes and transmixing through the selective partitions only in those cases when flows:

$$w_{1,1}, w_{1,2}, \ldots, w_{1,n-1}$$

and

$$w_{2,2}, w_{2,3}, \ldots, w_{2,n}$$

through the connecting tubes and flows:

$$w_{F_1}, w_{F_2}, \ldots, w_{F_n}$$

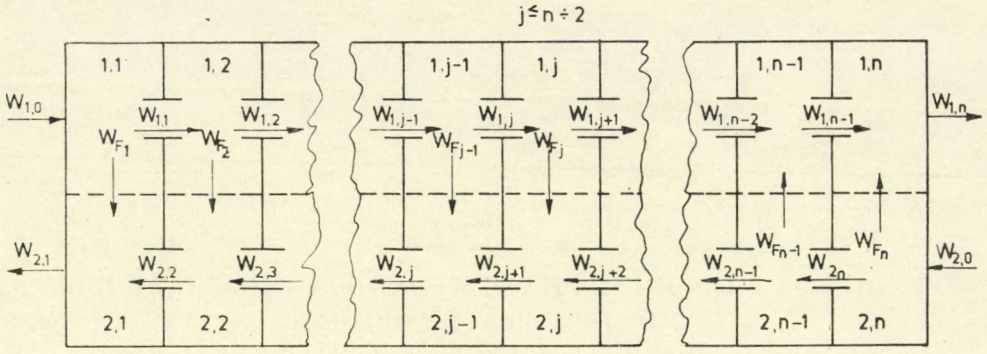

Fig. 1.
Schematics of the convective flow system of the counter-current cascade

through the partitions are also determined along with the input and output flows. Experience has proved that the earlier assumptions used [1], i.e.:

$$w_{F_1,} = w_{F_2,} = \ldots = w_{F_n} = 0 \tag{1}$$

and consequently:

$$w_{1,1} = w_{1,2} = \ldots = w_{1,n-1} = w_{1,0} = w_{1,n} \tag{2}$$

and:

$$w_{2,2} = w_{2,3} = \ldots = w_{2,n} = 2,1 = 2,0 \tag{3}$$

hold only in the case of specially designed systems. In the majority of cases the formal term "counter- current" can be used only because the directions of input and output flows at the primary and secondary sides of the cascade are opposite. The liquid flow inside and between the units can no longer be considered to be countercurrent. The experimental determination of the components of the complex flow pattern is extremely difficult.

Computation of the Components of the Convective Flow System

The flow through the connecting tube, $w_{i,j}$ and through the partition, w_{F_j} can be calculated due to the almost obvious realization that the formation of the complex flow pattern is governed by the principle of minimum energy. Flows $w_{i,j}$ and w_{F_j} assume values determined by input and output flow rates, apparatus design and operation parameters which ensure that energy losses in flows inside the system are minimum. When the overall energy loss is the smallest all the flows through the connecting tubes and the partitions are stabilized with respect to time. This stabilized condition can be described by energy balance equations in which the energy losses corresponding to flows $w_{i,j}$ and w_{F_j} are the terms. Energy loss appears as a pressure drop over the connecting tubes and partitions, i.e. over resistances against liquid flow. Thus, changes in the pressure drop over connecting tubes and partitions as functions of design and operation parameters have to be determined to facilitate the construction of the energy balance. Experiments were carried out to obtain these functions presented as empirical relationships [2].

The calculation of the pressure drop balance equation of the counter-current cascade is shown here for the simplest and most frequently encountered case [1, 3], i.e. when:

$$w_{1,0} = w_{1,n} = w_{2,1} = w_{2,0} \tag{4}$$

Naturally, calculations can be carried out in other cases as well [2]. If Eq. (4) is valid and the major design parameters of each cascade unit are equal, then due to the symmetry of the system the relationship:

$$w_{1,j} = w_{2,j+1} = w_{1,n-1} = w_{2,n-j+1} \tag{5}$$

relating to the flows through the connecting tubes is also fulfilled (cf. *Fig. 1*). The directions of flows $w_{1,j}$ and $w_{1,0}$ as well as $w_{2,j}$ and $w_{2,0}$ are the same. It also holds for the flows through the partitions that:

$$w_{Fj} = w_{F_{n-j}} \tag{6}$$

but their directions are opposite. If $j \leq n \div 2$ (where the symbol $\div$ is used to represent a division operation with integers) then the direction of w_F points from side $i=1$ towards side $i=2$.

Naturally, due to Eqns. (5) and (6) the corresponding pressure drop values are also equal:

$$\Delta p_{1,j} = \Delta p_{2,j+1} = \Delta p_{1,n-j} = \Delta p_{2,n-j+1} \tag{7}$$

$$\Delta p_{Fj} = \Delta p_{F_{n-j}} \tag{8}$$

It follows that the liquid from any unit in which there is a branching (i.e. there are flows leaving the system both through one of the connecting tubes and the partition) can reach the exit port of the apparatus on no more than two routes. In steady state conditions, the pressure drops along the two routes are equal. In the case of $j \leq n \div 2$ the following pressure drop balance equation can be constructed for the jth cell at the $i=1$ side:

$$\Delta p_{1,j} + \Delta p_{1,j+1} + \ldots + \Delta p_{1,n-1} = \Delta p_{Fj} + \Delta p_{2,1} + \ldots + \Delta p_{2,j}. \tag{9}$$

Allowing for Equations (5) and (6), Eq. (9) can be rewritten when the number of units is an odd number, n:

$$2(\Delta p_{1,j} + \Delta p_{1,j+1} + \ldots + \Delta p_{1,n\div 2}) + \Delta p_{1,1} + \ldots + \Delta p_{1,j-1} = \Delta p_{Fj} + \Delta p_{1,1} + \ldots + \Delta p_{1,j-1}. \tag{10}$$

After eliminations:

$$2\left(\sum_{j}^{n\div 2} \Delta p_{1,j}\right) = \Delta p_{Fj}. \tag{11}$$

Thus, an equation set consisting of $2(n-1)$ equations can be constructed for a cascade consisting of n unit pairs. The equation set contains $n \div 2$ pressure drop balance equations and $n \div 2$ flow rate balance equations. Together with the empirical relationships [2] the equation system can be solved resulting in flow rates $w_{1,j}$ and w_{Fj}. For example, if n is an odd number the equation set becomes:

$$\begin{cases} 2\sum_{j=1}^{n\div 2} \Delta p_{1,j} = \Delta p_{F_1} \\ \vdots \\ 2\sum_{j}^{n\div 2} \Delta p_{1,j} = \Delta p_{F_j} \\ \vdots \\ 2\Delta p_{1,\,n\div 2} = \Delta p_{F\,n\div 2} \\ w_{1,0} = w_{1,1} + w_{F_1} \\ w_{1,1} = w_{1,2} + w_{F_2} \\ \vdots \\ w_{1,j} = w_{1,j+1} + w_{F_{j+1}} \\ \vdots \\ w_{1,\,n\div 2} = w_{1,\,n\div 2+1} + w_{F\,n\div 2+1} \end{cases} \tag{12}$$

A similar equation set can be constructed when n is an even number.

A comprehensive physical picture relating to the flow conditions in countercurrent bubble and sieve-plate columns equipped with selective partitions could be derived from the results presented in *Part 1* [6] and the determination of the flow rates through the connecting tubes and selective partitions.

The countercurrent cascade system consists of pairs of bubble or sieve-plate columns separated by selective partitions and the column pairs are connected by connecting tubes. Flow rates through the connecting tubes and selective partitions are determined by the input liquid flow rates, design and operation parameters (as detailed in *Part 1*) allowing for the principle of minimum energy. Transmixing and backmixing processes take place in the connecting tubes and through the selective partitions, respectively. (Their properties were also detailed in *Part 1.*)

Model of the Cascade System

A mathematical model was developed to describe the cascade system operating in steady state conditions. An important prerequisite of the model was that use could be made of the previous numerical data as input data. The model is based on the so-called internal recirculation model [4] and the column pair model described in *Part 1* [6].

The schematics of the model are shown in *Fig. 2.*

The following assumptions hold:

- liquid phase is perfectly mixed in the units,
- useful volumes of the units are equal, V,
- $i=1,2;\quad 0\leq j\leq n+1$,
- flows between the units have the following meaning:
  ${}_{j}w_{j+1}^{(i)}$: flow from the jth unit into the $j+1^{\text{th}}$ unit in the ith row,
  ${}_{j+1}w_{j}^{(i)}$: flow rate of opposite direction between the same units,
  $w_j^{(i)}$: flow from the jth unit in the ith row into the jth unit in the other row,
- the equivalencies:

$$ {}_{1}w_{0}^{(1)} = {}_{n+1}w_{n}^{(1)} = {}_{0}w_{1}^{(2)} = {}_{n}w_{n+1}^{(2)} = 0 \tag{13}$$

are valid.

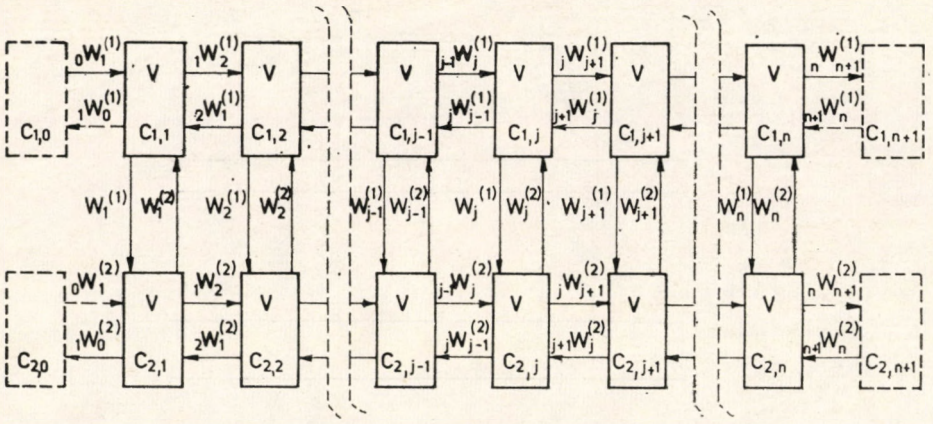

Fig. 2.
Schematics of the cascade model

The balance equations constructed for the units $1 \leq j \leq n$ form a constant coefficient first order linear differential equation set, which in the case of steady state conditions, becomes simply a linear equation set. The vector-matrix representation of this equation is shown in *Table 1.*

The coefficients used in the *Table 1* are as follows

$$a_{i,j} = -({}_{j}w_{j+1}^{(i)} + {}_{j}w_{j-1}^{(i)} + w_{j}^{(i)});$$

$$b_{1,j} = {}_{j}w_{j-1}^{(i)};$$

$$d_{i,j} = {}_{j}w_{j+1}^{(i)};$$

$$e_{i,j} = w_{j}^{(i)};$$

$$f_{1,0} = {}_{0}w_{1}^{(1)};$$

$$f_{2,n+1} = {}_{n+1}w_{n}^{(2)}.$$

The model can be advantageously used in this form for computerized processing. However, a modified version was also required for input flow rates $w_{i,j}$ and w_{F_j} and the mixing parameters as initial data. The schematics of the modified model are shown in *Fig. 3.*

a) for the input flows:

$$w_{1,0} = {}_{0}w_{1}^{(1)} \quad \text{and} \quad w_{2,0} = {}_{n+1}w_{n}^{(2)} \tag{14}$$

b) for the output flows:

$$w_{1,n} = {}_{n}w_{n+1}^{(1)} \quad \text{and} \quad w_{2,1} = {}_{1}w_{0}^{(1)} \tag{15}$$

c) for flows $w_{i,j}$ between the neighbouring units:
if $i = 1$ then:

$$w_{1,j} = \left|{}_{j+1}w_{j}^{(1)} - {}_{j}w_{j+1}^{(1)}\right| \tag{16}$$

if $i = 2$ then:

$$w_{2,j} = \left|{}_{j-1}w_{j}^{(2)} - {}_{j}w_{j-1}^{(2)}\right| \tag{17}$$

Table 1.

$1,1$	$1,2,\ldots,1,j-1$	$1,j$	$1,j+1,\ldots,1,n-1$	$1,n$	$2,1$	$2,2,\ldots,2,j-1$	$2,j$	$2,j+1,\ldots,2,n-1$	$2,n$	$c_{i,j}$	const.
$a_{1,1}$	$b_{1,2}$				$e_{2,1}$					$c_{1,1}$	$-f_{1,0}c_{1,0}$
$d_{1,1}$	$a_{1,2}\ \ldots$					$e_{2,2}$				$c_{1,2}$	0
	$\ddots$					$\ddots$				$\vdots$	$\vdots$
	$\ddots$					$\ddots$				$\vdots$	$\vdots$
	$\ldots\ a_{1,j-1}$	$b_{1,j}$				$e_{2,j-1}$				$c_{1,j-1}$	0
	$d_{1,j-1}$	$a_{1,j}$	$b_{1,j+1}$				$e_{2,j}$			$c_{1,j}$	0
		$d_{1,j}$	$a_{1,j+1}\ \ldots$					$e_{2,j+1}$		$c_{1,j+1}$	0
			$\ddots$					$\ddots$		$\vdots$	$\vdots$
			$\ddots$					$\ddots$		$\vdots$	$\vdots$
			$\ldots\ a_{1,n-1}$	$e_{1,n}$					$e_{2,n-1}$	$c_{1,n-1}$	0
			$d_{1,n-1}$	$a_{1,n}$					$a_{2,n}$	$c_{1,n}$	0
$e_{1,1}$					$a_{2,1}$	$d_{2,2}$				$c_{2,1}$	0
	$e_{1,2}$				$b_{2,1}$	$a_{2,2}\ \ldots$				$c_{2,2}$	0
	$\ddots$					$\ddots$				$\vdots$	$\vdots$
	$\ddots$					$\ddots$				$\vdots$	$\vdots$
	$e_{1,j-1}$					$\ldots\ a_{2,j-1}$	$d_{2,j}$			$c_{2,j-1}$	0
		$e_{1,j}$				$b_{2,j-1}$	$a_{2,j}$	$d_{2,j+1}$		$c_{2,j}$	0
			$e_{1,j+1}$				$b_{2,j}$	$a_{2,j+1}\ \ldots$		$c_{2,j+1}$	0
			$\ddots$					$\ddots$		$\vdots$	$\vdots$
			$\ddots$					$\ddots$		$\vdots$	$\vdots$
			$e_{1,n-1}$					$\ldots\ a_{2,n-1}$	$d_{2,n}$	$c_{2,n-1}$	0
				$e_{1,n}$				$b_{2,n-1}$	$a_{2,n}$	$c_{2,n}$	$-f_{2,n+1}c_{2,0}$

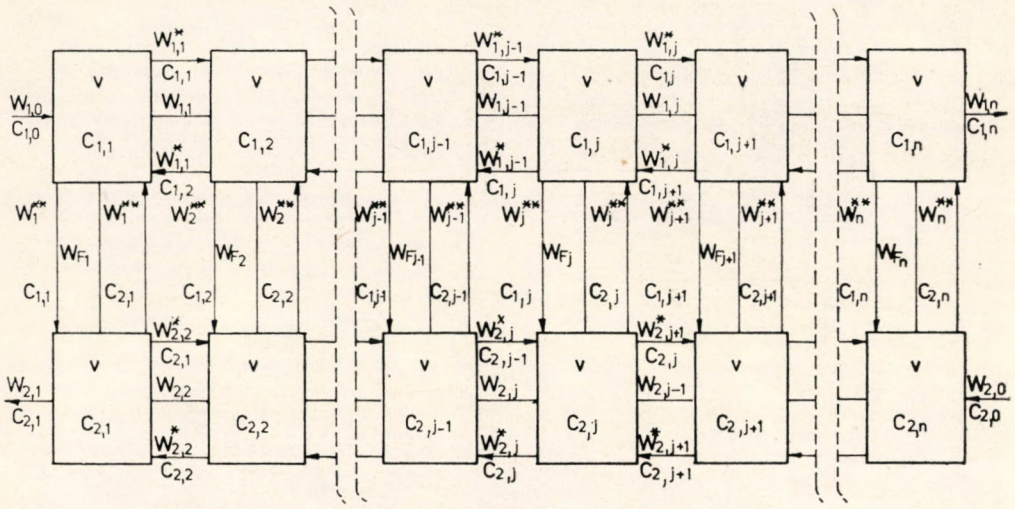

Fig. 3.
Schematics of the modified cascade model

d) for flow w_{F_j} between units of the same "column":

$$w_{F_j} = |w_j^{(1)} - w_j^{(2)}| \tag{18}$$

e) flows $w_{i,j}^*$ are defined as in the model in *Part 1* or as the backmixing flow rate w^* in the internal recirculation model.
If $i = 1$ then:

$$w_{1,j}^* = \frac{{}_j w_{j+1}^{(1)} + {}_{j+1} w_j^{(1)} - w_{1,j}}{2} \tag{19}$$

If $i = 2$ then:

$$w_{2,j}^* = \frac{{}_{j-1} w_1^{(2)} + {}_j w_{j-1}^{(2)} - w_{2,j}}{2} \tag{20}$$

f) flows w_j^{**} are defined as in the model in *Part 1*, as the transmixing flow rate w^{**}:

$$w_j^{**} = \frac{w_j^{(1)} - w_j^{(2)} - w_{F_j}}{2}. \tag{21}$$

The above cascade model was used for the mathematical description of the flow conditions in the counter-current cascade system. The criteria for the applicability of the system are as follows:

a) Liquid phase is almost perfectly mixed in the units;
b) Volume differences between the successive units are negligable;
c) Characteristic dimensions of the connecting tubes and selective partitions in the units are equal.

It was mentioned in *Part 1* [7] that former observations [1, 5] substantiated condition *a)*. With respect to condition *b)* it was determined that liquid

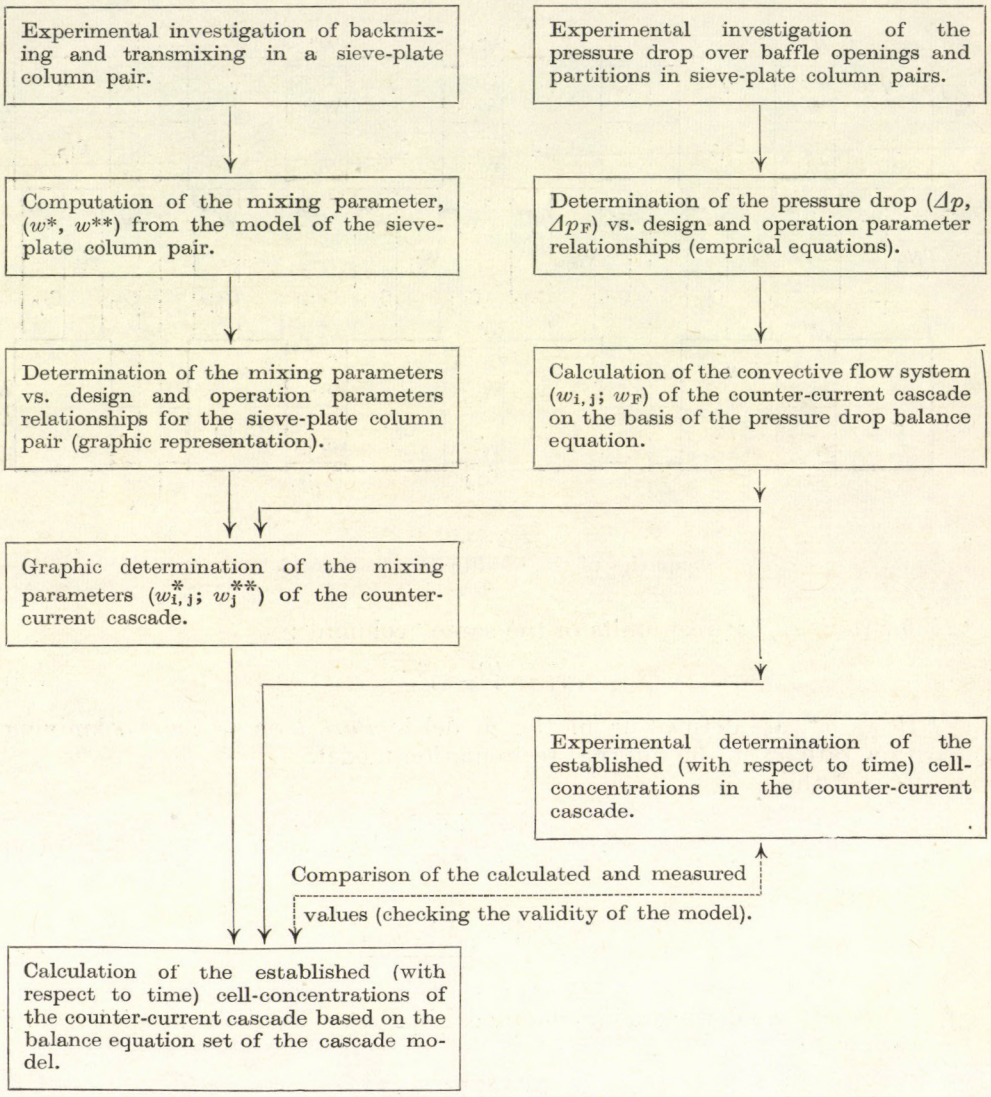

Fig. 4.

Application of the cascade model for the calculation of the counter-current cascade (Calculations schematics)

volumes held in the units of the counter-current cascade were equal within $\pm 10-15\%$. This difference can be considered negligable. Condition *c)* was ensured by the appropriate design of the apparatus.

The model and the apparatus were fitted as follows:

- cells of the apparatus correspond to units of the model,
- concentrations $c_{i,j}$ mean the steady state concentrations in the respective cells,

— flow rates $w_{F,j}$ and $w_{i,j}$ flow through the partitions and the connecting tubes,
— backmixing flow rate $w^{*}_{i,j}$, is considered with the quantitative characteristics of backmixing taking place in the connecting tubes,
— transmixing flow rate w^{**}_{j} is considered with the quantitative characteristics of transmixing taking place through the selective partitions.

The validity of the model was checked as follows:

Based on the equation set describing the model, the results of pressure drop balance equations and mixing studies in the column pairs at different parameter settings the equilibrium concentration achieved in the cells of the counter-current cascade were determined according to the computation scheme shown in *Fig. 4.* Measurements were also carried out to determine the equilibrium concentration series in the cells at equal parameter settings. Computed and measured values were compared and the adequacy of the model was determined.

Relative deviations of the calculated and measured value are presented in *Tables 2, 3* and *4.* Concentrations are expressed in a dimensionless form by dividing the successive values with the respective input concentrations, $c_{1,0}$. Relative deviations also relate to $c_{1,0}$. It can be concluded from the comparison that there is a sufficient agreement between the measured and calculated values, so the model can be considered adequate for the mathematical description of flow conditions in a bubble and sieve-plate column cascade equipped with selective partitions. Regardless of the complicated nature of the model, its development can be considered a significant step in the field of the calculations relating to counter-current cascades.

SYMBOLS

$a_{i,j}$, $b_{i,j}$, $d_{i,j}$, $e_{i,j}$, $f_{i,j}$ — algebraical expressions;
A — surface area of the selective partition, m²;
$c_{i,j}$ — liquid phase concentration in the $(i, j)^{th}$ unit of the cascade, kg/m³;
$c^{*}_{i,j}$ — dimensionless concentration in the $(i, j)^{th}$ unit of the cascade, (—);
i, j — natural numbers;
Δc — deviation between measured and calculated dimensionless concentrations, %.
n — number of unit pairs in the cascade;
$\Delta p_{i,j}$ — pressure drop of the liquid flowing from the $(i, j)^{th}$ unit over the connecting tube, kg/ms²;
$\Delta p_{F,j}$ — pressure drop of the liquid flowing through the partitions between members of the unit pairs of the cascade, kg/ms²;
q — cross section area of the connecting tube, m²;
v' — linear gas velocity with respect to the empty cross section, m/s;
V — useful volume of the apparatus, m³;
${}_{j}w^{(1)}_{j+1}$ — flow from the jth unit into the $(j+1)^{th}$ unit in the ith row of the model, m³/s;
${}_{j+1}w^{(i)}_{j}$ — flow from the $(j+1)^{th}$ unit into the jth unit in the ith row of the model, m³/s;
$w^{(i)}_{j}$ — flow from the jth unit in the ith row of the model into the jth unit in the other row, m³/s;
$w_{i,j}$ — flow from the $(i, j)^{th}$ unit of the cascade into the $(i, j+1)^{th}$ unit, m³/h;
$w_{F,j}$ — flow between the jth unit pairs of the cascade, m³/s;
$w^{*}_{i,j}$ — backmixing flow rate corresponding to flow rate $w_{i,j}$ defined in both directions, m³/s;
w^{**}_{j} — transmixing flow rate between the jth unit pairs of the cascade defined in both directions, m³/s;

Table 2.

Constants $v' = 0.6$ m/s $A = 2 \times 10^{-4}$ m^2 $q = 1.04 \times 10^{-4}$ m^2
$l = 4 \times 10^{-2}$ m

n (−)	$w_{1,0} = w_{2,0}$ (10^{-6} m^3/s)	j (−)	$c^*_{1,j}$ (−)		Δc (%)	$c^*_{2,j}$ (−)		Δc (%)
			measured	calculated		measured	calculated	
		1	0.860	0.846	1.4	0.724	0.683	4.1
4	2.78	2	0.625	0.666	−4.1	0.516	0.526	−1.0
		3	0.425	0.474	−4.9	0.286	0.334	−4.8
		4	0.240	0.317	−7.7	0.109	0.154	−4.5
		1	0.977	0.932	4.5	0.758	0.689	2.9
4	5.56	2	0.725	0.760	−3.5	0.447	0.474	−2.7
		3	0.487	0.526	−3.9	0.212	0.240	−2.8
		4	0.231	0.311	−8.0	0.028	0.068	−4.0
		1	0.997	0.965	3.2	0.750	0.706	4.4
4	8.33	2	0.829	0.825	0.4	0.363	0.447	−8.4
		3	0.568	0.551	1.7	0.135	0.185	−5.0
		4	0.270	0.294	−2.4	0.004	0.034	−3.0
		1	0.841	0.807	3.4	0.597	0.592	0.5
3	2.78	2	0.623	0.599	2.4	0.375	0.400	−2.5
		3	0.379	0.408	−2.9	0.133	0.193	−6.0
		1	0.950	0.905	4.5	0.577	0.569	0.8
3	5.56	2	0.766	0.688	7.8	0.274	0.313	−3.9
		3	0.417	0.430	−1.3	0.039	0.095	−5.6
		1	0.976	0.948	2.8	0.519	0.566	−4.7
3	8.33	2	0.784	0.741	4.3	0.195	0.259	−6.4
		3	0.444	0.434	1.0	0.007	0.052	−4.5
2	2.78	1	0.774	0.751	2.3	0.420	0.464	−4.4
		2	0.533	0.536	−0.3	0.144	0.249	−10.5
2	5.56	1	0.920	0.859	6.1	0.370	0.398	−2.8
		2	0.621	0.602	1.9	0.039	0.141	−10.2
2	8.33	1	0.948	0.919	2.9	0.339	0.384	−4.5
		2	0.625	0.616	0.9	0.008	0.081	−7.3

Table 3.

Constants $w_{1,0} = w_{2,0} = 8.33 \times 10^{-6}$ m³/s $n = 5$ $l = 3 \times 10^{-2}$ m
$A = 2 \times 10^{-4}$ m²

q (m²×10⁻⁴)	v' (m/s)	j (−)	$c^*_{1,j}$ (−) measured	$c^*_{1,j}$ (−) calculated	Δc (%)	$c^*_{2,j}$ (−) measured	$c^*_{2,j}$ (−) calculated	Δc (%)
		1	0.986	0.984	0.2	0.829	0.814	1.5
		2	0.895	0.903	−0.8	0.569	0.634	−6.5
0.53	0.3	3	0.516	0.664	−14.8	0.396	0.336	6.0
		4	0.253	0.366	−11.3	0.088	0.097	−5.9
		5	0.126	0.191	−6.5	0.003	0.016	−1.9
		1	0.976	0.973	0.3	0.803	0.820	−1.7
		2	0.878	0.897	−1.9	0.563	0.643	−8.0
0.53	0.4	3	0.491	0.650	−15.9	0.365	0.350	1.5
		4	0.227	0.356	−12.9	0.018	0.103	−8.5
		5	0.151	0.180	−2.9	−0.004	0.015	−1.9
		1	0.990	0.981	0.9	0.806	0.823	−1.7
		2	0.860	0.891	−3.1	0.565	0.649	−1.5
0.53	0.5	3	0.490	0.640	−15.0	0.193	0.360	−16.7
		4	0.212	0.351	−13.9	0.021	0.109	−8.8
		5	0.140	0.176	−3.6	−0.005	0.018	2.3
		1	0.953	0.980	−2.7	0.831	0.824	0.7
		2	0.853	0.887	−3.4	0.594	0.651	−5.7
0.53	0.6	3	0.457	0.635	−17.8	0.221	0.363	−14.2
		4	0.207	0.349	−14.2	0.033	0.111	−7.8
		5	0.140	0.175	−3.5	−0.004	0.019	−2.3
		1	0.994	0.976	1.8	0.676	0.744	−6.8
		2	0.933	0.875	5.8	0.438	0.553	−11.5
1.04	0.3	3	0.655	0.679	−2.4	0.165	0.324	−15.9
		4	0.456	0.450	0.6	0.043	0.128	−8,5
		5	0.277	0.255	2.2	0.002	0.027	−2.5
		1	0.971	0.972	−0.1	0.681	0.750	−6.9
		2	0.907	0.865	4.2	0.482	0.562	−8.0
1.04	0.4	3	0.644	0.665	−2.1	0.196	0.336	−14.0
		4	0.445	0.440	0.5	0.057	0.136	−7.9
		5	0.277	0.250	2.7	0.003	0.030	−2.7
		1	0.979	0.972	0.7	0.678	0.753	−7.5
		2	0.901	0.861	4.0	0.483	0.586	−10.3
1.04	0.5	3	0.644	0.662	−1.8	0.203	0.355	−15.2
		4	0.432	0.434	−0.2	0.064	0.142	−7.8
		5	0.267	0.247	2.0	0.002	0.031	−2.9
		1	1.000	0.972	2.8	0.712	0.755	−4.3
		2	0.899	0.859	4.0	0.517	0.573	−5.6
1.04	0.6	3	0.632	0.654	−2.2	0.218	0.349	−13.1
		4	0.397	0.430	−3.3	0.067	0.144	−7.7
		5	0.239	0.246	−0.7	0.002	0.032	−3.0

Table 4.

Constants: $n = 5$ $v' = 0.6$ m/s $q = 1.04 \times 10^{-4}$ m^2
$l = 4 \times 10^{-2}$ m

A ($m^2 \cdot 10^{-4}$)	$w_{1,0}/w_{2,0}$ (−)	j (−)	$c^*_{1,j}$ (−) measured	$c^*_{1,j}$ (−) calculated	Δc (%)	$c^*_{2,j}$ (−) measured	$c^*_{2,j}$ (−) calculated	Δc (%)
		1	0.982	0.983	−0.1	0.475	0.511	−3.6
	1:1	2	0.952	0.945	0.7	0.305	0.331	−2.6
0.5		3	0.825	0.860	−3.5	0.140	0.140	0.0
		4	0.651	0.669	−1.8	0.042	0.055	−1.3
		5	0.464	0.488	−2.4	−0.003	0.017	−1.9
		1	0.954	0.933	2.1	0.341	0.384	−4.3
	1:2	2	0.814	0.793	2.1	0.200	0.212	−1.2
0.5		3	0.650	0.599	5.1	0.085	0.083	0.2
		4	0.411	0.381	3.0	0.025	0.032	0.7
		5	0.263	0.233	3.0	−0.007	0.008	−1.5
		1	0.903	0.991	−8.8	0.661	0.768	−10.7
	2:1	2	0.937	0.968	−3.1	0.517	0.619	−10.2
0.5		3	0.868	0.916	−4.8	0.297	0.401	−10.3
		4	0.768	0.789	−2.3	0.145	0.206	−6.1
		5	0.621	0.616	0.5	0.034	0.068	−3.4
		1	0.850	0.828	2.2	0.249	0.297	−4.8
	3:1	2	0.598	0.582	1.6	0.139	0.143	−0.4
0.5		3	0.373	0.360	1.3	0.056	0.048	1.2
		4	0.231	0.196	3.5	0.015	0.017	−0.2
		5	0.145	0.108	3.7	0.003	0.004	−0.7
		1	0.988	0.978	1.0	0.606	0.643	−3.7
	1:1	2	0.923	0.909	1.4	0.396	0.432	−3.6
1		3	0.730	0.770	−4.0	0.179	0.230	−5.9
		4	0.542	0.568	−2.6	0.054	0.091	−3.7
		5	0.348	0.357	−0.9	0.007	0.022	−2.9
		1	0.913	0.880	3.3	0.423	0.461	−3.7
	1:2	2	0.654	0.605	4.9	0 236	0.238	−0.2
1		3	0.367	0.340	2.7	0.094	0.091	0.3
		4	0.194	0.167	2.7	0.027	0.027	0.0
		5	0.106	0.077	2.9	−0.007	−0.005	−1.2
		1	0.984	0.984	0.0	0.886	0.923	−3.7
	2:1	2	0.961	0.973	−1.2	0.797	0.833	−3.6
1		3	0.892	0.909	−4.7	0.591	0.659	−6.8
		4	0.730	0.761	−3.1	0.332	0.395	−6.3
		5	0.528	0.539	−1.1	0.103	0.120	−1.7
		1	0.723	0.696	2.7	0.277	0.327	−5.0
	1:3	2	0.381	0.358	2.3	0.130	0.125	0.5
1		3	0.161	0.134	2.7	0.040	0.035	0.5
		4	0.065	0.045	2.0	0.009	0.008	0.1
		5	0.031	0.018	1.3	−0.003	0.001	−0.4

REFERENCES

1. Balla, L.: Studies on the Mass Transfer through Selective Partitions between Dynamic Foam Systems. Thesis, Univ. Chem. Engng., Veszprém, 1969 (in the Hungarian).
2. Sisak, Cs.: Studies on the Liquid Phase Mixing Processes in Sieve-plate Column Cascades with Selective Partitions. Thesis, Univ. Chem. Engng., Veszprém, 1977 (in the Hungarian).
3. Blickle, T. und Balla, L.: Chem. Anlagen + Verfahren, *1974* (9), 57, 61.
4. Haddad, A. H. and Wolf, D.: Can. J. Chem. Eng., *45*, 100 (1967).
5. Nagy, E.: Studies on the Mass Transfer Processes in Bubble Columns. Thesis, Univ. Chem. Engng., 1974 (in the Hungarian).
6. Balla, L., Sisak, Cs.: J. Hung. Ind. Chem., *6*, 000 (1978).

РЕЗЮМЕ

Согласно экспериментальным наблюдениям авторов т. н. противоточные каскады барботажных и пенных колонн с селективными переборками нельзя считать чисто противоточными, поскольку в них образуется сложная система конвективных потоков. На основе закона энергетического минимума был разработан расчётный метод для определения количества жидкости, проходящего по переходным трубам и через переборку. Для описания гидродинамики жидкой фазы была построена каскадная модель. Используя метод, разработанный для расчёта системы конвективных потоков, а также результаты, приведённые в предыдущей статье касательно пар пенных колонн, были рассчитаны стационарные концентрационные соотношения, образующиеся в установке. Между рассчитанными и измеренными данными было установлено хорошее совпадение.

HUNGARIAN JOURNAL
OF INDUSTRIAL CHEMISTRY
VESZPRÉM
Vol. 6. pp. 409–422 (1978)

ANNÄHERNDE ANALYTISCHE BESCHREIBUNG EINER REAKTION ERSTEN GRADES IN EINEM DÜNNSCHICHTREAKTOR

T. VAJDA

(Forschungsinstitut für Technische Chemie der Ungarischen Akademie der Wissenschaften, Budapest)

Eingegangen am 30 August, 1978.

Gegenwärtige Arbeit untersucht in Anlehnung auf frühere Resultate die Möglichkeit der annähernden analytischen Beschreibung einer Reaktion ersten Grades in einem Dünnschichtreaktor. Der Fehler der Annäherungslösung im Vergleich zu der exakten Lösung wird mittels analytischer Fehlerschätzung festgestellt.

Einleitung

Wie bekannt, werden die Transportprozesse in der chemischen Verfahrenstechnik im allgemeinen mittels partieller Differentialgleichungssysteme beschrieben. Die analytische Lösung dieser Gleichungen erfordert einem umfangreichen mathematischen Apparat, die erhaltenen Resultate sind von komplizierter Struktur und daher bei — für die Praxis wichtigen — Berechnungen nur in beschränktem Maße anwendbar.

Aus oben erwähnten Gründen schien es notwendig, eine solche für die Anforderungen der Praxis noch genügend genaue, annähernde analytische Lösungsmethode auszuarbeiten, deren Anwendung relativ einfach ist, wobei die erhaltenen Resultate übersichtlich und für numerische Berechnungen unmittelbar verwendbar sind. Die Methode haben wir in früheren Arbeiten für gewisse Prozeßtypen, und zwar für Fälle von reinem Ausgleichungscharakter [1], sowie für Transportsysteme, die auch Quellen enthielten [2], ausführlich beschrieben.

In gegenwärtiger Arbeit wird auf der Basis obiger Methode die annähernde analytische Lösung des mathematischen Modells einer sich in einem Dünnschichtreaktor abspielenden Reaktion ersten Grades erzeugt. Es wird gezeigt, daß im Vergleich zu den in [1] und [2] untersuchten Prozeßtypen im Gange der Berechnungen neue Überlegungen getroffen werden müssen.

Das physikalisch-mathematische Modell

Betrachten wir den Dünnschichtreaktor auf *Abbildung 1:*
Bei der Stelle $z=0$ tritt die Flüssigkeit und das Gas im Gleichstrom in den Reaktor ein. Letzteres wird absorbiert und tritt mit dem entsprechenden

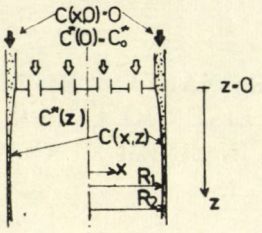

Bild 1.

Komponenten der Flüssigkeit in eine Reaktion ersten Grades. Die Konzetration des Gases in der Dünnschicht wird von der im Cartesischen Koordinatensystem aufgeschriebenen Funktion $C(x, z)$, im Gasraum mit $C^*(z)$ gemessen. Dadurch wird zwar die Krümmung der Dünnschicht vernachlässigt, was aber wegen ihrer im Vergleich mit dem Apparatendurchmesser geringen Dicke zuläßig ist. Nehmen wir weiterhin an, daß im Gasraum in den einzelnen horizontalen Ebenen die gleiche Konzentration vorhanden ist (dann ist C^* nur von der z-Koordinate abhängig), und daß der Geschwindigkeitsfeld der Flüssigkeit in der im Apparat gebildeten Dünnschicht — bei Annahme einer entsprechenden Durchschnittsgeschwindigkeit v in Richtung z — als homogen betrachtet werden kann. Der Prozeßverlauf wird nur in stationärem Zustand geprüft.

Um das physikalisch-mathematische Modell aufstellen zu können, muß der globale Prozeß in Teilprozeße gegliedert werden. Betrachten wir erst den Transport des in der Flüssigkeitsschicht absorbierten Stoffes. Nehmen wir an, daß — wie völlig plausibel — der Transport in der Dünnschicht in Richtung z nur konvektiv, in Querrichtung jedoch nur diffusiv ist. In diesem Fall bleiben aus der im Cartesischen Koordinatensystem aufgeschriebenen Erhaltungsgleichung folgende Glieder übrig:

$$v\frac{\partial C}{\partial z}=D\frac{\partial^2 C}{\partial x^2}+KC. \tag{1}$$

Hier ist D die Diffusionskonstante des in der Flüssigkeitsschicht absorbierten Gases, K die Geschwindigkeitskonstante des die Reaktion ersten Grades repräsentierenden Quellengliedes.

Der Transport des absorbierenden Gases im Gasraum besteht nur aus der Konvektion in Richtung z, da der innerhalb einer horizontalen Schicht verlaufende Ausgleichsprozeß vernachlässigt wird. Hier muß jedoch die Absorption bei der Innenfläche der Dünnschicht berücksichtigt werden, was das Auftreten eines Quellengliedes in der Gastransportgleichung bedeutet. Dieses Glied ist notwendigerweise proportional mit dem auf der Innenfläche $x=R_1$

der Dünnschicht auftretenden Stofftransport in normaler Richtung. Unter Berücksichtigung obiger Gesichtspunkte lautet die Transportgleichung für das Gas:

$$v^* \frac{dC^*}{dz} = B \left(\frac{\partial C}{\partial x}\right)_{x=R_1}, \tag{2}$$

wobei v^* die lineare Geschwindigkeit des Gases im Apparat und B ein Proportionalitätsfaktor bedeutet.

Das Differentialgleichungssystem (1)—(2) stellt die mathematische Beschreibung des untersuchten Problems dar. Der Definitionsbereich der unabhängigen Veränderlichen in den Gleichungen umfaßt $0 \leq z < +\infty$, $R_1 \leq x \leq R_2$. Unsere Aufgabe besteht im weiteren in der Feststellung der zu obigem Gleichungssystem gehörenden Anfangs- und Randbedingungen. Es ist vor allem bekannt, daß das Gas an Stelle $z = 0$ in den Apparat mit gegebener Konzentration C_0^* eintritt, daher ist

$$C^*(0) = C_0^*. \tag{3}$$

Anderseits wird angenommen, daß sich zwischen der Hauptmasse des Gases und der Flüssigkeitsschicht eine Grenzschicht bildet, und dadurch die Newtonsche Randbedingung geltend ist:

$$\left(\frac{\partial C}{\partial x}\right)_{x=R_1} = -h[C^*(z) - \mu C(R_1, z)], \tag{4}$$

wobei h der Stoffaustauschfaktor, μ die Henrysche Konstante ist.

Es kann weiterhin offenbar angenommen werden, daß die in den Reaktor eintretende Flüssigkeit kein Absorbeat enthält, und daher

$$C(x, 0) = 0. \tag{5}$$

In der Dünnschicht hat der Diffusionsstrom in Querrichtung bei der Reaktorwand natürlich den Wert von Null:

$$\left(\frac{\partial C}{\partial x}\right)_{x=R_2} = 0. \tag{6}$$

Die Zusammenhänge (3)—(6) geben die kompletten Anfangs- und Randbedingungen des Differentialgleichungssystems (1)—(2) an. Im weiteren verfolgen wir das Ziel, die annähernde analytische Lösungsmöglichkeit des gezeigten mathematischen Problems zu untersuchen.

Beschreibung der annähernden analytischen Lösungsmethode

Die Annäherung besteht darin, daß statt der Funktion $C(x, z)$ mit zwei Variablen, versucht wird, deren Durchschnitt nach der Variablen x annähernd aufzuschreiben:

$$\overline{C}(z) = \frac{1}{R_2 - R_1} \int_{R_1}^{R_2} C(x, z)\, dx. \tag{7}$$

Wir integrieren daher Gleichung (1) nach der Variablen x zwischen den Grenzen R_1 und R_2 und erhalten unter Berücksichtigung von (7):

$$v\frac{d\bar{C}}{dz}=\frac{D}{R_2-R_1}\left(\left(\frac{\partial C}{\partial x}\right)_{x=R_2}-\left(\frac{\partial c}{\partial x}\right)_{x=R_1}\right)+K\bar{C}. \tag{8}$$

In (8) kann das erste Glied der rechten Seite unter Berücksichtigung von (4) bzw. (6) umgeformt werden. Das Resultat ergibt:

$$v\frac{d\bar{C}}{dz}=\frac{Dh}{R_2-R_1}(C^*-\mu C(R_1,z))+K\bar{C}. \tag{9}$$

Substituieren wir schließlich (4) in (2), so erhalten wir folgenden Zusammenhang:

$$v^*\frac{dC^*}{dz}=-Bh(C^*-\mu C(R_1,z)). \tag{10}$$

Das Gleichungssystem (9)—(10) wäre bereits genügend zur Erzeugung von $\bar{C}$ und C^*, ist jedoch nicht lösbar, da in ihm auch der Wert der Funktion C bei der Grenze R_1 figuriert. Es wird daher folgende Hilfsfunktion eingeführt:

$$\zeta(z)=\frac{C^*(z)-\mu C(R_1,z)}{C^*(z)-\mu\bar{C}(z)}. \tag{11}$$

Die Hauptmerkmale der Verhaltensweise einer Funktion dieser Struktur ist bereits in [1] ausführlich analysiert worden. Mit Verwendung von (11) kann das Gleichungssystem (9)—(10) umgeformt werden:

$$v\frac{d\bar{C}}{dx}=\frac{Dh}{R_2-R_1}\zeta(z)(C^*-\mu\bar{C})+K\bar{C}, \tag{12}$$

$$v^*\frac{dC^*}{dx}=-Bh\zeta(z)(C^*-\mu\bar{C}). \tag{13}$$

Das Resultat von (12)—(13) ist noch exakt. Das Wesen der Annäherung besteht darin, daß die Funktion $\zeta(z)$ durch ihren im limes $z\to+\infty$ angenommenen Wert substituiert wird:

$$\zeta(z)\approx\lim_{z\to+\infty}\zeta(z)=\zeta_\infty. \tag{14}$$

Es wird behauptet — und dadurch wird eben die Annäherungsmethode gut anwendbar — daß, wie in den Fällen von [1] und [2], der Grenzwert ζ_∞ ohne Lösung des ursprünglichen mathematischen Problems aus den Laplace-Transformierten auch jetzt unmittelbar bestimmt werden kann.

Bestimmung des Grenzwertes ζ_∞

In [1] und [2] wird ausführlich die Frage untersucht, auf welche Weise der Grenzwert ζ_∞ sowohl bei Prozeßen von reinem Ausgleichungscharakter als auch in Fällen von Transportsystemen, die auch Quellen enthalten, bestimmt werden kann. In beiden Fällen erweist sich dazu die Bestimmung der Laplace-

Transformierten der Lösungsfunktionen — aus denen jene Variable eliminiert wurde, nach welcher kein Durchschnitt gebildet wird — als genügend. Obgleich in den Gleichungen unseres gegenwärtigen Problems Quellenglieder auftreten, kann die in [2] gezeigte Methode doch nicht angewandt werden. Wenn nämlich die Laplace-Transformierten nach den entsprechenden Variablen aufgeschrieben werden, so ist $p=0$ kein Pol derselben (p ist der Parameter der Transformation), und so tritt in der Lösungsfunktion keine nur von der zweiten Variablen abhängige, additiv separierbare Funktion auf.

Der Grund hierfür ist — aus physikalischen Überlegungen ausgehend — klar, da sich ja der untersuchte Prozeß jetzt nicht in einem Medium mit Reservoircharakter abspielt, und daher divergieren die Lösungsfunktionen C und C^* bei einer beliebig kleinen positiven Reaktionskonstante K im Grenzübergang $z \to +\infty$, bzw. sie tendieren im Falle eines ähnlichen negativen K-Wertes gegen Null. Die Methode laut [1] kann jedoch bereits angewendet werden, da nun notwendigerweise:

$$C(x,z)=\sum_{k=1}^{\infty} A_k(x)e^{p_k z}, \quad (15a) \qquad C^*(z)=\sum_{k=1}^{\infty} A_k^* e^{p_k z}, \quad (15b)$$

wo nun aus den Polstellen der Laplace-Transformierten festgestellt werden kann, daß (im Falle eines positiven K):

$$+\infty > p_1 > p_2 > \ldots > p_n > 0 > p_{n+1} > p_{n+2} > \ldots$$

Substituieren wir (15a)—(15b) in (11). Wenn der Grenzübergang $z \to +\infty$ bei $\zeta(z)$ durchgeführt wird, ist auch jetzt einzusehen, daß:

$$\zeta_\infty = \frac{A_1^* - \mu A_1(R_1)}{A_1^* - \mu \overline{A}_1}. \quad (16)$$

Wegen (16) kann jetzt unter Ausnützung der speziellen Struktur von (15a)—(15b) die in [1] gezeigte Berechnung durchgeführt werden:

$$\zeta_\infty = \lim_{p \to p_1} \frac{F^*(p) - \mu F(R_1, p)}{F^*(p) - \mu \overline{F}(p)}, \quad (17)$$

wobei F und F^* die Laplace-Transformierten der Lösungsfunktionen darstellen:

$$F(x,p)=\int_0^{\infty} C(x,z)e^{-pz}\,dz, \quad (18a) \qquad F^*(p)=\int_0^{\infty} C^*(z)e^{-pz}\,dz. \quad (18b)$$

Wir berechnen nun unter Benützung von (1)—(6) die Transformierten (18a)—(18b). Nach Durchführung der Laplace-Transformation von Gleichung (1), sowie unter Anwendung der Anfangsbedingung (5) erhalten wir folgenden Zusammenhang:

$$\frac{d^2F}{dx^2} + \frac{K - vp}{D} F = 0. \quad (19)$$

Durch Transformation der Gleichung (2), sowie Anwendung der Anfangs-

bedingung (3) und der Randbedingung (4) gewinnen wir den Zusammenhang wie folgt:

$$F^* = \frac{v^* C_0^* + Bh\mu F(R_1)}{Bh + v^* p}. \tag{20}$$

Die Transformierten der Randbedingungen (4) und (6) sind einfach:

$$\left(\frac{dF}{dx}\right)_{x=R_1} = -h[F^* - \mu F(R_1)], \quad \text{(21a)} \qquad \left(\frac{dF}{dx}\right)_{x=R_2} = 0. \tag{21b}$$

Die allgemeine Lösung von Gleichung (19):

$$F(x, p) = P\, sh\, \omega x + Q\, ch\, \omega x, \tag{22}$$

wobei

$$\omega = \sqrt{\frac{vp - K}{D}}, \tag{23}$$

P und Q sind zu bestimmende Konstanten. Substituieren wir (22) in (21b), so erhalten wir:

$$P\, ch\, \omega R_2 + Q\, sh\, \omega R_2 = 0, \tag{24}$$

sodann (20) in (21a), und in das Ergebnis (22) substituierend ergibt sich folgender Zusammenhang:

$$P\left[\omega\, ch\, \omega R_1 - \frac{hv^* p\mu}{Bh + v^* p}\, sh\, \omega R_1\right] + Q\left[\omega\, sh\, \omega R_1 - \frac{hv^* \mu p}{Bh + v^* p}\, ch\, \omega R_1\right] = -\frac{hv^* C_0^*}{Bh + v^* p}. \tag{25}$$

Durch Nebeneindarstellen der Zusammenhänge (24) und (25) ergeben sich für die Konstanten P und Q:

$$P = -\frac{hv^* C_0^*\, sh\, \omega R_2}{(Bh + v^* p)\omega\, sh\, \omega(R_2 - R_1) + hv^* \mu p\, ch\, \omega(R_2 - R_1)}, \tag{26a}$$

$$Q = \frac{hv^* C_0^*\, ch\, \omega R_2}{(Bh + v^* p)\omega\, sh\, \omega(R_2 - R_1) + hv^* \mu p\, ch\, \omega(R_2 - R_1)}. \tag{26b}$$

Nach Substituierung von (26a) und (26b) in (22) und Zusammenziehen des Resultats ergibt sich:

$$F(x, p) = \frac{hv^* C_0^*\, ch\, \omega(R_2 - x)}{(Bh + v^* p)\omega\, sh\, \omega(R_2 - R_1) + hv^* \mu p\, ch\, \omega(R_2 - R_1)}. \tag{27}$$

Schließlich substituieren wir (27) in (20):

$$F^*(p) = \frac{v^* C_0^*}{Bh + v^* p}\left[1 + \frac{Bh^2 \mu\, ch\, \omega(R_2 - R_1)}{(Bh + v^* p)\omega\, sh\, \omega(R_2 - R_1) + hv^* \mu p\, ch\, \omega(R_2 - R_1)}\right]. \tag{28}$$

Damit wurden die für die Bestimmung des Grenzwertes ζ_∞ notwendigen Transformierten erzeugt. Für die Substituierung der Ergebnisse in (17) muß noch der Durchschnitt von (27) festgestellt werden, der sich einfach als

$$\overline{F}(p)=\frac{hv^*C_0^* \; sh\,\omega(R_2-R_1)}{[(Bh+v^*p)\omega \; sh\,\omega(R_2-R_1)+hv^*\mu p \; ch\,\omega(R_2-R_1)]\omega(R_2-R_1)} \tag{29}$$

ergibt.

Durch Nebeneinanderstellung von (27), (28), (29), sowie (17) ergibt sich für den Grenzwert ζ_∞:

$$\zeta_\infty=\lim_{p\to p_1}\frac{\frac{1}{Bh+v^*p}[(Bh+v^*p)\omega \; sh\,\omega(R_2-R_1)+hv^*\mu p \; ch\,\omega(R_2-R_1)]+}{\frac{1}{Bh+v^*p}[(Bh+v^*p)\omega \; sh\,\omega(R_2-R_1)+hv^*\mu p \; ch\,\omega(R_2-R_1)]+}$$

$$\frac{+\frac{\mu Bh^2 \; ch\,\omega(R_2-R_1)}{Bh+v^*p}-\mu h \; ch\,\omega(R_2-R_1)}{+\frac{\mu Bh^2 \; ch\,\omega(R_2-R_1)}{Bh+v^*p}-\frac{\mu h \; sh\,\omega(R_2-R_1)}{\omega(R_2-R_1)}}. \tag{30}$$

Hier ist p_1 die größte Wurzel des sich aus der Laplace-Transformierten bzw. aus (23) ergebenden Eigenwertgleichung:

$$th\sqrt{\frac{vp-K}{D}}(R_2-R_1)=-\frac{hv^*\mu p}{(Bh+v^*p)\sqrt{\frac{vp-K}{D}}} \tag{31}$$

[und da die Wurzeln von (31) alle reell sind, kann man sagen, daß es der positivste Pol der Transformierten ist]. Nach Durchführung des Grenzüberganges und unter Berücksichtigung von (31) erhalten wir schließlich:

$$\zeta_\infty=\frac{v^*p_1(R_2-R_1)(K-vp_1)}{hv^*\mu p_1 D-Bh(R_2-R_1)(K-vp_1)}. \tag{32}$$

Der Grenzwert ζ_∞ konnte also auch jetzt schon aus den viel einfacher erhaltbaren Laplace-Transformierten erzeugt werden als Funktion der Parameter des untersuchten Systems.

Generierung der Annäherungslösungen

Unsere Aufgabe besteht schließlich in der Lösung des Gleichungssystems (12)—(13), wobei die Annäherung (14) angewandt wird. Die zum Gleichungssystem gehörenden Anfangsbedingungen bilden (3), sowie der Zusammenhang

$$\overline{C}(0)=0, \tag{33}$$

der durch die Durchschnittsbildung der Bedingung (5) gewonnen wird. Das Gleichungssystem wird vor allem in normale Form geordnet:

$$\frac{d\overline{C}}{dz}=\left(\frac{K}{v}-\frac{Dh\zeta_\infty\mu}{(R_2-R_1)v}\right)\overline{C}+\frac{Dh\zeta_\infty}{(R_2-R_1)v}C^*, \tag{34a}$$

$$\frac{dC^*}{dz}=\frac{Bh\zeta_\infty\mu}{v^*}\overline{C}-\frac{Bh\zeta_\infty}{v^*}C^*. \tag{34b}$$

Wie bekannt (z. B. aus [3]), hat die Lösung des Gleichungssystems (34a)—(34b) folgende Form:

$$\overline{C} = \overline{a}\, e^{\lambda_1 z} + \overline{b}\, e^{\lambda_2 z}, \tag{35a}$$

$$C^* = a^*\, e^{\lambda_1 z} + b^*\, e^{\lambda_2 z}, \tag{35b}$$

wobei $\overline{a}$, $\overline{b}$, a^* und b^* Konstante, λ_1 und λ_2 die Eigenwerte von folgendem Koeffizientenmatrix sind:

$$\begin{bmatrix} \dfrac{K}{v} - \dfrac{Dh\zeta_\infty \mu}{(R_2 - R_1)v} & \dfrac{Dh\zeta_\infty}{(R_2 - R_1)v} \\ \dfrac{Bh\zeta_\infty \mu}{v^*} & -\dfrac{Bh\zeta_\infty}{v^*} \end{bmatrix}. \tag{36}$$

Daraus folgt also:

$$\lambda_{1,2} = \frac{1}{2}\left\{\frac{K}{v} - \frac{Bh\zeta_\infty}{v^*} - \frac{Dh\zeta_\infty \mu}{(R_2 - R_1)v} \pm \left[\left(\frac{Dh\zeta_\infty \mu}{(R_2 - R_1)v} + \frac{Bh\zeta_\infty}{v^*} - \frac{K}{v}\right)^2 + \frac{4KBh\zeta_\infty}{vv^*}\right]^{1/2}\right\}. \tag{37}$$

Die in (35a)—(35b) auftretenden Konstanten sind aus den Bedingungen (3) und (33), sowie aus den Zusammenhängen zu bestimmen, die sich aus entsprechender Nebeneinanderstellung von (36) und (37) (siehe [3]) ergeben. Für letztere erhalten wir nach einigem Rechnen folgende Zusammenhänge:

$$\overline{a} = \frac{2Dh\zeta_\infty}{(R_2 - R_1)v\alpha}\, a^*, \tag{38a}$$

$$b^* = -\frac{2\mu Bh\zeta_\infty}{v^*\alpha}\, \overline{b}. \tag{38b}$$

Hier ist

$$\alpha = \frac{Dh\zeta_\infty \mu}{(R_2 - R_1)v} - \frac{Bh\zeta_\infty}{v^*} - \frac{K}{v} + \left[\left(\frac{Dh\zeta_\infty \mu}{(R_2 - R_1)v} + \frac{Bh\zeta_\infty}{v^*} - \frac{K}{v}\right)^2 + \frac{4KBh\zeta_\infty}{vv^*}\right]^{1/2}. \tag{39}$$

Nun wird (38a)—(38b) in (35a)—(35b) zurücksubstituiert, sodann werden die gewonnenen Werte $\overline{C}$ und C^* in (3) und (33) eingesetzt, und wir erhalten für die Konstanten a^* und $\overline{b}$:

$$a^* = \frac{(R_2 - R_1)vv^*\alpha^2 C_0^*}{(R_2 - R_1)vv^*\alpha^2 + 4D\mu Bh^2\zeta_\infty^2}, \tag{40a}$$

$$\overline{b} = -\frac{2Dhv^*\zeta_\infty C_0^*}{(R_2 - R_1)vv^*\alpha^2 + 4D\mu Bh^2\zeta_\infty^2}. \tag{40b}$$

Schließlich ergibt sich also durch die Nebeneinanderstellung von (35a)—(35b), (38a)—(38b) und (40a)—(40b) für die Annäherungslösungen:

$$\overline{C}(z) = \frac{2Dhv^*\alpha\zeta_\infty C_0^*}{(R_2 - R_1)vv^*\alpha^2 + 4D\mu Bh^2\zeta_\infty^2}\left(e^{\lambda_1 z} - e^{\lambda_2 z}\right), \tag{41a}$$

$$C^*(z) = \frac{(R_2 - R_1)vv^*\alpha^2 C_0^*}{(R_2 - R_1)vv^*\alpha^2 + 4D\mu Bh^2\zeta_\infty^2}\left(e^{\lambda_1 z} + \frac{4D\mu Bh^2\zeta_\infty^2}{(R_2 - R_1)vv^*\alpha^2}\, e^{\lambda_2 z}\right). \tag{41b}$$

Mit den Zusammenhängen (41a)—(41b) haben wir das uns gesetzte Ziel erreicht: Wir haben zu der mathematischen Beschreibung von Prozeßen, die sich in Dünnschichtreaktoren bei Reaktionen ersten Grades abspielen, eine Art einer analytischen Annäherungsformel aufgestellt.

Schätzung des Fehlers der Annäherungsmethode

Es werden folgende Vektorbezeichnungen eingeführt:

$$U=\begin{bmatrix}\overline{C}\\ C^*\end{bmatrix}_{ex}, \quad (42a) \qquad V=\begin{bmatrix}\overline{C}\\ C^*\end{bmatrix}_{ap}, \quad (42b) \qquad U_0=\begin{bmatrix}0\\ C_0^*\end{bmatrix}. \quad (42c)$$

Hier ist U der Vektor der exakten, V der Vektor der Annäherungslösung, U_0 ist der Anfangswert. Unter Verwendung der Bezeichnungen von (42) kann das Gleichungssystem (12)—(13) in folgender Form aufgeschrieben werden:

$$\frac{dU}{dz}=\zeta(z)GU+HU, \quad (43a) \qquad U(0)=U_0, \quad (43b)$$

und (34a)—(34b) in Form von:

$$\frac{dV}{dz}=\zeta_\infty GV+HV, \quad (44a) \qquad V(0)=U_0, \quad (44b)$$

wobei die Matrizen G und H die folgenden sind:

$$G=\begin{bmatrix}-\dfrac{Dh\mu}{(R_2-R_1)v} & \dfrac{Dh}{(R_2-R_1)v}\\ \dfrac{Bh\mu}{v^*} & -\dfrac{Bh}{v^*}\end{bmatrix}, \quad (45a) \qquad H=\begin{bmatrix}\dfrac{K}{v} & 0\\ 0 & 0\end{bmatrix}. \quad (45b)$$

Die Lösung der im V-ten Teil bereits ausgearbeiteten Aufgabe (44a)—(44b) kann jetzt auch in kompakter Form aufgeschrieben werden. Da der Matrix $\zeta_\infty G+H$ mit (36) identisch ist, sind die Eigenwerte des ersteren ebenfalls unter (37) anzutreffen, die Eigenvektoren aber sind auf Grund von (38a)—(38b) und (39) wie folgt:

$$S_1=\begin{bmatrix}2Dh\zeta_\infty\\ \alpha v(R_2-R_1)\end{bmatrix}, \quad (46a) \qquad S_2=\begin{bmatrix}-\alpha v^*\\ 2\mu Bh\zeta_\infty\end{bmatrix}. \quad (46b)$$

Wenn dann die aus den Säulenvektoren (46a)—(46b) zu bildende Transformation P eingeführt wird, sowie deren Inverse P^{-1}:

$$P=\begin{bmatrix}2Dh\zeta_\infty & -\alpha v^*\\ \alpha v(R_2-R_1) & 2\mu Bh\zeta_\infty\end{bmatrix}, \quad (47a)$$

$$P^{-1}=[4D\mu Bh^2\zeta_\infty^2+\alpha^2(R_2-R_1)vv^*]^{-1}\begin{bmatrix}2\mu Bh\zeta_\infty & \alpha v^*\\ -\alpha v(R_2-R_1) & 2Dh\zeta_\infty\end{bmatrix}, \quad (47b)$$

so erhält man durch Transformation der Gleichung (44a)—(44b):

$$\frac{d\tilde{V}}{dz}=\zeta_\infty\tilde{G}\tilde{V}+\tilde{H}\tilde{V}, \quad (48a) \qquad \tilde{V}(0)=\tilde{U}_0. \quad (48b)$$

Hier sind $\tilde{V}=P^{-1}V$, $\tilde{U}=P^{-1}U_0$, $\tilde{G}=P^{-1}GP$, $\tilde{H}=P^{-1}HP$, und da $\zeta_\infty\tilde{G}+\tilde{H}$ bereits ein Diagonalmatrix ist, ergibt sich für die Lösung von (48a)—(48b), bzw. durch deren sofortige Rücktransformation für die Lösung von (44a)—(44b):

$$V(z)=Pe^{(\zeta_\infty\tilde{G}+\tilde{H})z}P^{-1}U_0. \quad (49)$$

Durch Umformen der Gleichung (43a) erhalten wir:

$$\frac{dU}{dz} = \zeta_\infty GU + HU + (\zeta(z) - \zeta_\infty)GU. \tag{50}$$

Es kann festgestellt werden, daß beim Abtrennen des letzten Gliedes der rechten Seite von (50) die Lösung der erhaltenen homogenen Gleichung gerade (49) ergibt. Mit Hilfe der Methode der Variation der Konstanten kann (50) unter Benutzung von (43b) zu folgender Integralgleichung umgebildet werden:

$$U(z) = P\mathrm{e}^{(\zeta_\infty \tilde{G} + \tilde{H})z} P^{-1} U_0 + P \int_0^z \mathrm{e}^{(\zeta_\infty \tilde{G} + \tilde{H})(z-s)} P^{-1} (\zeta(s) - \zeta_\infty) GU(s)\, ds. \tag{51}$$

Führen wir schließlich die $\| \ \|$ Normen der in (51) figurierenden Mengen — als die Summe der absoluten Werte der Komponenten — ein, dann kann obige Integralgleichung in nachstehende Integralungleichung umgeformt werden:

$$\| U \| \leq M\mathrm{e}^{mz} + N \int_0^z \mathrm{e}^{m(z-s)} |\zeta(s) - \zeta_\infty| \, \| U \| \, ds. \tag{52}$$

Hier ist

$$M = \|P\| \, \|P^{-1}\| \, \|U_0\| = \frac{[\alpha(v^* + v(R_2 - R_1)) + 2h\zeta_\infty(D + \mu B)]^2 \cdot C_0^*}{4D\mu h^2 \zeta_\infty^2 + \alpha^2 (R_2 - R_1) v v^*}, \tag{53}$$

und

$$N = \|P\| \, \|P^{-1}\| \, \|G\| = \frac{[\alpha(v^* + v(R_2 - R_1)) + 2h\zeta_\infty(D + \mu B)]^2 \cdot (1 + \mu) \left(\dfrac{Dh}{(R_2 - R_1)v} + \dfrac{Bh}{v^*} \right)}{4D\mu B h^2 \zeta_\infty^2 + \alpha^2 (R_2 - R_1) v v^*}. \tag{54}$$

Die Konstante m ist um einen beliebig kleinen positiven Wert ε größer als der positivste Eigenwert des Matrix $\zeta_\infty G + H$.

Man multipliziere beide Seiten der Ungleichung (52) mit e^{-mz}:

$$\| U \| \, \mathrm{e}^{-mz} \leq M + N \int_0^z |\zeta(s) - \zeta_\infty| \, \| U \| \, \mathrm{e}^{-ms} \, ds, \tag{55}$$

dann folgt aus (55) aufgrund der GRONWALL—LEMMA:

$$\| U \| \, \mathrm{e}^{-mz} \leq M \, \mathrm{e}^{N \int_0^z |\zeta(s) - \zeta_\infty| \, ds}. \tag{56}$$

Multiplizieren wir beide Seiten des Ausdrucks (56) mit e^{mz}, so gewinnen wir einen oberen Schätzungswert hinsichtlich der Norm des exakten Lösungsvektors U:

$$\| U \| \leq M \, \mathrm{e}^{mz + N \int_0^z |\zeta(s) - \zeta_\infty| \, ds}. \tag{57}$$

Der Fehler der Annäherungsmethode wird durch die von oben her vorgenommene Schätzung der Norm der Menge $U-V$ angegeben. Durch den Vergleich der Resultate (49) und (51) ist zu sehen, daß das zweite Glied der rechten Seite von (51) gerade den Fehler ausdrückt. Daher ist es zutreffend, wenn man auf die Normen übergeht, daß

$$||U-V|| \leq N \int_0^z e^{m(z-s)} |\zeta(s)-\zeta_\infty| \, ||U|| \, ds. \tag{58}$$

Wir erhöhen den Wert der rechten Seite von (58), wenn an die Stelle von $||U||$ ein größerer Wert als dieser geschrieben wird. So ergibt sich durch Anwendung von (57) für den Fehler der Annäherungsmethode schließlich:

$$||U-V|| \leq MN \, e^{mz} \int_0^z |\zeta(s)-\zeta_\infty| e^{N\int_0^s |\zeta(t)-\zeta_\infty| \, dt} \, ds. \tag{59}$$

Betrachtet man die Struktur des Ausdrucks unter (59), so ist es sofort offensichtlich, daß das Verhalten desselben entscheidend vom Vorzeichen der Konstante m abhängt. Aus diesem Grunde sind vor allem die Vorzeichenverhalten der Eigenwerte λ — infolge der physikalischen Natur des ursprünglich modellierten Prozeßes — in jenen Fällen, wenn die Geschwindigkeitskonstante K einen negativen Wert, den Wert Null, bzw. einen positiven Wert annimmt, zu untersuchen. Aufgrund von (37) ist es leicht einzusehen, daß unter den Eigenwerten folgende Relationen bestehen:

$$\begin{aligned} &a)\ \lambda_2 < \lambda_1 < 0, && \text{wenn} && K<0; \\ &b)\ \lambda_2 < 0,\ \lambda_1 = 0, && \text{wenn} && K=0; \\ &c)\ \lambda_2 < 0 < \lambda_1, && \text{wenn} && K>0, \end{aligned}$$

falls die übrigen auftretenden Prozeßparameter richtige Werte annehmen.

Anderseits kann hinsichtlich des Verhaltens der Funktion $|\zeta(z)-\zeta_\infty|$ aufgrund von (11) und (14), sowie mit Hilfe physikalischer Überlegungen festgestellt werden, daß:

$$\begin{aligned} &a)\ |\zeta(0)-\zeta_\infty| = 1-\zeta_\infty < 1; \\ &b)\ \lim_{z\to+\infty} |\zeta(z)-\zeta_\infty| = 0, \end{aligned}$$

und im Hinblick darauf, daß die Ausgleichsprozeße des Wärme- und Stofftransportes jederzeit exponentialen Charakter haben, ist:

$$c)\ \int_0^{+\infty} |\zeta(s)-\zeta_\infty| \, ds < +\infty.$$

Unter Anwendung obiger Bedingungen beträgt der Annäherungsfehler von (59) — im Falle eines negativen Wertes der Geschwindigkeitskonstante K — Null, wenn $z=0$, und tendiert zumindest exponential abnehmend gegen Null im Grenzwert $z \to +\infty$, daher nimmt seine Größe in irgendeinem inneren — in Kenntnis der Funktion $\zeta(z)$ aus dem Zusammenhang (59) annähernd

festellbaren Punkt des untersuchten Intervalls notwendigerweise einen maximalen Wert an.

Wenn $K=0$ ist, so kann die Formel unter (59) nicht angewendet werden, bzw. sie ergibt einen sehr schlechten Schätzungswert. Es ist jedoch einzusehen, daß — da in diesem Fall $\tilde{H}=0$ ist — das zweite Glied der rechten Seite von (51) folgende einfachere Form annimmt:

$$U-V=\int_0^z e^{\lambda_k(z-s)}(\zeta(s)-\zeta_\infty)GU(s)\,ds. \tag{60}$$

Unter Berücksichtigung des über die Eigenwerte λ und über das Verhalten der Funktion $\zeta(z)-\zeta_\infty$ Gesagten, sowie in Anbetracht der Begrenztheit des Lösungsvektors U folgt aus (60) sofort, daß sich der Annäherungsfehler auch jetzt genau so verhält, wie im vorhin angeführten Fall.

Im Falle einer positiven Geschwindigkeitskonstante nimmt der Fehler laut (59) vom anfanglichen Nullwert ausgehend monoton wachsend zu, und divergiert im Grenzwert $z\to+\infty$. Diese Tatsache bedeutet jedoch kein Hindernis dabei, daß im Falle eines endlichen Reaktors der Fehler der Annäherung auch in diesem Falle geschätzt werden kann.

SYMBOLVERZEICHNIS

$\left.\begin{matrix}\overline{a}\\ a^*\end{matrix}\right\}$ — Koeffizienten;
A_k^* — Koeffizienten;
A_k — Funktionskoeffizienten;
$\left.\begin{matrix}\overline{b}\\ b^*\end{matrix}\right\}$ — Koeffizienten;
B — Proportionalitätsfaktor;
C — Konzentration des Gases in der Flüssigkeit;
C^* — Konzentration des Gases im Gasraum;
C_0^* — Konzentration des Gases im Gasraum bei der Stelle $z=0$;
$\overline{C}$ — Durchschnittskonzentration in der Dünnschicht;
D — Diffusionskonstante des Gases im Flüssigkeitsfilm;
F — Laplace-Transformierte von C;
F^* — Laplace-Transformierte von C*;
$\left.\begin{matrix}G\\ H\\ \tilde{G}\\ \tilde{H}\end{matrix}\right\}$ — Koeffizientenmatrizen bzw. deren Transformierte;
h — Stoffaustauschfaktor;
K — Reaktionsgeschwindigkeitskonstante;
k — laufender Index;
$\left.\begin{matrix}m\\ M\\ N\end{matrix}\right\}$ — Konstanten;
$\left.\begin{matrix}P\\ P^{-1}\end{matrix}\right\}$ — Diagonalisiertransformation bzw. deren Inverse;
p — Parameter der Laplace-Transformation;
p_k — Polstellen der Laplace-Transformierten;
$\left.\begin{matrix}P\\ Q\end{matrix}\right\}$ — Koeffizienten;
R_1 — Radius bei der Innenseite der Dünnschicht;

R_2 — Innenradius des Dünnschichtreaktors;
s, t — Integrationsvariablen;
S — Eigenvektor des Koeffizientenmatrix;
U — Vektor der exakten Lösung;
$U_0, \tilde{U}_0$ — Anfangswert, bzw. dessen Transformierte;
$V, \tilde{V}$ — Vektor der Annäherungslösung bzw. deren Transformierte;
v — Durchschnittsgeschwindigkeit der Flüssigkeit in der Dünnschicht;
v^* — Durchschnittsgeschwindigkeit des Gases im Gasraum;
x — Ortskoordinate in der Dünnschichtdicke gemessen;
z — Ortskoordinate entlag der Länge des Reaktors;
α — Parameterkomplex;
ζ — Hilfsfunktion;
ζ_∞ — Grenzwert der Hilfsfunktion;
λ — Eigenwerte des Koeffizientenmatrix;
μ — Henrysche Konstante;
ω — Parameterkomplex.

LITERATUR

1. Polinszky, K. et al.: Acta Chim. Acad. Sci. Hung., *85*, 161 (1975).
2. Polinszky, K. et al.: Hung. J. Ind. Chem., *4*, 151 (1976).
3. Kneschke, A.: Differentialgleichungen I., Teubner Verl. Ges., Leipzig, 1965.

SUMMARY

With reference to the previous results the author investigated the possibility of the approximate analytical solution of the chemical reactions of first order carried out in a rotary film reactor. The error of the approximate solution—compared to the result of the exact solution—was determined by analytical error estimation method.

РЕЗЮМЕ

В настоящей работе, на основе полученных ранее результатов исследуются возможности приближённого аналитического описания реакций первого порядка, происходящих в плёночном реакторе. Ошибка приближённого метода по сравненню с точным решением была установлена с помощью аналитического расчёта ошибки.

HUNGARIAN JOURNAL
OF INDUSTRIAL CHEMISTRY
VESZPRÉM
Vol. 6. pp. 423–434 (1978)

ALGORYTHM FOR THE ANALYTICAL APPROXIMATION OF A DIFFUSION MODEL OF DIPHASIC PROCESSES OCCURRING IN HEAT AND MASS TRANSFER

T. VAJDA and T. BLICKLE

(Research Institute for Technical Chemistry of the Hungarian Academy of Sciences, Veszprém, Hungary)

Received: August 30, 1978.

The heuristic method described is used for approximate analytical study of special processes in nonlinear two-phase transport systems. Starting from the usual diffusion model, the method gives a relationship between the input data, the parameters and the output data of the system. An analytical estimate of the error is used to show that in the case of the source functions occurring in practice, the approximate method does not diverge, and its accuracy is satisfactory over the whole range of the independent variable.

Introduction

One of the frequently occurring tasks of the operational science of the chemical industry is the mathematical description of diphasic, one-dimensional, stationary transport systems, which can be characterized by axial mixing, and by a term of source of an arbitrary shape depending only on the value of the relevant potentials. As it is known, this description is carried out, taking the mixing into account by the formalism of the diffusion models, by means of common, second order, homogeneous, non-linear systems of differential equations with two unknowns and of the pertinent boundary conditions of partly inhomogeneous type. However, the second order nature of the mathematical problem, from the aspect of the operational science of the chemical industry, which prefers the use of equations of first order, raises certain problems of contemplation and interpretation, whose solution appeared to be practical. In addition, the possibilities of the analytical solution of the problem of second order are also essentially more limited than those of problem of first order, which are otherwise commensurable from other aspects.

Although a number of authors have already dealt with the approximative solution of the mathematical models of transport processes of various chemical industry types (e.g. [1–6]), the performed investigations have not been

extended to the above mentioned field of problems. On the other hand, certain initial investigations [7] allowed us to assume that the above discussed aims could be fulfilled by means of heuristic considerations. In the present work, by an adequate heuristic reinterpretation of the problem of the second order serving for the mathematical treatment of diffusion models, an approximative mathematical model is developed for the approximative analytical description of the examined transport system in this sense, which description being carried out by means of equations of first order. On transforming the problems of the second and of the first order into appropriate systems of integral equations and on their comparison with each other, it can be proved that the solutions generated by the equation system of first order can be considered in fact as approximative solutions of the equation system of the second order.

If the production of only the outlet potential values, i.e. of the outgoing signals is satisfactory, we shall prove that even the effective solution of the differential equation system of first order can be avoided, and ultimately an algebraic equation system will be obtained for the determination of the outgoing signals. On the other hand, it follows from the generalized character of the initial model that the method is suitable for the approximative analytic description of not only the processes of heat or mass transfer of two interacting phases, but also for that of the parallel processes of heat and mass transfer of one single phase. Furthermore, the method can be further generalized in principle, within the framework of the basic model, for the case of equations of any arbitrary number.

We shall prove by means of an analytical error estimation that the error of the approximation does not diverge in the case of source functions, bounded and satisfying the Lipschitz condition on the set of potential values to be considered in the course of the given process. On applying the exact and the approximative mathematical models in numerical calculations of the same aim and on comparing the obtained results, it can be seen that the suggested method is in the parameter interval of interest from practical aspects, essentially more accurate than that expectable on the basis of the error formula.

The Basic Model and its Approximation

It is known from relevant literature (e.g. [8]) that the transport processes of the systems characterized in the foregoing discussion can be described conventionally by an equation system transformed to the normal form:

$$-A_i \frac{d^2u_i}{dx^2} + \frac{du_i}{dx} - f_i(u_1, u_2) = 0, \quad i = 1, 2 \tag{1}$$

(for the sake of simplicity we deal here only with the direct current systems, but it can be seen that the derivations which will be presented can also be carried out in the case of counter-current). In the above problem (1), the generalized mixing factors A_i are $0 < A_i < +\infty$, the normal co-ordinate x is $0 \leq x \leq 1$, u_i denotes the desired potential functions the transport of the extensive quantities pertaining to which are examined. With regard to later discussions, we presume that on the set of potential values to be taken into account during the given process the source functions f_i are bounded and

satisfy in their all variables the Lipschitz condition with the exponent one. These conditions are always satisfied at the source functions occurring in practice.

The boundary conditions pertaining to the equation system (1), are obtained automatically [9, 10] when the eventual mixing occurring in the environment of the investigated transport system is also described by a diffusion model:

$$u_i(0) - A_i\left(\frac{du_i}{dx}\right)_{x=0} = u_{e_i}, \tag{2}$$

$$\left(\frac{du_i}{dx}\right)_{x=1} = 0, \tag{3}$$

$$i = 1, 2,$$

where the relationships (2) and (3) are also transformed into a normal shape corresponding to the equations (1), u_{e_i} are the input potential values. It can be seen that besides the statements concerning the source functions, the existence and uniqueness of the potential functions generated by the problem (1)—(2)—(3) within the system are ensured.

The equation system (1) is denoted as the diffusion model of the investigated transport system owing to its analogy with an equation of the general mass transport of such a shape, when in this so-called continuity equation the mass flow generated by the phenomenon of diffusion is represented by a term proportional to the gradient of concentration. In the case of a one-dimensional stationary system, on expanding the continuity equation, this obviously denotes the appearance of a term proportional to the second derivative of the potential present, according to the space co-ordinate. Although a term of second order is similarly applied in the diffusion model of transport systems with axial mixing for the description of the mixing process, this term has no physical meaning whatever. Its sole function in the system is the formal representation of the mechanical and thermal effects inducing the mixing process. It is suitable for this purpose, because these latter effects after all alter the system in the sense of homogenization in the same way as common diffusion does.

Let us now discuss the equation system constructed on the basis of heuristic considerations:

$$(1 + A_i)\frac{dv_i}{dx} - f_i(v_1, v_2) = 0, \tag{4}$$

and the boundary conditions pertaining to it:

$$(1 + A_i)v_i(0) - A_i v_i(1) = u_{e_i}, \qquad i = 1, 2, \tag{5}$$

where the functions v_i satisfy the problem (4)—(5), whereas the interpretation of the other quantities present is unchanged. Our next aim is to examine whether the above functions v_i can be used and at which accuracy, as the approximative solutions of the problem (1)—(2)—(3).

The following formal physical interpretation of the approximative mathematical model (4)—(5) is quite obvious. According to the equations (4) corresponding to the formalism of the normal forms under (1), the volume rate of the convective flows of the transport system in the approximative model is taken higher by A_i than the real value. This is attained, as understandable

from the boundary conditions (5), as nodal point equations, in a way that the surplus is allowed to recirculate from the outlet of the system to the inlet, meanwhile maintaining the volume rate of the convective flows leaving the system at a constant level. Thus, the basic and the approximative models differ from each other, from formal physical aspects only in the way of interpretation of mixing. However, this does not obviously determine the interrelations of the adequate mathematical models.

Returning now to the former field of problems, it is obvious that the direct comparison of the problems (1)—(2)—(3) and (4)—(5) is not successful. However, by the formal implicit generation of the solutions, integral relationships can be obtained, which may be considered as integral equation inverses of the original differential equations also comprising the boundary conditions, and thus they are equivalent to the basic problem and to its approximation, respectively. On finding the basis systems of the differential operators present in the equations (1) and (4) respectively, then applying the method of varying the constant [11], the following integral equations are obtained:

$$u_i(x) = u_{e_i} + \int_0^x f_i(u_1(\xi), u_2(\xi))\, d\xi + \int_x^1 e^{\frac{x-\xi}{A_i}} f_i(u_1(\xi), u_2(\xi))\, d\xi, \tag{6}$$

$$v_i(x) = u_{e_i} + \int_0^x f_i(v_1(\xi), v_2(\xi))\, d\xi + \frac{A_i}{1+A_i} \int_x^1 f_i(v_1(\xi), v_2(\xi))\, d\xi, \tag{7}$$

$$i = 1, 2.$$

The formal similarity of the results (6) and (7) is at once conspicuous. On examining the multiplying factors of the third terms at the right sides, which factors distinguish the two equations from each other, it can be stated that this latter appears to be the analytical approximative form of the former. Namely, it can be proved by a simple functional analysis that the integral deviation of the terms $e^{\frac{x-\xi}{A_i}}$ and $\frac{A_i}{1+A_i}$ in the set of the relevant values x and ξ is very small for all A_i. Consequently, the exact and the approximative problems are in a similar relation to each other, as this is generally the case at the construction of approximative analytical forms.

Finally, it was noted that the form of the boundary conditions (5), which differs from that of the usual initial conditions of equations of first order, is an essential feature of the approximative model. It can be seen in turn that on considering what has been said above regarding the source functions f_i, the approximative potential functions, which can be determined from problem (4)—(5) always exist and are unique in cases of practical importance.

Estimation of the Error of Approximation

Let us now briefly survey the analytical method of determining the deviation of the results obtained on using the two types of mathematical models. Let us characterize the accuracy of the approximative model by estimating from

above the quantities:

$$\delta_i(x) = |u_i(x) - v_i(x)|, \qquad i = 1, 2. \tag{8}$$

Then, on using the results of (6) and (7), we obtain from relationship (8) after repeated transformations:

$$\delta_i(x) \leq \int_0^x |f_i(u_1, u_2) - f_i(v_1, v_2)|\, d\xi + \frac{A_i}{1+A_i} \int_x^1 |f_i(u_1, u_2) - f_i(v_1, v_2)|\, d\xi +$$

$$+ \int_x^1 \left| \left(e^{\frac{x-\xi}{A_2}} - \frac{A_i}{1+A_i} \right) f_i(u_1, u_2) \right| d\xi, \tag{9}$$

$$i = 1, 2.$$

Since according to our presumptions concerning the source functions f_i, values of M_i and K_i can be given by means of wich in the set of potential values relevant in the course of the given process:

$$M_i = \max [|f_i(u_1, u_2)|], \tag{10}$$

furthermore:

$$|f_i(u_1, u_2) - f_i(v_1, v_2)| \leq K_i \sum_{j=1}^{2} |u_j - v_j|, \tag{11}$$

$$i = 1, 2.$$

So the system of unequalities (9) can be further transformed on using the relationships (8), (10) and (11):

$$\delta_i(x) \leq K_i \int_0^x \sum_{j=1}^{2} \delta_j(\xi)\, d\xi + \frac{K_i A_i}{1+A_i} \int_x^1 \sum_{j=1}^{2} \delta_j(\xi)\, d\xi + \varphi_i(x, A_i, M_i), \tag{12}$$

$$i = 1, 2,$$

where:

$$\varphi_i(x, A_i, M_i) = M_i \int_x^1 \left| e^{\frac{x-\xi}{A_i}} - \frac{A_i}{1+A_i} \right| d\xi =$$

$$\begin{cases} M_i A_i \left(1 + e^{\frac{x-1}{A_i}}\right) + \dfrac{M_i A_i}{1+A_i}(1-x) + \dfrac{2M_i A_i^2}{1+A_i}\left(\ln \dfrac{A_i}{1+A_i} - 1\right), \\ \text{if } \ 0 \leq x \leq 1 + A_i \ln \dfrac{A_i}{1+A_i}, \\ M_i A_i \left(1 - e^{\frac{x-1}{A_i}}\right) + \dfrac{M_i A_i}{1+A_i}(x-1), \quad \text{if } 1 + A_i \ln \dfrac{A_i}{1+A_i} < x \leq 1, \end{cases} \tag{13}$$

$$i = 1, 2.$$

On introducing the denotions:

$$\Delta(x) = \int_0^x \sum_{i=1}^{2} \delta_i(\xi)\, d\xi, \qquad \alpha = \sum_{i=1}^{2} \frac{K_i}{1+A_i},$$
$$\beta = \sum_{i=1}^{2} \frac{A_i K_i}{1+A_i}, \qquad \Phi(x) = \sum_{i=1}^{2} \varphi_i(x), \tag{14}$$

we obtain from the system of integral inequalities (12) with the use of the denotions under (14) the differential inequality:

$$\frac{d\Delta}{dx} \leq \alpha\Delta + \beta\Delta(1) + \Phi \tag{15}$$

to which the initial condition:

$$\Delta(0) = 0 \tag{16}$$

attaches itself. Finally, on finding a solution to the problem (15)—(16), and resubstituting this in (15) we obtained an upper estimation for the total sum of the errors under (8):

$$\sum_{i=1}^{2} \delta_i(x) < \alpha e^{\alpha x} \int_0^x \Phi(\xi) e^{-\alpha\xi}\, d\xi + \Phi(x) + \beta e^{\alpha} \int_0^1 \Phi(\xi) e^{-\alpha\xi}\, d\xi. \tag{17}$$

The estimation (17) is not the sharpest of those derivable from the inequality (15). Anyhow, it can already be stated from the relationship (17) that due to the readily understandable properties:

$$\lim_{A_i \to 0} \varphi_i(x, A_i, M_i) = \lim_{A_i \to +\infty} \varphi_i(x, A_i, M_i) = 0, \tag{18}$$
$$i = 1, 2$$

of the functions under (13) the error, i.e. the deviation between the results provided by the problems of the second order and those of the first order tends towards zero if the mixing factors A_i tend according to any arbitrary system towards the limit values zero or infinite. These are just the cases without mixing and with complete mixing, which are both of major pratical importance. The numerical analysis of the functions φ_i allows us to guess that the error is in general rather small in the case of source functions f_i which are of small value and do not vary too quickly.

Use of the Approximation for the Mathematical Description of Special Heat and Mass Transfer Processes

In the following, the mathematical description of some important operations of the chemical industry will be carried out by means of the approximative method. First of all, an important remark must be made concerning the structure of the source functions f_i present in the equations. Namely, these differ from each other in general, in cases relevant from the aspect of

applications only in a multiplication factor, and thus a separate method can be given for the determination of the potential values in the end point from the problem (4)—(5).

On taking into account what has been said above, let us now to deal with the case:

$$f_2(v_1, v_2) = Bf_1(v_1, v_2), \tag{19}$$

where B is constant. On comparing the equations of the equation system (4) and applying equation (19) we obtain:

$$(1+A_1)\frac{dv_1}{dx} = \frac{1+A_2}{B}\frac{dv_2}{dx}. \tag{20}$$

Relationship (20) can be at once integrated between the limits zero and x. Thus:

$$(1+A_1)(v_1 - v_1(0)) = \frac{1+A_2}{B}(v_2 - v_2(0)). \tag{21}$$

There is a possibility to use the boundary conditions (5), therefore a novel form of (21) will be:

$$(1+A_1)v_1 - A_1 v_1(1) - u_{e_1} = \frac{1+A_2}{B}v_2 - \frac{A_2}{B}v_2(1) - \frac{u_{e_2}}{B}. \tag{22}$$

Let us now create a relationship between the potential values in the end point, from equation (22) on substituting $x = 1$:

$$v_2(1) = Bv_1(1) - Bu_{e_1} + u_{e_2}. \tag{23}$$

Since (23) can be considered as an independent equation, it can be resubstituted into equation (22), affording for the potential function of subscript 2:

$$v_2 = B\frac{1+A_1}{1+A_2}v_1 + B\frac{A_2 - A_1}{1+A_2}v_1(1) - Bu_{e_1} + u_{e_2} \equiv v_2(v_1). \tag{24}$$

It can be seen that in the case satisfying the condition (19) we obtain a linear relationship of the potential functions present, in which relationship the end point value of one of the potentials occurs as a parameter.

On applying the formula (24) the first equation of the equation system (4) becomes integrable, and with the use of the adequate one of the boundary conditions (5) an algebraic equation is obtained for the determination of the value $v_1(1)$:

$$(1+A_1)\int_{\frac{u_{e1}+A_1v_1(1)}{1+A_1}}^{v_1(1)} \frac{dv_1}{f_1(v_1, v_2(v_1))} = 1. \tag{25}$$

The value $v_2(1)$ is obtained by resubstituting $v_1(1)$ into the relationship (23). Obviously, $v_2(1)$ may also be obtained in a direct way with the use of the inverse form corresponding to relationship (24):

$$v_1 = \frac{1+A_2}{B(1+A_1)}v_2 + \frac{A_1 - A_2}{B(1+A_1)}v_2(1) - \frac{u_{e_2}}{B} + u_{e_1} \equiv v_1(v_2) \tag{26}$$

from the other equation of the equation system (4) respectively, on using the other boundary condition. For that, the algebraic equation is as follows:

$$(1+A_2)\int\limits_{\frac{u_{e_2}+A_2v_2(1)}{1+A_2}}^{v_2(1)}\frac{dv_2}{f_2(v_1(v_2),\,v_2)}=1. \tag{27}$$

Investigation of the Adsorption Process Characterizable by the Langmuir Isotherm

Let us consider the following technical problem. A gas mixture and a granular mass are fed continuously into an adsorber whose cross section is small in comparison to its length. One of the components of the mixture is adsorbed by the grain mass along the length of the equipment (here we must assume conditions under which the volume rate of the gas phase does not change on the effect of the process occurring there along the equipment). We presume that grains adjacent to each other change places during their motion and that, respectively, the gas is mixed up forward and backward in an axial direction during its flow among the grains. We assume that the intensity of the adsorption process is proportional to the deviation of the actual saturation degree of grains by adsorbate and of the equilibrium value, which can be calculated on the basis of the Langmuir isotherm [12].

The mathematical description of the above transport system can be adequately carried out by the problem (1)—(2)—(3). The occurring source functions f_i are in the normal form corresponding to the problem and are as follows:

$$f_1=\frac{a_1L}{V_1}\left(\frac{a_2u_2}{a_3+u_2}-u_1\right),$$

$$f_2=-\frac{a_1LT}{V_2}\left(\frac{a_2u_2}{a_3+u_2}-u_1\right), \tag{28}$$

where the subscript 1 indicates the phase of the adsorbent, subscript 2 the phase of the adsorbate, values V denoting the volume rates of the phases, values a suitable constants, L the length of the equipment and T a proportionality factor. It is quite obvious that owing to the non-linearity of the source functions (28) no analytical solution of problem (1)—(2)—(3) in closed form exists.

On the basis of problem (4)—(5) let us now determine the concentration $v_2(1)$ of the adsorbate at the outlet of the equipment. In this case, the values u of the source functions (28) are according to the sense replaced by values v, furthermore, on comparing relationships (19) and (28) it can be seen at once that:

$$B=-\frac{TV_1}{V_2}. \tag{29}$$

On introducing the denotions:

$$\alpha_2=\frac{1+A_2}{B(1+A_1)},\qquad \beta_2=\frac{A_1-A_2}{B(1+A_1)}\,v_2(1)-\frac{u_{e_2}}{B}+u_{e_1} \tag{30}$$

and comparing expressions (26)—(30) we obtain the following relationship:

$$\frac{a_1 TL}{V_2(1+A_2)} = -\int\limits_{\frac{u_{e_2}+A_2 v_2(1)}{1+A_2}}^{v_2(1)} \left(\frac{a_2 v_2}{a_3+v_2} - \alpha_2 v_2 - \beta_2\right)^{-1} dv_2 . \tag{31}$$

In order to integrate let us arrange the right side of expression (31) to the usual form:

$$\frac{a_1 TL}{V_2(1+A_2)} = \int\limits_{\frac{u_{e_2}+A_2 v_2(1)}{1+A_2}}^{v_2(1)} \frac{(v_2+a_3)\,dv_2}{\alpha_2 v_2^2 + (\alpha_2 a_3 + \beta_2 - a_2) v_2 + \beta_2 a_3} . \tag{32}$$

On carrying out the integration under (32) [14] we obtain the below given algebraic equation for the determination of $v_2(1)$:

$$\frac{a_1 TL}{V_2(1+A_2)} = \frac{1}{2\alpha_2} \ln \frac{\alpha_2 v_2^2(1) + (\alpha_2 a_3 + \beta_2 - a_2) v_2(1) + \beta_2 a_3}{\alpha_2 \left(\frac{u_{e_2}+A_2 v_2(1)}{1+A_2}\right)^2 + (\alpha_2 a_3 + \beta_2 - a_2)\left(\frac{u_{e_2}+A_2 v_2(1)}{1+A_2}\right) + \beta_2 a_3} +$$

$$+ \frac{\alpha_2 a_3 + a_2 - \beta_2}{4\alpha_2 \left(\frac{(\alpha_2 a_3 + \beta_2 - a_2)^2}{4} - \alpha_2 \beta_2 a_3\right)^{1/2}} \cdot \tag{33}$$

$$\cdot \left[\ln \frac{2\alpha_2 v_2 + \beta_2 + \alpha_2 a_3 - a_2 - 2\left(\frac{(\alpha_2 a_3 + \beta_2 - a_2)^2}{4} - \alpha_2 \beta_2 a_3\right)^{1/2}}{2\alpha_2 v_2 + \beta_2 + \alpha_2 a_3 - a_2 + 2\left(\frac{(\alpha_2 a_3 + \beta_2 - a_2)^2}{4} - \alpha_2 \beta_2 a_3\right)^{1/2}} \right]_{\frac{u_{e_2}+A_2 v_2(1)}{1+A_2}}^{v_2(1)},$$

since on investigating the possible values of the occurring physical parameters it can be seen that:

$$\frac{(\alpha_2 a_3 + \beta_2 - a_2)^2}{4} - \alpha_2 \beta_2 a_3 > 0.$$

For the sake of conspicuity we did not indicate the limits of integration in the second term at the right side.

The solution of equation (33) for the value of $v_2(1)$ can be carried out only by numerical methods. However, we obtain a direct reply to the question of much greater importance from practical aspects, i.e. which equipment length is needed in the given case of other process parameters for a change of determined extent of the adsorbate concentration.

Investigation of Absorption in the Case of a Transfer Term of General Form

Let us introduce a liquid continuously at the lower end of an absorber of longitudinal shape, located vertically, and spray a gas mixture into it. One of the components of the mixture representing a small portion of the total volume is absorbed by the liquid. However, under such conditions the volume rate of the gas phase along the equipment cannot change appreciably. From the aspect of its volume elements, the liquid is intensively mixed up by the bubbles moving upwards in the liquid. This movement reacts and creates to a small extent dispersion of the given bubble front. The intensity of the material flow from the gas phase into the liquid phase can be determined on the

basis of the two-film theory [12], consequently the diffusion model applied for the equipment has the following source functions:

$$f_1 = \frac{a_1 L}{V_1}(u_2 - a_2 u_1)^P,$$

$$f_2 = -\frac{a_1 TL}{V_2}(u_2 - a_2 u_1)^P, \tag{34}$$

where 1 is the subscript of the liquid phase, 2 the subscript of the gas phase, P the general exponent of the transfer term, whereas the interpretation of the other quantities corresponds to those given previously (the particular name of the parameter a_2 is: Henry constant).

On the basis of the approximative model, the algebraic equation obtained with the use of the relationships (26), (27), and (29), (30), and (34) for the determination of the outlet concentration of $v_2(1)$ is:

$$-\frac{a_1 TL}{V_2(1+A_2)} = \int_{\frac{u_{e_2}+A_2 v_2(1)}{1+A_2}}^{v_2(1)} (v_2 - a_2(\alpha_2 v_2 + \beta_2))^{-P}\, dv_2. \tag{35}$$

Then, on carrying out the integration in equation (35) and arranging the result, we obtain:

$$\frac{a_1 TL}{V_2(1+A_2)} = \frac{1}{(1-\alpha_2 a_2)(P-1)}\left[((1-\alpha_2 a_2)v_2(1) - a_2\beta_2)^{1-P} - \right.$$

$$\left. -\left((1-\alpha_2 a_2)\frac{u_{e_2}+A_2 v_2(1)}{1+A_2} - a_2\beta_2\right)^{1-P}\right]. \tag{36}$$

In connection with equation (36), the same considerations can be made as those in the case of the example of adsorption.

Description of a Reaction of First Order on Taking into Account the Reaction Heat of the Process

A gas continuously enters an adiabatic tube reactor packed with a catalyst, at one of the ends of the reactor. The gas is isomerized by an exothermic reaction of first order. The increase of the specific volume of the gas mixture, due to the rise of temperature, is neglected. In this case, the volume rate along the equipment is unchanged. Let us assume that the mechanical action of the catalyst bed on the flow of gas is similar to the conditions described in the adsorber. The heat and material balance of the process is described correctly by problem (1)–(2)–(3), the source functions are according to the Arrhenius relationship [12] as follows:

$$f_1 = -\frac{a_1 L u_1}{V_1} e^{-\frac{a_2}{u_2}},$$

$$f_2 = \frac{a_1 TL u_1}{V_2} e^{-\frac{a_2}{u_2}}, \tag{37}$$

where 1 is the subscript of the material balance, 2 the subscript of the heat balance, thus u_1 indicates the concentration of the still not isomerized component, whereas u_2 is the temperature of the gas mixture.

On the basis of the approximative model, let us determine the outlet concentration $v_1(1)$ from which we can reach conclusions concerning the efficiency of the reactor. On introducing the denotions:

$$\alpha_1 = B\,\frac{1+A_1}{1+A_2}, \qquad \beta_1 = B\,\frac{A_2-A_1}{1+A_2}\,v_1(1) - Bu_{e_1} + u_{e_2}, \tag{38}$$

and comparing the relationships (24), (25), and (37) and (38), we obtain for the determination of $v_1(1)$ the equation:

$$-\frac{a_1 L}{V_1(1+A_1)} = \int\limits_{\frac{u_{e_1}+A_1 v_1(1)}{1+A_1}}^{v_1(1)} \frac{1}{v_1}\,e^{\frac{a_2}{\alpha_1 v_1+\beta_1}}\,dv_1 . \tag{39}$$

In order to carry out the integration let us introduce the new variable: $w = \dfrac{1}{\alpha_1 v_1 + \beta_1}$. Subsequently, after repeated transformations of the integrand and distribution to partial fractions, we obtain from equation (39):

$$\frac{a_1 L}{V_1(1+A_1)} = \int\limits_{\frac{1}{\alpha_1\frac{u_{e_1}+A_1 v_1(1)}{1+A_1}+\beta_1}}^{\frac{1}{\alpha_1 v_1(1)+\beta_1}} \frac{1}{w}\,e^{a_2 w}\,dw - \int\limits_{\frac{1}{\alpha_1\frac{u_{e_1}+A_1 v_1(1)}{1+A_1}+\beta_1}}^{\frac{1}{\alpha_1 v_1(1)+\beta_1}} \frac{1}{w-\frac{1}{\beta_1}}\,e^{a_2 w}\,dw. \tag{40}$$

On introducing the so-called integral-exponential function [13]:

$$Ei(x) = \int\limits_{-\infty}^{x} \frac{e^t}{t}\,dt = \lim_{\varepsilon\to 0}\left[\int\limits_{-\infty}^{-\varepsilon} \frac{e^t}{t}\,dt + \int\limits_{\varepsilon}^{x} \frac{e^t}{t}\,dt\right], \tag{41}$$

whose function values are given in tables, the final form of equation (40), after carrying out the integration [14], will be as follows:

$$\frac{a_1 L}{V_1(1+A_1)} = Ei\left(\frac{a_2}{\alpha_1 v_1(1)+\beta_1}\right) - Ei\left(\frac{a_2}{\alpha_1\dfrac{u_{e_1}+A_1 v_1(1)}{1+A_1}+\beta_1}\right) +$$

$$+ e^{\frac{a_2}{\beta_1}}\,Ei\left(\frac{a_2}{\alpha_1\dfrac{u_{e_1}+A_1 v_1(1)}{1+A_1}+\beta_1} - \frac{a_2}{\beta_1}\right) - e^{\frac{a_2}{\beta_1}}\,Ei\left(\frac{a_2}{\alpha_1 v_1(1)+\beta_1} - \frac{a_2}{\beta_1}\right). \tag{42}$$

Although the numerical determination of the potential value in the end point is not a simple task, the inverse formula can still be well used for the determination of the geometrical length of the reactor carrying out the given conversion.

REFERENCES

1. Kondratiew, G. M.: Regularny Teplovy Rezhim., Gostehizdat, Moscow, 1954.
2. Heiligenstädt, W.: Wärmetechnische Rechnungen für Industrieöfen, Stahleisen, Düsseldorf, 1951.
3. Sasvári, G.: Acta Chim. Acad. Sci. Hung., *40*, 343 (1964).
4. Polinszky, K. et al.: Acta Chim. Acad. Sci. Hung., *85*, 161 (1975).
5. Polinszky, K. et al.: Hung. J. Ind. Chem., *4*, 151 (1976).
6. Fülöp, J. et al.: Preprint, Inst. Teplo i Massoobmena Ak. Nauk BSSR. Minsk, 1977.
7. Blickle, T. et al.: Hung. J. Ind. Chem. *5*, 403 (1977).
8. Bird, R. B. et al.: Transport Phenomena. J. Wiley and Sons, New York, 1966.
9. Danckwerts, P. V.: Chem. Eng. Sci., *2*, 1 (1953).
10. Wehner, J. F. et al.: Chem. Eng. Sci., *6*, 89 (1956).
11. Kneschke, A.: Differentialgleichungen I. Teubner Verlagsgesellschaft, Leipzig, 1965.
12. Perry, J. H.: Chemical Engineers' Handbook. McGraw-Hill, New York, 1964.
13. Jahnke, E. et al.: Tafeln Höherer Funktionen, Teubner Verlagsgesellschaft, Stuttgart, 1966.
14. Gröbner, W. et al.: Integraltafeln, Springer Verlag, Wien, 1961.

РЕЗЮМЕ

В данной работе описывается эвристический метод приближённого аналитического исследования двухфазных, нелинейных систем переноса. Исходя из традиционной диффузионной модели, данный метод даёт зависимости медлу входными данными, параметрами системы и выходным сигналом. Путём аналитической оценки ошибки показано, что в случае встречающихся на практике функций источников данный метод не расходится, и его точность удовлетворительна в пределах всего интервала независимой переменной.

HUNGARIAN JOURNAL
OF INDUSTRIAL CHEMISTRY
VESZPRÉM
Vol. 6. pp. 435–440 (1978)

DETERMINATION OF THE FILTRATE OUTPUT OF THE INDUSTRIAL FILTRATION CENTRIFUGE WITH THE AID OF A MODEL SIZED CENTRIFUGE

G. HALÁSZ

(Research Institute for Technical Chemistry of the Hungarian Academy of Sciences, Veszprém, Hungary)

Received: September 16, 1978.

As a starting relation, the general filtration equation was adapted for the filtration in centrifugal force. After transforming the equation into a appropriate form, the reciprocal rate of filtration was plotted against $ln\ (r_3/r_2)$. The slope of the curve gave $\alpha(1-\varepsilon)$.

To determinate $\alpha(1-\varepsilon)$, it was necessary to test the time changes of cake thickness and filtrate output at a constant pressure. "In situ" determining the $\alpha(1-\varepsilon)$ one can estimate the filtrate output of the industrial-sized filtration centrifuge at the same filtering suspension, filter medium and centrifugal force.

This project was aimed at the development of an appropiate method to calculate the volumetric performance of industrial filtration centrifuges. The multiple of the specific resistance and porosity of the filter cake measured on a pilot plant centrifuge was used for the input parameter. In the case of compressible filter cakes, the multiple of porosity and specific resistance is measured in situ in the pilot plant filtration centrifuge.

Calculation starts with Grace's equations [1]:

$$\frac{dV}{dt}\cdot\frac{\mu R_m}{2\pi r_3 h}-\frac{\varrho\omega^2(r_2^2-r_1^2)}{2}=\varrho\omega^2\int_{r_2}^{r_3} r\,dr+\frac{\varrho}{(2\pi h)^2}\left(\frac{dV}{dt}\right)^2\int_{r_2}^{r_3}\frac{dr}{r^3}+\frac{\mu}{2\pi h}\cdot\frac{dV}{dt}\int_{r_2}^{r_3}\alpha(1-\varepsilon)\,\frac{dr}{r}. \qquad (1)$$

Geometrical data are shown in *Fig. 1.*

In the case of compressible filter cakes Eq. (1) can be integrated according to the space co-ordinates only when the specific resistance and porosity are known functions of the cake layer thickness, and the layer thickness is a known function of time. Changes in the cake thickness are assumed to follow the

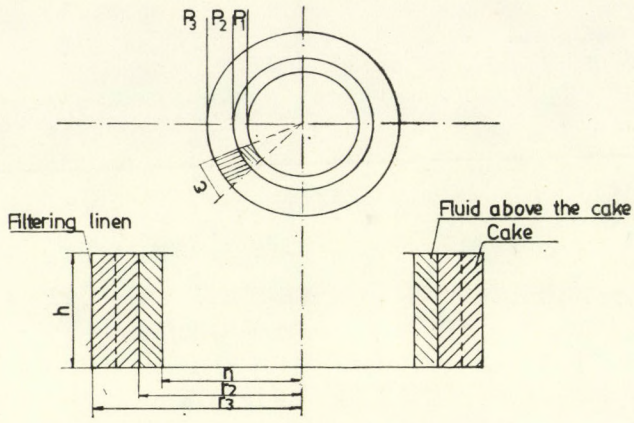

Fig. 1.
Nomenclature of the filtration in centrifuge

„first order rule", i.e.:

$$\frac{dr_2}{dt} = -a \cdot r_2 + b$$

$$r_2|_{t=0} = r_3 \qquad r_2|_{t=\infty} = r_1 \tag{2}$$

Having allowed for the boundary conditions, the solution of Eq. (2) becomes:

$$r_2 = (r_3 - r_1)e^{-at} + r_1 \tag{3}$$

where parameter a is obtained by fitting Eq. (3) to the measured cake layer thickness as time values determined in a pilot plant centrifuge.

Grace's equation can be applied only for incompressible cakes. Let us therefore divide the filtration run into small time segments, Δt, during which the cake can be considered incompressible.

If Eq. (3) is known then Eq. (1) can be integrated in all these time segments and dV/dt data can be obtained:

$$\frac{dV}{dt} = \frac{\pi^3 n^2 \varrho h (r_3^2 - r_1^2)}{30^2 \mu \left[\bar{\alpha}_{\Delta t}(1 - \bar{\varepsilon}_{\Delta t}) \ln\left(\frac{r_3}{r_2}\right) + \frac{R_m}{r_3} \right]} \tag{4}$$

Let us introduce two compounded parameters which are constant for any given machine and materials to be filtered:

$$C = \frac{\pi^3 n^2 \varrho h (r_3^2 - r_1^2)}{30^2 \mu} \qquad c = \frac{R_m}{r_3} \tag{5}$$

Thus Eq. 4 can be rewritten as:

$$C \frac{dt}{dV} = \bar{\alpha}_{\Delta t}(1 - \bar{\varepsilon}_{\Delta t}) \ln\left(\frac{r_3}{r_2}\right) + c \tag{6}$$

So if $C.dt/dV$ is plotted against $\ln (r_3/r_2)$ then the slope of the line yields the multiple of the specific resistance and porosity. If the output flow rate of the filtrate is measured and the kinetics of the cake layer thickness increase is detected, then the curve corresponding to Eq. 6 can be obtained for the filtration period *(Fig. 2)*:

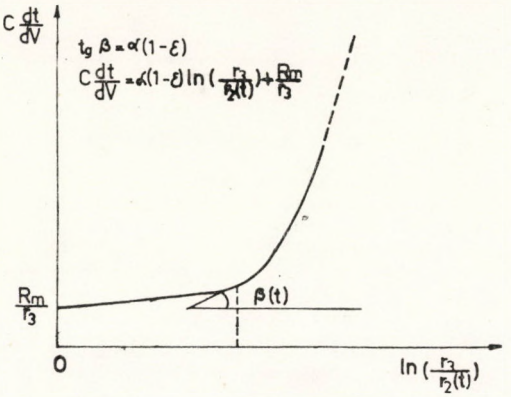

Fig. 2.
Illustration to Eq. (6)

Based on experiments carried out in a pilot plant centrifuge, the multiple of porosity and specific resistance can be obtained for each Δt interval.

The geometrical (r_1, r_2, r_3, h) and operational (n) parameters of an industrial centrifuge are known to aid the selection of the appropriate type. If geometrical and operational parameters, as well as the porosity and specific resistance belonging to a given time interval are suitable for Grace's equation (Eq. 4), then the numerical integration can be carried out. If the computation is repeated for all the successive time intervals, then the volumetric performance of the filtration is obtained.

The above mentioned computation method necessitated the development of a new experimenthal technique. As regards the model centrifuge, the main requirements of the theory are as follows:

The liquid level should be maintained at a constant level by a controlled feed rate for filtration carried out at a constant pressure and in the knowledge of dV/dt required for Eq. (6).

The changes of the layer thickness of the filtration cake should be measured during the course of filtration with parameter a in Eq. (3) obtained by parameter fitting.

SYMBOLS

a — parameter in eq. (2);
h — height of the filter cake;
t — time;
R_m — resistance of the filter cloth;
V — volumetric performance of the centrifuge;
r_1 — distance of fluid above the cake
r_2 — distance of cake surface
r_3 — distance of filtering linen
} from the axis of the centrifuge;

α — relative resistance;
ε — porosity;
ϱ — density;
μ — dynamic viscosity;
ω — angular velocity.

REFERENCE

1. Szűrés (Filtration) (ed. Szabó Zoltán) Műszaki Kiadó, Budapest, 1966.

РЕЗЮМЕ

Взятое за основу общее уравнение фильтрации используется автором применительно к процессу фильтрации в поле центробежных сил. После приведения данного уравнения в соответствующую форму, обратное значение скорости фильтрации изображалось, как функция от $ln\ (r_3/r_2)$. Крутизна кривой даёт значение $(1-\varepsilon)$.

Для определения $\alpha(1-\varepsilon)$ необходимо исследовать изменение во времени толщины лепёшки на фильтре и выхода фильтрата, при условии постоянного давления. Определив $\alpha(1-\varepsilon)$ в данной модельной пилотной центрифуге, можно оценить выход фильтрата промышленной фильтрующей центрифуги для тех же: фильтруемой суспензии, материала фильтра, и центробежного поля сил.

Tájékoztató a közlemények szerzői részére

1. A „Hungarian Journal of Industrial Chemistry" a veszprémi vegyipari tudományos intézmények közös kiadványa, amely angol, orosz, francia vagy német nyelven írt, a vegyipart közvetlenül érintő alkalmazott és alapkutatások eredményeivel, a vegyipari folyamat-, eljárás- vagy művelettannal foglalkozó eredeti közleményeket tartalmaz. A szerkesztő bizottság a veszprémi intézmények alkalmazottain kívül azok részére is lehetővé teszi eredményeik közlését, akik a megjelölt tudományterületen dolgoznak és a megjelenő kémiai tárgyú folyóirataink adott profilja miatt nincs megfelelő lehetőségük munkáik hazai publikálására.

2. A fent említett és/vagy magyar nyelven írt kéziratot két példányban közvetlenül a főszerkesztő címére (Dr. Bodor Endre, Veszprém, Postafiók 28; 8201) küldhetik a szerzők, rövid levél kíséretében, amelynek tartalmaznia kell a következőket:

a) A beküldött kézirat önálló munka, a közölt eredmények ebben a formában más tudományos folyóiratban nem kerülhetnek publikálásra;

b) Amennyiben a közlemény magyar nyelven íródott, a fenti négy nyelv közül melyiken kívánja közleményét megjelentetni?

c) A cikk elfogadása után maguk kívánják-e a fordítást elvégezni, vagy a szerkesztő bizottság gondoskodjék a fordítás elvégzéséről?

d) Közlendő annak a szerzőnek a neve, címe és telefonszáma, akivel a szerkesztőség a nyomdai munkák végzése idején a kapcsolatot felveheti.

A kísérőlevelet a kutatóintézet, a tanszék vagy az üzem vezetőjének a közlést engedélyező láttamozásával kell ellátni.

3. Az A/4 formátumú papírra gépelt kézirat első oldalára csak a közlemény címét, a szerző(k) nevét és munkahelyét továbbá *legfeljebb 15 sor* terjedelemben (soronként 50 leütés!) a közlemény összefoglalóját kérjük gépeltetni.

A *legfeljebb A/4 méretű* ábrákat külön kérjük mellékelni. Részükre a kéziratban helyet nem kell biztosítani. — Külön papíron kérjük az ábrák szövegét az ábraszám feltüntetése mellett felsorolni.

A táblázatok a szöveg közé gépelendők. A táblázatokat is számjelzéssel kell ellátni.

A lábjegyzeteket az illető oldal aljára kell gépeltetni.

Az irodalom felsorolásánál kérjük a Chemical Abstracts-ban alkalmazott közlési mód használatát. (A keresztnév(ek) első betűinek feltüntetése szükséges!)

CONTENTS

PARTI, M.: Transport Processes in Packed Beds 333

DENCS, B. and ORMÓS, Z.: Particle Formation from Solutions in Gas Fluidized Beds. IV. Determination of Average Particle Size and Solid Material Feed Ratio 343

FRATZSCHER, W., HEBECKER, D. und GAFFKE, G.: Zur Gleichgewichtsberechnung und Bewertung gasförmiger Energieträger bei Hochtemperaturprozessen (To the Equilibrium Calculation and Estimation of Gaseous Energy Carriers of High Temperature Processes) 351

GARTSMAN, A. N., CHERKASHIN, V. V. and RASSADNIKOVA, N. I.: Chemical Reaction Accompanied by Mass Transfer in Liquid-Gas Systems. II. Consecutive First and Second Order Chemical Reactions (in the Russian) 361

BIEHOUNEK, J.: The Throughput Availability of a Capacity-Divided Parallel Connection with Internal Capacity Reserve 369

BALLA, L. and SISAK, Cs.: Studies on the Liquid Phase Hydrodynamics in Bubble and Sieve-Plate Columns Equipped with Selective Partitions. I. Liquid Mixing Processes in the Connecting Tubes and on the Selective Partitions Installed between Pairs of Bubble or Sieve-Plate Columns 383

BALLA, L. and SISAK, Cs.: Studies on the Liquid-Phase Hydrodynamics in Bubble and Sieve-Plate Columns Equipped with Selective Partitions. II. Modelling of the Flow Conditions in Counter-Current Cascades 395

VAJDA, T.: Annähernde analytische Beschreibung einer Reaktion ersten Grades in einem Dünnschichtreaktor (Approximate Analytic Description of a First Order Reaction Carried Out in a Rotary Film Reactor) 409

VAJDA, T. and BLICKLE, T.: Algorithm for the Analytical Approximation of a Diffusion Model of Diphasic Processes Occurring in Heat and Mass Transfer ... 423

HALÁSZ, G.: Determination of the Filtrate Output of the Industrial Filtration Centrifuge with the Aid of a Model Sized Centrifuge 435

Egyetemi Nyomda — 78.3547 Budapest, 1979. Felelős vezető: Sümeghi Zoltán igazgató

THE FOLLOWING ARE PLEASED TO ACCEPT SUBSCRIPTIONS TO THIS JOURNAL:

AUSTRALIA

C.B.D. Library and Subscription Service
Box 4886 G.P.O.
Sydney 2000

Cosmos Book and Record Shop
145 Acland Street
St. Kilda 3182

Globe and Co.
694—696 George Street
Sydney 2000

AUSTRIA

Globus (VAZ)
Höchstädtplatz 3
A—1200 Wien XX

BELGIUM

"Du Monde Entier" S. A.
Rue du Midi 162
B—1000 Bruxelles

Office International de Librairie
Avenue Marnix 30
B—1050 Bruxelles

CANADA

Pannonia Books
P.O. Box 1017
Postal Station "B"
Toronto, Ontario M5T 2T8

DENMARK

Munksgaard's Boghandel
Norregade 6
DK—1165 Copenhagen K

FINLAND

Akateeminen Kirjakauppa
Keskuskatu 2, P.O.B. 128
SF—00 100 Helsinki 10

FRANCE

Office International de Documentation et Librairie
48 Rue Gay Lussac
75 Paris 5

GERMAN FEDERAL REPUBLIC

Kubon und Sagner
Pf 68
D—8 München 34
BRD

GREAT BRITAIN

Bailey Bros and Swinfen Ltd.
Warner House, Folkestone
Kent CT 19 6PH England

HOLLAND

Martinus Nijhoff
Periodicals Department
P.O. Box 269
The Hague

Swets and Zeitlinger
Keizersgracht 487
Amsterdam C

ITALY

Licosa
P.O.B. 552, Via Lamarmora 45
50121 Firenze

JAPAN

Igaku Shoin Ltd.
Foreign Department
Tokyo International P.O. Box 5063
Tokyo

Maruzen Co. Ltd.
P.O. Box 5050
Tokyo International 100—31

Nauka Ltd.
Yasutomi Bldg. 5F 2—12 Kanda
Jinbocho, Chiyoda-ku
Tokyo 101

NORWAY

Tanum—Cammermayer
Karl Johangt. 41—43
Oslo 1

SWEDEN

Almqvist and Wiksell Förlag A. B.
Box 2120
S—103 13 Stockholm 2

Wennegren—Williams AB
Subscription Department Fack
S—104 Stockholm 30

SWITZERLAND

Karger Libri A. G.
Petersgraben 31
CH—4011 Basel

USA

Ebsco Subs. Services
1 st Ave North at 13th street
Birmingham, Ala. 35201